Computational Modeling of Immune Signals

Ravi Starzl

CMU-LTI-12-008

Language Technologies Institute
School of Computer Science
Carnegie Mellon University
5000 Forbes Ave., Pittsburgh, PA 15213
www.lti.cs.cmu.edu

Thesis Committee:

Jaime Carbonell Ph.D., Carnegie Mellon University
Raj Reddy Ph.D., Carnegie Mellon University
Tom Mitchell Ph.D., Carnegie Mellon University
Chien Ho Ph.D., Carnegie Mellon University
Stefan Schneeberger M.D., Johns Hopkins University School of Medicine and Innsbruck Medical University

Submitted in partial fulfillment of the requirements
for the degree of Doctor of Philosophy
In Language and Information Technologies

Abstract

The primary obstacle to enabling wide spread adoption of composite tissue transplantation, as well as to improving long-term solid organ transplant outcomes, is establishing a personalized medication regimen optimizing the balance between immunosuppression and immune function - the individual minimum effective level of immunosuppression. Presently, the clinical gold standard for monitoring immune function is histologic inspection of biopsy for tissue damage, or monitoring blood chemistry for signs of organ failure. These trailing indicators reflect damage that has already accumulated, and are of little use in proactively determining the immunologic state of a patient.

Samples collected from small animal surgical models were used to quantify the amount of immune signaling protein present (cytokines and chemokines) under various experimental conditions. Patterns in protein expression that reliably discriminate amongst the groups were then investigated with statistical inference methods such as the logistic classifier, decision tree, and random forest, operating in both the original feature space and in transformed feature spaces.

This work demonstrates computational methods are effective in elucidating and classifying cytokine profiles, allowing the detection of rejection in composite tissue allografts well in advance of the current clinical gold standard, and shows that the methods can be effective in solid organ contexts as well. This work further determines that cytokine patterns of inflammation associated with rejection are specific to the structure and composition of the tissue in which they occur, and can be distinguished from immune signaling patterns associated with unspecific inflammation, wound-healing, or immunosuppressed tissue.

Clinical translation of these findings may provide novel computational tools that enable physicians to design personalized immunosuppression strategies for patients. The methods described in this work also provide information that can be used to investigate the biological basis for the observed immune signaling patterns. Further development may provide a computational framework for identifying novel therapeutic strategies in other pathologies.

Chapter 1 Introduction **1**
Current State of the Art **1**
What is Needed **5**
The Approach of this Work **5**
Thesis Hypotheses **7**
Hypothesis 1: Detection of rejection 8
Hypothesis 2: Separation of tissues 8
Hypothesis 3: Isolating Specific Forms of Inflammation in a Heterogeneous Set 8
Chapter 2 Literature Review **9**
Organ Transplantation **9**
Rejection Marker Literature **11**
Composite Tissue Allotransplantation 12
Similarities in Early Skin Rejection and Other Sources of Skin Inflammation 13
Computational Literature **15**
Alternative and Experimental Methods for Detecting Rejection **16**
Chapter 3 Methods **18**
Data from the Literature is Necessary but Not Sufficient 18
The Necessity of the Small Animal Model 18
Experiment Design **19**
Selection of Surgical Models 19
Cohorts, Groups, and Sampling 20
Orthotopic Limb Transplantation 21
Contact Hypersensitivity (CHS) 22
Delayed Type Hypersensitivity (DTH) 23
Incisional Wound Healing 24
Heterotopic Heart and Lung Transplant 24
Rejection Grade Assessment 25
Sample Selection, Quantification, and Mass Normalization 26
Computation Modeling and Analysis 26
Data Conditioning 27
Classification Tasks 28
Classification Methods 29
Feature Transformation: Multivariate Analysis of Variance (MANOVA) 30
Performance Evaluation Metrics 31
Baseline Performance 33
Chapter 4 Results **34**
Histology **34**
Raw Cytokine Concentrations **36**
Tissue Specific Patterns of Inflammation **41**
Baseline Performance for Separation of Tissues 41
Enhanced Performance for Separation of Tissues 43
Identification of Rejection in Allograft vs Isograft **53**
Baseline Performance for Identification of Allograft vs Isograft 57
Enhanced Performance for Identification of Allograft vs Isograft 60
Identifying Specific Forms of Inflammation in a Heterogeneous Set **69**
Baseline Performance for Detection of Rejection Associated Inflammation 71
Enhanced Performance in Detection of Rejection Associated Inflammation 74
Baseline in Identification of Inflammation Type 80
Performance in Enhanced Identification of Inflammation Type 85

Combined Tissue Model Performance **93**
Solid Organ Performance **94**
Baseline Heart Performance 94
Enhanced Heart Performance 96
Baseline Lung Performance 97
Enhanced Lung Performance 99

Chapter 5 Discussion **101**
Separation of Tissues **101**
Separation of allograft from Isograft **102**
Isolating Specific Forms of Inflammation in a Heterogeneous Set **103**
Separation of Rejection from Not Rejection Associated Inflammation **103**
Going One Step Further: Identification of Inflammation Type **104**
Extension to Solid Organs **105**
Future Work **106**

Chapter 6 Summary and Conclusion **107**
Acknowledgements **109**
Research Support 111
References **112**

Appendix A Data Tables **121**
Histology **121**
Hypothesis 1 Skin **125**
Allograft vs Isograft 125
All Time Points 125
POD <= 5 128
POD > 5 131
Rejecting versus Suppressed Tissue 134
Hypothesis 1 Muscle **137**
Allograft vs Isograft 137
All Time Points 137
POD <= 5 140
POD > 5 143
Rejecting versus Suppressed Muscle 146
Hypothesis 2 Allograft **148**
All Time Points 148
POD <= 5 148
POD > 5 150
Hypothesis 2 Isograft **151**
All Time Points 151
POD <= 5 151
POD > 5 153
Hypothesis 2 FK-Treated **154**
Hypothesis 2 FK-Treatment Withdrawn **154**
Hypothesis 2 Naïve **155**
Hypothesis 3 Skin **156**
Rejection vs Not Rejection 156
All Time Points 156
POD <= 5 159
POD > 5 163
Type of Inflammation 166

All Time Points 166
POD <= 5 169
POD > 5 174
Hypothesis 3 Muscle 179
Rejection vs Not Rejection 179
All Time Points 179
POD <= 5 181
POD > 5 183
Type of Inflammation 186
All Time Points 186
POD <= 5 189
POD > 5 193
Cytokine Intergroup r Statistic Values 197
Appendix B Hypothesis 1 Figures 198
Allograft vs Isograftin Skin (all time points) 198
Original 14-Dimensional Feature Space 198
5-Dimensional Feature Selected Space 199
MANOVA Transformed Feature Space 201
Hybrid Feature Space 202
ROC Curves in Skin 204
Original Feature Space 204
Hybrid Feature Space 207
Allograft vs Isograftin Skin (POD <= 5) 209
Original 14-Dimensional Feature Space 209
5-Dimensional Feature Selected Space 212
MANOVA Transformed Feature Space 213
Allograft vs Isograftin Skin (POD > 5) 215
Original 14-Dimensional Feature Space 215
5-Dimensional Feature Selected Space 218
MANOVA Transformed Feature Space 219
Allograft vs Isograft in Muscle (all time points) 221
Original 14-Dimensional Feature Space 221
5-Dimensional Feature Selected Space 223
MANOVA Transformed Feature Space 224
Hybrid Feature Space 226
ROC Curves in Muscle 228
Original Features 228
Hybrid Features 230
Allograft vs Isograft in Muscle (POD <= 5) 232
Original 14-Dimensional Feature Space 232
5-Dimensional Feature Selected Space 235
MANOVA Transformed Feature Space 237
Allograft vs Isograft in Muscle (POD > 5) 238
Original 14-Dimensional Feature Space 238
5-Dimensional Feature Selected Space 241
MANOVA Transformed Feature Space 243
Rejecting vs Suppressed in FK Treated Skin 244
Original 14-Dimensional Feature Space 244
5-Dimensional Feature Selected Space 246
MANOVA Transformed Feature Space 247

Rejecting vs Suppressed in FK Treated Muscle **249**
Original 14-Dimensional Feature Space 249
5-Dimensional Feature Selected Space 250
MANOVA Transformed Feature Space 251
Appendix C Hypothesis 2 Figures **254**
Skin vs Muscle in Allograft **254**
All Time Points 254
POD <= 5 255
POD > 5 258
Skin vs Muscle in Isograft **261**
All Time Points 261
POD <= 5 262
POD > 5 265
Skin vs Muscle in FK-Treated **268**
All Time Points 268
Skin vs Muscle in FK-Treatment Withdrawn **270**
All Time Points 270
Skin vs Muscle in Naive **271**
Appendix D Hypothesis 3 Figures **274**
Rejecting vs. Not Rejecting in Skin (all time points) **274**
Original 14-Dimensional Feature Space 274
5-Dimensional Feature Selected Space 276
MANOVA Transformed Feature Space 278
Hybrid Feature Space 279
ROC Curves in Skin: Rejection 281
Rejection in Original Feature Space 281
Rejection in Hybrid Feature Space 284
Rejection vs. Not Rejection in Skin (POD <= 5) **286**
Original 14-Dimensional Feature Space 286
5-Dimensional Feature Selected Space 289
MANOVA Transformed Feature Space 291
Rejecting vs. Not Rejecting in Skin (POD > 5) **292**
Original 14-Dimensional Feature Space 292
5-Dimensional Feature Selected Space 295
MANOVA Transformed Feature Space 297
Rejecting vs. Not Rejecting in Muscle (all time points) **298**
Original 14-Dimensional Feature Space 298
5-Dimensional Feature Selected Space 300
MANOVA Transformed Feature Space 302
Hybrid Features 303
ROC Curves in Muscle: Rejection 306
Rejection in Original Feature Space 306
Rejection in Hybrid Feature Space 308
Rejection vs. Not Rejection in Muscle (POD <= 5) **310**
Original 14-Dimensional Feature Space 310
5-Dimensional Feature Selected Space 313
MANOVA Transformed Feature Space 315
Rejection vs. Not Rejection in Muscle (POD > 5) **316**
Original 14-Dimensional Feature Space 316

5-Dimensional Feature Selected Space 319
MANOVA Transformed Feature Space 321
Type of Inflammation in Skin (all time points) 323
Original 14-Dimensional Feature Space 323
5-Dimensional Feature Selected Space 324
MANOVA Transformed Feature Space 325
Hybrid Feature Space 327
ROC Curves in Skin: Wound Healing and Unspecific Inflammation 330
Wound Healing in Original Feature Space 330
Wound Healing in Hybrid Feature Space 332
Unspecific Inflammation in Original Feature Space 334
Unspecific Inflammation in Hybrid Feature Space 337
Type of Inflammation in Skin (POD <= 5) 339
Original 14-Dimensional Feature Space 339
5-Dimensional Feature Selected Space 342
MANOVA Transformed Feature Space 343
Type of Inflammation in Skin (POD > 5) 345
Original 14-Dimensional Feature Space 345
5-Dimensional Feature Selected Space 348
MANOVA Transformed Feature Space 349
Type of Inflammation in Muscle (all time points) 351
Original 14-Dimensional Feature Space 351
5-Dimensional Feature Selected Space 353
MANOVA Transformed Feature Space 355
Hybrid Features 356
ROC Curves in Muscle: Wound Healing and Unspecific Inflammation 358
Wound Healing in Original Feature Space 358
Wound Healing in Hybrid Feature Space 360
Unspecific Inflammation in Original Feature Space 363
Unspecific Inflammation in Hybrid Feature Space 365
Type of Inflammation in Muscle (POD <= 5) 367
Original 14-Dimensional Feature Space 367
5-Dimensional Feature Selected Space 370
MANOVA Transformed Feature Space 372
Type of Inflammation in Muscle (POD > 5) 373
Original 14-Dimensional Feature Space 373
5-Dimensional Feature Selected Space 376
MANOVA Transformed Feature Space 378

Appendix E Related Literature 380
Cytokines, Chemokines, and Their Role in the Immune System 380
Themes in Transplantation 381
Immunosuppression and Immunsuppressive Agents (specifically Tacrolimus) 381
Rejection and Markers of Rejection 382
Tolerogenic and Minimal Immunosuppression Therapy 382
Classifiers and Statistical Learning 383
Feature Transformation Methods 383
Complexity, Efficiency, Signaling, and Systems 383
Prior Publications and Refereed Conference Presentations in the Area 384

Chapter 1 Introduction

Rejection is the name given to the powerful and destructive inflammatory response of the body to transplanted organs that have different histocompatibility features from the host. Rejection is characterized by a powerful cell-mediated cytotoxic response that inexorably destroys the allograft, unless it is moderated or suppressed by therapeutic intervention. It is the bane of clinical transplantation and it is the underlying reason why toxic immunosuppression therapy is required.

Simply maximizing immunosuppression dosage is not a viable option. Instead, it is necessary to minimize both rejection and immunosuppression to achieve an optimal outcome. Achieving this goal requires the ability to assess whether rejection is developing in advance of gross histological damage.

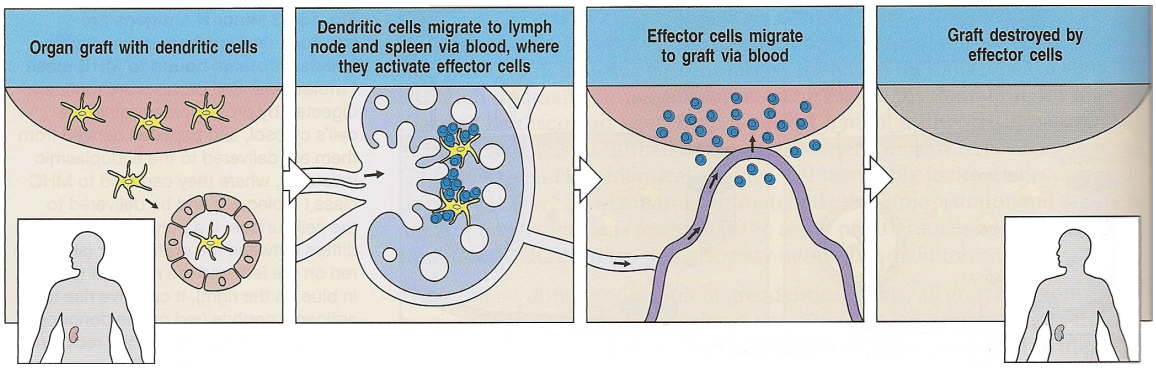

Figure 1.1 from (Murphy 2011) p. 656

While the detection of a wide range of markers is now technically possible at a reasonable price with excellent accuracy, clinicians have not yet found a way to make use of these newly accessible informational features to detect rejection in advance of gross histological damage.

Sample collection, marker quantification, and immunosuppressive treatment are all areas with sophisticated solutions, but they cannot currently be integrated to full effect. Timely information about the current state and likely course of rejection, or the balance between rejection and immunosuppression, is not available. In part this is because no method of analysis using these markers has emerged with sufficient sensitivity, specificity, and cost efficiency to be clinically relevant.

This thesis lays the foundations for a system to provide such information by demonstrating that rejection can be detected in advance of gross histological damage, with high specificity and sensitivity, through the computational modeling of currently quantifiable proteomic immune signaling factors.

Current State of the Art

The current gold standard method for detecting rejection in allografts is the pathologist examination of a tissue biopsy. Biopsies can be collected as part of a standard post-operative care routine, or in response to observed abnormalities in the organ or its function.

In this procedure, pathologists examine a slide-mounted slice of the biopsy and measure three factors; lymphocytic infiltrate, structural compromise of the tissue, and blood vessel damage. Pathologist readings result in gradings that label the current state of the tissue on a scale of rejection, such as the Banff scale. We shall refer to this method of detecting rejection as detecting rejection by histology. A diagrammatic overview of the current clinical process is provided in (Figure 1.2).

When information about the underlying pathology of the sample is not provided, the histology of rejection is often difficult or impossible to distinguish from contact hypersensitivity (CHS), insect bites or dermatophyte infections (Kanitakis et al. Transplantation 2000).

From the perspective of managing patient immunosuppression, detecting rejection by histology suffers from serious drawbacks:

- The measured factors reflect damage that has already occurred (following indicators), and the factors become visible as the damaging runaway inflammation is approaching its peak (as inflammation activity is exponentially accelerating).
- Once advanced rejection has been detected by histology rescue by a bolus of immunosuppressants, such as corticosteroids, is usually required.
- Histopathological changes associated with rejection are very similar to several common inflammatory dermatoses (e.g. contact hypersensitivity)

The detection of rejection by histology followed by one or more rescue bolus treatments sets the stage for undesirable potential outcomes:

- Opportunistic infection allowed by a weakened immune system
- Chronic rejection from vasculopathy caused by damage from inflammation
- Inappropriate treatment for inflammation from a different source (e.g. CHS)

Failure to properly identify and manage rejection carries substantial penalties in mortality and financial cost associated with rehospitalizations.

Because of the high human and financial cost of rejection the standard clinical practice has become treatment with high levels of multiple immunosuppressants, commonly termed multi-drug or triple therapy. This therapy commonly applies a corticosteroid (e.g. Prednisone), calcineurin inhibitor (e.g. Tacrolimus), and anti-proliferative agent (e.g. Azathioprene).

Although this approach often prevents the manifestation of rejection, over immunosuppression creates its own serious problems that can be just as serious as rejection. Opportunistic infections in patients with weakened immune systems often lead to morbidities, and routinely requires rehospitalization. The immunosuppressant regimen is also toxic to many of the body's organs, especially the kidney. Transplant recipients (of any kind) frequently require downstream kidney transplants due to immunosuppressant toxicity.

The conflicting objectives of preventing rejection and minimizing immunosuppression create a situation where clinicians and their patients must

balance on a razor's edge. An imbalance in therapy leading to over or under immunosuppression can rapidly and permanently affect patient morbidity and mortality.

Adding to the difficulty of the task is the lack of methods to assess the effect that any given level of immunosuppression will have on a patient's immune system. Inevitably this has led to the clinical standard becoming a trial-and-error method to try to find the appropriate balance of immunosuppression and quality of life.

The amount of immunosuppression in a patient is measured as a combination of regular dose amounts and trough levels in the patient's body. Clinicians attempt to achieve a delicate balance between immunosuppression and rejection by optimizing immunosuppressant dose, immunosuppressant trough level, rejection, morbidity, and patient quality of life. Immunosuppressant dose is the driving factor for these tightly linked effects. Changes in dosing will affect immunosuppressant trough levels, which in turn will affect rejection, morbidity, and patient quality of life. This can also be seen as optimizing the balance between immunosuppression and rejection.

Changes in dosing can take up to several days to affect trough levels. Changes in immune system activity allowed by changes in trough levels in turn can take from one to three additional days to manifest at the histological level. Thus it can take up to a week (or possibly more) for a clinician to assess changes to immunosuppression therapy. This effectively limits the ability of clinicians to be responsive to the fluid and evolving immunologic state of an individual. It also locks clinicians into a reactive management mode that encourages error on the side of over immunosuppression.

Patients with inadequate immunosuppression develop a clear rejection pathology for which grading has been well established. Clinicians currently infer the extent to which a patient is over-immunosuppressed on a case-by-case basis through morbidity and quality of life measures.

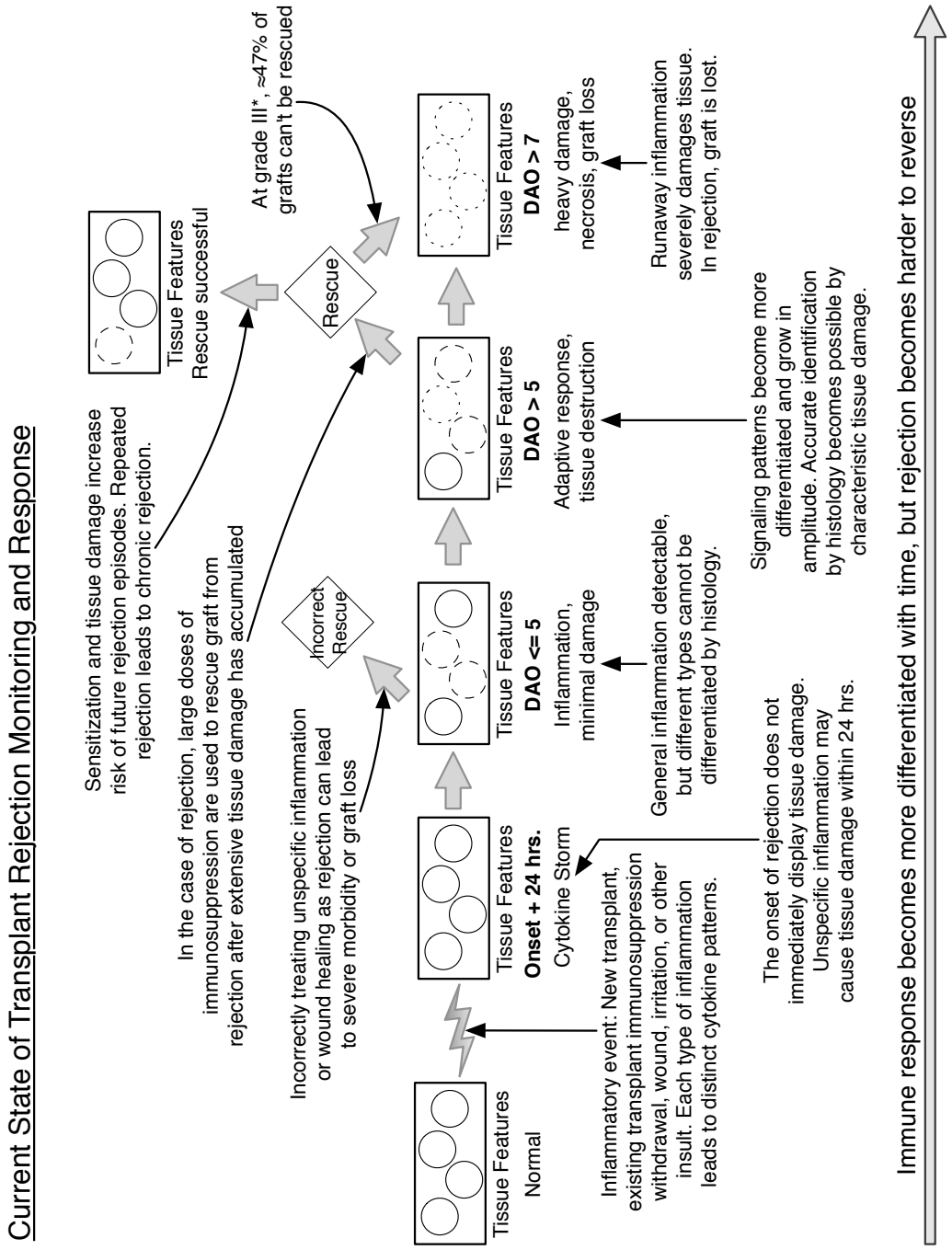

DAO = Days After Onset of Immune Response
**Graded by Banff 2007 rejection grading criterion*
Figure 1.2 Diagram illustrating standard current clinical process of monitoring for and responding to rejection in allografts.

What is Needed

While effective sampling, marker quantitation, and immune suppression options are available, the missing piece for clinicians is a system that can guide them in making decisions about immunosuppressant dosing (Figure 1.3). This system needs to provide information about whether rejection has developed in tissue before the damage manifests visibly (histologically), and it needs to be able to provide immediate feedback about the downstream effects of changes in dosing. The system also must be robust to false positives from inflammation that is not associated with rejection.

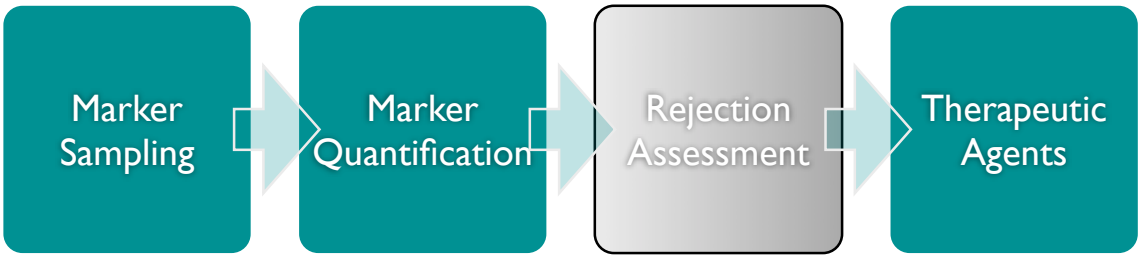

Figure 1.3 Accurate and information rich assessment of rejection state and trend is needed

A reduction in the time needed to assess treatment changes would allow clinicians to much more rapidly home in on the correct dosing regimen for each individual patient. A turnaround time of one to two days would allow novel approaches such as immunomodulation, minimal immunosuppression, and tolerogenic protocols to become a common clinical reality.

Although far more information than the factors currently measured by pathologists is now available, these additional dimensions of data have not yielded the improved predictive power they seem to promise. The primary factor contributing to this is the complexity of the immune system itself.

The Approach of this Work

The immune system is truly a complex adaptive system, and our understanding of it is still in its infancy. The immune system is ubiquitous and continuously active. It operates on multiple scales, is an integral part of homeostasis in nearly all tissues, and is the coordinating system for responses to pathologies. These complexities, with interdependent variables, context dependence, and the scarcity of mechanistic information have all made the area challenging to further elucidate with traditional methods described in the immunology or transplant literature.

However, new computational methods that have enabled significant advances in complex symmetrical problems from other areas of science, such as language technologies and machine learning, have the potential to enable significant improvements in modeling the immunology and transplant areas. The application of these methods requires an understanding of immunology, complexity, and computer science, as it is necessary to adapt the utility of computational algorithms

to the actual biology, and it is likewise necessary to translate the numerical results into biologically relevant (and accurate) elucidations.

The application of the methods described in this work provides a framework with which the current standard clinical process of monitoring and responding to rejection (Figure 1.2) may be transformed. By changing the metric of rejection from tissue damage to the biochemical signaling patterns that are the signature of rejection, the ability to identify and differentiate inflammation, as well as use existing therapies more effectively, becomes immediately available to clinicians. One diagrammatic example of how this technology can be applied in practice is provided in (Figure 1.4), where tissue damage is not visually assessed and the only metric of assessment is immune signaling.

Further development may also lead to an important new therapeutic capability, the direct intervention in regulatory immune signaling pathways through highly targeted cytokines, chemokines, or other agents with specific immune signaling regulatory functions. The ability to elucidate and differentiate specific states associated with specific conditions, to modulate specific signaling pathways, and the ability to rapidly observe the response to these interventions could enable an entirely new paradigm for more effective rejection management.

While this thesis demonstrates the application of these methods specifically to rejection management, it is clear that the ability to analytically map and intervene in specific regulatory and inflammatory immune signaling pathways would have enormous implications for many other areas of immunology and medicine such as oncology, autoimmunity, infectious disease, trauma and burn, and others.

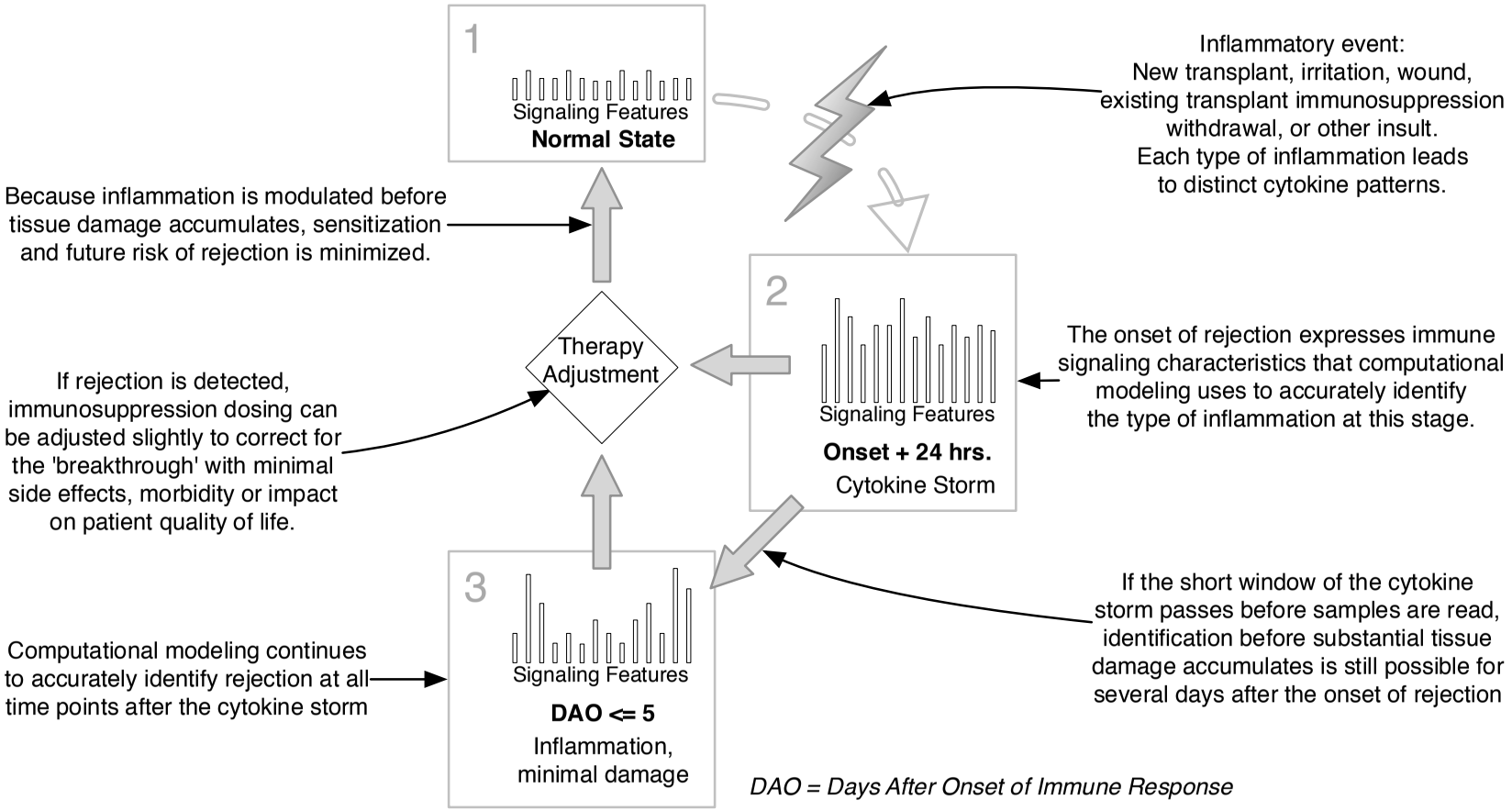

Figure 1.4 Diagram illustrating the computational modeling enhanced process of monitoring and responding to allograft rejection .

Thesis Hypotheses

This thesis examines the validity of three key hypotheses that lead to a system utilizing computational modeling methods applied to immune signaling (cytokine) profiles quantified from tissue samples that provides information about rejection before damage manifests visibly (histologically), and which provides rapid feedback about the effects of changes in dosing.

Hypothesis 1: Detection of rejection

The onset of rejection can be reliably and accurately detected in advance of the current clinical standard by measuring proteomic immune signaling factors associated with inflammation, and using computational models to predict whether these factors are indicative of rejection.

Hypothesis 2: Separation of tissues

Immune signaling patterns that drive rejection within each tissue are distinct.

Hypothesis 3: Isolating Specific Forms of Inflammation in a Heterogeneous Set

Cytokine patterns of inflammation associated with rejection can be distinguished from other unspecific, wound-induced, or immunosuppressed patterns.

All three of these hypothesis were confirmed, as discussed in greater detail in the remainder of this dissertation.

Chapter 2 Literature Review

This work builds upon the current state of the art in multiple fields of science and medicine. A historically oriented introduction to the areas of solid organ transplantation, composite tissue transplantation, and computational/statistical literature most relevant to this work is provided.

Organ Transplantation

The concept of replacing organs or limbs that have become diseased or damaged is a deeply rooted human dream, so old it that has been incorporated into our mythology in chimeric beings like the Hindu Ganesha(Narain 1991). The oldest recorded attempted transplant was the use of skin from a donor to conduct a reconstructive rhinoplasty on another man, performed by the classical Indian surgeon Sushruta, sometime between 1000 and 600 BCE (Ackerknecht 1982; Hauben 1984; Saraf 2007). Throughout the ages surgeons have attempted transplantation time and again, but it was not until key contributions from Medawar, Brent, and Billingham at the turn of the 20th century that real progress in understanding the biology underlying host-allograft interactions was made(Medawar 1944; Billingham, Brent, and Medawar 1956; Billingham and Silvers 1961). At approximately the same time, important insights into the circulation and role of lymphocytes in relevant immunologic response were being made(Gowans 1959; Farr 1951; PERRY et al. 1959; Keohane 1958; Hulse 1959). This essential work came on the heels of important early descriptions of lymphocyte activity in inflammation (Bunting 1921; Yoffey 1933; Yoffey 1936; Kolouch 1939).

As the scientific foundations for transplant biology rapidly evolved, the first successful kidney transplant between identical twins was conducted in 1954 (Murray, Merrill, and Harrison 2001; Merrill et al. 1956). Although a surgical success, little immunologic information was generated because the transplant was not an allograft (or homograft). The monozygotic twins were genetically identical and therefore shared the same major histocompatibility complex (MHC). Rejection virtually never occurs in such cases. The identical twin transplant of 1954 was an isograft, sidestepping entirely the potent unresolved issues of allogenicity, and immunologically more similar to an autograft than an allograft. It would not be until the 1960's that appreciable graft survival was achieved in MHC mismatched patients (Thomas E Starzl 1963; THOMAS E STARZL 1963; T E STARZL 1963; Murray, Merrill, and Harrison 1963)

Throughout the 1960's and 1970's, attempts to control rejection included irradiation of the recipient to neutralize the host immune system (Hulse 1959; Hume, Magee, and Kauffman 1963; Gleason 1967; Wolf, McGavic, and Hume 1969; Jones, Wilson, and Bealmear 1971; Penn and Starzl 1972), the administration of azathioprine (Thomas E Starzl 1963; THOMAS E STARZL 1963; T E STARZL 1963; Murray, Merrill, and Harrison 1963), and eventually treatment with anti-lymphocyte globulin (ALG/ALS) (Lwason, Ellis, and Hodges 1966; Greaves et al. 1967; T. E. Starzl, Groth, and Brettschneider 1967; GRAY, MONACO, and RUSSELL 1964; Huntley et al. 1966). Although these were shown to have beneficial effects on

graft survival, morbidities were extensive (RIFKIND, Marchioro, WADDELL, and Starzl 1964; RIFKIND, Starzl, Marchioro, WADDELL, ROWLANDS, and HILL 1964; T. E. Starzl, Marchioro, Porter, MOORE, RIFKIND, and WADDELL 1964), rejection was still a threat (T. E. Starzl, Marchioro, Brittain, Holmes, and WADDELL 1964), and graft-versus-host disease would sometimes overtake patients (Billingham 1966; Glucksberg et al. 1974; G E Sale 1977; LAWLEY and PECK 1977; Korngold 1978; Graze 1979; Shulman et al. 1980; Matsuoka 1981).

With the arrival of cyclosporine in the late 1970's, a new era in the clinical viability of transplantation as a therapeutic intervention dawned. Significant improvements in outcome and graft survival were achieved first in liver (T. Starzl, Klintmalm, and Porter 1981), then in kidney (Group 1983) patients. A new class of immunosuppressant, cyclosporine was powerful enough to provide the high levels of immunosuppression required for managing transplants, with fewer of the morbidities associated with prior treatment regimens.

However, these improvements came with a price. Cyclosporine was shown to be nephrotoxic over time (Shulman, Striker, and Kennedy 1981; Myers, Ross, and Newton 1984; GoranBG 1981), and care still had to be taken to avoid the morbidities associated with a suppressed immune system, such as infection (Dummer, Hardy, and Poorsattar 1983). Despite these drawbacks, the level of clinical improvement cyclosporine offered over previous methods was very compelling, and cyclosporine fueled much of the explosive growth in transplantation during the 1980s and beyond (Colombo and Ammirati 2011; Furukawa 2004; Borel 2002).

In late 1987 a report from Japan introduced FK-506 (Tacrolimus) as a new and potent immunosuppressive agent (Ochiai et al. 1987). Additional studies rapidly followed in more animal models, confirming FK-506's effectiveness in suppressing and rescuing grafts from rejection (Venkataramanan et al. 1987; Zeevi et al. 1987; Todo et al. 1987; Murase et al. 1987; Makowka et al. 1987; Nalesnik et al. 1987; Thiru, Collier, and Calne 1987). Synergistic effects with cyclosporine were also observed (Sanghvi et al. 1987; Zeevi et al. 1987). The potency of FK-506, and its synergistic effects with other drugs, would open the door for future therapeutic strategies to leverage immunosuppression dosage as a controller for modulating the tolerance/rejection balance in transplants (T. E. Starzl 1988).

The search for cyclosporine's mechanism of action began almost immediately after it was shown to have clinical promise, but it was not until after the introduction and clinical adoption of FK-506 in the early 1990's that both FK-506 and cyclosporine were discovered to inhibit the calcineurin phosphatase pathway (Schreiber and Crabtree 1992; Russell et al. 1992; Erlanger 1992; Siekierka and Sigal 1992). Further studies rapidly elucidated additional mechanism details in subsequent years.

Although mainstream clinical practice had vigorously adopted high-dose combination immunosuppression therapy as the treatment of choice because of the specter of rejection, in 1992 the notion that more immunosuppression was not necessarily better emerged. A group of patients were discovered to have become chimeric, or developed tolerance towards their allograft (T. E. Starzl et al. 1992), helping to elucidate the fact that allografts carried passenger leukocytes that

conducted an immune response against the host, much as the host carries out an immune reaction against the allograft (Rao et al. 1996). This became known as the double-immune response or clonal exhaustion and deletion (T. E. Starzl and Fung 2010). Further investigation of these cases revealed that moderate levels of immunosuppression, carefully timed and tailored to each individual, was at least partially successful in eliminating patient dependence on lifelong immunosuppression (Shapiro et al. 2003). Prior to these observations the clinical view was that the immune response needed to be quashed as early and completely as possible, in order to prevent the leviathan of rejection from emerging. However after the chimeric patients were discovered, the door to the consideration of more nuanced application of immunosuppression was opened.

Organ transplantation has evolved from a non-existent field to one of the most prominent disciplines in medicine over the past half century.

Rejection Marker Literature

Skin rejection is is of particular interest in this thesis because of its high immunogenicity, and because the process of rejection in skin is likely to be elucidating for other tissues. It is also a component of the composite tissue allograft that has historically been more difficult to manage with minimal immunosuppression protocols than other tissue (such as muscle).

The Banff 97 working classification of renal allograft pathology (Racusen et al. 1999) provided a uniform basis for the grading rejection in allograft biopsies. It has been subsequently updated, most recently by Banff 07 classification of renal allograft pathology: updates and future directions (Solez et al. 2008). Grading schemes relevant to skin and composite tissue allotransplantation were also defined in The Banff 2007 Working Classification of Skin-Containing Composite Tissue Allograft Pathology (Cendales et al. 2008).

Cytokines are signaling proteins that are essential to both organ and immune function (Nicola 1995), influencing the behavior of cells by binding to surface receptors (Ihle 1995). Suppressors of cytokine signaling and immunity (Kubo, Hanada, and Yoshimura 2003)provides a thorough review of how suppression of cytokine signaling can significantly alter an immune response, and provide potential therapeutic alternatives to systemic immunosuppression.

A description of the properties of cytokine ligands and receptors, as well as a listing of the currently known cytokines, is provided in (Murphy 2011). Several signaling proteins that have a function in the immune system are sometimes also classified as chemokines. A broad review of this class of signaling proteins is given in (Charo 2006). Cytokines are generally considered the class of proteins involved in regulation of immune activity (Brunton 2010), while chemokines are involved in inducing cell movement (chemotaxis) (Murdoch and Finn 2000).

Cytokine expressions associated with CHS, and discussion of the role of individual cytokines in the pathology of CHS, are given in (Piguet et al. 1991; Lu et al. 1998; Wang et al. 1999).

Composite Tissue Allotransplantation

With the first human hand transplantation performed in the modern era of immunosuppression in 1998 composite tissue allotransplantation (CTA) has become a clinical reality. Over the past decade it has become a treatment option for the many patients suffering from complex tissue injuries or defects not amenable to conventional reconstruction (Dubernard et al. 1999). The more than 60 hand/forearm and most recently arm transplants as well as 12 face transplants performed throughout the world have also shown that allograft survival with good functional outcomes can be routinely achieved after CTA (Lanzetta et al. 2007; Schneeberger and Ninkovic 2006; Cooney and Hentz 2001; Schuind et al. 2006; Petruzzo et al. 2006). However, despite the fact that surgical procedures and functional outcomes are highly successful, the need for long-term and high-dose immunosuppression to enable graft survival and to treat/reverse acute rejection episodes are the remaining and pace-limiting obstacles towards wide spread application (Schneeberger, Zelger, Ninkovic, and Margreiter 2005; Abramowicz and Schneeberger 2007). The toxicity profile of such drug treatment is considerable and includes serious side effects, such as opportunistic infections, malignancy and end organ damage (Stratta 1997; Hettiaratchy et al. 2004; Gander et al. 2006; First and Peddi 1998).

CTA recipients are unique in that they undergo a transplant procedure for what is considered to be a non-life-threatening condition. Therefore, there is a critical need to develop immunosuppression minimization strategies to reduce the risks of chronic immunosuppression.

The skin is the principal target of rejection after CTA transplantation, making it an obstacle to tolerance induction or minimizing immunosuppression. On the other hand, due to its external location, the skin provides a unique clinical opportunity for monitoring, early diagnosis, prevention and treatment of CTA rejection, including the possibility of therapies applied directly/topically to the skin.

Acute rejection in hand transplantation appears with maculopapular skin lesions (Figure 2.1), which can be limited to a small area of the skin or can spread over large parts of the transplant (Schneeberger and Ninkovic 2006; Cooney and Hentz 2001; Cendales et al. 2006; Cendales et al. 2008; Schneeberger, Lucchina, Lanzetta, Brandacher, Bösmüller, Steurer, Baldanti, Dezza, Margreiter, and Bonatti 2005; Steinmuller 2001).

Figure 2.1 Examples of acute skin rejection

Clinical macroscopic manifestations can range from mild pink discoloration or erythema to lichenoid papules, edema and onychomadesis. The main histological

feature of acute rejection is a mononuclear cell infiltrate. It first appears in the perivascular space of the dermis and then spreads to the interface between dermis and epidermis and/or adnexal structures. A perivascular, cellular infiltrate within the epidermis is typical for a moderate grade of rejection with the immunologic response reaching the outermost layer. If rejection is not successfully treated at that stage, necrosis of single keratinocytes can be observed, resulting in focal dermal-epidermal separation and significant graft damage (Cendales et al. 2006; Schneeberger, Lucchina, Lanzetta, Brandacher, Bösmüller, Steurer, Baldanti, Dezza, Margreiter, and Bonatti 2005; Steinmuller 2001). If rejection progresses further, necrosis and loss of the epidermis, as the ultimate stage of skin rejection, are considered irreversible. However, very limited information is available on the involvement of components other than the skin in this acute rejection process (Schneeberger, Lucchina, Lanzetta, Brandacher, Bösmüller, Steurer, Baldanti, Dezza, Margreiter, and Bonatti 2005). The histological findings in CTA patients are in line with results from experimental studies indicating that the skin is highly immunogenic and hence the primary/sentinel target for rejection. This is further substantiated by the fact that immunological tolerance can be achieved towards all components of a CTA experimentally except the skin. It was also shown that skin alterations in a CTA are not exclusively limited to alloimmune-mediated injury. The clinical and histopathological features of immune-related and non-rejection processes are potentially overlapping or may coincide with acute rejection. The underlying mechanisms are largely unknown and represent a current major clinical challenge in differentiating between acute rejection and other forms of skin inflammation.

Similarities in Early Skin Rejection and Other Sources of Skin Inflammation

Skin rejection in CTA presents with erythematous macules that may progress if not treated to infiltrated scaly violaceous lichenoid papules covering the complete surface of the graft (Kanitakis et al. 2000). These alterations are not specific for rejection and may mimic inflammatory dermatoses. Kanitakis et al. emphasized the diagnostic challenges in early or mild skin rejection. Early rejection (grades 1 and 2) can be especially difficult to differentiate from contact dermatitis (Figure 2.2 and Figure 2.3), insect bites, or dermatophyte infections. While the geographic limitation of lesions to the skin of the allograft can be an important and helpful hint, atypical cases of skin rejection with regard to the anatomical site, progression or the clinical manifestation have been described (Kreczy, Brandacher, and Steurer 2004) and the location alone cannot be considered proof. Early and accurate diagnosis, however, are critical to either prevent progression of rejection or incorrect treatment of the patient.

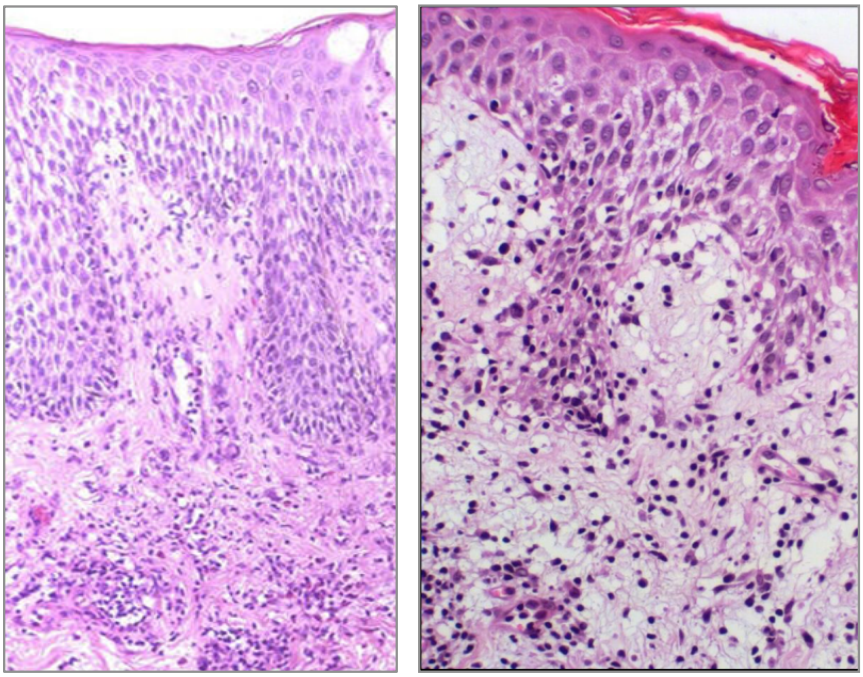

Figure 2.2 The histopathology of CHS (left) and early rejection (right) are similar

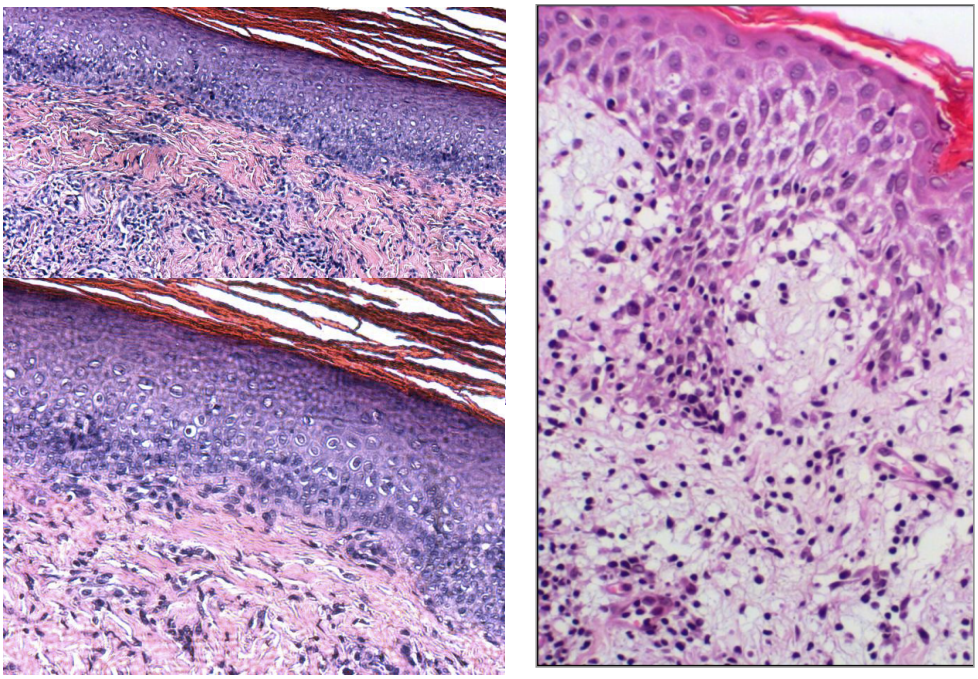

Figure 2.3 The histopathology of DTH (left top and bottom) and early rejection (right) are similar

Parallels between acute skin rejection and inflammatory dermatoses (e.g. contact dermatitis, psoriasis and atopic dermatitis) also exist on the molecular and cellular level. Allergic contact dermatitis for example is a T cell-mediated delayed type hypersensitivity reaction that occurs upon hapten challenge in sensitized individuals (Gober and Gaspari 2008). Therefore the differentiation mainly based on histological and macroscopic criteria can be difficult. It has been demonstrated, that

T-cells (CD4+ and CD8+ cells) are critical effectors and that elements of the innate immune system (e.g. natural killer cells) may play a key role (Saint-Mezard et al. 2004). Epidermal Langerhans cells as the most powerful antigen presenting cells in skin as well as keratinocytes are regulating this inflammatory process. Cytokines derived from Langerhans cells (e.g. IL-12) and from T-cells (IFN-gamma, IL-4 and IL-10) play a pivotal role in the induction and initiation of this common skin disease (Gober and Gaspari 2008; Pastore et al. 2004).

Computational Literature

Concise and thorough coverage of the statistical inference and modeling methods this thesis uses are given in (Wasserman 2010b) and (Wasserman 2010a). Both discriminative and generative methods are important to this thesis. Discriminative methods are often able to produce classifiers that have superior performance to their generative counterparts, however generative methods allow data to be generated from the model (effectively allowing *in silico* simulation of changes in model parameters).

Initial discriminative efforts begin with a logistic regression implementation and expand to other methods. Recall that a logistic classifier uses

$$f(z) = \frac{1}{1 + e^{-z}}$$

Equation 1 The logistic function

to take input of any real-numbered value and produce output R that is $0 \leq R \leq 1$. Generally the input to this function is

$$z = \beta_0 + \beta_1 x_1 + \beta_2 x_2 + \ldots + \beta_k x_k$$

where each beta represents a regression coefficient of each independent variable x.

Equation 2 A common logit definition

Although the parameters measured in this thesis are not independent, logistic regression can still give useful results. These can provide the insight needed to apply multi-variate regression and other generalized linear models (Freedman 2005)

Decision trees are useful for data exploration, classification along non-linear decision boundaries, or in selectively applying other models. They can take the form of classification trees, regression trees, or the hybrid classification and regression (CART) trees (Breiman et al. 1984). As predictive models, the nodes represent decision criterion, the branches represent conjunctions of parameters, and the leaves are the final classes assigned by the decision tree function. Thorough and accessible coverage of this area of statistical learning is given in (Hastie, Tibshirani, and Friedman 2008a).

When decision trees are combined into an ensemble, the form the random forest classifier (Liaw 2002). This method is particularly powerful and is able to capture highly non-linear decision surfaces (Breiman 2001; Hastie, Tibshirani, and Friedman 2008b). The methods by which random forests are grown and trained

provide unbiased built-in estimation of performance because part of the data is left out in each bootstrap sample, protecting against overfitting.

Feature transformation methods allow high dimensional data to be understood in new and possibly more intuitive ways. Highly complex data sets frequently contain important patterns that are obscured by the method of data collection. For example, important immune signaling patterns may exist in a given context, but because the features that can be measured are constrained, the raw data may not provide a clear picture of what those important patterns are. Without feature transformation methods, the data would be opaque to clinical interpretation, and any decision criterion that statistical inference algorithms learn on the raw data could be sub-optimal.

The feature transformation methods of most utility in this thesis are Singular Vector Decompisition (SVD), Principle Component Analysis (PCA), and Multivariate Analysis of Variance (MANOVA).

SVD decomposes a matrix by

$$M = U\Sigma V^T$$

Where M is the original matrix, U is a unitary matrix, $\sum$ is a rectilinear diagonal matrix, and V^T is again a unitary matrix.

Equation 3 The SVD factorization

PCA makes use of this decomposition. A detailed account of the complete decompisition and variations of it are given in (Strang 2005).

PCA is mathematically defined as an orthoganal linear transformation. PCA seeks to find the linear combination of observed features that fits into the smallest number of synthesized features possible. The effect of this is to "load" the maximum amount of observed variance (along orthoganal bases) into the top synthesized features. The actual transformation occurs by

$$Y^T = M^T U$$

Where Y is the transformed matrix, M is the original data matrix, and U is the first singular matrix yielded by SVD decomposition of M.

Equation 4 The PCA transform

Extensive coverage of PCA is given in (Jolliffe 2010).

While PCA seeks to find the combination of observed features that are most informative of the underlying structure of variance, the MANOVA method seeks to maximize the separation of labeled classes. It is often possible for the same classifier to yield better classification performance with a MANOVA transformed data set than with a PCA transformed data set. (Eriksson et al. 2006), (Härdle and Simar 2003), and (Rencher 2002) provide insight and instruction in the method.

Alternative and Experimental Methods for Detecting Rejection

Interest in finding a better means of detecting or predicting rejection has spawned a range of research approaches. Although none of these methods has found

widespread clinical adoption, the technical innovations provide context for this thesis and are informative of the challenges faced by the field.

Utilizing little or no tissue data, the psychiatric analysis described by (Owen and Bonds 2006) concluded that although the features measured could be used to identify certain risk factors for rehospitalization, they were not predictive of rejection specifically. Rehospitalizations were due to a variety of causes, including immunosuppression-associated infection.

A significant amount of ongoing research is being invested in finding genetic markers for rejection. The most promising results to date have come from (Li et al. 2001) showing correlation between miRNA coding for cytotoxic proteins and rejection, as well as (Snyder et al. 2011) showing strong correlation between donor gene fragments in circulating blood and the progression of rejection. However in the presented results there is a high degree of variance in key metrics measured, and the detection of rejection is thought to occur at the onset of graft damage. This may eventually provide an improvement over current clinical standards by reducing unneccessary biopsies, and results from this thesis may eventually be adapted to work with this method. Additional work in the area of genetic rejection detection has been done by (Sindhi et al. 2008) and (Lande et al. 2007).

Cellular analysis is perhaps the most popular alternative approach to assessing rejection. A large number of biomarkers have been identified and catalogued by (Jain 2010), however *in-vivo* most biomarkers suffer from high false positive rates, or are not cost-effective to assess. For kidney transplant cases, (Kotb et al. 1999) describes a method that is a reliable indicator in about 62% of studied cases. (Bishop et al. 1986) identifies cells associated with rejection in circulating blood, but like (Snyder et al. 2011), these cells provide very limited or no predictive value beyond what is technically achievable by pathologist examination of biopsy.

Doppler tissue imaging as described by (Stengel et al. 2001) may eventually provide a non-invasive alternative to heart biopsy. As described, the system is capable of 82% sensitivity but only 53% specificity, and again does not confer predictive power.

Significant recent advances in proteomic analysis have been made by (Phillips et al. 2004) who proposed a breath-test for heart transplant rejection that is capable of 71.4% sensitivity and 62.4% specificity. (Maier et al. 2011) shows excellent performance in predicting corneal transplant rejection with the application of linear discriminant analysis to selected cytokines, reinforcing the underlying approach of this thesis.

Efforts to map the measured semantic properties of rejection by (Stanley, McManus, and Rockey) resulted in a system that shows promise in predicting post-transplant mortality, but is not effective in predicting rejection or infection. A literature derived networks of interactions between cells and cytokines was described in (Shen-Orr et al. 2009), although this is primarily a data exploration tool, as no mechanism for providing predictions or state assessments is present in the system.

Additional literature and suggestions for further reading is provided in Appendix E Related Literature

Chapter 3 Methods

Data available in the literature does not provide the necessary time points or features required for the analyses presented in this work. To achieve statistical significance and control for variance not related to the experiment design, large quantities of original experimental data was collected from hind-limb composite tissue transplants in an established rat small animal model. The concentration of immune signaling proteins (cytokines) was quantified by Luminex multiplexing platform, which provided the features for analysis by statistical and computational methods. These patterns provide the discriminative classifiers substantial predictive power.

Data from the Literature is Necessary but Not Sufficient

The literature is useful to this work by providing modeling parameters, biological explanations for analytic results, and scientific context for this research. While extensive information about the behavior of individual cytokines (or small cliques of cytokines) is available in the literature, this data alone is not suitable for the purpose of elucidating the hypothesis of this thesis.

Cytokines are by nature pleomorphic, and have a wide range of cellular effects that are context dependent. For this reason, *in vitro* studies of specific cytokine behaviors are often not consistent with *in vivo* observations. Similarly, *in vivo* observations can be inconsistent with each other and vary with sampling conditions, anatomical location, pathology, and many more factors.

The literature lacks data sets that contain measurements from a wide range of cytokines, over time, sampled from a uniform surgical model. Therefore the hypotheses proposed here can not be verified to the extent required for clinical relevance from analysis of the literature alone.

Because of these factors, has been critical to incorporate a program into this thesis to build a dataset that captures the high-dimensional information about in-vivo cytokine profiles over time. This data is essential to separating the portions of immune signaling meaningfully associated with rejection, from signaling activity that is related to other types of inflammation or other body processes.

In vitro models of immune function are not sophisticated enough to capture the inherent dynamism of a higher order living organism (e.g. small animal). The influence of processes, both known and unknown, have substantial effect on the development and regulation of immune system activity. Although complimentary in vitro studies are helpful to clarify specific interaction or mechanism questions, in vivo examination is a pre-requisite for accurate systems-level understanding of the immune signaling associated with the experimental groups examined in this work.

The Necessity of the Small Animal Model

Because of the need to exert as much control over the number of variable conditions as possible, it became clear that a small-animal surgical model is the only platform able to provide data that controlled for genetic variation across animals. By

utilizing animals of the same age, weight, and health, and by housing the animals under identical conditions, as well as administering treatments at identical time points, additional sources of variation are able to be moderated.

By observing the "similarities in the differences, and the differences in the similarities" of the immune signaling in animals as the factors are varied across groups, clarity about what is associated with the relevant immune response versus what is associated with other biological functions became possible. This is something that would not be possible to accomplish within reasonable time and resource constraints in humans.

Experiment Design

Selection of Surgical Models

The primary tissues of interest in this thesis are the skin and muscle. Their immediate visibility and the ease with which biopsies can be obtained make them ideal tissues for the elucidation of the hypothesis in this thesis. Beyond the convenient accessibility of the tissues, there are some important physiological properties that make them relevant.

Skin is an epithelial tissue, with very high levels of resident immune cells such as dendritic cells, macrophages, and others. This makes the skin a tissue with powerful innate immunity capacities, as well as an unusually efficient initiator of the adaptive immune response. These are properties that are shared to some extent by all epithelial tissues, including those found in the lung, intestine, and in certain areas of other solid organs or vessels.

Muscle on the other hand is not an epithelial tissue, and has a very different cellular constitution. It is more extensively vascularized, and is not considered a specialized immunologic barrier like skin.

Under routine immunosuppression, the muscle and bone components of a composite tissue allograft (e.g. a complete rat hind limb) can be engrafted. However, the skin component will often continue to experience episodes of rejection even under immunosuppression, an effect widely observed and very problematic in composite tissue transplantation. These episodes frequently require rescue treatment with one or more large bolus doses of corticosteroids. This implies that the immunologic mechanisms of the two tissues are distinct to some extent. This thesis will seek to prove that the methods derived here will be applicable to both tissues, despite their biological distinctiveness.

In order to verify that the distinctive immune signaling properties of rejection observed in skin or muscle are also a valid basis for differentiation in other solid organ contexts, additional samples were gathered from a rat cardiac transplant model that included sampling from a wide range of organs. This will allow direct comparison of the predictive methods across at least four tissue types: skin, muscle, heart, and lung. It will also allow the features that are most predictive in each tissue to be analyzed and compared.

The limb transplant model in rats is a standard model for investigating the immune response towards a composite tissue allograft. This model has been

established in the Lee/Brandacher/Schneeberger laboratory and is routinely utilized to investigate inflammatory and immune phenomena, including inflammation, ischemia reperfusion injury and CTA rejection. The limb allograft carries all of the components that would comprise a composite tissue allograft such as the hand. The Lewis (LEW) to Brown Norway (BN) combination is an established rat strain combination providing predictable patterns of rejection. Without treatment, early signs of acute rejection with edema and erythema of the skin can be observed at 5 days after transplantation. Rejection then progresses resulting in scaling and ultimately necrosis of the skin at POD 11-13.

Cohorts, Groups, and Sampling

To facilitate collaborative multi-center data collection with surgeons at the University of Pittsburgh, Johns Hopkins Medical, and Carnegie Mellon University, sample collection has been divided into cohorts, each of which provide data about a specific inflammatory process.

Four cohorts of data were collected, each divided into further groups to provide more information about relevant changes in signaling. A summary of the cohorts and the conditions they represent are presented in table 1.

Cohort	Hypothesis	Surgery	Time Point	Tissue	n	Sample Types Provided
1	1, 2	Orthotopic Hind limb Tx	3, 5, 7, 9, 11	Skin, Muscle	> 230	Allograft, Isograft, Naive, Immunosuppressed, Histology
2	3	Hind limb Tx and CHS	1, 2, 3, 4, 5, 6	Skin	> 150	Allograft, Isograft, Naive, Unspecific Inflammation
3	2, 3	Wounding with shock	N/A	Skin, Muscle	> 32	Wound Healing, Unspecific Inflammation
4	1, 2 in solid organ	Heterotopic heart/lung Tx	0, 1, 3, 5, 7, 9	Heart, Lung	> 30	Allograft, Native

Table 3 Summary of Experimental Groups

Cohort 1 was designed to provide a large amount of cytokine signaling data about the distinguishing signaling characteristics of allogeneic, syngeneic, naive, and immunosuppressed hind limb transplants. In untreated skin the adaptive immune response takes approximately two to three days to develop and the course of rejection runs over approximately 11 days, so samples will be taken at post-operative days 3,5,7,9, and 11 in the untreated allogeneic and syngeneic groups. To collect data about how immunosuppression alters immune signaling, samples from treated allogeneic and syngeneic groups will also be taken at the same time points. To observe how immunosuppression may have changed the immune signaling process leading to rejection, immunosuppression is stopped in the treated groups at POD 20, and samples are then taken at intervals synchronized to development of

visible rejection grading criteria (such as erythema, etc). At each time point, biopsy samples are taken from both skin and muscle. Surgery and sampling in collaboration with surgeons from the University of Innsbruck School of Medicine, Johns Hopkins School of Medicine Department of Plastic Surgery, and University of Pittsburgh Medical Center Department of Plastic and Reconstructive Surgery.

Cohort 2 will provide information about the separation of inflammation associated with rejection from unspecific inflammation. An induced contact hypersensitivity and delayed type hypersensitivity model in hind-limb allograft, hind-limb isograft, and naive animals provides information required to isolate immune signaling patterns associated with unspecific inflammation. Samples are taken from the skin and muscle at POD 1, 2, 3, 4, 5, and 6. Surgery and sampling in collaboration with surgeons from the University of Innsbruck School of Medicine.

Cohort 3 elucidates wound healing, both with and without cardiogenic shock. An unavoidable consequence of any transplant is surgical trauma, as well as cardiogenic shock in the allograft. This cohort collects data about the associated cytokine profiles. Surgery and sampling in collaboration with surgeons from the University of Innsbruck School of Medicine and the University of Pittsburgh School of Medicine.

Cohort 4 performs heterotopic heart and lung transplant. Because internal solid organs are part of the program biopsy in this surgical model, additional internal organs are sampled to develop a broad picture of complementary changes in organ systems in response to rejection. The graft heart, native heart, graft lung, native lung, skin, muscle, kidney, liver, spleen, lymph node, and plasma were sampled. Heart and lung rejection reaches its necrotic stage earlier than skin, so samples were taken at POD 1, 3, 5, 7, and 9. Surgery and sampling in collaboration with surgeons from the Carnegie Mellon University Nuclear Magnetic Resonance Center.

All animal procedures, care, and housing were reviewed and approved by the University of Pittsburgh or Carnegie Mellon University Institutional Animal Care and Use Committee, and followed the National Institutes of Health guidelines for the care and use of laboratory animals.

Orthotopic Limb Transplantation

This procedure is used in the rat CTA model. In brief, the femoral nerve, artery and vein are isolated and divided sharply, ensuring adequate length for subsequent vascular anastomoses. The remaining thigh muscle groups, including the sciatic nerve, are then transected to completely expose the mid-portion of the femur. A transverse osteotomy is performed through the femur completing the allograft harvest. Following amputation, the donor limb is perfused through the femoral artery with 3 ml of lactated ringer flush. The recipient animal is prepared in a similar fashion. Transplantation of the allograft starts with a femur osteosynthesis. The femoral vein and then femoral artery are anastomosed. The sciatic as well as the femoral nerve are apposed with 10-0 nylon sutures in an interrupted fashion. The ventral and dorsal muscle groups are then repaired, and the skin closed.

Animals were monitored daily for signs of rejection. The primary clinical diagnosis of rejection was based on Banff skin rejection criterion . Biopsies were

fixed in 10% buffered formalin and processed routinely for H&E staining, and some biopsies were preserved with RNALater for future immunohistochemical studies.

Figure 3.1 Hind-limb allograft (showing signs of rejection at POD 5)

Contact Hypersensitivity (CHS)

Type 1 T cells produce cytokines, which activate resident skin cells allowing the production of inflammatory cytokines and chemokines. This is responsible for the recruitment of leucocytes from blood to skin leading to the development of skin lesions. This process is illustrated in Figure 3.2.

Sensitization phase:

1. Haptens penetrate the epidermis and are uptaken by skin LC
2. Which migrate to draining lymph nodes
3. Where they present haptenated peptides to T cells
4. Specific T cell precursors clonally expand in draining lymph nodes, recirculate via the blood and migrate into tissues including the skin.

Elicitation phase:

5. When the same hapten is applied on the skin, it penetrates the epidermis and is uptaken by epidermal cells, including skin LC and keratinocytes
6. Which can present haptenated peptides to recirculating T cells

Male LEW-rats are sensitized with 100µl of 1% DNFB (2,4-dinitro-1-fluorobenzene) in 4:1 acetone/olive oil on the shaved abdomen. On day 5 the dorsal surface of the right pinna is challenged with 50µl of 1% DNFB in 4:1 acetone/olive oil whereas the left pinna is only treated with vehicle (acetone/olive oil). Every 24 hours (for 5 days) animals were sacrificed and the complete right and left pinna harvested. Samples were then processed for histology, immunohistochemistry, protein and RNA isolation.

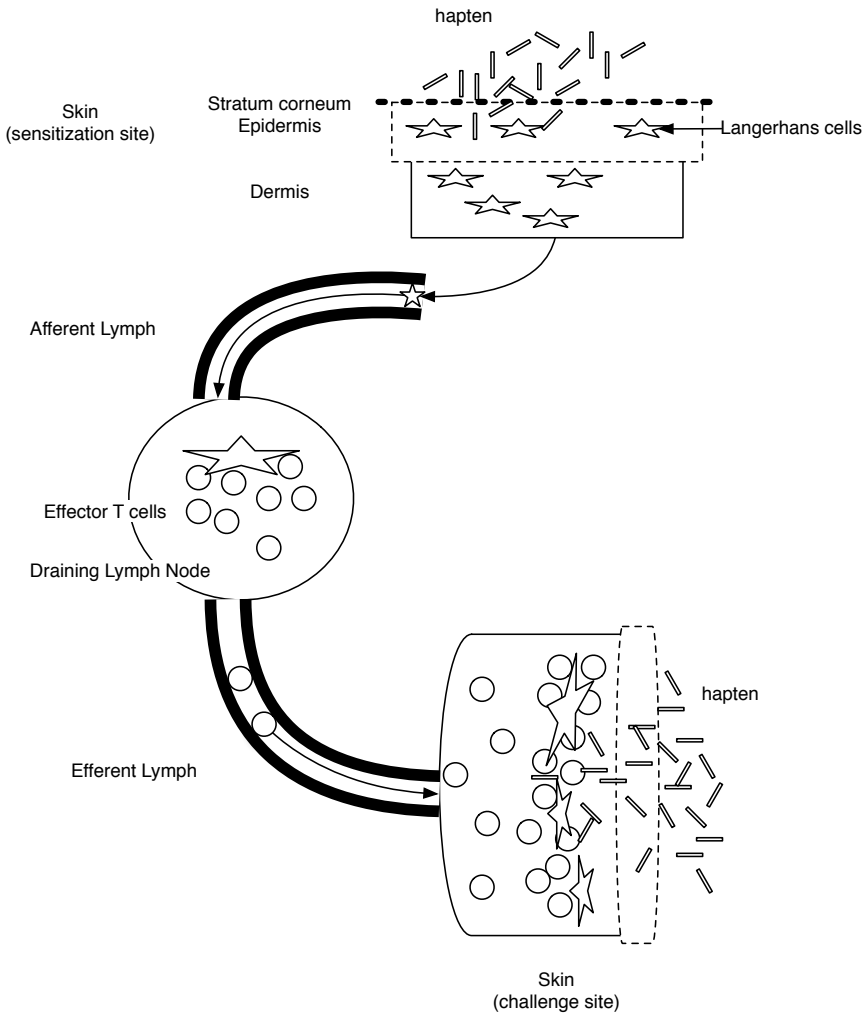

Figure 3.2 Illustration of the pathophysiology of contact hypersensitivity

This protocol is a modification of the footpad-swelling test described by (Catalina et al. 1996; Engeman et al. 2000).

Delayed Type Hypersensitivity (DTH)

DTH is a form of contact hypersensitivity mediated by T cells (mainly CD4+ cells) that respond to protein antigens introduced by contact with the skin. In this procedure, male LEW-rats are injected with 300µl mBSA (2 mg/ml) in PBS +complete Freund's adjuvant as sensitization (intradermal/abdomen). After 7 days (challenging) an injection of 100µl mBSA suspended in PBS is injected into footpad, while the other footpad is given PBS only (Figure 3.3). Measurement of the footpad swelling is taken with a digital caliper 24h to 48h after challenge.

Figure 3.3 Footpad with induced DTH

Incisional Wound Healing

Lewis rats were anesthetized and an excision biopsy was taken from the lateral aspect of the thigh on one of the hind limbs in each of the rats. In the "shock group", four Lewis rats were sacrificed with a fatal sodium pentobarbital (Lundbeck Inc, Deerfield, IL) overdose and excision biopsy taken 15-30 seconds after cessation of heartbeat. The surgical biopsy is itself considered the wounding event in both groups. Tissue was drawn away from the body and held in forceps while surgical scissors cut 15mm x 10mm of tissue from the lateral aspect of the thigh.

Heterotopic Heart and Lung Transplant

A working heart transplantation model with transplanting an en bloc heart and lung from DA to BN as allograft. The surgical procedure has been described elsewhere ((Ye et al. 2008; Wu et al. 2006)). In brief, donors were anesthetized by inhalation of isofluorane (Abbott Laboratories, North Chicago, IL). The chest wall was opened after injected 500U/kg body weight of heparin sodium into the inferior vena cava (IVC). 10 ml of cold lactated Ringer's solution (Abbott Laboratories, IL) was infused into the IVC followed by ligation and division of the IVC. The left lung was ligated and excised. The right superior vena cava (SVC) were ligated and divided, and the ascending aorta was dissected and transected. The grafts were then placed into cold lactated Ringer's solution until transplantation.

The recipient rat was intubated and ventilated with 2% isoflurane in a 2:1 O2: N2O gas mixture at 1.0 mL/100 g body weight and 60 bpm. Both the abdominal aorta and the IVC were dissected and clamped. The graft aorta and SVC were anastomosed to the recipient aorta and IVC respectively, in an end-to-side fashion with continuous 8-0 polypropylene suture (Ethicon, Inc. Somerville, NJ). Rhythmic heartbeats commenced spontaneously after unclamping. The transplanted hearts exhibited similar cardiac output (working path) to that of native hearts. The abdominal wall was sutured with 6-0 silk (Ethico. Inc.). Graft survival was monitored daily following transplantation for one week, and then weekly by palpating the transplanted heart.

Rejection Grade Assessment

Rejection is graded by transplant surgeon assessment of biopsy histology, according to the Banff 2007 criterion.

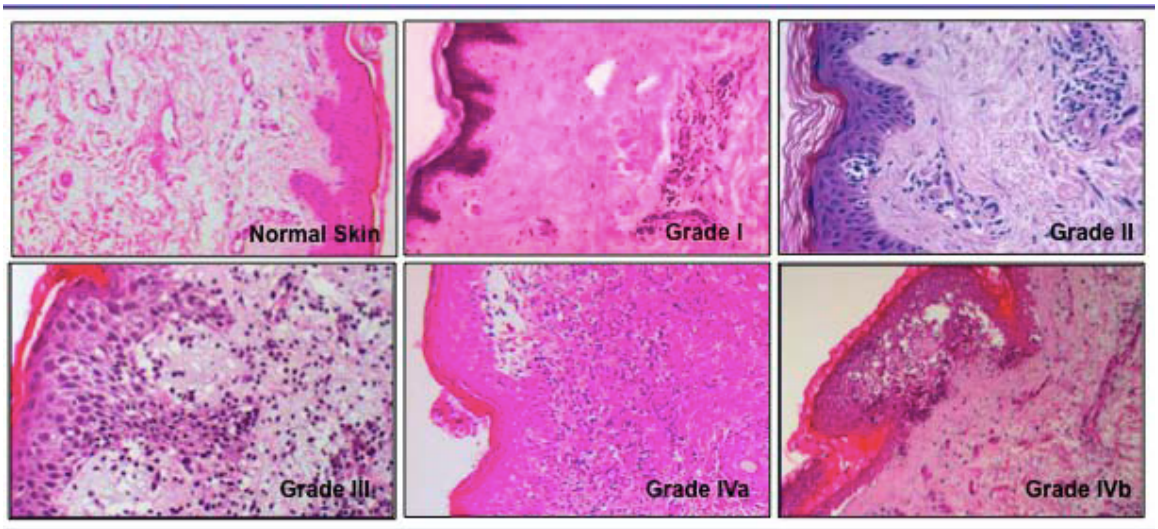

Figure 3.4 Allograft histology rejection grades

Grade 0: No or rare inflammatory cells
Grade I: Mild perivascular infiltration. No involvement of overlying epidermis
Grade II: Moderate. Perivascular inflammation with/without mild epidermal or adnexal involvement (limited to spongiosis and exocytosis). No epidermal dyskeratosis or apoptosis.
Grade III: Dense inflammation and epidermal involvement with apoptosis, dyskeratosis and/or keratinolysis.
Grade IV: Necrotizing acute rejection. Frank necrosis of epidermis or other skin structures.

Histology readings were conducted on tissue samples affixed to slides, where physiological indicators such (as desquamation) are not available for consideration. The transplant surgeon used these specific features in grading skin samples:
Grade 0: Normal skin, only few single infiltrating cells.
Grade 1: perivascular infiltrate, infiltrate around adnexal structures, mild infiltrate in dermis and deep tissue.
Grade 2: Dense diffuse infiltrate in dermis, interface reaction, infiltrating cells also in epidermis, single apoptotic keratocytes.
Grade 3: Dermal epidermal separation, dense infiltrate.

These features were used in the scoring of muscle samples:
Grade 0: Normal muscle, only single infiltrating cells.
Grade 1: Perivascular infiltrate, intact muscle.
Grade 2: Diffuse infiltrate, onset of fibrosis, degeneration.
Grade 3: Necrosis, fibrosis, degeneration of muscle fibers.

Sample Selection, Quantification, and Mass Normalization

All tissue samples are immediately sectioned into ≤ 0.5 cm^3 pieces and placed into individual sample tubes filled with RNALater™ and stored at -4ºC overnight, then moved to -80ºC storage, as per manufacturer instructions.

For tissue processing, approximately 50 mg of the tissue is transferred to a 2.0 ml microcentrifuge tube containing 0.6 ml of 1x BioSource tissue extraction reagent (San Diego, CA) supplemented with 10µl of 100mM phenylmethanesulfonyl fluoride in ethanol as a protease inhibitor. The tissue is homogenized using a tissue homogenizer for 25-45 seconds until the sample is in a consistent solution. The sample is placed on ice, if processing multiple samples, then centrifuged at 4 C for 10 min at 10,000xg. After centrifugation, the supernatant is collected and placed in a new microcentrifuge tube, placed on ice and assayed for protein content using the biocinchoninic acid (BCA) protein assay (Pierce, Rockford, IL) according to the manufacturer's protocol.

Per sample protein levels are assessed by BCA assay and subsequently titrated to a total protein concentration of 1 mg/ml. All samples were assayed for inflammatory cytokines and chemokines using the Luminex™ multiplexing platform (100 IS; MiraiBio, Alameda, CA) and a Millipore™ 14-plex rat cytokine bead set (Millipore, Billerica, MA) that included interferon (IFN)-γ, IL-1α, IL-1β, IL-2, IL-4, IL-5, IL-6, IL-10, IL-12p70, IL-18, monocyte chemotactic protein (MCP-1), GRO/KC, TNF-α, and granulocyte-macrophage colony stimulating factor (GM-CSF). These pro-inflammatory cytokines/chemokines play important roles inflammation. While all cytokines measured are not expected to play a major role in every context, measurement of the uniform set provides a broad coverage of in-vivo inflammatory activity, allowing important distinctions between groups and tissues to be learned. Results were read in pg/ml, then subsequently normalized to total mass of sample protein (pg cytokine/mg protein) for each of the 14 cytokines by the formula x=(a/b)*1000, where x=(pg of cytokine/mg of protein), a= (pg/ml cytokine) and b= (µg/ml protein).

Final raw data is aggregated into a matrix with each row representing an individual observation, and each column representing a feature. The basic features upon which analysis was conducted included tissue type and cytokine level readings, with grouping variables for measure classifier performance. Additional feature interaction variables were added as described in data conditioning below.

Computation Modeling and Analysis

Statistical analyses were performed using MathWorks MatLab™ and Microsoft Excel™. Excel was used for data conditioning and preparation, while in-depth statistical analysis and classification was conducted in MatLab. Where possible, pre-existing MatLab classification routines were utilized and extended as required. In this work the terms computational modeling, computational analysis, statistical inference, and statistical analysis are used interchangeably. The fields of computer science and statistics are both foundational to making this work possible. The term computational modeling is used most prevalently because it evokes the particular perspective of this work on the nature of the immune system.

Data Conditioning

Data were organized into matrices where each row indicated a distinct observation, and each column a feature (i.e. cytokine or interaction feature). Categorical labels grouped data and all predictions were for these labels. All feature values were real-valued numbers.

Performance of mass-normalized cytokine data versus [0,1] interval normalized data were assessed across the majority of classifiers and groups. While some improvement in the classification performance of a subset of classifiers was seen (particularly in LDA and QDA), the improvements were not statistically significant. Therefore, all results reported are from analysis conducted on the unaltered mass-normalized scale of pg cytokine/mg protein.

In addition to the matrix of mass-normalized data, a hybrid matrix was formed in both skin and muscle data sets by adding feature interaction variables to the original 14 -ytokine feature set (Table 6.280, Table 6.281, Table 6.282, Table 6.283). The selection of these features was driven by the intuition that feature interactions which are present in one group or the other but not both will provide the additional information relevant to the separation of groups and consequently improvement in classifier performance.

To minimize the risk of overfitting, after each feature interaction variable is added performance is re-tested to evaluate improvement in accuracy, p-value, and AUROC score. If the improvement is sufficient for stable performance, additional feature interaction variables are not added. The maximum number of feature interaction variables added in this work was up to four.

Three of these features were selected by partitioning the original data matrix for each tissue by group ("rejecting" or "not rejecting"), then calculating the Pearson's r statistic for each matrix to measure pairwise correlation between the 14 cytokines, yielding a 14 x 14 square matrix of r values that represents intra-group correlation among features.

$$r = \frac{1}{n-1}\sum_{i=1}^{n}\left(\frac{X_i - \bar{X}}{s_X}\right)\left(\frac{Y_i - \bar{Y}}{s_Y}\right)$$

where $\bar{X}$, and s_X represent the sample mean and sample standard deviation.

Equation 5 Pearson's r statistic

For each tissue, the square matrix of r-values for each group was subtracted from each other. For example, the matrix of r-values for the group "rejecting" was subtracted from the matrix of r-values for "not rejecting." This yielded a new 14 x 14 square matrix that represents pairwise correlation between features present in one group but not both. Feature pairs with higher values (either positive or negative) are more desirable. This process was performed for both muscle and skin data. By this process, the interaction between GM-CSF, IL-2, and TNFa scored highly in skin while the interactions between MCP-1, GRO/KC, and IL-18 scored highly in muscle.

To select the fourth feature interaction variable the MANOVA coefficients for each cytokine's contribution to the separation of groups were assessed. The cytokine with the highest coefficients in the first and second canonical variable of

the MANOVA analysis defines the first half of the new feature interaction variable. The coefficient scores of this cytokine also define a point on a plot drawn with the X-axis as the first canonical variable, and the Y-axis as the second canonical variable. Next, a line is drawn from the origin (0,0) to the coordinates (termed Line 1). The second feature selected for calculation of the feature interaction variable is the cytokine with the next highest coefficients in the first and second canonical variable *and* that is the most orthogonal to Line 1.

In skin (Table 6.280) the feature interactions selected by r-value comparison were GM-CSF*TNFa and IL-2*TNFa, while in muscle (Table 6.281) they were MCP-1*IL-18 and GRO/KC*IL-18.

In heart the feature interactions selected by r-value comparison (Table 6.282) were GM-CSF*IL-6, GM-CSF*TNFa, and IL-5*IFN-g, while the feature interaction selected by MANOVA coefficient analysis (Figure 4.56) was GM-CSF*IL-5. In lung the feature interactions selected by r-value comparison (Table 6.283) were GM-CSF*IL-5, GM-CSF*GRO/KC, and GM-CSF*IL-1a, while the feature interaction selected by MANOVA coefficient analysis (Figure 4.60) was IL-5*TNFa.

In this work, the terms extended feature space and hybrid feature space are treated synonymously, and both refer to the original feature space plus feature interaction variables as defined here.

Classification Tasks

The classification tasks to demonstrate the three hypotheses of this work are:

Hypothesis 1

In each tissue of skin and muscle, discriminate between allograft and isograft groups, as well as between fk-treated and fk-treatment withdrawn groups. Make this distinction when including all time points, when including only time points earlier than POD 5, and when including only time points greater than or equal to POD 5.

Hypothesis 2

For each surgical group measured, discriminate between skin and muscle tissue. Make each of these distinctions when including all time points, when including only time points earlier than POD 5, and when including only time points greater than or equal to POD 5.

Hypothesis 3

In each tissue of skin and muscle distinguish between rejection-associated inflammation and not rejection-associated inflammation. Also attempt to classify the type of inflammation of each observation as rejection, wound healing, or unspecific inflammation. Further, make these distinctions when including all time points, when including only time points earlier than POD 5, and when including only time points greater than or equal to POD 5.

Extension to Solid Organ

To evaluate the effectiveness of the modeling approach described in this work in detecting rejection in contexts beyond composite tissue allotransplantation, the method with top performance marks on the composite tissue data set was then applied to heterotopic heart and lung transplant data. In the solid organ context, the ability to separate the transplanted organ (rejecting) from the native organ (not rejecting) provides an indication of how this work may generalize to other settings. Because rejection in heart and lung transplant can be visually discerned at POD 5, only time points at or prior to POD 3 are included in this classification task.

Classification Methods

Linear Discriminant Analysis (LDA)

LDA seeks to find a linear combination of cytokines that separates the categorically labeled data, and is used here as a linear classifier. One notable aspect of LDA is that it assumes the conditional probability density functions of each class are normally distributed, and that class covariances are full rank as well as identical. This method provides data about the performance of a linear classifier under various contexts. Although the normality and homoscedasticity assumptions are violated in much of the cytokine data analyzed in this work, good performance in discriminating groups can be seen in many contexts.

$$\vec{w} \cdot \vec{x} < c$$

where

$$\vec{w} = \Sigma^{-1}(\vec{\mu}_1 - \vec{\mu}_0)$$

where x = feature set, w = coefficients, mu = class means, c = threshold constant between classes

Equation 6 Linear Discriminant Classifier

Quadratic Discriminant Analysis

The quadratic discriminant is an extension of LDA, where the assumption of identical covariances is removed. This allows more flexible decision boundaries to be learned, but requires enough observations from each class to properly calculate the class covariance.

$$(\vec{x} - \vec{\mu}_0)^T \Sigma_{y=0}^{-1} (\vec{x} - \vec{\mu}_0) + \ln|\Sigma_{y=0}| - (\vec{x} - \vec{\mu}_1)^T \Sigma_{y=1}^{-1} (\vec{x} - \vec{\mu}_1) - \ln|\Sigma_{y=1}| \; < \; T$$

where x = feature set, mu0,1 = class means, y = class, T = Threshold for classification

Equation 7 QDA Classifier

In some experimental groups examined, the additional flexibility in the decision surface that the quadratic extension of LDA (QDA) allows provides slightly better performance.

Multinomial Logistic Regression Classifier

This regression model generalizes logistic regression to allow more than two classification outcomes. This method does not assume statistical independence of

the features. The probability of membership in each class is compared, and the most likely class is selected.
For the reference class,

$$P(Y_i = 1) = \frac{1}{1 + \sum_{h=2}^{M} \exp(Z_{hi})}$$

and for each of the m = 2… M classes,

$$P(Y_i = m) = \frac{\exp(Z_{mi})}{1 + \sum_{h=2}^{M} \exp(Z_{hi})}$$

where $Z = x_i * b_i$
where x_i = observation i, and b_i = coefficient i

Equation 8 Multinomial Logistic Regression

Classification Tree

The classification tree is constructed starting from a root node where the binary distinction of the data that provides the most information (as calculated by information gain) about the class is made. A new node is made for each distinction, and for each node the process is repeated until a stopping criterion, such as purity or minimum number of objects, is met. The resulting tree is then pruned with cross-validation to control over-fitting. Generally, information gain is defined as

$$IG(T, a) = H(T) - H(T|a)$$

Where T = set of training examples, a = some feature, and H = entropy
Equation 9 Information Gain

$$H(X) = -\sum_{i=1}^{n} p(x_i) \log_b p(x_i)$$

Equation 10 Shannon's Entropy

Random Forest

An ensemble classifier that aggregates many individual decision trees and makes a classification that is the mode of the classes output by the ensemble of decision trees. Each tree in the ensemble is grown to make a decision on a subset of the data set features, and a training set for the tree is selected by taking a bootstrap sample. The remaining observations are used to estimate the error of the tree. For each subsequent node in the tree, randomly choose another subset of features on which to base the next split. This is continued until the tree is fully grown. This method combines bootstrap aggregation (bagging), and random feature selection. It is capable of very high classification accuracy in non-linear problem spaces.

Feature Transformation: Multivariate Analysis of Variance (MANOVA)

MANOVA is a generalization of the Analysis of Variance (ANOVA) method that tests for the difference in two or more vectors of means. The primary advantage

of MANOVA is its ability to measure changes to multiple dependent variables simultaneously. The MANOVA method also generates a set of linear coefficients for the features and calculates the orthogonal axes along which group separation is maximized. An informal description of MANOVA is given by

The total sum of squares is split into the sum of squares between groups and within groups

$$SS_{tot} = SS_{bg} + SS_{wg}$$

The sum of squares between groups is then split into the variance for each independent variable and the interaction between them. A series of computations yields a cross-product S matrix that is composed of

$$S_{tot} = S_{IV1} + S_{IV2} + \ldots + S_{IVn} + S_{\text{interaction}} + S_{\text{within group error}}$$

Determinants of the S matrices are then found. Using Wilks' λ the variance accounted for by the best linear combination of dependent variables

$$\eta^2 = 1 - \Lambda$$

Equation 11 Summary of the Multivariate Analysis of Variance (MANOVA) method

Manova helps to discern a coordinate space upon which group differentiation may be more efficient, as well as to quantify the extent to which each cytokine is contributing to the separation of classes.

Performance Evaluation Metrics

Classifier performance metrics are reported as accuracy, p-value, and the confusion matrix. Accuracy is measured as a percentage, calculated by (1-misclassification rate)*100.

Classification performance is compared to a numeric system baseline and the gold-standard human performance baseline. The numeric system baseline is random class selection, while the human performance baseline is transplant surgeon classification and grading based on evaluation of histology (current gold standard). All misclassification rates, error, or other performance metrics are calculated by 10-fold cross validation. Complete confusion matrices are presented for easy classifier error analysis. Random forest classification performance is also evaluated against a stratified 30% held-out test set to provide additional perspective on performance.

Statistical significance (p-values) are calculated by independent two-sample t-test with unequal variance (Welch's t-test).

$$t = \frac{\overline{X}_1 - \overline{X}_2}{\sqrt{\frac{s_1^2}{N_1} + \frac{s_2^2}{N_2}}}$$

Equation 12 Welch's t-test

Where $\overline{X}_i$ is the sample mean, s_i^2 is the sample variance and N_i is the sample size. Sample one is the trace of the confusion matrix (correct classifications), and sample two is the off-diagonal elements of the matrix (false classifications). Each row of the off-diagonal elements is summed so that the vectors for correct and incorrect classifications are equal in length (Figure 3.5).

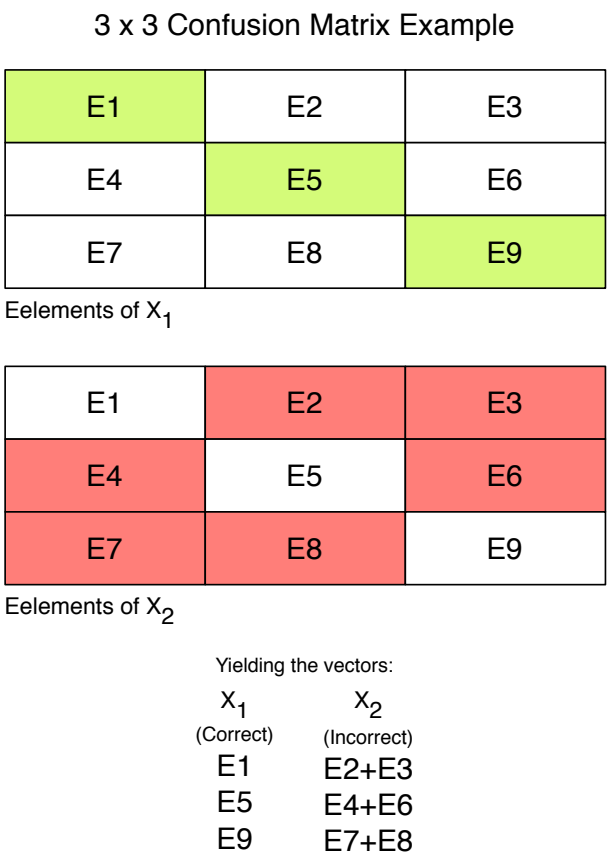

Figure 3.5 Diagram illustrating the calculation of p-values from the confusion matrix

Receiver Operating Characteristic (ROC) plots were created for select classifiers. The ROC plot is a representation of the true positive versus false positive rate, and is well established as a tool for selecting optimal classifiers in diagnostic decision-making. These plots were made by forming a plane with the interval 0 to 1 on both the X and Y-axes, then plotting the ratio of true positives in the classified-as-positive group over false positives in the classified-as-negative group. The X-axis represents the false positive rate and the Y-axis represents the true positive rate. Point-wise bootstrap confidence intervals are computed by with the bias corrected and accelerated percentile method, utilizing 100 replicas. A complete description of this method is provided in (Efron 1987). The bootstrapping method is justified in this case because there is insufficient data for more traditional statistical inference, and the theoretical distribution underlying the cytokine distributions is unknown and possibly highly complex. Area under the ROC curve values were also calculated for the ROC plots using trapezoidal approximated to estimate the area.

The area under the curve between j and i can be estimated by the equation

$$T = \frac{j-i}{n}\left[f(x_0) + 2f(x_1) + \ldots + 2f(x_{n-1}) + f(x_n)\right]$$

where T = the total area estimated, n = the number of trapezoids, x_0 = i, x_1 … x_n are the x-coordinates (equally spaced) of the right edges of trapezoids 1 … n, and f(x) is the function to calculate the area of a trapezoid.

Equation 13 Approximation of the area under a curve with the trapezoid rule

The area of a trapezoid can be calculated by

$$a = \left(\frac{b1 + b2}{2}\right)h$$

where a = the area of the trapezoid, b_1 and b_2 are the lengths of each base, and h is the height of the trapezoid.

Equation 14 Area of a trapezoid

The data used to generate the ROC plots and the AUROC values were the results of leave-one-out, or jackknifing, cross-validation. In jackknifing cross-validation, the entire data set except for one instance is used for training the model, and the held out observation is classified with that model. The held out observation is then replaced and a new observation is held out for classification. This process is repeated until each observation in the data set has been held out for classification. This method is identical to k-fold cross validation where k is equal to the number of observations in the data set.

Baseline Performance

To help assess performance of the modeling approaches presented in this work, baseline classification performance for experiment is provided here. Baseline performance is measured by random selection, linear discriminant analysis (LDA), and quadratic discriminant analysis (QDA).

For each experiment, LDA and QDA classification was performed in the original feature space, a 5-feature selected space (selected with OOB feature importance), as well as in a MANOVA transformed space (where cytokine features were replaced with the canonical variables of the MANOVA transform). The original feature space consistently yielded the best results and the MANOVA transformed space yields nearly equivalent results to the original feature space. The feature-selected space expresses bias as well as lower overall accuracy rates, however retains a level of accuracy that is more than proportional to the reduction in dimensionality, and is therefore worth consideration.

Chapter 4 Results

Because of the scale of this work, we refer to figures that are both in-line with text and provided as supplemental material in appendices. This allows systematic elucidation of the results while maintaining accessibility to key findings. Results are presented by section for each of the hypothesis 1 (early detection), 2 (each tissue is distinct), and 3 (identify specific type of inflammation) that are confirmed. Raw cytokine concentrations and features are presented first. Next, Hypothesis 2 is presented, as the separation of skin and muscle provides a convenient structure for elucidation of further findings. The results for hypothesis 1 are then shown, followed finally by the results of the most challenging tasks from hypothesis 3.

To summarize the results, skin and muscle tissue are separated (hypothesis 2) at all timepoints with strong statistical significance by MANOVA analysis (Figure 4.13, Figure 4.16, Figure 4.19) as well as successful classification with random forest classifier at 92.28% average accuracy (Figure 4.8,Table 4.16).

In skin, the classifier with top performance for hypothesis 1 at all timepoints is the random forest classifier using the feature space that includes interaction variables (hybrid features) achieving accuracy of 96.15% (Table 4.34), and an AUROC score of .995 (Figure 4.30). The top performer for hypothesis 3 at all timepoints for the differentiation of rejection associated inflammation from not rejection associated inflammation is the random forest classifier, using hybrid features achieving accuracy of 92.55% (Table 4.54) and an AUROC score of .968 (Figure 4.41). A model where skin an muscle are considered together performs poorly compared to the models where they are considered separately.

In muscle, the classifier with top performance for hypothesis 1 at all timepoints is the random forest classifier using the feature space that includes interaction variables (hybrid features) achieving accuracy of 95.16% (Table 4.38), and an AUROC score of .9895 (Figure 4.32). The top performer for hypothesis 3 at all timepoints for the differentiation of rejection associated inflammation from not rejection associated inflammation is the random forest classifier, using hybrid features achieving accuracy of 86.80% (Table 4.58) and an AUROC score of .955 (Figure 4.43).

Histology

The mode of allograft and Isograft samples at or prior to POD 5 is zero, while after POD 5 the mode of allografts was three or greater (Table 4.1). The average grade of allograft and Isograft samples were less than one at or prior to POD 5. After POD 5 the Isograft average remained close to zero and the allograft average increased to three (Table 4.2).

Group (skin)	Mode of grade	
	POD<=5	*POD>5*
Allograft	0	3
Isograft	0	0

Table 4.1

Group (skin)	Average grade	
	POD<=5	*POD>5*
Allograft	0.765	3
Isograft	0.133	0.104

Table 4.2

In muscle the mode of allograft and Isograft groups were zero at or prior to POD 5, while at three in allografts and zero in isografts after POD 5 (Table 4.3). Average grade levels in muscle were below one at or prior to POD 5, and after POD 5 remained below one in Isografts and elevated to over two in allografts (Table 4.4).

Group (muscle)	Mode of grade	
	POD<=5	*POD>5*
Allograft	0	3
Isograft	0	0

Table 4.3

Group (muscle)	Average grade	
	POD<=5	*POD>5*
Allograft	0.467	2.222
Isograft	0.1875	0.75

Table 4.4

While being treated with FK-506 groups in skin had a mode of grade 0 (Table 4.5) and average grade below one (Table 4.6). In the five days following withdrawal of treatment the mode remained at zero but the average grade increased to over one. Beyond five days after treatment with FK-506 was stopped, the mode of grade becomes three, and the average grade is over two.

Group (skin)	Mode of grade
FK-Treated	0
FK-Withdrawn (Early)	0
FK-Withdrawn (Late)	3

Table 4.5

Group (skin)	Average grade
FK-Treated	0.436
FK-Withdrawn (Early)	1.143
FK-Withdrawn (Late)	2.286

Table 4.6

Muscle groups treated with FK-506 have a similar pattern to that seen in treated skin. Mode of grade is 0 under treatment (Table 4.7) and average grade is near zero under treatment (Table 4.8). Within the five days following cessation of treatment, the mode remains zero, and average grade of rejection increases to over

one. Beyond five days after treatment was withdrawn, the mode of grade becomes 2 and average grade increases to over 2.

Group (muscle)	Mode of grade
FK-Treated	0
FK-Withdrawn (Early)	0
FK-Withdrawn (Late)	2

Table 4.7

Group (muscle)	Average grade
FK-Treated	0.1
FK-Withdrawn (Early)	1.214
FK-Withdrawn (Late)	2.438

Table 4.8

The transplant surgeon made additional notes when reading muscle samples:

- The ATC group showed severe signs of rejection after day 9.
- The same was observed in the FK animals after day 25-27 (including infiltration and so on).
- Interestingly, the ISO group showed signs of degeneration after day 27, hardly any infiltrate (no rejection, of course). In grade 3 hardly any muscle was left, but a lot of fibrosis and connective tissue (Bindegewebe) – this phenomenon was not found to the same degree in all animals, but all showed at least some degree of degeneration.

Details of the readings for Allograft group are in (Table 6.1), Isograft in (Table 6.2), FK-Treated groups in (Table 6.3), and FK-Withdrawn groups in (Table 6.4).

Raw Cytokine Concentrations

In Cohort 1 skin, high concentrations of IL-1a and IL-18 were seen in all groups (Figure 4.1). Allografts display particularly elevated levels of IL-6, IL-1b, and GRO/KC. Larger variance and more outliers are also characteristics of the allograft group.

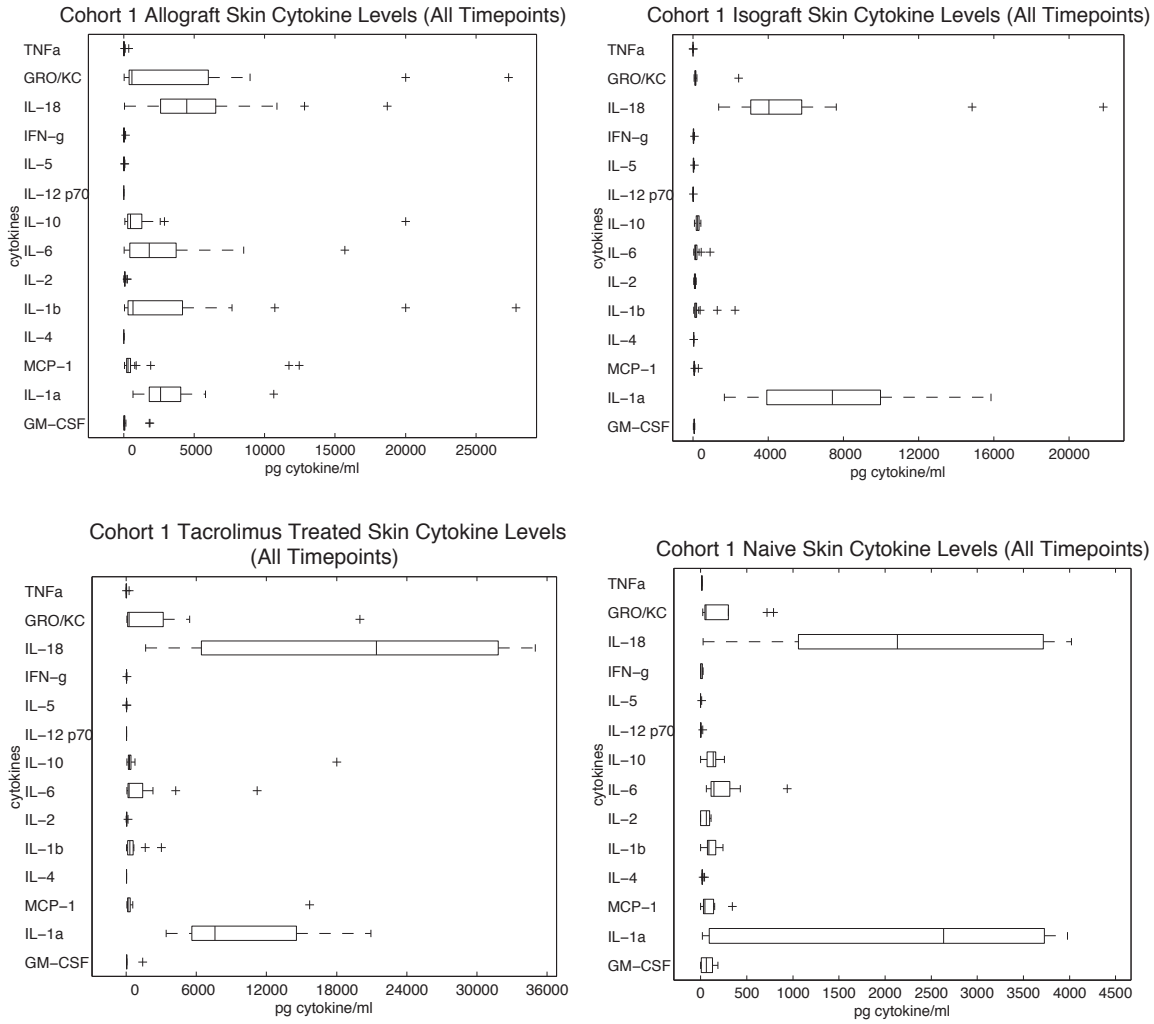

Figure 4.1 Cohort 1 Raw Skin Cytokine Levels of Allograft, Isograft, Tacrolimus Treated, and Naive.

In the box plots presented above, the bisecting line of each box represents represents the cytokine median concentration. The edges of box itself represent the 25th and 75th percentile, the whiskers represent extreme data points not considered outliers, and the plus symbols represent data points considered outliers. No outliers were eliminated from examination in this work.

A different set of cytokines appears to be activated in the muscle of Cohort 1 (Figure 4.2). There is little overlap with the cytokine profiles of skin, and there are clearly distinct cytokine profiles between each group. IL-18 or IL-1b also seem to play an important role in muscle. Similar to what is seen in skin, high levels of variance in cytokine levels are also a characteristic of allograft muscle.

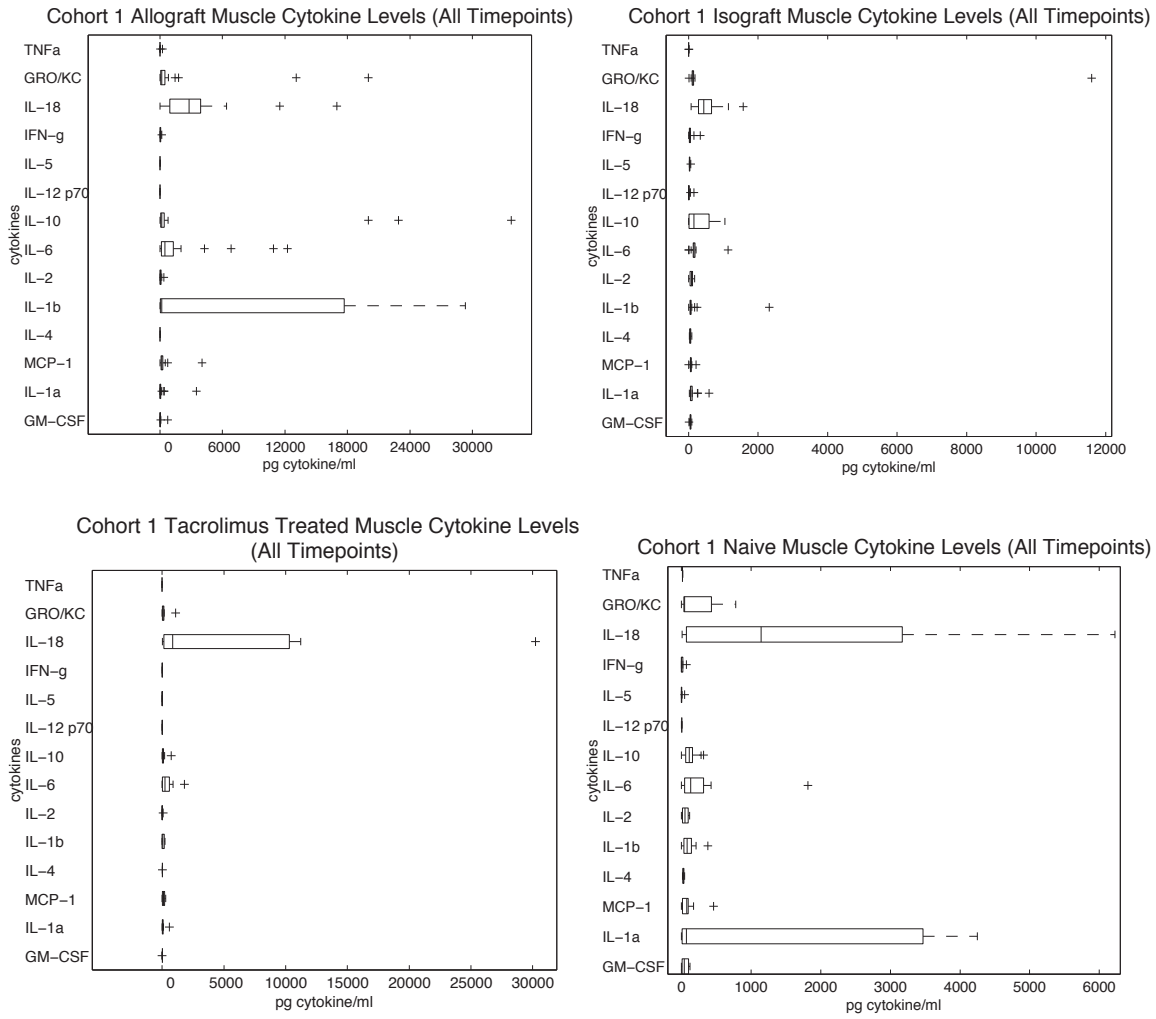

Figure 4.2 Cohort 1 Raw Muscle Cytokine Levels of Allograft, Isograft, Tacrolimus Treated, and Naive.

Skin allograft and isograft groups in Cohort 2 display qualitative similarities, as do CHS and DTH groups. However the allograft and isograft groups are visually distinct from the CHS and DTH groups (Figure 4.3). Many of the prominent cytokines shown are shared with cohort 1, although MCP-1 appears to be more pronounced in cohort 2.

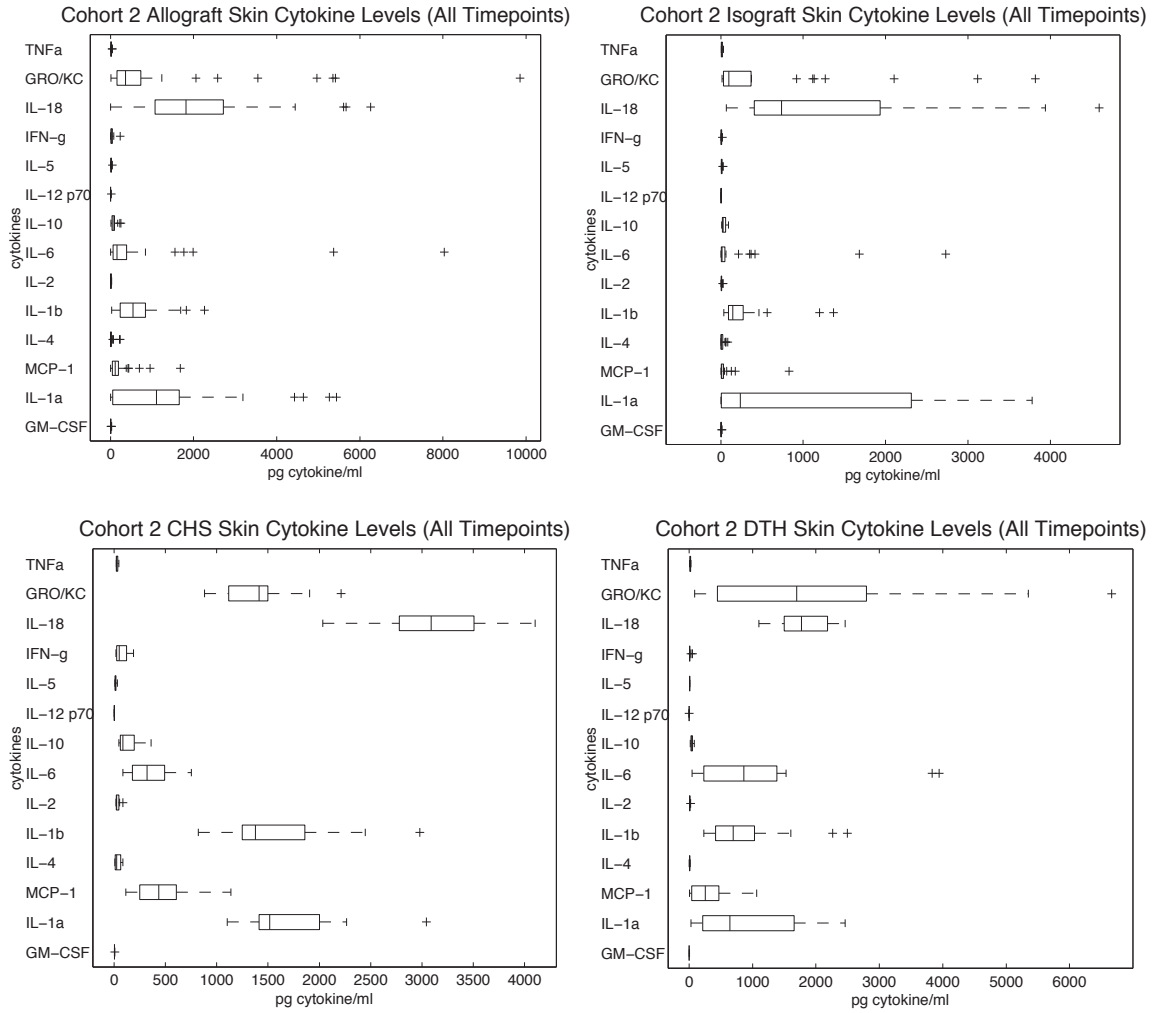

Figure 4.3 Cohort 2 Raw Skin Cytokine Levels of Allograft, Isograft, Contact Hypersensitivity (CHS) and Delayed Type Hypersensitivity (DTH).

The wound healing and associated reperfusion injury (shock) response shows a distinct overall cytokine expression (Figure 4.4). Several cytokines prominent in other cohorts (such as IL-1a, IL-18, and IL-6) are also seen here. However, the delta in the scale of cytokine activity between the wound and the shock groups is large, and may provide an important clue to the range of the wound-healing inflammatory response.

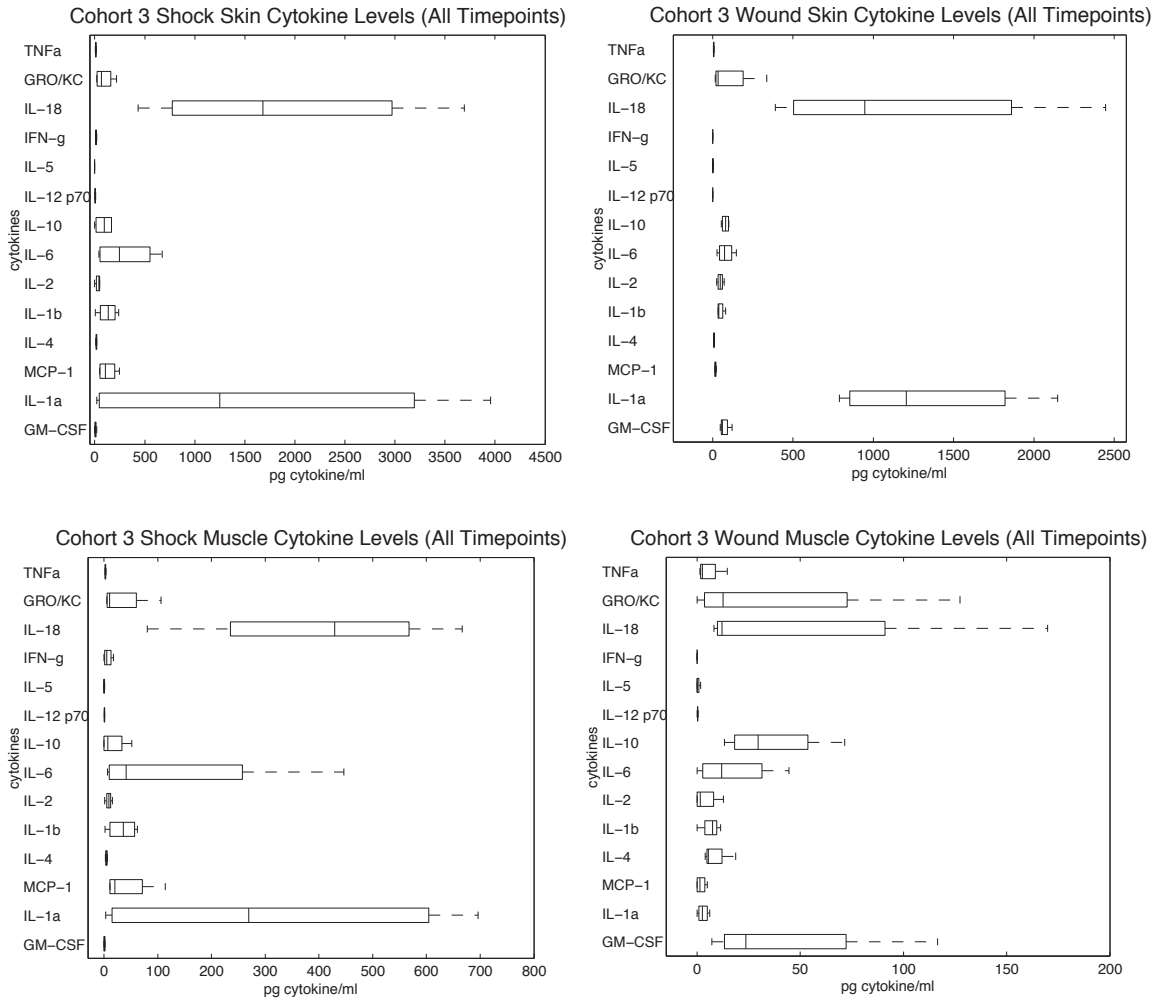

Figure 4.4 Cohort 3 Raw Skin and Muscle Cytokine Levels.

The cytokines prominent in heart rejection show a different profile from that seen in lung rejection (Figure 4.5). Heart rejection and lung rejection are also distinctive from skin or muscle rejection. IL-1a, which is prominently expressed in the skin and muscle of other cohorts, is not found in high concentrations in this cohort.

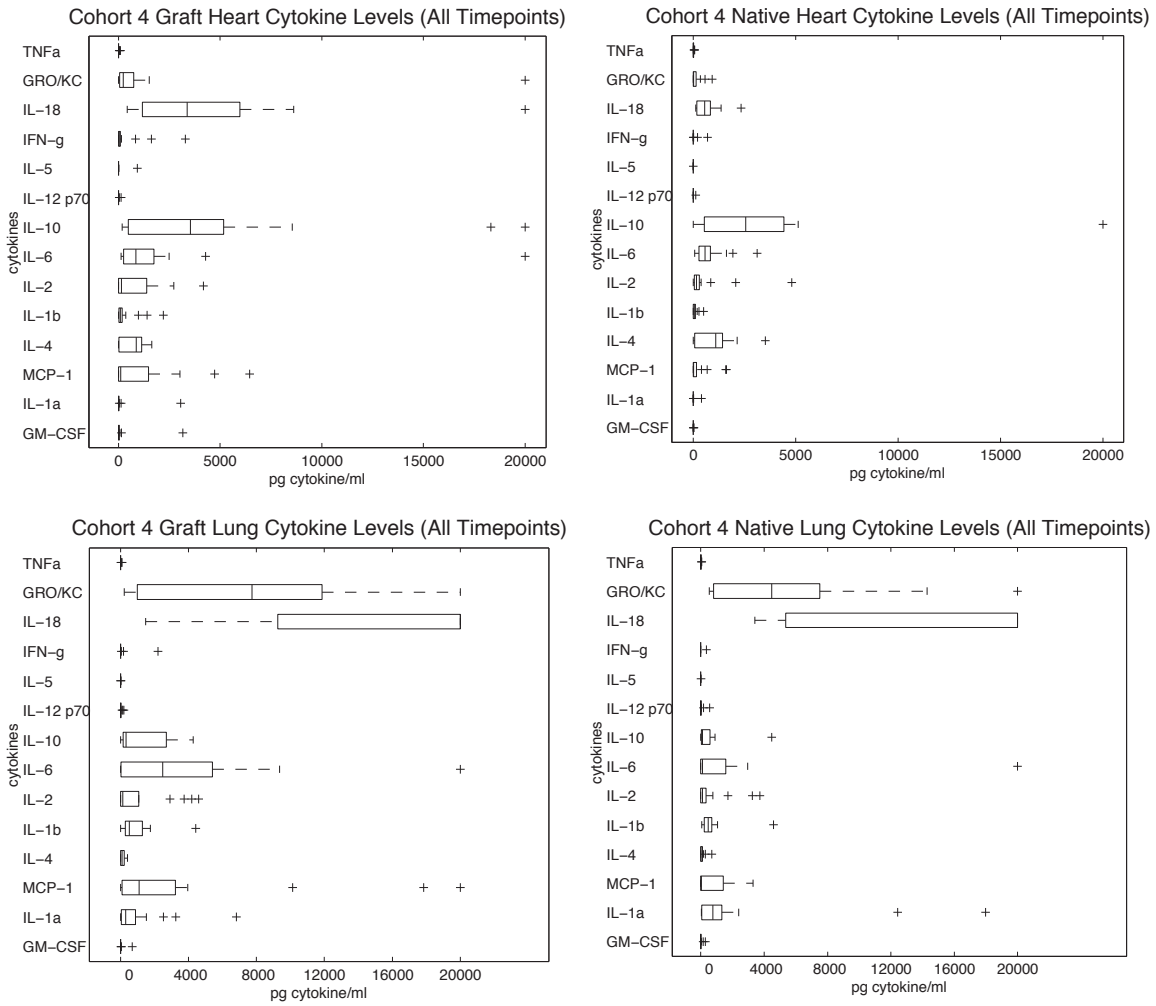

Figure 4.5 Cohort 4 Raw Heart and Lung Cytokine Levels.

Although some patterns in inflammation present themselves at a qualitative level during visual analysis of this data, more comprehensive and quantitative information about the changes in cytokine network profiles under the different experimental conditions is needed. The following sections provide this deeper analysis in relation to the relevant hypothesis.

Tissue Specific Patterns of Inflammation

Baseline Performance for Separation of Tissues

CTA Allograft Skin vs Muscle Random Classification (all time points)

Accuracy	**Confusion Matrix**			
46.81%	*Classified As*			
p-value	Muscle	Skin		
.8438	19	22	Muscle	*True Class*
	26	27	Skin	

Table 4.9 Baseline: Random classifier performance in allograft skin vs muscle

CTA Isograft Skin vs Muscle Random Classification (all time points)

Accuracy	**Confusion Matrix**			
47.90%	*Classified As*			
p-value	Muscle	Skin		
.2999	27	30	Muscle	*True Class*
	32	30	Skin	

Table 4.10 Baseline: Random classifier performance in isograft skin vs muscle

CTA Allograft Skin vs Muscle Linear Discriminant (all time points)

Accuracy	**Confusion Matrix**			
74.47%	*Classified As*			
p-value	Muscle	Skin		
.1663	39	2	Muscle	*True Class*
	22	31	Skin	

Table 4.11

CTA Allograft Skin vs Muscle Quadratic Discriminant (all time points)

Accuracy	**Confusion Matrix**			
71.28%	*Classified As*			
p-value	Muscle	Skin		
.0433	31	10	Muscle	*True Class*
	17	36	Skin	

Table 4.12

CTA Isograft Skin vs Muscle Linear Discriminant (all time points)

Accuracy	**Confusion Matrix**			
86.56%	*Classified As*			
p-value	Muscle	Skin		
.0161	54	3	Muscle	*True Class*
	13	49	Skin	

Table 4.13

CTA Isograft Skin vs Muscle Quadratic Discriminant (all time points)

Accuracy	**Confusion Matrix**			
92.44%	*Classified As*			
p-value	Muscle	Skin		
.0261	48	9	Muscle	*True Class*
	0	62	Skin	

Table 4.14

Naive Skin vs Muscle Linear Discriminant

Accuracy	**Confusion Matrix**			
70.37%	*Classified As*			
p-value	Muscle	Skin		
.2699	6	3	Muscle	*True Class*
	5	13	Skin	

Table 4.15

LDA classifiers were able to achieve moderate but unstable success in separating tissue at all time points in allograft (Table 4.11), isograft (Table 4.13), and Naïve (Table 4.15) groups. Similar results are seen for time points at or prior to POD 5 in allograft (70%, Table 6.103) and isograft (93.75%, Table 6.113), as well as after POD 5 in allograft (85.29%, Table 6.107) and isograft (87.32%, Table 6.117). QDA classifiers achieved marginally higher accuracy than LDA, but significantly higher significance in allograft (Table 4.12) and isograft (Table 4.14) when evaluating samples from all time points.

Enhanced Performance for Separation of Tissues

Following the intuition that different tissue types may express different inflammation patterns, the data was separated into sub-matrices grouped by tissue (i.e. skin and muscle). This ultimately enables significant gains in accuracy and significance in the isolation of specific forms of inflammation.

Distinctive cytokine network patterns in skin and muscle are shown here for each experimental condition, specifically allograft, isograft, under Tacrolimus treatment, withdrawn from Tacrolimus treatment, and naïve.

The naïve tissue expresses the narrowest margin of difference between skin and muscle tissue, but the distinction is evident even at the level of qualitative visual analysis of cytokine concentration levels (Figure 4.6). Quantitative analysis with MANOVA reveals the groups to follow significantly different distributions (Figure 4.7). IL-5 and IL-12p70 are important drivers of this distinction (Figure 6.148).

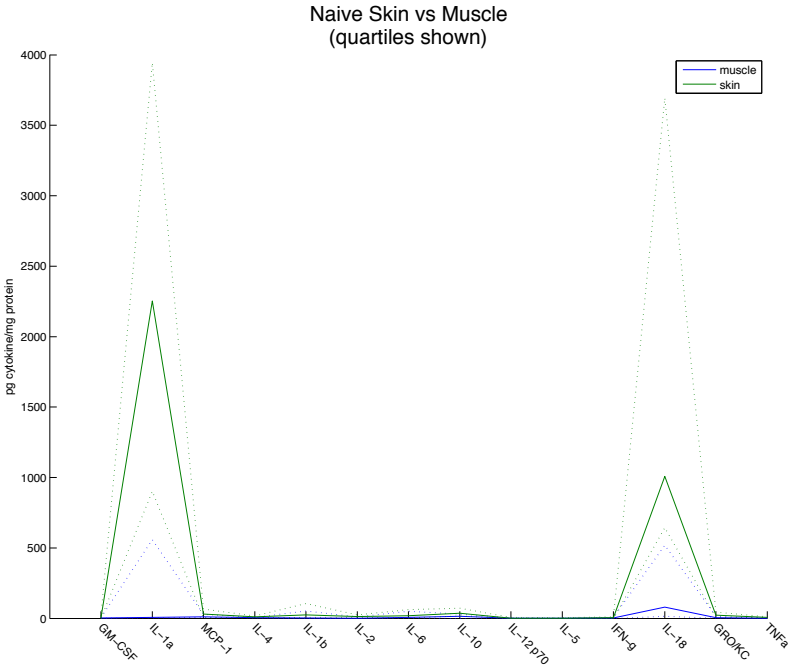

Figure 4.6 Parallel plot of skin and muscle cytokine concentrations in naïve

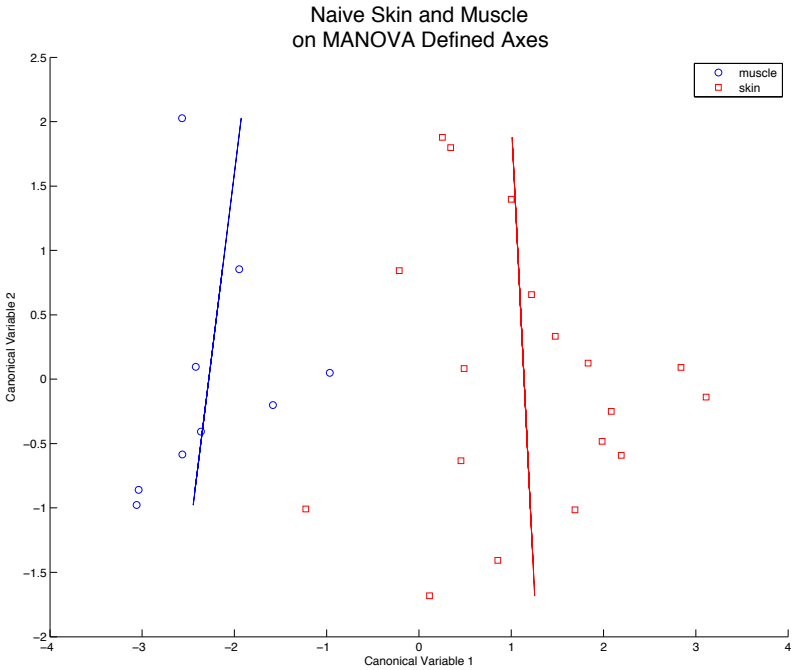

Figure 4.7 Skin and muscle cytokine network patterns follow significantly different distributions in naïve as determined by MANOVA ($p<0.05$)

The underlying distinction between skin and muscle in naïve animals that is clearly evident in the MANOVA transformed space is less evident in the original untransformed feature space, as can be seen by the performance of the baseline LDA classifier at approximately 70% (Table 4.15), as well as the logistic classifier with accuracy at about 74% (Table 6.125). The decision tree (85.19%, Table 6.126,

Figure 6.149 and Figure 6.150) is more successful in capturing the distinction, while the random forest (Table 4.16, Figure 4.8) classifier is most accurate.

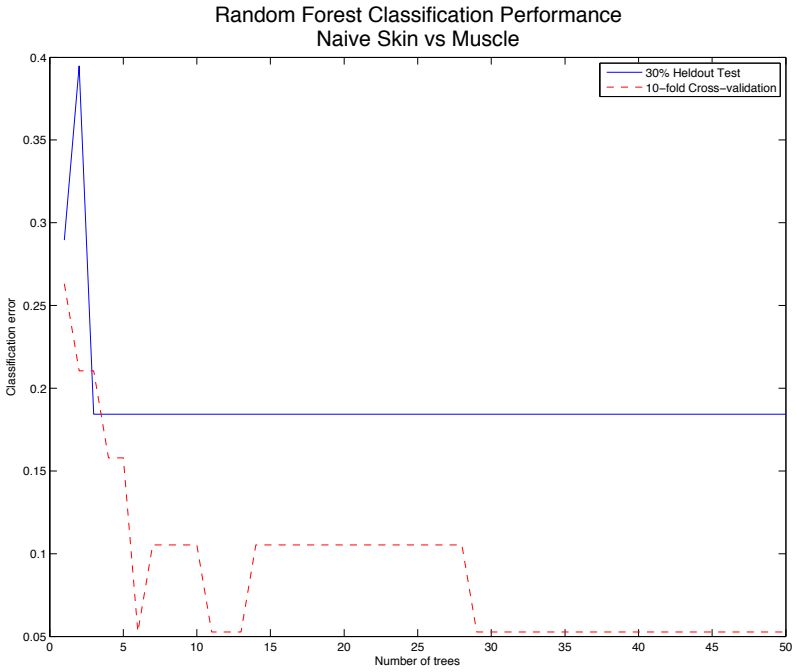

Figure 4.8

Naive Skin vs Muscle Random Forest (50 trees)				
Accuracy	**Confusion Matrix**			
85.19%	*Classified As*			
p-value	Muscle	Skin		
.1718	7	2	Muscle	*True Class*
	1	17	Skin	

Table 4.16

Isograft animals also showed distinction in cytokine expression between skin and muscle components that was qualitatively evident (Figure 4.9) as well quantitatively evident (Figure 4.10), with the distinction being driven largely by IL-5, TNFa, and GM-CSF (Figure 6.127).

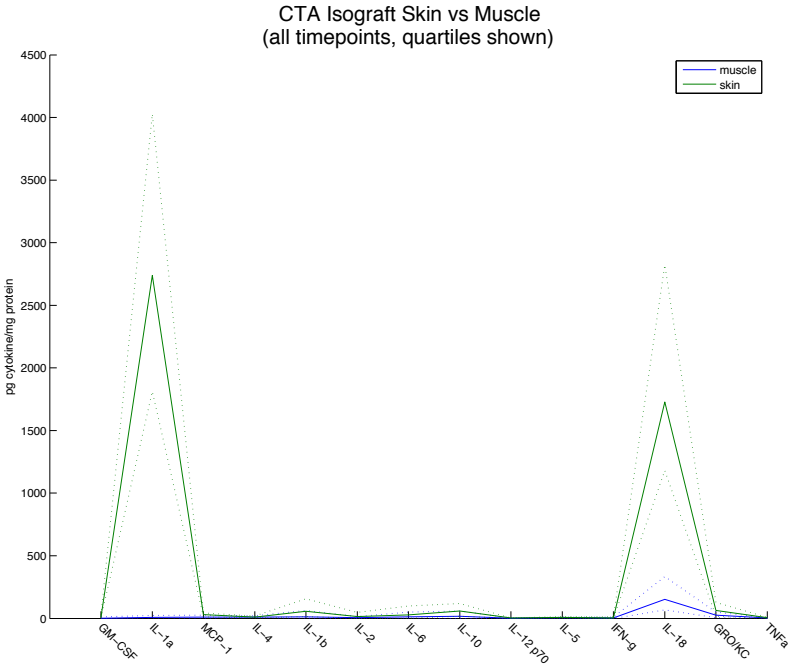

Figure 4.9 Parallel plot of skin and muscle cytokine concentrations in isograft

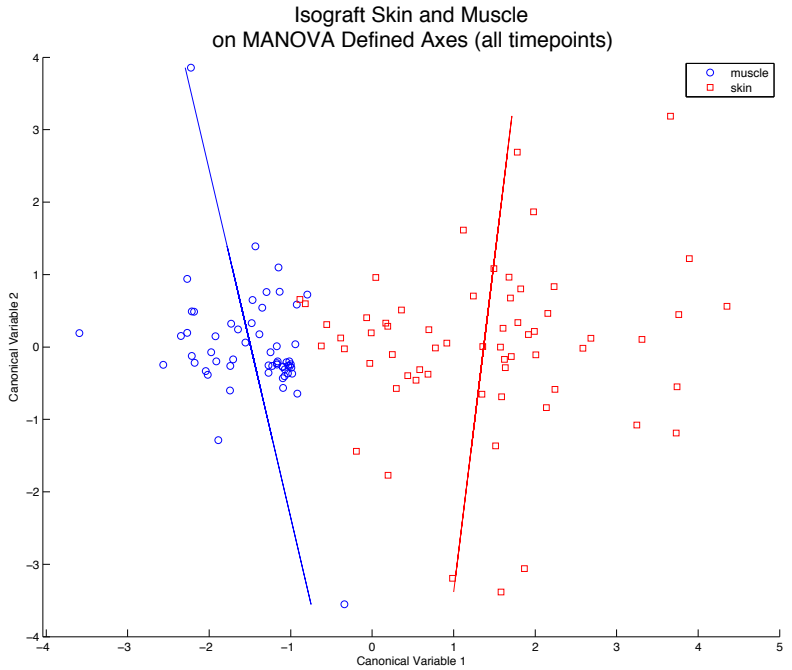

Figure 4.10 Skin and muscle cytokine network patterns follow significantly different distributions in isograft as determined by MANOVA (p<0.01)

Logistic (94.12%, Table 6.111), decision tree (96.64%, Table 6.112, Figure 6.128 and Figure 6.129), and random forest (97.48%, Table 4.17, Figure 4.11) classifiers are all able to separate the cytokine patterns of skin from muscle in isografts at all time points.

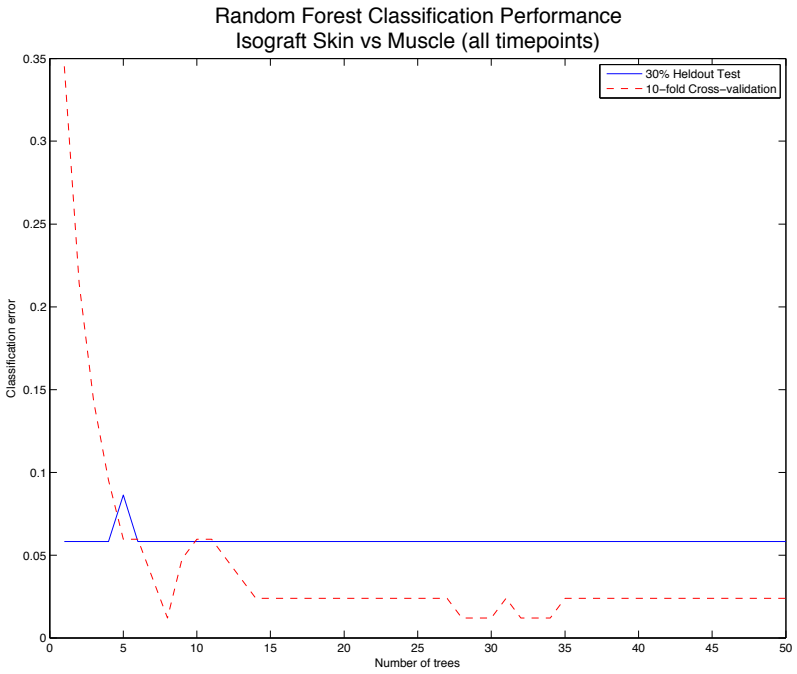

Figure 4.11

CTA Isograft Skin vs Muscle Random Forest (all time points, 50 trees)

Accuracy	**Confusion Matrix**			
97.48%	*Classified As*			
p-value	Muscle	Skin		
.0013	56	1	Muscle	*True Class*
	2	60	Skin	

Table 4.17

Isograft tissues also have separate distributions at time points at or prior to POD 5 (Figure 6.130, Figure 6.131, Figure 6.132), as well as after POD 5 (Figure 6.136, Figure 6.137, Figure 6.138). Logistic (77.08%), decision tree (97.92%), and random forest (98.5%) achieve good performance at or prior to POD 5 (Table 6.114, Table 6.115, Table 6.116, and Figure 6.133, Figure 6.134, Figure 6.135) as well as after POD 5 with logistic (88.73%), decision tree (97.18%), and random forest (98.59%) (Table 6.118, Table 6.119, Table 6.120, and Figure 6.139, Figure 6.140, Figure 6.141).

The distinction between skin and muscle continues to hold in allografts with the additional source of inflammation introduced by rejection (Figure 4.12 and Figure 4.13). This process is driven by a more complex plurality of cytokines that includes IL-12p70, TNFa, IL-5, GM-CSF, and others (Figure 6.112).

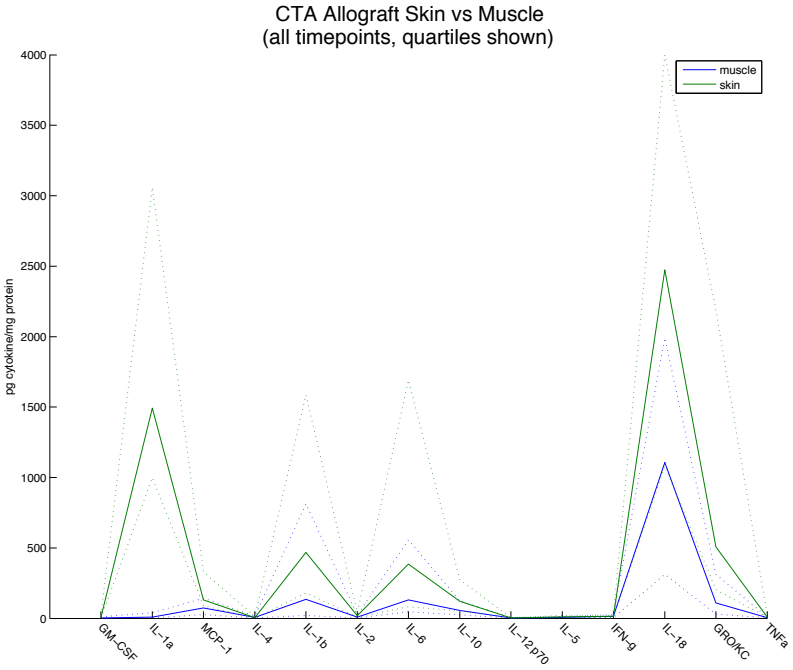

Figure 4.12 Parallel plot of skin and muscle cytokine concentrations in allograft

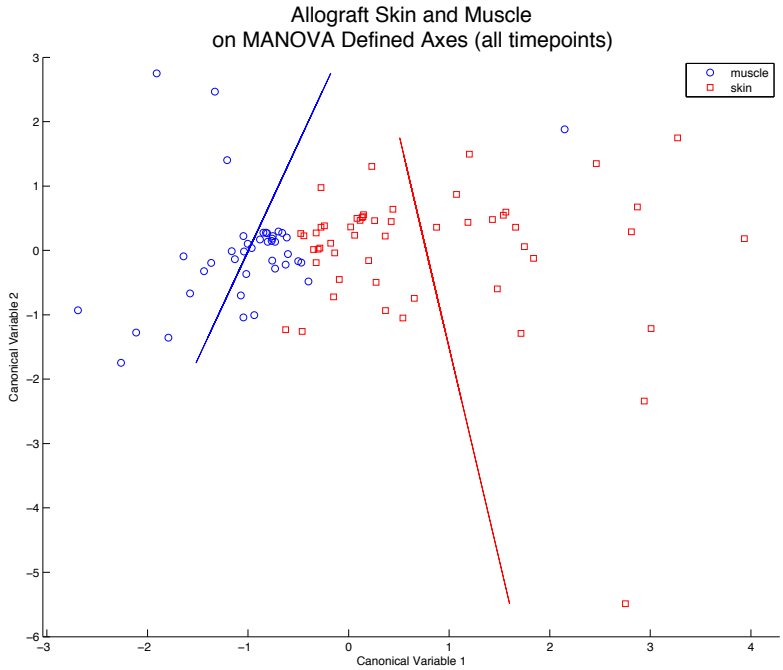

Figure 4.13 Skin and muscle cytokine network patterns follow significantly different distributions in allograft as determined by MANOVA ($p<0.01$)

Skin and muscle tissue in allograft continue to follow separate distributions at time points prior to and including POD 5 (prior to visible rejection, Figure 6.115, Figure 6.116, and Figure 6.117), as well as after POD 5 (Figure 6.121, Figure 6.122, and Figure 6.123).

The logistic (86.17%, Table 6.101), decision tree (95.74%, Table 6.102, Figure 6.113 and Figure 6.114), and random forest (94.68%, Table 4.18, Figure

4.14) classifiers are able to separate the cytokine patterns of skin from muscle in allografts at all time points.

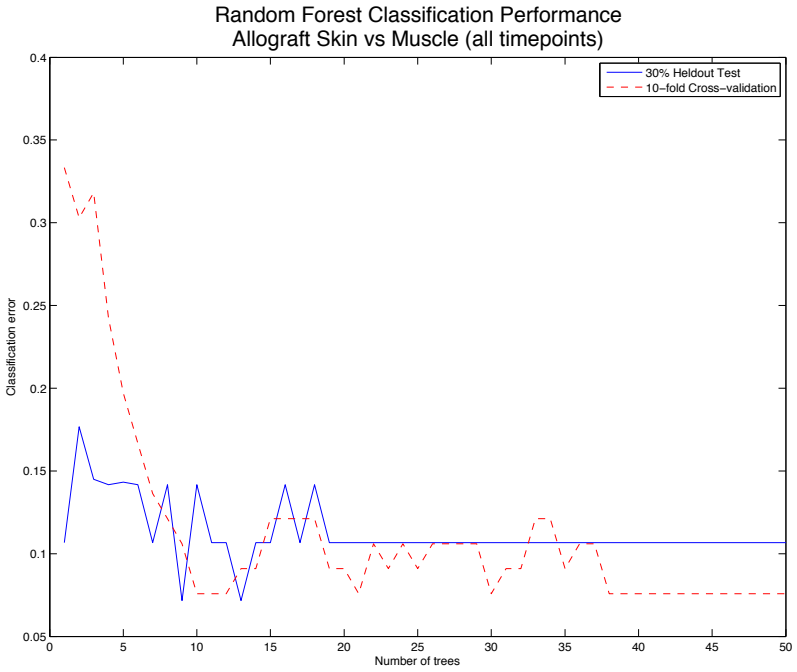

Figure 4.14

CTA Allograft Skin vs Muscle Random Forest (all time points, 50 trees)

Accuracy	**Confusion Matrix**			
94.68%	*Classified As*			
p-value	Muscle	Skin		
.0233	38	3	Muscle	*True Class*
	2	51	Skin	

Table 4.18

Good performance at or prior to POD 5 is also achieved in logistic (78.33%), decision tree (98.33%), and random forest (96.67%) (Table 6.104, Table 6.105, Table 6.106, and Figure 6.118, Figure 6.119, Figure 6.120) as well as after POD 5 in logistic (76.47%), decision tree (91.18%), and random forest (91.18%) (Table 6.108, Table 6.109, Table 6.110, and Figure 6.124, Figure 6.125, Figure 6.126).

Muscle and skin components retain their distinctiveness under active immunosuppression (Figure 4.15 and Figure 4.16). IL-5 appears to play the principal distinguishing role under conditions of immunosuppression (Figure 6.142).

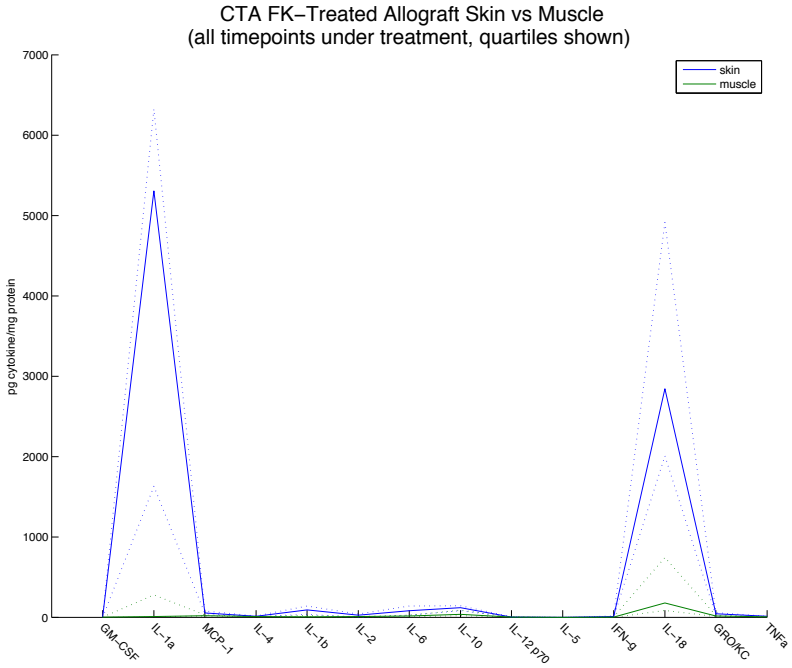

Figure 4.15 Parallel plot of skin and muscle cytokine concentrations in FK-Treated

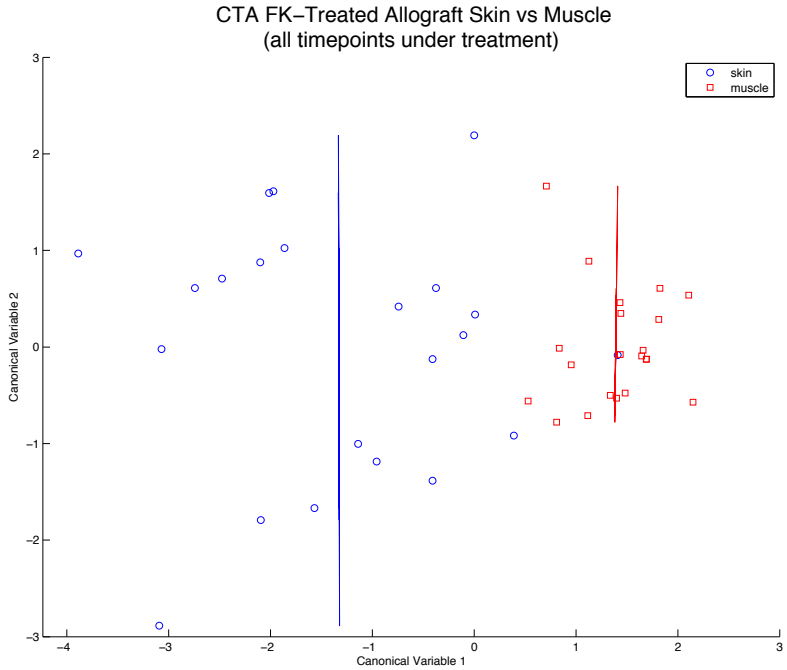

Figure 4.16 Skin and muscle cytokine network patterns follow significantly different distributions in FK-Treated as determined by MANOVA ($p<0.01$)

Reasonable separation of tissues can be achieved with the logistic classifier (74.42%, Table 6.121), although better separation is achieved with the decision tree (90.97%, Table 6.122, Figure 6.143, Figure 6.144) and best stable performance with random forest (86.05%, Table 4.19, Figure 4.17).

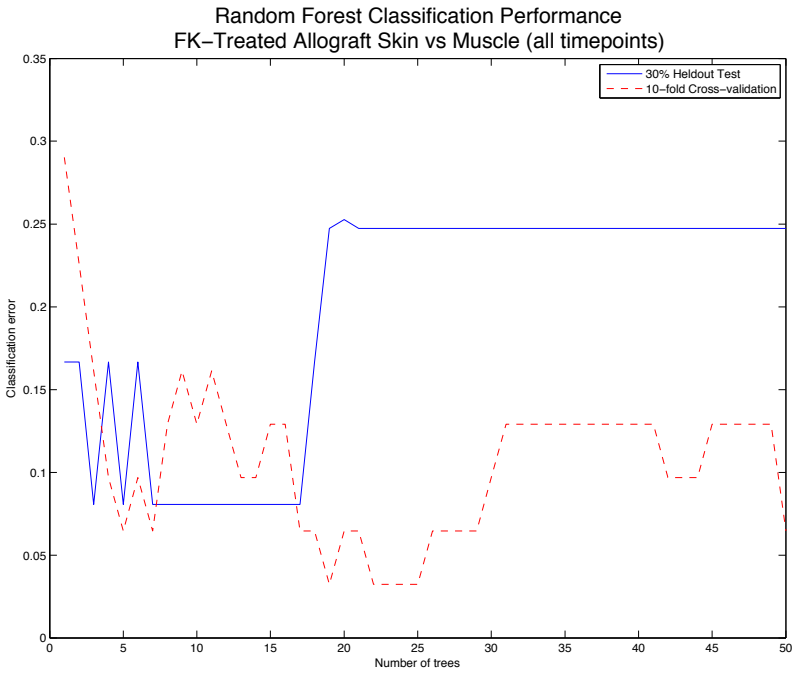

Figure 4.17

CTA FK-Treated Allograft Skin vs Muscle Random Forest (all time points under treatment, 50 trees)

Accuracy	**Confusion Matrix**			
86.05%	*Classified As*			*True Class*
p-value	Muscle	Skin		
.0104	18	3	Muscle	
	1	21	Skin	

Table 4.19

Even after immunosuppression is withdrawn skin and muscle continue to express distinctive cytokine patterns (Figure 4.18 and Figure 4.19). A larger plurality of cytokines appears to drive the distinctions than under conditions of immunosuppression, although TNFa and IL-5 again are primary contributors (Figure 6.145).

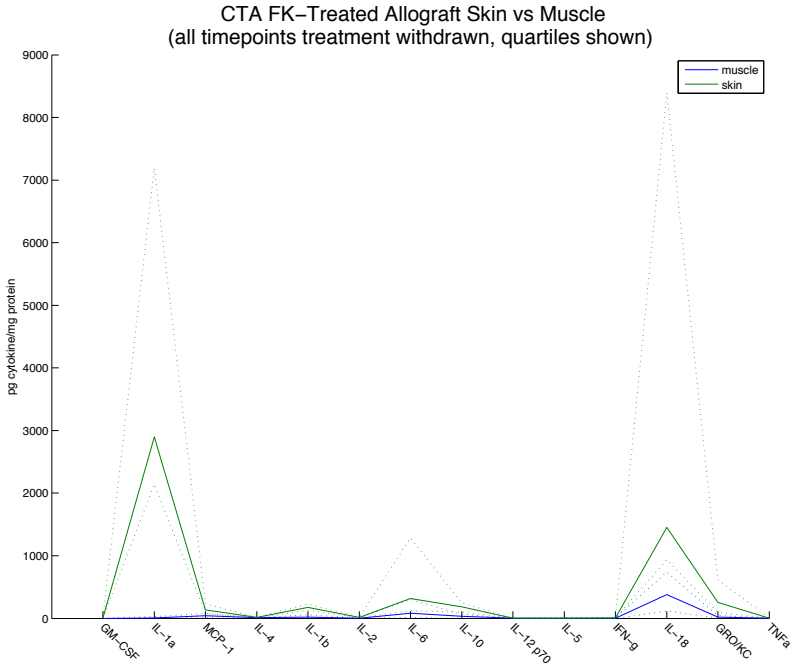

Figure 4.18 Parallel plot of skin and muscle cytokine concentrations in FK-Treatment Withdrawn

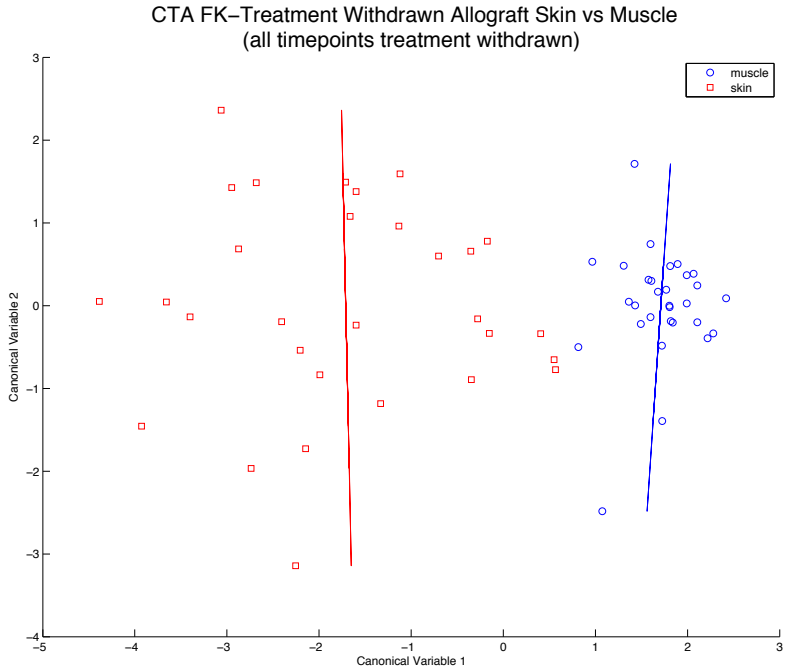

Figure 4.19 Skin and muscle cytokine network patterns follow significantly different distributions in FK-Treatment Withdrawn as determined by MANOVA ($p<0.01$)

The additional inflammation enables excellent separation of skin and muscle tissue by logistic classifier (95.00%, Table 6.123), decision tree (100%, Table 6.124, Figure 6.146, Figure 6.147), and random forest (98.33%, Table 4.20, Figure 4.20).

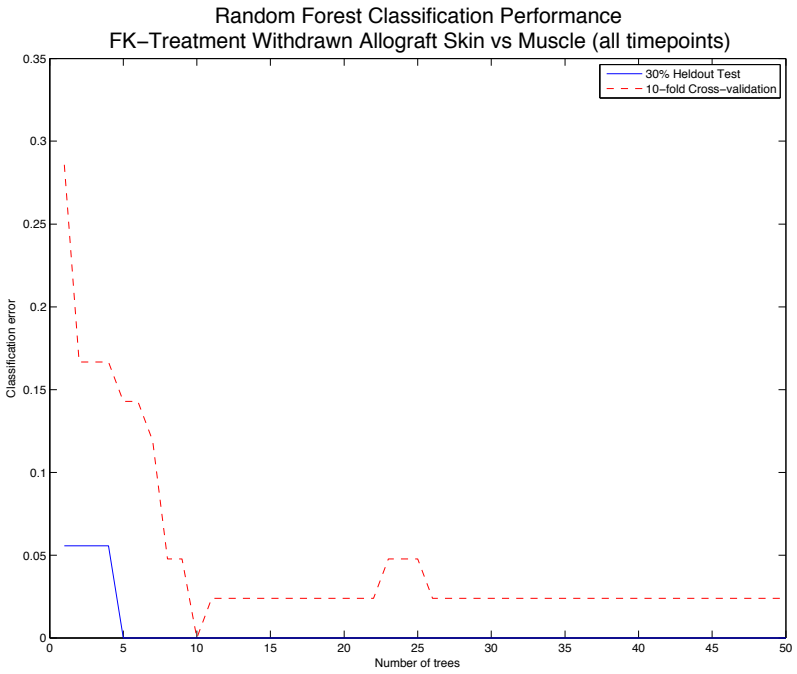

Figure 4.20

CTA FK-Treatment Withdrawn Allograft Skin vs Muscle Random Forest (all time points treatment withdrawn, 50 trees)

Accuracy	**Confusion Matrix**			
98.33%	*Classified As*			
p-value	Muscle	Skin		
<.0001	30	0	Muscle	*True Class*
	0	30	Skin	

Table 4.20

Identification of Rejection in Allograft vs Isograft

Differences in concentration of IL-1a, IL-1b, IL-6, IL-18, and MCP-1 are evident from the parallel plot of allograft versus isograft in skin (Figure 4.21), and MCP-1, IL-1b, IL-6, and IL-18 in muscle (Figure 4.23).

When transformed by MANOVA and the samples plotted on the axis defined by the first and second canonical variable of the MANOVA transformation, the degree of separation between allograft and Isograft becomes clearer in both skin (Figure 4.22) and muscle (Figure 4.24). On the MANOVA defined axes separation of groups in skin is driven primarily by IL-12p70, IFN-g, TNFa, IL-4, GM-CSF, and IL-5 (Figure 6.1), and in muscle separation is driven primarily by IL-5, IL-12p70, GM-CSF, TNFa, and IFN-g (Figure 6.48).

When feature interaction variables are added to the data set, the MANOVA transformed plot shows even greater contrast between groups (Figure 6.11), driven primarily by IL-12p70, IFN-g, IL-4, GM-CSF, and TNFa (Figure 6.12).

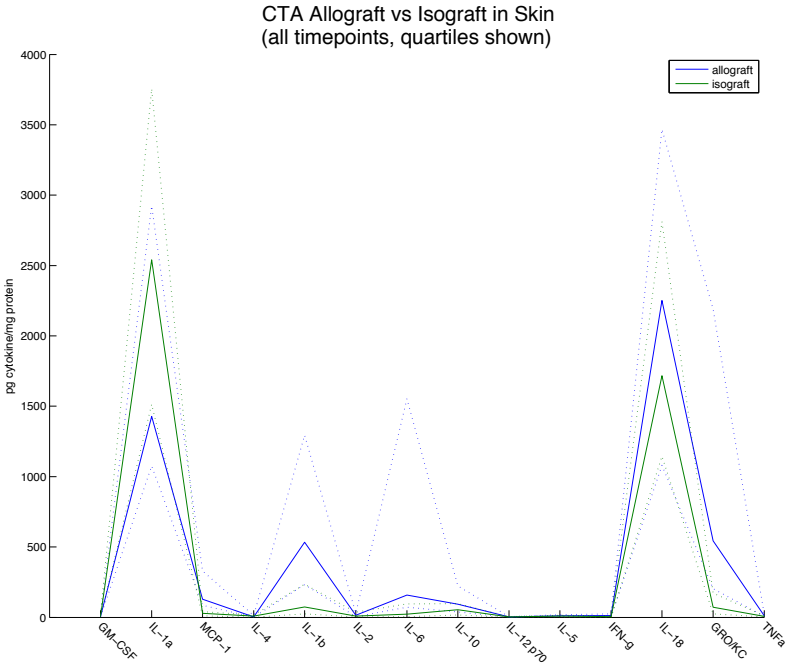

Figure 4.21

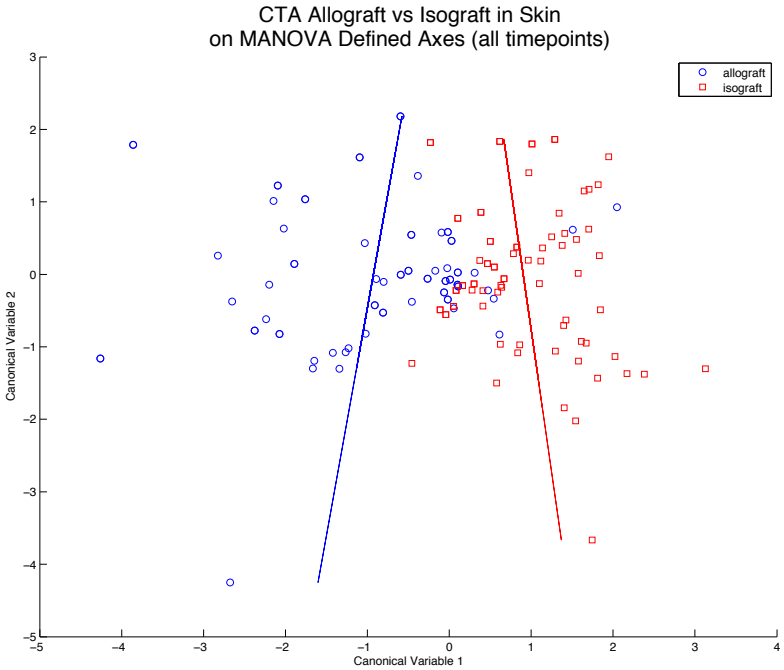

Figure 4.22

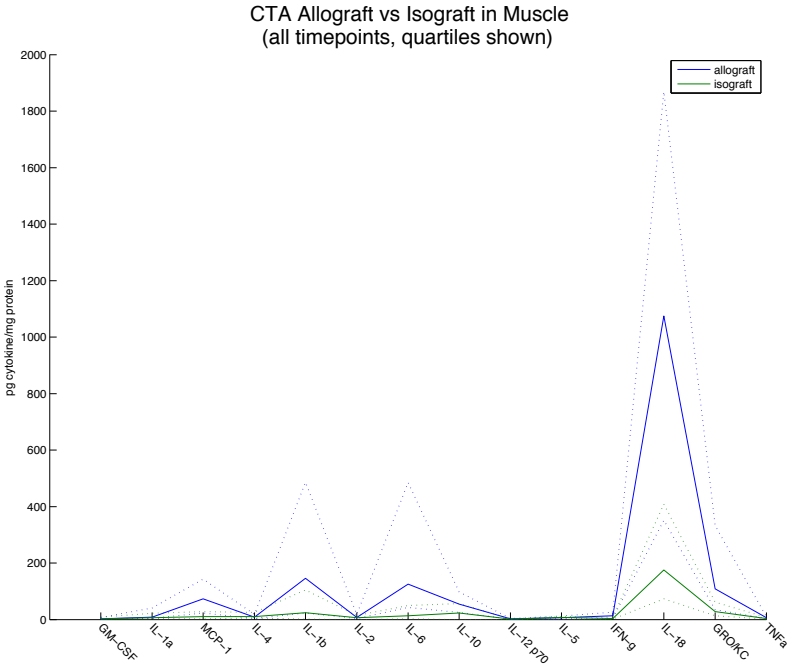

Figure 4.23

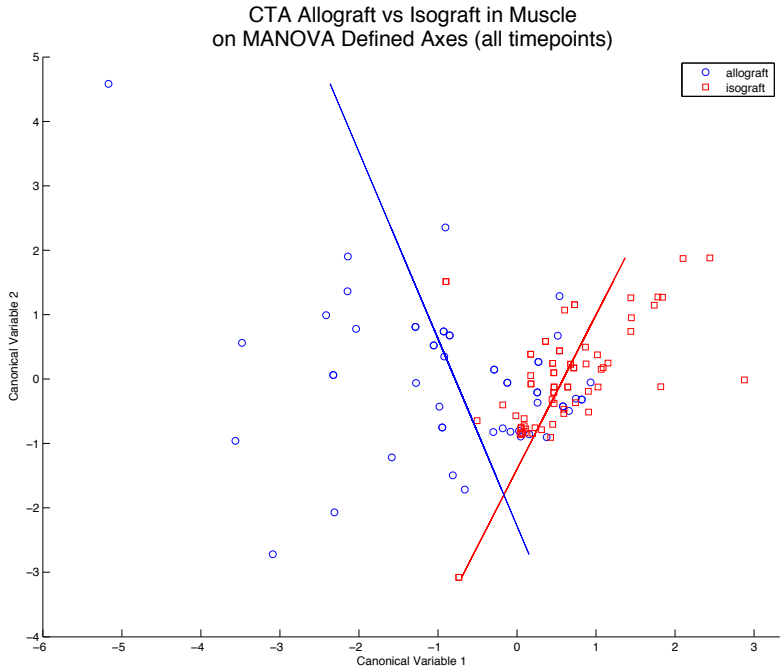

Figure 4.24

In allograft samples that are either immunosuppressed or withdrawn from immunosuppression and rejecting show differences in concentration of IL-1a, IL-6, IL-18, and GRO/KC in the parallel plot of rejecting versus suppressed in skin (Figure 4.25). Differences in the concentration of MCP-1, IL-1b, IL-6, and IL-18 are evident in the parallel plot of muscle sample cytokine concentrations (Figure 4.26).

When transformed by MANOVA and the samples plotted on the axis defined by the first and second canonical variable of the MANOVA transformation, the separation between rejecting and suppressed becomes clearer in skin (Figure 4.27) and muscle (Figure 4.28). On the MANOVA defined axes separation of groups in skin is driven primarily by IL-5, IL-12p70, TNFa, and IL-4 (Figure 6.95), and in muscle separation is driven primarily by IL-12p70, IL-5, TNFa, GM-CSF, and IFN-g (Figure 6.104).

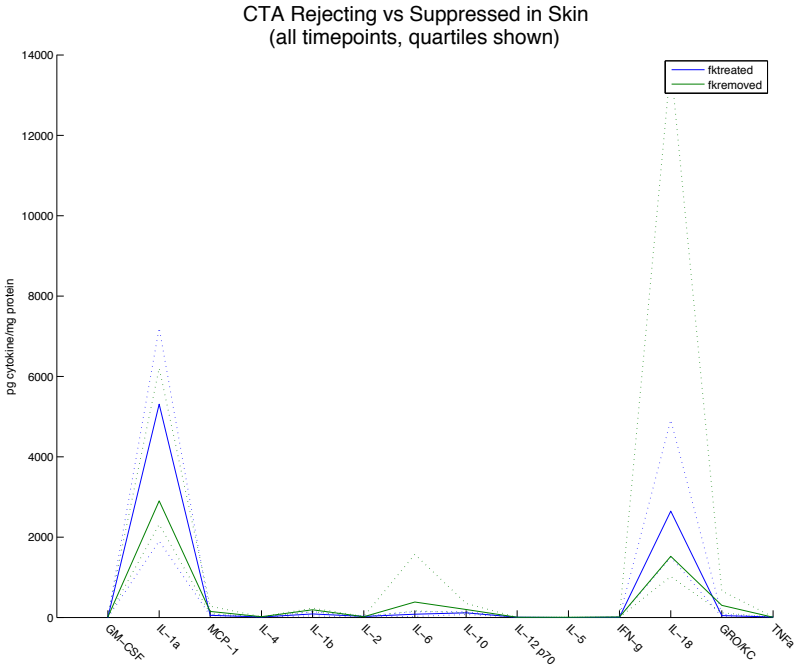

Figure 4.25

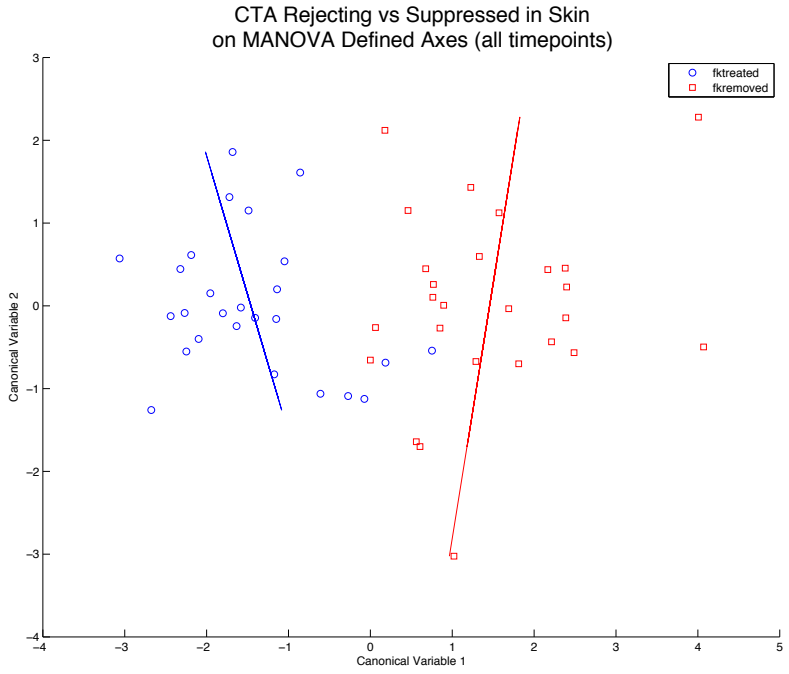

Figure 4.26

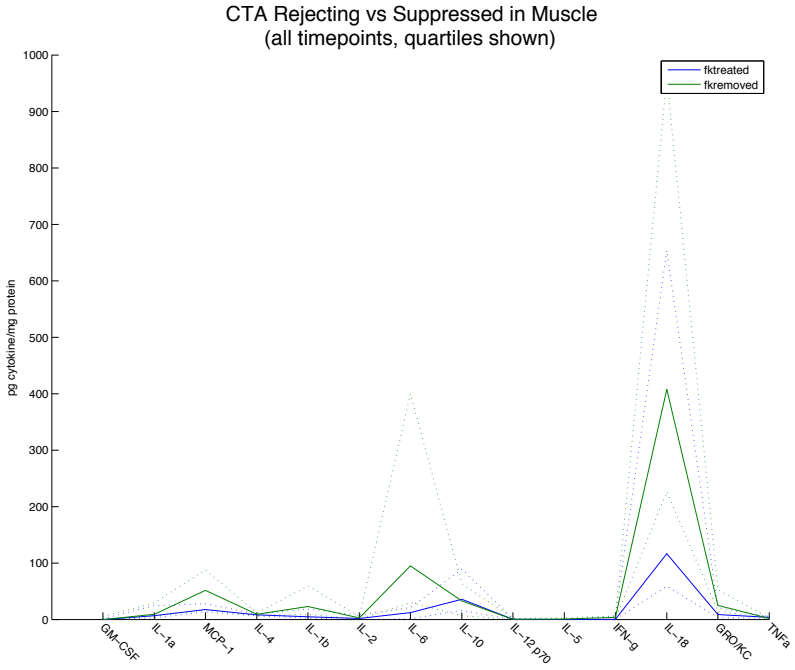

Figure 4.27

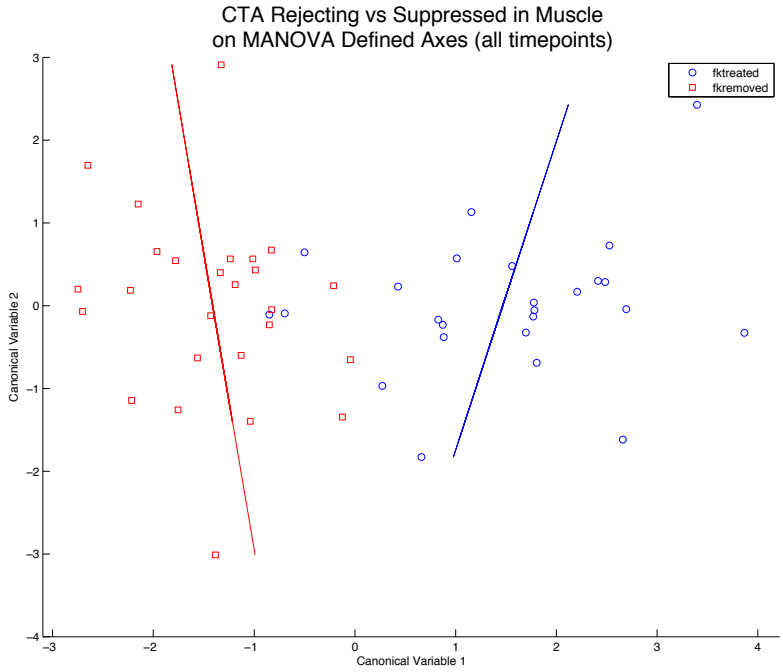

Figure 4.28

Baseline Performance for Identification of Allograft vs Isograft

Random classification was able to select the correct class approximately half the time in both skin and muscle with very little bias (Table 4.21, Table 4.22). When considering samples from all time points, LDA classification performed at about 80% accuracy in skin (Table 4.23) with an AUROC score of .885 (Figure 6.15), and in muscle accuracy was also about 80% (Table 4.27) with an AUROC score of .714 (Figure 6.62). QDA classification achieved about 81% accuracy in skin (Table 4.24)

with an AUROC score of .915 (Figure 6.16), and about 86% accuracy in muscle (Table 4.28) with AUROC of .832 (Figure 6.63). The confusion matrices show evidence of bias in both cases.

Adding feature interaction variables to the data improved the AUROC score of LDA in skin to .873 (Figure 6.20), and QDA in skin to .921 (Figure 6.21). Similar improvements were seen in muscle with the AUROC score of LDA in muscle increasing to .833 (Figure 6.67), and QDA in muscle reaching .869 (Figure 6.68).

CTA Allograft vs Isograft in Skin Random Classification (all time points)

Accuracy	**Confusion Matrix**			
50.64%	*Classified As*			
p-value	Allograft	Isograft		
.3828	35	44	Allograft	*True Class*
	38	39	Isograft	

Table 4.21 Baseline: Random classifier performance in skin allograft vs isograft

CTA Allograft vs Isograft in Muscle Random Classification (all time points)

Accuracy	**Confusion Matrix**			
52.42%	*Classified As*			
p-value	Allograft	Isograft		
.8922	35	36	Allograft	*True Class*
	25	28	Isograft	

Table 4.22 Baseline: Random classifier performance in muscle allograft vs isograft

CTA Allograft vs Isograft in Skin Linear Discriminant (all time points)

Accuracy	**Confusion Matrix**			
80.77%	*Classified As*			
p-value	Allograft	Isograft		
.0457	60	17	Allograft	*True Class*
	8	71	Isograft	

Table 4.23 CTA Allograft vs Isograft in Skin Linear Discriminant (all time points)

Feature selected (69.87%, Table 6.5), MANOVA transformed (80.12%, Table 6.6)

CTA Allograft vs Isograft in Skin Quadratic Discriminant (all time points)

Accuracy	**Confusion Matrix**			
81.41%	*Classified As*			
p-value	Allograft	Isograft		
.0387	56	21	Allograft	*True Class*
	8	71	Isograft	

Table 4.24

Feature selected (71.15%, Table 6.7), MANOVA transformed (84.41%, Table 6.8)

CTA Rejecting vs Suppressed in Skin Linear Discriminant (FK Groups)

Accuracy	Confusion Matrix			
82.69%	*Classified As*			
p-value	Rejecting	Suppressed		
.0017	21	5	Rejecting	*True Class*
	4	22	Suppressed	

Table 4.25

Feature selected (75.00%, Table 6.43), MANOVA transformed (82.69%, Table 6.44)

CTA Rejecting vs Suppressed in Skin Quadratic Discriminant (FK Groups)

Accuracy	Confusion Matrix			
86.54%	*Classified As*			
p-value	Rejecting	Suppressed		
.0122	24	2	Rejecting	*True Class*
	5	21	Suppressed	

Table 4.26

Feature selected (78.85%, Table 6.45), MANOVA transformed (84.62%, Table 6.46)

CTA Allograft vs Isograft in Muscle Linear Discriminant (all time points)

Accuracy	Confusion Matrix			
70.16%	*Classified As*			
p-value	Allograft	Isograft		
.3018	27	26	Allograft	*True Class*
	11	60	Isograft	

Table 4.27

Feature selected (73.39%, Table 6.53), MANOVA transformed (73.39%, Table 6.54)

CTA Allograft vs Isograft in Muscle Quadratic Discriminant (all time points)

Accuracy	Confusion Matrix			
78.23%	*Classified As*			
p-value	Allograft	Isograft		
.1526	34	19	Allograft	*True Class*
	8	63	Isograft	

Table 4.28

Feature selected (70.97%, Table 6.55), MANOVA transformed (80.65%, Table 6.56)

CTA Rejecting vs Suppressed in Muscle Linear Discriminant (FK Groups)

Accuracy	Confusion Matrix			
80.39%	*Classified As*			
p-value	Rejecting	Suppressed		
.0010	21	5	Rejecting	*True Class*
	5	20	Suppressed	

Table 4.29

Feature selected (72.55%, Table 6.91), MANOVA transformed (82.35%, Table 6.92)

CTA Rejecting vs Suppressed in Muscle Quadratic Discriminant (FK Groups)

Accuracy	**Confusion Matrix**			
84.31%	*Classified As*			
p-value	Rejecting	Suppressed		
.0008	22	4	Rejecting	*True Class*
	4	21	Suppressed	

Table 4.30
Feature selected (62.75%, Table 6.93), MANOVA transformed (84.31%, Table 6.94)

In addition to analysis at all time points, baseline performance was measured at or prior to POD 5 in skin with LDA (76.92%, Table 6.17), feature selected LDA (61.54%, Table 6.18), MANOVA LDA (69.23%, Table 6.19), and feature selected QDA (60.44%, Table 6.20), as well as in muscle with LDA (81.57%, Table 6.65), feature selected LDA (68.42%, Table 6.66), MANOVA LDA (82.89%, Table 6.67), and feature selected QDA (71.05%, Table 6.68).

After POD 5 baseline performance in skin was measured by LDA (93.85%, Table 6.30), feature selected LDA (84.62%, Table 6.31), MANOVA LDA (90.77%, Table 6.32), and feature selected QDA (95.38%, Table 6.33), as well as in muscle by LDA (87.50%, Table 6.78), feature selected LDA (87.50%, Table 6.79), MANOVA LDA (89.53%, Table 6.80), and feature selected QDA (91.67%, Table 6.81). The original feature space yields the best results, MANOVA nearly equivalent to the original feature space, and feature selected space the least accurate. Baseline performance trends indicate early classification is the more challenging task.

Performance in separating tissue under immunosuppression from tissue withdrawn from immunosuppression (rejecting) was also measured in skin by LDA (75.00%, Table 6.43), feature selected LDA (82.65%, Table 6.44), MANOVA LDA (78.85%, Table 6.45), and feature selected QDA (84.62%, Table 6.46). Performance in muscle with LDA (72.55%, Table 6.91), feature selected LDA (82.35%, Table 6.92), MANOVA LDA (62.75%, Table 6.93), and feature selected QDA (84.31%, Table 6.94) were also measured.

Enhanced Performance for Identification of Allograft vs Isograft

When analyzing all time points in skin, in the original feature space the logistic classifier is able to separate allograft from isograft groups with good performance (83.97% accuracy) and significance (Table 4.31) with an AUROC of .915 (Figure 6.17), but some bias towards misclassification of isografts as allografts is evident. The addition of feature interaction variables slightly improves AUROC to .919 (Figure 6.22). In the decision tree classifier (Figure 6.2) the inverse bias is seen although the stable accuracy increases to 91.03% (Table 4.32, Figure 6.3) with AUROC of .956 (Figure 6.18). Feature interaction variables do not improve the decision tree AUROC (.953, Figure 6.23). Superior performance (95.55% accuracy) and significance is achieved with the random forest classifier grown to 50 trees (Table 4.33, Figure 6.4) with AUROC of .989 (Figure 6.19). The accuracy increases further to 96.15% if the extended feature interaction variables are added (Table 4.34, Figure 4.29) and AUROC reaches .995 (Figure 4.30).

CTA Allograft vs Isograft in Skin Logistic Classifier (all time points)

Accuracy	**Confusion Matrix**			
83.97%	*Classified As*			
p-value	Allograft	Isograft		
.0175	60	17	Allograft	*True Class*
	8	71	Isograft	

Table 4.31

Feature selected (80.77%,Table 6.9), MANOVA transformed (83.33%,Table 6.10), Hybrid features (82.69%,Table 6.11)

CTA Allograft vs Isograft in Skin Decision Tree (all time points, pruned tree)

Accuracy	**Confusion Matrix**			
91.03%	*Classified As*			
p-value	Allograft	Isograft		
.0069	72	5	Allograft	*True Class*
	13	66	Isograft	

Table 4.32

Feature selected (91.67%,Table 6.12), MANOVA transformed (91.67%,Table 6.13), Hybrid features (89.10%,Table 6.14)

CTA Allograft vs Isograft in Skin Random Forest (all time points, 50 trees)

Accuracy	**Confusion Matrix**			
95.55%	*Classified As*			
p-value	Allograft	Isograft		
.0005	74	3	Allograft	*True Class*
	2	77	Isograft	

Table 4.33

Feature selected (95.55%,Table 6.15), MANOVA transformed (92.31%,Table 6.16)

CTA Allograft vs Isograft in Skin Random Forest (all time points, hybrid features, 50 trees)

Accuracy	**Confusion Matrix**			
96.15%	*Classified As*			
p-value	Allograft	Isograft		
.0002	74	3	Allograft	*True Class*
	3	76	Isograft	

Table 4.34

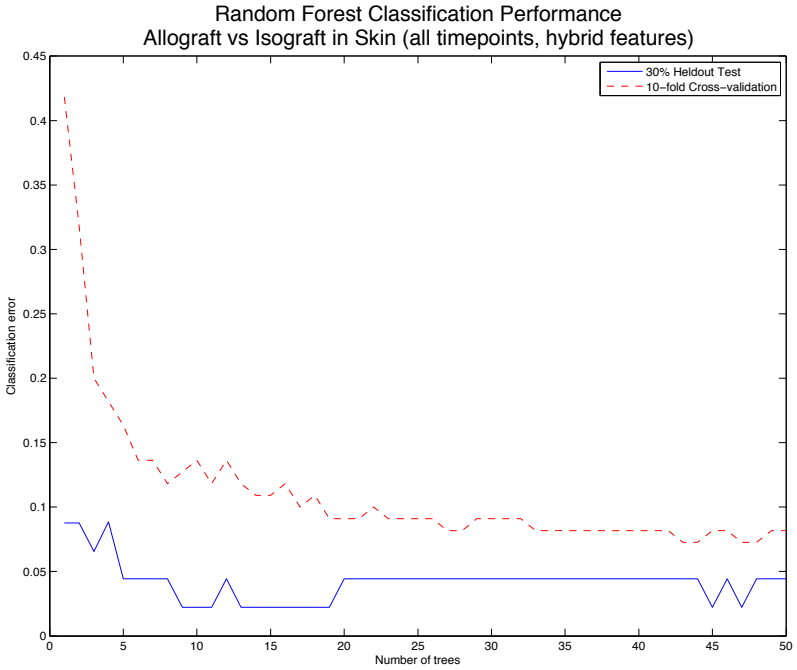

Figure 4.29

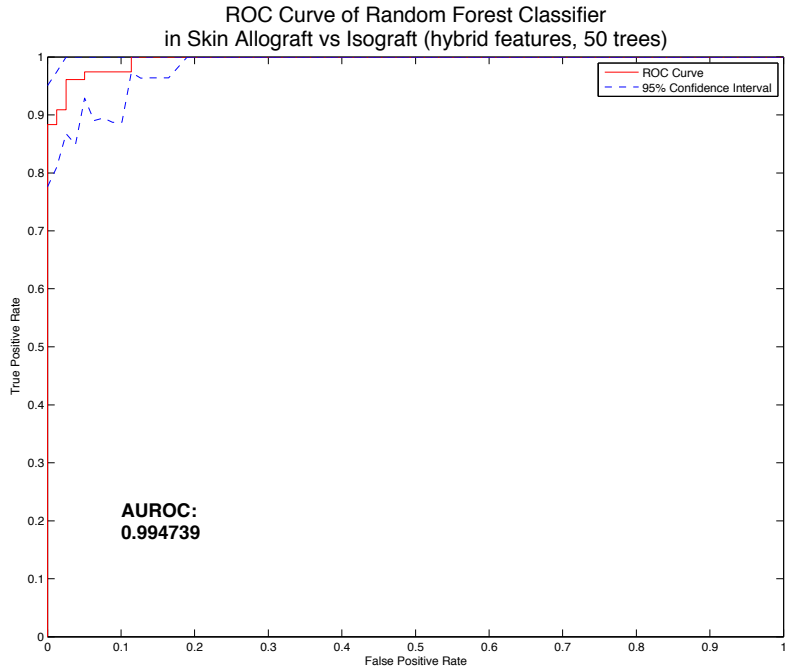

Figure 4.30

Parallel plot (Figure 6.24) and MANOVA transformation (Figure 6.25) show distinction between allograft and Isograft groups in skin at or prior to POD 5, driven primarily by IL-12p70 (Figure 6.26).

In skin, at or prior to POD 5 logistic classification separates allograft from Isograft groups with 83.52% accuracy with statistical significance and little bias (Table 6.21). MANOVA transformation does not significantly alter these results

(Table 6.23), while feature selection (Table 6.22) reduces accuracy to 76.92% and introduces some bias towards misclassifying allograft as Isograft.

The decision tree classifier (Figure 6.27) improves accuracy to 82.42%, but without statistical significance and introduces bias towards misclassifying Isograft as allograft (Table 6.24, Figure 6.28), which are problems also seen with performance on feature selected data (81.32% accuracy, Table 6.25, Figure 6.30, Figure 6.31). Performance on MANOVA transformed data is much better at 84.62% accuracy with statistical significance and less bias (Table 6.26, Figure 6.33, Figure 6.34).

Better performance (93.41% accuracy) and significance is seen in random forest classifier grown to 50 trees (Table 6.27, Figure 6.29), which is effectively the same performance seen with random forest on MANOVA transformed data (Table 6.29, Figure 6.35). Accuracy on feature-selected data is 91.21% with significance (Table 6.28, Figure 6.32).

Distinction between allograft and Isograft groups after POD 5 in skin is also evident in the parallel plot (Figure 6.36) and MANOVA transformation (Figure 6.37), driven primarily by IFN-g, IL-4, and TNF-a, as well as a second level of influence by IL-12p70, IL-5, GM-CSF, and MCP-1 (Figure 6.38).

After POD 5 in skin, logistic classification separates allograft from Isograft groups with 92.31% accuracy with statistical significance and little bias (Table 6.34). MANOVA transformation reduces accuracy and significance slightly (Table 6.36), while feature selection (Table 6.35) increases accuracy to 93.85% but reduces significance and introduces some bias towards misclassifying allograft as Isograft.

The decision tree classifier (Figure 6.39) reaches 96.92% accuracy with statistical significance (Table 6.37, Figure 6.40), while on feature selected data it achieves perfect accuracy (Table 6.38, Figure 6.42, Figure 6.43). Performance on MANOVA transformed data is 96.92% accuracy with statistical significance (Table 6.39, Figure 6.45, Figure 6.46).

Better performance (96.92% accuracy) is seen in random forest classifier grown to 50 trees (Table 6.40,Figure 6.41), which is effectively the same performance seen with random forest on MANOVA transformed data (Table 6.42, Figure 6.47). Nearly perfect accuracy on feature-selected data with significance is also achieved (Table 6.41, Figure 6.44).

In muscle analysis including all time points, logistic classification separates allograft from isograft groups with an AUROC of .792 (Figure 6.64), 75.81% accuracy, low significance, and evident bias towards classification of isografts as allografts (Table 4.35). With feature interaction variables the AUROC of logistic regression increases to .801 (Figure 6.69). The decision tree classifier (Figure 6.49, Figure 6.50) reaches an AUROC of .896 (Figure 6.65), improves accuracy to 83.87%, reduces the bias and improves significance (Table 4.36, Figure 6.51). With feature interaction variable, decision tree AUROC decreases to .893 (Figure 6.70). Better performance (95.97% accuracy) and significance is seen in random forest classifier grown to 50 trees (Table 4.37) with an AUROC of .987 (Figure 6.66), and the best performance (95.16% accuracy with improved significance) is seen when the extended feature interaction variables are added to the data matrix (Table 4.38, Figure 4.31) with AUROC of .9895 (Figure 4.32).

CTA Allograft vs Isograft in Muscle Logistic Classifier (all time points)

Accuracy	**Confusion Matrix**			
75.81%	*Classified As*			
p-value	Allograft	Isograft		
.2306	30	23	Allograft	*True Class*
	7	64	Isograft	

Table 4.35

Feature selected (75.81%,Table 6.57), MANOVA transformed (78.23%,Table 6.58), Hybrid features (78.23%,Table 6.59)

CTA Allograft vs Isograft in Muscle Decision Tree (all time points, pruned tree)

Accuracy	**Confusion Matrix**			
83.87%	*Classified As*			
p-value	Allograft	Isograft		
.0733	39	14	Allograft	*True Class*
	11	60	Isograft	

Table 4.36

Feature selected (80.65%,Table 6.60), MANOVA transformed (82.26%,Table 6.61), Hybrid features (84.68%,Table 6.62)

CTA Allograft vs Isograft in Muscle Random Forest (all time points, 50 trees)

Accuracy	**Confusion Matrix**			
95.97%	*Classified As*			
p-value	Allograft	Isograft		
.0403	47	6	Allograft	*True Class*
	2	69	Isograft	

Table 4.37

Feature selected (91.94%,Table 6.63), MANOVA transformed (87.10%,Table 6.64)

CTA Allograft vs Isograft in Muscle Random Forest (all time points, hybrid features, 50 trees)

Accuracy	**Confusion Matrix**			
95.16%	*Classified As*			
p-value	Allograft	Isograft		
.0352	48	5	Allograft	*True Class*
	2	69	Isograft	

Table 4.38

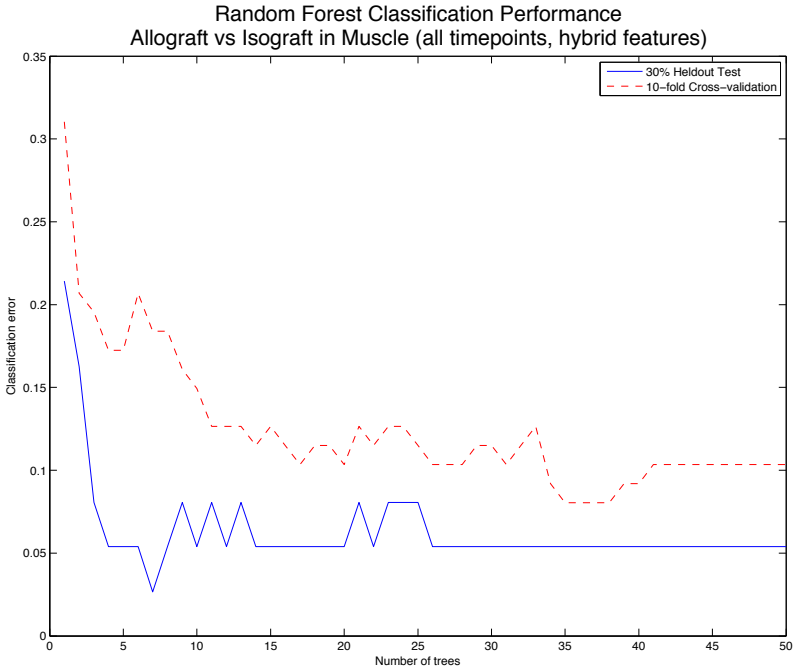

Figure 4.31

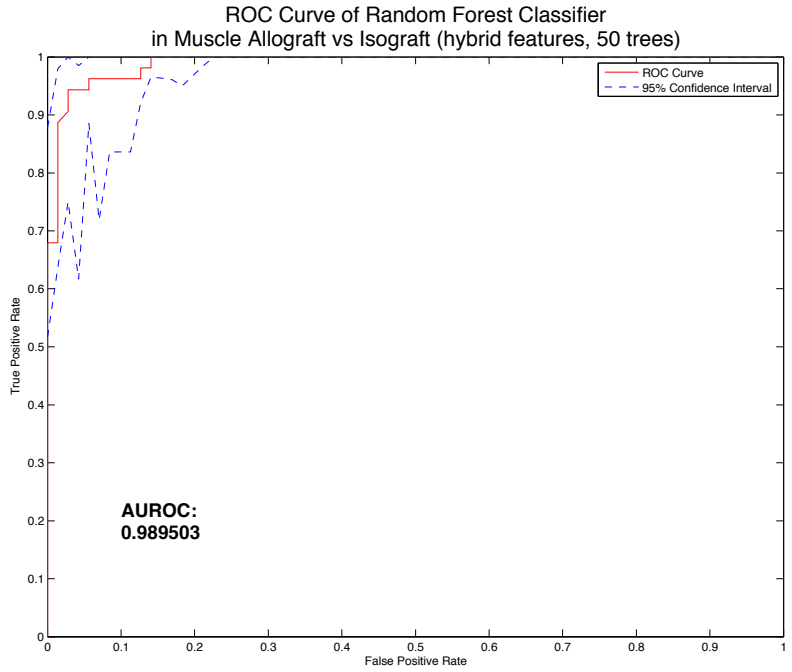

Figure 4.32

At or prior to POD 5 in muscle, the parallel plot (Figure 6.71) and MANOVA transformation (Figure 6.72) show distinction between allograft and isograft, driven primarily by IL-12p70, IL-5, and GM-CSF (Figure 6.73).

At POD 5 or earlier in muscle, logistic classification separates allograft from Isograft groups with 77.63% but without statistical significance (Table 6.69). MANOVA transformation increases accuracy to 81.58% with significance (Table

6.71), while feature selection (Table 6.70) reduces accuracy to 60.53% and also reduces significance.

The decision tree classifier (Figure 6.74) reaches 85.53% accuracy with strong significance (Table 6.72, Figure 6.75), while on feature selected data it achieves 77.63% accuracy with strong significance (Table 6.73, Figure 6.77, Figure 6.78). Performance on MANOVA transformed data is 82.90% accuracy again with statistical significance (Table 6.74, Figure 6.80, Figure 6.81).

Better performance (98.68% accuracy) is seen in random forest classifier grown to 50 trees (Table 6.75, Figure 6.76), on MANOVA transformed data the accuracy was 84.21% (Table 6.77, Figure 6.82), while with feature-selected data accuracy reached 94.74% (Table 6.76, Figure 6.79), all with significance.

After POD 5 in muscle, the parallel plot (Figure 6.83) and MANOVA transformation (Figure 6.84) show distinction between allograft and isograft, driven primarily by TNFa and IL-5 (Figure 6.85).

In muscle after POD 5, logistic classification separates allograft from Isograft groups with 91.67% but without statistical significance (Table 6.82). MANOVA transformation increases accuracy to 95.83% although still without significance (Table 6.84), while feature selection (Table 6.83) further increases accuracy to 97.92%, also without significance.

The decision tree classifier (Figure 6.86) reaches 95.83% accuracy but without significance (Table 6.85, Figure 6.87), while on feature selected data it achieves 93.75% again without significance (Table 6.86, Figure 6.89, Figure 6.90), and on MANOVA transformed data performance is 93.75% accuracy but again with no statistical significance (Table 6.87, Figure 6.92, Figure 6.93).

Better performance (97.92% accuracy) is seen in random forest classifier grown to 50 trees (Table 6.88, Figure 6.88), on MANOVA transformed data the accuracy was 93.75% (Table 6.90, Figure 6.94), while with feature-selected data accuracy reached 95.83% (Table 6.89, Figure 6.91), all nearly significant but with definitive confusion matrices.

In allograft skin, when separating tissue that is under immunosuppression from tissue that has been withdrawn from immunosuppression and is rejecting, logistic classifier performance is 88.46% accurate and stable (Table 4.36). The decision tree (Figure 6.96) is also 88.46% accurate, although slightly more biased towards misclassifying rejecting samples and suppressed (Table 4.37, Figure 6.97). The random forest classifier grown to 50 trees achieves the best stable performance at 92.31% accuracy (Table 4.38, Figure 4.33).

CTA Rejecting vs Suppressed in Skin Logistic Classifier (FK Groups)

Accuracy	**Confusion Matrix**			
88.46%	*Classified As*			
p-value	Rejecting	Suppressed		
<.0001	23	3	Rejecting	*True Class*
	3	23	Suppressed	

Table 4.39

Feature selected (88.46%,Table 6.47), MANOVA transformed (80.77%,Table 6.48)

CTA Rejecting vs Suppressed in Skin Decision Tree (FK Groups, pruned tree)

Accuracy	**Confusion Matrix**			
88.46%	*Classified As*			
p-value	Rejecting	Suppressed		
.0101	25	1	Rejecting	*True Class*
	4	22	Suppressed	

Table 4.40

Feature selected (84.62%,Table 6.49), MANOVA transformed (94.23%,Table 6.50)

CTA Rejecting vs Suppressed in Skin Random Forest (FK Groups, 50 trees)

Accuracy	**Confusion Matrix**			
92.31%	*Classified As*			
p-value	Rejecting	Suppressed		
.0041	25	1	Rejecting	*True Class*
	3	23	Suppressed	

Table 4.41

Feature selected (84.62%,Table 6.51), MANOVA transformed (90.38%,Table 6.52)

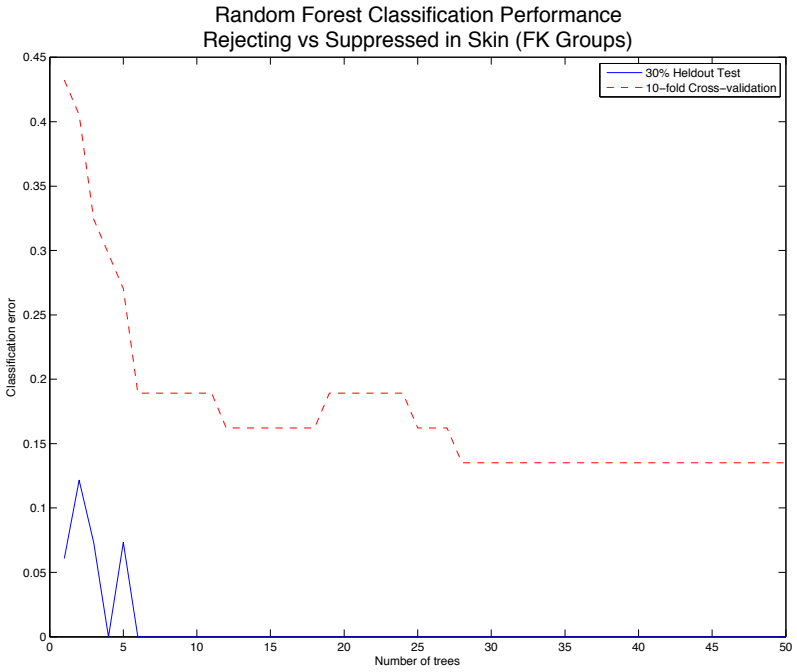

Figure 4.33

In allograft muscle, when separating tissue that is under immunosuppression from tissue that has been withdrawn from immunosuppression and is rejecting, the logistic classifier is 78.43% accurate (Table 4.42). Decision tree classifier (Figure 4.34) performance is the most stable and at 96.08%, the most accurate (Table 4.43,

Figure 4.35). Random forest grown to 50 trees reaches 86.27% accuracy (Table 4.44, Figure 6.105).

CTA Rejecting vs Suppressed in Muscle Logistic Classifier (FK Groups)

Accuracy	**Confusion Matrix**			
78.43%	*Classified As*			
p-value	Rejecting	Suppressed		
.0151	7	19	Rejecting	*True Class*
	21	4	Suppressed	

Table 4.42

Feature selected (70.59%,Table 6.95), MANOVA transformed (74.51%,Table 6.96)

CTA Rejecting vs Suppressed in Muscle Decision Tree (FK Groups, pruned tree)

Accuracy	**Confusion Matrix**			
96.08%	*Classified As*			
p-value	Rejecting	Suppressed		
.0006	23	3	Rejecting	*True Class*
	2	23	Suppressed	

Table 4.43

Feature selected (74.51%,Table 6.97), MANOVA transformed (94.12%,Table 6.98)

CTA Rejecting vs Suppressed in Muscle Random Forest (FK Groups, 50 trees)

Accuracy	**Confusion Matrix**			
86.27%	*Classified As*			
p-value	Rejecting	Suppressed		
.0008	22	4	Rejecting	*True Class*
	4	21	Suppressed	

Table 4.44

Feature selected (72.55%,Table 6.99), MANOVA transformed (88.24%,Table 6.100)

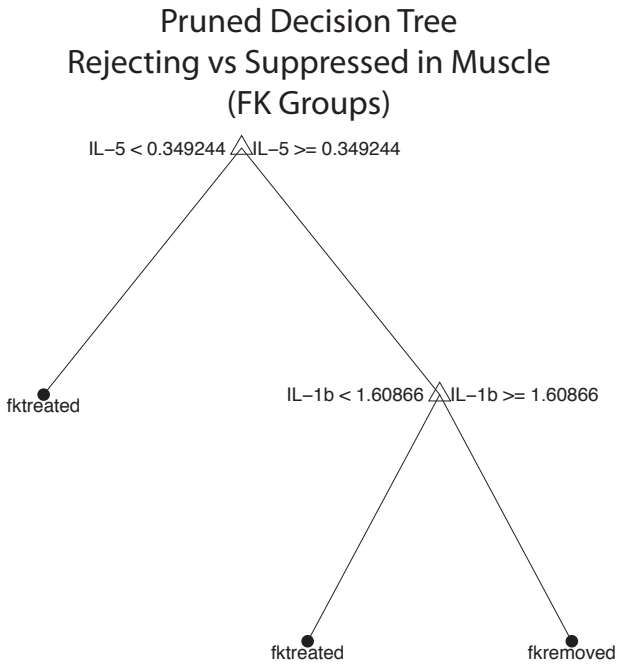

Figure 4.34

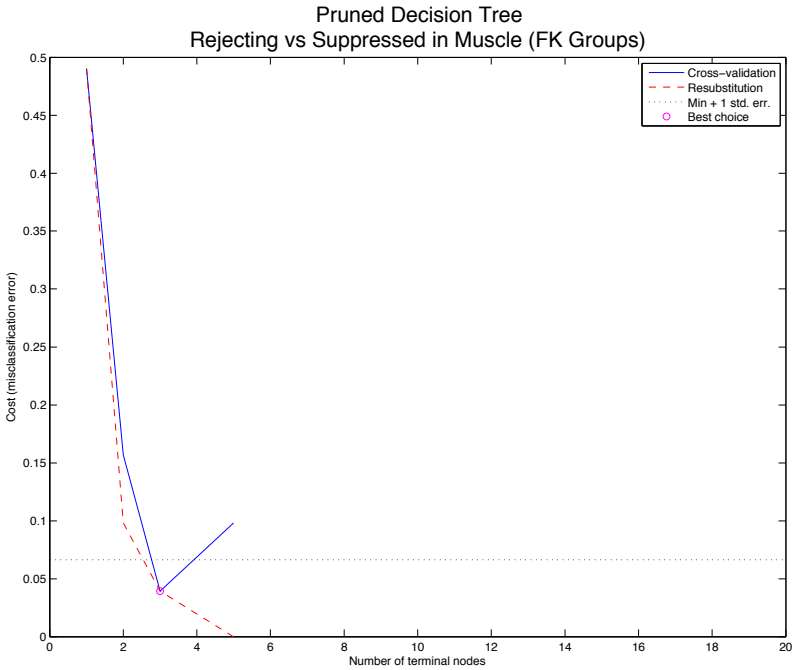

Figure 4.35

Identifying Specific Forms of Inflammation in a Heterogeneous Set

Differences in concentration of IL-1a, MCP-1, IL-6, IL-10, IL-18, and GRO/KC are evident from the parallel plot of inflammation associated with rejection versus inflammation not associated with rejection in skin (Figure 4.36), and MCP-1, IL-1b, IL-6, IL-10IL-18, and GRO/KC in muscle (Figure 4.38).

When transformed by MANOVA and the samples plotted on the axis defined by the first and second canonical variable of the MANOVA transformation, the degree of separation between groups with rejection associated inflammation from those with inflammation not rejection associated becomes clearer in skin (Figure 4.37) driven primarily by IL12-p70, IL-5, and TNFa (Figure 6.151), and in muscle (Figure 4.39) driven primarily by IL-12p70, IL-5, GM-CSF, TNFa, and IFNg (Figure 6.199).

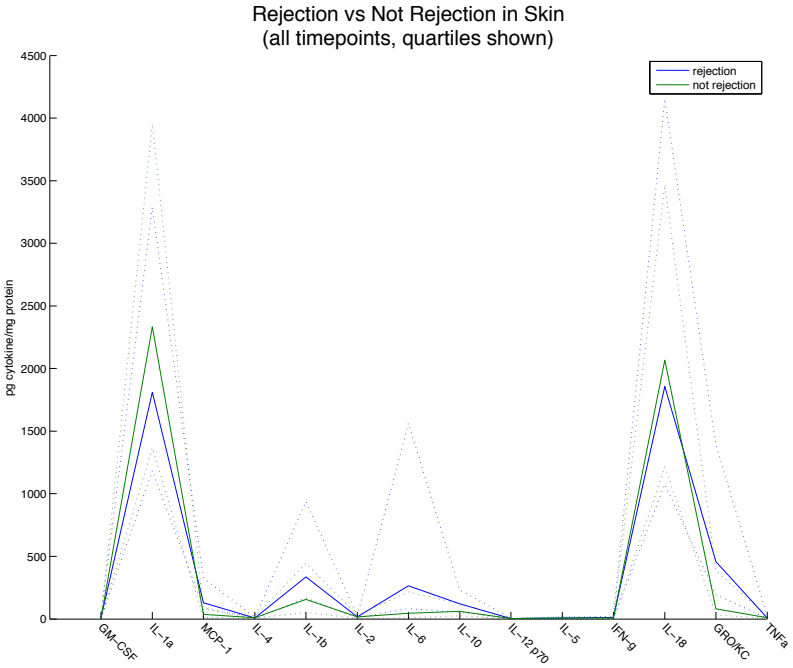

Figure 4.36

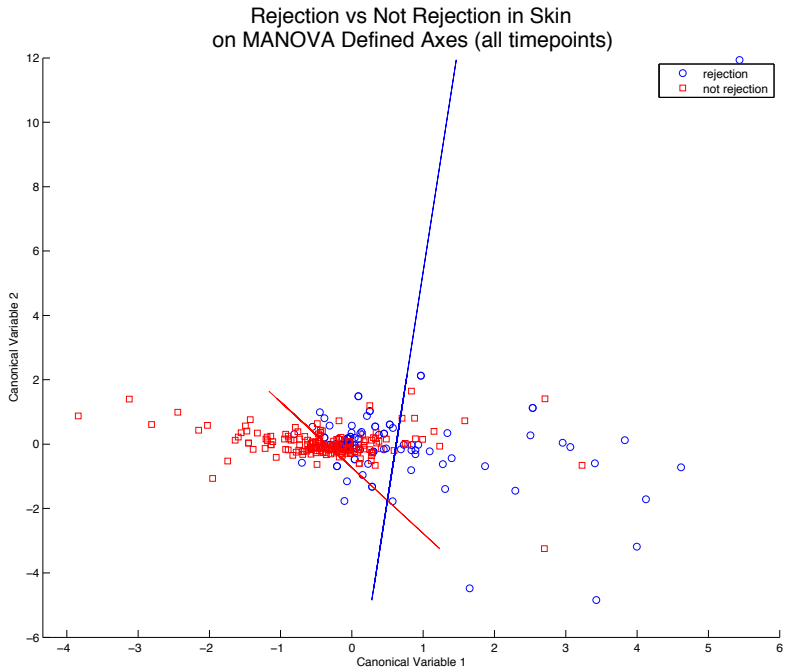

Figure 4.37

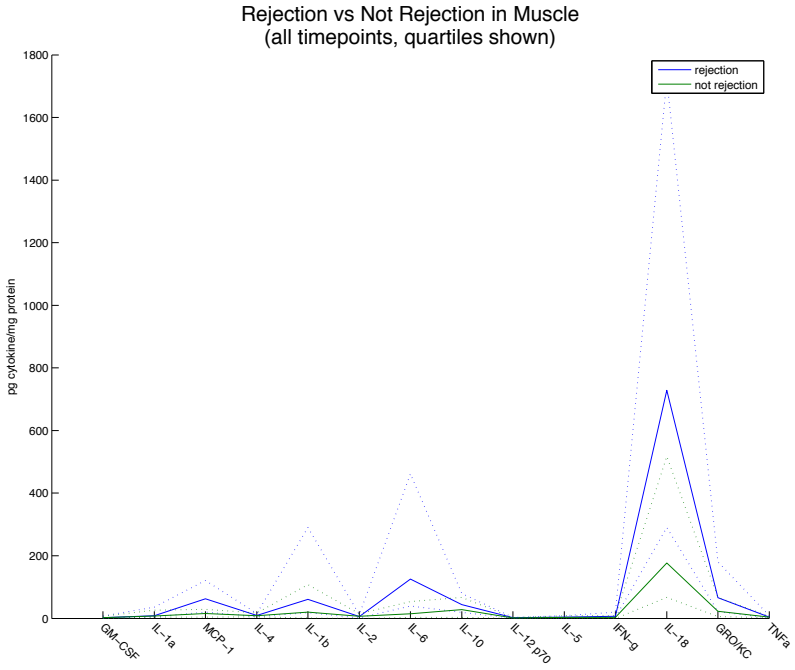

Figure 4.38

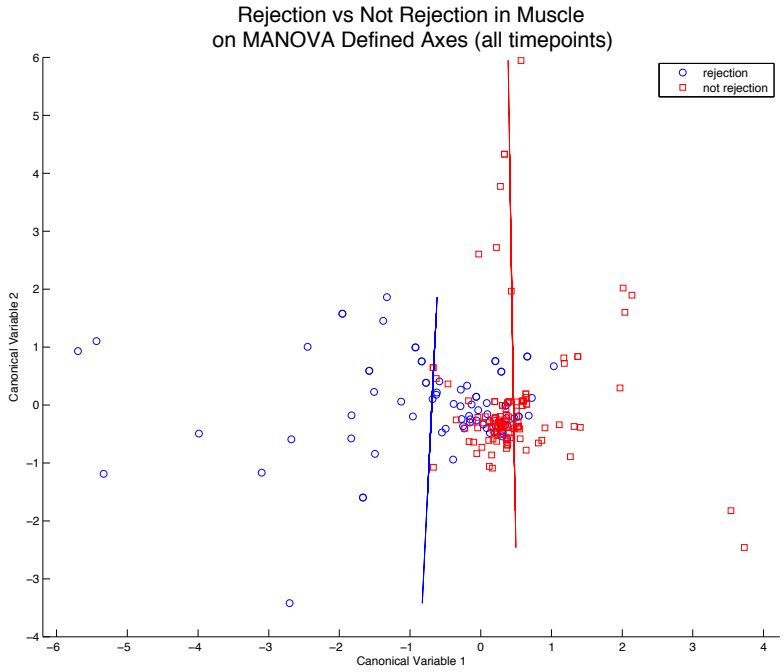

Figure 4.39

Baseline Performance for Detection of Rejection Associated Inflammation

In a heterogeneous set of inflammation samples, those with rejection-associated inflammation are separated from those with inflammation that is not associated with rejection.

Random classification was able to select the correct class slightly less than half the time in both skin and muscle with very little bias (Table 4.45, Table 4.46). When considering samples from all time points, LDA classification performed at about 68.09% accuracy without significance in skin (Table 4.47) with an AUROC score of .257 (Figure 6.165), and in muscle accuracy was 70.56% (Table 4.49) with an AUROC score of .275 (Figure 6.214). QDA classification achieved about 77.66% accuracy in skin with no significance (Table 4.48) with an AUROC score of .123 (Figure 6.166), and about 72.59% accuracy in muscle without significance (Table 4.50) with AUROC of .185 (Figure 6.215).

Adding feature interaction variables to the data improved the AUROC score of LDA in skin to .265 (Figure 6.170), and QDA in skin to .139 (Figure 6.171). Similar improvements were seen in muscle with the AUROC score of LDA in muscle increasing to .213 (Figure 6.219), and to .202 with QDA in muscle (Figure 6.220).

Rejection vs Not Rejection in Skin Random Classification (all time points)

Accuracy	**Confusion Matrix**			
45.74%	*Classified As*			
p-value	Not Rejection	Rejection		
1.000	88	91	Not Rejection	*True Class*
	50	53	Rejection	

Table 4.45 Baseline: Random classifier performance in rejecting vs not rejecting skin

Rejection vs Not Rejection in Muscle Random Classification (all time points)

Accuracy	**Confusion Matrix**			
44.67%	*Classified As*			
p-value	Not Rejection	Rejection		
.8748	56	62	Not Rejection	*True Class*
	39	40	Rejection	

Table 4.46 Baseline: Random classifier performance in rejecting vs not rejecting muscle

Rejection vs Not Rejection in Skin Linear Discriminant (all time points)

Accuracy	**Confusion Matrix**			
68.09%	*Classified As*			
p-value	Not Rejection	Rejection		
.3887	142	37	Not Rejection	*True Class*
	53	50	Rejection	

Table 4.47

Feature selected (64.89%,Table 6.127), MANOVA transformed (68.09%,Table 6.128)

Rejection vs Not Rejection in Skin Quadratic Discriminant (all time points)

Accuracy	**Confusion Matrix**

77.66%	*Classified As*			
p-value	Not Rejection	Rejection		
.3651	172	7	Not Rejection	*True Class*
	56	47	Rejection	

Table 4.48

Feature selected (71.28%,Table 6.129), MANOVA transformed (76.60%,Table 6.130)

Rejection vs Not Rejection in Muscle Linear Discriminant (all time points)

Accuracy	**Confusion Matrix**			
70.56%	*Classified As*			
p-value	Not Rejection	Rejection		
.3668	102	16	Not Rejection	*True Class*
	42	37	Rejection	

Table 4.49

Feature selected (67.51%,Table 6.211), MANOVA transformed (73.10%,Table 6.212)

Rejection vs Not Rejection in Muscle Quadratic Discriminant (all time points)

Accuracy	**Confusion Matrix**			
72.59%	*Classified As*			
p-value	Not Rejection	Rejection		
.3315	104	14	Not Rejection	*True Class*
	40	39	Rejection	

Table 4.50

Feature selected (71.28%,Table 6.129), MANOVA transformed (76.60%,Table 6.130)

In addition to analysis at all time points, baseline performance was measured at or prior to POD 5 in skin with LDA (72.25%,Table 6.139), feature selected LDA (66.47%,Table 6.140), MANOVA LDA (71.01%,Table 6.141), QDA (75.14%,Table 6.142), feature selected QDA (66.47%,Table 6.143), and MANOVA QDA (74.57%,Table 6.144), as well as in muscle with LDA (74.29%,Table 6.221), feature selected LDA (67.62%,Table 6.222), and MANOVA LDA (74.29%,Table 6.223).

After POD 5 baseline performance in skin was measured by LDA (80.00%, Table 6.154), feature selected LDA (67.88%,Table 6.155), MANOVA LDA (76.36%,Table 6.156), QDA (83.64%,Table 6.157), feature selected QDA (77.58%,Table 6.158), and MANOVA QDA (84.24%, Table 6.159), as well as in muscle by LDA (77.19%,Table 6.233), feature selected LDA (69.30%,Table 6.234), and MANOVA LDA (80.70%,Table 6.235). The original feature space once more yields the best results in this experiment, while MANOVA provides nearly equivalent results to the original feature space, and the feature-selected space performs least well. Baseline performance indicates differentiation amongst groups at an early time point remains more challenging than differentiation at a late time point.

Enhanced Performance in Detection of Rejection Associated Inflammation

When analyzing samples at all time points in skin, the logistic regression classifier achieves 70.57% accuracy while evincing bias and lack of significance (Table 4.51) with an AUROC of .775 (Figure 6.167). Adding feature interaction variables to the data improved the AUROC score of the logistic classifier to .877 (Figure 6.268). The decision tree (Figure 6.152) yields an AUROC score of .893 (Figure 6.168), improves accuracy to 87.59%, ameliorates bias, and improves significance (Table 4.52, Figure 6.153) but not to significant levels. Adding feature interaction variables changed the AUROC score of the decision tree to .885 (Figure 6.269). Random forest grown to 100 trees reaches an AUROC of .970 (Figure 6.174), 93.62% accuracy with significance and little bias (Table 4.53, Figure 6.154). When feature interaction variables were included Random Forest AUROC increased to .977 (Figure 4.41), accuracy slightly changes to 92.55% accuracy but with no substantial change in significance although cross validation results indicate slightly improved performance (Table 4.54, Figure 4.40).

Rejection vs Not Rejection in Skin Logistic Classifier (all time points)

Accuracy	**Confusion Matrix**			
70.57%	*Classified As*			
p-value	Not Rejection	Rejection		
.4637	19	160	Not Rejection	*True Class*
	39	64	Rejection	

Table 4.51

Feature selected (68.09%,Table 6.131), MANOVA transformed (72.70%,Table 6.132), Hybrid features (76.95%,Table 6.133)

Rejection vs Not Rejection in Skin Decision Tree (all time points, pruned tree)

Accuracy	**Confusion Matrix**			
87.59%	*Classified As*			
p-value	Not Rejection	Rejection		
.1122	158	21	Not Rejection	*True Class*
	19	84	Rejection	

Table 4.52

Feature selected (79.08%,Table 6.134), MANOVA transformed (81.56%,Table 6.135), Hybrid features (87.59%,Table 6.136)

Rejection vs Not Rejection in Skin Random Forest (all time points, 100 trees)

Accuracy	**Confusion Matrix**			
93.62%	*Classified As*			
p-value	Not Rejection	Rejection		
.0829	169	10	Not Rejection	*True Class*
	9	94	Rejection	

Table 4.53

Feature selected (84.04%,Table 6.137), MANOVA transformed (87.23%,Table 6.138)

Rejection vs Not Rejection in Skin Random Forest (all time points, hybrid features, 100 trees)

Accuracy	**Confusion Matrix**			
92.55%	*Classified As*			
p-value	Not Rejection	Rejection		
.0852	172	7	Not Rejection	*True Class*
	9	94	Rejection	

Table 4.54

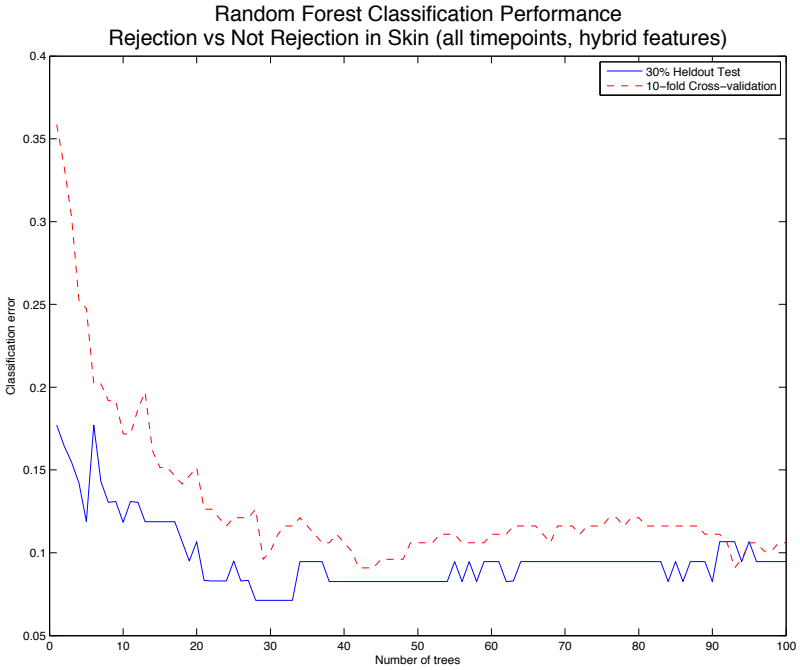

Figure 4.40

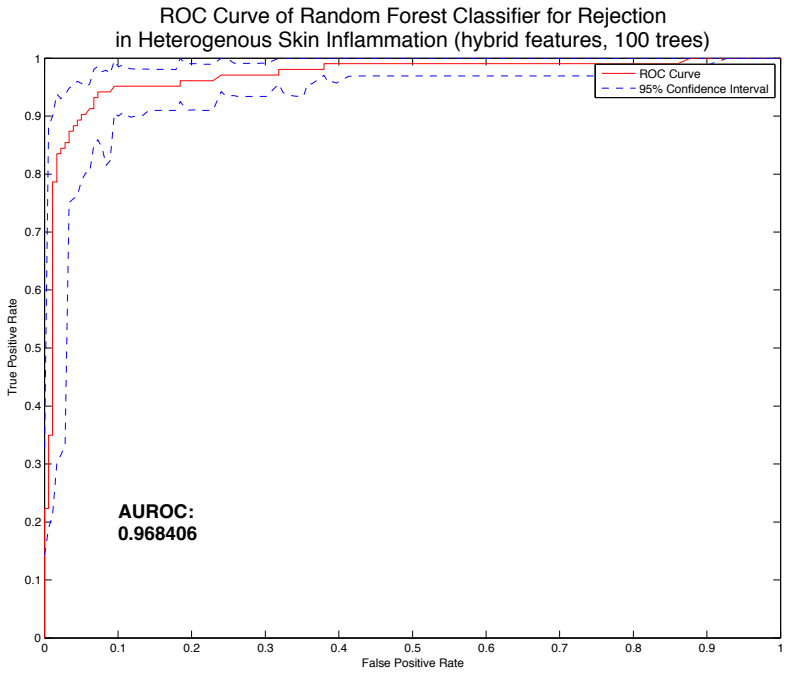

Figure 4.41

At or prior to POD 5 in skin, the parallel plot (Figure 6.175) and MANOVA transformation (Figure 6.176) show distinction between rejection and not rejection associated inflammation, driven primarily by TNFa, IL-4, IL-12p70, GM-CSF, and IL-5 (Figure 6.177).

In skin at or prior to POD 5, logistic classification separates rejection from not rejection associated inflammation with 74.57% but without statistical significance (Table 6.145). MANOVA transformation enables 72.83% accuracy still without significance (Table 6.147), while feature selection (Table 6.146) allows accuracy of 68.21%, also without significance.

The decision tree classifier (Figure 6.178) reaches 80.92% accuracy but without significance (Table 6.148, Figure 6.179), on feature selected data it achieves 78.61% again without significance (Table 6.149, Figure 6.181, Figure 6.182), and on MANOVA transformed data performance is 87.86% accuracy but again with no statistical significance (Table 6.150, Figure 6.184, Figure 6.185).

Random forest grown to 100 trees reaches 95.95% accuracy (Table 6.151, Figure 6.180), on MANOVA transformed data the accuracy was 91.33% (Table 6.153, Figure 6.186), both are near significance but with definitive confusion matrices. Feature-selected data accuracy reached 84.39% (Table 6.152, Figure 6.183), without significance.

After POD 5 in skin, the parallel plot (Figure 6.187) and MANOVA transformation (Figure 6.188) show distinction between rejection and not rejection associated inflammation, driven primarily by IL-12p70 (Figure 6.189).

In skin after POD 5, logistic classification separates rejection from not rejection associated inflammation with 76.97% but without statistical significance (Table 6.160). MANOVA transformation enables 80.00% accuracy still without

significance (Table 6.162), while feature selection (Table 6.161) allows accuracy of 72.12%, also without significance.

The decision tree classifier (Figure 6.190) reaches 88.48% accuracy but without significance (Table 6.163, Figure 6.191), on feature selected data it achieves 83.03% again without significance (Table 6.164, Figure 6.193, Figure 6.194), and on MANOVA transformed data performance is 86.06% accuracy but again with no statistical significance (Table 6.165, Figure 6.196, Figure 6.197).

Random forest grown to 100 trees reaches 93.94% accuracy (Table 6.166, Figure 6.192), and feature-selected data accuracy reached 90.91% (Table 6.167, Figure 6.195), both near significance but with definitive confusion matrices. On MANOVA transformed data the accuracy was 89.09% (Table 6.168, Figure 6.198), without significance.

Analyzing samples at all time points in muscle, logistic regression reaches AUROC of .777 (Figure 6.216), and 75.63% accuracy but again with bias and no significance (Table 4.55). With feature interaction variables logistic regression yields an AUROC of .816 (Figure 6.221). Decision tree (Figure 6.200) accuracy reaches 80.20%, but still shows bias and some insignificance (Table 4.56, Figure 6.201) and yields an AUROC of .845 (Figure 6.217). With feature interaction variables the AUROC is .827 (Figure 6.222). Random forest grown to 100 trees (Figure 6.202) achieves an AUROC of .944 (Figure 6.218) with 89.85% accuracy and significance, but still shows some signs of bias in classifying rejecting samples as not rejecting (Table 4.57). When feature interaction variables are included, Random Forest accuracy decreases to 86.55% while significance increases slightly (Table 4.58, Figure 4.42) and the AUROC changes to .955 (Figure 4.43).

Rejection vs Not Rejection in Muscle Logistic Classifier (all time points)

Accuracy	**Confusion Matrix**			
75.63%	*Classified As*			
p-value	Not Rejection	Rejection		
.2728	106	12	Not Rejection	*True Class*
	36	43	Rejection	

Table 4.55

Feature selected (74.11%,Table 6.213), MANOVA transformed (74.11%,Table 6.214), Hybrid features (77.16%,Table 6.215)

Rejection vs Not Rejection in Muscle Decision Tree (all time points, pruned tree)

Accuracy	**Confusion Matrix**			
80.20%	*Classified As*			
p-value	Not Rejection	Rejection		
.1937	100	18	Not Rejection	*True Class*
	30	49	Rejection	

Table 4.56

Feature selected (78.17%,Table 6.216), MANOVA transformed (73.60%,Table 6.217), Hybrid features (79.70%,Table 6.218)

Rejection vs Not Rejection in Muscle Random Forest (all time points, 100 trees)

Accuracy	Confusion Matrix			
89.85%	*Classified As*			
p-value	Not Rejection	Rejection		
.0844	114	4	Not Rejection	*True Class*
	14	65	Rejection	

Table 4.57

Feature selected (86.29%,Table 6.219), MANOVA transformed (88.32%,Table 6.220)

Rejection vs Not Rejection in Muscle Random Forest (all time points, hybrid features, 100 trees)

Accuracy	Confusion Matrix			
86.80%	*Classified As*			
p-value	Not Rejection	Rejection		
0.0779	110	8	Not Rejection	*True Class*
	14	65	Rejection	

Table 4.58

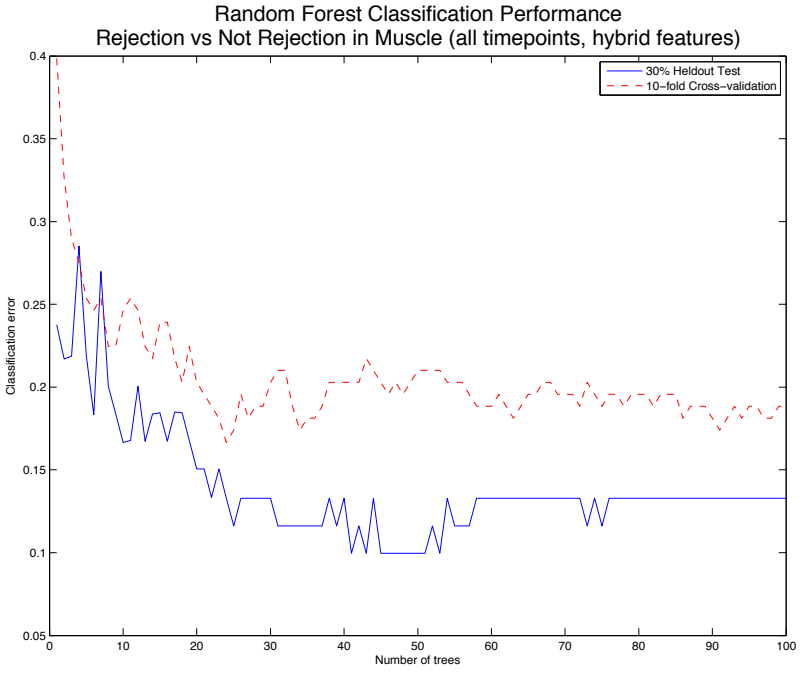

Figure 4.42

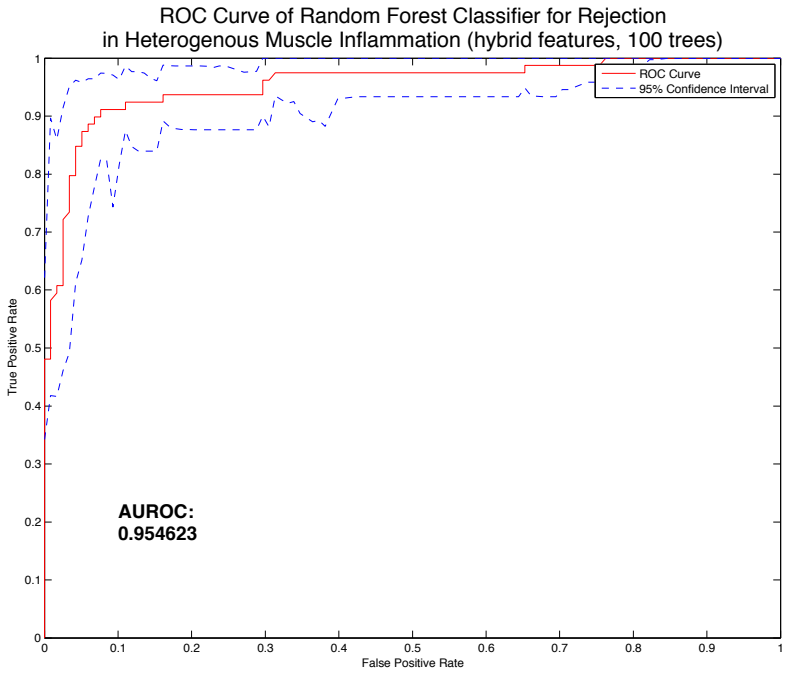

Figure 4.43

At or prior to POD 5 in muscle, the parallel plot (Figure 6.223) and MANOVA transformation (Figure 6.224) show distinction between rejection and not rejection associated inflammation, driven primarily by TNFa, IFN-g, IL-12p70, GM-CSF, and IL-5 (Figure 6.225).

In muscle at or prior to POD 5, logistic classification separates rejection from not rejection associated inflammation with 70.48% but without statistical significance (Table 6.224). MANOVA transformation enables 68.57% accuracy still without significance (Table 6.226), while feature selection (Table 6.225) allows accuracy of 73.33%, also without significance.

The decision tree classifier (Figure 6.226) reaches 81.90% accuracy near significance (Table 6.227, Figure 6.227), on feature selected data it achieves 73.33% again without significance (Table 6.228, Figure 6.229, Figure 6.230), and on MANOVA transformed data performance is also 73.33% accuracy but again with no statistical significance (Table 6.229, Figure 6.232, Figure 6.233).

Random forest grown to 100 trees reaches 88.57% accuracy (Table 6.230, Figure 6.228) just on the threshold of significance, while on MANOVA transformed data the accuracy was 86.67% (Table 6.232, Figure 6.234), near significance. Feature-selected data accuracy reached 83.81% (Table 6.231, Figure 6.231), without significance.

After POD 5 in muscle, the parallel plot (Figure 6.235) and MANOVA transformation (Figure 6.236) show distinction between rejection and not rejection associated inflammation, driven primarily by IL-TNFa, and IL-5 (Figure 6.237).

In muscle after POD 5, logistic classification separates rejection from not rejection associated inflammation with 87.72% near statistical significance (Table 6.236). MANOVA transformation enables 87.72% accuracy also near significance

(Table 6.238), while feature selection (Table 6.237) allows accuracy of 64.04%, without significance.

The decision tree classifier (Figure 6.238) reaches 82.46% near significance (Table 6.239, Figure 6.239), on feature selected data it achieves 85.96% without significance (Table 6.240, Figure 6.241, Figure 6.242), and on MANOVA transformed data performance is 83.33% accuracy but again with no statistical significance (Table 6.241, Figure 6.244, Figure 6.245).

Random forest grown to 100 trees reaches 88.60% accuracy (Table 6.242, Figure 6.240), and feature-selected data accuracy reached 85.96% (Table 6.243, Figure 6.243), both near significance but with strong confusion matrices. On MANOVA transformed data the accuracy was 88.60% (Table 6.244, Figure 6.246), near significance and also with a strong confusion matrix.

Baseline in Identification of Inflammation Type

Going one step beyond the ability to differentiate rejection from not rejection associated inflammation, the ability to separate and identify three different classes of inflammation is examined. In a heterogeneous set of inflammation samples with three group labels, the class label (inflammation type) of each sample is predicted.

Differences in concentration of IL-1a, MCP1, IL-1b, IL-6, IL-18, and GRO/KC are evident from the parallel plot of allograft versus isograft in skin (Figure 4.44), and MCP-1, IL-1b, IL-6, IL-18, and GRO/KC in muscle (Figure 4.46).

When transformed by MANOVA and plotted on the axis defined by the first and second canonical variable of the MANOVA transformation, the degree of separation between allograft and Isograft becomes clearer in skin (Figure 4.45) driven primarily by IL-5, TNFa, and IL-12p70 (Figure 6.248), as well as clearer in muscle (Figure 4.47) driven primarily by IL-5, TNFa, IL-12p70, GM-CSF and IFNg (Figure 6.304).

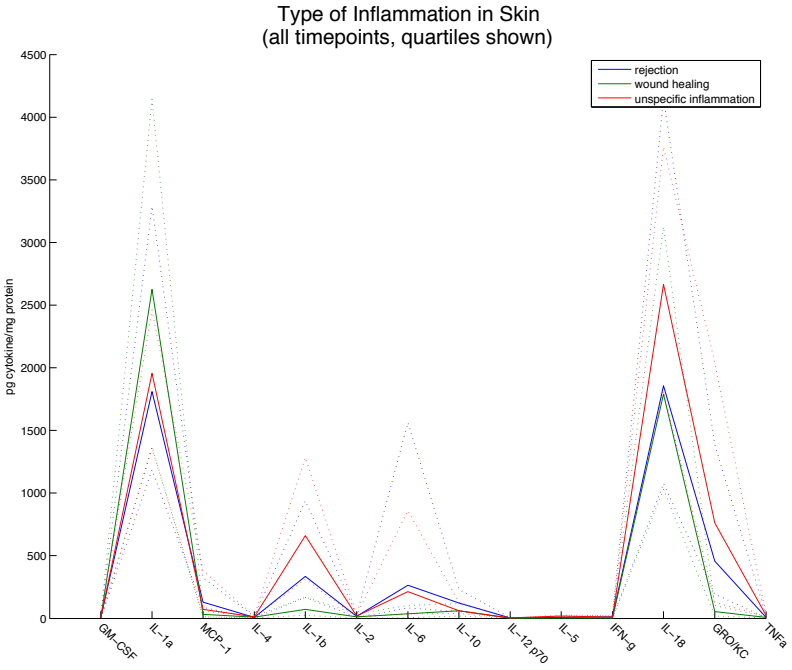

Figure 4.44

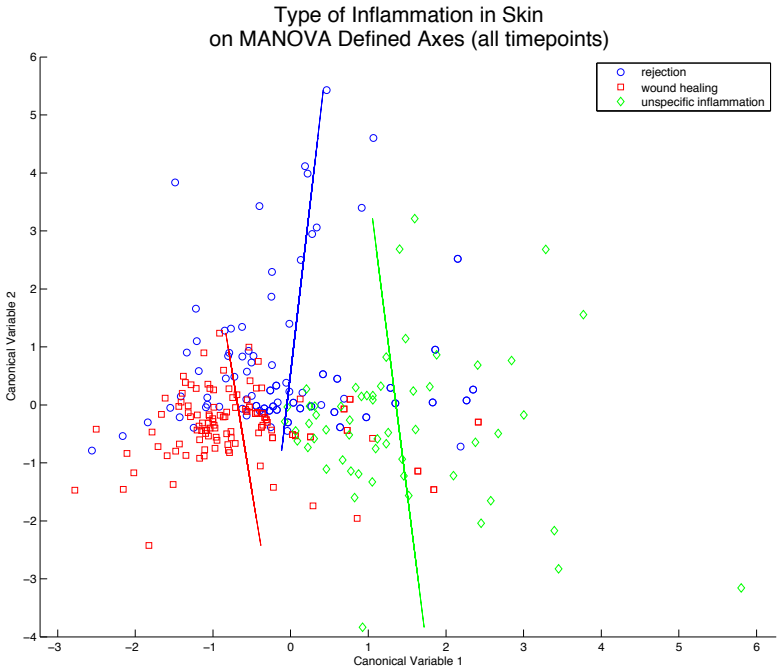

Figure 4.45

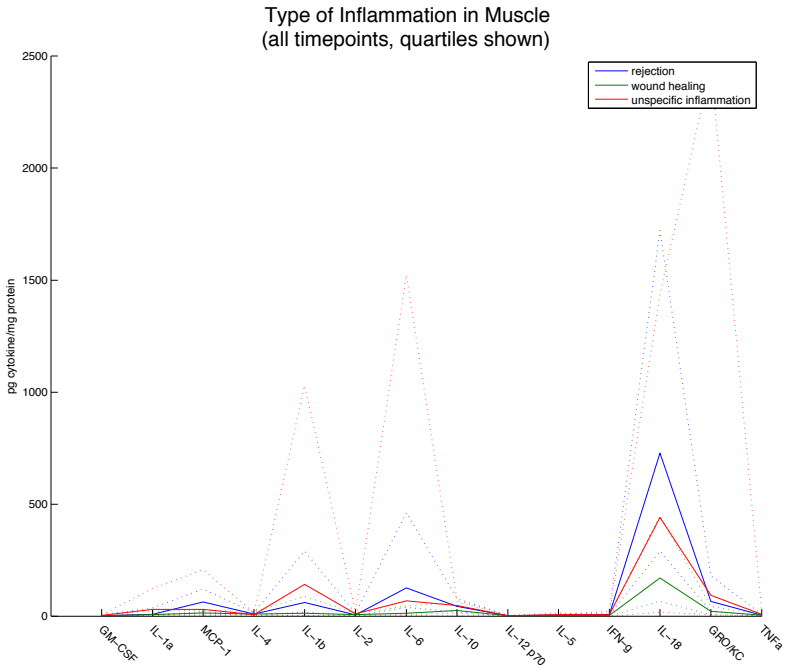

Figure 4.46

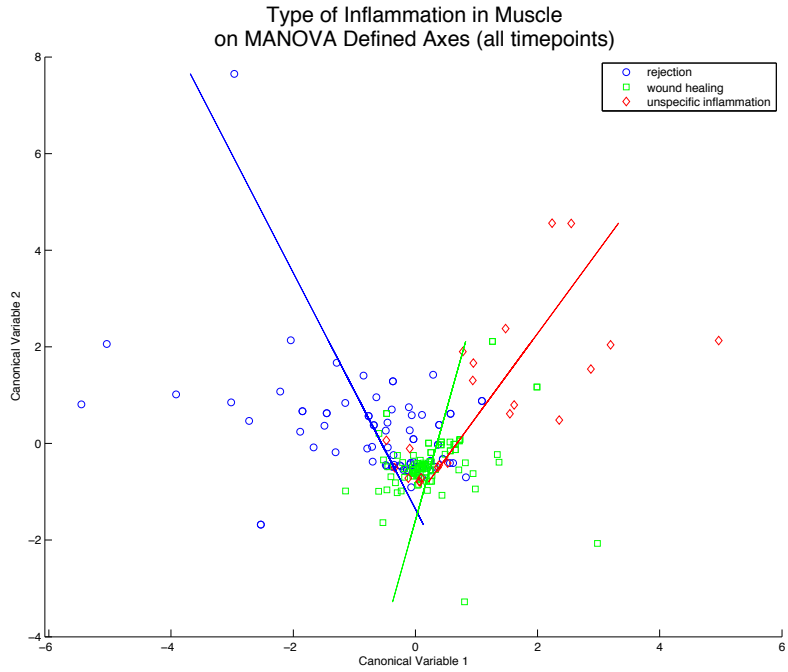

Figure 4.47

Random classification was able to identify the type of inflammation correctly 28.72% of the time in skin and 28.43% of the time in muscle with very little bias (Table 4.59, Table 4.62). The identification of rejection is isomorphic to the task of differentiating rejection from not rejection described in the previous section, and is therefore not repeated here.

When considering samples from all time points, LDA classification performed with 64.54% accuracy without significance in skin (Table 4.60). In skin LDA yielded

AUROC scores of .827 (Figure 6.261) in identifying wound healing, and .870 (Figure 6.270) in identifying unspecific inflammation in the original feature space, and yielded AUROC scores of .819 (Figure 6.266) in identifying wound healing, and .871(Figure 6.275) in identifying unspecific inflammation with feature interaction variables. In muscle LDA classification performed with 63.45% accuracy without significance (Table 4.63). In muscle LDA yielded AUROC scores of .675 (Figure 6.318) in identifying wound healing, and .633 (Figure 6.327) in identifying unspecific inflammation in the original feature space, and yielded AUROC scores of .723 (Figure 6.322) in identifying wound healing, and .682 (Figure 6.331) in identifying unspecific inflammation with feature interaction variables.

QDA classification performed with 64.54% accuracy without significance in skin (Table 4.61). In skin QDA yielded AUROC scores of .894 (Figure 6.262) in identifying wound healing and .792 (Figure 6.271) in identifying unspecific inflammation in the original feature space, while yielding AUROC scores of .891 (Figure 6.267) in identifying wound healing and .808 (Figure 6.276) in identifying unspecific inflammation with feature interaction variables. In muscle QDA classification performed with 63.45% accuracy without significance (Table 4.64). In muscle QDA yielded AUROC scores of .760 (Figure 6.319) in identifying wound healing, and .539 (Figure 6.323) in identifying unspecific inflammation in the original feature space, and yielded AUROC scores of .773 (Figure 6.328) in identifying wound healing, and .576 (Figure 6.332) in identifying unspecific inflammation with feature interaction variables.

Type of Inflammation in Skin Random Classification (all time points)

Accuracy	**Confusion Matrix**				
28.72%	*Classified As*				
p-value	Rejection	Unspecific Inflammation	Wound Healing		
.1407	31	38	34	Rejection	*True Class*
	19	22	15	Unspecific Inflammation	
	33	44	46	Wound Healing	

Table 4.59 Baseline: Random classifier performance for identifying type of inflammation in skin

Type of Inflammation in Skin Linear Discriminant (all time points)

Accuracy	**Confusion Matrix**				
64.54%	*Classified As*				
p-value	Rejection	Unspecific Inflammation	Wound Healing		
.2878	46	21	36	Rejection	*True Class*
	11	38	7	Unspecific Inflammation	
	12	13	98	Wound Healing	

Table 4.60

Feature selected (50.71%,Table 6.169), MANOVA transformed (64.18%,Table 6.170)

Type of Inflammation in Skin Quadratic Discriminant (all time points)

Accuracy	**Confusion Matrix**				
67.73%	*Classified As*				
p-value	Rejection	Unspecific Inflammation	Wound Healing		
.2696	50	22	31	Rejection	*True Class*
	5	32	19	Unspecific Inflammation	
	4	10	109	Wound Healing	

Table 4.61

Feature selected (59.57%,Table 6.171), MANOVA transformed (67.02%,Table 6.172)

Type of Inflammation in Muscle Random Classification (all time points)

Accuracy	**Confusion Matrix**				
28.43%	*Classified As*				
p-value	Rejection	Unspecific Inflammation	Wound Healing		
.2210	30	26	23	Rejection	*True Class*
	11	4	7	Unspecific Inflammation	
	32	36	28	Wound Healing	

Table 4.62 Baseline: Random classifier performance for identifying type of inflammation in muscle

Type of Inflammation in Muscle Linear Discriminant (all time points)

Accuracy	**Confusion Matrix**				
63.45%	*Classified As*				
p-value	Rejection	Unspecific Inflammation	Wound Healing		
.4930	33	10	36	Rejection	*True Class*
	1	11	10	Unspecific Inflammation	
	9	6	81	Wound Healing	

Table 4.63

Feature selected (57.36%,Table 6.245), MANOVA transformed (62.44%,Table 6.246)

Type of Inflammation in Muscle Quadratic Discriminant (all time points)

Accuracy	**Confusion Matrix**				
67.51%	*Classified As*				
p-value	Rejection	Unspecific Inflammation	Wound Healing		
.3749	42	10	27	Rejection	*True Class*
	7	8	7	Unspecific Inflammation	
	8	5	83	Wound Healing	

Table 4.64

Feature selected (58.89%,Table 6.247)

In addition to analysis at all time points, baseline performance was measured at or prior to POD 5 in skin with LDA (65.32%,Table 6.181), feature selected LDA (49.13%,Table 6.182), MANOVA LDA (64.16%,Table 6.183), QDA (69.36%,Table 6.184), feature selected QDA (47.40%,Table 6.185), and MANOVA QDA (71.10%,Table 6.186), as well as in muscle with LDA (54.29%,Table 6.256), feature selected LDA (55.24%,Table 6.257), and MANOVA LDA (51.43%,Table 6.258).

After POD 5 baseline performance in skin was measured by LDA (75.76%, Table 6.196), feature selected LDA (52.12%,Table 6.197), MANOVA LDA (76.36%, Table 6.198), QDA (78.79%,Table 6.199), feature selected QDA (63.64%,Table 6.200), and MANOVA QDA (80.61%,Table 6.201), as well as in muscle by LDA (64.04%,Table 6.268), feature selected LDA (57.89%,Table 6.269), and MANOVA LDA (65.79%,Table 6.270). Again original feature space results are best, MANOVA nearly equivalent, and feature-selected least accurate. Early time point samples remain more challenging to accurately classify than late time point samples.

Performance in Enhanced Identification of Inflammation Type

Analyzing samples from all time points in skin, the logistic classifier identifies the sample inflammation type 68.09% of the time, but not with significance (Table 4.65). The logistic classifier delivers an AUROC of .885 (Figure 6.263) in the detection of wound healing in the original feature space, and an AUROC of .877 (Figure 6.268) when the feature interaction variables are included. It also delivers an AUROC of .893 (Figure 6.272) in the detection of unspecific inflammation in the original feature space, and an AUROC of .886 (Figure 6.277) with feature interaction variables.

Decision tree (Figure 6.249) identifies the sample inflammation type 77.66% of the time, with near significance (Table 4.66, Figure 6.250). The decision tree yields an AUROC of .843 (Figure 6.264) in the detection of wound healing in the original feature space, and an AUROC of .885 (Figure 6.269) when the feature interaction variables are included. It also delivers an AUROC of .878 (Figure 6.273) in the detection of unspecific inflammation in the original feature space, and an AUROC of .877 (Figure 6.278) with feature interaction variables.

Random forest identifies the sample inflammation type 82.98% of the time with significance (Table 6.179, Figure 6.213), and with feature interaction variables reaches 90.43% accuracy with significance (Table 4.68,Figure 4.48). Random forest yields an AUROC of .973 (Figure 6.265) in the detection of wound healing in the original feature space, and an AUROC of .977 (Figure 4.49) when the feature interaction variables are included. It also delivers an AUROC of .992 (Figure 6.274) in the detection of unspecific inflammation in the original feature space, and an AUROC of .987 (Figure 4.50) with feature interaction variables.

Type of Inflammation in Skin Logistic Classifier (all time points)

Accuracy	**Confusion Matrix**				
68.09%	*Classified As*				
p-value	Rejection	Unspecific Inflammation	Wound Healing		
.2964	61	16	26	Rejection	*True Class*
	15	23	18	Unspecific Inflammation	
	6	9	108	Wound Healing	

Table 4.65

Feature selected (60.99%,Table 6.173), MANOVA transformed (68.09%,Table 6.174), Hybrid features (70.21%,Table 6.175)

Type of Inflammation in Skin Decision Tree (all time points, pruned tree)

Accuracy	**Confusion Matrix**				
77.66%	*Classified As*				
p-value	Rejection	Unspecific Inflammation	Wound Healing		
.1316	76	7	20	Rejection	*True Class*
	18	26	12	Unspecific Inflammation	
	9	7	107	Wound Healing	

Table 4.66

Feature selected (75.18%,Table 6.176), MANOVA transformed (71.28%,Table 6.177), Hybrid features (79.43%,Table 6.178)

Type of Inflammation in Skin Random Forest (all time points, 100 trees)

Accuracy	**Confusion Matrix**				
89.01%	*Classified As*				
p-value	Rejection	Unspecific Inflammation	Wound Healing		
.0259	93	0	10	Rejection	*True Class*
	9	43	4	Unspecific Inflammation	

	7	3	113	Wound Healing	

Table 4.67

Feature selected (82.98%,Table 6.179), MANOVA transformed (82.98%,Table 6.180)

Type of Inflammation in Skin Random Forest (all time points, hybrid features, 100 trees)

Accuracy

90.43%

p-value

.0231

Confusion Matrix

Classified As				
Rejection	Unspecific Inflammation	Wound Healing		
93	0	10	Rejection	*True Class*
7	45	4	Unspecific Inflammation	
5	1	117	Wound Healing	

Table 4.68

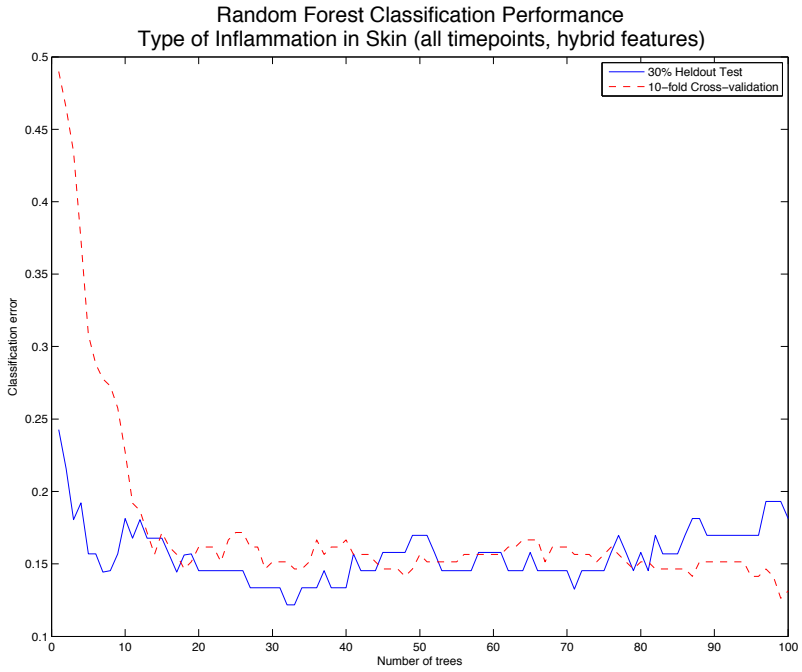

Figure 4.48

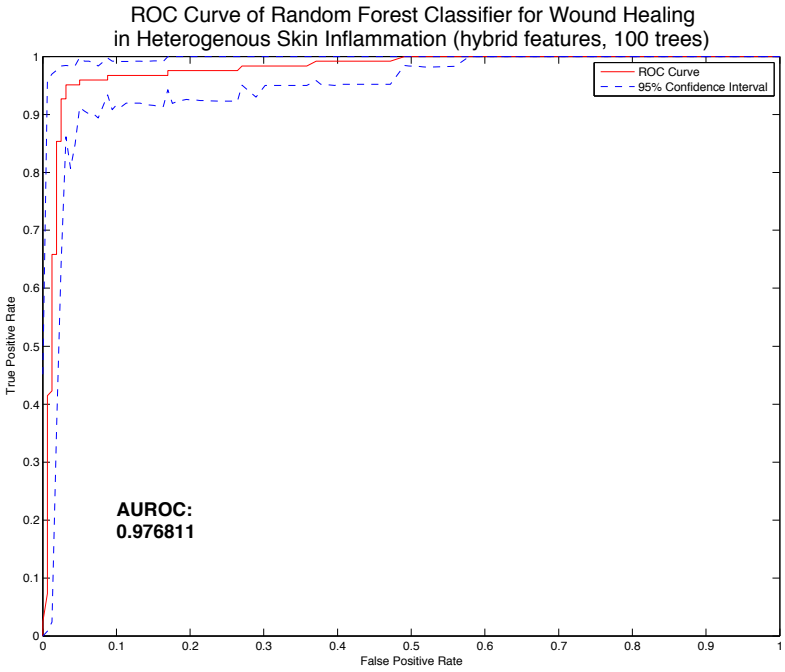

Figure 4.49

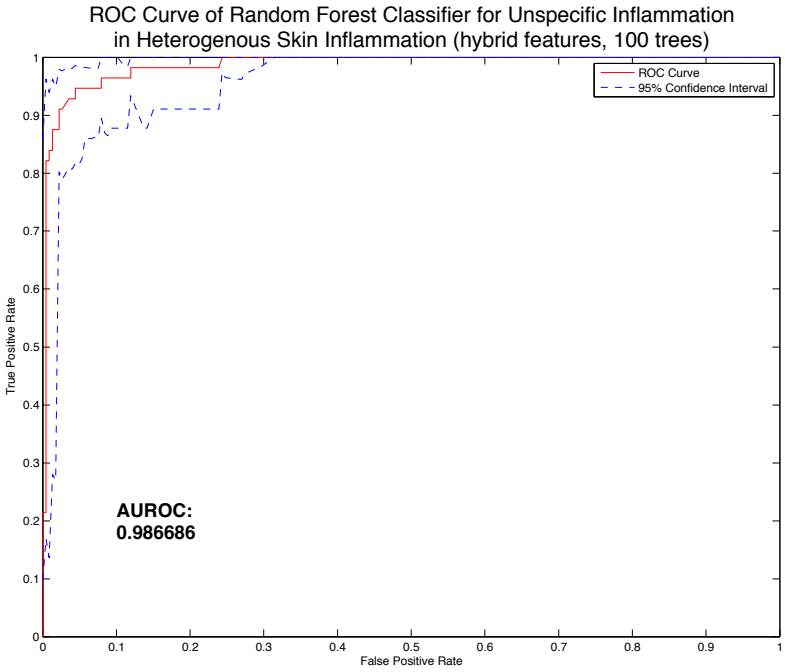

Figure 4.50

At or prior to POD 5 in skin, the parallel plot (Figure 6.279) and MANOVA transformation (Figure 6.280) show distinction between rejection and not rejection associated inflammation, driven primarily by TNFa, IL-4, IL-12p70, GM-CSF, IL-2, and IL-5 (Figure 6.281).

In skin at or prior to POD 5, logistic classification separates rejection from not rejection associated inflammation with 68.79% accuracy in the original feature

space (Table 6.187), MANOVA transformation enables 65.32% accuracy (Table 6.189), while feature selection (Table 6.188) allows accuracy of 54.34%, all with significance.

The decision tree classifier (Figure 6.282) reaches 73.41% accuracy in the original feature space (Table 6.190, Figure 6.283), on feature selected data it achieves 63.58% (Table 6.191, Figure 6.285, Figure 6.286), and on MANOVA transformed data performance is 73.99% (Table 6.192, Figure 6.288, Figure 6.289) , all with significance.

Random forest grown to 100 trees reaches 86.71% accuracy (Table 6.193, Figure 6.284) with significance, on MANOVA transformed data the accuracy was 87.28% (Table 6.195, Figure 6.290) with significance, and on feature-selected data accuracy reached 79.19% (Table 6.194, Figure 6.287) with significance.

After POD 5 in skin, the parallel plot (Figure 6.291) and MANOVA transformation (Figure 6.292) show distinction between rejection and not rejection associated inflammation, driven primarily by IL-12p70, TNFa, and IL-5 (Figure 6.293).

In skin after POD 5, logistic classification separates rejection from not rejection associated inflammation with 81.21% (Table 6.202), and MANOVA transformation enables 81.21% accuracy (Table 6.203), both without siginificance. Feature selection (Table 6.204) allows 62.42% with statistical significance.

The decision tree classifier (Figure 6.294) reaches 78.18% in the original feature space (Table 6.205, Figure 6.295), and on feature selected data it achieves 77.58% (Table 6.206, Figure 6.297, Figure 6.298), both with significance. On MANOVA transformed data performance is 64.48% accuracy but with no statistical significance (Table 6.207, Figure 6.300, Figure 6.301).

Random forest grown to 100 trees reaches 89.70% accuracy (Table 6.208, Figure 6.296), feature-selected data accuracy reached 87.27% (Table 6.209, Figure 6.299), and MANOVA transformed data the accuracy was 86.06% (Table 6.210, Figure 6.302), all with strong significance.

Analyzing muscle samples from all time points, the logistic classifier identifies the sample inflammation type 68.02% of the time, but not with significance (Table 4.69). The logistic classifier delivers an AUROC of .738 (Figure 6.320) in the detection of wound healing in the original feature space, and an AUROC of .745 (Figure 6.324) when the feature interaction variables are included. It also delivers an AUROC of .641 (Figure 6.329) in the detection of unspecific inflammation in the original feature space, and an AUROC of .677 (Figure 6.333) with feature interaction variables.

Decision tree (Figure 6.305) identifies the sample inflammation type 70.56% of the time, without significance (Table 4.70, Figure 6.306). The decision tree yields an AUROC of .727 (Figure 6.321) in the detection of wound healing in the original feature space, and an AUROC of .748 (Figure 6.325) when the feature interaction variables are included. It also delivers an AUROC of .529 (Figure 6.330) in the detection of unspecific inflammation in the original feature space, and an AUROC of .529 (Figure 6.334) with feature interaction variables.

Random forest identifies the sample inflammation type 81.73% of the time with significance (Table 4.71, Figure 6.307), and with feature interaction variables

reaches 83.25% accuracy with better significance (Table 4.72, Figure 4.51). Random forest yields an AUROC of .936 (Figure 4.52) in the detection of wound healing in the original feature space, and an AUROC of .923 (Figure 6.326) when the feature interaction variables are included. It also delivers an AUROC of .863 (Figure 4.53) in the detection of unspecific inflammation in the original feature space, and an AUROC of .856 (Figure 6.335) with feature interaction variables.

Type of Inflammation in Muscle Logistic Classifier (all time points)

Accuracy
68.02%
p-value
.4140

Confusion Matrix

Classified As				
Rejection	Unspecific Inflammation	Wound Healing		
46	3	30	Rejection	*True Class*
5	6	11	Unspecific Inflammation	
10	4	82	Wound Healing	

Table 4.69

Feature selected (59.90%,Table 6.248), MANOVA transformed (67.01%,Table 6.249), Hybrid features (67.51%,Table 6.250)

Type of Inflammation in Muscle Decision Tree (all time points, pruned tree)

Accuracy
70.56%
p-value
.3737

Confusion Matrix

Classified As				
Rejection	Unspecific Inflammation	Wound Healing		
48	2	29	Rejection	*True Class*
5	5	12	Unspecific Inflammation	
13	5	78	Wound Healing	

Table 4.70

Feature selected (68.53%,Table 6.251), MANOVA transformed (73.10%,Table 6.252), Hybrid features (68.02%,Table 6.253)

Type of Inflammation in Muscle Random Forest (all time points, 100 trees)

Accuracy
81.73%
p-value
.1532

Confusion Matrix

Classified As				
Rejection	Unspecific Inflammation	Wound Healing		
66	2	11	Rejection	*True Class*
3	8	11	Unspecific Inflammation	
6	3	87	Wound Healing	

Table 4.71

Feature selected (79.19%,Table 6.254), MANOVA transformed (79.19%,Table 6.255)

Type of Inflammation in Muscle Random Forest (all time points, hybrid features, 100 trees)

Accuracy	**Confusion Matrix**				
83.25%	*Classified As*				
p-value	Rejection	Unspecific Inflammation	Wound Healing		
.1350	70	0	9	Rejection	*True Class*
	2	8	12	Unspecific Inflammation	
	5	1	90	Wound Healing	

Table 4.72

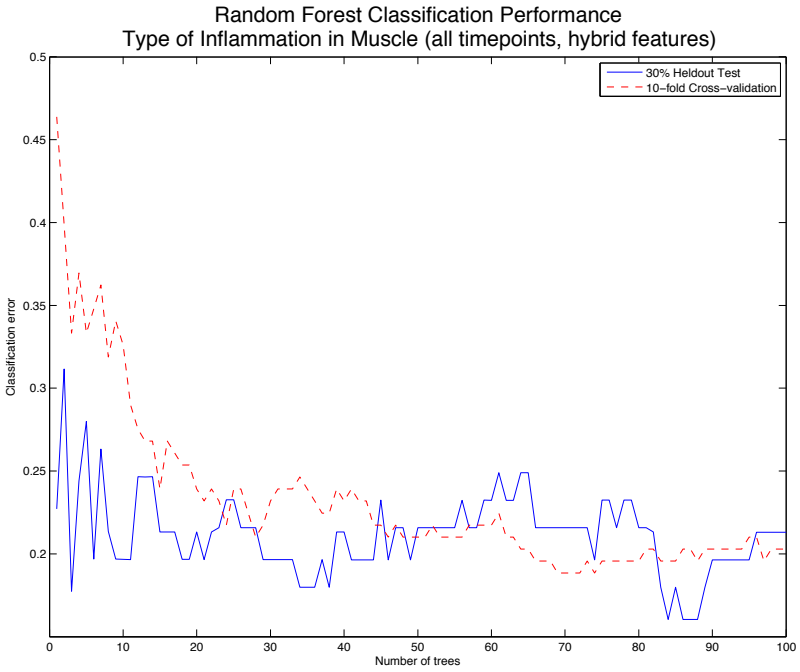

Figure 4.51

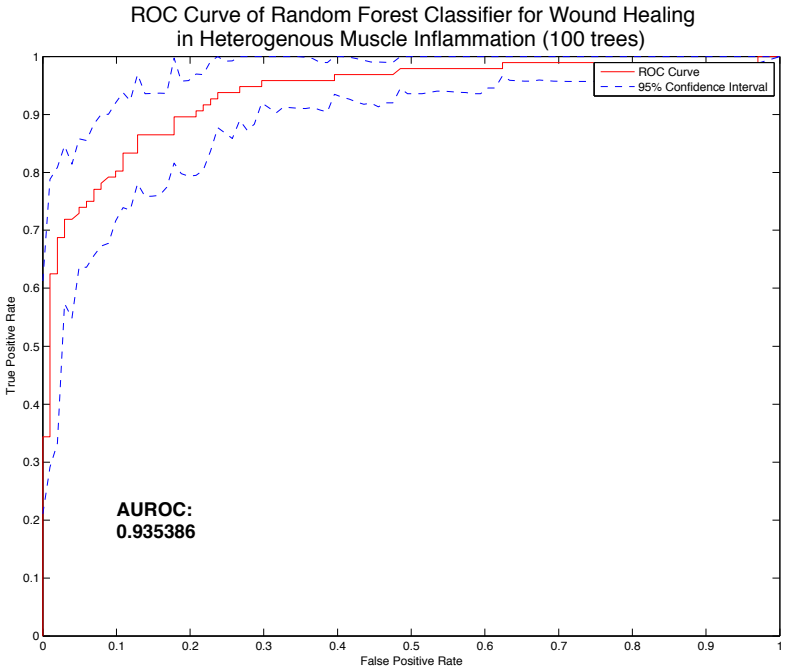

Figure 4.52

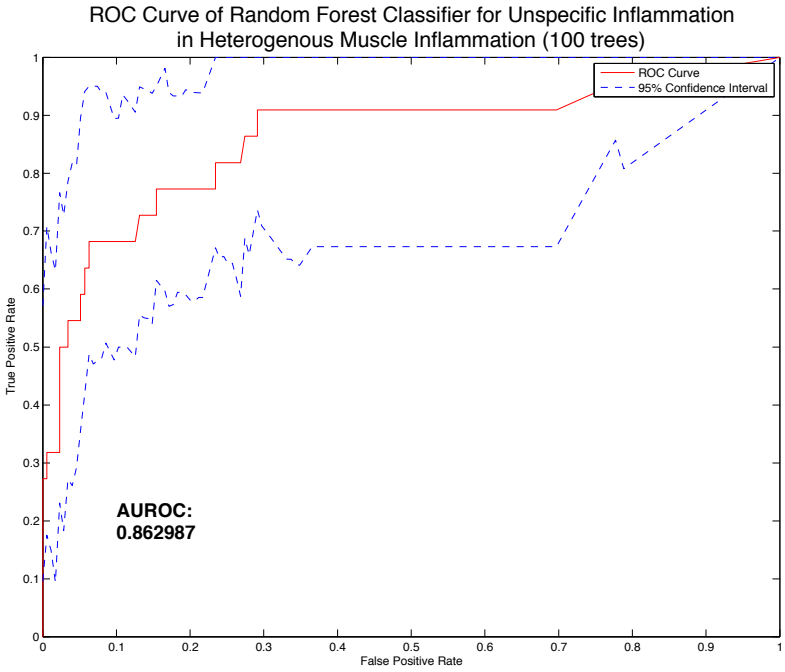

Figure 4.53

At or prior to POD 5 in muscle, the parallel plot (Figure 6.336) and MANOVA transformation (Figure 6.337) show distinction between rejection and not rejection associated inflammation, driven primarily by TNFa, IL-12p70, and IL-5 (Figure 6.338).

In muscle at or prior to POD 5, logistic classification separates rejection from not rejection associated inflammation with 60.95% accuracy but without statistical

significance (Table 6.259). MANOVA transformation enables 63.81% accuracy still without significance (Table 6.260), while feature selection (Table 6.261) allows accuracy of 61.90%, also without significance.

The decision tree classifier (Figure 6.339) reaches 66.67% accuracy (Table 6.262, Figure 6.340), on feature selected data it achieves 64.76% (Table 6.263, Figure 6.342, Figure 6.343), and on MANOVA transformed data performance is also 65.71% accuracy but all without statistical significance (Table 6.264, Figure 6.345, Figure 6.346).

Random forest grown to 100 trees reaches 74.29% accuracy (Table 6.265, Figure 6.341) near significance, while on MANOVA transformed data the accuracy was 76.19% (Table 6.267, Figure 6.347), with significance. Feature-selected data accuracy reached 78.10% (Table 6.266, Figure 6.344), with significance.

After POD 5 in muscle, the parallel plot (Figure 6.348) and MANOVA transformation (Figure 6.349) show distinction between rejection and not rejection associated inflammation, driven primarily by IL-TNFa, and IL-5 (Figure 6.350).

In muscle after POD 5, logistic classification separates rejection from not rejection associated inflammation with 74.46% without statistical significance (Table 6.271). MANOVA transformation enables 74.56% accuracy also without significance (Table 6.272), while feature selection (Table 6.273) allows accuracy of 70.18%, without significance.

The decision tree classifier (Figure 6.351) reaches 70.18% (Table 6.274, Figure 6.352), on feature selected data it also reaches 70.18% (Table 6.275, Figure 6.354, Figure 6.355), and on MANOVA transformed data performance is 77.19% accuracy all with no statistical significance (Table 6.276, Figure 6.357, Figure 6.358).

Random forest grown to 100 trees reaches 79.82% accuracy (Table 6.277, Figure 6.353), and feature-selected data accuracy reached 77.19% (Table 6.278, Figure 6.356), both near significance. On MANOVA transformed data the accuracy was 82.46% (Table 6.279, Figure 6.359), with significance.

Combined Tissue Model Performance

To verify the tissue-specific models are superior to combined tissue models, data from both muscle and tissue (all time points) were merged into a single matrix for analysis. In this framework no information about tissue, time (POD), or pathology is available as a feature in the data; the only features were concentrations of the fourteen cytokines quantified. Initial results for the detection of rejection in allograft vs. isograft groups were promising (Table 4.73) but below those of the tissue-specific models (Table 4.31, Table 4.32, Table 4.33 in skin and Table 4.35, Table 4.36, Table 4.37 in muscle).

Classifier	Accuracy	p-Value
Logistic	81.07%	.0775
Decision Tree	88.93%	.0129
Random Forest	94.64%	.0109

Table 4.73 Classifier performance for allograft vs isograft in combined tissue set

When the rejecting samples were mixed with a more heterogenous sample set that included various wound healing and unspecific inflammation samples, results for the detection of rejection in the combined tissue model were less compelling for logistic and decision tree classifiers, although random forest continued to perform, despite the added noise (Table 4.74). The performance marks of these models remains below those of the tissue specific models (Table 4.51, Table 4.52, and Table 4.53 in skin or Table 4.55, Table 4.56, and Table 4.57 in muscle).

Classifier	Accuracy	p-Value
Logistic	70.35%	.4888
Decision Tree	84.34%	.1281
Random Forest	92.69%	.0689

Table 4.74 Classifier performance in identifying rejection associated inflammation in heterogeneous combined tissue set

In the most challenging task of correctly classifying samples among three forms of inflammation (rejection, wound healing, and unspecific inflammation), logistic and decision tree classifiers performed poorly, while the random forest classifier continued to show decent performance (Table 4.75). Again, the tissue specific models are superior performers (Table 4.65, Table 4.66, and Table 4.67 in skin or Table 4.69, Table 4.70, and Table 4.71 in muscle).

Classifier	Accuracy	p-Value
Logistic	68.48%	.3409
Decision Tree	74.73%	.1685
Random Forest	88.10%	.0608

Table 4.75 Classifier performance in identifying specific inflammation type in heterogeneous combined tissue set

Solid Organ Performance

Rejecting allograft and not-rejecting native organs were compared in heterotopic heart and lung transplantation to evaluate performance of these methods in the solid organ context.

Baseline Heart Performance

Differences in concentration of IL-4 and IL-18 are evident from the parallel plot of allograft versus native heart (Figure 4.54). When transformed by MANOVA and the samples plotted on the axis defined by the first and second canonical variable of the MANOVA transformation, the degree of separation between allograft and native groups becomes clearer (Figure 4.55). On the MANOVA defined axes separation of groups in heart is driven primarily by IL-5 and GM-CSF (Figure 4.56).

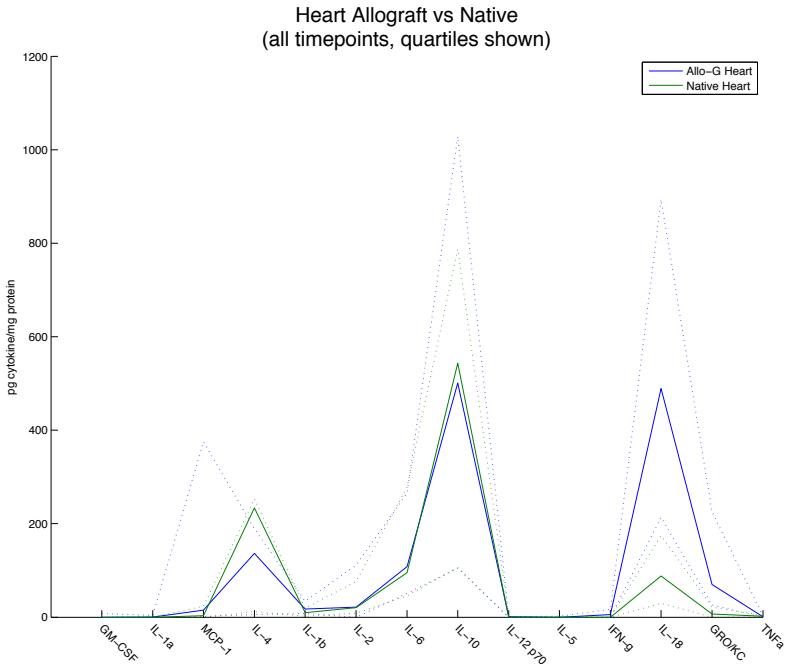

Figure 4.54

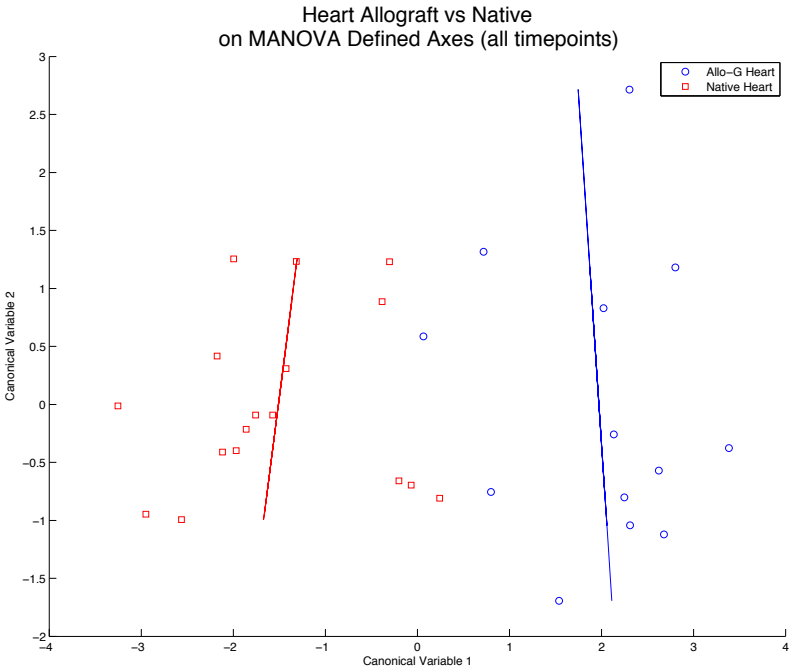

Figure 4.55

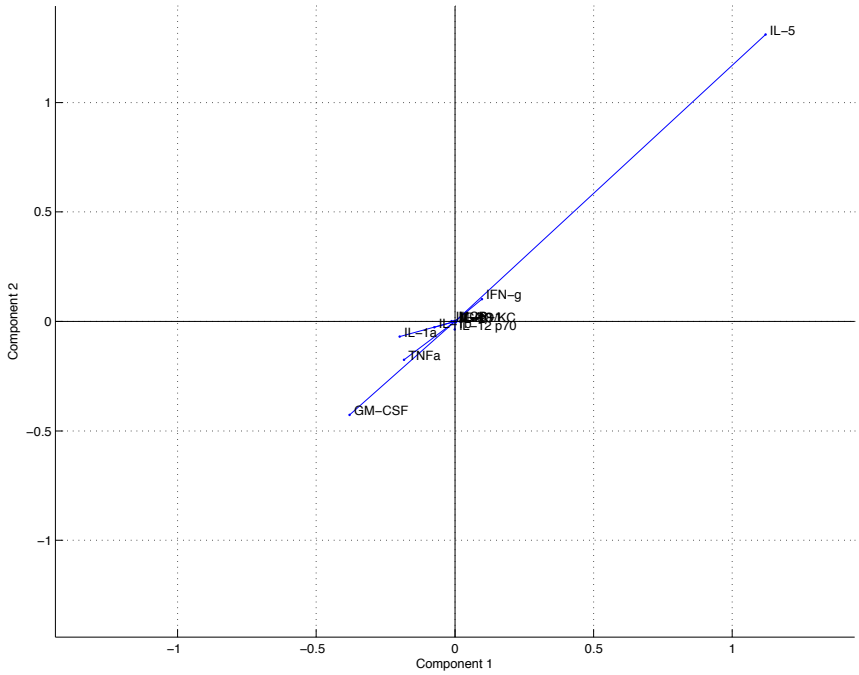

Figure 4.56

The LDA classifier was able to correctly identify the rejecting heart 70% of the time and with little evidence of bias (Table 4.76).

Allograft vs Native Heart with LDA (POD <= 3, Original Feature Space)				
Accuracy	**Confusion Matrix**			
%70.00	*Classified As*			
p-value	Not Rejecting	Rejecting		
.0630	9	4	Not Rejecting	*True Class*
	5	12	Rejecting	

Table 4.76

Enhanced Heart Performance

In heart, the accuracy reached 96.67% with significance with the random forest classifier on the MANOVA transformed hybrid feature space (Table 4.77,Figure 4.57).

Allograft vs Native Heart with Random Forest (POD <= 3, MANOVA on hybrid features, 50 trees)		
Accuracy	**Confusion Matrix**	
%96.67	*Classified As*	*True*

p-value	Rejecting	Not Rejecting		
.0169	12	1	Not Rejecting	
	2	15	Rejecting	

Table 4.77

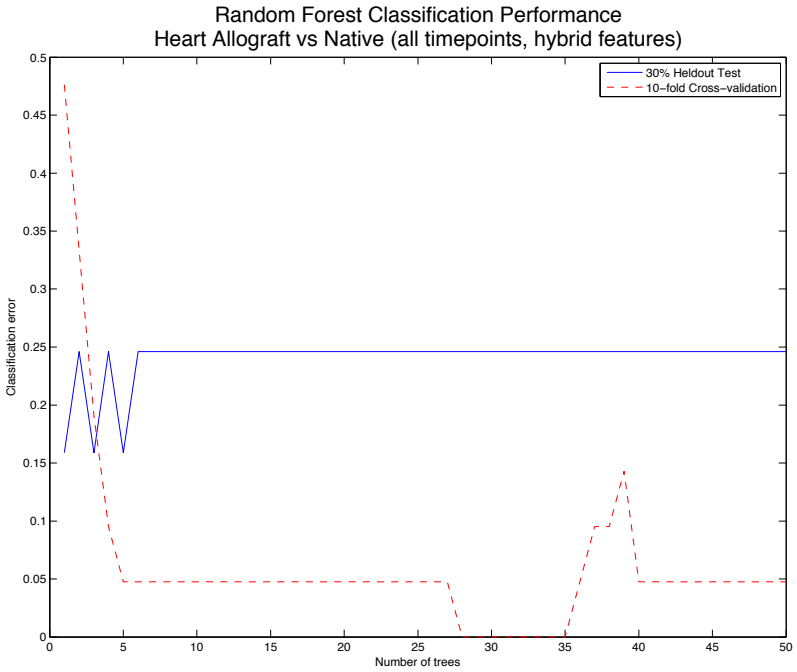

Figure 4.57

Baseline Lung Performance

Differences in concentration of MCP-1, IL-6, IL-10, IL-18, GRO/KC, and IFNg are evident from the parallel plot of allograft versus native lung (Figure 4.58). When transformed by MANOVA and the samples plotted on the axis defined by the first and second canonical variable of the MANOVA transformation, the degree of separation between allograft and native groups becomes clearer (Figure 4.59). On the MANOVA defined axes separation of groups in lung is driven primarily by IL-5, TNFa, and GM-CSF (Figure 4.60).

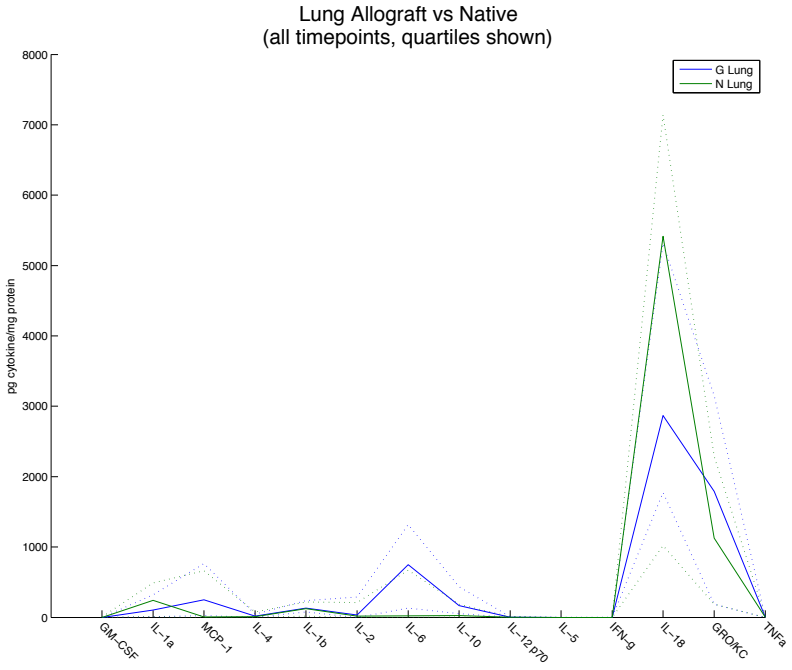

Figure 4.58

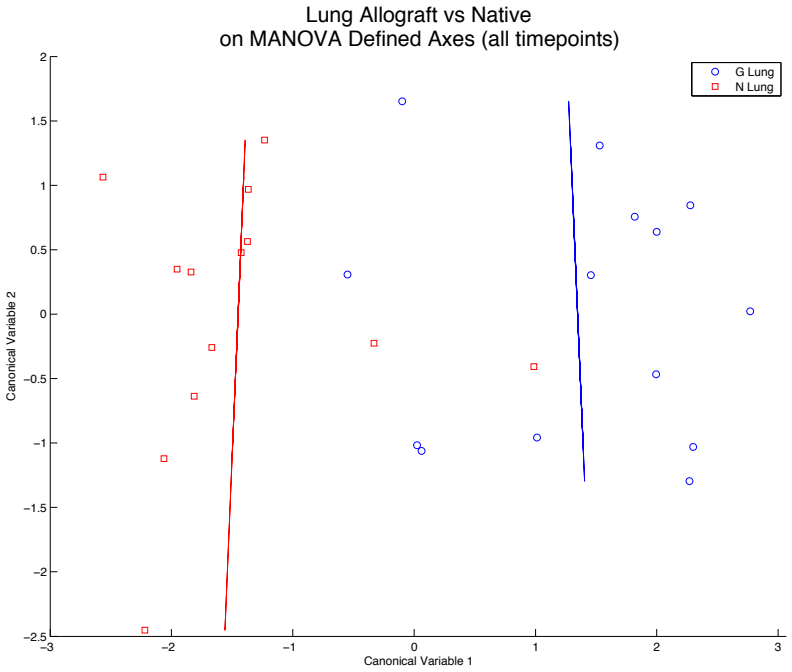

Figure 4.59

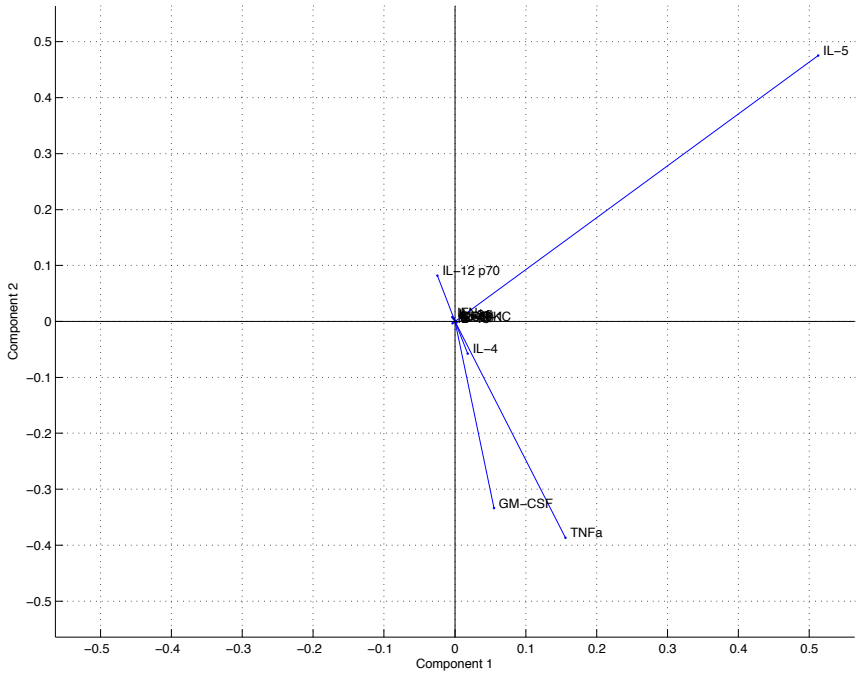

Figure 4.60

The LDA classifier was able to correctly identify the rejecting lung approximately 70% of the time and did not show signs of bias (Table 4.78).

Allograft vs Native Lung with LDA (POD <= 3, Original Feature Space)				
Accuracy	**Confusion Matrix**			
%70.37	*Classified As*			
p-value	Not Rejecting	Rejecting		
.0082	10	4	Not Rejecting	*True Class*
	4	9	Rejecting	

Table 4.78

Enhanced Lung Performance

In lung, the random forest classifier on the MANOVA transformed hybrid feature space reached 85.19% accuracy with significance (Table 4.79,Figure 4.61).

Allograft vs Native Lung with Random Forest (POD <= 3, MANOVA on hybrid features, 50 trees)				
Accuracy	**Confusion Matrix**			
%88.89	*Classified As*			
p-value	Not Rejecting	Rejecting		
.0019	13	1	Not Rejecting	*True Class*
	1	12	Rejecting	

Table 4.79

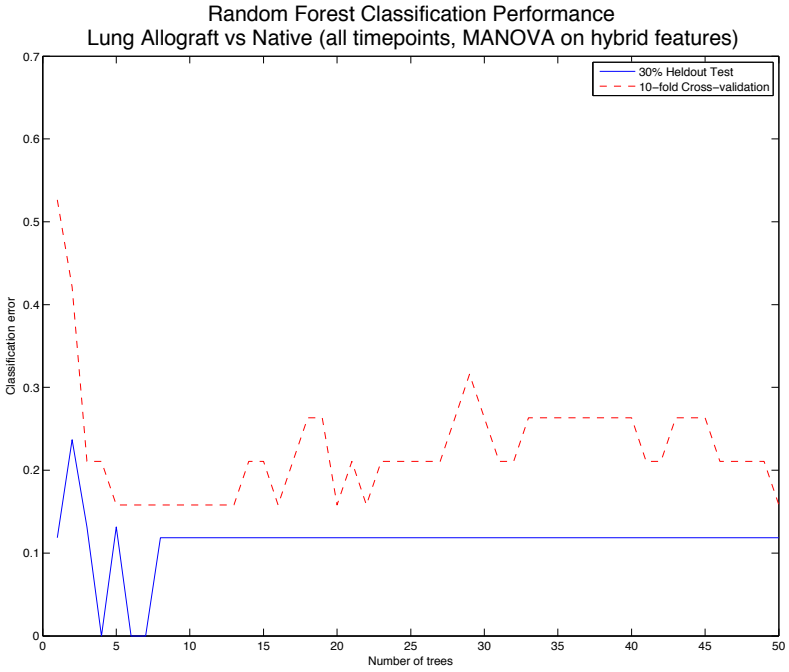
Random Forest Classification Performance
Lung Allograft vs Native (all timepoints, MANOVA on hybrid features)
30% Heldout Test
10−fold Cross−validation
Classification error
Number of trees
0
0.1
0.2
0.3
0.4
0.5
0.6
0.7
0
5
10
15
20
25
30
35
40
45
50

Figure 4.61

Chapter 5 Discussion

Separation of Tissues

Hypothesis 2 of this thesis states that: "immune signaling patterns that drive rejection within each tissue are distinct." This work demonstrates that indeed *the immune signaling patterns that drive rejection within each tissue are distinct*, as measured by the 14 pro-inflammatory cytokines and chemokines described in the methods section. This means that patterns of rejection follow different patterns of expression that are dependent on the type of tissue within which the inflammation is occurring.

Hypothesis 2 was originally proposed as a consequence of the observation that different tissues are comprised of significantly different populations of cells, and that this would logically have an effect on the composition and strength of the local immune response.

Despite the general knowledge that different types of tissue are composed of distinct cell populations, quantitative analysis of the differences in skin and muscle immune signaling profiles has not been found in the literature. This tissue-specific variation in immune signaling has likely been a confounding factor in the analysis of immune signaling, and no doubt has contributed to the reputation of immune signaling as notoriously difficult to model.

Hypothesis 2 was proposed to demonstrate that differences in tissue type are an important source of variance, and that the information content of immune signals is linked to the tissue-context. Incorporating this concept resolves a potentially large source of variance within the data, and provides a structured approach for analyzing the immune signaling associated with rejection and other types of inflammation in the appropriate tissue-context.

The results of the experiments testing separation of tissues provides strong evidence that, holding experimental and sampling conditions constant, skin and muscle coordinate and regulate immune activity distinctly from each other, yet maintain high intra-group consistency.

This is most intuitively obvious in the MANOVA group plots of naïve (Figure 4.7), Isograft (Figure 4.10), allograft (Figure 4.13), and immunosuppressed tissue (Figure 4.16). The same separation of skin from muscle is reliably made by logistic regression, decision tree, and random forest classifiers as described in the results. This separation holds when all time points are analyzed together, when only time points at or prior to POD 5 are considered, or when only time points after POD 5 are considered.

The naïve model is the closest experimental condition to a healthy and stable natural state currently available. Under these conditions inflammation is expected to be minimal although some animal-to-animal variance and biopsy-induced inflammation is unavoidable. We also see that it is more challenging to separate skin from muscle in the naïve case than in any of the other experimental conditions. We also see that separating skin from muscle in the immunosuppressed tissue is more challenging than in the allograft, post immune suppression rejecting, or even

Isograft tissue. Allografts and post immunosuppression rejecting tissue are most easily distinguishable. This seems to imply that the basal state of tissue is most similar to each other, and that as inflammation is induced the dynamics specific to each tissue become more and more clear.

Although it may be technically possible to learn this distinction implicitly in a machine learning model with enough data, such as in a combined tissue random forest model, the time and financial cost involved in collecting sufficient number of samples to learn this distinction under all possible conditions makes such an approach unrealistic. By incorporating knowledge that context (tissue) is essential for interpreting the meaning of immune signals, better modeling decisions are being made, and therefore more accurate models can be built with less data.

Separation of allograft from Isograft

Hypothesis 1 of this thesis states that: "The onset of rejection can be reliably and accurately detected in advance of the current clinical standard by measuring proteomic immune signaling factors associated with inflammation, and using computational models to predict whether these factors are indicative of rejection."

The findings in this work demonstrates that indeed *rejection can be reliably detected in advance of the current clinical gold standard of histologic evaluation*, by modeling the 14 pro-inflammatory cytokines and chemokines described in the methods section. This means that patterns of rejection follow different patterns of expression that are dependent on the type of tissue within which the inflammation is occurring.

Baseline performance of linear discriminant and quadratic discriminant classifier's in skin are approximately 80 to 81% accurate, with robust statistical significance. This indicates that the patterns of cytokine expression in skin are fundamentally different in Isograft and allograft skin tissue, and this difference can be captured with reasonable performance by computationally efficient linear algorithms such as LDA or QDA. Baseline performance in discriminating between immunosuppressed and post immunosuppression rejecting tissue is even stronger, at approximately 82% accuracy with LDA And approximately 86% with QDA respectively, both with high statistical significance. Again, the implication of the strong baseline outcomes is that the cytokine expression patterns of skin tissue under immunosuppression are fundamentally different from those expressed by skin tissue that has been withdrawn from immunosuppression and is now rejecting. The consistency with which this distinction is made across a rather complex set of features implies a high level of biological significance. In other words, not only is the specific cytokine or immune signaling protein important, but the specific combination of cytokines in the local cytokine milieu plays a determinative role in the nature and progression of inflammation expressed.

These baseline results can be improved upon significantly by more sophisticated classifiers. The logistic classifier achieves almost 84% accuracy in skin, the decision tree achieves over 91% accuracy, and random forest achieves over 95% accuracy with very high statistical significance. The addition of feature interaction variables improves the random forest performance to over 96%, and

improves statistical significance, lending validity to the method by which the feature interaction variables were selected. This also implies that there are specific cytokine interactions that are relevant only under certain conditions, and that these interactions can be leveraged to more effectively interpret cytokine network meaning. The identification and elucidation of additional feature interaction variables would most likely further improve the results presented in this work. Based on the observations and findings in this work, it is also likely that there are other feature interactions beyond those identified here, including amongst cytokines that have a predominantly immunologic role and other signaling proteins that are not commonly identified with the immune system.

The significance of the accuracy with which allograft can be separated from Isograft is highlighted when the mode of the grade of rejection at or prior to POD 5 is considered. In this time segment both Isograft and allograft samples, in both skin and muscle, are read at grade 0 or 1 and cannot be distinguished from one another. It is interesting to note that such high levels of classification accuracy can be achieved even when no information about time is provided to the algorithm.

Isolating Specific Forms of Inflammation in a Heterogeneous Set

Hypothesis 3 of this thesis states that "Cytokine patterns of inflammation associated with rejection can be distinguished from other unspecific, wound-induced, or immunosuppressed cytokine patterns of inflammation." The findings reported here confirm this hypothesis and show that *specific types of inflammation can be distinguished from one another through the analysis of cytokine expression patterns*. This is demonstrated by 2 experiments.

In the first experiment, inflammation that is associated with rejection is separated from inflammation that is not associated with rejection in a heterogenous sample set that includes multiple types of inflammation (such as wound healing, endotoxic shock, contact hypersensitivity, etc.). This experimental configuration is different from separation of allograft from Isograft, because of the additional noise introduced by the various types of inflammation, and is therefore a more complex task.

In the second experiment, the heterogenous sample set is grouped into 3 types of inflammation; rejection, wound healing, and unspecific inflammation. The classification task is to identify the type of inflammation associated with each sample. Although the focus of this thesis is on the identification of rejection-associated inflammation, the results of this experiment imply the conversational modeling of cytokine signals has application far beyond transplantation.

Separation of Rejection from Not Rejection Associated Inflammation

LDA and QDA classifiers only achieved 68% and 77% accuracy in skin respectively, and with no statistical significance. In muscle LDA achieved 70% while QDA achieved 72% accuracy. The poor performance of baseline classifiers indicates that while the difference between Isograft and allograft samples may be clear and

relatively linear, consideration of additional forms of inflammation introduces nonlinear decision boundaries.

This is reinforced by contrasting the performance of the logistic classifier in skin, which reaches only 70% accuracy and no statistical significance, with the decision tree classifier, which reaches 87% accuracy and almost reaches statistical significance. Random forest is the classifier most able to capture nonlinear decision boundaries, and perhaps for this reason is also the top performer with over 93% accuracy and statistical significance. When additional feature interaction variables are provided to the random forest classifier, there is a slight reduction in the misclassification of "not rejection" as "rejection" (Table 4.54).

Going One Step Further: Identification of Inflammation Type

When analyzing samples from all time points, the LDA classifier is 64% accurate (not statistically significant) in identifying sample inflammation type in skin, while QDA is 67% accurate (also not statistically significant) in skin. In muscle accuracy is diminished with LDA reaching only 63% (not statistically significant), while QDA again reaches 67% accuracy (again not statistically significant).

The logistic classifier achieves 68% accuracy in skin - not much improved beyond that of the baseline LDA model. The decision tree improves to 77% accuracy and almost reaches statistical significance, but the best performance is provided by random forest, with 89% accuracy and statistical significance. When feature interaction variables are incorporated, random forest delivers over 90% accuracy with very high statistical significance.

In muscle the logistic classifier again reaches 68% accuracy (with no statistical significance), while the decision tree reaches 70% accuracy (with no statistical significance). The decision tree performs more poorly in muscle than in skin, implying that identification of information type in muscle is a more complex task than in skin. Random forest is able to achieve 81% accuracy, but does not quite achieve statistical significance. When feature interaction variables are incorporated random forest improves to over 83% accurate, and almost reaches statistical significance.

A closer analysis of the confusion matrix of the random forests with hybrid features reveals the largest source of error to be a bias for misclassifying unspecific inflammation samples as wound healing. The next largest source of error is misclassification of rejection as wound healing. Interestingly, the accuracy of the random forest when only analyzing samples at or prior to POD 5 is approximately 74%, while analyzing only samples after POD 5 the accuracy is approximately 79%. In both cases statistical significance is not quite achieved. However the bias in misclassification does change between early and late time points, with rejection almost never being misclassified as wound healing and a larger number of wound healing samples being misclassified as unspecific inflammation at early time points. This could indicate the classification labels that show excellent performance in skin do not as accurately reflect the underlying inflammation patterns of muscle, however sufficient accuracy is achieved to show that distinctive cytokine patterns are indeed expressed under different inflammatory conditions.

Because muscle is more extensively perfused than skin, and because the native population of immune cells has important differences from that of the skin (such as the absence of Langerhans cells), it is reasonable to expect that the immune reaction in muscle is being driven by a different set of primary factors from those driving the immune reaction in skin. The features primarily responsible for separation of groups in MANOVA transformation of muscle are more extensive than the features responsible for separation of groups in skin, specifically including GM-CSF and IFNg. Both of these cytokines are highly multifunctional, and could be indicative of additional processes regulating immune function and muscle that are not present in skin. The intuitive interpretation of these findings is that although muscle is less immunogenic than skin, reduced immunogenicity actually makes a distinction between types of inflammation more complex. It may be possible that the skin, being a natural immunologic barrier organ, has evolved more sophisticated and effective immune responses. It may also be possible that because of the large surface area of the skin and its exposure to the external environment that consequently skin has evolved a more sophisticated immunologic repertoire in order to both provide specific, effective, contained responses to antigen, as well as provide a more challenging target for adversarial adaptation by pathogens and parasites.

Extension to Solid Organs

The methodology that yields high-performance in the composite tissue allograft approach also provides high-performance in the heterotopic heart and lung transplant models. Baseline performance with LDA classifier in both heart and long is approximately 70%, however with random forest using the extended feature set, accuracy is able to reach 96.67% in heart, and 88.89% in lung, both with statistical significance. This indicates that the fundamental approach described in this work of relating patterns in the cytokine features with outcome in pathology holds true in solid organs as well as in skin and muscle.

The specific features selected differ in heart, lung, skin, and muscle, reinforcing the finding that each tissue type follows distinct inflammation activity, and this is reflected in the cytokine expression patterns since they are one of the primary communication channels of the immune system.

Interestingly, separation of allograft from native organ is more complicated in the lung than heart, as evidence by the accuracy rate and confusion matrix. This may have its biological roots in the fact that the long has extremely dense populations of alveolar macrophages, and therefore has higher native levels of immune activity than the heart, which is primarily a muscle and is not known to have particularly high levels of basal immune activity.

Further elucidation of the specific cellular composition of a tissue, and incorporating that information into the feature interactions and weightings of a model, is likely to provide even further improvements in accuracy and generalization across a wide range of contexts.

Future Work

My hope is that the findings of this thesis will be rapidly extended into human data, validated, and applied in the clinic to improve the lives of transplant patients. The ability to interpret the communication stream of the immune system at a computational level is an exciting development that should be pursued and elucidated. Through the application of the techniques described in this thesis, and the reconciliation of the findings described herein with the literature, it may be possible to identify novel methods for diagnosing, treating, and ultimately curing a variety of immune system centric illnesses.

An area requiring additional elucidation is the discovery, incorporation, and optimization of interactions amongst the features, both at an explicit level (such as represented in pairwise r-statistics), as well as through a latent entity (such as a common emitter, regulator, or receiver cell). This work provides one approach that has been shown to work empirically, but a more formal exploration of the underlying mechanics at a biological and mathematical level would be worthwhile.

The development of a classifier able to identify rejection from cytokine expression patterns enables the development of a new generation of noninvasive diagnostic devices. The National Endowment for Plastic Surgery and the Department of Plastic Surgery at Johns Hopkins Medical School have already provided funding for the development of a noninvasive skin rejection diagnostic based on this work. Preliminary results are very promising, and suggest that even more advanced noninvasive detection methods are possible for solid organ application, including a cytokine breath test capable of detecting rejection as early and reliably as direct biopsy methods.

The application of the analytic methods and approach described in this thesis to further elucidate the cellular infiltration and regulation dynamics in heart and lung transplant are being pursued at the Pittsburgh NMR Center as part of its P 41 grant renewal proposal, as well as new R01 and other NIH applications. The collaboration with the Pittsburgh NMR Center has led to the early exploration of a novel potential combination immunosuppression therapy, as well as a method by which the local cell population of the sample can be inferred from the cytokine signaling activity measured. We have just scratched the surface of the potential for this technology to enhance and extend the capabilities of bioimaging.

Ongoing work with Prof. Nyberg (Language Technologies Institute, Carnegie Mellon University) into methods by which the results of numerical analysis in biological experiments can be reconciled with observations reported in the literature has also yielded exciting and novel extensions of information representation and learning methods that may be able to more effectively answer questions from researchers, as well as more effectively represent information gained from biological experiments.

Chapter 6 Summary and Conclusion

This work has demonstrated that patterns of inflammation, particularly those associated with rejection, are specific to the type of tissue within which they occur (their context). Frequently the immunological characteristics of tissue are generalized in source texts and the literature, giving the impression that the immune response is similar across a variety of tissues and pathologies. However, the experimental data gathered here emphasizes that different tissue types behave with distinct immune signaling characteristics that when taken into account, improve modeling performance markedly. MANOVA analysis determined that skin and muscle tissue followed distinct distributions ($p < 0.05$,Figure 4.7). Random forest was 97.48% ($p<0.05$,Table 4.17) accurate in separating skin from muscle in Isograft groups, 94.68% ($p<0.05$, Table 4.18) accurate in allograft, and 86.05% accurate ($p<0.05$, Table 4.19) even when tissue was treated with immunosuppression (FK-506). This may be an important factore to take into consideration when modeling and interpreting immune signals or cell activity patterns in future work.

Another main finding of this work is that rejection can be detected well in advance of the current clinical gold standard of histology through the application of statistical inference models to capture distinctive patterns in immune signaling expression. The combinatorial complexity of these immune signaling patterns makes them intractable to human analysis, but the patterns inherent to the data are sufficiently distinct that classifiers such as the random forest are able to achieve very high levels of accuracy, statistical significance, and low false-positive/false-negative rates. This is particularly true when feature interaction variables are added to the original set of quantified cytokine signal features. Several combinations of classifiers and feature transformation methods are provided to show the progressive changes in accuracy as each method is applied to the data, to help provide additional insight into the characteristics of immune signaling and how those characteristics relate to the pathology. The most successful method in identifying rejection at all timepoints was the random forest classifier applied to the data set that included feature interaction variables.

When comparing the immune signaling patterns of untreated allograft with isografts, very high levels of classification accuracy are reached. In skin MANOVA analysis determined that allograft and Isograft groups follow separate distributions ($p<0.05$,Figure 4.26), and the random forest classifer is able to separate allograft from Isograft 96.15% of the time ($p<0.05$,Table 4.34). After withdrawal of immunosuppression random forest performs with 92.31% accuracy ($p<0.05$,Table 4.41). In muscle, MANOVA analysis also shows allograft and Isograft follow different distributions ($p<0.05$, Figure 4.28) and random forest is 95.16% accurate ($p<0.05$, Table 4.38) when separating the groups. After immunosuppression is withdrawn, performance is 86.27% accurate ($p<0.05$,Table 4.44). The random forest classifier reaches an AUROC score of .9947 in skin (Figure 4.30), and .9895 in muscle (Figure 4.32).

Beyond separating allograft from Isograft, this work shows that immune signaling patterns can be used to differentiate and identify different types of inflammation, including the classification of inflammation in samples at stages that are not currently differentiable through histologic analysis. The clinical gold standard of histologic evaluation is currently unable to differentiate between early signs of rejection (at approximately POD 5 in skin or muscle), and other unspecific causes of inflammation such as infection, mechanical stress, insect bites, or other wounding. However, the random forest classifier, particularly when provided with feature interaction data, is able to correctly identify inflammation patterns associated with rejection, wound healing, and unspecific inflammation. This implies that the approach and methods described in this work have application well beyond the field of transplant immunology. In skin, MANOVA analysis indicated that rejection associated inflammation followed a different distribution from inflammation not associated with rejection ($p<0.05$,Figure 4.37), and the random forest classifier was 92.55% accurate ($p = 0.0852$,Table 4.54). It reached an AUROC score of .9684 for rejection (Figure 4.41), .9768 for wound healing (Figure 4.49), and .9867 for unspecific inflammation (Figure 4.50). In muscle, MANOVA analysis indicated that rejection associated inflammation followed a different distribution from inflammation not associated with rejection ($p<0.05$,Figure 4.39), and the random forest classifier was 86.80% accurate ($p = 0.0779$,Table 4.58). It reached an AUROC score of .9684 for rejection (Figure 4.43), .9354 for wound healing (Figure 4.52), and .8630 for unspecific inflammation (Figure 4.53).

These findings are also effective in identifying rejection at early time points in the solid organ context. In the heterotopic heart and lung transplant model, the rejecting heart allograft was able to be distinguished from the non-rejecting native heart, and the rejecting lung allograft was distinguished from the non-rejecting native lung with very high accuracy and statistical significance. In heart, MANOVA analysis shows allograft and native organs follow different distributions ($p<0.05$,Figure 4.55), and the random forest classifier on the extended feature space is 96.67% accureate ($p<0.05$, Table 4.77). In lung, MANOVA analysis shows allograft and native organs follow different distributions ($p<0.05$, Figure 4.59), and the random forest classifier on the extended feature space is 88.89% accureate ($p<0.05$, Table 4.79).

Perhaps most importantly this work has demonstrated that patterns in the communication and coordination of the immune system, as expressed through immune signaling proteins, can be modeled successfully as a fundamentally computational system where the features and the determination of the roles that they play in predicting outcome may be determined through inference, rather than exclusively modeling based on physical interactions, spatial location, or signaling pathways.

A generic procedure for deriving computational models that will be able to provide separation between groups where the features are composed primarily of immune signaling factors (such as cytokines) has also been derived by this work:

1) Measure pro-inflammatory cytokine or other biomarkers of inflammation.
2) Measure correlation coefficients for each group within the sample space (r-value).

3) Subtract r-values from each other to find the highest inter-group r-values (i.e. values that are high in one group or another but not both).
4) Multiply the features identified from procedure (3) above to create new "interaction features".
5) Add these features to the original feature space.
6) Apply MANOVA transformation to the extended (hybrid) feature data matrix.
7) Apply a classifier to the MANOVA transformed extended feature space.

This procedure represents a first generation modeling methodology characteristic of computational immunology. Improvements to this methodology, and the development of additional approaches, will benefit from additional future work in exploring feature interactions as well as correlation of numeric analysis with biological function.

Computational immunology, represented in part by the approaches and methods described in this work, makes tractable the use of data and patterns that may otherwise be intractably sparse, complex, or noisy, and provides a structured approach to derive from that data potential biomarkers, novel therapies, compounds, or conclusions of high practical value.

Acknowledgements

I would like to thank Dr. Stefan Schneeberger, Dr. Gerald Brandacher, and Dr. WP Andrew Lee for their extensive support and early commitment to this project, and for providing me with excellent source material on the history of composite tissue allotransplantation, the current challenges facing the field of transplantation and transplant immunology, and guidance in helping to understand what research will make important practical impacts in the clinic. I would also like to thank them for taking time and effort to train me in microsurgery, the rat hindlimb transplant surgical model, and providing me with credentials and access to be able to develop the skills. This work would not have been possible without their participation and belief.

I would also like to thank Dr. Dolores Wolfram, for her amazing commitment to this research, and for being a highly intelligent sounding board for an endless stream of ideas. In particular I would like to thank her for conducting the majority of small animal surgeries represented by the data in this work, as well as the extensive post surgery animal care, sampling, laboratory work, and record keeping. Without her collaboration, it would not have been possible for me to conduct the extensive number of surgeries represented by this work.

Ms. Nadine Eberhardt was instrumental in the collection, and Luminex quantitation of samples in the contact hypersensitivity groups. Her bright and intelligent discussions with me on the pathophysiology of contact hypersensitivity provided me with many great ideas about how to incorporate the data into this work.

Dr. Theresa Hautz provided all the histological greetings and readings represented in this work. This was an enormous undertaking, which she completed with remarkable speed and accuracy. I would also like to thank her for the many

conversations we had regarding what is and is not differentiable at early time points with histology.

Dr. Chien Ho has been a constant and powerful positive influence on the scope direction and speed of this research. His early commitments to this work, and recognition of the biological potential of these computational methods, have been a driving force in my research. I would also like to thank him for incorporating this research into his existing NIH program grants, and for making computational immunology apart of the Pittsburgh NMR Center. His numerous discussions regarding the immunology of rejection, and the potential roles of various immune cells at different stages of rejection have influenced the approach represented in this work significantly.

Dr. Qing Ye conducted all the surgeries for the heterotopic heart and lung transplant groups, including old postsurgery animal care, sampling, and recordkeeping. She has also been a continuous supporter of this research.

Dr. Yoram Vodovotz has been working in the area of mathematical modeling of biological systems, and the many discussions we have had regarding methods to capture the complexity of processes have been invaluable. He has generously provided material, personnel, and expertise for the Luminex quantitation of samples collected by the collaborating surgeons or myself, as well as investing extensive time and effort into editing papers that we have submitted for publication based on data presented in this work. I would also like to thank him for inviting me to present on numerous occasions at the center for inflammation and regenerative modeling group meetings. The feedback I received from these presentations was extremely helpful.

Mr. Derek Barclay for his investment of time and energy in homogenizing tissue samples, conducting protein quantification assays, and operating the Luminex machine in the Vodovotz lab. The majority of cytokine quantifications presented in this work were prepared and read by him.

Dr. Ruben Zamora has provided me with extensive, energetic, and positive feedback on how to make this work more biologically relevant, and has always provided honest insight into the significance of the findings. He has contributed extensive time and effort into editing papers that we have submitted for publication based on data presented in this work.

Dr. Jaime Carbonell, my advisor, has provided guidance and instruction at every critical stage on all aspects of computational modeling, as well as how to reconcile numerical analysis with biological function. His early belief in this novel approach to quantifying and elucidating immune signaling has made this work possible.

I would also like to thank Dr. Raj Reddy for his insightful comments and guidance on how to improve this work, its accessibility, validity, as well as significance. I would also like to thank Dr. Reddy for inspiring me to take the 1st step's towards finding novel means of elucidating immune function, by applying methods that have been proven successful in other fields (such as language technologies).

I owe an extensive, rich, and enlightening education in machine learning and statistical inference to Dr. Tom Mitchell. His guidance in understanding how the

numerical transformation of data can provide perspective on scenarios represented by the data that would otherwise be invisible or inaccessible has had a life altering effect on me personally, as well as on my research. I also would like to thank him for being an extraordinarily positive and calm influence on my development.

My grandfather Thomas Starzl has been a lifelong source of information and inspiration about what could be accomplished with creativity, determination, biology, and medicine.

And finally I would like to thank my father, Tim Starzl, for his help in formatting and editing this work for consistency, grammar, and spelling.

Although every effort was made to survey the full range of relevant literature in each of the fields examined, it is an everpresent possibility work pre-dating that cited here was accidentaly not included because I was not aware of it.

Research Support

Support for the research in this thesis has been received from the Armed Forces Institute for Regenerative Medicine Advanced Regenerative Medicine (ARM) 3 Program, the ARM 4 Program, the Department of Defense Telemedicine and Advanced Technology Research Center, the Plastic Surgery Department at Johns Hopkins School of Medicine, the National Endowment for Plastic Surgery, the Austrian Science Fund, the Tyrolian Zukunftsstiftung, the Pittsburgh NMR Center NIH grants R01HL-081349 and P41EB-001977, the Vodovotz Laboratory at the University of Pittsburgh Medical Center, the Department of Plastic and Reconstructive Surgery at the University of Pittsburgh Medical Center, and the Pennsylvania Department of Health Commonwealth Universal Research Enhancement (CURE) program.

References

Abramowicz, D, and S Schneeberger. 2007. "Hand Transplantation: the State-of-the-Art." *The Journal of Hand Surgery*.

Ackerknecht, Erwin Heinz. 1982. *A Short History of Medicine*. Johns Hopkins Univ Pr.

Billingham, R E. 1966. "The Biology of Graft-Versus-Host Reactions.." *Harvey Lectures* 62: 21–78.

Billingham, Rupert E, and Willys Silvers. 1961. *Transplantation of Tissues and Cells*.

Billingham, Rupert E, Leslie Brent, and Peter Brian Medawar. 1956. *Quantitative Studies on Tissue Transplantation Immunity*. III. Actively Acquired Tolerance.

Bishop, G A, B M Hall, G G Duggin, J S Horvath, A G Sheil, and D J Tiller. 1986. "Immunopathology of Renal Allograft Rejection Analyzed with Monoclonal Antibodies to Mononuclear Cell Markers.." *Kidney International* 29 (3) (March): 708–717.

Borel, JF. 2002. *History of the Discovery of Cyclosporin and of Its Early Pharmacological Development.* Wiener Klinische Wochenschrift.

Breiman, L. 2001. "Random Forests." *Machine Learning*.

Breiman, Leo, Jerome Friedman, Charles J Stone, and R A Olshen. 1984. *Classification and Regression Trees*. 1st ed. Chapman and Hall/CRC.

Brunton, Laurence. 2010. *Goodman and Gilman's the Pharmacological Basis of Therapeutics, Twelfth Edition*. 12th ed. McGraw-Hill Professional.

Bunting, C H. 1921. "Fate of the Lymphocyte." *Journal of Experimental Medicine* 33 (5) (April 30): 593–600. doi:10.1084/jem.33.5.593.

Catalina, M D, M C Carroll, H Arizpe, A Takashima, P Estess, and M H Siegelman. 1996. "The Route of Antigen Entry Determines the Requirement for L-Selectin During Immune Responses.." *The Journal of Experimental Medicine* 184 (6) (December 1): 2341–2351.

Cendales, L C, J Kanitakis, S Schneeberger, C Burns, P Ruiz, L Landin, M Remmelink, et al. 2008. "The Banff 2007 Working Classification of Skin-Containing Composite Tissue Allograft Pathology.." In, 8:1396–1400. doi:10.1111/j.1600-6143.2008.02243.x.

Cendales, Linda C, Allan D Kirk, J Margaret Moresi, Phillip Ruiz, and David E Kleiner. 2006. "Composite Tissue Allotransplantation: Classification of Clinical Acute Skin Rejection.." *Transplantation Proceedings* 81 (3) (February 15): 418–422. doi:10.1097/01.tp.0000185304.49987.d8.

Charo, IF. 2006. "The Many Roles of Chemokines and Chemokine Receptors in Inflammation." *New England Journal of Medicine*.

Colombo, D, and E Ammirati. 2011. "Cyclosporine in Transplantation - a History of Converging Timelines.." *Journal of Biological Regulators and Homeostatic Agents* 25 (4) (September): 493–504.

Cooney, WP, and VR Hentz. 2001. "Successful Hand Transplantation—One-Year Follow-Up." *New England Journal of Medicine*.

Dubernard, J M, E Owen, G Herzberg, M Lanzetta, X Martin, H Kapila, M Dawahra, and N S Hakim. 1999. "Human Hand Allograft: Report on First 6 Months.." *The Lancet* 353 (9161) (April 17): 1315–1320. doi:10.1016/S0140-6736(99)02062-

0.
Dummer, JS, A Hardy, and A Poorsattar. 1983. "Early Infections in Kidney, Heart, and Liver Transplant Recipients on Cyclosporine.." *Transplantation Proceedings*.
Efron, B. 1987. "Better Bootstrap Confidence Intervals." *Journal of the American Statistical Association*.
Engeman, T M, A V Gorbachev, R P Gladue, P S Heeger, and R L Fairchild. 2000. "Inhibition of Functional T Cell Priming and Contact Hypersensitivity Responses by Treatment with Anti-Secondary Lymphoid Chemokine Antibody During Hapten Sensitization.." *Journal of Immunology (Baltimore, Md. : 1950)* 164 (10) (May 15): 5207–5214.
Eriksson, L, E Johansson, N Kettaneh-Wold, J Trygg, C Wikstrom, and S Wold. 2006. *Multivariate and Megavariate Data Analysis Basic Principles and Applications (Part I)*. Umetrics.
Erlanger, B F. 1992. "Do We Know the Site of Action of Cyclosporin?." *Immunology Today* 13 (12) (December): 487–490.
Farr, RS. 1951. "Experiments on the Fate of the Lymphocyte." *The Anatomical Record*.
First, M R, and V R Peddi. 1998. "Malignancies Complicating Organ Transplantation.." *Transplantation Proceedings* 30 (6) (September): 2768–2770.
Freedman, David. 2005. *Statistical Models*. Theory and Practice. Cambridge Univ Pr.
Furukawa, H. 2004. "Evolution of Immunosuppression in Liver Transplantation: Contribution of Cyclosporine." *Transplantation Proceedings*.
G E Sale, K. G. Lerner E A Barker H M Shulman E D Thomas. 1977. "The Skin Biopsy in the Diagnosis of Acute Graft-Versus-Host Disease in Man.." *The American Journal of Pathology* 89 (3) (December 1): 621.
Gander, Brian, Charles S Brown, Dalibor Vasilic, Allen Furr, Joseph C Banis, Michael Cunningham, Osborne Wiggins, et al. 2006. "Composite Tissue Allotransplantation of the Hand and Face: a New Frontier in Transplant and Reconstructive Surgery.." *Transplant International : Official Journal of the European Society for Organ Transplantation* 19 (11) (November): 868–880. doi:10.1111/j.1432-2277.2006.00371.x.
Gleason, RE. 1967. "Report From Kidney Transplant Registry: Analysis of Variables in the Function of Human Kidney Transplants." *Transplantation Proceedings*.
Glucksberg, H, R Storb, A Fefer, C. D. BUCKNER, P. E. NEIMAN, R. A. CLIFT, K. G. LERNER, and E. D. THOMAS. 1974. "Clinical Manifestations of Graft-Versus-Host Disease in Human Recipients of Marrow From Hl-a-Matched Sibling Donor,S." *Transplantation Proceedings* 18 (4) (October 1): 295.
Gober, Michael D, and Anthony A Gaspari. 2008. "Allergic Contact Dermatitis.." *Current Directions in Autoimmunity* 10: 1–26. doi:10.1159/000131410.
GoranBG, K. 1981. *Cyclosporine a Hapatotoxicity in 66 Renal Allograft Recipients*. Transplantation.
Gowans, JL. 1959. "The Recirculation of Lymphocytes From Blood to Lymph in the Rat." *The Journal of Physiology*.
GRAY, J G, A P MONACO, and P S RUSSELL. 1964. "Heterologous Mouse Anti-Lymphocyte Serum to Prolong Skin Homografts.." *Surgical Forum* 15: 142–144.
Graze, PR. 1979. "Chronic Graft Versus Host Disease: a Syndrome of Disordered

Immunity." *The American Journal of Medicine*.
Greaves, M F, I M Roitt, R Zamir, and R B Carnaghan. 1967. "Effect of Anti-Lymphocyte Serum on Responses of Human Peripheral-Blood Lymphocytes to Specific and Non-Specific Stimulants in Vitro.." *The Lancet* 2 (7530) (December 23): 1317–1319.
Group, Canadian Multicentre Transplant Study. 1983. "A Randomized Clinical Trial of Cyclosporine in Cadaveric Renal Transplantation." *New England Journal of Medicine*.
Hastie, Trevor, Robert Tibshirani, and Jerome H Friedman. 2008a. *The Elements of Statistical Learning*. Data Mining, Inference, and Prediction. Springer Verlag.
Hastie, Trevor, Robert Tibshirani, and Jerome H Friedman. 2008b. *The Elements of Statistical Learning*. Data Mining, Inference, and Prediction. Springer Verlag.
Hauben, D J. 1984. *Sushruta Samhita (Sushruta'a Collection) (800-600 B.C.?). Pioneers of Plastic Surgery. Acta Chirurgiae Plasticae*. Vol. 26.
Härdle, Wolfgang, and Léopold Simar. 2003. *Applied Multivariate Statistical Analysis*. Springer Verlag.
Hettiaratchy, Shehan, Mark A Randolph, François Petit, W P Andrew Lee, and Peter E M Butler. 2004. "Composite Tissue Allotransplantation--a New Era in Plastic Surgery?." *British Journal of Plastic Surgery* 57 (5) (July): 381–391. doi:10.1016/j.bjps.2004.02.012.
Hulse, E V. 1959. "Lymphocyte Depletion of the Blood and Bone Marrow of the Irradiated Rat: a Quantitative Study." *British Journal of Haematology* 5 (3) (July): 278–283. doi:10.1111/j.1365-2141.1959.tb04035.x.
Hume, DM, JH Magee, and HM Kauffman Jr. 1963. "Renal Homotransplantation in Man in Modified Recipients." *Annals of Surgery*.
Huntley, R T, P D Taylor, Y Iwasaki, T L Marchioro, H Jeejeebhoy, K A Porter, and T E Starzl. 1966. "Use of Anti-Lymphocyte Serum to Prolong Dog Homograft Survival.." *Surgical Forum* 17: 230–233.
Ihle, JN. 1995. "Cytokine Receptor Signalling.." *Nature*.
Jain, Kewal K. 2010. *The Handbook of Biomarkers*. Humana Pr Inc.
Jolliffe, I T. 2010. *Principal Component Analysis (Springer Series in Statistics)*. 2nd ed. Springer.
Jones, J Miriam, Raphael Wilson, and Patricia M Bealmear. 1971. "Mortality and Gross Pathology of Secondary Disease in Germfree Mouse Radiation Chimeras."
Kanitakis, J, D Jullien, J F Nicolas, C Frances, A Claudy, J P Revillard, E Owen, and J M Dubernard. 2000. "Sequential Histological and Immunohistochemical Study of the Skin of the First Human Hand Allograft.." *Transplantation Proceedings* 69 (7) (April 15): 1380–1385.
Keohane, KW. 1958. *Some Experiments in Fluorescent Microscopy Designed to Elucidate the Fate of the Lymphocyte*. Experimental Physiology.
Kolouch, F, Jr. 1939. "The Lymphocyte in Acute Inflammation." *The American Journal of Pathology*.
Korngold, B. 1978. "Lethal Graft-Versus-Host Disease After Bone Marrow Transplantation Across Minor Histocompatibility Barriers in Mice. Prevention by Removing Mature T Cells From Marrow." *Journal of Experimental Medicine* 148 (6) (December 1): 1687–1698. doi:10.1084/jem.148.6.1687.

Kotb, Malak, Wendy C Russell, Donna K Hathaway, Lillian W Gaber, and A Osama Gaber. 1999. "The Use of Positive B Cell Flow Cytometry Crossmatch in Predicting Rejection Among Renal Transplant Recipients." *Clinical Transplantation* 13 (1pt2) (February): 83–89. doi:10.1034/j.1399-0012.1999.130104.x.

Kreczy, A, G Brandacher, and W Steurer. 2004. "Steroid-and ATG-Resistant Rejection After Double Forearm Transplantation Responds to Campath-1H." *American Journal of Transplantation : Official Journal of the American Society of Transplantation and the American Society of Transplant Surgeons*.

Kubo, M, T Hanada, and A Yoshimura. 2003. "Suppressors of Cytokine Signaling and Immunity." *Nature Immunology*.

Lande, Jeffrey D, Jagadish Patil, Na Li, Todd R Berryman, Richard A King, and Marshall I Hertz. 2007. "Novel Insights Into Lung Transplant Rejection by Microarray Analysis.." *Proceedings of the American Thoracic Society* 4 (1) (January): 44–51. doi:10.1513/pats.200605-110JG.

Lanzetta, Marco, Palmina Petruzzo, Jean-Michel Dubernard, Raimund Margreiter, Frederic Schuind, Warren Breidenbach, Roberta Nolli, et al. 2007. "Second Report (1998-2006) of the International Registry of Hand and Composite Tissue Transplantation.." *Transplant Immunology* 18 (1) (July): 1–6. doi:10.1016/j.trim.2007.03.002.

LAWLEY, TJ, and GL PECK. 1977. "Scleroderma, Sjögren-Like Syndrome, and Chronic Graft-Versus-Host Disease." *Annals of Internal Medicine*.

Li, B, C Hartono, R Ding, and VK Sharma. 2001. "Noninvasive Diagnosis of Renal-Allograft Rejection by Measurement of Messenger RNA for Perforin and Granzyme B in Urine — NEJM." *New England Journal of Medicine*.

Liaw, A. 2002. "Classification and Regression by randomForest." *R News*.

Lu, B, C Ebensperger, Z Dembic, Y Wang, M Kvatyuk, T Lu, R L Coffman, S Pestka, and P B Rothman. 1998. "Targeted Disruption of the Interferon-Gamma Receptor 2 Gene Results in Severe Immune Defects in Mice.." *Proceedings of the National Academy of Sciences of the United States of America* 95 (14) (July 7): 8233–8238.

Lwason, R K, L R Ellis, and C V Hodges. 1966. "Anti-Lymphocyte Serum in Prolongation of Dog Renal Homografts.." *Surgical Forum* 17: 515–516.

Maier, Philip, Ulrike Heizmann, Daniel Böhringer, Yvonne Kern, and Thomas Reinhard. 2011. "Predicting the Risk for Corneal Graft Rejection by Aqueous Humor Analysis.." *Molecular Vision* 17: 1016–1023.

Makowka, L, F Chapman, S Qian, A Zerbe, P H Lee, N Murase, R Saunders, S Todo, and T E Starzl. 1987. "The Effect of FK-506 on Hyperacute Rejection in Presensitized Rats.." *Transplantation Proceedings* 19 (5 Suppl 6) (October): 79–83.

Matsuoka, LY. 1981. "Graft Versus Host Disease." *Journal of the American Academy of Dermatology*.

Medawar, P B. 1944. "The Behaviour and Fate of Skin Autografts and Skin Homografts in Rabbits: a Report to the War Wounds Committee of the Medical Research Council.." *Journal of Anatomy* 78 (Pt 5) (October): 176–199.

Merrill, J P, J E Murray, J H Harrison, and W R Guild. 1956. "Successful Homotransplantation of the Human Kidney Between Identical Twins." *JAMA : the Journal of the American Medical Association* 160 (4) (January 28): 277–282.

doi:10.1001/jama.1956.02960390027008.
Murase, N, S Todo, P H Lee, H S Lai, F Chapman, M A Nalesnik, L Makowka, and T E Starzl. 1987. "Heterotopic Heart Transplantation in the Rat Receiving FK-506 Alone or with Cyclosporine.." *Transplantation Proceedings* 19 (5 Suppl 6) (October): 71–75.
Murdoch, C, and A Finn. 2000. "Chemokine Receptors and Their Role in Inflammation and Infectious Diseases." *Blood*.
Murphy, Kenneth. 2011. *Janeway's Immunobiology (Immunobiology: the Immune System (Janeway))*. 8th ed. Garland Science.
Murray, J E, J P Merrill, and J H Harrison. 2001. *Renal Homotransplantation in Identical Twins. 1955. Journal of the American Society of Nephrology : JASN*. Vol. 12.
Murray, JE, JP Merrill, and JH Harrison. 1963. "Prolonged Survival of Human-Kidney Homografts by Immunosuppressive Drug Therapy." *New England Journal of Medicine*.
Myers, BD, J Ross, and L Newton. 1984. "Cyclosporine-Associated Chronic Nephropathy." *New England Journal of Medicine*.
Nalesnik, M A, S Todo, N Murase, S Gryzan, P H Lee, L Makowka, and T E Starzl. 1987. "Toxicology of FK-506 in the Lewis Rat.." *Transplantation Proceedings* 19 (5 Suppl 6) (October): 89–92.
Narain, AK. 1991. *Ganesa: a Protohistory of the Idea and the Icon*. Ganesh: Studies of an Asian god. Albany: State ….
Nicola, Nicos A. 1995. *Guidebook to Cytokines and Their Receptors (Guide Book Series)*. Ed. Nicos A Nicola. 1st ed. A Sambrook and Tooze Publication at Oxford University Press.
Ochiai, T, K Nakajima, M Nagata, T Suzuki, T Asano, T Uematsu, T Goto, S Hori, T Kenmochi, and T Nakagoori. 1987. "Effect of a New Immunosuppressive Agent, FK 506, on Heterotopic Cardiac Allotransplantation in the Rat.." *Transplantation Proceedings* 19 (1 Pt 2) (February): 1284–1286.
Owen, JE, and CL Bonds. 2006. "Psychiatric Evaluations of Heart Transplant Candidates: Predicting Post-Transplant Hospitalizations, Rejection Episodes, and Survival." *Psychosomatics*.
Pastore, Saveria, Francesca Mascia, Feliciana Mariotti, Cristina Dattilo, and Giampiero Girolomoni. 2004. "Chemokine Networks in Inflammatory Skin Diseases.." *European Journal of Dermatology : EJD* 14 (4) (June): 203–208.
Penn, I, and TE Starzl. 1972. "A Summary of the Status of De Novo Cancer in Transplant Recipients." *Transplantation Proceedings*.
PERRY, SEYMOUR, CHARLES G. Jr CRADDOCK, GLORIA PAUL, and JOHN S. LAWRENCE. 1959. "Lymphocyte Production and Turnover." *Archives of Internal Medicine* 103 (2) (February 1): 224. doi:10.1001/archinte.1959.00270020052006.
Petruzzo, P, L Badet, A Gazarian, M Lanzetta, H Parmentier, J Kanitakis, A Sirigu, X Martin, and J M Dubernard. 2006. "Bilateral Hand Transplantation: Six Years After the First Case.." *American Journal of Transplantation : Official Journal of the American Society of Transplantation and the American Society of Transplant Surgeons* 6 (7) (July): 1718–1724. doi:10.1111/j.1600-6143.2006.01369.x.

Phillips, Michael, John P Boehmer, Renee N Cataneo, Taseer Cheema, Howard J Eisen, John T Fallon, Peter E Fisher, et al. 2004. "Prediction of Heart Transplant Rejection with a Breath Test for Markers of Oxidative Stress.." *The American Journal of Cardiology* 94 (12) (December 15): 1593–1594. doi:10.1016/j.amjcard.2004.08.052.

Piguet, P F, G E Grau, C Hauser, and P Vassalli. 1991. "Tumor Necrosis Factor Is a Critical Mediator in Hapten Induced Irritant and Contact Hypersensitivity Reactions.." *The Journal of Experimental Medicine* 173 (3) (March 1): 673–679.

Racusen, L C, K Solez, R B Colvin, S M Bonsib, M C Castro, T Cavallo, B P Croker, et al. 1999. "The Banff 97 Working Classification of Renal Allograft Pathology.." *Kidney International* 55 (2) (February): 713–723. doi:10.1046/j.1523-1755.1999.00299.x.

Rao, A S, T E Starzl, A J Demetris, M Trucco, A Thomson, S Qian, N Murase, and J J Fung. 1996. "The Two-Way Paradigm of Transplantation Immunology.." *Clinical Immunology and Immunopathology* 80 (3 Pt 2) (September): S46–51.

Rencher, Alvin C. 2002. *Methods of Multivariate Analysis*. Wiley-Interscience.

RIFKIND, D, T E Starzl, T L Marchioro, W R WADDELL, D T ROWLANDS, and R B HILL. 1964. "Transplantation Pneumonia.." *JAMA : the Journal of the American Medical Association* 189 (September 14): 808–812.

RIFKIND, D, T L Marchioro, W R WADDELL, and T E Starzl. 1964. "Infectious Diseases Associated with Renal Homotransplantation.." *JAMA : the Journal of the American Medical Association* 189 (August 10): 397–407.

Russell, R G, R Graveley, F Coxon, H Skjodt, E Del Pozo, P Elford, and A Mackenzie. 1992. "Cyclosporin a. Mode of Action and Effects on Bone and Joint Tissues.." *Scandinavian Journal of Rheumatology. Supplement* 95: 9–18.

Saint-Mezard, Pierre, Frédéric Berard, Bertrand Dubois, Dominique Kaiserlian, and Jean-François Nicolas. 2004. "The Role of CD4+ and CD8+ T Cells in Contact Hypersensitivity and Allergic Contact Dermatitis.." *European Journal of Dermatology : EJD* 14 (3) (April): 131–138.

Sanghvi, A, V Warty, A Zeevi, W Diven, R Duquesnoy, L Makowka, and T E Starzl. 1987. "FK-506 Enhances Cyclosporine Uptake by Peripheral Blood Lymphocytes.." *Transplantation Proceedings* 19 (5 Suppl 6) (October): 45–49.

Saraf, S. 2007. "Sushruta: Rhinoplasty in 600 BC." *The Internet Journal of Plastic Surgery*.

Schneeberger, S, and M Ninkovic. 2006. "Status 5 Years After Bilateral Hand Transplantation." *American Journal of Transplantation : Official Journal of the American Society of Transplantation and the American Society of Transplant Surgeons*.

Schneeberger, Stefan, Bettina Zelger, Marina Ninkovic, and Raimund Margreiter. 2005. "Transplantation of the Hand." *Transplantation Reviews* 19 (2) (April): 100–107. doi:10.1016/j.trre.2005.07.001.

Schneeberger, Stefan, Stefano Lucchina, Marco Lanzetta, Gerald Brandacher, Claudia Bösmüller, Wolfgang Steurer, Fausto Baldanti, Clara Dezza, Raimund Margreiter, and Hugo Bonatti. 2005. "Cytomegalovirus-Related Complications in Human Hand Transplantation.." *Transplantation Proceedings* 80 (4) (August 27): 441–447.

Schreiber, S L, and G R Crabtree. 1992. "The Mechanism of Action of Cyclosporin a and FK506.." *Immunology Today* 13 (4) (April): 136–142.

Schuind, F, C Van Holder, D Mouraux, Ch Robert, A Meyer, P Salvia, N Vermeylen, and D Abramowicz. 2006. "The First Belgian Hand Transplantation--37 Month Term Results.." *Journal of Hand Surgery (Edinburgh, Scotland)* 31 (4) (August): 371–376. doi:10.1016/j.jhsb.2006.01.003.

Shapiro, Ron, Mark L Jordan, Amit Basu, Velma Scantlebury, Santosh Potdar, Henkie P Tan, Edward A Gray, et al. 2003. "Kidney Transplantation Under a Tolerogenic Regimen of Recipient Pretreatment and Low-Dose Postoperative Immunosuppression with Subsequent Weaning.." *Annals of Surgery* 238 (4) (October): 520–5; discussion 525–7. doi:10.1097/01.sla.0000089853.11184.53.

Shen-Orr, Shai S, Ofir Goldberger, Yael Garten, Yael Rosenberg-Hasson, Patricia A Lovelace, David L Hirschberg, Russ B Altman, Mark M Davis, and Atul J Butte. 2009. "Towards a Cytokine-Cell Interaction Knowledgebase of the Adaptive Immune System.." *Pacific Symposium on Biocomputing. Pacific Symposium on Biocomputing*: 439–450.

Shulman, H, G Striker, and M Kennedy. 1981. "Nephrotoxicity of Cyclosporin a After Allogeneic Marrow Transplantation." *New England Journal of Medicine*.

Shulman, Howard M, Keith M Sullivan, Paul L Weiden, George B McDonald, Gary E Striker, George E Sale, Robert Hackman, Mang-So Tsoi, Rainer Storb, and E Donnall Thomas. 1980. "Chronic Graft-Versus-Host Syndrome in Man." *The American Journal of Medicine* 69 (2) (August): 204–217. doi:10.1016/0002-9343(80)90380-0.

Siekierka, J J, and N H Sigal. 1992. "FK-506 and Cyclosporin a: Immunosuppressive Mechanism of Action and Beyond.." *Current Opinion in Immunology* 4 (5) (October): 548–552.

Sindhi, Rakesh, Brandon W Higgs, Daniel E Weeks, Chethan Ashokkumar, Ronald Jaffe, Cecilia Kim, Patrick Wilson, et al. 2008. "Genetic Variants in Major Histocompatibility Complex-Linked Genes Associate with Pediatric Liver Transplant Rejection.." *Gastroenterology* 135 (3) (September): 830–9, 839.e1–10. doi:10.1053/j.gastro.2008.05.080.

Snyder, Thomas M, Kiran K Khush, Hannah A Valantine, and Stephen R Quake. 2011. "Universal Noninvasive Detection of Solid Organ Transplant Rejection.." *Proceedings of the National Academy of Sciences of the United States of America* 108 (15) (April 12): 6229–6234. doi:10.1073/pnas.1013924108.

Solez, K, R B Colvin, L C Racusen, M Haas, B Sis, M Mengel, P F Halloran, et al. 2008. "Banff 07 Classification of Renal Allograft Pathology: Updates and Future Directions.." *American Journal of Transplantation : Official Journal of the American Society of Transplantation and the American Society of Transplant Surgeons* 8 (4) (April): 753–760. doi:10.1111/j.1600-6143.2008.02159.x.

Stanley, C, B McManus, and C Rockey. "Case Study: Applied Semantic Knowledgebase for Detection of Patients at Risk of Organ Failure Through Immune Rejection." *Http://Www.W3.org/2001/Sw/Sweo/Public/UseCases/IOInformatics/*. W3C Semantic Web Use Cases. http://www.w3.org/2001/sw/sweo/public/UseCases/IOInformatics/.

Starzl, T E. 1988. "New Approaches in the Use of Cyclosporine: with Particular

Reference to the Liver.." *Transplantation Proceedings* 20 (3 Suppl 3) (June): 356–360.
Starzl, T E, A J Demetris, M Trucco, H Ramos, A Zeevi, W A Rudert, M Kocova, C Ricordi, S Ildstad, and N Murase. 1992. "Systemic Chimerism in Human Female Recipients of Male Livers.." *The Lancet* 340 (8824) (October 10): 876–877.
Starzl, T E, T L Marchioro, K A Porter, C A MOORE, D RIFKIND, and W R WADDELL. 1964. "Renal Homotransplantation; Late Function and Complications.." *Annals of Internal Medicine* 61 (September): 470–497.
Starzl, T E, T L Marchioro, R S Brittain, J H Holmes, and W R WADDELL. 1964. "Problems in Renal Homotransplantation." *JAMA : the Journal of the American Medical Association* 187 (10) (March 7): 734–740. doi:10.1001/jama.1964.03060230062016.
Starzl, TE, GBG Klintmalm, and KA Porter. 1981. "Liver Transplantation with Use of Cyclosporin a and Prednisone." *New England Journal of Medicine*.
Starzl, Thomas E, and John J Fung. 2010. *Themes of Liver Transplantation. Hepatology (Baltimore, Md.)*. Vol. 51. doi:10.1002/hep.23595.
Starzl, Thomas E, Carl G Groth, and Lawrence Brettschneider. 1967. "The Use of Heterologous Antilymphocyte Globulin (Alg) in Human Renal and Liver Transplantation.." *International Congress Series / Excerpta Medica* 162: 83–90.
Steinmuller, D. 2001. "Skin Allograft Rejection by Stable Hematopoietic Chimeras That Accept Organ Allografts Sill Is an Enigma.." *Transplantation Proceedings* 72 (1) (July 15): 8–9.
Stengel, S M, Y Allemann, M Zimmerli, E Lipp, N Kucher, P Mohacsi, and C Seiler. 2001. "Doppler Tissue Imaging for Assessing Left Ventricular Diastolic Dysfunction in Heart Transplant Rejection.." *Heart (British Cardiac Society)* 86 (4) (October): 432–437.
Strang, Gilbert. 2005. *Linear Algebra and Its Applications*. 4th ed. Brooks Cole.
Stratta, R J. 1997. "Simultaneous Use of Tacrolimus and Mycophenolate Mofetil in Combined Pancreas-Kidney Transplant Recipients: a Multi-Center Report. the FK/MMF Multi-Center Study Group.." *Transplantation Proceedings* 29 (1-2) (January): 654–655.
T E STARZL, T. L. MARCHIORO K N VON KAULLA G HERMANN R S BRITTAIN W R WADDELL. 1963. "Homotransplantation of the Liver in Humans." *Surgery, Gynecology & Obstetrics* 117 (December 1): 659.
Thiru, S, D S Collier, and R Calne. 1987. "Pathological Studies in Canine and Baboon Renal Allograft Recipients Immunosuppressed with FK-506.." *Transplantation Proceedings* 19 (5 Suppl 6) (October): 98–99.
Thomas E Starzl, T. L. Marchioro G Hermann R S Brittain William R Waddell. 1963. "Renal Homografts in Patients with Major Donor-Recipient Blood Group Incompatibilities." *Surgical Forum* 14: 214.
THOMAS E STARZL, THOMAS L. MARCHIORO WILLIAM R WADDELL. 1963. "The Reversal of Rejection in Human Renal Homografts with Subsequent Development of Homograft Tolerance." *Surgery, Gynecology & Obstetrics* 117 (October 1): 385.
Todo, S, L Podesta, P ChapChap, D Kahn, C E Pan, Y Ueda, K Okuda, O Imventarza, A Casavilla, and A J Demetris. 1987. "Orthotopic Liver Transplantation in Dogs

Receiving FK-506.." *Transplantation Proceedings* 19 (5 Suppl 6) (October): 64–67.

Venkataramanan, R, V S Warty, M A Zemaitis, A T Sanghvi, G J Burckart, H Seltman, S Todo, L Makowka, and T E Starzl. 1987. "Biopharmaceutical Aspects of FK-506.." *Transplantation Proceedings* 19 (5 Suppl 6) (October): 30–35.

Wang, B, L Zhuang, H Fujisawa, G A Shinder, C Feliciani, G M Shivji, H Suzuki, P Amerio, P Toto, and D N Sauder. 1999. "Enhanced Epidermal Langerhans Cell Migration in IL-10 Knockout Mice.." *Journal of Immunology (Baltimore, Md. : 1950)* 162 (1) (January 1): 277–283.

Wasserman, Larry. 2010a. *All of Nonparametric Statistics (Springer Texts in Statistics)*. Springer.

Wasserman, Larry. 2010b. *All of Statistics: a Concise Course in Statistical Inference (Springer Texts in Statistics)*. Springer.

Wolf, J.S., J.D. McGavic, and D.M. Hume. 1969. "Inhibition of the Effector Mechanism of Transplant Immunity by Local Graft Irradiation.." *Sur. Gynecol. Obstet., 128: 584-90(Mar. 1969).* (January 1).

Wu, Y.L., Q Ye, L.M. Foley, T.K. Hitchens, K Sato, J.B. Williams, and C. Ho. 2006. "In Situ Labeling of Immune Cells with Iron Oxide Particles: an Approach to Detect Organ Rejection by Cellular MRI." *Proceedings of the National Academy of Sciences of the United States of America* 103 (6): 1852–1857. doi:10.1073/iti0606103.

Ye, Q, Y.L. Wu, L.M. Foley, T.K. Hitchens, D.F. Eytan, H. Shirwan, and C. Ho. 2008. "Longitudinal Tracking of Recipient Macrophages in a Rat Chronic Cardiac Allograft Rejection Model with Noninvasive Magnetic Resonance Imaging Using Micrometer-Sized Paramagnetic Iron Oxide Particles." *Circulation* 118 (2): 149–156. doi:10.1161/CIRCULATIONAHA.108.189734.

Yoffey, J M. 1936. "Variation in Lymphocyte Production." *Journal of Anatomy* 70 (Pt 4) (July 1): 507.

Yoffey, JM. 1933. "The Quantitative Study of Lymphocyte Production." *Journal of Anatomy*.

Zeevi, A, R Duquesnoy, G Eiras, H Rabinowich, S Todo, L Makowka, and T E Starzl. 1987. "Immunosuppressive Effect of FK-506 on in Vitro Lymphocyte Alloactivation: Synergism with Cyclosporine a.." *Transplantation Proceedings* 19 (5 Suppl 6) (October): 40–44.

Appendix A Data Tables

Histology

Group	Number	POD	Skin grade	Muscle grade
Allograft	7	0	0	0
Allograft	10	0	0	0
Allograft	11	0	0	0
Allograft	1	3	0	0
Allograft	3	3	1	1
Allograft	5	3	0	0
Allograft	6	3	0	miss.
Allograft	7	3	0	1
Allograft	10	3	0	0
Allograft	12	3	0	0
Allograft	1	5	2	0
Allograft	2	5	1	0
Allograft	3	5	2	1
Allograft	4	5	1	1
Allograft	8	5	1	miss.
Allograft	9	5	2	1
Allograft	11	5	3	2
Allograft	1	7	3	miss.
Allograft	3	7	3	1
Allograft	6	7	3	1
Allograft	7	7	3	1
Allograft	10	7	3	1
Allograft	12	7	3	1
Allograft	1	9	3	3
Allograft	2	9	3	2
Allograft	8	9	3	1
Allograft	9	9	3	2
Allograft	11	9	3	3
Allograft	1	11	3	3
Allograft	3	11	3	3
Allograft	4	11	3	3
Allograft	6	11	3	3
Allograft	7	11	3	3
Allograft	8	11	3	3
Allograft	9	11	3	3
Allograft	10	11	3	3

Table 6.1

Group	Number	POD	Skin grade	Muscle grade
Isograft	4	0	0	0
Isograft	6	0	0	0

Isograft	8	0	0	0
Isograft	10	0	0	0
Isograft	16	0	0	0
Isograft	18	0	0	0
Isograft	1	3	1	0
Isograft	2	3	0	1
Isograft	4	3	0	0
Isograft	7	3	0	0
Isograft	10	3	1	1
Isograft	3	5	0	1
Isograft	5	5	0	0
Isograft	6	5	miss.	0
Isograft	8	5	0	0
Isograft	9	5	0	0
Isograft	1	7	2	1
Isograft	2	7	0	0
Isograft	4	7	0	0
Isograft	7	7	0	0
Isograft	10	7	0	0
Isograft	3	9	0	0
Isograft	5	9	0	0
Isograft	6	9	1	0
Isograft	8	9	0	0
Isograft	9	9	0	1
Isograft	1	11	2	1
Isograft	2	11	0	0
Isograft	3	11	0	1
Isograft	4	11	0	0
Isograft	5	11	miss.	0
Isograft	10	11	0	0
Isograft	6	20	0	0
Isograft	7	20	0	1
Isograft	8	20	0	1
Isograft	9	20	0	0
Isograft	13	20	0	0
Isograft	14	20	0	0
Isograft	17	20	0	0
Isograft	20	20	0	0
Isograft	11	23	0	0
Isograft	12	23	0	0
Isograft	15	23	0	1
Isograft	16	23	0	1
Isograft	18	23	0	0
Isograft	13	25	0	0
Isograft	14	25	0	miss.
Isograft	17	25	0	1
Isograft	19	25	0	1
Isograft	20	25	0	1
Isograft	11	27	0	2

Isograft	15	27	0	2
Isograft	16	27	0	2
Isograft	18	27	0	0
Isograft	13	29	0	0
Isograft	14	29	0	2
Isograft	17	29	0	2
Isograft	20	29	0	1
Isograft	11	31	0	1
Isograft	12	31	0	1
Isograft	15	31	0	3
Isograft	20	31	0	3
Isograft	13	34	0	1
Isograft	14	34	0	3
Isograft	15	34	0	2

Table 6.2

Group	Number	POD	Skin grade	Muscle grade
FK-Treated	1	0	0	0
FK-Treated	4	0	0	0
FK-Treated	5	0	0	0
FK-Treated	7	0	0	0
FK-Treated	13	0	0	0
FK-Treated	19	0	0	0
FK-Treated	11	3	0	0
FK-Treated	12	3	0	0
FK-Treated	15	3	0	0
FK-Treated	16	3	0	0
FK-Treated	17	3	0	0
FK-Treated	13	5	0	0
FK-Treated	14	5	0	0
FK-Treated	18	5	0	0
FK-Treated	19	5	1	0
FK-Treated	20	5	1	0
FK-Treated	11	7	0	0
FK-Treated	12	7	0	0
FK-Treated	15	7	0	0
FK-Treated	16	7	0	0
FK-Treated	17	7	1	0
FK-Treated	13	9	1	0
FK-Treated	14	9	2	0
FK-Treated	18	9	0	1
FK-Treated	19	9	0	0
FK-Treated	20	9	1	0
FK-Treated	11	11	0	0
FK-Treated	12	11	3	0
FK-Treated	13	11	1	1
FK-Treated	14	11	1	0
FK-Treated	15	11	1	1

FK-Treated	16	11	miss.	0
FK-Treated	17	11	0	0
FK-Treated	18	11	0	0
FK-Treated	19	11	1	0
FK-Treated	20	11	0	0
FK-Treated	3	20	0	0
FK-Treated	7	20	0	0
FK-Treated	8	20	0	0
FK-Treated	10	20	3	1

Table 6.3

Group	Number	POD	Skin grade	Muscle grade
FK-Withdrawn	1	23	2	0
FK-Withdrawn	2	23	1	0
FK-Withdrawn	5	23	0	0
FK-Withdrawn	6	23	0	0
FK-Withdrawn	3	25	2	2
FK-Withdrawn	4	25	1	0
FK-Withdrawn	7	25	0	1
FK-Withdrawn	8	25	0	1
FK-Withdrawn	10	25	3	3
FK-Withdrawn	1	27	3	3
FK-Withdrawn	2	27	2	3
FK-Withdrawn	5	27	2	3
FK-Withdrawn	6	27	0	1
FK-Withdrawn	9	27	0	0
FK-Withdrawn	3	29	2	2
FK-Withdrawn	4	29	2	2
FK-Withdrawn	7	29	2	2
FK-Withdrawn	8	29	2	2
FK-Withdrawn	10	29	3	3
FK-Withdrawn	1	31	3	3
FK-Withdrawn	2	31	3	2
FK-Withdrawn	4	31	3	2
FK-Withdrawn	5	31	3	3
FK-Withdrawn	6	31	1	2
FK-Withdrawn	9	31	2	2
FK-Withdrawn	2	34	3	3
FK-Withdrawn	5	34	3	3
FK-Withdrawn	6	34	3	2
FK-Withdrawn	7	34	3	3
FK-Withdrawn	9	34	3	3

Table 6.4

Hypothesis 1 Skin

Allograft vs Isograft

All Time Points

CTA Allograft vs Isograft in Skin Linear Discriminant (all time points, feature selected)

Accuracy	Confusion Matrix			
69.87%	*Classified As*			
p-value	Allograft	Isograft		
.3264	56	21	Allograft	*True Class*
	9	70	Isograft	

Table 6.5

CTA Allograft vs Isograft in Skin Linear Discriminant (all time points, MANOVA transformed)

Accuracy	Confusion Matrix			
80.12%	*Classified As*			
p-value	Allograft	Isograft		
.0535	61	16	Allograft	*True Class*
	10	69	Isograft	

Table 6.6

CTA Allograft vs Isograft in Skin Quadratic Discriminant (all time points, feature selected)

Accuracy	Confusion Matrix			
71.15%	*Classified As*			
p-value	Allograft	Isograft		
.2602	40	37	Allograft	*True Class*
	8	71	Isograft	

Table 6.7

CTA Allograft vs Isograft in Skin Quadratic Discriminant (all time points, MANOVA transformed)

Accuracy	Confusion Matrix			
84.41%	*Classified As*			
p-value	Allograft	Isograft		
.0387	56	21	Allograft	*True Class*
	8	71	Isograft	

Table 6.8

CTA Allograft vs Isograft in Skin Logistic Classifier (all time points, feature selected)

Accuracy	Confusion Matrix			
80.77%	*Classified As*			
p-value	Allograft	Isograft		
.0350	56	21	Allograft	*True Class*
	9	70	Isograft	

Table 6.9

CTA Allograft vs Isograft in Skin Logistic Classifier (all time points, MANOVA transformed)

Accuracy	Confusion Matrix			
83.33%	*Classified As*			
p-value	Allograft	Isograft		
.0091	61	16	Allograft	*True Class*
	10	69	Isograft	

Table 6.10

CTA Allograft vs Isograft in Skin Logistic Classifier (all time points, hybrid features)

Accuracy	Confusion Matrix			
82.69%	*Classified As*			
p-value	Allograft	Isograft		
.0123	60	17	Allograft	*True Class*
	10	69	Isograft	

Table 6.11

CTA Allograft vs Isograft in Skin Decision Tree (all time points, pruned tree, feature selected)

Accuracy	Confusion Matrix			
91.67%	*Classified As*			
p-value	Allograft	Isograft		
.0011	73	4	Allograft	*True Class*
	8	71	Isograft	

Table 6.12

CTA Allograft vs Isograft in Skin Decision Tree (all time points, MANOVA transformed, pruned tree)

Accuracy	Confusion Matrix			
91.67%	*Classified As*			
p-value	Allograft	Isograft		
.0011	70	7	Allograft	*True Class*

	5	74	Isograft	

Table 6.13

CTA Allograft vs Isograft in Skin Decision Tree (all time points, hybrid features, pruned tree)

Accuracy	**Confusion Matrix**			
89.10%	*Classified As*			
p-value	Allograft	Isograft		
.0123	71	6	Allograft	*True Class*
	17	62	Isograft	

Table 6.14

CTA Allograft vs Isograft in Skin Random Forest (all time points, 50 trees, feature selected)

Accuracy	**Confusion Matrix**			
95.55%	*Classified As*			
p-value	Allograft	Isograft		
.0002	72	5	Allograft	*True Class*
	5	74	Isograft	

Table 6.15

CTA Allograft vs Isograft in Skin Random Forest (all time points, MANOVA transformed, 50 trees)

Accuracy	**Confusion Matrix**			
92.31%	*Classified As*			
p-value	Allograft	Isograft		
.0003	69	8	Allograft	*True Class*
	4	75	Isograft	

Table 6.16

POD <= 5

CTA Allograft vs Isograft in Skin Linear Discriminant (POD <= 5)

Accuracy	**Confusion Matrix**			
76.92%	*Classified As*			
p-value	Allograft	Isograft		
.0596	38	16	Allograft	*True Class*
	5	32	Isograft	

Table 6.17

CTA Allograft vs Isograft in Skin Linear Discriminant (POD <= 5, feature selected)

Accuracy	**Confusion Matrix**			
61.54%	*Classified As*			
p-value	Allograft	Isograft		
.4702	25	29	Allograft	*True Class*
	6	31	Isograft	

Table 6.18

CTA Allograft vs Isograft in Skin Linear Discriminant (POD <= 5, MANOVA transformed)

Accuracy	**Confusion Matrix**			
69.23%	*Classified As*			
p-value	Allograft	Isograft		
.1032	35	19	Allograft	*True Class*
	9	28	Isograft	

Table 6.19

CTA Allograft vs Isograft in Skin Quadratic Discriminant (POD <= 5, feature selected)

Accuracy	**Confusion Matrix**			
60.44%	*Classified As*			
p-value	Allograft	Isograft		
.4467	26	28	Allograft	*True Class*
	8	29	Isograft	

Table 6.20

CTA Allograft vs Isograft in Skin Logistic Classifier (POD <= 5)

Accuracy	**Confusion Matrix**			
83.52%	*Classified As*			
p-value	Allograft	Isograft		
.0509	45	9	Allograft	*True Class*
	6	31	Isograft	

Table 6.21

CTA Allograft vs Isograft in Skin Logistic Classifier (POD <= 5, feature selected)

Accuracy	Confusion Matrix			
76.92%	*Classified As*			
p-value	Allograft	Isograft		
.0596	38	16	Allograft	*True Class*
	5	32	Isograft	

Table 6.22

CTA Allograft vs Isograft in Skin Logistic Classifier (POD <= 5, MANOVA transformed)

Accuracy	Confusion Matrix			
83.52%	*Classified As*			
p-value	Allograft	Isograft		
.0626	46	8	Allograft	*True Class*
	7	30	Isograft	

Table 6.23

CTA Allograft vs Isograft in Skin Decision Tree (POD <= 5, pruned tree)

Accuracy	Confusion Matrix			
82.42%	*Classified As*			
p-value	Allograft	Isograft		
.6308	52	2	Allograft	*True Class*
	29	8	Isograft	

Table 6.24

CTA Allograft vs Isograft in Skin Decision Tree (POD <= 5, pruned tree, feature selected)

Accuracy	Confusion Matrix			
81.32%	*Classified As*			
p-value	Allograft	Isograft		
.4089	53	1	Allograft	*True Class*
	22	15	Isograft	

Table 6.25

CTA Allograft vs Isograft in Skin Decision Tree (POD <= 5, pruned tree, MANOVA transformed)

Accuracy	Confusion Matrix			
84.62%	*Classified As*			
p-value	Allograft	Isograft		
.0378	45	9	Allograft	*True Class*
	4	33	Isograft	

Table 6.26

CTA Allograft vs Isograft in Skin Random Forest (POD <= 5, 50 trees)

Accuracy	Confusion Matrix			
93.41%	*Classified As*			
p-value	Allograft	Isograft		
.0370	51	3	Allograft	*True Class*
	2	35	Isograft	

Table 6.27

CTA Allograft vs Isograft in Skin Random Forest (POD <= 5, 50 trees, feature selected)

Accuracy	Confusion Matrix			
91.21%	*Classified As*			
p-value	Allograft	Isograft		
.0507	51	3	Allograft	*True Class*
	4	33	Isograft	

Table 6.28

CTA Allograft vs Isograft in Skin Random Forest (POD <= 5, 50 trees, MANOVA transformed)

Accuracy	Confusion Matrix			
93.41%	*Classified As*			
p-value	Allograft	Isograft		
.0384	49	5	Allograft	*True Class*
	3	34	Isograft	

Table 6.29

POD > 5

CTA Allograft vs Isograft in Skin Linear Discriminant (POD > 5)

Accuracy	Confusion Matrix			
93.85%	*Classified As*			
p-value	Allograft	Isograft		
.1140	20	3	Allograft	*True Class*
	1	41	Isograft	

Table 6.30

CTA Allograft vs Isograft in Skin Linear Discriminant (POD > 5, feature selected)

Accuracy	Confusion Matrix			
84.62%	*Classified As*			
p-value	Allograft	Isograft		
.2801	13	10	Allograft	*True Class*
	0	42	Isograft	

Table 6.31

CTA Allograft vs Isograft in Skin Linear Discriminant (POD > 5, MANOVA transformed)

Accuracy	Confusion Matrix			
90.77%	*Classified As*			
p-value	Allograft	Isograft		
.1512	18	5	Allograft	*True Class*
	1	41	Isograft	

Table 6.32

CTA Allograft vs Isograft in Skin Quadratic Discriminant (POD > 5, feature selected)

Accuracy	Confusion Matrix			
95.38%	*Classified As*			
p-value	Allograft	Isograft		
.0684	23	0	Allograft	*True Class*
	3	39	Isograft	

Table 6.33

CTA Allograft vs Isograft in Skin Logistic Classifier (POD > 5)

Accuracy	Confusion Matrix			
92.31%	*Classified As*			
p-value	Allograft	Isograft		
.0927	21	2	Allograft	*True Class*
	3	39	Isograft	

Table 6.34

CTA Allograft vs Isograft in Skin Logistic Classifier (POD > 5, feature selected)

Accuracy	**Confusion Matrix**			
93.85%	*Classified As*			
p-value	Allograft	Isograft		
.1347	19	4	Allograft	*True Class*
	0	42	Isograft	

Table 6.35

CTA Allograft vs Isograft in Skin Logistic Classifier (POD > 5, MANOVA transformed)

Accuracy	**Confusion Matrix**			
90.77%	*Classified As*			
p-value	Allograft	Isograft		
.1286	19	4	Allograft	*True Class*
	2	40	Isograft	

Table 6.36

CTA Allograft vs Isograft in Skin Decision Tree (POD > 5, pruned tree)

Accuracy	**Confusion Matrix**			
96.92%	*Classified As*			
p-value	Allograft	Isograft		
.0705	23	0	Allograft	*True Class*
	2	40	Isograft	

Table 6.37

CTA Allograft vs Isograft in Skin Decision Tree (POD > 5, pruned tree, feature selected)

Accuracy	**Confusion Matrix**			
100%	*Classified As*			
p-value	Allograft	Isograft		
.0759	23	0	Allograft	*True Class*
	0	42	Isograft	

Table 6.38

CTA Allograft vs Isograft in Skin Decision Tree (POD > 5, pruned tree, MANOVA transformed)

Accuracy	**Confusion Matrix**			
96.92%	*Classified As*			
p-value	Allograft	Isograft		
.0820	22	1	Allograft	*True Class*
	2	40	Isograft	

Table 6.39

CTA Allograft vs Isograft in Skin Random Forest (POD > 5, 50 trees)

Accuracy	**Confusion Matrix**			
96.92%	*Classified As*			
p-value	Allograft	Isograft		
.0705	23	0	Allograft	*True Class*
	2	40	Isograft	

Table 6.40

CTA Allograft vs Isograft in Skin Random Forest (POD > 5, 50 trees, feature selected)

Accuracy	**Confusion Matrix**			
100%	*Classified As*			
p-value	Allograft	Isograft		
.0730	23	0	Allograft	*True Class*
	1	41	Isograft	

Table 6.41

CTA Allograft vs Isograft in Skin Random Forest (POD > 5, 50 trees, MANOVA transformed)

Accuracy	**Confusion Matrix**			
96.92%	*Classified As*			
p-value	Allograft	Isograft		
.0849	22	1	Allograft	*True Class*
	1	41	Isograft	

Table 6.42

Rejecting versus Suppressed Tissue

CTA Rejecting vs Suppressed in Skin Linear Discriminant (FK Groups, feature selected)

Accuracy	Confusion Matrix			
75.00%	*Classified As*			
p-value	Rejecting	Suppressed		*True Class*
.2366	14	12	Rejecting	
	1	25	Suppressed	

Table 6.43

CTA Rejecting vs Suppressed in Skin Linear Discriminant (FK Groups, MANOVA transformed)

Accuracy	Confusion Matrix			
82.69%	*Classified As*			
p-value	Rejecting	Suppressed		*True Class*
.0017	21	5	Rejecting	
	4	22	Suppressed	

Table 6.44

CTA Rejecting vs Suppressed in Skin Quadratic Discriminant (FK Groups, feature selected)

Accuracy	Confusion Matrix			
78.85%	*Classified As*			
p-value	Rejecting	Suppressed		*True Class*
.0938	17	9	Rejecting	
	2	24	Suppressed	

Table 6.45

CTA Rejecting vs Suppressed in Skin Quadratic Discriminant (FK Groups, MANOVA transformed)

Accuracy	Confusion Matrix			
84.62%	*Classified As*			
p-value	Rejecting	Suppressed		*True Class*
.0061	23	3	Rejecting	
	5	21	Suppressed	

Table 6.46

CTA Rejecting vs Suppressed in Skin Logistic Classifier (FK Groups, feature selected)

Accuracy	Confusion Matrix	
88.46%	*Classified As*	*True*
p-value		

.0194	Rejecting	Suppressed		
	5	21	Rejecting	
	25	1	Suppressed	

Table 6.47

CTA Rejecting vs Suppressed in Skin Logistic Classifier (FK Groups, MANOVA transformed)

Accuracy	**Confusion Matrix**			
80.77%	*Classified As*			
p-value	Rejecting	Suppressed		
<.0001	5	21	Rejecting	*True Class*
	21	5	Suppressed	

Table 6.48

CTA Rejecting vs Suppressed in Skin Decision Tree (FK Groups, pruned tree, feature selected)

Accuracy	**Confusion Matrix**			
84.62%	*Classified As*			
p-value	Rejecting	Suppressed		
.0194	25	1	Rejecting	*True Class*
	5	21	Suppressed	

Table 6.49

CTA Rejecting vs Suppressed in Skin Decision Tree (FK Groups, pruned tree, MANOVA transformed)

Accuracy	**Confusion Matrix**			
94.23%	*Classified As*			
p-value	Rejecting	Suppressed		
<.0001	23	3	Rejecting	*True Class*
	3	23	Suppressed	

Table 6.50

CTA Rejecting vs Suppressed in Skin Random Forest (FK Groups, 50 trees, feature selected)

Accuracy	**Confusion Matrix**			
84.62%	*Classified As*			
p-value	Rejecting	Suppressed		
.0019	25	1	Rejecting	*True Class*
	5	21	Suppressed	

Table 6.51

CTA Rejecting vs Suppressed in Skin Random Forest (FK Groups, 50 trees,

MANOVA transformed)

Accuracy	**Confusion Matrix**			
90.38%	*Classified As*			
p-value	Rejecting	Suppressed		
.0101	25	1	Rejecting	*True Class*
	4	22	Suppressed	

Table 6.52

Hypothesis 1 Muscle

Allograft vs Isograft

All Time Points

CTA Allograft vs Isograft in Muscle Linear Discriminant (all time points, feature selected)

Accuracy	Confusion Matrix			
73.39%	*Classified As*			
p-value	Allograft	Isograft		
.3206	26	27	Allograft	*True Class*
	6	65	Isograft	

Table 6.53

CTA Allograft vs Isograft in Muscle Linear Discriminant (all time points, MANOVA transformed)

Accuracy	Confusion Matrix			
73.39%	*Classified As*			
p-value	Allograft	Isograft		
.2979	27	26	Allograft	*True Class*
	7	64	Isograft	

Table 6.54

Allograft vs Isograft in Muscle Quadratic Discriminant (all time points, feature selected)

Accuracy	Confusion Matrix			
70.97%	*Classified As*			
p-value	Allograft	Isograft		
.3496	25	28	Allograft	*True Class*
	8	63	Isograft	

Table 6.55

CTA Allograft vs Isograft in Muscle Quadratic Discriminant (all time points, MANOVA transformed)

Accuracy	Confusion Matrix			
80.65%	*Classified As*			
p-value	Allograft	Isograft		
.1616	34	19	Allograft	*True Class*
	5	66	Isograft	

Table 6.56

CTA Allograft vs Isograft in Muscle Logistic Classifier (all time points, feature selected)

Accuracy	Confusion Matrix			
75.81%	*Classified As*			
p-value	Allograft	Isograft		
.1861	32	21	Allograft	*True Class*
	9	62	Isograft	

Table 6.57

CTA Allograft vs Isograft in Muscle Logistic Classifier (all time points, MANOVA transformed)

Accuracy	Confusion Matrix			
78.23%	*Classified As*			
p-value	Allograft	Isograft		
.1526	34	19	Allograft	*True Class*
	8	63	Isograft	

Table 6.58

CTA Allograft vs Isograft in Muscle Logistic Classifier (all time points, hybrid features)

Accuracy	Confusion Matrix			
78.23%	*Classified As*			
p-value	Allograft	Isograft		
.1727	33	20	Allograft	*True Class*
	7	64	Isograft	

Table 6.59

CTA Allograft vs Isograft in Muscle Decision Tree (all time points, pruned tree, feature selected)

Accuracy	Confusion Matrix			
80.65%	*Classified As*			
p-value	Allograft	Isograft		
.0385	42	11	Allograft	*True Class*
	15	56	Isograft	

Table 6.60

CTA Allograft vs Isograft in Muscle Decision Tree (all time points, MANOVA transformed, pruned tree)

Accuracy	Confusion Matrix			
82.26%	*Classified As*			
p-value	Allograft	Isograft		
.1672	33	20	Allograft	*True Class*

	9	62	Isograft	

Table 6.61

CTA Allograft vs Isograft in Muscle Decision Tree (all time points, hybrid features, pruned tree)

Accuracy	**Confusion Matrix**			
84.68%	*Classified As*			
p-value	Allograft	Isograft		
.1284	36	17	Allograft	*True Class*
	6	65	Isograft	

Table 6.62

CTA Allograft vs Isograft in Muscle Random Forest (all time points, 50 trees, feature selected)

Accuracy	**Confusion Matrix**			
91.94%	*Classified As*			
p-value	Allograft	Isograft		
.0309	47	6	Allograft	*True Class*
	6	65	Isograft	

Table 6.63

CTA Allograft vs Isograft in Muscle Random Forest (all time points, MANOVA transformed, 50 trees)

Accuracy	**Confusion Matrix**			
87.10%	*Classified As*			
p-value	Allograft	Isograft		
.0394	44	9	Allograft	*True Class*
	9	62	Isograft	

Table 6.64

POD <= 5

CTA Allograft vs Isograft in Muscle Linear Discriminant (POD <= 5)

Accuracy	Confusion Matrix			
81.57%	*Classified As*			
p-value	Allograft	Isograft		
.0299	28	10	Allograft	*True Class*
	4	34	Isograft	

Table 6.65

CTA Allograft vs Isograft in Muscle Linear Discriminant (POD <= 5, feature selected)

Accuracy	Confusion Matrix			
68.42%	*Classified As*			
p-value	Allograft	Isograft		
.3861	17	21	Allograft	*True Class*
	3	35	Isograft	

Table 6.66

CTA Allograft vs Isograft in Muscle Linear Discriminant (POD <= 5, MANOVA transformed)

Accuracy	Confusion Matrix			
82.89%	*Classified As*			
p-value	Allograft	Isograft		
.0194	29	9	Allograft	*True Class*
	4	34	Isograft	

Table 6.67

CTA Allograft vs Isograft in Muscle Quadratic Discriminant (POD <= 5, feature selected)

Accuracy	Confusion Matrix			
71.05%	*Classified As*			
p-value	Allograft	Isograft		
.2000	21	17	Allograft	*True Class*
	5	33	Isograft	

Table 6.68

CTA Allograft vs Isograft in Muscle Logistic Classifier (POD <= 5)

Accuracy	Confusion Matrix			
77.63%	*Classified As*			
p-value	Allograft	Isograft		
.0101	28	10	Allograft	*True Class*
	7	31	Isograft	

Table 6.69

CTA Allograft vs Isograft in Muscle Logistic Classifier (POD <= 5, feature selected)

Accuracy	Confusion Matrix			
60.53%	*Classified As*			
p-value	Allograft	Isograft		
.4453	17	21	Allograft	*True Class*
	9	29	Isograft	

Table 6.70

CTA Allograft vs Isograft in Muscle Logistic Classifier (POD <= 5, MANOVA transformed)

Accuracy	Confusion Matrix			
81.58%	*Classified As*			
p-value	Allograft	Isograft		
.0035	30	8	Allograft	*True Class*
	6	32	Isograft	

Table 6.71

CTA Allograft vs Isograft in Muscle Decision Tree (POD <= 5, pruned tree)

Accuracy	Confusion Matrix			
85.53%	*Classified As*			
p-value	Allograft	Isograft		
.0007	33	5	Allograft	*True Class*
	6	32	Isograft	

Table 6.72

CTA Allograft vs Isograft in Muscle Decision Tree (POD <= 5, pruned tree, feature selected)

Accuracy	Confusion Matrix			
77.63%	*Classified As*			
p-value	Allograft	Isograft		
.0007	33	5	Allograft	*True Class*
	6	32	Isograft	

Table 6.73

CTA Allograft vs Isograft in Muscle Decision Tree (POD <= 5, pruned tree, MANOVA transformed)

Accuracy	Confusion Matrix			
82.90%	*Classified As*			
p-value	Allograft	Isograft		
.0017	27	11	Allograft	*True Class*

	10	28	Isograft	

Table 6.74

CTA Allograft vs Isograft in Muscle Random Forest (POD <= 5, 50 trees)

Accuracy	Confusion Matrix			
98.68%	*Classified As*			*True Class*
p-value	Allograft	Isograft		
<.0001	36	2	Allograft	
	2	36	Isograft	

Table 6.75

CTA Allograft vs Isograft in Muscle Random Forest (POD <= 5, 50 trees, feature selected)

Accuracy	Confusion Matrix			
94.74%	*Classified As*			*True Class*
p-value	Allograft	Isograft		
.0012	34	4	Allograft	
	2	36	Isograft	

Table 6.76

CTA Allograft vs Isograft in Muscle Random Forest (POD <= 5, 50 trees, MANOVA transformed)

Accuracy	Confusion Matrix			
84.21%	*Classified As*			*True Class*
p-value	Allograft	Isograft		
.0025	34	4	Allograft	
	6	32	Isograft	

Table 6.77

POD > 5

CTA Allograft vs Isograft in Muscle Linear Discriminant (POD > 5)

Accuracy	Confusion Matrix			
87.50%	*Classified As*			
p-value	Allograft	Isograft		
.2152	11	4	Allograft	*True Class*
	2	31	Isograft	

Table 6.78

CTA Allograft vs Isograft in Muscle Linear Discriminant (POD > 5, feature selected)

Accuracy	Confusion Matrix			
87.50%	*Classified As*			
p-value	Allograft	Isograft		
.2487	10	5	Allograft	*True Class*
	1	32	Isograft	

Table 6.79

CTA Allograft vs Isograft in Muscle Linear Discriminant (POD > 5, MANOVA transformed)

Accuracy	Confusion Matrix			
89.53%	*Classified As*			
p-value	Allograft	Isograft		
.2151	11	4	Allograft	*True Class*
	1	32	Isograft	

Table 6.80

CTA Allograft vs Isograft in Muscle Quadratic Discriminant (POD > 5, feature selected)

Accuracy	Confusion Matrix			
91.67%	*Classified As*			
p-value	Allograft	Isograft		
.1109	15	0	Allograft	*True Class*
	4	29	Isograft	

Table 6.81

CTA Allograft vs Isograft in Muscle Logistic Classifier (POD > 5)

Accuracy	Confusion Matrix			
91.67%	*Classified As*			
p-value	Allograft	Isograft		
.1313	14	1	Allograft	*True Class*
	3	30	Isograft	

Table 6.82

CTA Allograft vs Isograft in Muscle Logistic Classifier (POD > 5, feature selected)

Accuracy	Confusion Matrix			
97.92%	*Classified As*			
p-value	Allograft	Isograft		
.1368	14	1	Allograft	*True Class*
	0	33	Isograft	

Table 6.83

CTA Allograft vs Isograft in Muscle Logistic Classifier (POD > 5, MANOVA transformed)

Accuracy	Confusion Matrix			
95.83%	*Classified As*			
p-value	Allograft	Isograft		
.1344	14	1	Allograft	*True Class*
	1	32	Isograft	

Table 6.84

CTA Allograft vs Isograft in Muscle Decision Tree (POD > 5, pruned tree)

Accuracy	Confusion Matrix			
95.83%	*Classified As*			
p-value	Allograft	Isograft		
.2155	11	4	Allograft	*True Class*
	0	33	Isograft	

Table 6.85

CTA Allograft vs Isograft in Muscle Decision Tree (POD > 5, pruned tree, feature selected)

Accuracy	Confusion Matrix			
93.75%	*Classified As*			
p-value	Allograft	Isograft		
.2155	11	4	Allograft	*True Class*
	0	33	Isograft	

Table 6.86

CTA Allograft vs Isograft in Muscle Decision Tree (POD > 5, pruned tree, MANOVA transformed)

CV Accuracy	Confusion Matrix			
93.75%	*Classified As*			
p-value	Allograft	Isograft		
.2155	11	4	Allograft	*True Class*
	0	33	Isograft	

Table 6.87

CTA Allograft vs Isograft in Muscle Random Forest (POD > 5, 50 trees)

Accuracy	Confusion Matrix			
97.92%	*Classified As*			
p-value	Allograft	Isograft		
.1368	14	1	Allograft	*True Class*
	0	33	Isograft	

Table 6.88

CTA Allograft vs Isograft in Muscle Random Forest (POD > 5, 50 trees, feature selected)

Accuracy	Confusion Matrix			
95.83%	*Classified As*			
p-value	Allograft	Isograft		
.1368	14	1	Allograft	*True Class*
	0	33	Isograft	

Table 6.89

CTA Allograft vs Isograft in Muscle Random Forest (POD > 5, 50 trees, MANOVA transformed)

Accuracy	Confusion Matrix			
93.75%	*Classified As*			
p-value	Allograft	Isograft		
.1580	13	2	Allograft	*True Class*
	1	32	Isograft	

Table 6.90

Rejecting versus Suppressed Muscle

CTA Rejecting vs Suppressed in Muscle Linear Discriminant (FK Groups, feature selected)

Accuracy	Confusion Matrix			
72.55%	*Classified As*			
p-value	Rejecting	Suppressed		
.1629	15	11	Rejecting	*True Class*
	3	22	Suppressed	

Table 6.91

CTA Rejecting vs Suppressed in Muscle Linear Discriminant (FK Groups, MANOVA transformed)

Accuracy	Confusion Matrix			
82.35%	*Classified As*			
p-value	Rejecting	Suppressed		
.0046	22	4	Rejecting	*True Class*
	5	20	Suppressed	

Table 6.92

CTA Rejecting vs Suppressed in Muscle Quadratic Discriminant (FK Groups, feature selected)

Accuracy	Confusion Matrix			
62.75%	*Classified As*			
p-value	Rejecting	Suppressed		
.6134	24	2	Rejecting	*True Class*
	17	8	Suppressed	

Table 6.93

CTA Rejecting vs Suppressed in Muscle Quadratic Discriminant (FK Groups, MANOVA transformed)

Accuracy	Confusion Matrix			
84.31%	*Classified As*			
p-value	Rejecting	Suppressed		
.0008	22	4	Rejecting	*True Class*
	4	21	Suppressed	

Table 6.94

CTA Rejecting vs Suppressed in Muscle Logistic Classifier (FK Groups, feature selected)

Accuracy	Confusion Matrix			
70.59%	*Classified As*			
p-value	Rejecting	Suppressed		
.0817	10	16	Rejecting	*True Class*
	20	5	Suppressed	

Table 6.95

CTA Rejecting vs Suppressed in Muscle Logistic Classifier (FK Groups, MANOVA transformed)

Accuracy	**Confusion Matrix**			
74.51%	*Classified As*			
p-value	Rejecting	Suppressed		
.0201	8	18	Rejecting	*True Class*
	20	5	Suppressed	

Table 6.96

CTA Rejecting vs Suppressed in Muscle Decision Tree (FK Groups, pruned tree, feature selected)

Accuracy	**Confusion Matrix**			
74.51%	*Classified As*			
p-value	Rejecting	Suppressed		
.0282	17	9	Rejecting	*True Class*
	6	19	Suppressed	

Table 6.97

CTA Rejecting vs Suppressed in Muscle Decision Tree (FK Groups, pruned tree, MANOVA transformed)

Accuracy	**Confusion Matrix**			
94.12%	*Classified As*			
p-value	Rejecting	Suppressed		
.4319	12	14	Rejecting	*True Class*
	7	18	Suppressed	

Table 6.98

CTA Rejecting vs Suppressed in Muscle Random Forest (FK Groups, 50 trees, feature selected)

Accuracy	**Confusion Matrix**			
72.55%	*Classified As*			
p-value	Rejecting	Suppressed		
.0019	19	7	Rejecting	*True Class*
	7	18	Suppressed	

Table 6.99

CTA Rejecting vs Suppressed in Muscle Random Forest (FK Groups, 50 trees, MANOVA transformed)

Accuracy	**Confusion Matrix**			
88.24%	*Classified As*			
p-value	Rejecting	Suppressed		
.0036	23	3	Rejecting	*True Class*
	4	21	Suppressed	

Table 6.100

Hypothesis 2 Allograft

All Time Points

CTA Allograft Skin vs Muscle Logistic Classifier (all time points)

Accuracy	**Confusion Matrix**			
86.17%	*Classified As*			
p-value	Muscle	Skin		
.0254	35	6	Muscle	*True Class*
	7	46	Skin	

Table 6.101

CTA Allograft Skin vs Muscle Decision Tree (all time points, pruned tree)

Accuracy	**Confusion Matrix**			
95.74%	*Classified As*			
p-value	Muscle	Skin		
.0260	38	3	Muscle	*True Class*
	1	52	Skin	

Table 6.102

POD <= 5

CTA Allograft Skin vs Muscle Linear Discriminant (POD <= 5)

Accuracy	**Confusion Matrix**			
70.00%	*Classified As*			
p-value	Muscle	Skin		
.1429	22	4	Muscle	*True Class*
	14	20	Skin	

Table 6.103

CTA Allograft Skin vs Muscle Logistic Classifier (POD <= 5)

Accuracy	**Confusion Matrix**			
78.33%	*Classified As*			
p-value	Muscle	Skin		
.0406	20	6	Muscle	*True Class*
	7	27	Skin	

Table 6.104

CTA Allograft Skin vs Muscle Decision Tree (POD <= 5 pruned tree)

Accuracy	**Confusion Matrix**			
98.33%	*Classified As*			
p-value	Muscle	Skin		
.0316	24	2	Muscle	*True Class*
	0	34	Skin	

Table 6.105

CTA Allograft Skin vs Muscle Random Forest (POD <= 5, 50 trees)

Accuracy	**Confusion Matrix**			
96.67%	*Classified As*			*True Class*
p-value	Muscle	Skin		
.0235	25	1	Muscle	
	0	34	Skin	

Table 6.106

POD > 5

CTA Allograft Skin vs Muscle Linear Discriminant (POD > 5)

Accuracy	Confusion Matrix			
85.29%	*Classified As*			
p-value	Muscle	Skin		
.0169	14	1	Muscle	*True Class*
	4	15	Skin	

Table 6.107

CTA Allograft Skin vs Muscle Logistic Classifier (POD > 5)

Accuracy	Confusion Matrix			
76.47%	*Classified As*			
p-value	Muscle	Skin		
.0630	10	5	Muscle	*True Class*
	6	13	Skin	

Table 6.108

CTA Allograft Skin vs Muscle Decision Tree (POD > 5 pruned tree)

Accuracy	Confusion Matrix			
91.18%	*Classified As*			
p-value	Muscle	Skin		
.0316	13	2	Muscle	*True Class*
	1	18	Skin	

Table 6.109

CTA Allograft Skin vs Muscle Random Forest (POD > 5, 50 trees)

Accuracy	Confusion Matrix			
91.18%	*Classified As*			
p-value	Muscle	Skin		
.0417	13	2	Muscle	*True Class*
	0	19	Skin	

Table 6.110

Hypothesis 2 Isograft

All Time Points

CTA Isograft Skin vs Muscle Logistic Classifier (all time points)

Accuracy	Confusion Matrix			
94.12%	*Classified As*			
p-value	Muscle	Skin		
.0015	54	3	Muscle	*True Class*
	4	58	Skin	

Table 6.111

CTA Isograft Skin vs Muscle Decision Tree (all time points, pruned tree)

Accuracy	Confusion Matrix			
96.64%	*Classified As*			
p-value	Muscle	Skin		
.0014	55	2	Muscle	*True Class*
	3	59	Skin	

Table 6.112

POD <= 5

CTA Isograft Skin vs Muscle Linear Discriminant (POD <= 5)

Accuracy	Confusion Matrix			
93.75%	*Classified As*			
p-value	Muscle	Skin		
.0101	24	0	Muscle	*True Class*
	3	21	Skin	

Table 6.113

CTA Isograft Skin vs Muscle Logistic Classifier (POD <= 5)

Accuracy	Confusion Matrix			
77.08%	*Classified As*			
p-value	Muscle	Skin		
.0194	18	6	Muscle	*True Class*
	8	16	Skin	

Table 6.114

CTA Isograft Skin vs Muscle Decision Tree (POD <= 5 pruned tree)

Accuracy	Confusion Matrix			
97.92%	*Classified As*			
p-value	Muscle	Skin		
.0009	24	0	Muscle	*True Class*
	1	23	Skin	

Table 6.115

CTA Isograft Skin vs Muscle Random Forest (POD <= 5, 50 trees)				
Accuracy	**Confusion Matrix**			
98.50%	*Classified As*			
p-value	Muscle	Skin		
.0041	24	0	Muscle	*True Class*
	2	22	Skin	

Table 6.116

POD > 5

CTA Isograft Skin vs Muscle Linear Discriminant (POD > 5)

Accuracy	Confusion Matrix			
87.32%	*Classified As*			
p-value	Muscle	Skin		
.0329	33	0	Muscle	*True Class*
	9	29	Skin	

Table 6.117

CTA Isograft Skin vs Muscle Logistic Classifier (POD > 5)

Accuracy	Confusion Matrix			
88.73%	*Classified As*			
p-value	Muscle	Skin		
.0043	30	3	Muscle	*True Class*
	5	33	Skin	

Table 6.118

CTA Isograft Skin vs Muscle Decision Tree (POD > 5 pruned tree)

Accuracy	Confusion Matrix			
97.18%	*Classified As*			
p-value	Muscle	Skin		
.0055	32	1	Muscle	*True Class*
	1	37	Skin	

Table 6.119

CTA Isograft Skin vs Muscle Random Forest (POD > 5, 50 trees)

Accuracy	Confusion Matrix			
98.59%	*Classified As*			
p-value	Muscle	Skin		
.0049	33	0	Muscle	*True Class*
	0	38	Skin	

Table 6.120

Hypothesis 2 FK-Treated

CTA FK-Treated Allograft Skin vs Muscle Logistic Classifier (all time points under treatment)

Accuracy	Confusion Matrix			
74.42%	*Classified As*			
p-value	Muscle	Skin		
.0014	17	4	Muscle	*True Class*
	4	18	Skin	

Table 6.121

CTA FK-Treated Allograft Skin vs Muscle Decision Tree (all time points under treatment)

Accuracy	Confusion Matrix			
90.97%	*Classified As*			
p-value	Muscle	Skin		
.0133	17	4	Muscle	*True Class*
	2	20	Skin	

Table 6.122

Hypothesis 2 FK-Treatment Withdrawn

CTA FK-Treatment Withdrawn Allograft Skin vs Muscle Logistic Classifier (all time points treatment withdrawn)

Accuracy	Confusion Matrix			
95.00%	*Classified As*			
p-value	Muscle	Skin		
.0011	26	4	Muscle	*True Class*
	5	25	Skin	

Table 6.123

CTA FK-Treatment Withdrawn Allograft Skin vs Muscle Decision Tree (all time points treatment withdrawn)

Accuracy	Confusion Matrix			
100%	*Classified As*			
p-value	Muscle	Skin		
<.0001	30	0	Muscle	*True Class*
	0	30	Skin	

Table 6.124

Hypothesis 2 Naïve

Naive Skin vs Muscle Logistic Classifier

Accuracy	**Confusion Matrix**			
74.07%	*Classified As*			
p-value	Muscle	Skin		
.3884	6	3	Muscle	*True Class*
	7	11	Skin	

Table 6.125

Naive Skin vs Muscle Decision Tree (pruned tree)

Accuracy	**Confusion Matrix**			
85.19%	*Classified As*			
p-value	Muscle	Skin		
.1692	7	2	Muscle	*True Class*
	2	16	Skin	

Table 6.126

Hypothesis 3 Skin

Rejection vs Not Rejection

All Time Points

Rejection vs Not Rejection in Skin Linear Discriminant (all time points, feature selected)

Accuracy	Confusion Matrix			
64.89%	*Classified As*			
p-value	Not Rejection	Rejection		
.5954	154	25	Not Rejection	*True Class*
	74	29	Rejection	

Table 6.127

Rejection vs Not Rejection in Skin Linear Discriminant (all time points, MANOVA transformed)

Accuracy	Confusion Matrix			
68.09%	*Classified As*			
p-value	Not Rejection	Rejection		
.3792	141	38	Not Rejection	*True Class*
	52	51	Rejection	

Table 6.128

Rejection vs Not Rejection in Skin Quadratic Discriminant (all time points, feature selected)

Accuracy	Confusion Matrix			
71.28%	*Classified As*			
p-value	Not Rejection	Rejection		
.5267	172	7	Not Rejection	*True Class*
	74	29	Rejection	

Table 6.129

Rejection vs Not Rejection in Skin Quadratic Discriminant (all time points, MANOVA transformed)

Accuracy	Confusion Matrix			
76.60%	*Classified As*			
p-value	Not Rejection	Rejection		
.3838	171	8	Not Rejection	*True Class*
	58	45	Rejection	

Table 6.130

Rejection vs Not Rejection in Skin Logistic Classifier (all time points, feature selected)

Accuracy	Confusion Matrix			
68.09%	*Classified As*			
p-value	Not Rejection	Rejection		
.5816	12	167	Not Rejection	*True Class*
	25	78	Rejection	

Table 6.131

Rejection vs Not Rejection in Skin Logistic Classifier (all time points, MANOVA transformed)

Accuracy	Confusion Matrix			
72.70%	*Classified As*			
p-value	Not Rejection	Rejection		
.4104	18	161	Not Rejection	*True Class*
	44	59	Rejection	

Table 6.132

Rejection vs Not Rejection in Skin Logistic Classifier (all time points, hybrid features)

Accuracy	Confusion Matrix			
76.95%	*Classified As*			
p-value	Not Rejection	Rejection		
.3304	15	164	Not Rejection	*True Class*
	52	51	Rejection	

Table 6.133

Rejection vs Not Rejection in Skin Decision Tree (all time points, feature selected, pruned tree)

Accuracy	Confusion Matrix			
79.08%	*Classified As*			
p-value	Not Rejection	Rejection		
.1426	138	41	Not Rejection	*True Class*
	26	77	Rejection	

Table 6.134

Rejection vs Not Rejection in Skin Decision Tree (all time points, MANOVA transformed, pruned tree)

Accuracy	Confusion Matrix			
81.56%	*Classified As*			
p-value	Not Rejection	Rejection		
.2249	157	22	Not Rejection	*True Class*
	38	65	Rejection	

Table 6.135

Rejection vs Not Rejection in Skin Decision Tree (all time points, hybrid features, pruned tree)

Accuracy	**Confusion Matrix**			
87.59%	*Classified As*			
p-value	Not Rejection	Rejection		
.1417	159	20	Not Rejection	*True Class*
	25	78	Rejection	

Table 6.136

Rejection vs Not Rejection in Skin Random Forest (all time points, feature selected, 100 trees)

Accuracy	**Confusion Matrix**			
84.04%	*Classified As*			
p-value	Not Rejection	Rejection		
.1095	153	26	Not Rejection	*True Class*
	19	84	Rejection	

Table 6.137

Rejection vs Not Rejection in Skin Random Forest (all time points, MANOVA transformed, 100 trees)

Accuracy	**Confusion Matrix**			
87.23%	*Classified As*			
p-value	Not Rejection	Rejection		
.0942	161	18	Not Rejection	*True Class*
	14	89	Rejection	

Table 6.138

POD <= 5

Rejection vs Not Rejection in Skin Linear Discriminant (POD <= 5)

Accuracy	Confusion Matrix			
72.25%	*Classified As*			
p-value	Not Rejection	Rejection		
.3023	90	29	Not Rejection	*True Class*
	19	35	Rejection	

Table 6.139

Rejection vs Not Rejection in Skin Linear Discriminant (POD <= 5, feature selected)

Accuracy	Confusion Matrix			
66.47%	*Classified As*			
p-value	Not Rejection	Rejection		
.5406	96	23	Not Rejection	*True Class*
	35	19	Rejection	

Table 6.140

Rejection vs Not Rejection in Skin Linear Discriminant (POD <= 5, MANOVA transformed)

Accuracy	Confusion Matrix			
71.01%	*Classified As*			
p-value	Not Rejection	Rejection		
.3216	89	30	Not Rejection	*True Class*
	20	34	Rejection	

Table 6.141

Rejection vs Not Rejection in Skin Quadratic Discriminant (POD <= 5)

Accuracy	Confusion Matrix			
75.14%	*Classified As*			
p-value	Not Rejection	Rejection		
.2226	88	31	Not Rejection	*True Class*
	12	42	Rejection	

Table 6.142

Rejection vs Not Rejection in Skin Quadratic Discriminant (POD <= 5, feature selected)

Accuracy	Confusion Matrix			
66.47%	*Classified As*			
p-value	Not Rejection	Rejection		
.6081	103	16	Not Rejection	*True Class*
	42	12	Rejection	

Table 6.143

Rejection vs Not Rejection in Skin Quadratic Discriminant (POD <= 5, MANOVA transformed)

Accuracy	Confusion Matrix			
74.57%	*Classified As*			
p-value	Not Rejection	Rejection		
.2265	87	32	Not Rejection	*True Class*
	12	42	Rejection	

Table 6.144

Rejection vs Not Rejection in Skin Logistic Classifier (POD <= 5)

Accuracy	Confusion Matrix			
74.57%	*Classified As*			
p-value	Not Rejection	Rejection		
.4435	108	11	Not Rejection	*True Class*
	33	21	Rejection	

Table 6.145

Rejection vs Not Rejection in Skin Logistic Classifier (POD <= 5, feature selected)

Accuracy	Confusion Matrix			
68.21%	*Classified As*			
p-value	Not Rejection	Rejection		
.6202	110	9	Not Rejection	*True Class*
	46	8	Rejection	

Table 6.146

Rejection vs Not Rejection in Skin Logistic Classifier (POD <= 5, MANOVA transformed)

Accuracy	Confusion Matrix			
72.83%	*Classified As*			
p-value	Not Rejection	Rejection		
.4558	105	14	Not Rejection	*True Class*
	33	21	Rejection	

Table 6.147

Rejection vs Not Rejection in Skin Decision Tree (POD <= 5, pruned tree)

Accuracy	Confusion Matrix	
80.92%	*Classified As*	*True*
p-value		

.3195	Not Rejection	Rejection		
	103	16	Not Rejection	
	23	31	Rejection	

Table 6.148

Rejection vs Not Rejection in Skin Decision Tree (POD <= 5, feature selected, pruned tree)

Accuracy	**Confusion Matrix**			
78.61%	*Classified As*			
p-value	Not Rejection	Rejection		
.3850	100	19	Not Rejection	*True Class*
	27	27	Rejection	

Table 6.149

Rejection vs Not Rejection in Skin Decision Tree (POD <= 5, MANOVA transformed, pruned tree)

Accuracy	**Confusion Matrix**			
87.86%	*Classified As*			
p-value	Not Rejection	Rejection		
.2243	104	15	Not Rejection	*True Class*
	15	39	Rejection	

Table 6.150

Rejection vs Not Rejection in Skin Random Forest (POD <= 5, 100 trees)

Accuracy	**Confusion Matrix**			
95.95%	*Classified As*			
p-value	Not Rejection	Rejection		
.1505	116	3	Not Rejection	*True Class*
	6	48	Rejection	

Table 6.151

Rejection vs Not Rejection in Skin Random Forest (POD <= 5, feature selected, 100 trees)

Accuracy	**Confusion Matrix**			
84.39%	*Classified As*			
p-value	Not Rejection	Rejection		
.2320	108	11	Not Rejection	*True Class*
	16	38	Rejection	

Table 6.152

Rejection vs Not Rejection in Skin Random Forest (POD <= 5, MANOVA transformed, 100 trees)

Accuracy	**Confusion Matrix**	
91.33%	*Classified As*	*True*

p-value	Not Rejection	Rejection		
.1943	112	7	Not Rejection	
	12	42	Rejection	

Table 6.153

POD > 5

Rejection vs Not Rejection in Skin Linear Discriminant (POD > 5)

Accuracy	Confusion Matrix			
80.00%	*Classified As*			
p-value	Not Rejection	Rejection		
.3251	104	12	Not Rejection	*True Class*
	21	28	Rejection	

Table 6.154

Rejection vs Not Rejection in Skin Linear Discriminant (POD > 5, feature selected)

Accuracy	Confusion Matrix			
67.88%	*Classified As*			
p-value	Not Rejection	Rejection		
.5991	102	14	Not Rejection	*True Class*
	39	10	Rejection	

Table 6.155

Rejection vs Not Rejection in Skin Linear Discriminant (POD > 5, MANOVA transformed)

Accuracy	Confusion Matrix			
76.36%	*Classified As*			
p-value	Not Rejection	Rejection		
.3845	102	14	Not Rejection	*True Class*
	25	24	Rejection	

Table 6.156

Rejection vs Not Rejection in Skin Quadratic Discriminant (POD > 5)

Accuracy	Confusion Matrix			
83.64%	*Classified As*			
p-value	Not Rejection	Rejection		
.2917	108	8	Not Rejection	*True Class*
	19	30	Rejection	

Table 6.157

Rejection vs Not Rejection in Skin Quadratic Discriminant (POD > 5, feature selected)

Accuracy	Confusion Matrix			
77.58%	*Classified As*			
p-value	Not Rejection	Rejection		
.4504	111	5	Not Rejection	*True Class*
	32	17	Rejection	

Table 6.158

Rejection vs Not Rejection in Skin Quadratic Discriminant (POD > 5, MANOVA transformed)

Accuracy	**Confusion Matrix**			
84.24%	*Classified As*			
p-value	Not Rejection	Rejection		
.2828	108	8	Not Rejection	*True Class*
	18	31	Rejection	

Table 6.159

Rejection vs Not Rejection in Skin Logistic Classifier (POD > 5)

Accuracy	**Confusion Matrix**			
76.97%	*Classified As*			
p-value	Not Rejection	Rejection		
.3813	13	103	Not Rejection	*True Class*
	24	25	Rejection	

Table 6.160

Rejection vs Not Rejection in Skin Logistic Classifier (POD > 5, feature selected)

Accuracy	**Confusion Matrix**			
72.12%	*Classified As*			
p-value	Not Rejection	Rejection		
.5804	4	112	Not Rejection	*True Class*
	7	42	Rejection	

Table 6.161

Rejection vs Not Rejection in Skin Logistic Classifier (POD > 5, MANOVA transformed)

Accuracy	**Confusion Matrix**			
80.00%	*Classified As*			
p-value	Not Rejection	Rejection		
.3463	10	106	Not Rejection	*True Class*
	26	23	Rejection	

Table 6.162

Rejection vs Not Rejection in Skin Decision Tree (POD > 5, pruned tree)

Accuracy	**Confusion Matrix**			
88.48%	*Classified As*			
p-value	Not Rejection	Rejection		
.1675	96	20	Not Rejection	*True Class*
	5	44	Rejection	

Table 6.163

Rejection vs Not Rejection in Skin Decision Tree (POD > 5, feature selected, pruned tree)

Accuracy	**Confusion Matrix**			
83.03%	*Classified As*			
p-value	Not Rejection	Rejection		
.4906	111	5	Not Rejection	*True Class*
	35	14	Rejection	

Table 6.164

Rejection vs Not Rejection in Skin Decision Tree (POD > 5, MANOVA transformed, pruned tree)

Accuracy	**Confusion Matrix**			
86.06%	*Classified As*			
p-value	Not Rejection	Rejection		
.2639	105	11	Not Rejection	*True Class*
	16	33	Rejection	

Table 6.165

Rejection vs Not Rejection in Skin Random Forest (POD > 5, 100 trees)

Accuracy	**Confusion Matrix**			
93.94%	*Classified As*			
p-value	Not Rejection	Rejection		
.1623	108	8	Not Rejection	*True Class*
	5	44	Rejection	

Table 6.166

Rejection vs Not Rejection in Skin Random Forest (POD > 5, feature selected, 100 trees)

Accuracy	**Confusion Matrix**			
90.91%	*Classified As*			
p-value	Not Rejection	Rejection		
.1775	107	9	Not Rejection	*True Class*
	7	42	Rejection	

Table 6.167

Rejection vs Not Rejection in Skin Random Forest (POD > 5, MANOVA transformed, 100 trees)

Accuracy	**Confusion Matrix**			
89.09%	*Classified As*			
p-value	Not Rejection	Rejection		
.2028	107	9	Not Rejection	*True Class*
	10	39	Rejection	

Table 6.168

Type of Inflammation

All Time Points

Type of Inflammation in Skin Linear Discriminant (all time points, feature selected)

Accuracy	Confusion Matrix				
50.71%	*Classified As*				
p-value	Rejection	Unspecific Inflammation	Wound Healing		
.9764	17	27	59	Rejection	*True Class*
	16	8	32	Unspecific Inflammation	
	2	3	118	Wound Healing	

Table 6.169

Type of Inflammation in Skin Linear Discriminant (all time points, MANOVA transformed)

Accuracy	Confusion Matrix				
64.18%	*Classified As*				
p-value	Rejection	Unspecific Inflammation	Wound Healing		
.3035	45	21	37	Rejection	*True Class*
	9	38	9	Unspecific Inflammation	
	12	13	98	Wound Healing	

Table 6.170

Type of Inflammation in Skin Quadratic Discriminant (all time points, feature selected)

Accuracy	Confusion Matrix				
59.57%	*Classified As*				
p-value	Rejection	Unspecific Inflammation	Wound Healing		
.6335	28	34	41	Rejection	*True Class*
	4	26	26	Unspecific Inflammation	
	1	8	114	Wound Healing	

Table 6.171

Type of Inflammation in Skin Quadratic Discriminant (all time points, MANOVA transformed)

Accuracy
67.02%
p-value
.2939

Confusion Matrix

Classified As			
Rejection	Unspecific Inflammation	Wound Healing	
48	26	29	Rejection
6	32	18	Unspecific Inflammation
4	10	109	Wound Healing

True Class

Table 6.172

Type of Inflammation in Skin Logistic Classifier (all time points, feature selected)

Accuracy
60.99%
p-value
.2905

Confusion Matrix

Classified As			
Rejection	Unspecific Inflammation	Wound Healing	
58	5	40	Rejection
32	1	23	Unspecific Inflammation
10	0	113	Wound Healing

True Class

Table 6.173

Type of Inflammation in Skin Logistic Classifier (all time points, MANOVA transformed)

Accuracy
68.09%
p-value
.3515

Confusion Matrix

Classified As			
Rejection	Unspecific Inflammation	Wound Healing	
62	15	26	Rejection
11	23	22	Unspecific Inflammation
6	20	107	Wound Healing

True Class

Table 6.174

Type of Inflammation in Skin Logistic Classifier (all time points, hybrid features)

Accuracy
70.21%

Confusion Matrix

Classified As	*True*

p-value
.3817

Rejection	Unspecific Inflammation	Wound Healing	
65	14	24	Rejection
10	25	21	Unspecific Inflammation
6	10	107	Wound Healing

Table 6.175

Type of Inflammation in Skin Decision Tree (all time points, feature selected, pruned tree)

Accuracy
75.18%
p-value
.1986

Confusion Matrix

Classified As			
Rejection	Unspecific Inflammation	Wound Healing	
80	4	19	Rejection
23	18	15	Unspecific Inflammation
16	4	103	Wound Healing

True Class

Table 6.176

Type of Inflammation in Skin Decision Tree (all time points, MANOVA transformed, pruned tree)

Accuracy
71.28%
p-value
.0790

Confusion Matrix

Classified As			
Rejection	Unspecific Inflammation	Wound Healing	
73	13	17	Rejection
15	35	6	Unspecific Inflammation
13	9	101	Wound Healing

True Class

Table 6.177

Type of Inflammation in Skin Decision Tree (all time points, hybrid features, pruned tree)

Accuracy
79.43%
p-value
.0604

Confusion Matrix

Classified As			
Rejection	Unspecific Inflammation	Wound Healing	
81	9	13	Rejection
13	35	8	Unspecific

True Class

			Inflammation	
12	7	104	Wound Healing	

Table 6.178

Type of Inflammation in Skin Random Forest (all time points, feature selected, 100 trees)

Accuracy	**Confusion Matrix**			
82.98%	*Classified As*			
p-value	Rejection	Unspecific Inflammation	Wound Healing	
.0719	90	0	13	Rejection
	21	30	5	Unspecific Inflammation
	11	1	111	Wound Healing
				True Class

Table 6.179

Type of Inflammation in Skin Random Forest (all time points, MANOVA transformed, 100 trees)

Accuracy	**Confusion Matrix**			
82.98%	*Classified As*			
p-value	Rejection	Unspecific Inflammation	Wound Healing	
.0421	84	1	18	Rejection
	13	39	4	Unspecific Inflammation
	10	3	110	Wound Healing
				True Class

Table 6.180

POD <= 5

Type of Inflammation in Skin Linear Discriminant (POD <= 5)

Accuracy	**Confusion Matrix**			
65.32%	*Classified As*			
p-value	Rejection	Unspecific Inflammation	Wound Healing	
.0724	29	7	18	Rejection
	12	34	10	Unspecific Inflammation
	9	4	50	Wound Healing
				True Class

Table 6.181

Type of Inflammation in Skin Linear Discriminant (POD <= 5, feature selected)

Accuracy	Confusion Matrix				
49.13%	*Classified As*				
p-value	Rejection	Unspecific Inflammation	Wound Healing		
.9579	15	13	26	Rejection	*True Class*
	14	14	28	Unspecific Inflammation	
	1	6	56	Wound Healing	

Table 6.182

Type of Inflammation in Skin Linear Discriminant (POD <= 5, MANOVA transformed)

Accuracy	Confusion Matrix				
64.16%	*Classified As*				
p-value	Rejection	Unspecific Inflammation	Wound Healing		
.0593	30	6	18	Rejection	*True Class*
	13	33	10	Unspecific Inflammation	
	11	4	48	Wound Healing	

Table 6.183

Type of Inflammation in Skin Quadratic Discriminant (POD <= 5)

Accuracy	Confusion Matrix				
69.36%	*Classified As*				
p-value	Rejection	Unspecific Inflammation	Wound Healing		
.0552	31	5	18	Rejection	*True Class*
	8	35	13	Unspecific Inflammation	
	0	9	54	Wound Healing	

Table 6.184

Type of Inflammation in Skin Quadratic Discriminant (POD <= 5, feature selected)

Accuracy	Confusion Matrix

47.40%

p-value

.8636

Classified As				
Rejection	Unspecific Inflammation	Wound Healing		
14	11	29	Rejection	*True Class*
11	15	30	Unspecific Inflammation	
3	7	53	Wound Healing	

Table 6.185

Type of Inflammation in Skin Quadratic Discriminant (POD <= 5, MANOVA transformed)

Accuracy

71.10%

p-value

.0432

Confusion Matrix

Classified As				
Rejection	Unspecific Inflammation	Wound Healing		
32	4	27	Rejection	*True Class*
8	36	12	Unspecific Inflammation	
1	7	55	Wound Healing	

Table 6.186

Type of Inflammation in Skin Logistic Classifier (POD <= 5)

Accuracy

68.79%

p-value

.0578

Confusion Matrix

Classified As				
Rejection	Unspecific Inflammation	Wound Healing		
27	11	16	Rejection	*True Class*
5	39	12	Unspecific Inflammation	
3	8	53	Wound Healing	

Table 6.187

Type of Inflammation in Skin Logistic Classifier (POD <= 5, feature selected)

Accuracy

54.34%

Confusion Matrix

Classified As	*True*

p-value
.0159

Rejection	Unspecific Inflammation	Wound Healing	
15	19	20	Rejection
15	22	19	Unspecific Inflammation
1	5	57	Wound Healing

Table 6.188

Type of Inflammation in Skin Logistic Classifier (POD <= 5, MANOVA transformed)

Accuracy
65.32%
p-value
.0515

Confusion Matrix

Classified As				
Rejection	Unspecific Inflammation	Wound Healing		
27	11	16	Rejection	*True Class*
10	37	9	Unspecific Inflammation	
5	9	49	Wound Healing	

Table 6.189

Type of Inflammation in Skin Decision Tree (POD <= 5, pruned tree)

Accuracy
73.41%
p-value
.0127

Confusion Matrix

Classified As				
Rejection	Unspecific Inflammation	Wound Healing		
38	6	10	Rejection	*True Class*
17	35	4	Unspecific Inflammation	
5	6	52	Wound Healing	

Table 6.190

Type of Inflammation in Skin Decision Tree (POD <= 5, feature selected, pruned tree)

Accuracy **Confusion Matrix**

63.58

p-value

.0427

Classified As				
Rejection	Unspecific Inflammation	Wound Healing		
31	12	11	Rejection	*True Class*
19	34	3	Unspecific Inflammation	
8	6	49	Wound Healing	

Table 6.191

Type of Inflammation in Skin Decision Tree (POD <= 5, MANOVA transformed, pruned tree)

Accuracy

73.99%

p-value

.0024

Confusion Matrix

Classified As				
Rejection	Unspecific Inflammation	Wound Healing		
42	7	5	Rejection	*True Class*
10	38	8	Unspecific Inflammation	
6	6	51	Wound Healing	

Table 6.192

Type of Inflammation in Skin Random Forest (POD <= 5, 100 trees)

Accuracy

86.71%

p-value

.0001

Confusion Matrix

Classified As				
Rejection	Unspecific Inflammation	Wound Healing		
47	2	5	Rejection	*True Class*
5	49	2	Unspecific Inflammation	
3	3	57	Wound Healing	

Table 6.193

Type of Inflammation in Skin Random Forest (POD <= 5, feature selected, 100 trees)

Accuracy

Confusion Matrix

79.19%

p-value

.0011

Classified As				
Rejection	Unspecific Inflammation	Wound Healing		
43	2	9	Rejection	*True Class*
13	41	2	Unspecific Inflammation	
6	4	53	Wound Healing	

Table 6.194

Type of Inflammation in Skin Random Forest (POD <= 5, MANOVA transformed, 100 trees)

Accuracy

87.28%

p-value

.0008

Confusion Matrix

Classified As				
Rejection	Unspecific Inflammation	Wound Healing		
45	3	6	Rejection	*True Class*
5	47	4	Unspecific Inflammation	
2	2	59	Wound Healing	

Table 6.195

POD > 5

Type of Inflammation in Skin Linear Discriminant (POD > 5)

Accuracy

75.76%

p-value

.0300

Confusion Matrix

Classified As				
Rejection	Unspecific Inflammation	Wound Healing		
27	11	11	Rejection	*True Class*
3	49	4	Unspecific Inflammation	
6	5	49	Wound Healing	

Table 6.196

Type of Inflammation in Skin Linear Discriminant (POD > 5, feature selected)

Accuracy

52.12%

p-value

.9151

Confusion Matrix

Classified As				
Rejection	Unspecific Inflammation	Wound Healing		
5	19	25	Rejection	*True Class*

5	22	29	Unspecific Inflammation	
0	1	59	Wound Healing	

Table 6.197

Type of Inflammation in Skin Linear Discriminant (POD > 5, MANOVA transformed)

Accuracy
76.36%
p-value
.0230

Confusion Matrix

Classified As				
Rejection	Unspecific Inflammation	Wound Healing		
27	11	11	Rejection	*True Class*
2	49	5	Unspecific Inflammation	
5	5	50	Wound Healing	

Table 6.198

Type of Inflammation in Skin Quadratic Discriminant (POD > 5)

Accuracy
78.79%
p-value
.0031

Confusion Matrix

Classified As				
Rejection	Unspecific Inflammation	Wound Healing		
38	6	5	Rejection	*True Class*
4	40	12	Unspecific Inflammation	
3	5	52	Wound Healing	

Table 6.199

Type of Inflammation in Skin Quadratic Discriminant (POD > 5, feature selected)

Accuracy
63.64%
p-value
.2697

Confusion Matrix

Classified As				
Rejection	Unspecific Inflammation	Wound Healing		
20	17	12	Rejection	*True Class*
2	32	22	Unspecific Inflammation	
1	6	53	Wound Healing	

Table 6.200

Type of Inflammation in Skin Quadratic Discriminant (POD > 5, MANOVA transformed)

Accuracy	**Confusion Matrix**				
80.61%	*Classified As*				
p-value	Rejection	Unspecific Inflammation	Wound Healing		
.0016	40	5	4	Rejection	*True Class*
	3	41	12	Unspecific Inflammation	
	3	5	52	Wound Healing	

Table 6.201

Type of Inflammation in Skin Logistic Classifier (POD > 5)

Accuracy	**Confusion Matrix**				
81.21%	*Classified As*				
p-value	Rejection	Unspecific Inflammation	Wound Healing		
.2429	36	10	3	Rejection	*True Class*
	3	45	8	Unspecific Inflammation	
	2	5	53	Wound Healing	

Table 6.202

Type of Inflammation in Skin Logistic Classifier (POD > 5, feature selected)

Accuracy	**Confusion Matrix**				
62.42%	*Classified As*				
p-value	Rejection	Unspecific Inflammation	Wound Healing		
.0091	10	21	18	Rejection	*True Class*
	3	35	18	Unspecific Inflammation	
	0	4	56	Wound Healing	

Table 6.203

Type of Inflammation in Skin Logistic Classifier (POD > 5, MANOVA transformed)

Accuracy	**Confusion Matrix**				
81.21%	*Classified As*				
p-value	Rejection	Unspecific Inflammation	Wound Healing		
.2123					*True Class*

	34	10	5	Rejection	
	2	44	10	Unspecific Inflammation	
	1	5	54	Wound Healing	

Table 6.204

Type of Inflammation in Skin Decision Tree (POD > 5, pruned tree)

Accuracy
78.18%
p-value
.0018

Confusion Matrix

Classified As				
Rejection	Unspecific Inflammation	Wound Healing		
36	7	6	Rejection	*True Class*
12	39	5	Unspecific Inflammation	
5	8	47	Wound Healing	

Table 6.205

Type of Inflammation in Skin Decision Tree (POD > 5, feature selected, pruned tree)

Accuracy
77.58%
p-value
.0103

Confusion Matrix

Classified As				
Rejection	Unspecific Inflammation	Wound Healing		
30	10	9	Rejection	*True Class*
9	44	3	Unspecific Inflammation	
6	12	42	Wound Healing	

Table 6.206

Type of Inflammation in Skin Decision Tree (POD > 5, MANOVA transformed, pruned tree)

Accuracy
68.48%
p-value
.5655

Confusion Matrix

Classified As				
Rejection	Unspecific Inflammation	Wound Healing		
3	17	29	Rejection	*True Class*
0	47	9	Unspecific Inflammation	
2	7	51	Wound Healing	

Table 6.207

Type of Inflammation in Skin Random Forest (POD > 5, 100 trees)

Accuracy
89.70%

p-value
.0006

Confusion Matrix

Classified As				*True Class*
Rejection	Unspecific Inflammation	Wound Healing		
46	0	3	Rejection	
5	51	0	Unspecific Inflammation	
5	4	51	Wound Healing	

Table 6.208

Type of Inflammation in Skin Random Forest (POD > 5, feature selected, 100 trees)

Accuracy
87.27%

p-value
.0001

Confusion Matrix

Classified As				*True Class*
Rejection	Unspecific Inflammation	Wound Healing		
43	1	5	Rejection	
4	50	2	Unspecific Inflammation	
6	1	53	Wound Healing	

Table 6.209

Type of Inflammation in Skin Random Forest (POD > 5, MANOVA transformed, 100 trees)

Accuracy
86.06%

p-value
.0004

Confusion Matrix

Classified As				*True Class*
Rejection	Unspecific Inflammation	Wound Healing		
40	3	6	Rejection	
4	50	2	Unspecific Inflammation	
8	2	50	Wound Healing	

Table 6.210

Hypothesis 3 Muscle

Rejection vs Not Rejection

All Time Points

Rejection vs Not Rejection in Muscle Linear Discriminant (all time points, feature selected)

Accuracy	Confusion Matrix			
67.51%	*Classified As*			
p-value	Not Rejection	Rejection		
.3516	94	24	Not Rejection	*True Class*
	40	39	Rejection	

Table 6.211

Rejection vs Not Rejection in Muscle Linear Discriminant (all time points, MANOVA transformed)

Accuracy	Confusion Matrix			
73.10%	*Classified As*			
p-value	Not Rejection	Rejection		
.3301	105	13	Not Rejection	*True Class*
	40	39	Rejection	

Table 6.212

Rejection vs Not Rejection in Muscle Logistic Classifier (all time points, feature selected)

Accuracy	Confusion Matrix			
74.11%	*Classified As*			
p-value	Not Rejection	Rejection		
.5445	107	11	Not Rejection	*True Class*
	54	25	Rejection	

Table 6.213

Rejection vs Not Rejection in Muscle Logistic Classifier (all time points, MANOVA transformed)

Accuracy	Confusion Matrix			
74.11%	*Classified As*			
p-value	Not Rejection	Rejection		
.3009	105	13	Not Rejection	*True Class*
	38	41	Rejection	

Table 6.214

Rejection vs Not Rejection in Muscle Logistic Classifier (all time points, hybrid features)

Accuracy	Confusion Matrix			
77.16%	*Classified As*			
p-value	Not Rejection	Rejection		
.2082	103	15	Not Rejection	*True Class*
	31	48	Rejection	

Table 6.215

Rejection vs Not Rejection in Muscle Decision Tree (all time points, feature selected, pruned tree)

Accuracy	Confusion Matrix			
78.17%	*Classified As*			
p-value	Not Rejection	Rejection		
.1409	93	25	Not Rejection	*True Class*
	26	53	Rejection	

Table 6.216

Rejection vs Not Rejection in Muscle Decision Tree (all time points, MANOVA transformed, pruned tree)

Accuracy	Confusion Matrix			
73.60%	*Classified As*			
p-value	Not Rejection	Rejection		
.1890	94	24	Not Rejection	*True Class*
	30	49	Rejection	

Table 6.217

Rejection vs Not Rejection in Muscle Decision Tree (all time points, hybrid features, pruned tree)

Accuracy	Confusion Matrix			
79.70%	*Classified As*			
p-value	Not Rejection	Rejection		
.1073	101	17	Not Rejection	*True Class*
	21	58	Rejection	

Table 6.218

Rejection vs Not Rejection in Muscle Random Forest (all time points, feature selected, 100 trees)

Accuracy	Confusion Matrix			
86.29%	*Classified As*			
p-value	Not Rejection	Rejection		
.0710	114	4	Not Rejection	*True Class*
	14	65	Rejection	

Table 6.219

Rejection vs Not Rejection in Muscle Random Forest (all time points, MANOVA transformed, 100 trees)

Accuracy	Confusion Matrix			
88.32%	*Classified As*			
p-value	Not Rejection	Rejection		
0.0682	107	11	Not Rejection	*True Class*
	13	66	Rejection	

Table 6.220

POD <= 5

Rejection vs Not Rejection in Muscle Linear Discriminant (POD <= 5)

Accuracy	Confusion Matrix			
74.29%	*Classified As*			
p-value	Not Rejection	Rejection		
.2987	57	10	Not Rejection	*True Class*
	17	21	Rejection	

Table 6.221

Rejection vs Not Rejection in Muscle Linear Discriminant (POD <= 5, feature selected)

Accuracy	Confusion Matrix			
67.62%	*Classified As*			
p-value	Not Rejection	Rejection		
.3815	52	15	Not Rejection	*True Class*
	19	19	Rejection	

Table 6.222

Rejection vs Not Rejection in Muscle Linear Discriminant (POD <= 5, MANOVA transformed)

Accuracy	Confusion Matrix			
74.29%	*Classified As*			
p-value	Not Rejection	Rejection		
.3216	58	9	Not Rejection	*True Class*
	18	20	Rejection	

Table 6.223

Rejection vs Not Rejection in Muscle Logistic Classifier (POD <= 5)

Accuracy	Confusion Matrix			
70.48%	*Classified As*			
p-value	Not Rejection	Rejection		
.3857	56	11	Not Rejection	*True Class*
	20	18	Rejection	

Table 6.224

Rejection vs Not Rejection in Muscle Logistic Classifier (POD <= 5, feature selected)

Accuracy	**Confusion Matrix**			
73.33%	*Classified As*			
p-value	Not Rejection	Rejection		
.3701	59	8	Not Rejection	*True Class*
	20	18	Rejection	

Table 6.225

Rejection vs Not Rejection in Muscle Logistic Classifier (POD <= 5, MANOVA transformed)

Accuracy	**Confusion Matrix**			
68.57%	*Classified As*			
p-value	Not Rejection	Rejection		
.4686	57	10	Not Rejection	*True Class*
	23	15	Rejection	

Table 6.226

Rejection vs Not Rejection in Muscle Decision Tree (POD <= 5, pruned tree)

Accuracy	**Confusion Matrix**			
81.90%	*Classified As*			
p-value	Not Rejection	Rejection		
.1543	57	10	Not Rejection	*True Class*
	10	28	Rejection	

Table 6.227

Rejection vs Not Rejection in Muscle Decision Tree (POD <= 5, feature selected, pruned tree)

Accuracy	**Confusion Matrix**			
73.33%	*Classified As*			
p-value	Not Rejection	Rejection		
.6567	67	0	Not Rejection	*True Class*
	34	4	Rejection	

Table 6.228

Rejection vs Not Rejection in Muscle Decision Tree (POD <= 5, MANOVA transformed, pruned tree)

Accuracy	**Confusion Matrix**			
73.33%	*Classified As*			
p-value	Not Rejection	Rejection		
.5365	65	2	Not Rejection	*True Class*
	28	10	Rejection	

Table 6.229

Rejection vs Not Rejection in Muscle Random Forest (POD <= 5, 100 trees)

Accuracy	Confusion Matrix			
88.57%	*Classified As*			
p-value	Not Rejection	Rejection		
.1097	62	5	Not Rejection	*True Class*
	6	32	Rejection	

Table 6.230

Rejection vs Not Rejection in Muscle Random Forest (POD <= 5, feature selected, 100 trees)

Accuracy	Confusion Matrix			
83.81%	*Classified As*			
p-value	Not Rejection	Rejection		
.1725	59	8	Not Rejection	*True Class*
	11	27	Rejection	

Table 6.231

Rejection vs Not Rejection in Muscle Random Forest (POD <= 5, MANOVA transformed, 100 trees)

Accuracy	Confusion Matrix			
86.67%	*Classified As*			
p-value	Not Rejection	Rejection		
.1351	63	4	Not Rejection	*True Class*
	8	30	Rejection	

Table 6.232

POD > 5

Rejection vs Not Rejection in Muscle Linear Discriminant (POD > 5)

Accuracy	Confusion Matrix			
77.19%	*Classified As*			
p-value	Not Rejection	Rejection		
.3990	71	2	Not Rejection	*True Class*
	24	17	Rejection	

Table 6.233

Rejection vs Not Rejection in Muscle Linear Discriminant (POD > 5, feature selected)

Accuracy	Confusion Matrix			
69.30%	*Classified As*			
p-value	Not Rejection	Rejection		*True Class*
.4260				

	61	12	Not Rejection	
	23	18	Rejection	

Table 6.234

Rejection vs Not Rejection in Muscle Linear Discriminant (POD > 5, MANOVA transformed)

Accuracy	Confusion Matrix			
80.70%	*Classified As*			
p-value	Not Rejection	Rejection		
.3184	71	2	Not Rejection	*True Class*
	20	21	Rejection	

Table 6.235

Rejection vs Not Rejection in Muscle Logistic Classifier (POD > 5)

Accuracy	Confusion Matrix			
87.72%	*Classified As*			
p-value	Not Rejection	Rejection		
.1275	67	6	Not Rejection	*True Class*
	8	33	Rejection	

Table 6.236

Rejection vs Not Rejection in Muscle Logistic Classifier (POD > 5, feature selected)

Accuracy	Confusion Matrix			
64.04%	*Classified As*			
p-value	Not Rejection	Rejection		
.6583	65	8	Not Rejection	*True Class*
	33	8	Rejection	

Table 6.237

Rejection vs Not Rejection in Muscle Logistic Classifier (POD > 5, MANOVA transformed)

Accuracy	Confusion Matrix			
87.72%	*Classified As*			
p-value	Not Rejection	Rejection		
.1409	68	5	Not Rejection	*True Class*
	9	32	Rejection	

Table 6.238

Rejection vs Not Rejection in Muscle Decision Tree (POD > 5, pruned tree)

Accuracy	Confusion Matrix	
82.46%	*Classified As*	*True*

p-value
.1460

Not Rejection	Rejection		
62	11	Not Rejection	
10	31	Rejection	

Table 6.239

Rejection vs Not Rejection in Muscle Decision Tree (POD > 5, feature selected, pruned tree)

Accuracy
85.96%
p-value
.1821

Confusion Matrix			
Classified As			
Not Rejection	Rejection		
69	4	Not Rejection	*True Class*
12	29	Rejection	

Table 6.240

Rejection vs Not Rejection in Muscle Decision Tree (POD > 5, MANOVA transformed, pruned tree)

Accuracy
83.33%
p-value
.2100

Confusion Matrix			
Classified As			
Not Rejection	Rejection		
63	10	Not Rejection	*True Class*
14	27	Rejection	

Table 6.241

Rejection vs Not Rejection in Muscle Random Forest (POD > 5, 100 trees)

Accuracy
88.60%
p-value
.1460

Confusion Matrix			
Classified As			
Not Rejection	Rejection		
71	2	Not Rejection	*True Class*
9	32	Rejection	

Table 6.242

Rejection vs Not Rejection in Muscle Random Forest (POD > 5, feature selected, 100 trees)

Accuracy
85.96%
p-value
.1378

Confusion Matrix			
Classified As			
Not Rejection	Rejection		
66	7	Not Rejection	*True Class*
9	32	Rejection	

Table 6.243

Rejection vs Not Rejection in Muscle Random Forest (POD > 5, MANOVA transformed, 100 trees)

Accuracy	Confusion Matrix			
88.60%	*Classified As*			
p-value	Not Rejection	Rejection		
.1309	69	4	Not Rejection	*True Class*
	8	33	Rejection	

Table 6.244

Type of Inflammation

All Time Points

Type of Inflammation in Muscle Linear Discriminant (all time points, feature selected)

Accuracy	Confusion Matrix				
57.36%	*Classified As*				
p-value	Rejection	Unspecific Inflammation	Wound Healing		
.7078	28	11	40	Rejection	*True Class*
	4	7	11	Unspecific Inflammation	
	11	7	78	Wound Healing	

Table 6.245

Type of Inflammation in Muscle Linear Discriminant (all time points, MANOVA transformed)

Accuracy	Confusion Matrix				
62.44%	*Classified As*				
p-value	Rejection	Unspecific Inflammation	Wound Healing		
.5031	34	10	35	Rejection	*True Class*
	2	11	9	Unspecific Inflammation	
	9	9	78	Wound Healing	

Table 6.246

Type of Inflammation in Muscle Quadratic Discriminant (all time points, feature selected)

Accuracy	Confusion Matrix				
58.89%	*Classified As*				
p-value	Rejection	Unspecific Inflammation	Wound Healing		*True Class*
.7117					

	19	9	51	Rejection	
	3	10	9	Unspecific Inflammation	
	3	6	87	Wound Healing	

Table 6.247

Type of Inflammation in Muscle Logistic Classifier (all time points, feature selected)

Accuracy	**Confusion Matrix**				
59.90%	*Classified As*				
p-value	Rejection	Unspecific Inflammation	Wound Healing		
.2419	30	2	47	Rejection	*True Class*
	7	2	13	Unspecific Inflammation	
	7	3	86	Wound Healing	

Table 6.248

Type of Inflammation in Muscle Logistic Classifier (all time points, MANOVA transformed)

Accuracy	**Confusion Matrix**				
67.01%	*Classified As*				
p-value	Rejection	Unspecific Inflammation	Wound Healing		
.4099	45	5	29	Rejection	*True Class*
	4	7	11	Unspecific Inflammation	
	10	6	80	Wound Healing	

Table 6.249

Type of Inflammation in Muscle Logistic Classifier (all time points, hybrid features)

Accuracy	**Confusion Matrix**				
67.51%	*Classified As*				
p-value	Rejection	Unspecific Inflammation	Wound Healing		
.4476	47	5	27	Rejection	*True Class*
	4	7	44	Unspecific Inflammation	
	10	7	79	Wound	

				Healing	

Table 6.250

Type of Inflammation in Muscle Decision Tree (all time points, feature selected, pruned tree)

Accuracy
68.53%
p-value
.4031

Confusion Matrix

Classified As				
Rejection	Unspecific Inflammation	Wound Healing		
49	0	30	Rejection	*True Class*
9	4	9	Unspecific Inflammation	
20	1	75	Wound Healing	

Table 6.251

Type of Inflammation in Muscle Decision Tree (all time points, MANOVA transformed, pruned tree)

Accuracy
73.10%
p-value
.2624

Confusion Matrix

Classified As				
Rejection	Unspecific Inflammation	Wound Healing		
49	2	28	Rejection	*True Class*
5	10	7	Unspecific Inflammation	
11	4	81	Wound Healing	

Table 6.252

Type of Inflammation in Muscle Decision Tree (all time points, hybrid features, pruned tree)

Accuracy
68.02%
p-value
.3093

Confusion Matrix

Classified As				
Rejection	Unspecific Inflammation	Wound Healing		
55	3	21	Rejection	*True Class*
7	5	10	Unspecific Inflammation	
15	6	75	Wound Healing	

Table 6.253

Type of Inflammation in Muscle Random Forest (all time points, feature

selected, 100 trees)

Accuracy	**Confusion Matrix**				
79.19%	*Classified As*				
p-value	Rejection	Unspecific Inflammation	Wound Healing		
.1654	64	1	14	Rejection	*True Class*
	5	8	9	Unspecific Inflammation	
	10	1	85	Wound Healing	

Table 6.254

Type of Inflammation in Muscle Random Forest (all time points, MANOVA transformed, 100 trees)

Accuracy	**Confusion Matrix**				
79.19%	*Classified As*				
p-value	Rejection	Unspecific Inflammation	Wound Healing		
.1530	65	0	14	Rejection	*True Class*
	6	9	7	Unspecific Inflammation	
	11	1	84	Wound Healing	

Table 6.255

POD <= 5

Type of Inflammation in Muscle Linear Discriminant (POD <= 5)

Accuracy	**Confusion Matrix**				
54.29%	*Classified As*				
p-value	Rejection	Unspecific Inflammation	Wound Healing		
.7438	15	5	18	Rejection	*True Class*
	3	8	11	Unspecific Inflammation	
	5	6	34	Wound Healing	

Table 6.256

Type of Inflammation in Muscle Linear Discriminant (POD <= 5, feature selected)

Accuracy	**Confusion Matrix**	
55.24%	*Classified As*	*True*
p-value		

.6890

Rejection	Unspecific Inflammation	Wound Healing	
18	0	20	Rejection
3	6	13	Unspecific Inflammation
9	2	34	Wound Healing

Table 6.257

Type of Inflammation in Muscle Linear Discriminant (POD <= 5, MANOVA transformed)

Accuracy	**Confusion Matrix**				
51.43%	*Classified As*				
p-value	Rejection	Unspecific Inflammation	Wound Healing		
.9234	13	7	18	Rejection	*True Class*
	4	6	12	Unspecific Inflammation	
	6	4	35	Wound Healing	

Table 6.258

Type of Inflammation in Muscle Logistic Classifier (POD <= 5)

Accuracy	**Confusion Matrix**				
60.95%	*Classified As*				
p-value	Rejection	Unspecific Inflammation	Wound Healing		
.3640	22	4	12	Rejection	*True Class*
	2	11	9	Unspecific Inflammation	
	6	8	31	Wound Healing	

Table 6.259

Type of Inflammation in Muscle Logistic Classifier (POD <= 5, feature selected)

Accuracy	**Confusion Matrix**				
61.90%	*Classified As*				
p-value	Rejection	Unspecific Inflammation	Wound Healing		
.3033	20	0	18	Rejection	*True Class*
	3	8	11	Unspecific Inflammation	
	6	2	37	Wound	

				Healing	

Table 6.260

Type of Inflammation in Muscle Logistic Classifier (POD <= 5, MANOVA transformed)

Accuracy
63.81%
p-value
.3317

Confusion Matrix

Classified As				
Rejection	Unspecific Inflammation	Wound Healing		
22	2	14	Rejection	*True Class*
2	11	9	Unspecific Inflammation	
6	5	34	Wound Healing	

Table 6.261

Type of Inflammation in Muscle Decision Tree (POD <= 5, pruned tree)

Accuracy
66.67%
p-value
.2275

Confusion Matrix

Classified As				
Rejection	Unspecific Inflammation	Wound Healing		
28	0	10	Rejection	*True Class*
2	7	13	Unspecific Inflammation	
3	5	37	Wound Healing	

Table 6.262

Type of Inflammation in Muscle Decision Tree (POD <= 5, feature selected, pruned tree)

Accuracy
64.76%
p-value
.2641

Confusion Matrix

Classified As				
Rejection	Unspecific Inflammation	Wound Healing		
25	4	9	Rejection	*True Class*
4	10	8	Unspecific Inflammation	
10	6	29	Wound Healing	

Table 6.263

Type of Inflammation in Muscle Decision Tree (POD <= 5, MANOVA transformed, pruned tree)

Accuracy	Confusion Matrix				
65.71%	*Classified As*				
p-value	Rejection	Unspecific Inflammation	Wound Healing		
.3169	29	2	7	Rejection	*True Class*
	6	6	10	Unspecific Inflammation	
	9	4	32	Wound Healing	

Table 6.264

Type of Inflammation in Muscle Random Forest (POD <= 5, 100 trees)

Accuracy	Confusion Matrix				
74.29%	*Classified As*				
p-value	Rejection	Unspecific Inflammation	Wound Healing		
.1177	36	2	0	Rejection	*True Class*
	4	9	9	Unspecific Inflammation	
	2	7	36	Wound Healing	

Table 6.265

Type of Inflammation in Muscle Random Forest (POD <= 5, feature selected, 100 trees)

Accuracy	Confusion Matrix				
78.10%	*Classified As*				
p-value	Rejection	Unspecific Inflammation	Wound Healing		
.0904	31	2	5	Rejection	*True Class*
	5	11	6	Unspecific Inflammation	
	6	2	37	Wound Healing	

Table 6.266

Type of Inflammation in Muscle Random Forest (POD <= 5, MANOVA transformed, 100 trees)

Accuracy	Confusion Matrix				
76.19%	*Classified As*				
p-value	Rejection	Unspecific Inflammation	Wound Healing		
.0561	31	0	7	Rejection	*True Class*
	2	14	6	Unspecific	

				Inflammation	
	7	6	32	Wound Healing	

Table 6.267

POD > 5

Type of Inflammation in Muscle Linear Discriminant (POD > 5)

Accuracy
64.04%
p-value
.4393

Confusion Matrix

Classified As				
Rejection	Unspecific Inflammation	Wound Healing		
16	3	22	Rejection	*True Class*
2	11	9	Unspecific Inflammation	
2	3	46	Wound Healing	

Table 6.268

Type of Inflammation in Muscle Linear Discriminant (POD > 5, feature selected)

Accuracy
57.89%
p-value
.6564

Confusion Matrix

Classified As				
Rejection	Unspecific Inflammation	Wound Healing		
16	3	22	Rejection	*True Class*
6	6	10	Unspecific Inflammation	
6	1	44	Wound Healing	

Table 6.269

Type of Inflammation in Muscle Linear Discriminant (POD > 5, MANOVA transformed)

Accuracy
65.79%
p-value
.3749

Confusion Matrix

Classified As				
Rejection	Unspecific Inflammation	Wound Healing		
17	3	21	Rejection	*True Class*
0	12	10	Unspecific Inflammation	
2	3	46	Wound	

				Healing	

Table 6.270

Type of Inflammation in Muscle Logistic Classifier (POD > 5)

Accuracy
74.46%
p-value
.4484

Confusion Matrix

Classified As				
Rejection	Unspecific Inflammation	Wound Healing		
28	4	9	Rejection	*True Class*
1	12	9	Unspecific Inflammation	
4	2	45	Wound Healing	

Table 6.271

Type of Inflammation in Muscle Logistic Classifier (POD > 5, feature selected)

Accuracy
70.18%
p-value
.2456

Confusion Matrix

Classified As				
Rejection	Unspecific Inflammation	Wound Healing		
21	2	18	Rejection	*True Class*
3	10	9	Unspecific Inflammation	
1	1	49	Wound Healing	

Table 6.272

Type of Inflammation in Muscle Logistic Classifier (POD > 5, MANOVA transformed)

Accuracy
74.56%
p-value
.5578

Confusion Matrix

Classified As				
Rejection	Unspecific Inflammation	Wound Healing		
30	2	9	Rejection	*True Class*
1	11	10	Unspecific Inflammation	
4	3	44	Wound Healing	

Table 6.273

Type of Inflammation in Muscle Decision Tree (POD > 5, pruned tree)

Accuracy
70.18%

Confusion Matrix

Classified As	*True*

p-value
.3487

Rejection	Unspecific Inflammation	Wound Healing	
28	4	9	Rejection
6	3	13	Unspecific Inflammation
2	1	48	Wound Healing

Table 6.274

Type of Inflammation in Muscle Decision Tree (POD > 5, feature selected, pruned tree)

Accuracy
70.18%
p-value
.7078

Confusion Matrix

Classified As				
Rejection	Unspecific Inflammation	Wound Healing		
21	0	20	Rejection	*True Class*
5	0	17	Unspecific Inflammation	
2	0	49	Wound Healing	

Table 6.275

Type of Inflammation in Muscle Decision Tree (POD > 5, MANOVA transformed, pruned tree)

Accuracy
77.19%
p-value
.5031

Confusion Matrix

Classified As				
Rejection	Unspecific Inflammation	Wound Healing		
25	0	16	Rejection	*True Class*
5	9	8	Unspecific Inflammation	
4	0	47	Wound Healing	

Table 6.276

Type of Inflammation in Muscle Random Forest (POD > 5, 100 trees)

Accuracy
79.82%

Confusion Matrix

Classified As	*True*

p-value
.1440

Rejection	Unspecific Inflammation	Wound Healing	
32	3	6	Rejection
4	9	9	Unspecific Inflammation
1	4	46	Wound Healing

Table 6.277

Type of Inflammation in Muscle Random Forest (POD > 5, feature selected, 100 trees)

Accuracy
77.19%
p-value
.1312

Confusion Matrix

Classified As				
Rejection	Unspecific Inflammation	Wound Healing		
32	3	6	Rejection	*True Class*
5	10	7	Unspecific Inflammation	
7	2	42	Wound Healing	

Table 6.278

Type of Inflammation in Muscle Random Forest (POD > 5, MANOVA transformed, 100 trees)

Accuracy
82.46%
p-value
.0546

Confusion Matrix

Classified As				
Rejection	Unspecific Inflammation	Wound Healing		
35	0	6	Rejection	*True Class*
3	14	5	Unspecific Inflammation	
5	3	43	Wound Healing	

Table 6.279

Cytokine Intergroup r Statistic Values

Pearson's r statistic values for the goup "Not Rejecting" subtracted from "Rejecting" in Skin

	GM-CSF	IL-1a	MCP-1	IL-4	IL-1b	IL-2	IL-6	IL-10	IL-12 p70	IL-5	IFN-g	IL-18	GRO/KC	TNFa
GM-CSF	0.000	-0.631	0.546	-0.807	0.164	0.808	0.150	0.105	-0.283	0.035	-0.334	-0.863	0.740	1.343
IL-1a		0.000	-0.301	-0.235	0.437	0.293	0.180	-0.692	0.084	0.154	-0.152	0.202	0.307	0.295
MCP-1			0.000	-0.280	-0.190	0.865	-0.300	0.467	-0.089	0.204	0.004	-0.534	0.154	0.855
IL-4				0.000	0.202	0.101	0.139	-0.730	0.105	0.036	0.220	-0.353	0.307	0.555
IL-1b					0.000	0.617	-0.028	0.080	0.084	-0.165	-0.049	0.532	-0.197	-0.470
IL-2						0.000	0.420	0.824	0.592	0.864	0.467	0.403	0.742	0.838
IL-6							0.000	0.050	0.229	0.113	0.035	0.196	-0.367	-0.017
IL-10								0.000	-0.348	0.024	-0.338	-0.761	0.639	1.199
IL-12 p70									0.000	0.107	-0.102	-0.097	0.319	0.410
IL-5										0.000	0.047	-0.136	0.278	0.473
IFN-g											0.000	-0.288	0.335	0.502
IL-18												0.000	0.324	-0.058
GRO/KC													0.000	0.042
TNFa														0.000

Table 6.280 Intergroup r statistic values for skin. Yellow highlight indicates feature pairs that are good candidates for inclusion in the hybrid matrix.

Pearson's r statistic values for the goup "Not Rejecting" subtracted from "Rejecting" in Muscle

	GM-CSF	IL-1a	MCP-1	IL-4	IL-1b	IL-2	IL-6	IL-10	IL-12 p70	IL-5	IFN-g	IL-18	GRO/KC	TNFa
GM-CSF	0.000	0.477	0.898	-0.205	0.199	-0.477	0.717	1.001	0.232	-0.113	0.080	0.237	0.144	1.152
IL-1a		0.000	0.514	0.004	-0.165	-0.020	0.429	0.517	-0.108	0.184	0.009	0.298	0.105	0.620
MCP-1			0.000	-0.330	-0.647	0.280	-0.099	0.942	0.393	0.306	0.497	-0.391	-0.573	0.522
IL-4				0.000	-0.455	-0.354	-0.433	0.022	-0.311	-0.660	-0.156	-0.539	-0.357	-0.760
IL-1b					0.000	0.531	-0.552	0.380	0.382	0.233	0.538	-0.112	-0.922	-0.382
IL-2						0.000	0.384	0.378	0.115	-0.047	0.082	0.484	-0.008	0.325
IL-6							0.000	0.985	0.419	0.301	0.563	-0.141	-0.519	0.274
IL-10								0.000	0.452	0.763	0.580	0.272	0.274	0.885
IL-12 p70									0.000	0.310	-0.269	0.458	0.059	0.394
IL-5										0.000	0.342	0.269	-0.269	0.089
IFN-g											0.000	0.518	0.089	0.499
IL-18												0.000	-0.528	-0.472
GRO/KC													0.000	-0.222
TNFa														0.000

Table 6.281 Intergroup r statistic values for muscle. Yellow highlight indicates feature pairs that are good candidates for inclusion in the hybrid matrix.

Pearson's r statistic values for the goup "Not Rejecting" subtracted from "Rejecting" in Heart

	GM-CSF	IL-1a	MCP-1	IL-4	IL-1b	IL-2	IL-6	IL-10	IL-12 p70	IL-5	IFN-g	IL-18	GRO/KC	TNFa
GM-CSF	0.000	1.054	0.283	0.596	0.845	0.617	1.293	0.838	-0.082	0.709	1.087	0.881	0.989	1.183
IL-1a		0.000	-0.288	0.199	0.169	-0.419	0.619	0.795	-0.033	1.108	0.046	-0.146	0.298	0.507
MCP-1			0.000	0.483	0.601	0.151	0.174	0.543	0.319	0.347	-0.153	0.136	0.077	0.099
IL-4				0.000	0.675	0.167	0.018	0.019	-0.010	0.752	0.069	-0.299	0.250	-0.155
IL-1b					0.000	-0.079	0.274	0.638	-0.141	0.016	0.282	0.791	0.280	0.104
IL-2						0.000	0.075	0.680	0.058	0.506	-0.329	-0.343	-0.075	0.199
IL-6							0.000	0.529	-0.299	1.083	0.552	0.048	0.984	0.033
IL-10								0.000	-0.225	0.873	0.679	0.063	0.905	0.514
IL-12 p70									0.000	-0.122	-0.281	-0.196	0.118	-0.244
IL-5										0.000	1.133	0.932	1.101	0.903
IFN-g											0.000	-0.123	0.367	0.450
IL-18												0.000	-0.142	-0.250
GRO/KC													0.000	0.781
TNFa														0.000

Table 6.282 Intergroup r statistic values for heart. Yellow highlight indicates feature pairs that are good candidates for inclusion in the hybrid matrix.

Pearson's r statistic values for the goup "Not Rejecting" subtracted from "Rejecting" in Lung

	GM-CSF	IL-1a	MCP-1	IL-4	IL-1b	IL-2	IL-6	IL-10	IL-12 p70	IL-5	IFN-g	IL-18	GRO/KC	TNFa
GM-CSF	0.000	-1.224	-0.423	-0.149	-0.527	-0.702	-0.918	-0.867	-0.229	1.013	0.013	-0.465	-1.012	-0.834
IL-1a		0.000	0.059	0.088	0.053	-1.002	-0.483	-0.171	-0.006	-0.226	0.237	-0.192	-0.128	-0.157
MCP-1				-0.787	-0.051	-0.152	-0.517	0.267	-0.598	-0.239	-0.285	-0.549	-0.183	-0.335
IL-4					-0.818	0.572	-0.312	-0.175	-0.354	0.006	-0.585	-0.690	0.224	-0.181
IL-1b					0.000	-0.039	-0.298	0.496	-0.584	-0.455	-0.116	-0.439	-0.206	-0.270
IL-2						0.000	-0.223	-0.908	0.798	0.174	0.646	-0.428	-0.322	0.017
IL-6							0.000	-0.418	-0.049	-0.058	0.214	-0.344	-0.462	-0.264
IL-10								0.000	0.029	-0.331	0.266	0.031	0.141	-0.241
IL-12 p70									0.000	-0.240	-0.622	-0.385	0.351	-0.123
IL-5										0.000	-0.099	-0.233	-0.473	-0.162
IFN-g											0.000	-0.564	0.002	0.034
IL-18												0.000	0.183	-0.565
GRO/KC													0.000	-0.229
TNFa														0.000

Table 6.283 Intergroup r statistic values for lung. Yellow highlight indicates feature pairs that are good candidates for inclusion in the hybrid matrix.

Appendix B Hypothesis 1 Figures

Allograft vs Isograftin Skin (all time points)

Original 14-Dimensional Feature Space

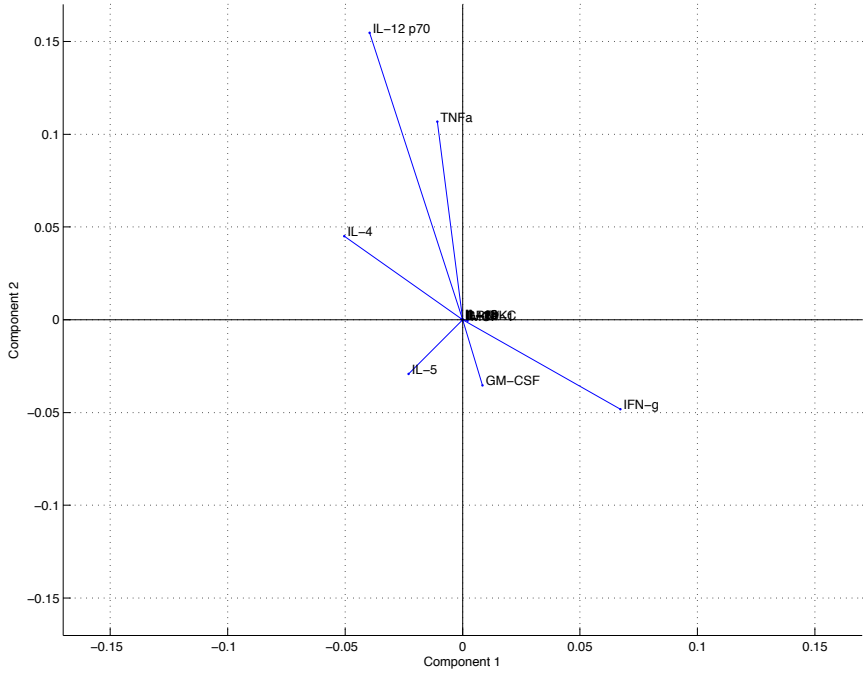

Figure 6.1

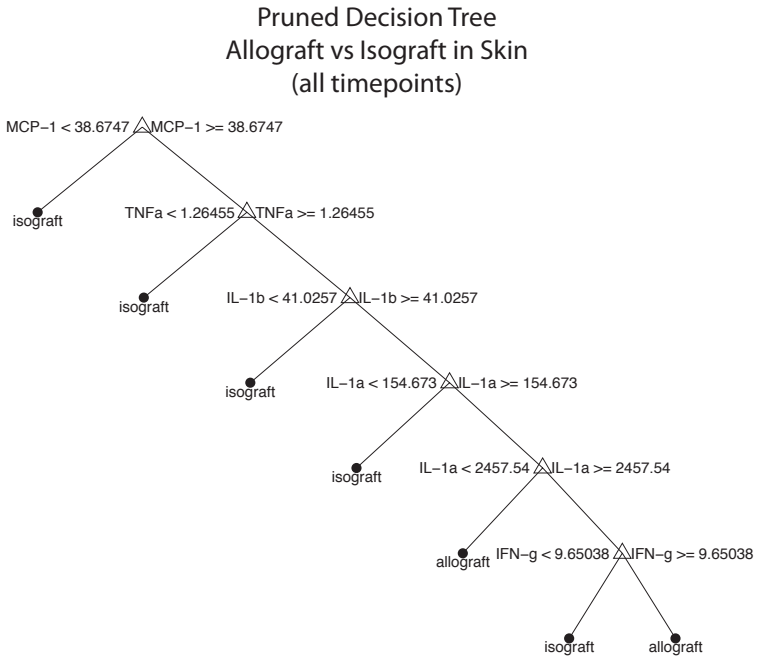

Figure 6.2

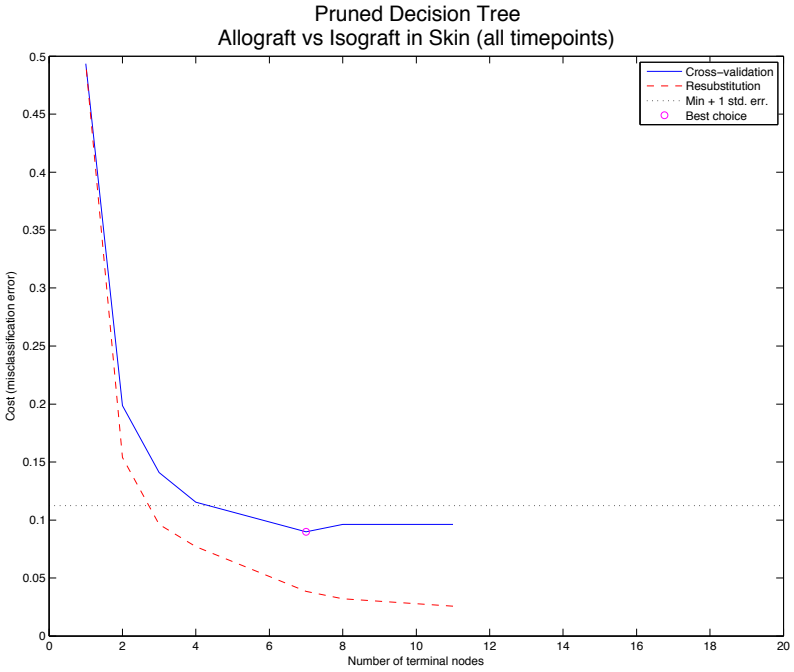

Figure 6.3

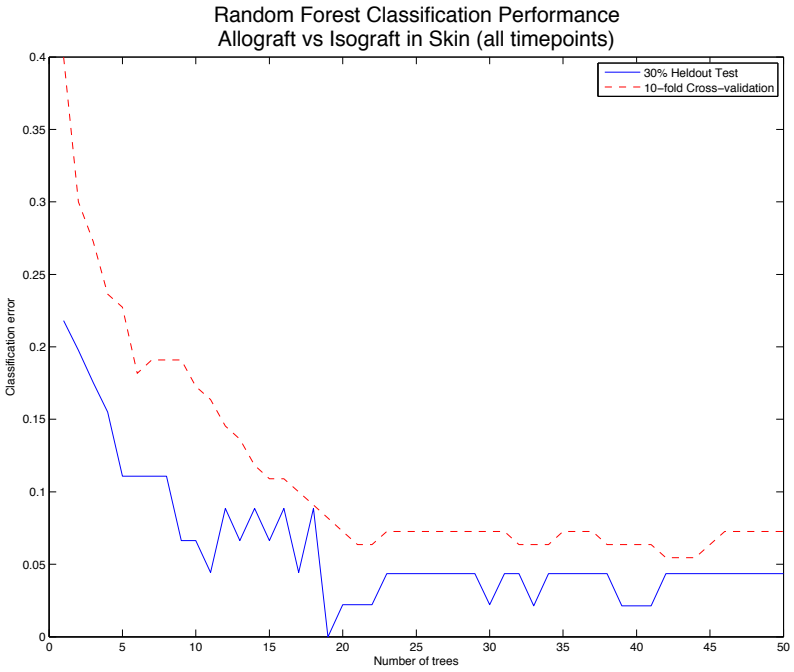

Figure 6.4

5-Dimensional Feature Selected Space

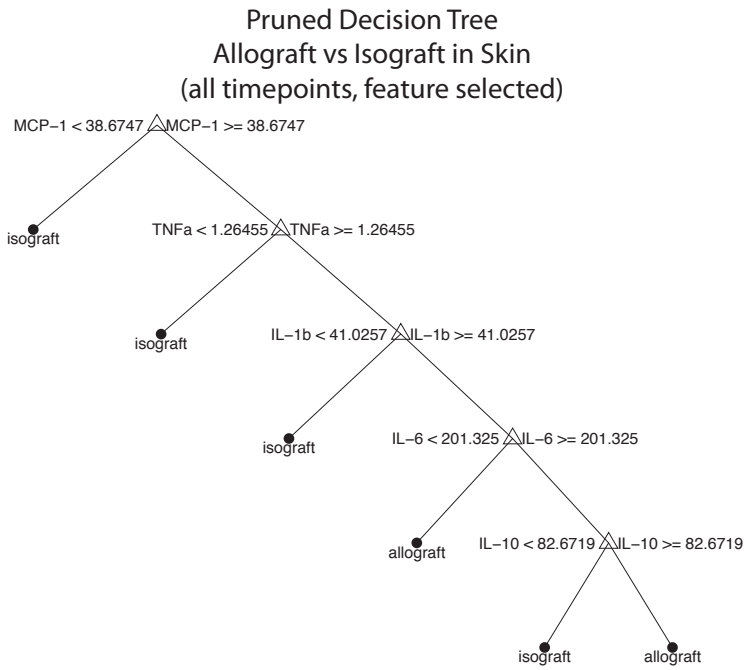

Figure 6.5

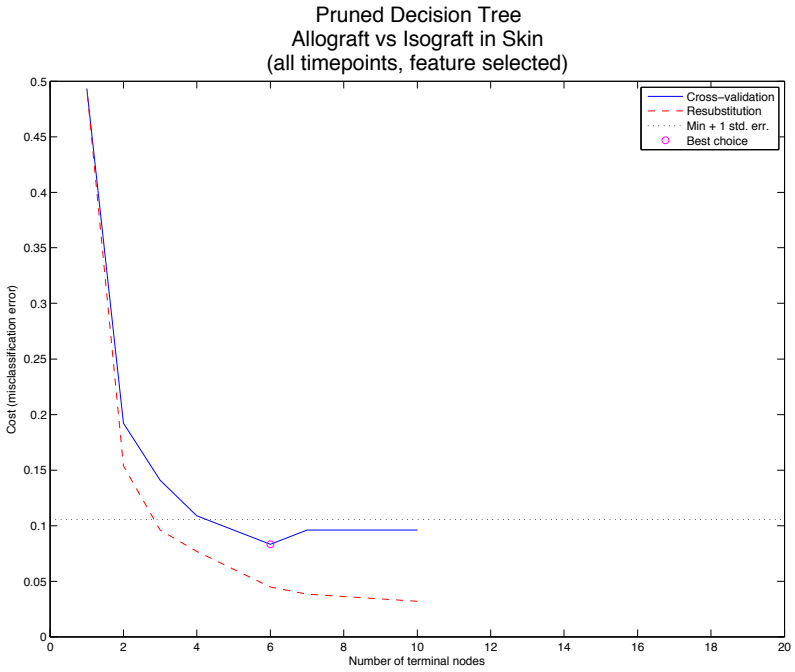

Figure 6.6

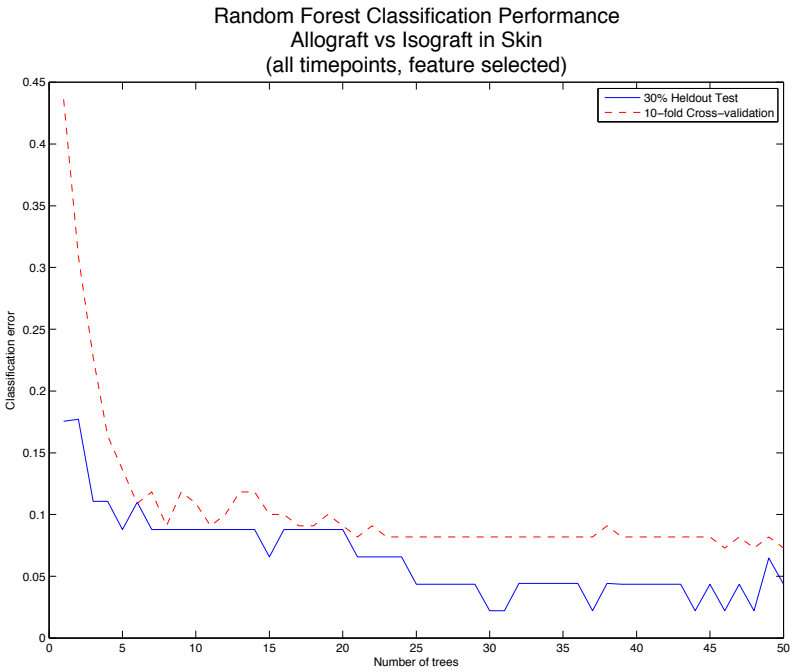

Figure 6.7

MANOVA Transformed Feature Space

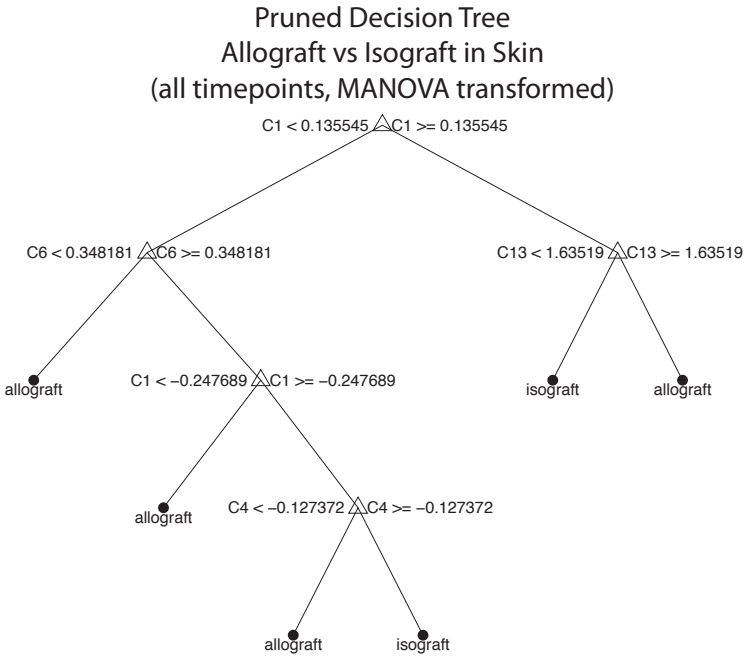

Figure 6.8

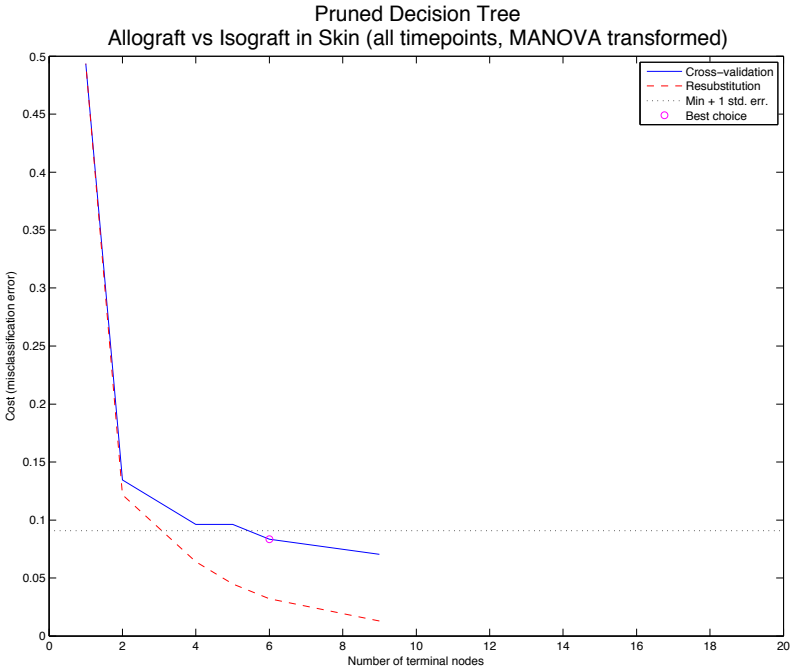

Figure 6.9

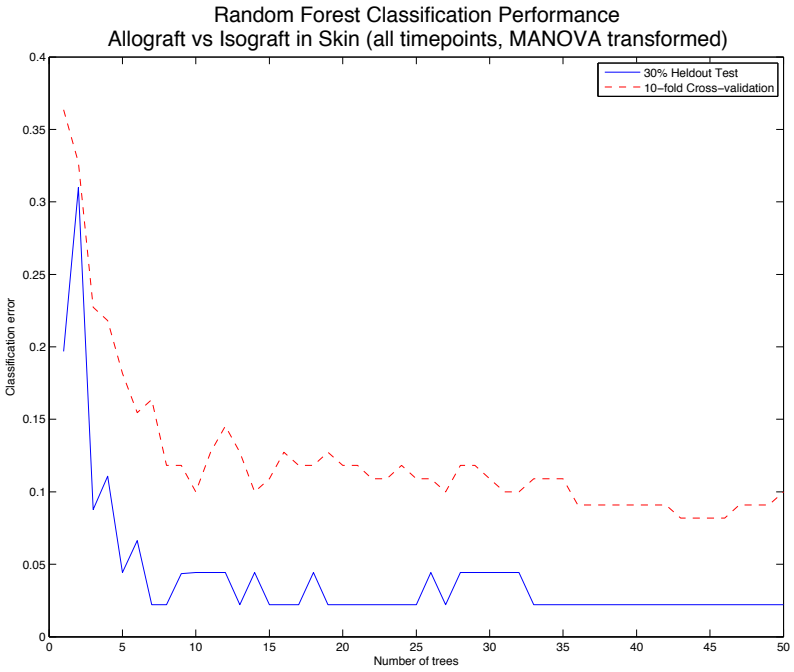

Figure 6.10

Hybrid Feature Space

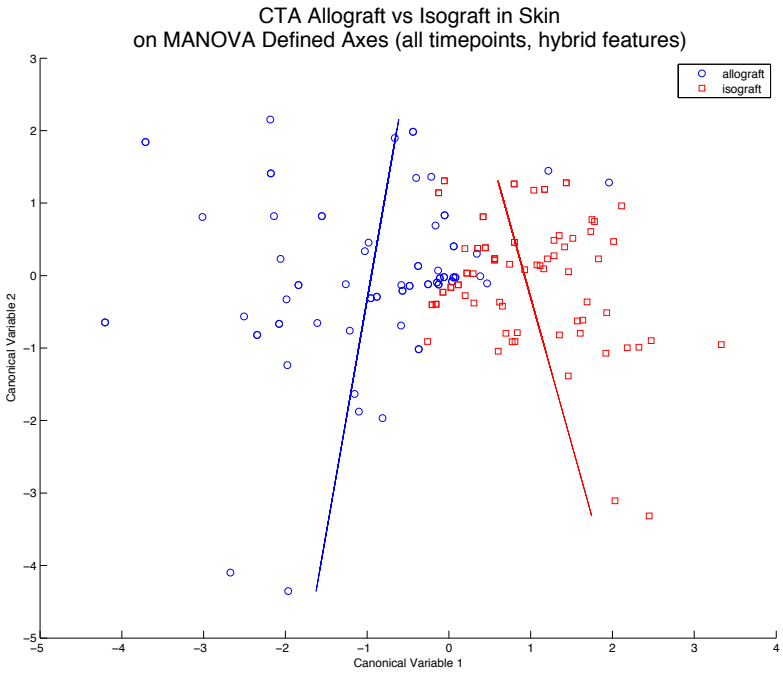

Figure 6.11

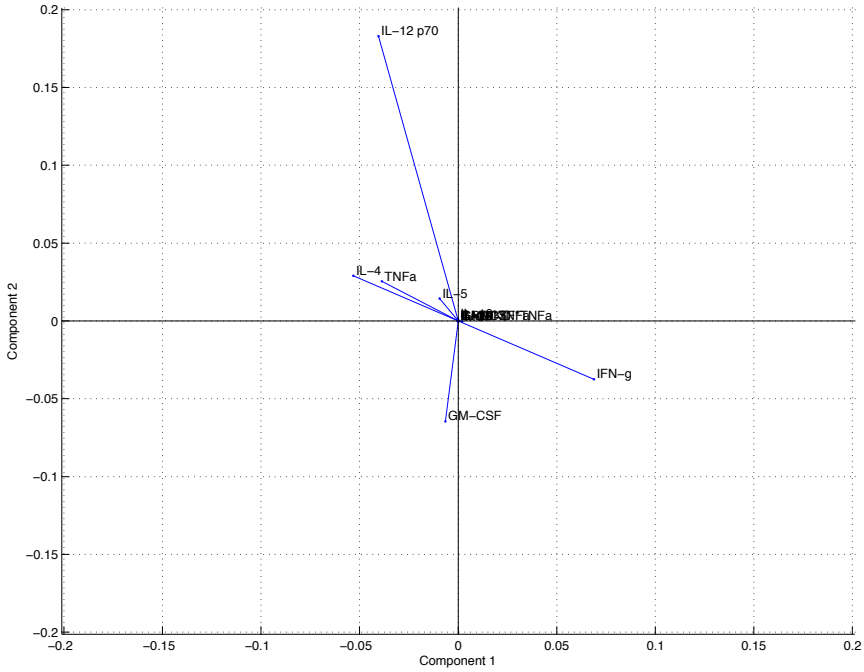

Figure 6.12

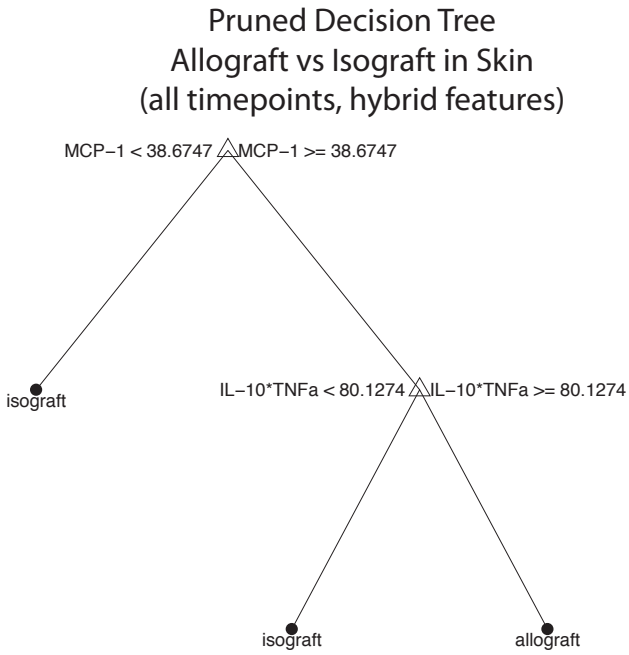

Figure 6.13

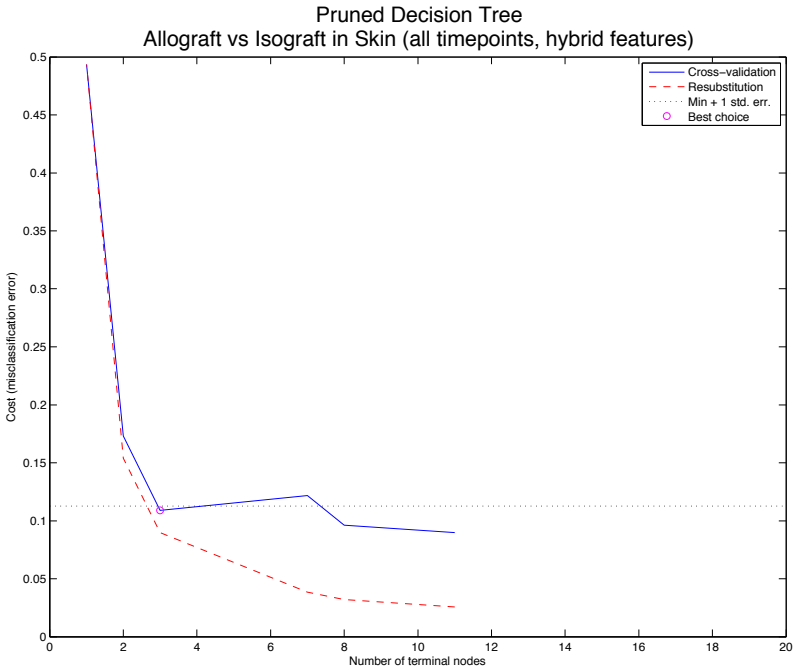

Figure 6.14

ROC Curves in Skin

Original Feature Space

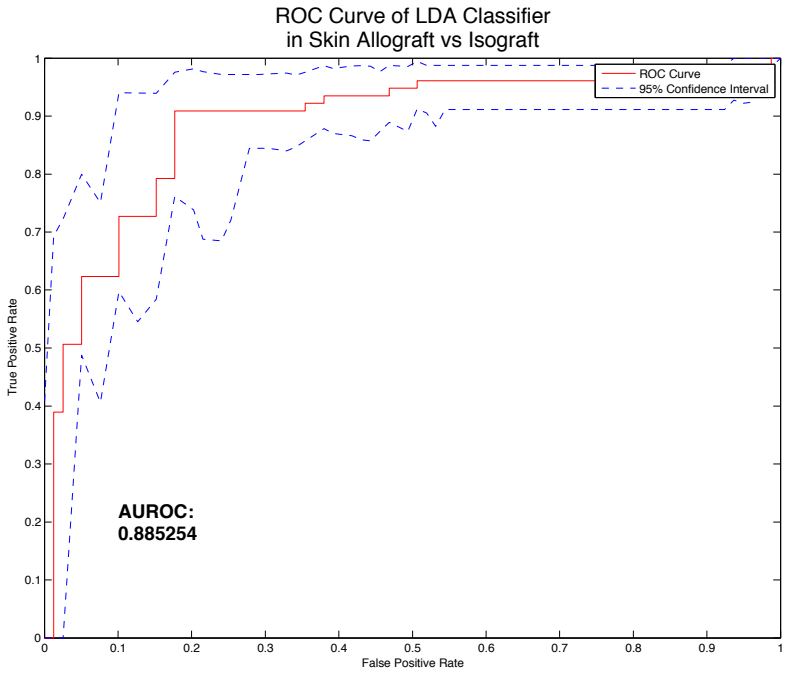

Figure 6.15

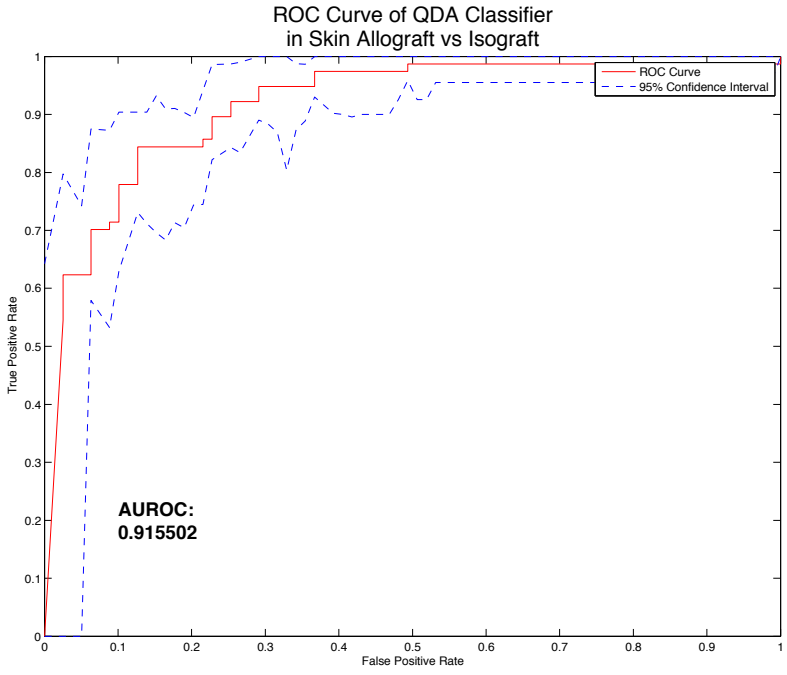

Figure 6.16

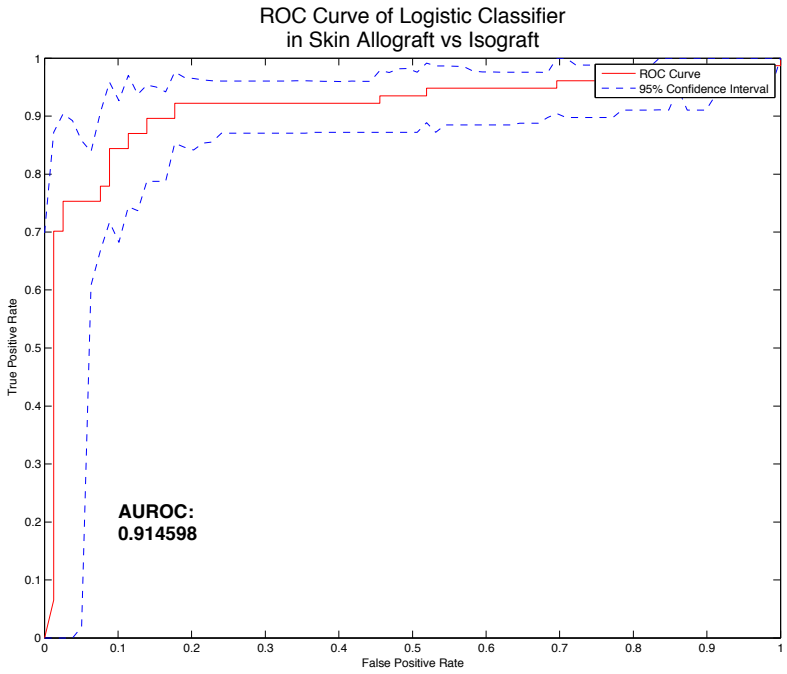

Figure 6.17

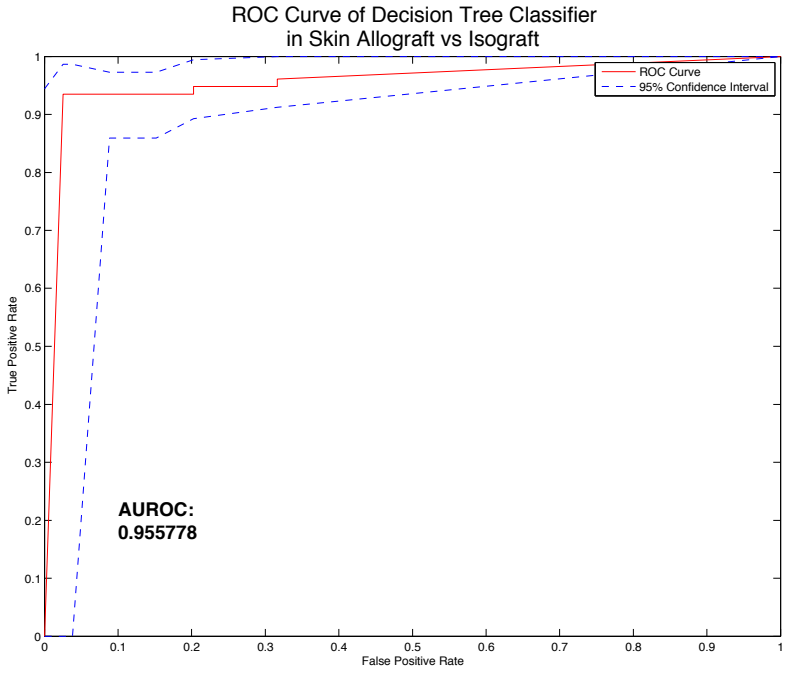

Figure 6.18

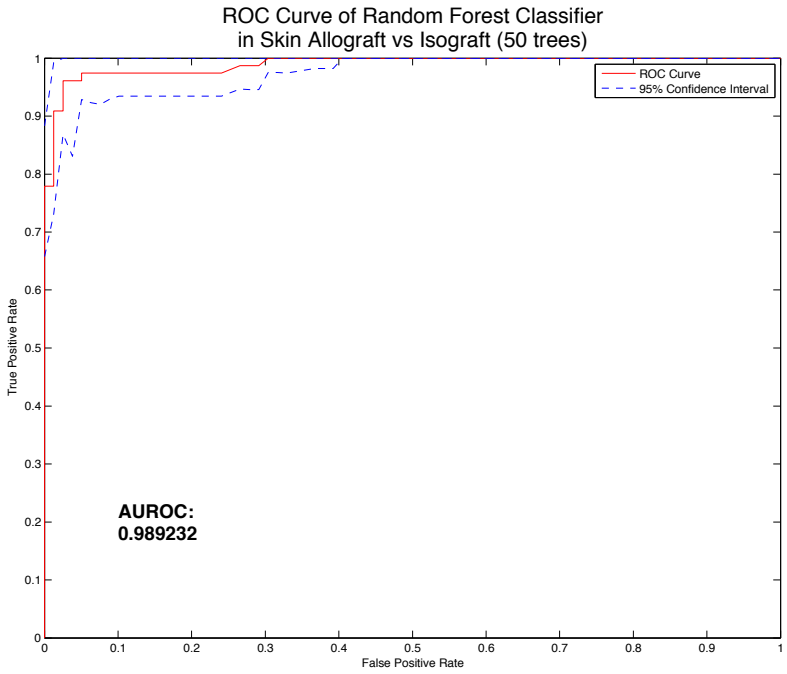

Figure 6.19

Hybrid Feature Space

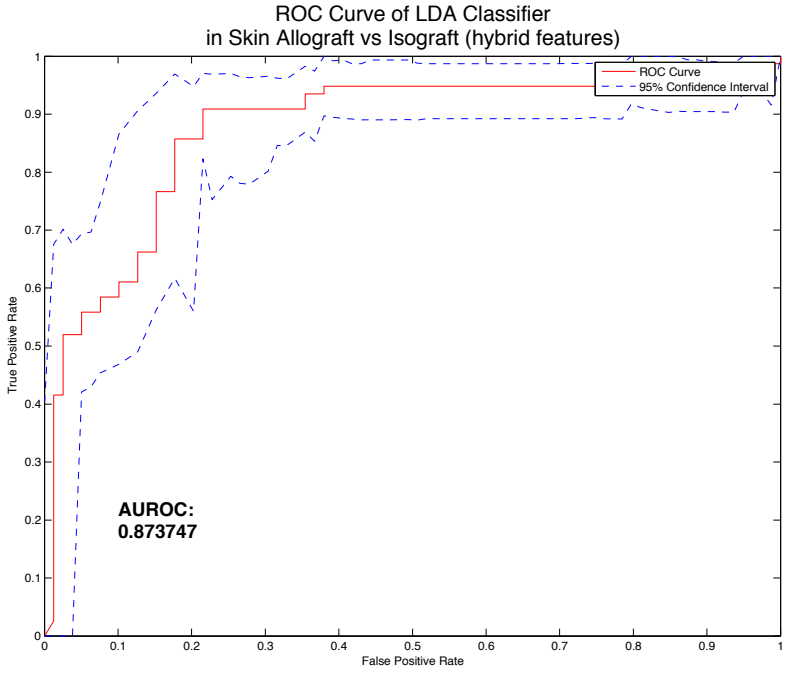

Figure 6.20

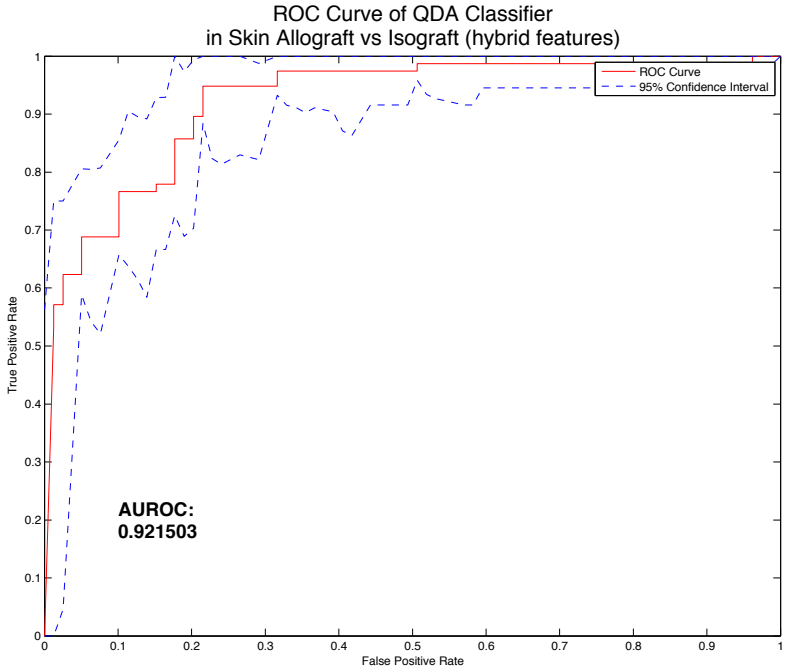

Figure 6.21

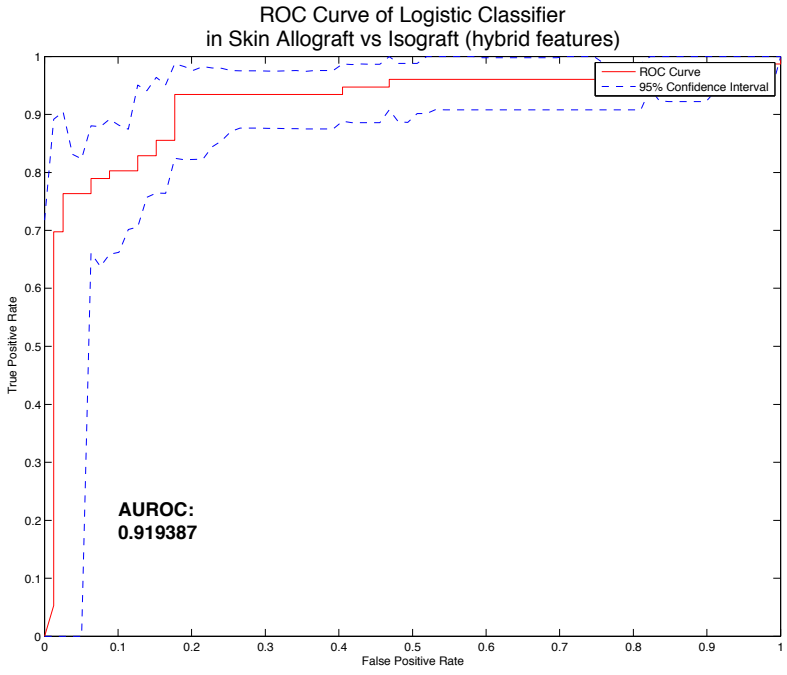

Figure 6.22

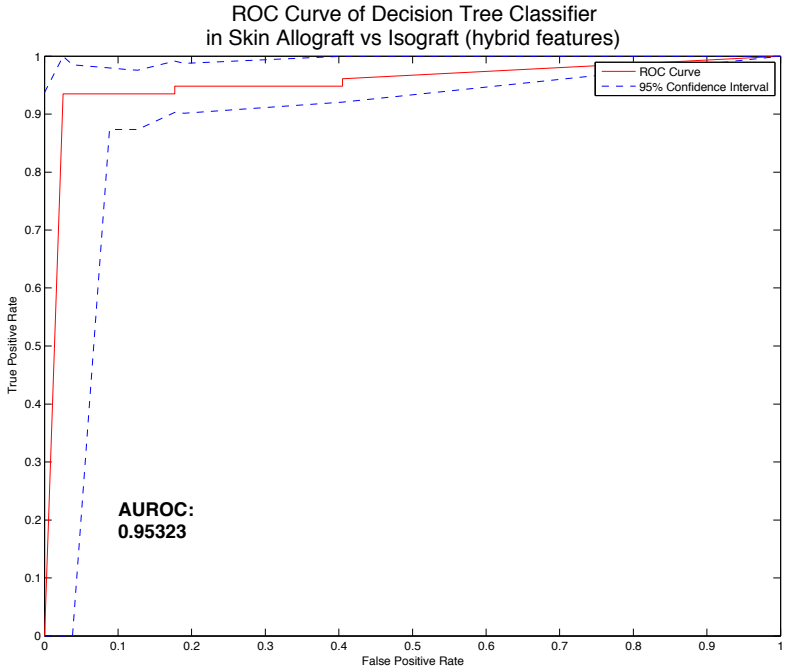

Figure 6.23

Allograft vs Isograftin Skin (POD <= 5)

Original 14-Dimensional Feature Space

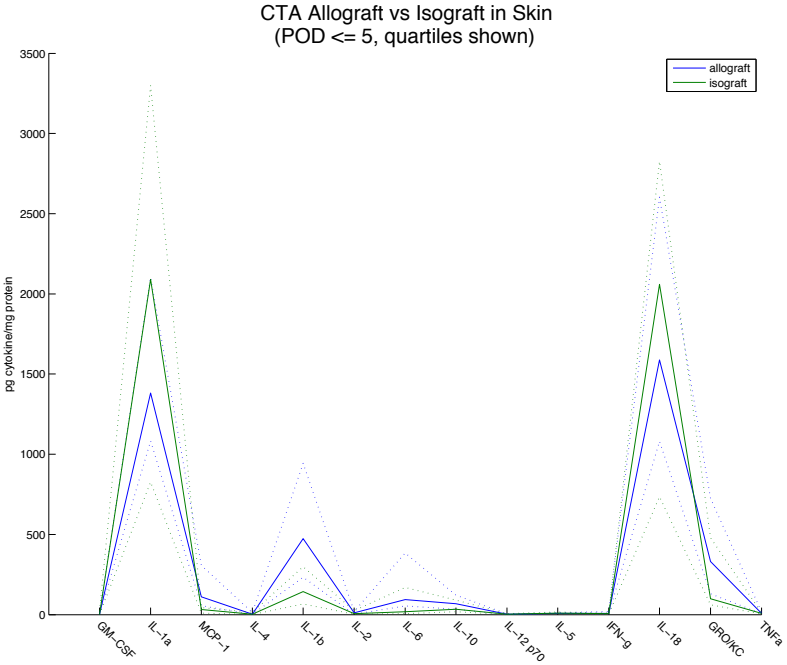

Figure 6.24

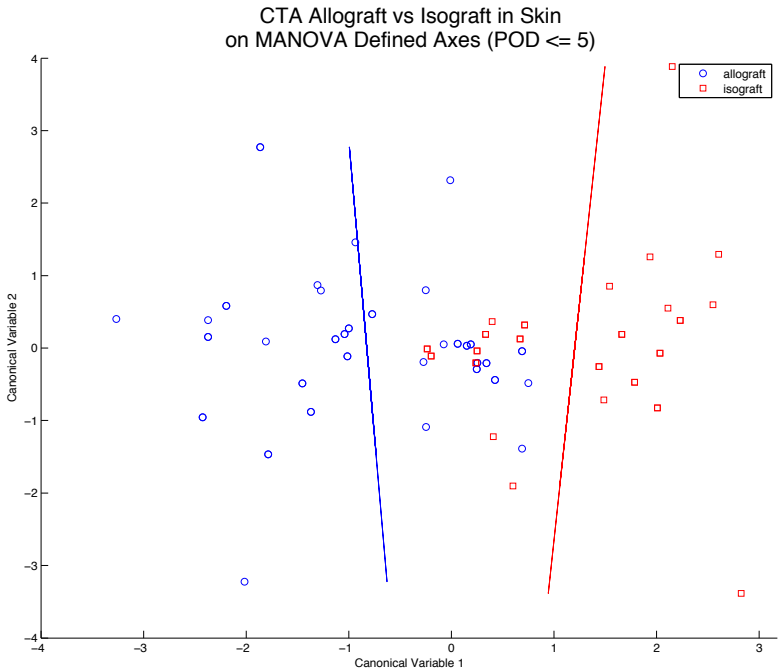

Figure 6.25

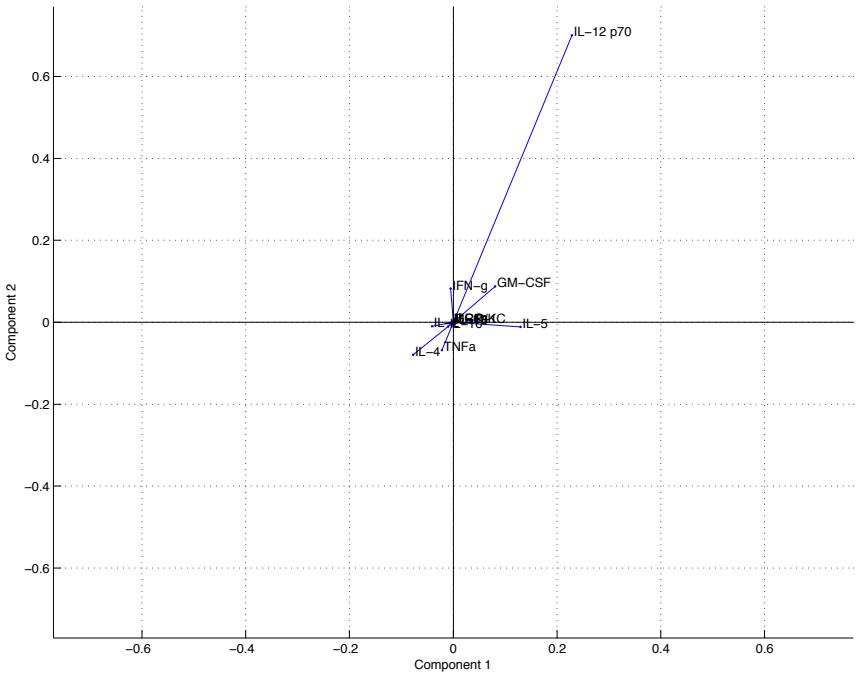

Figure 6.26

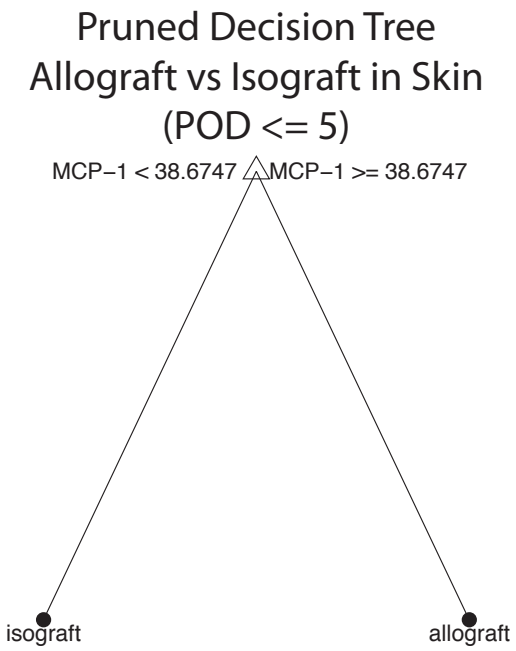

Figure 6.27

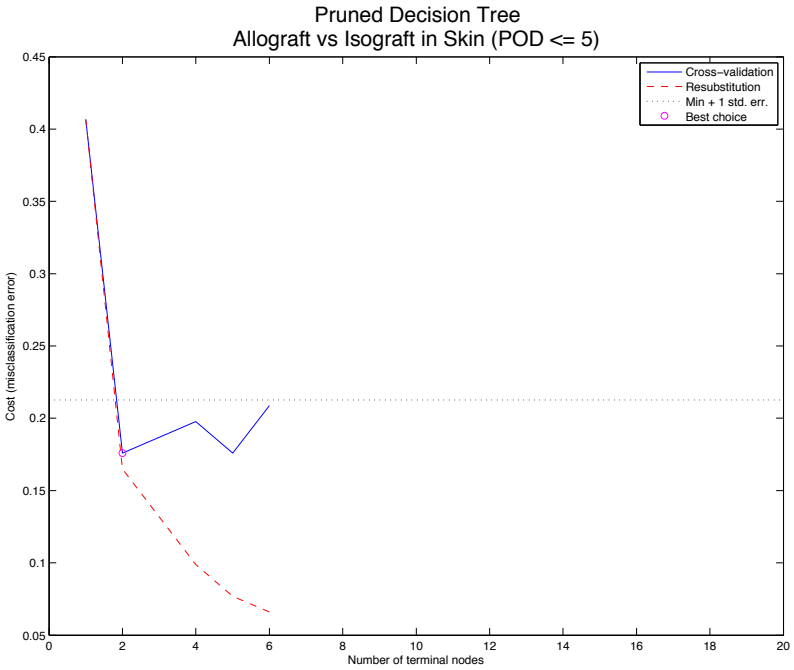

Figure 6.28

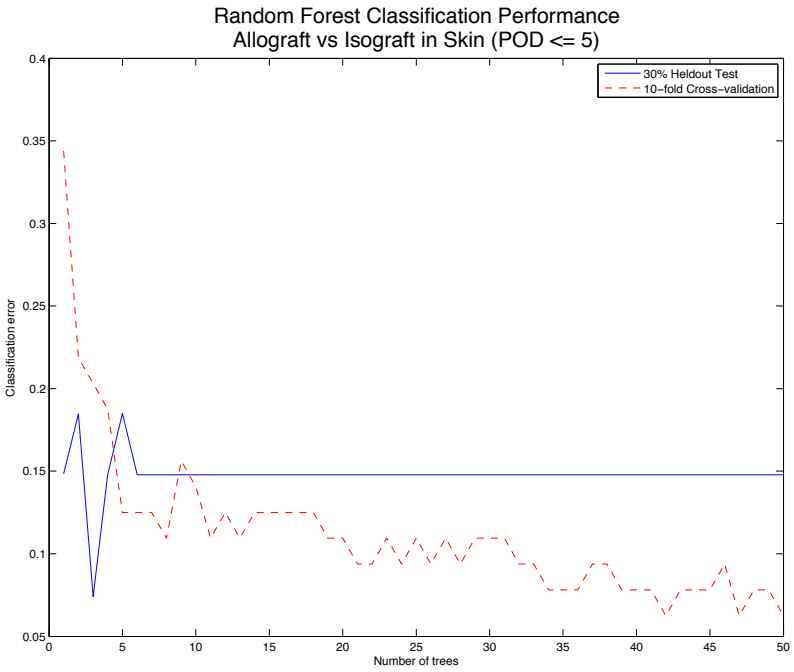

Figure 6.29

5-Dimensional Feature Selected Space

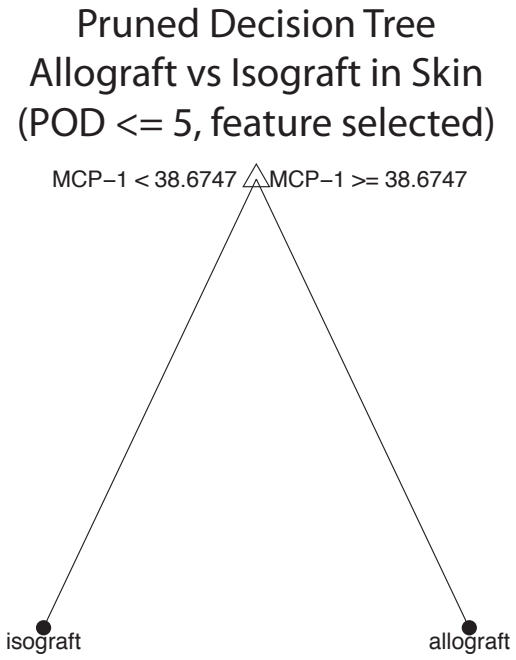

Figure 6.30

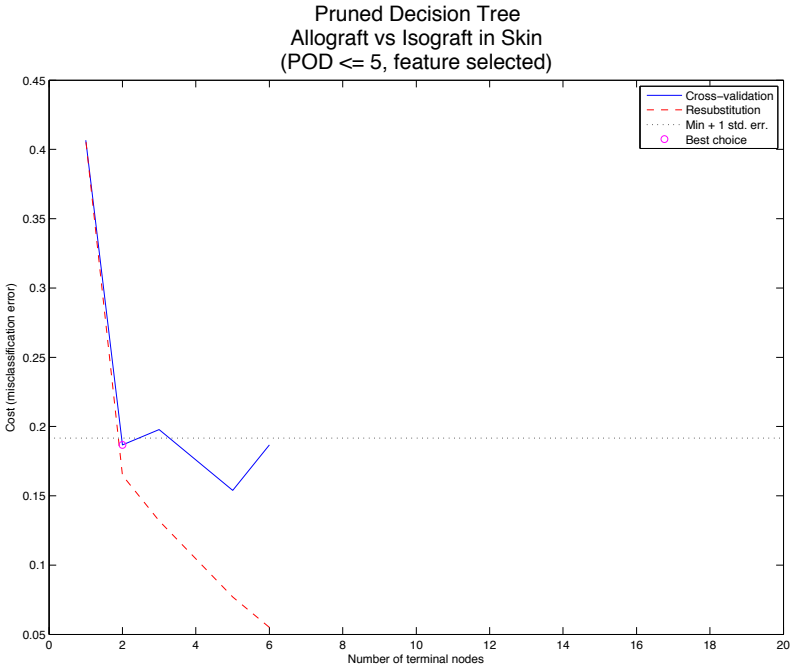

Figure 6.31

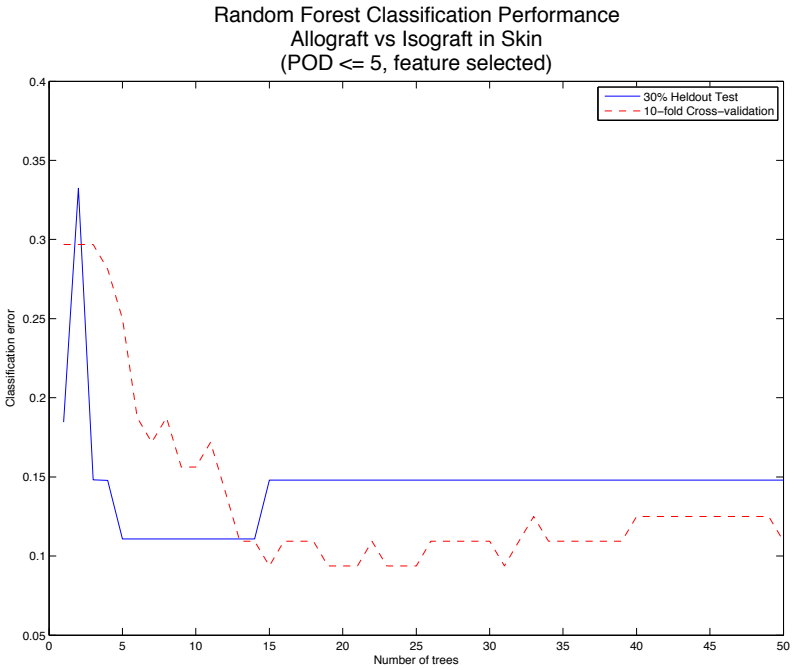

Figure 6.32

MANOVA Transformed Feature Space

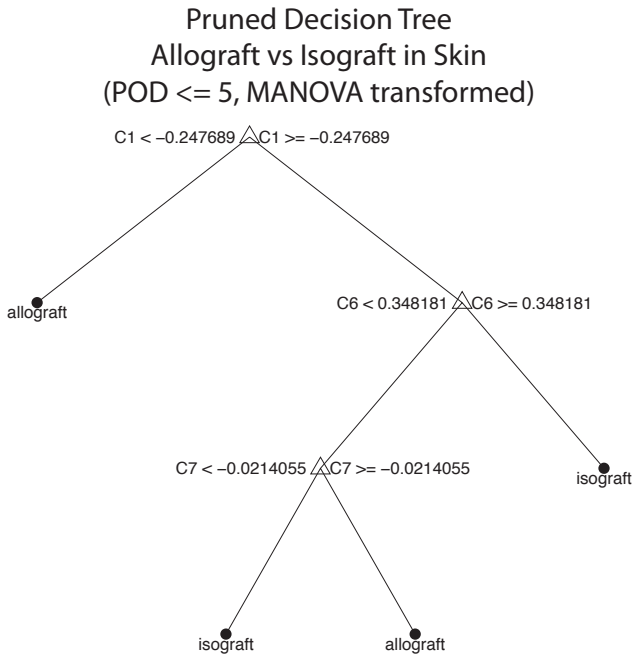

Figure 6.33

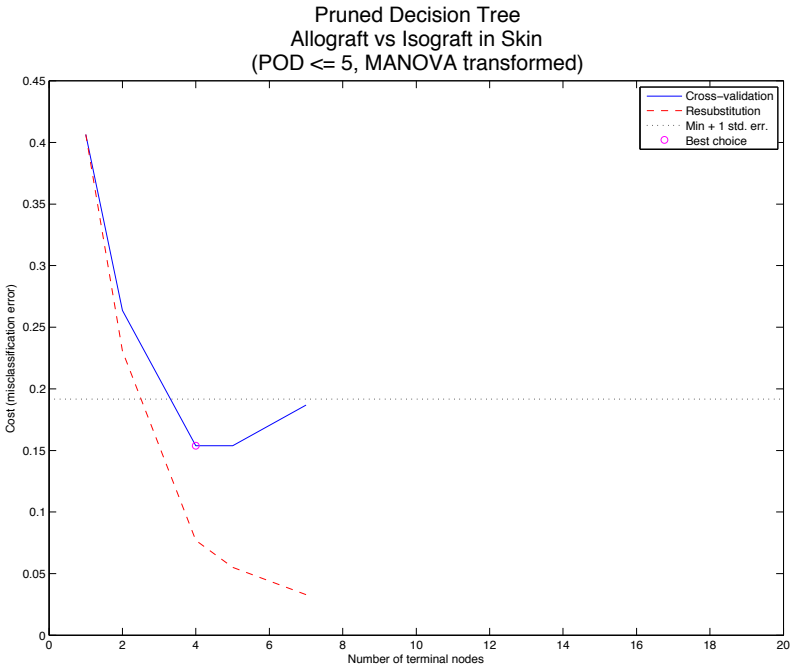

Figure 6.34

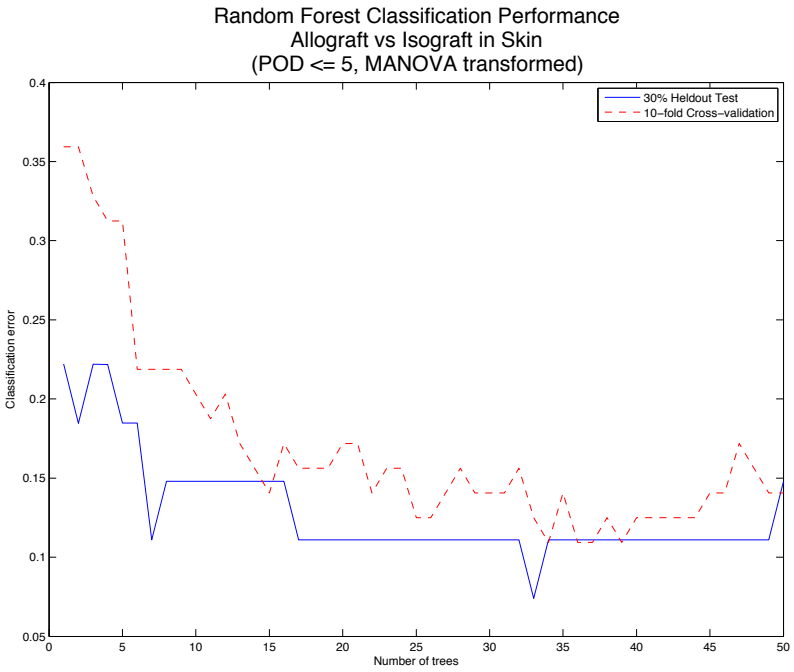

Figure 6.35

Allograft vs Isograftin Skin (POD > 5)

Original 14-Dimensional Feature Space

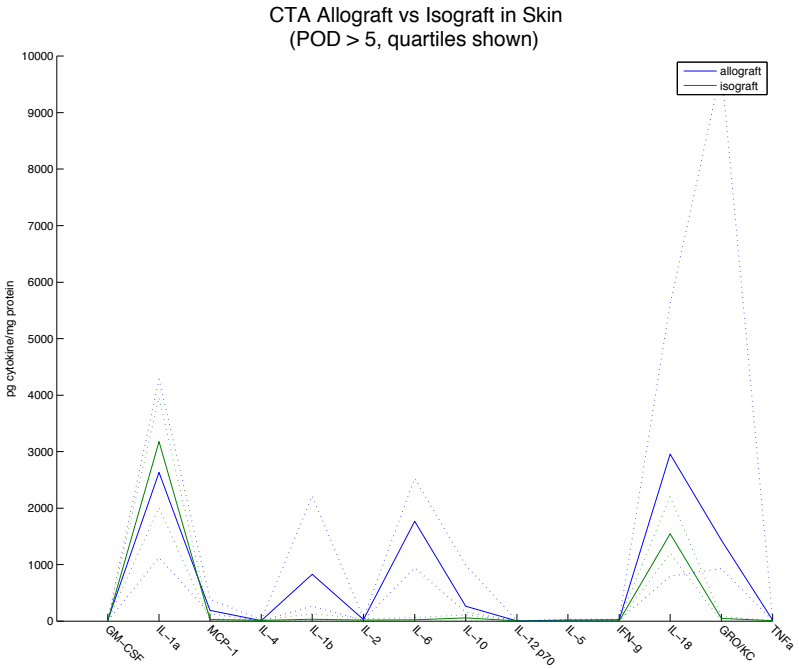

Figure 6.36

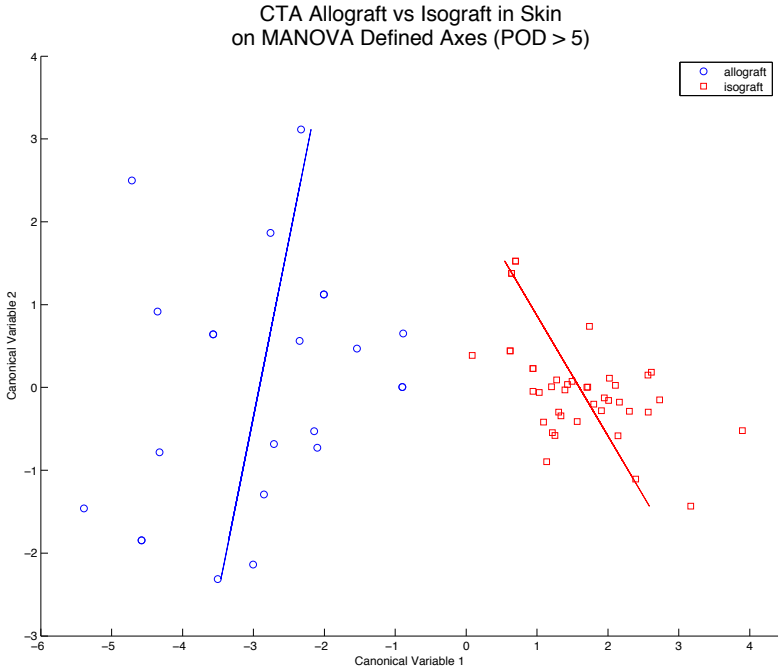

Figure 6.37

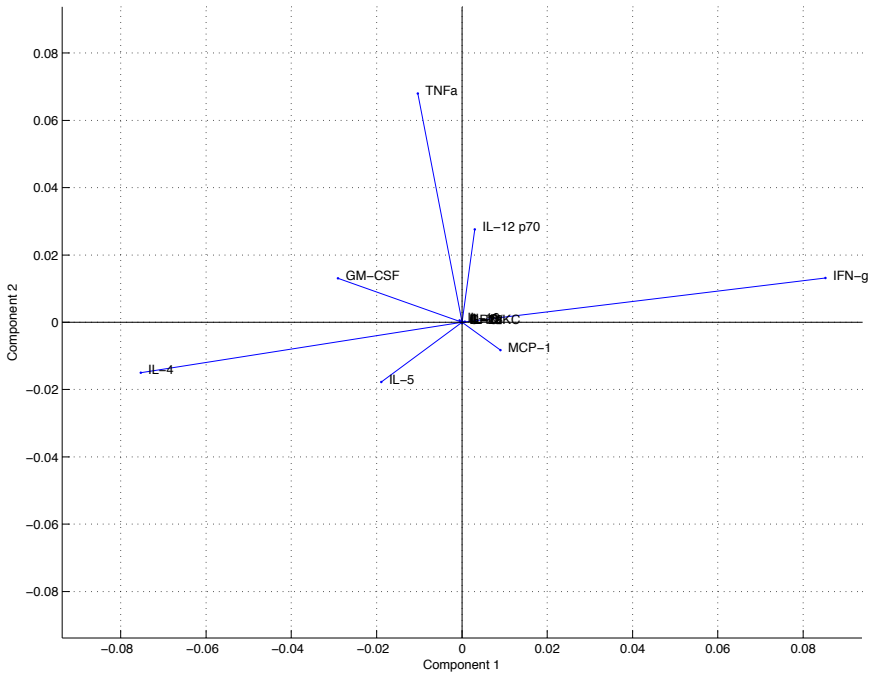

Figure 6.38

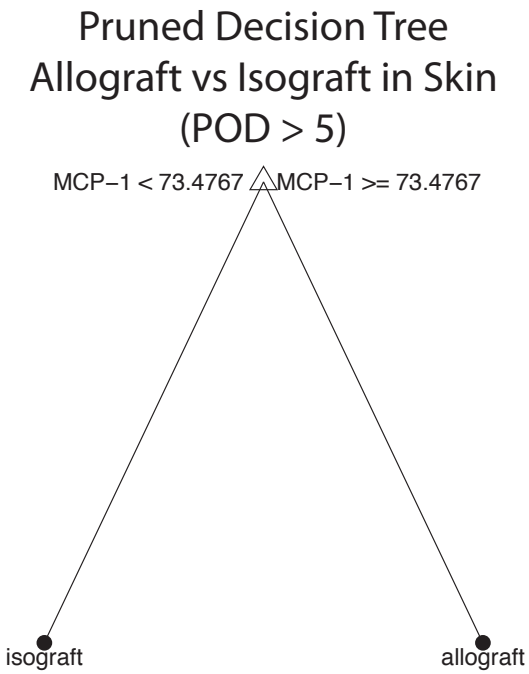

Figure 6.39

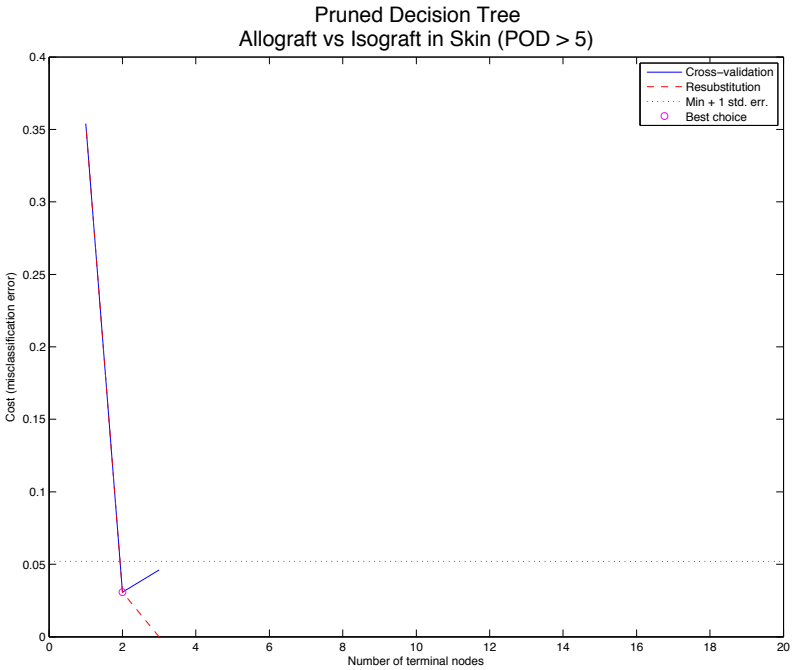

Figure 6.40

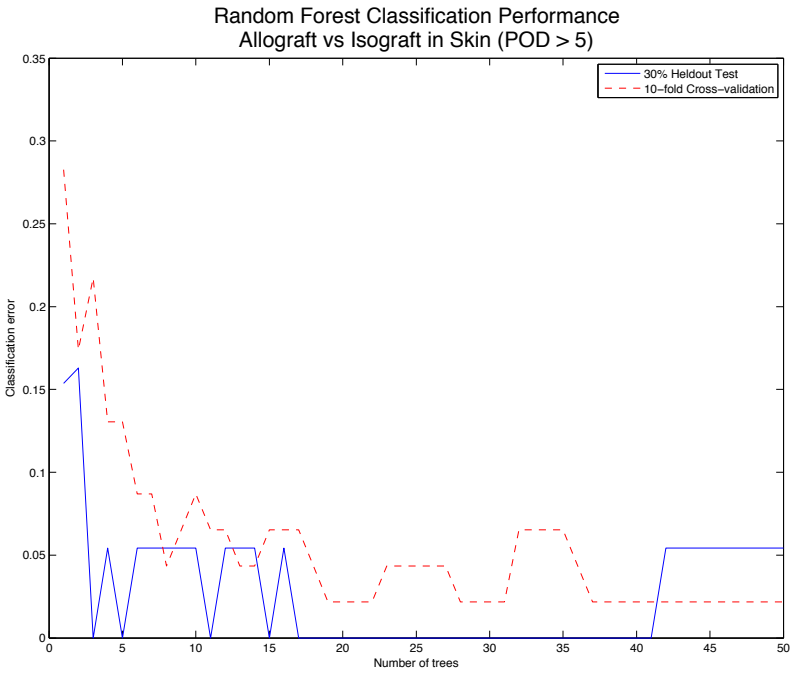

Figure 6.41

5-Dimensional Feature Selected Space

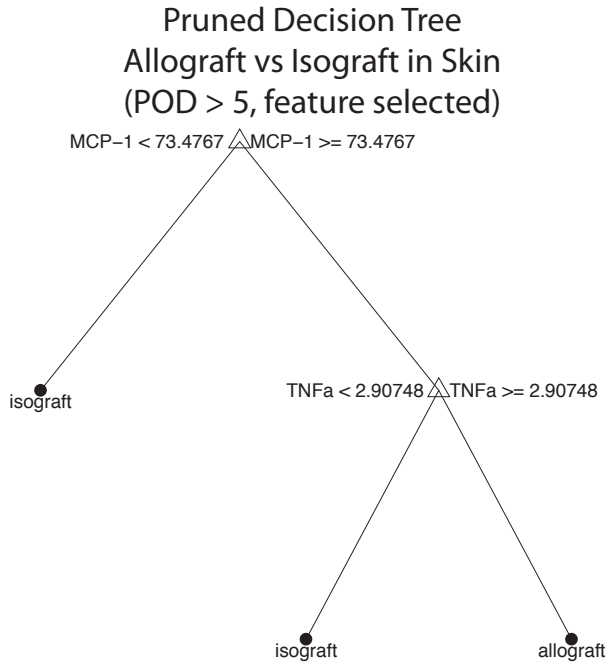

Figure 6.42

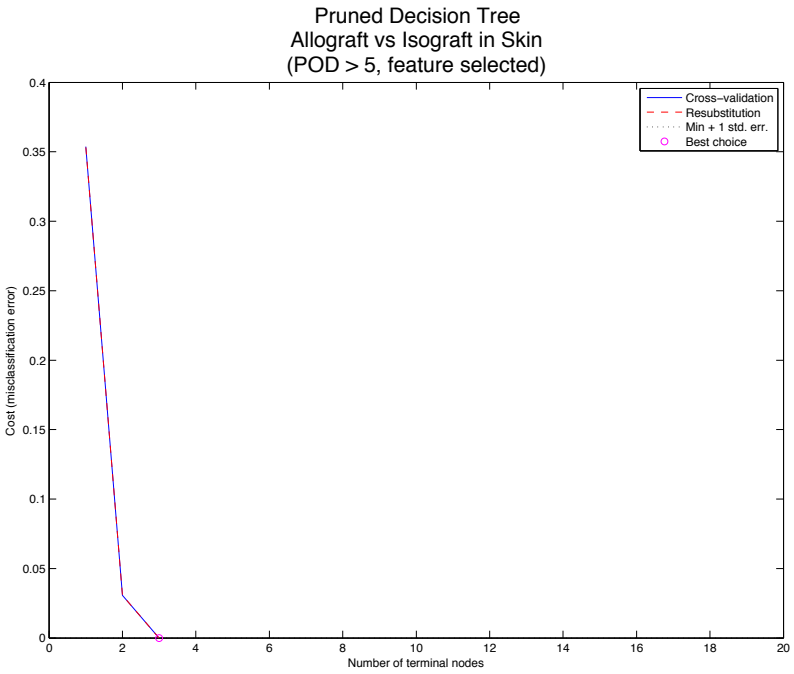

Figure 6.43

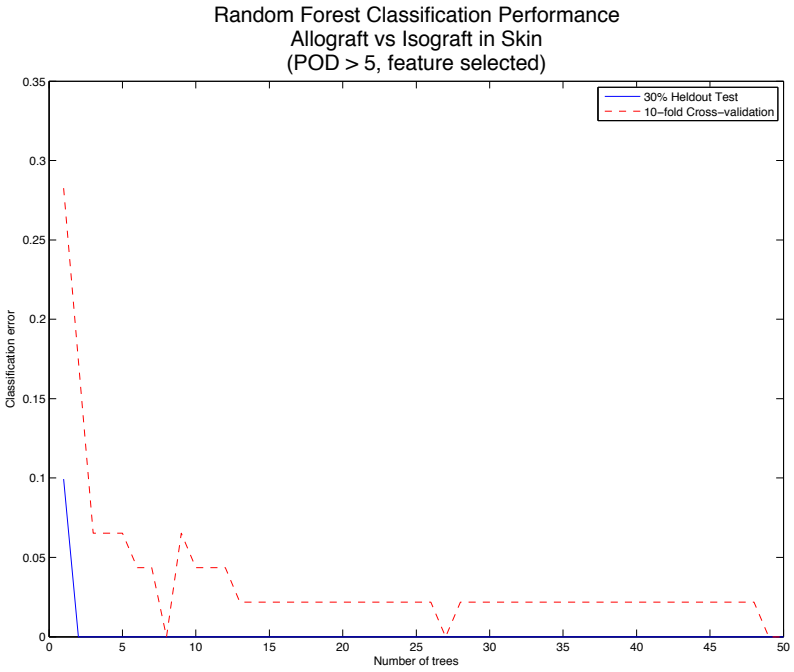

Figure 6.44

MANOVA Transformed Feature Space

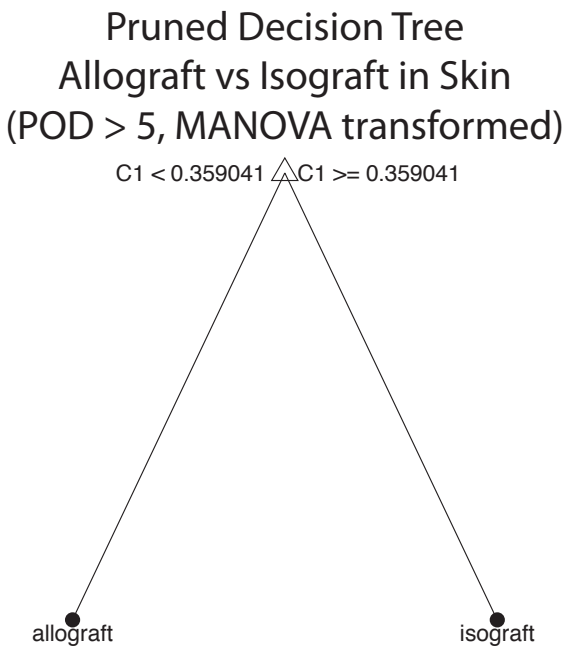

Figure 6.45

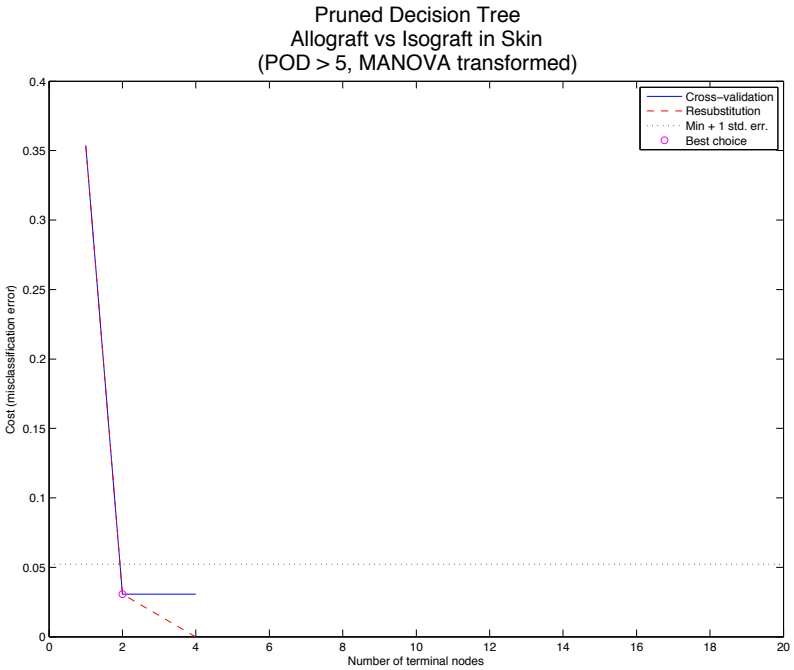

Figure 6.46

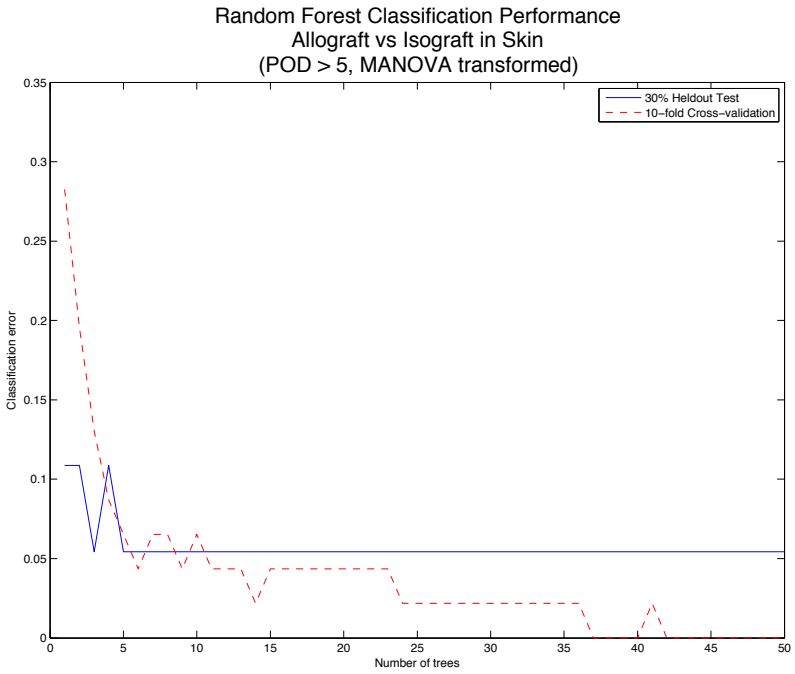

Figure 6.47

Allograft vs Isograft in Muscle (all time points)

Original 14-Dimensional Feature Space

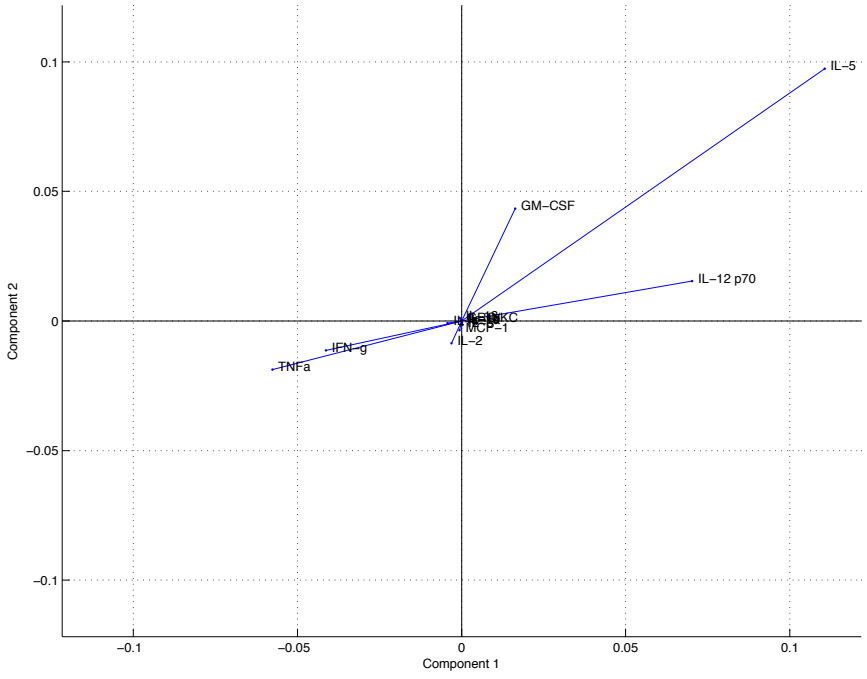

Figure 6.48

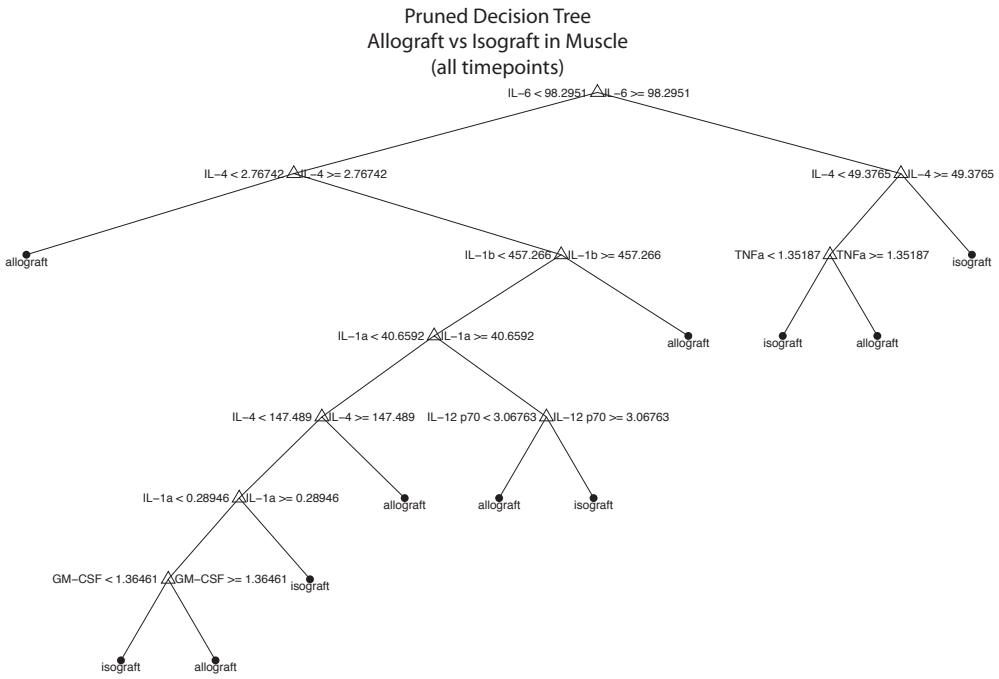

Figure 6.49

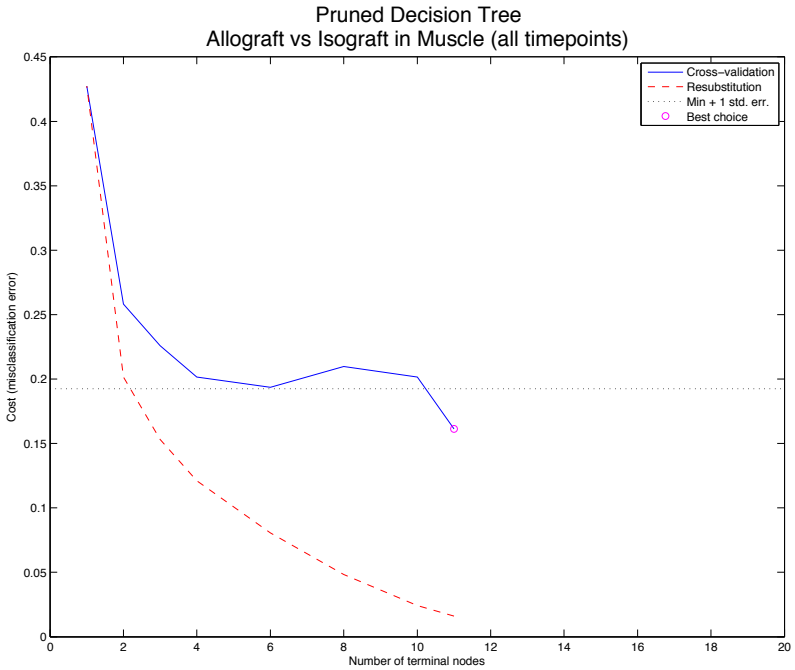

Figure 6.50

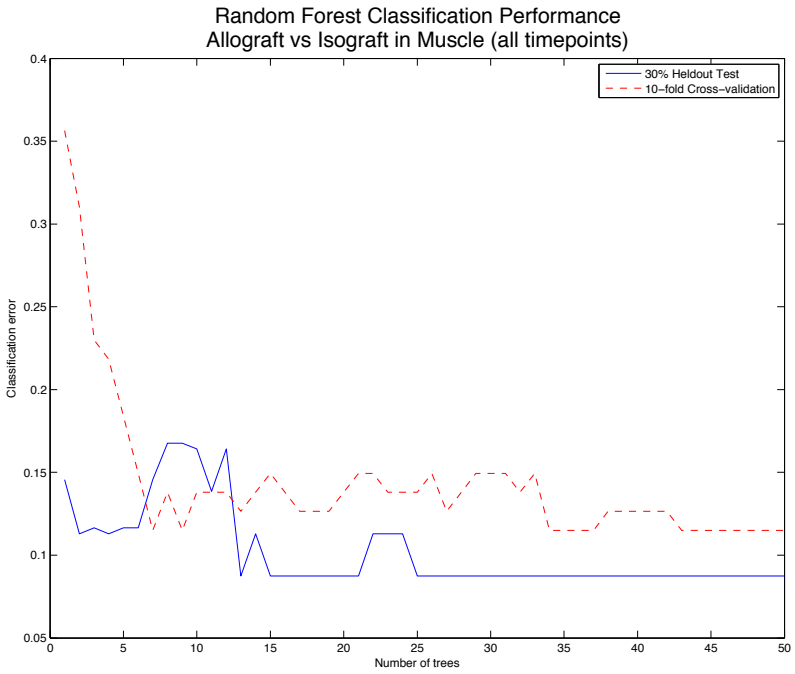

Figure 6.51

5-Dimensional Feature Selected Space

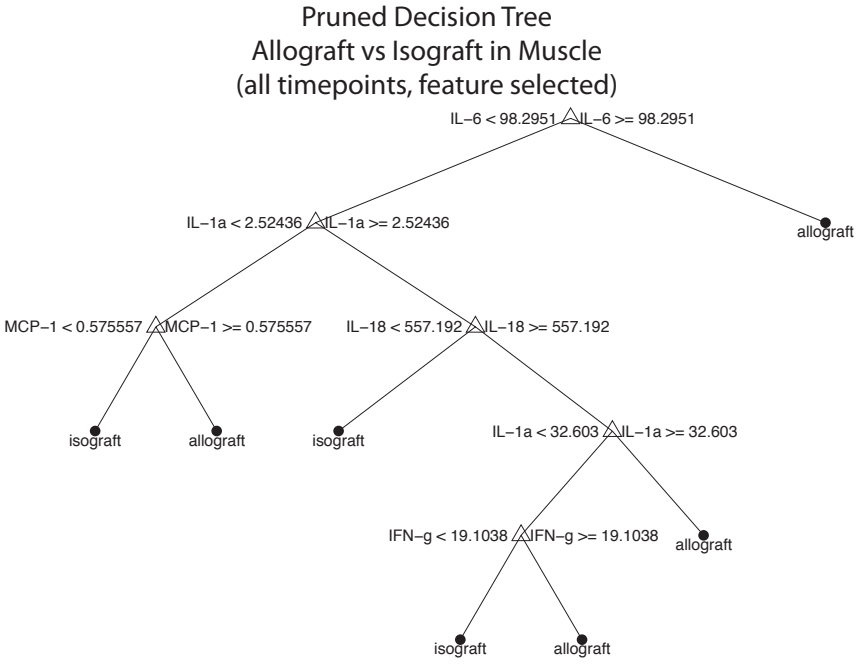

Figure 6.52

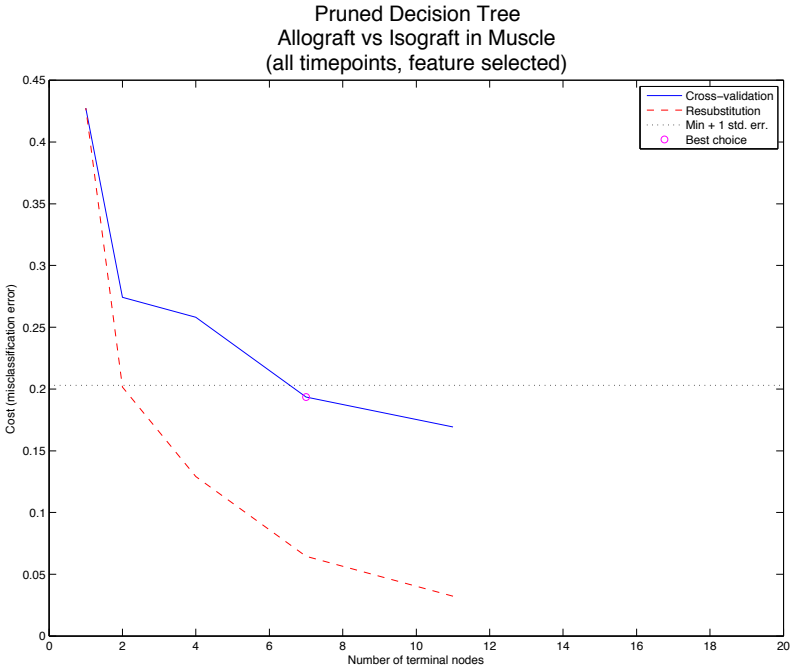

Figure 6.53

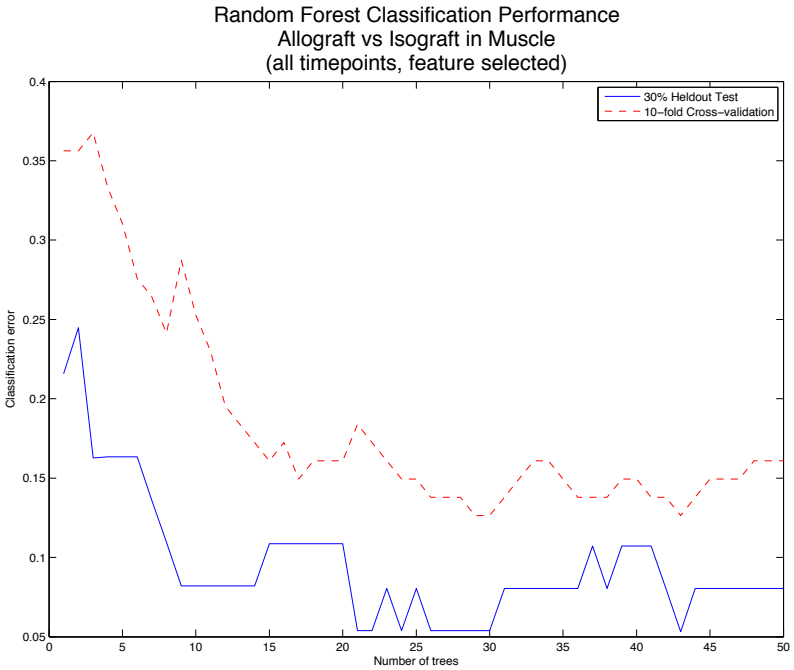

Figure 6.54

MANOVA Transformed Feature Space

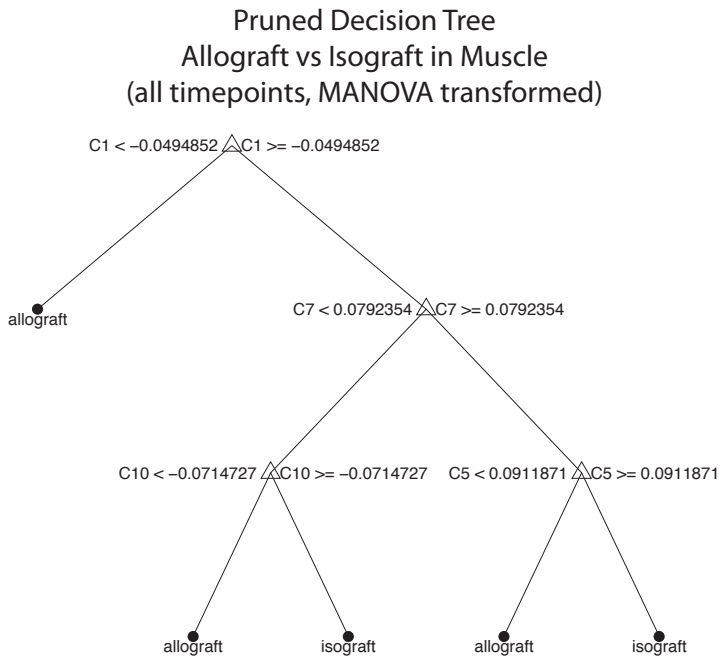

Figure 6.55

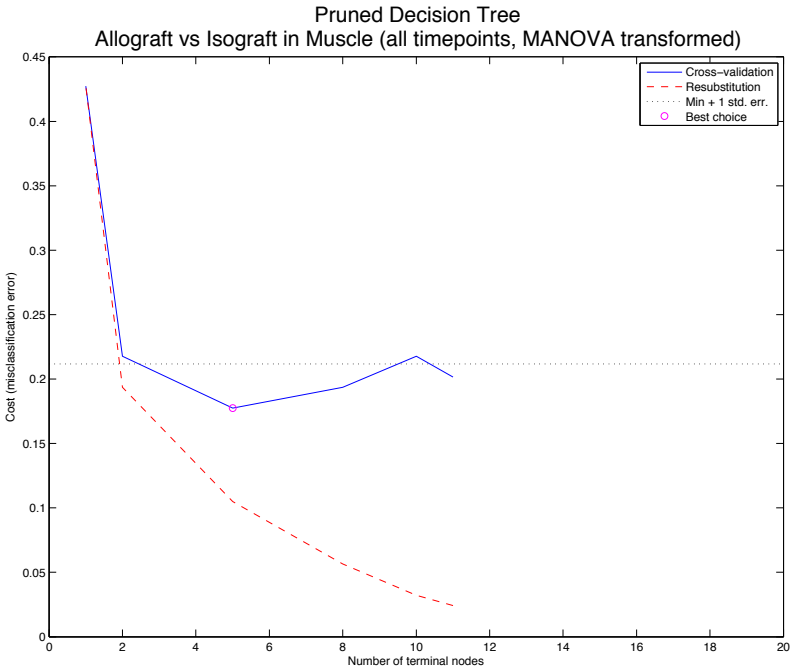

Figure 6.56

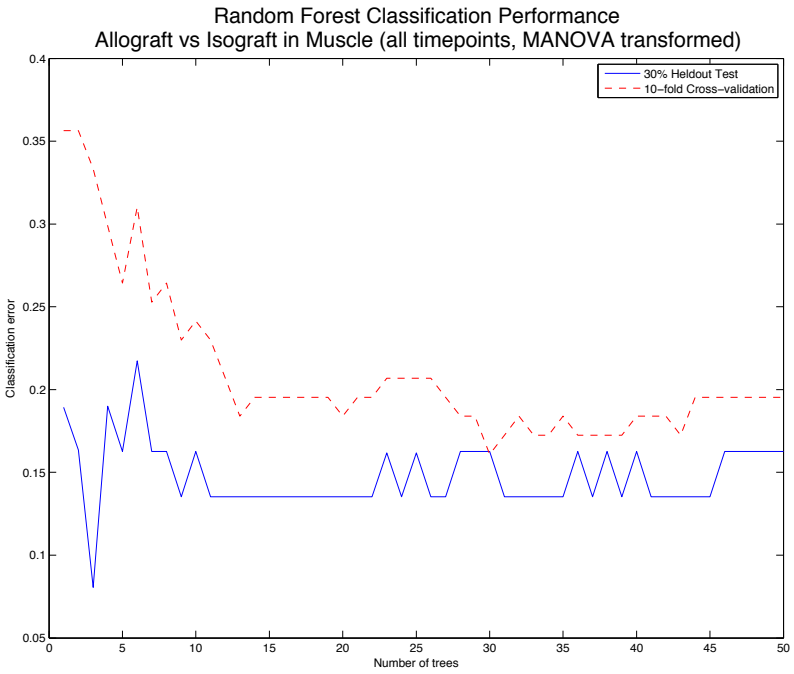

Figure 6.57

Hybrid Feature Space

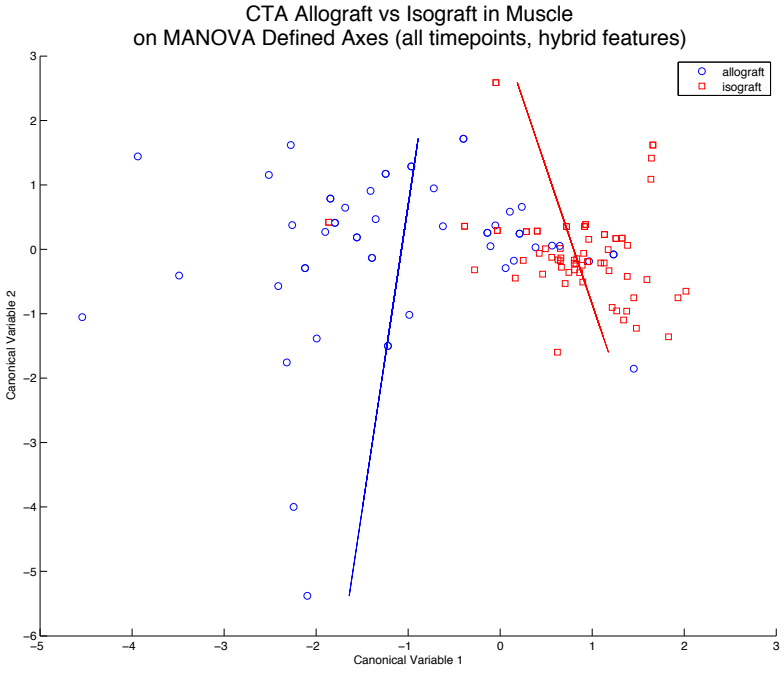

Figure 6.58

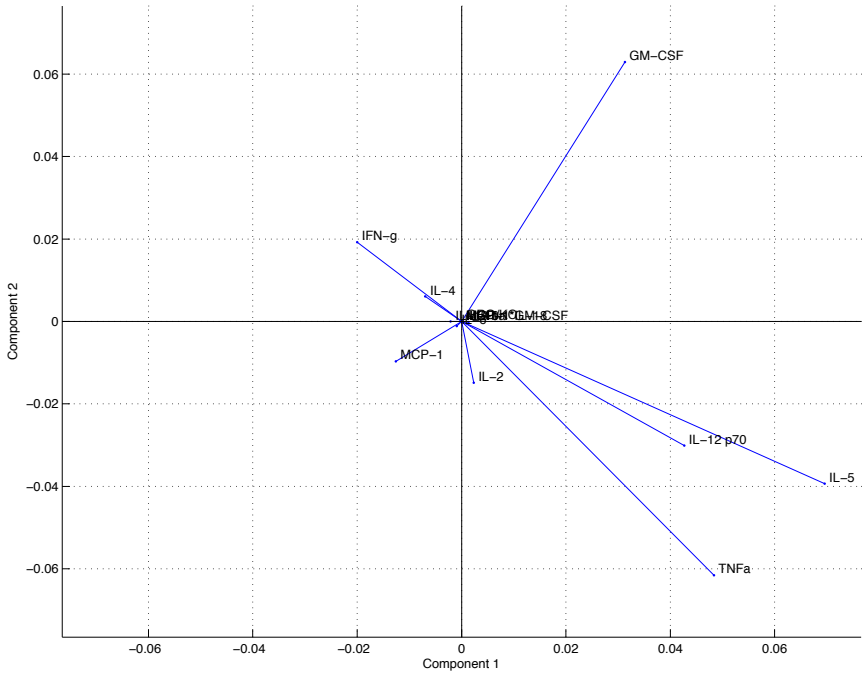

Figure 6.59

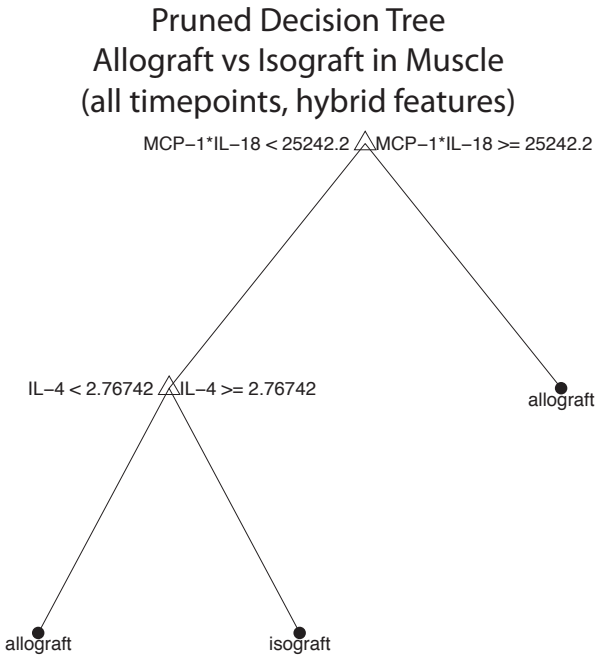

Figure 6.60

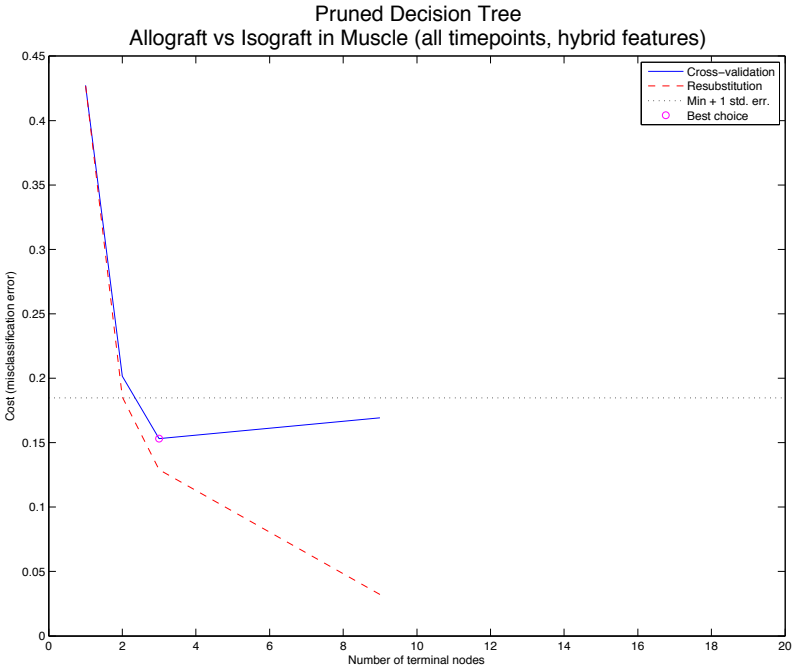

Figure 6.61

ROC Curves in Muscle

Original Features

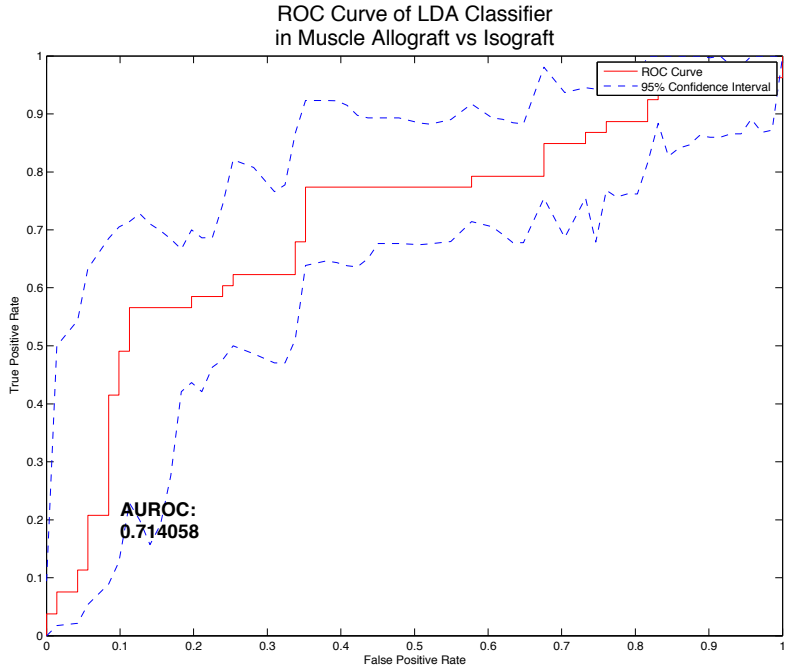

Figure 6.62

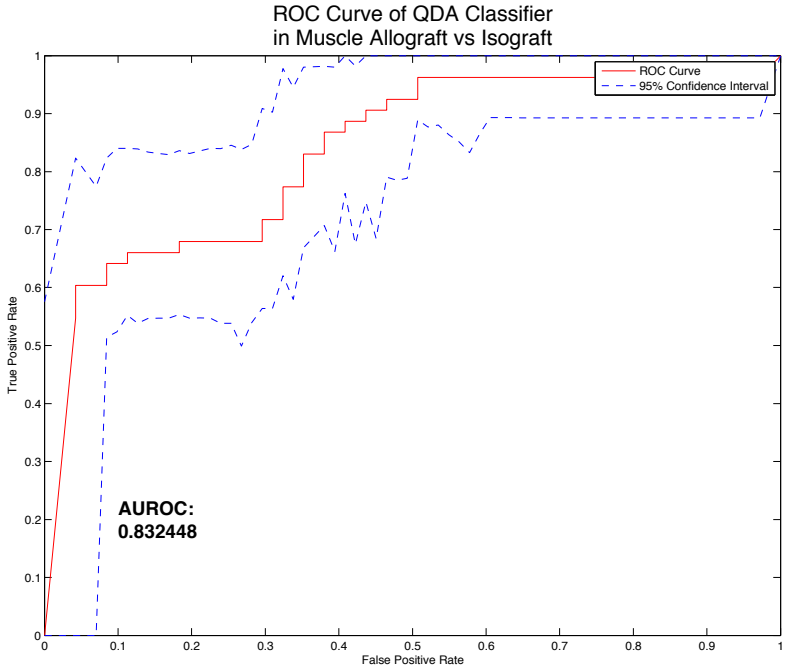

Figure 6.63

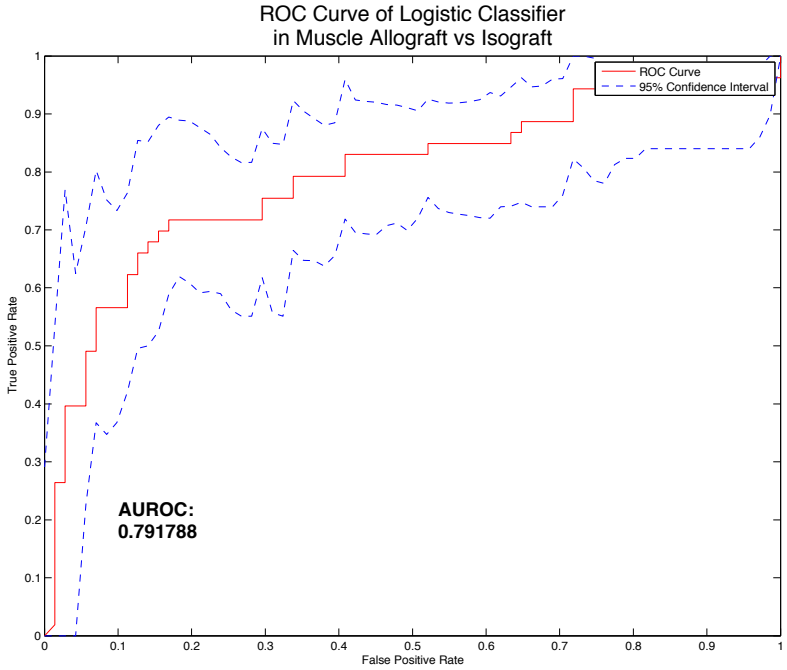

Figure 6.64

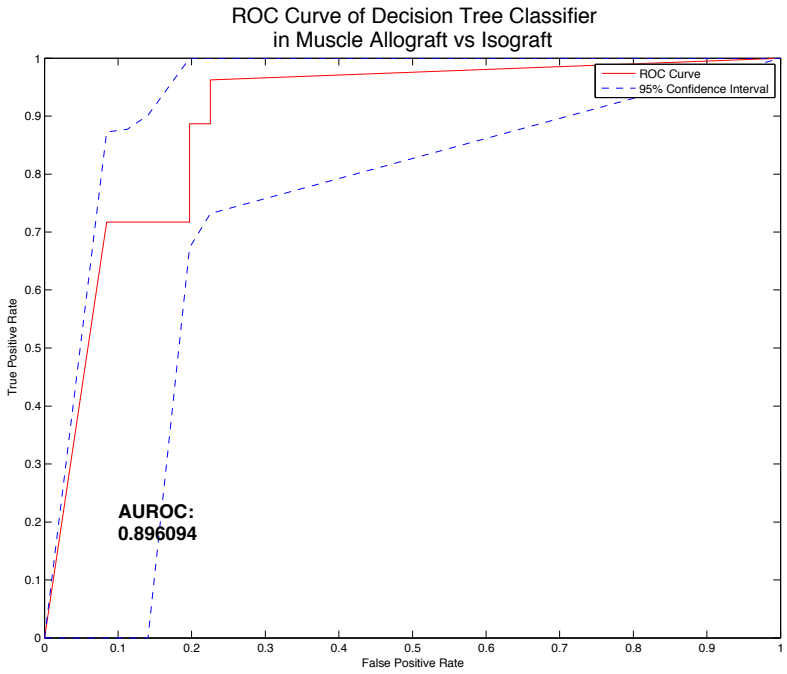

Figure 6.65

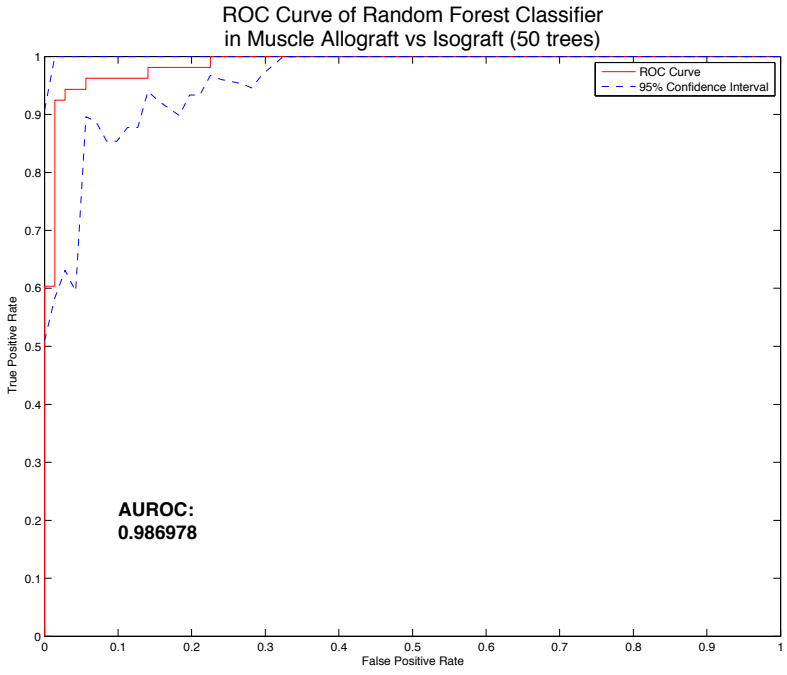

Figure 6.66

Hybrid Features

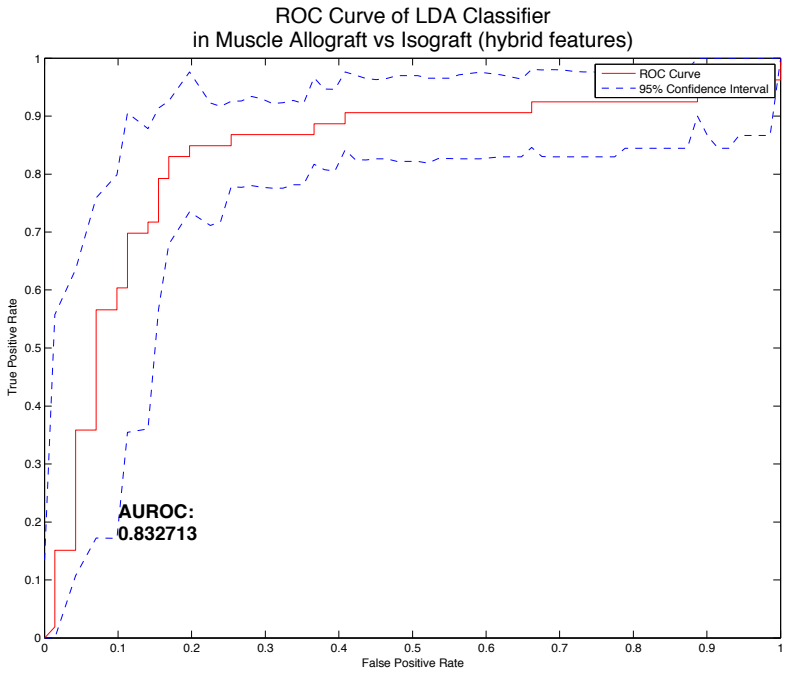

Figure 6.67

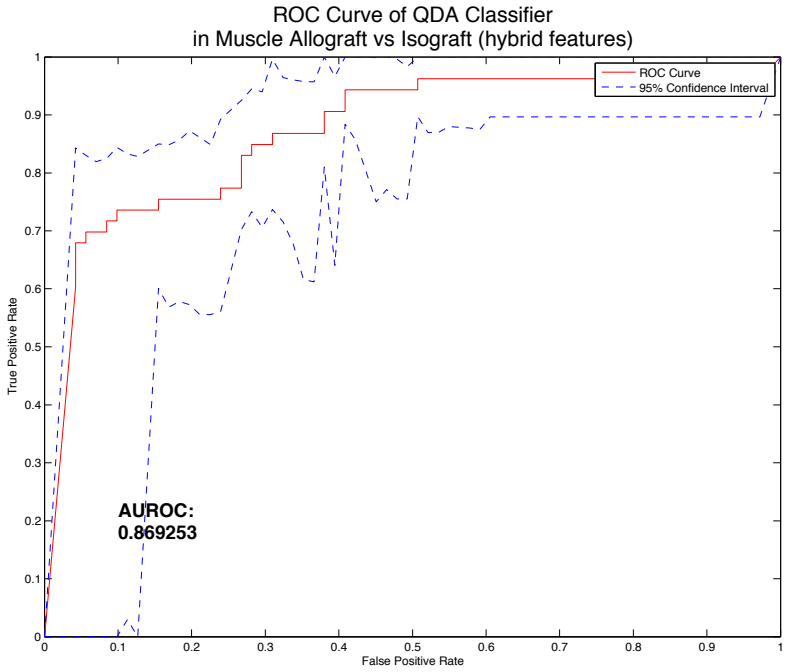

Figure 6.68

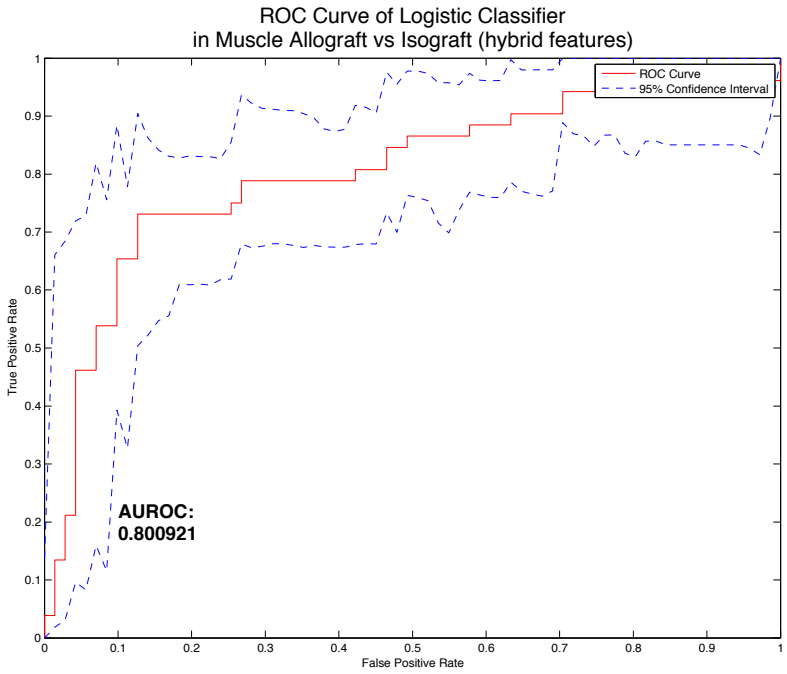

Figure 6.69

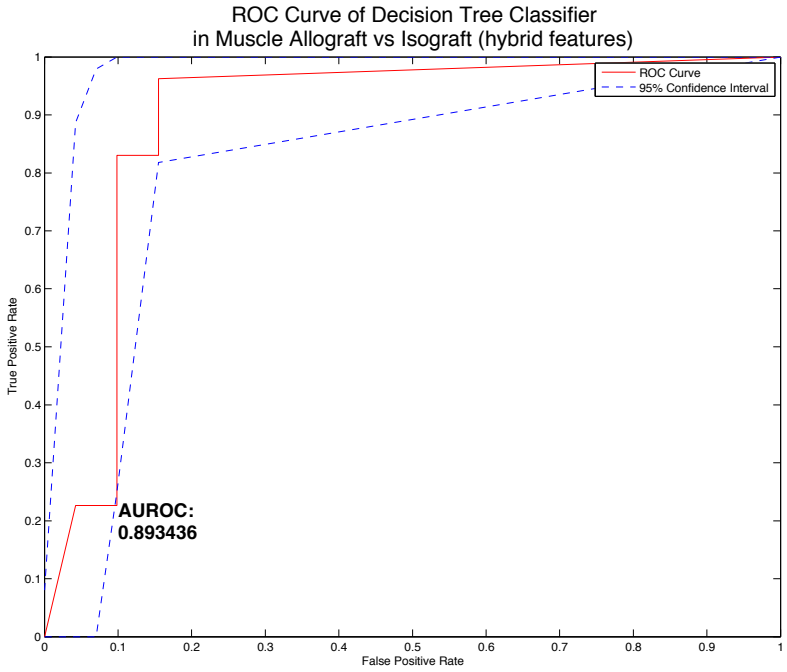

Figure 6.70

Allograft vs Isograft in Muscle (POD <= 5)

Original 14-Dimensional Feature Space

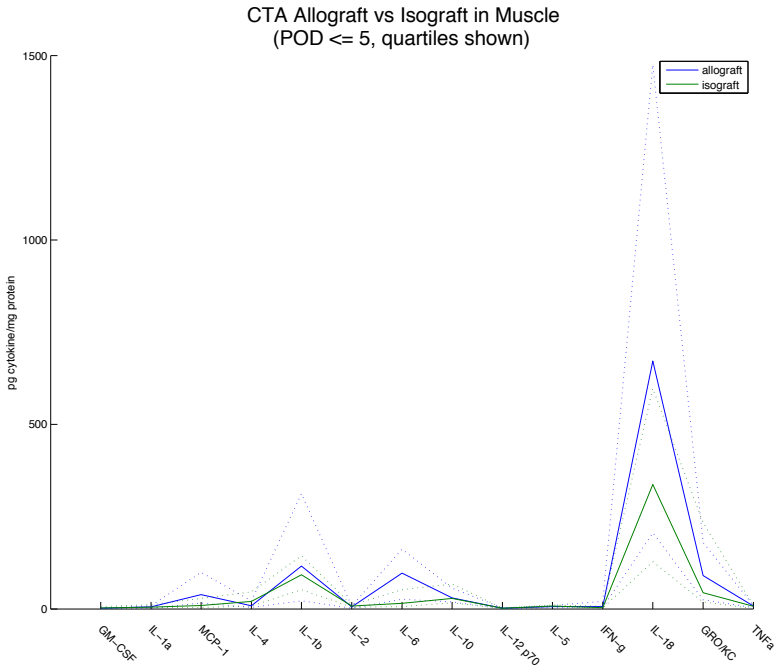

Figure 6.71

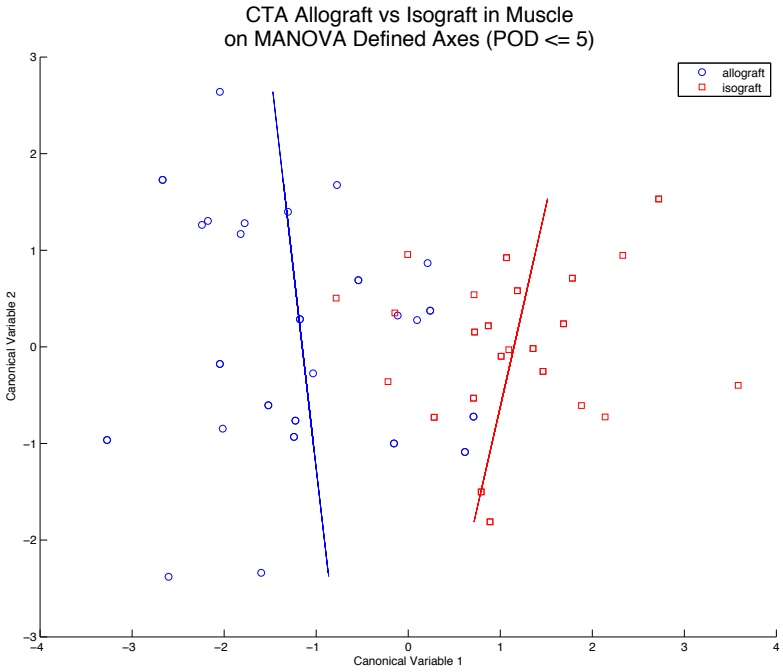

Figure 6.72

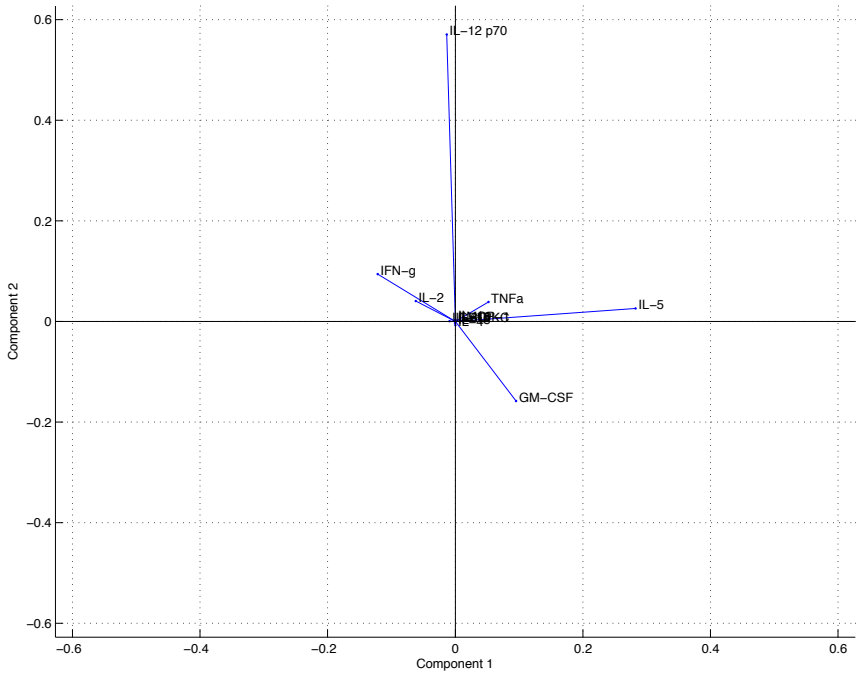

Figure 6.73

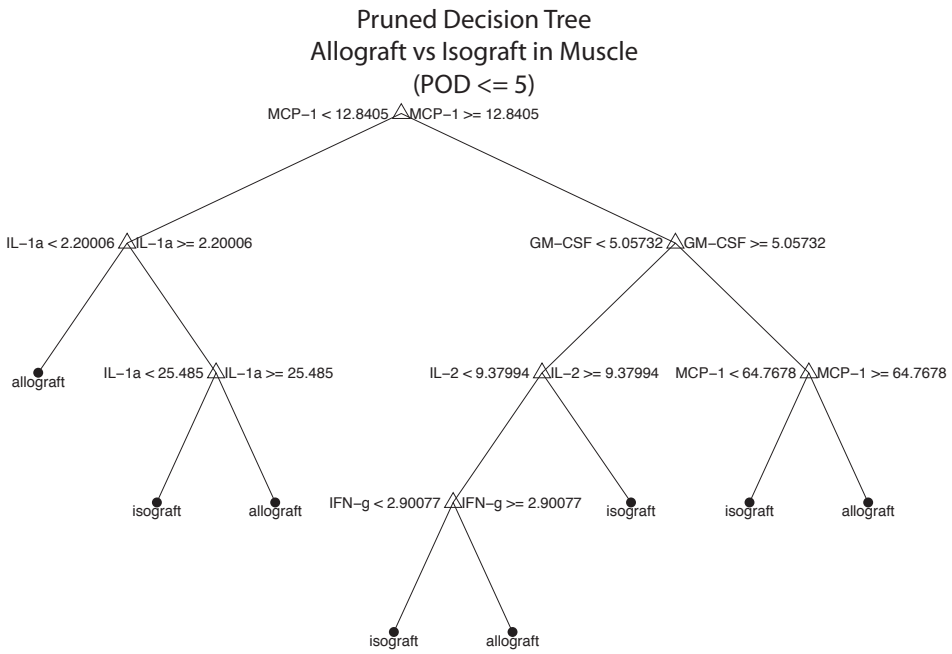

Figure 6.74

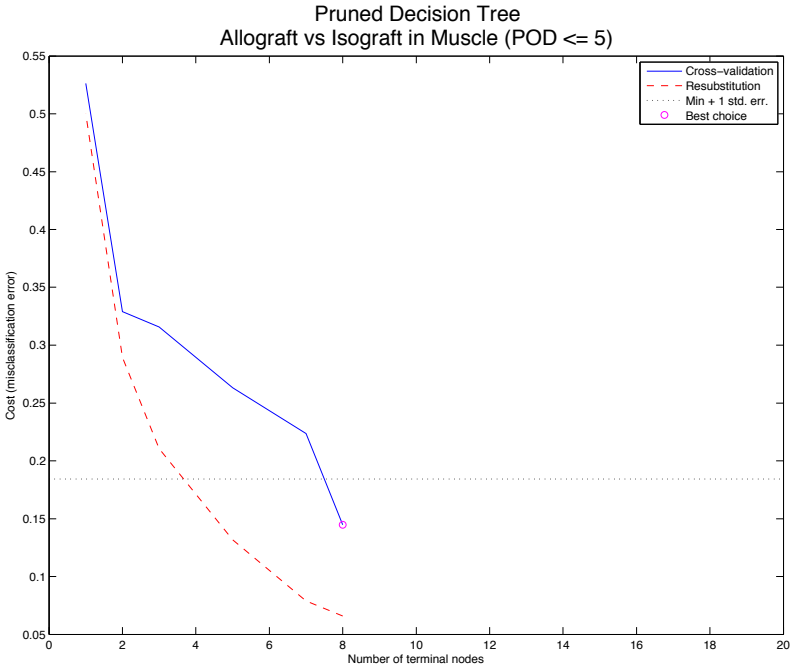

Figure 6.75

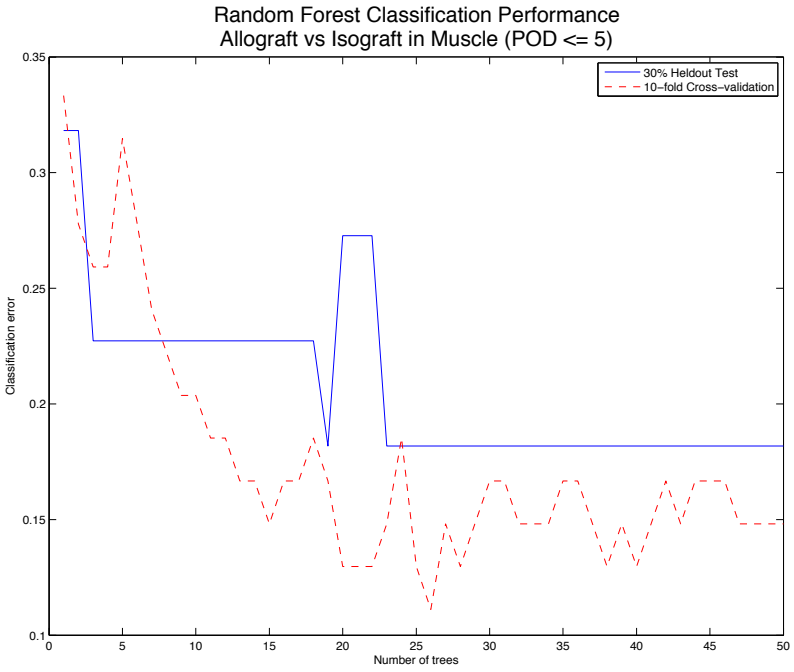

Figure 6.76

5-Dimensional Feature Selected Space

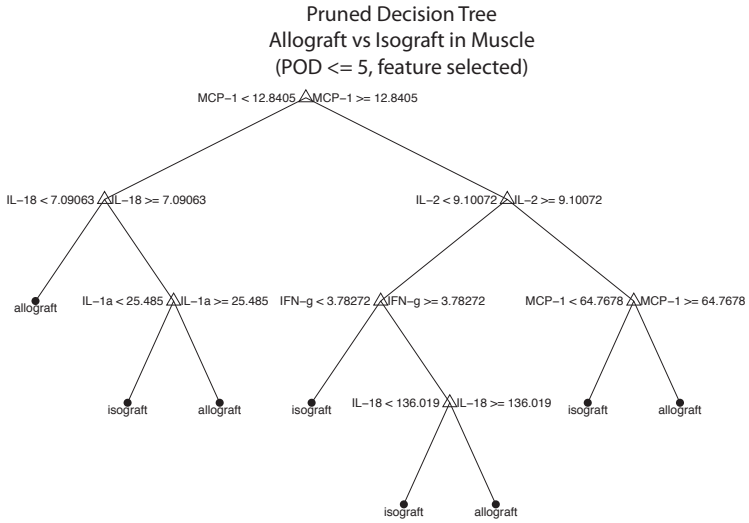

Figure 6.77

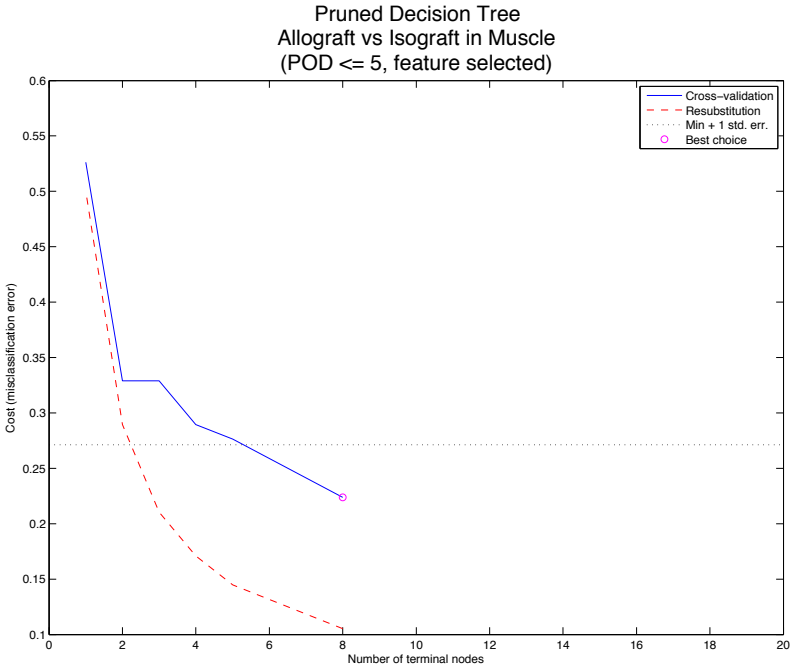

Figure 6.78

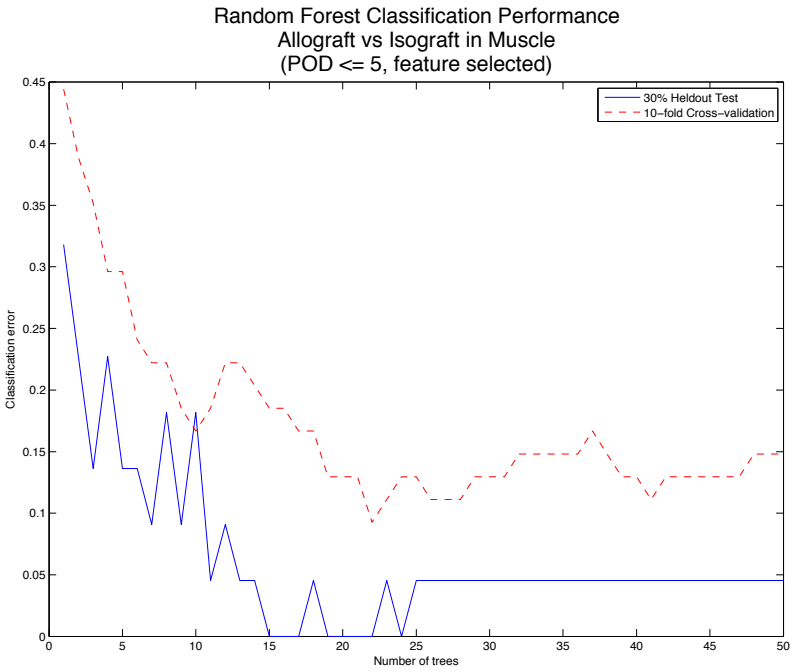

Figure 6.79

MANOVA Transformed Feature Space

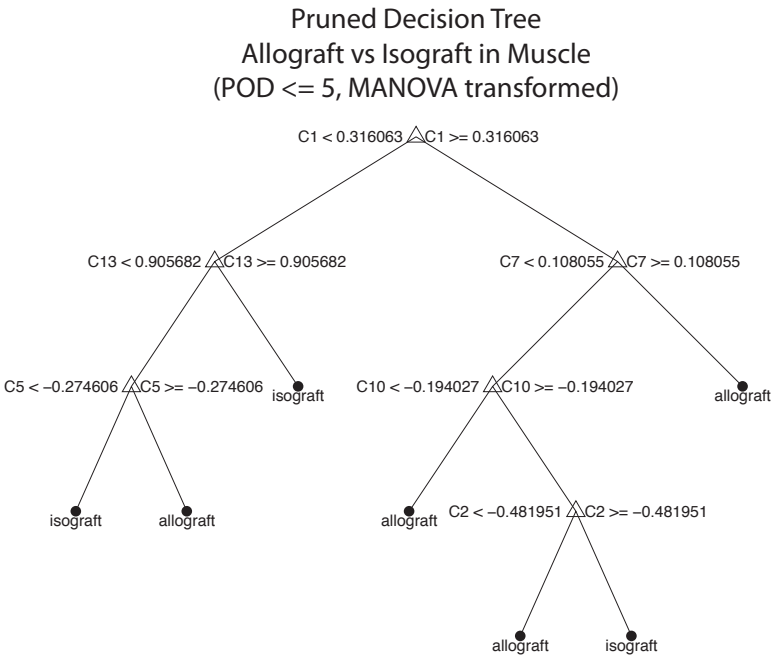

Figure 6.80

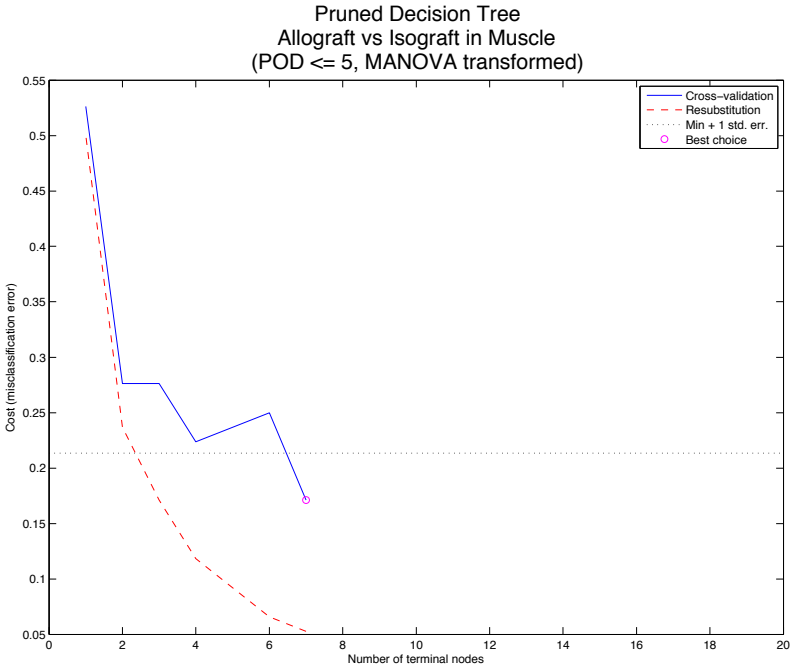

Figure 6.81

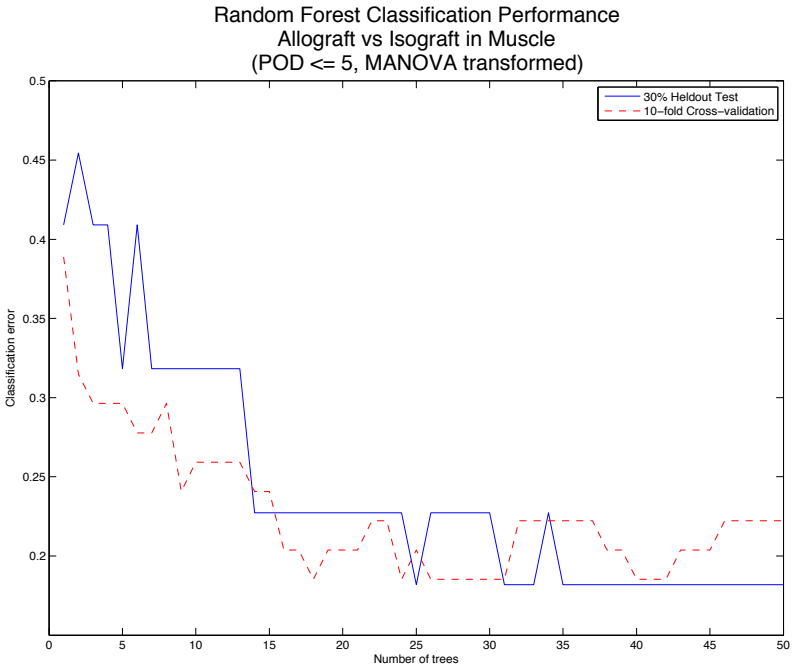

Figure 6.82

Allograft vs Isograft in Muscle (POD > 5)

Original 14-Dimensional Feature Space

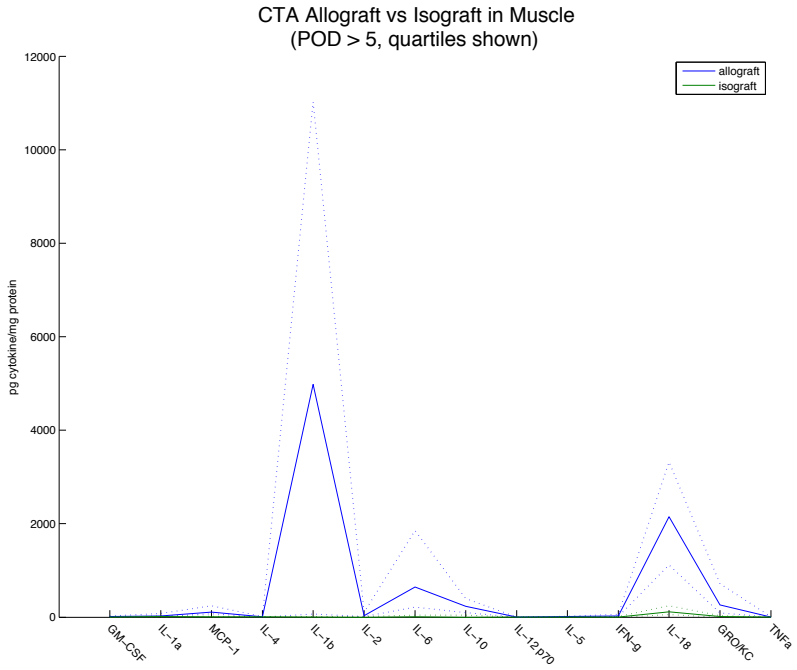

Figure 6.83

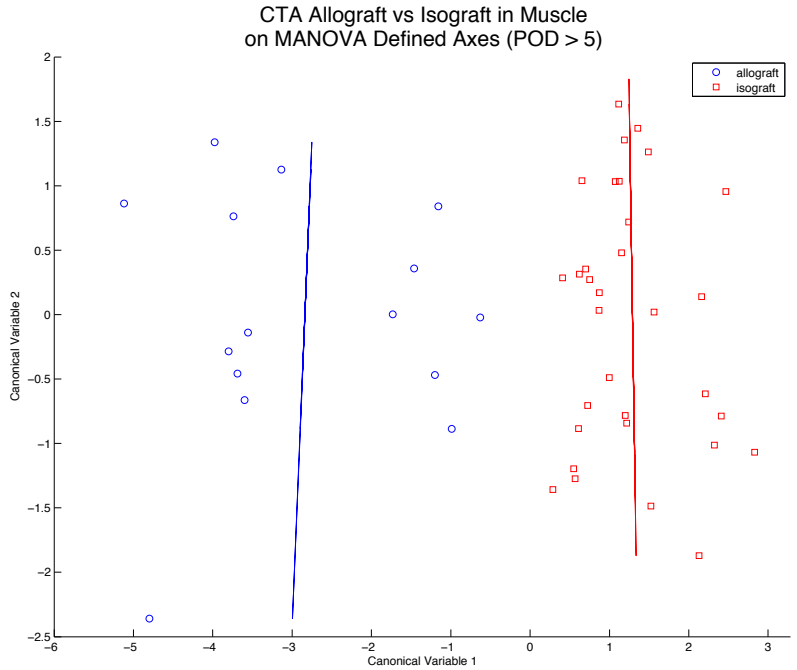

Figure 6.84

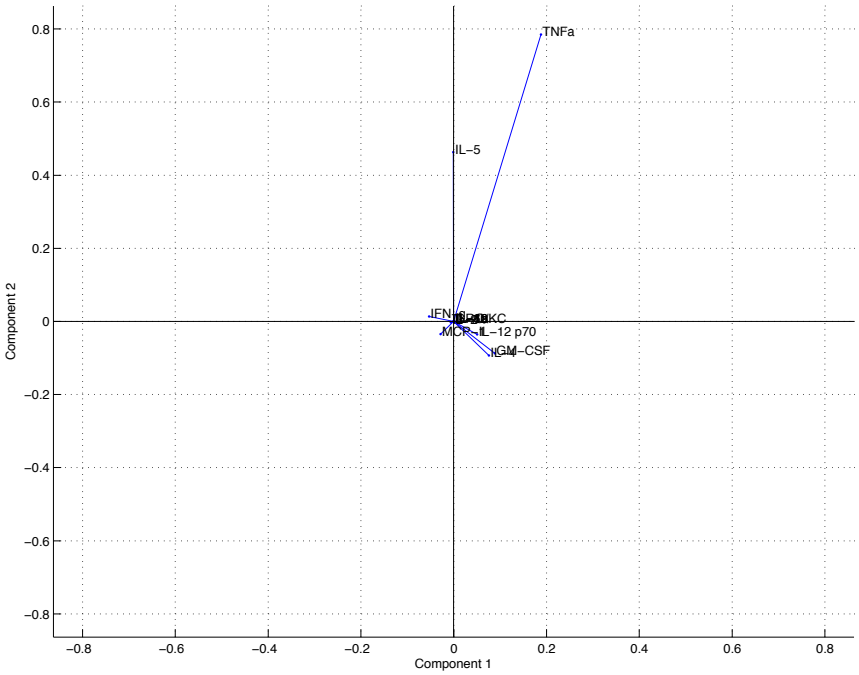

Figure 6.85

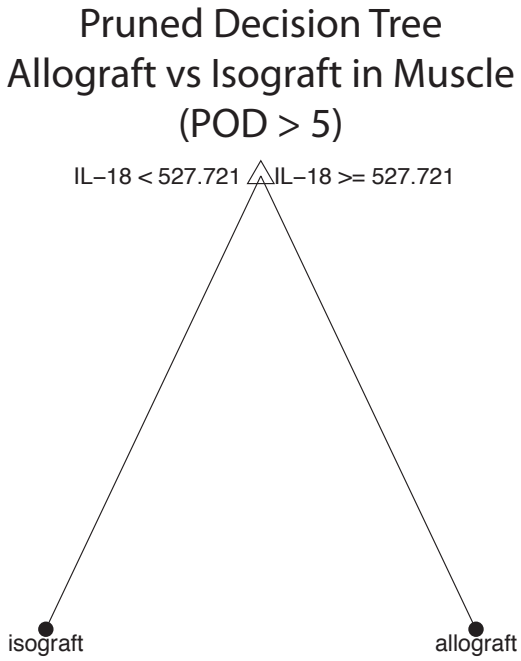

Figure 6.86

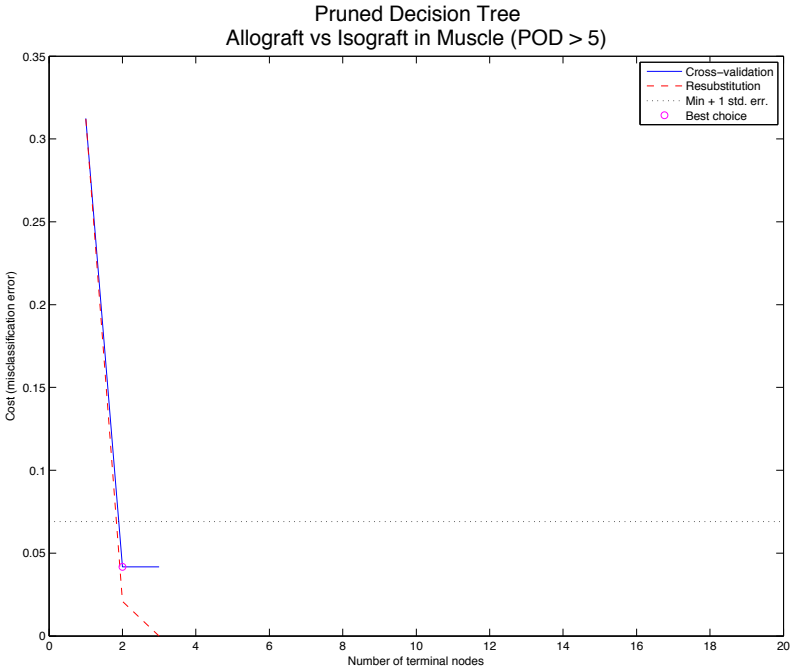

Figure 6.87

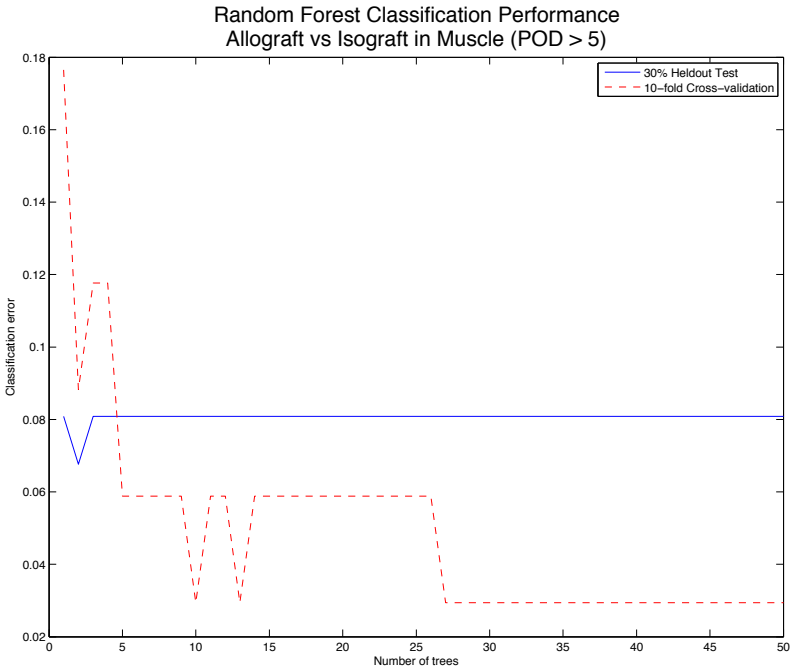

Figure 6.88

5-Dimensional Feature Selected Space

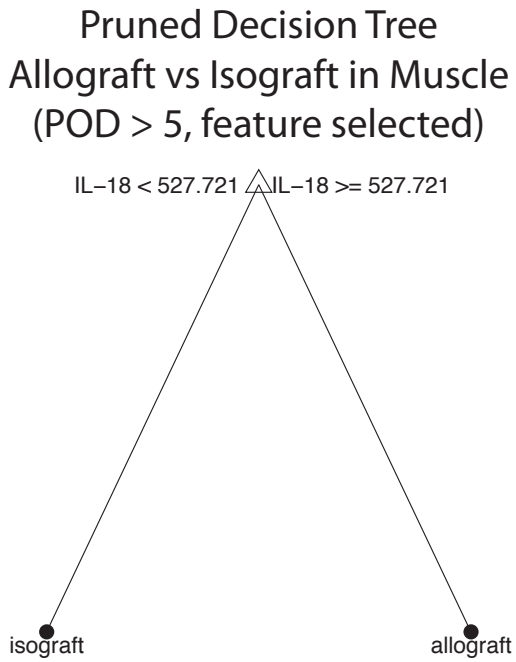

Figure 6.89

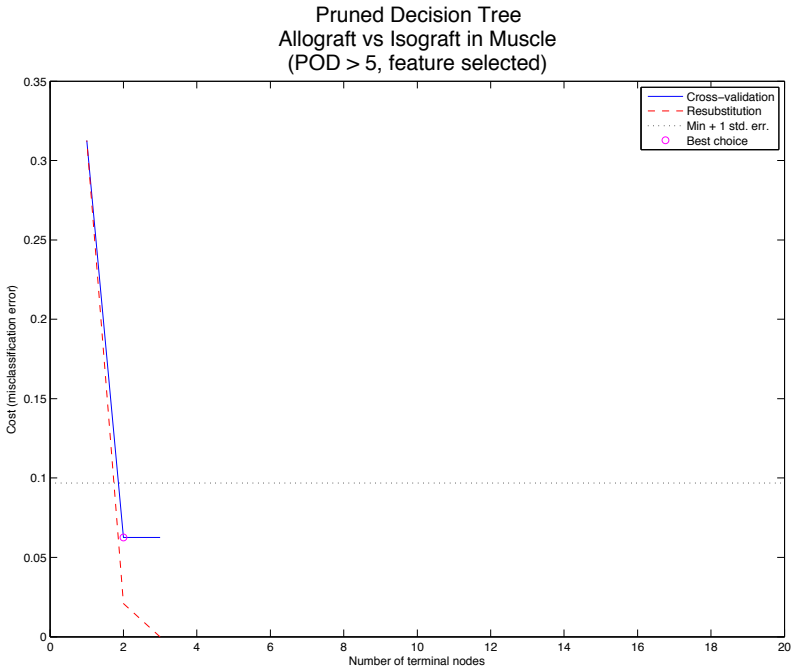

Figure 6.90

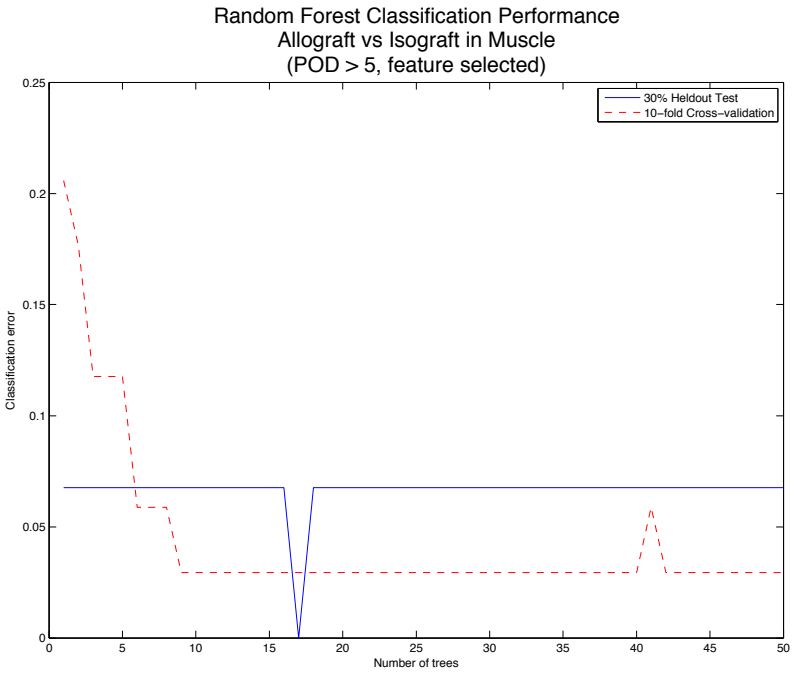

Figure 6.91

MANOVA Transformed Feature Space

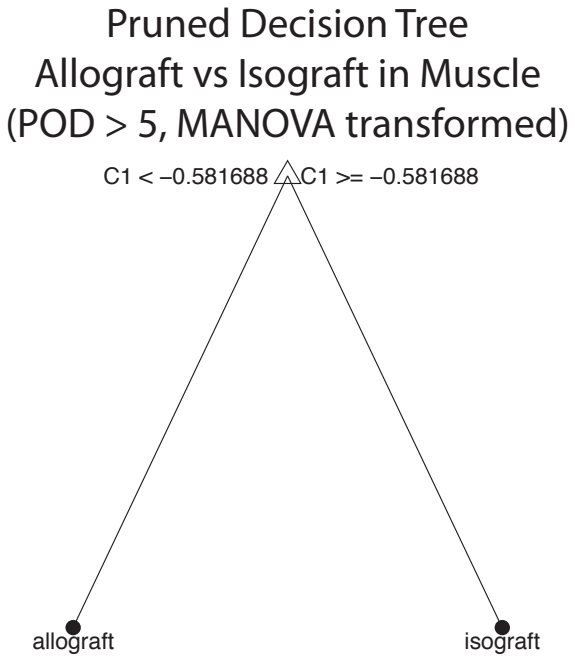

Figure 6.92

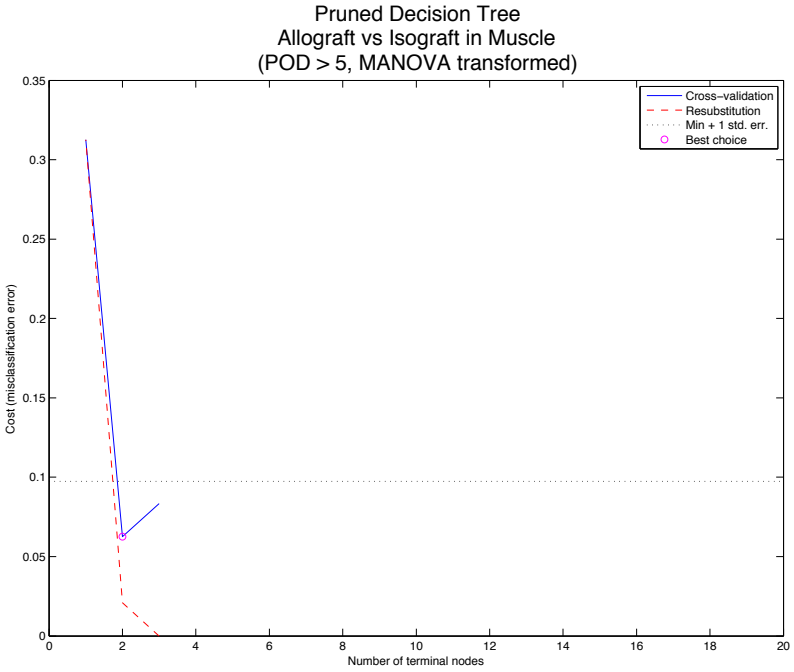

Figure 6.93

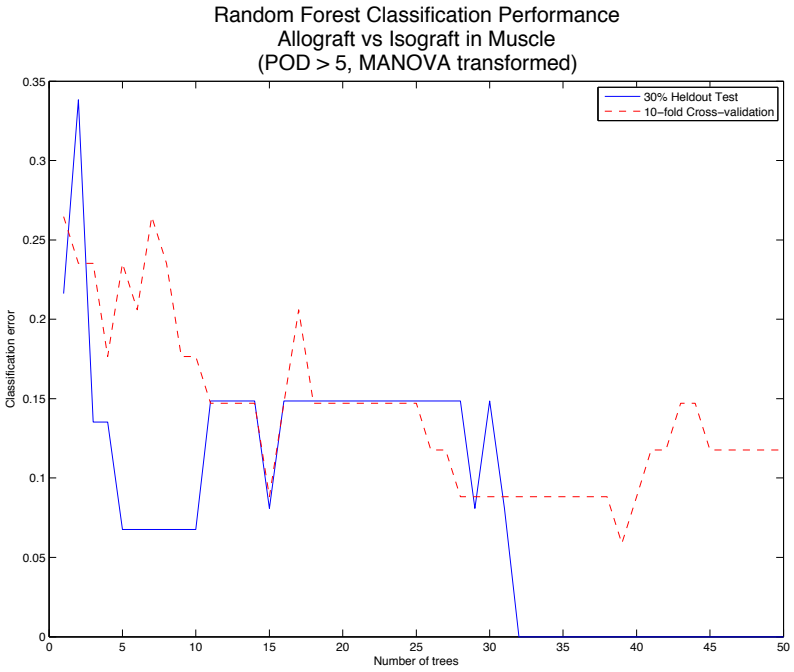

Figure 6.94

Rejecting vs Suppressed in FK Treated Skin

Original 14-Dimensional Feature Space

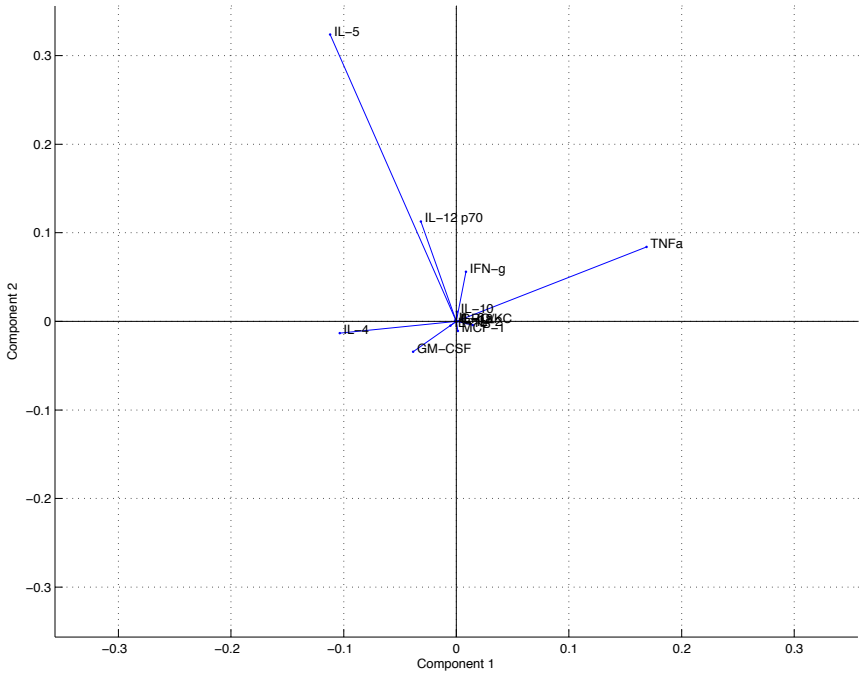

Figure 6.95

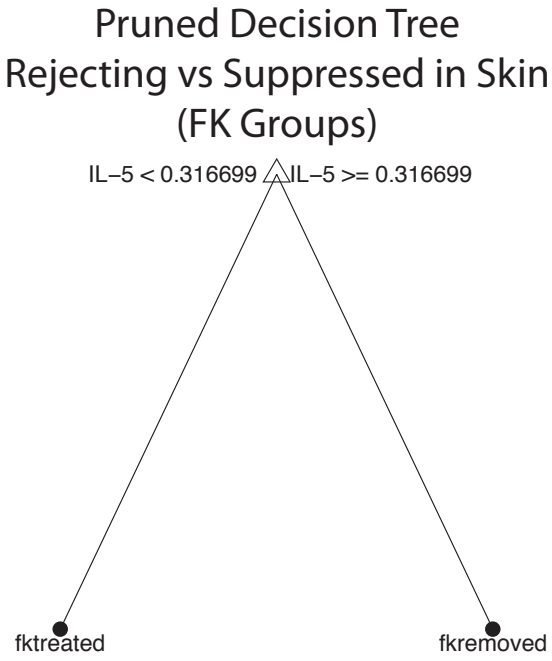

Figure 6.96

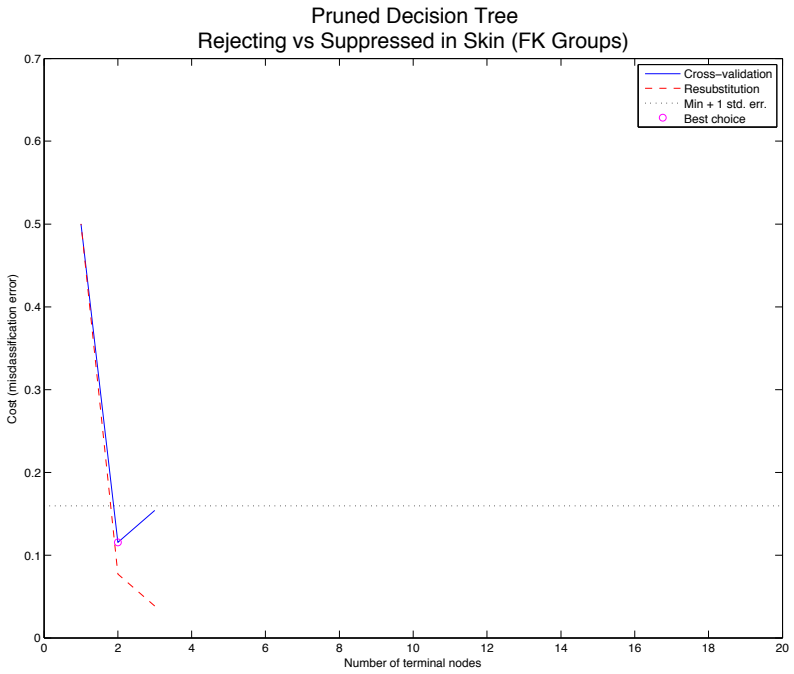

Figure 6.97

5-Dimensional Feature Selected Space

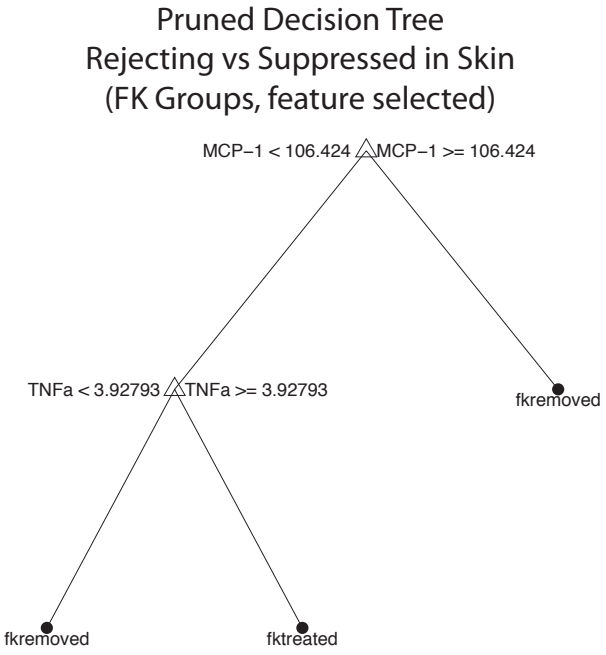

Figure 6.98

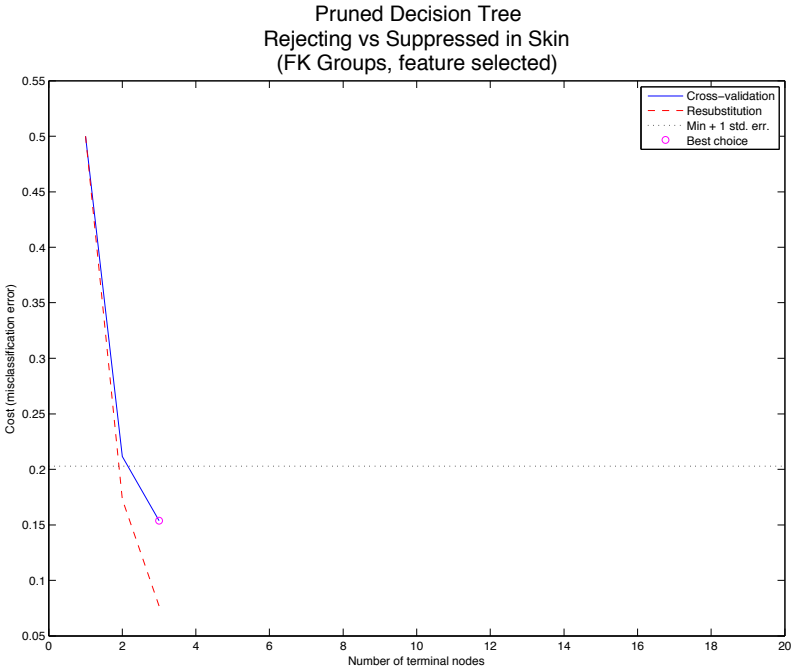

Figure 6.99

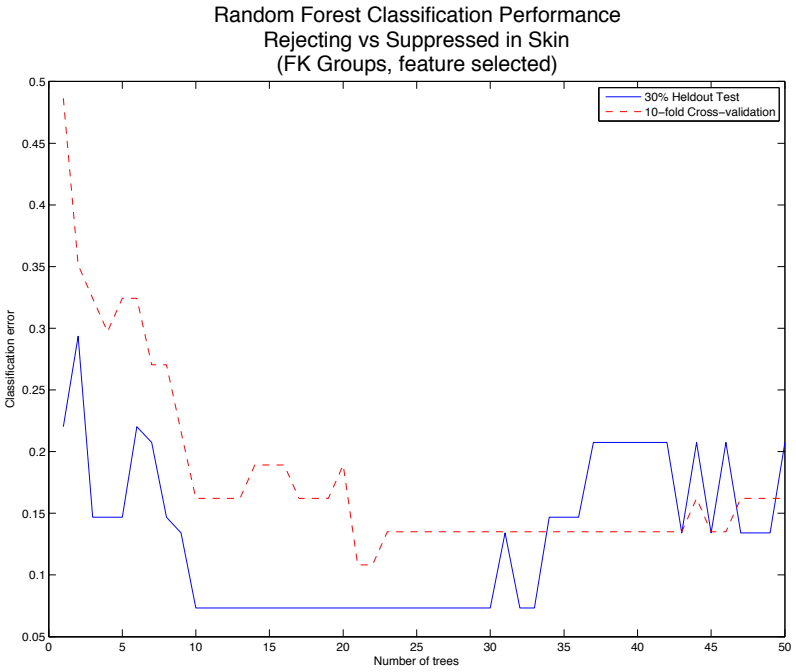

Figure 6.100

MANOVA Transformed Feature Space

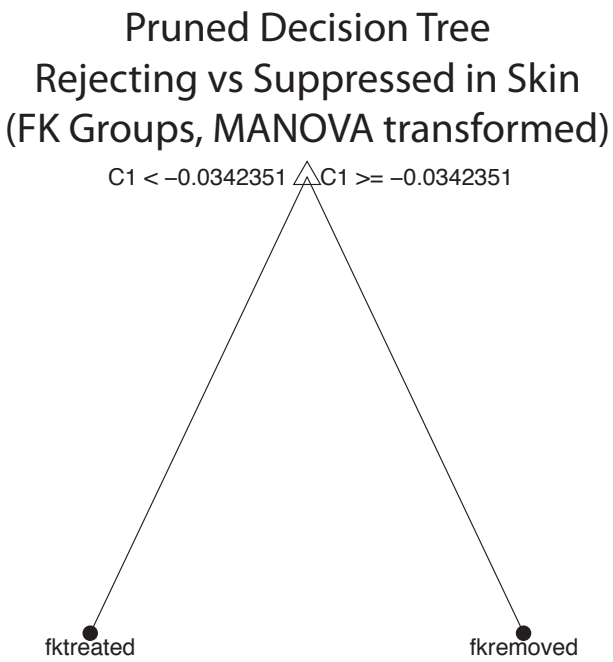

Figure 6.101

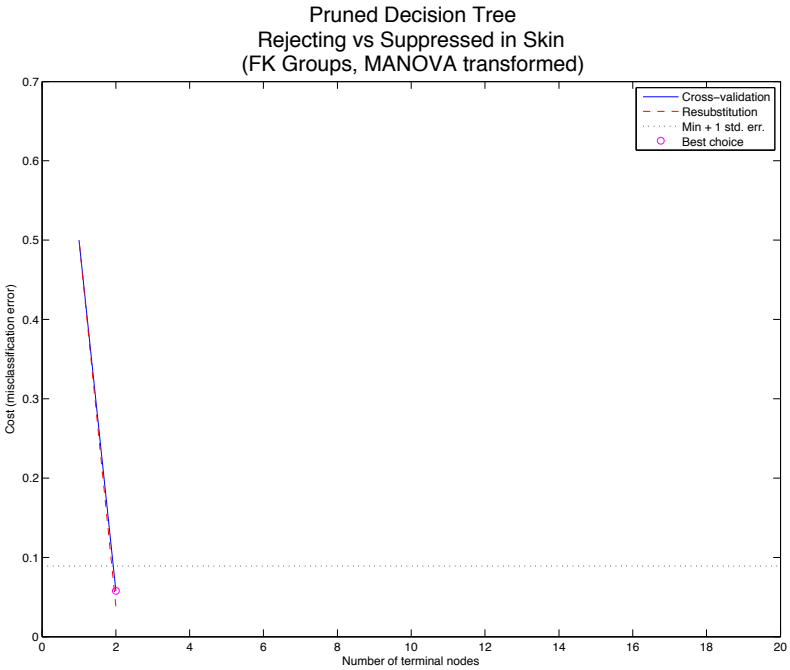

Figure 6.102

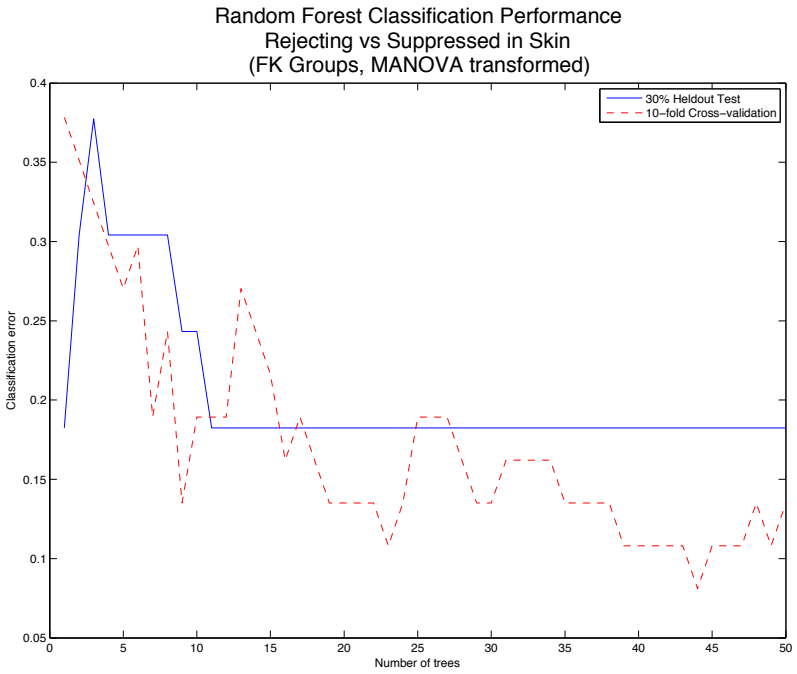

Figure 6.103

Rejecting vs Suppressed in FK Treated Muscle

Original 14-Dimensional Feature Space

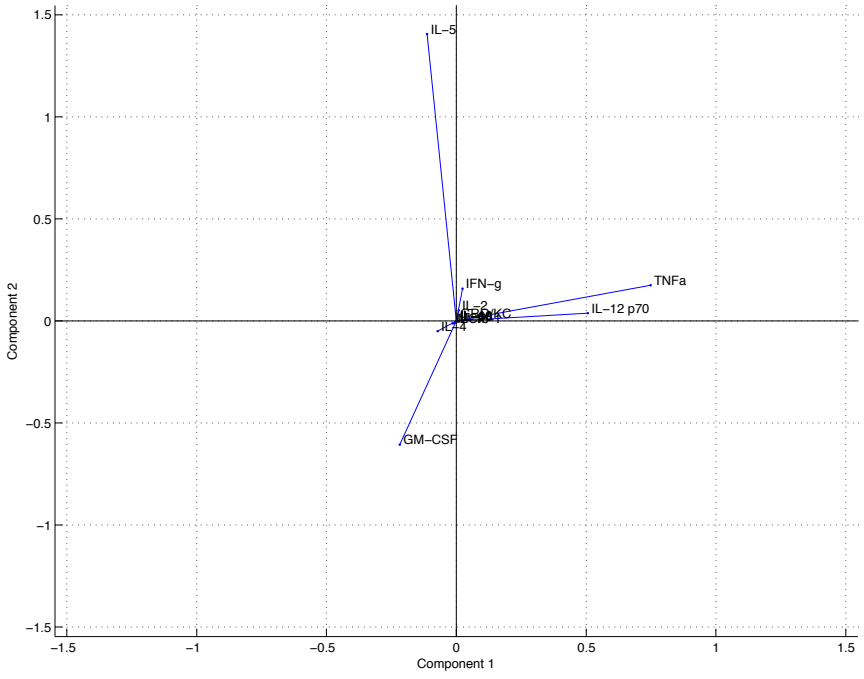

Figure 6.104

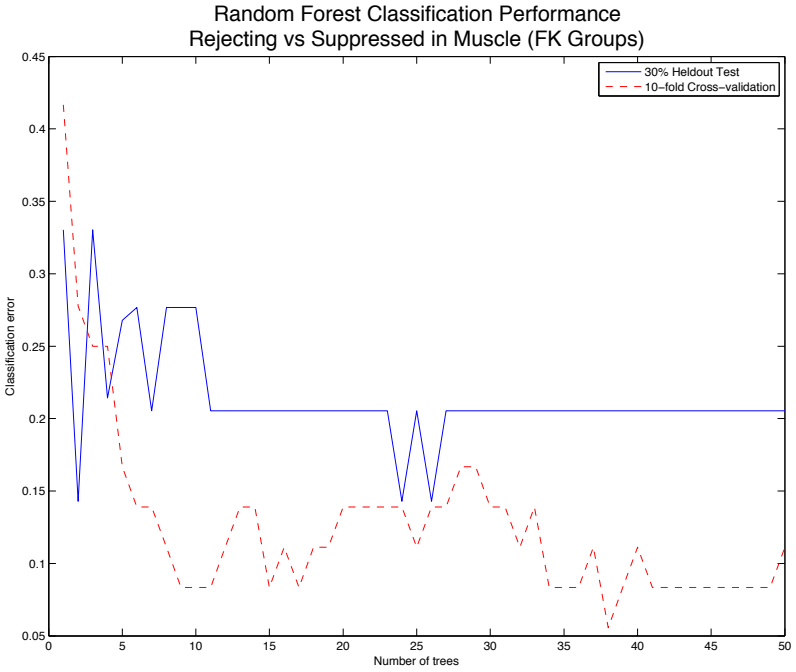

Figure 6.105

5-Dimensional Feature Selected Space

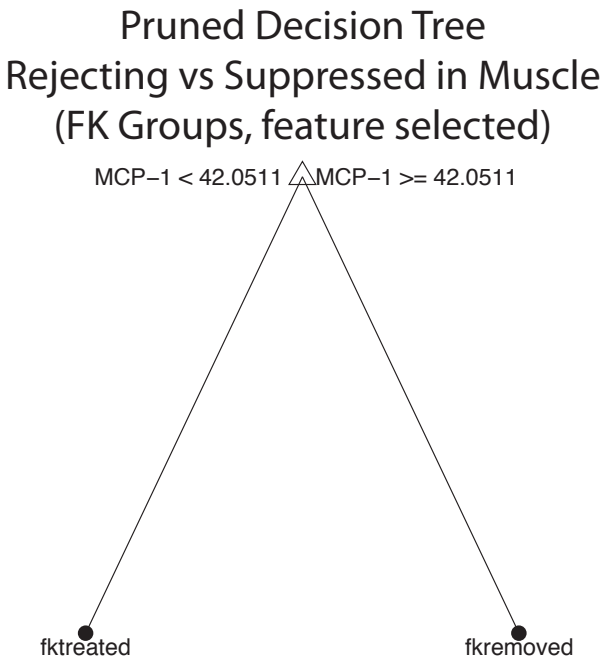

Figure 6.106

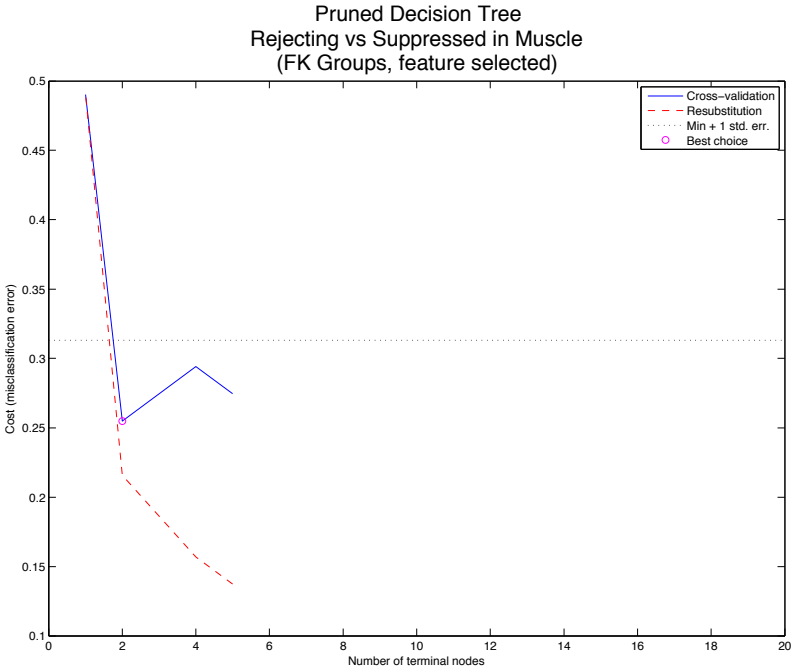

Figure 6.107

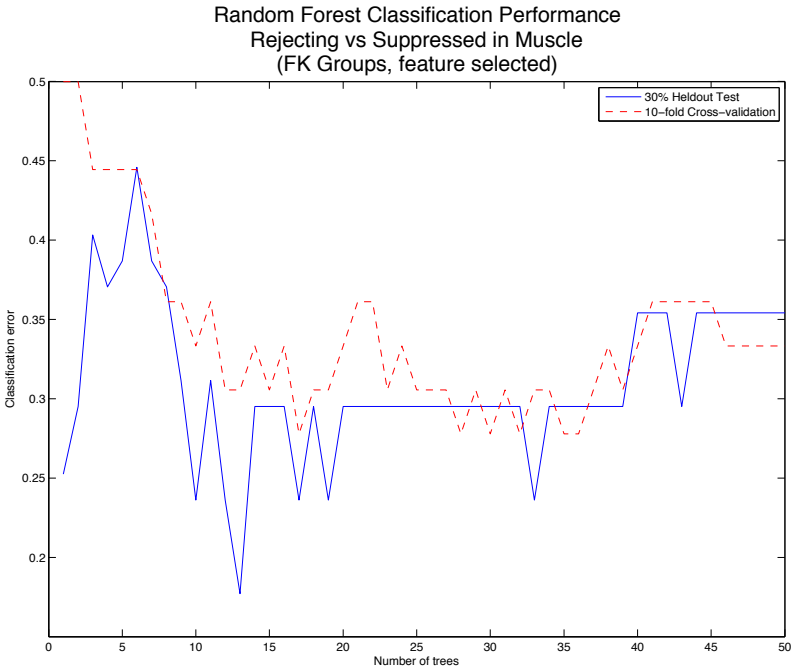

Figure 6.108

MANOVA Transformed Feature Space

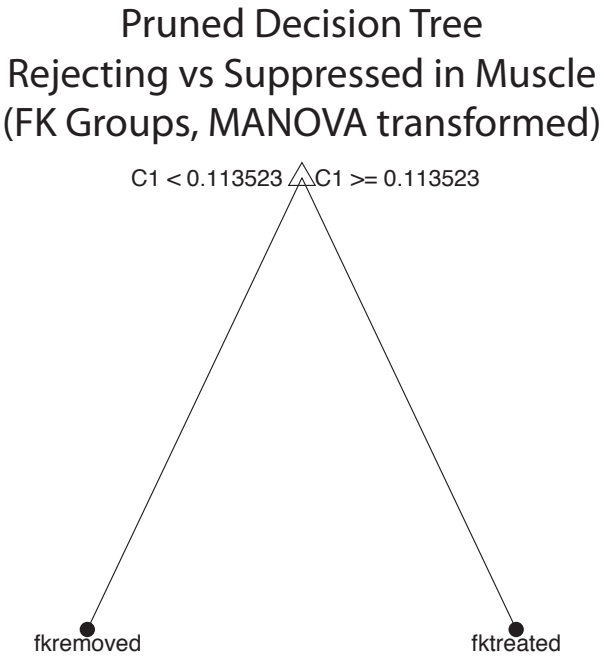

Figure 6.109

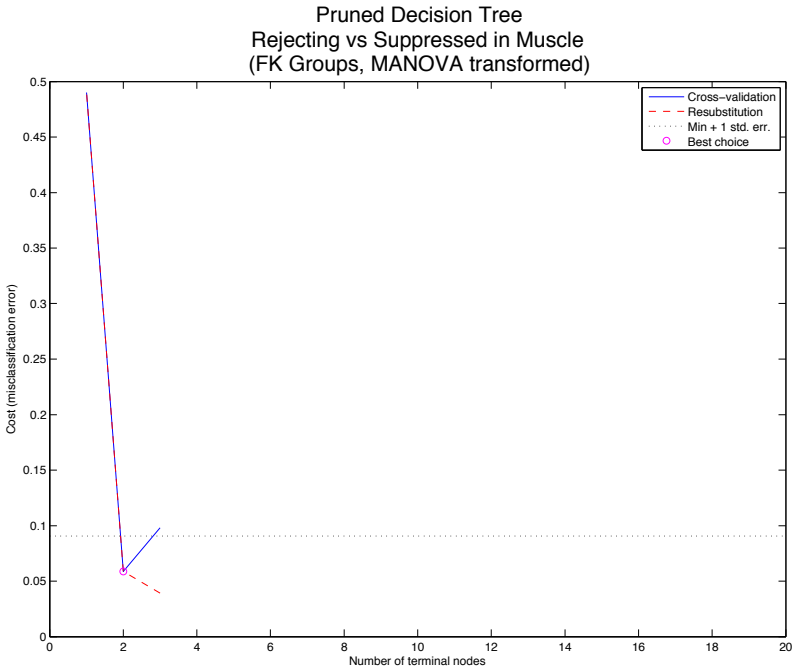

Figure 6.110

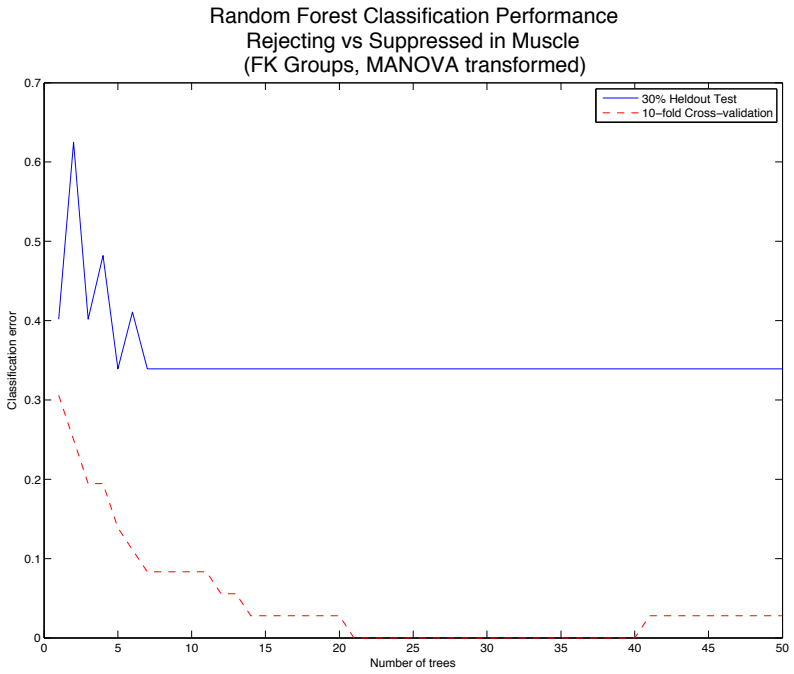
Random Forest Classification Performance
Rejecting vs Suppressed in Muscle
(FK Groups, MANOVA transformed)
30% Heldout Test
10−fold Cross−validation
Classification error
Number of trees
0
0.1
0.2
0.3
0.4
0.5
0.6
0.7
0
5
10
15
20
25
30
35
40
45
50

Figure 6.111

Appendix C Hypothesis 2 Figures

Skin vs Muscle in Allograft

All Time Points

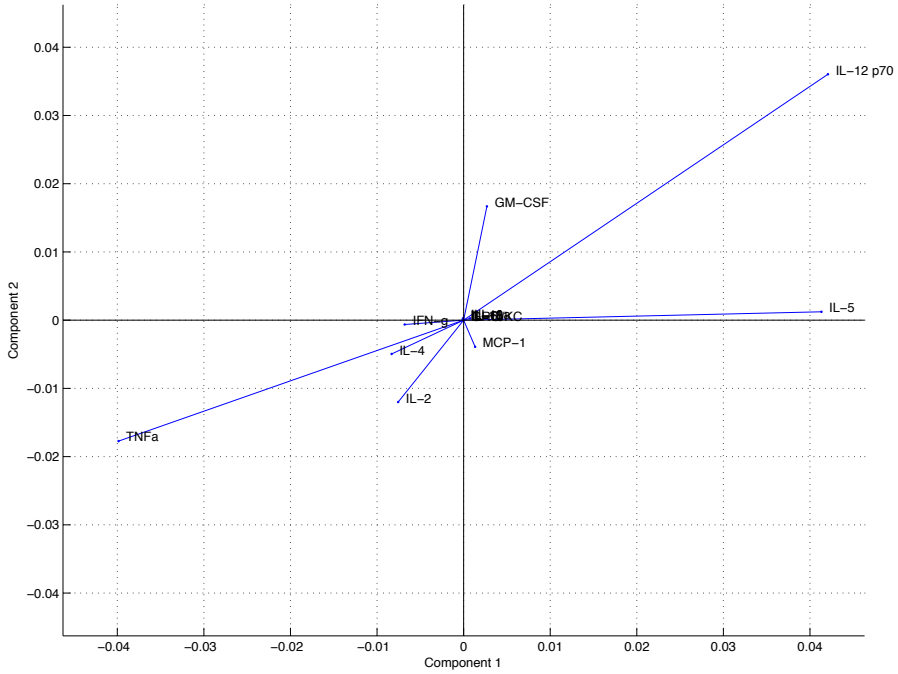

Figure 6.112 Cytokine contribution to MANOVA canonical variables 1 and 2 in allograft. Vector direction indicates which variable the cytokine is contributing to, while length indicates the strength of contribution.

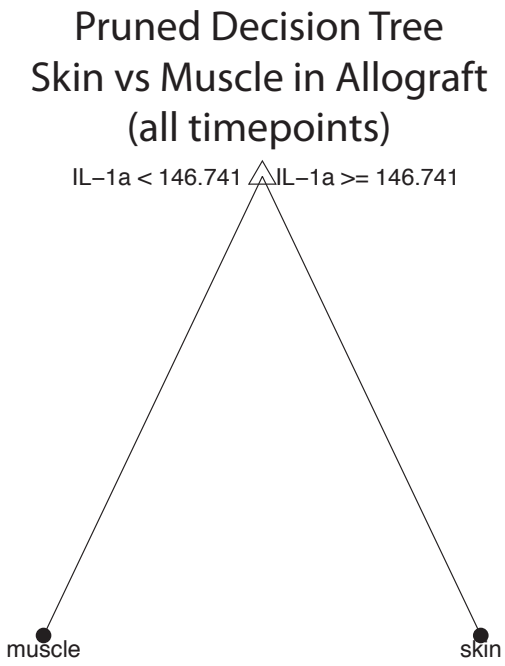

Figure 6.113

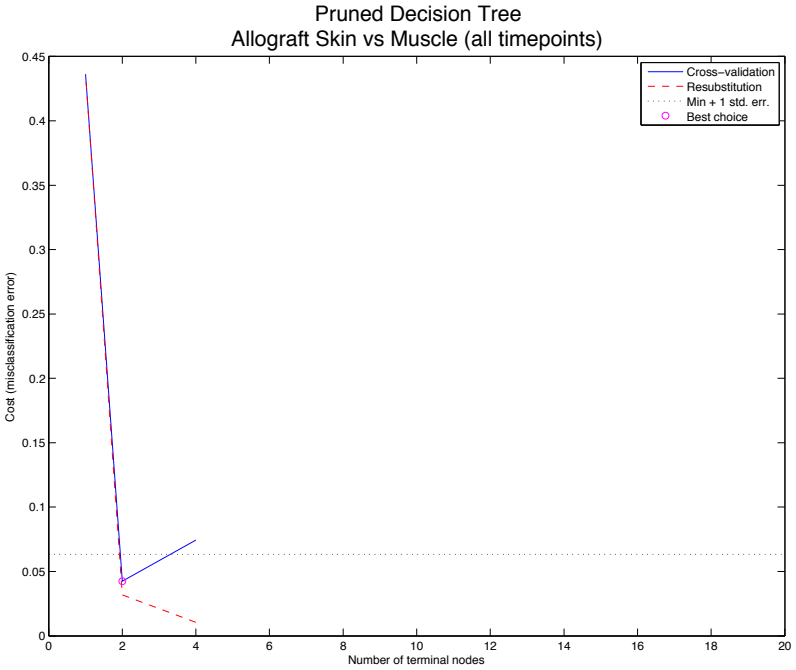

Figure 6.114

POD <= 5

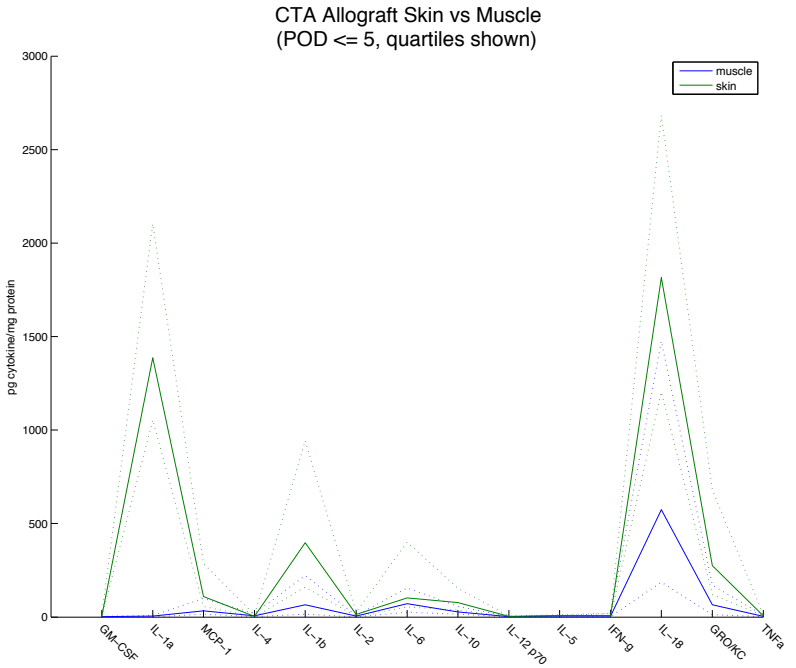

Figure 6.115

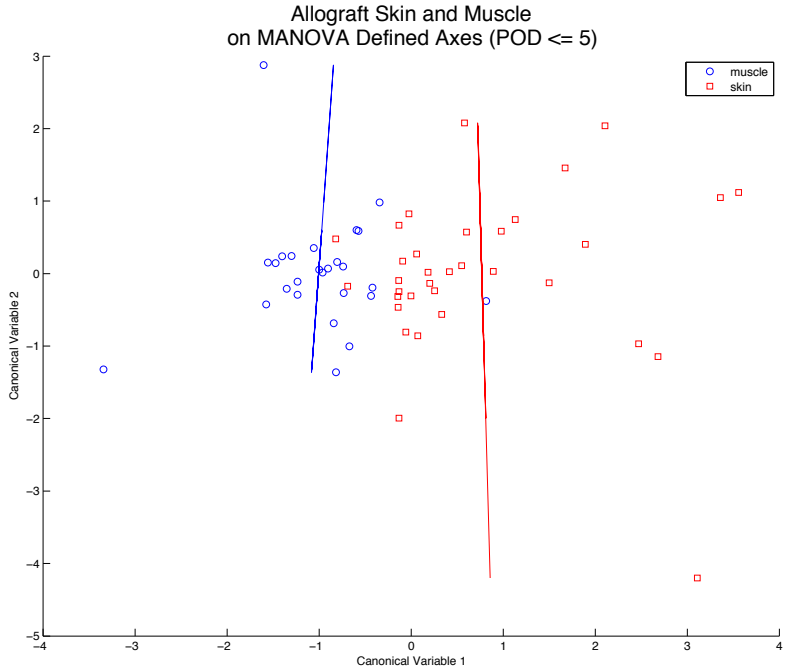

Figure 6.116

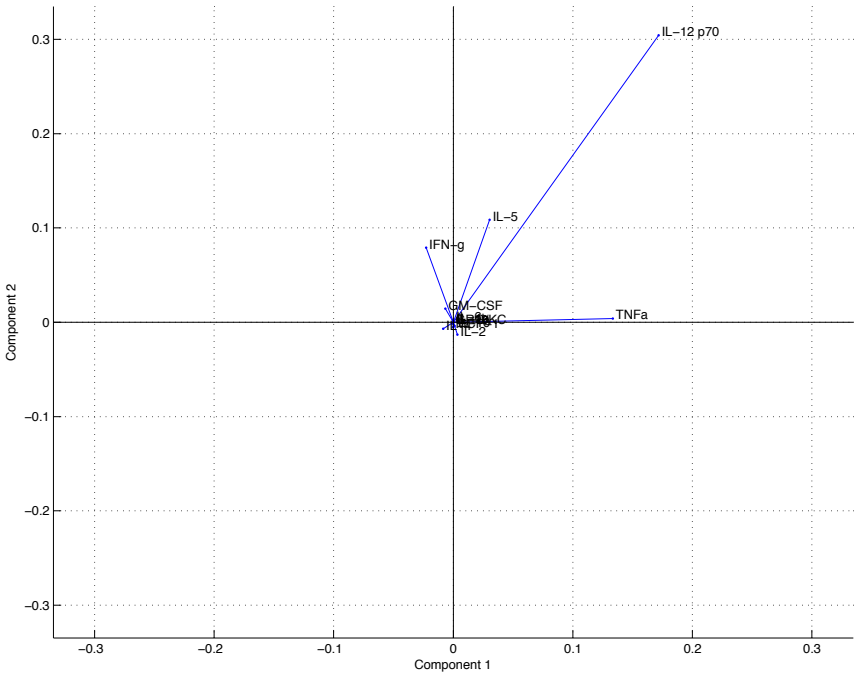

Figure 6.117

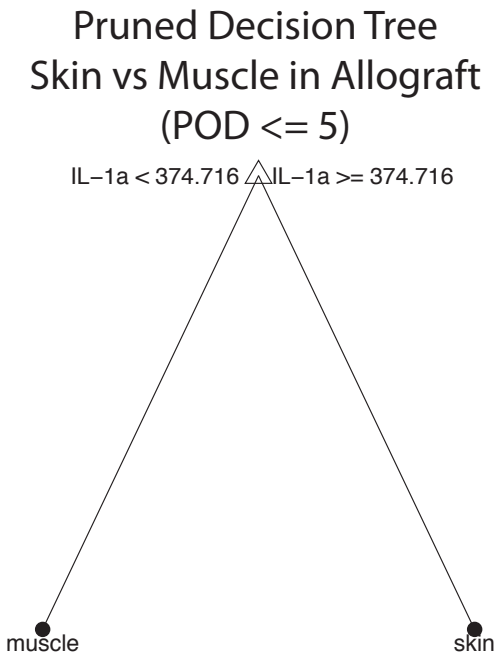

Figure 6.118

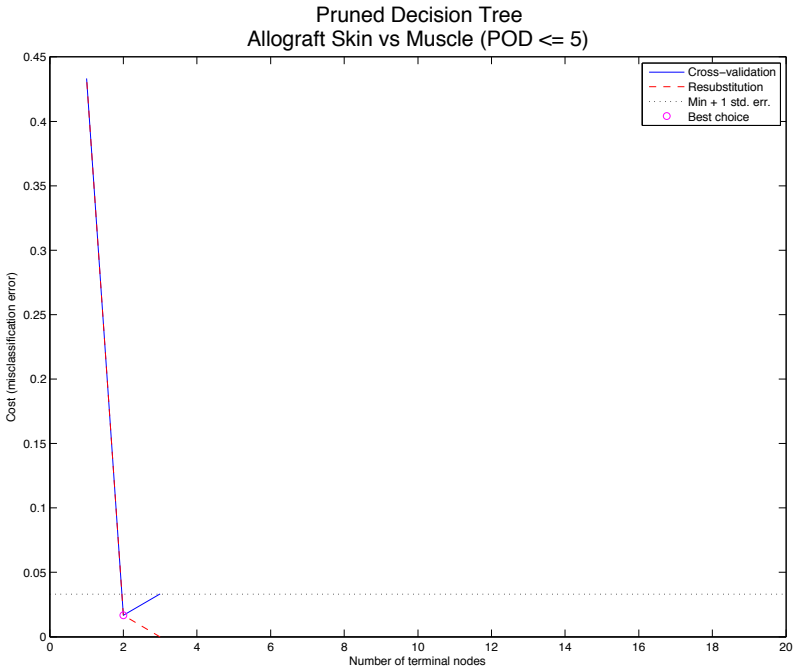

Figure 6.119

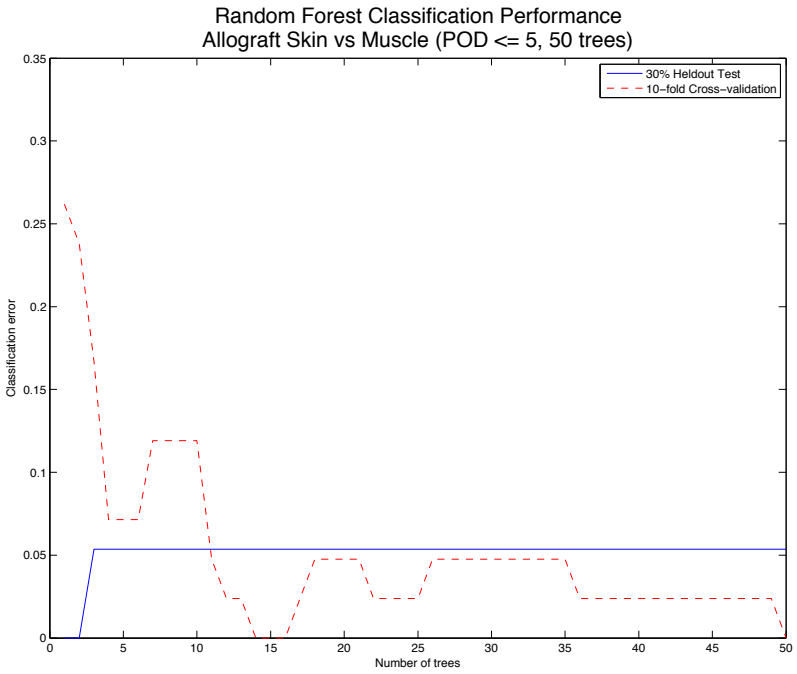

Figure 6.120

POD > 5

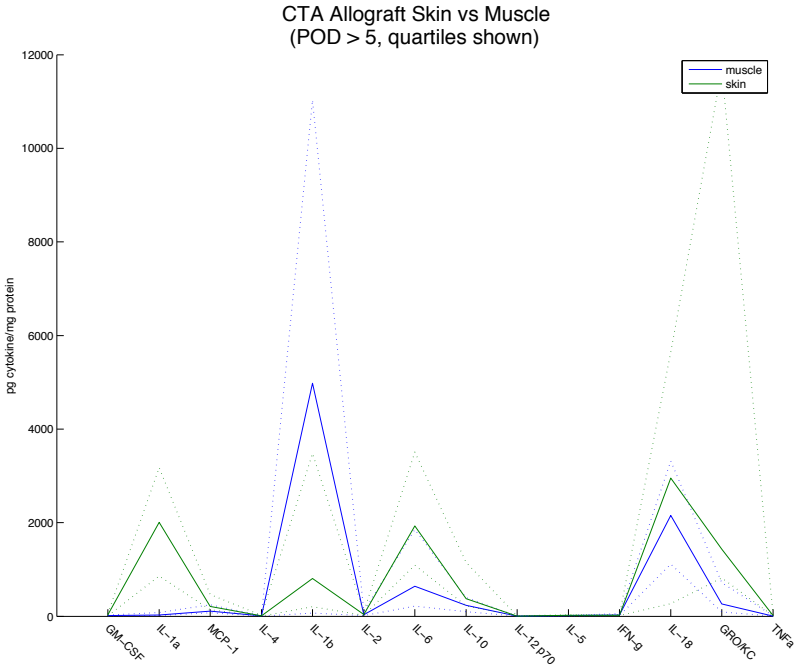

Figure 6.121

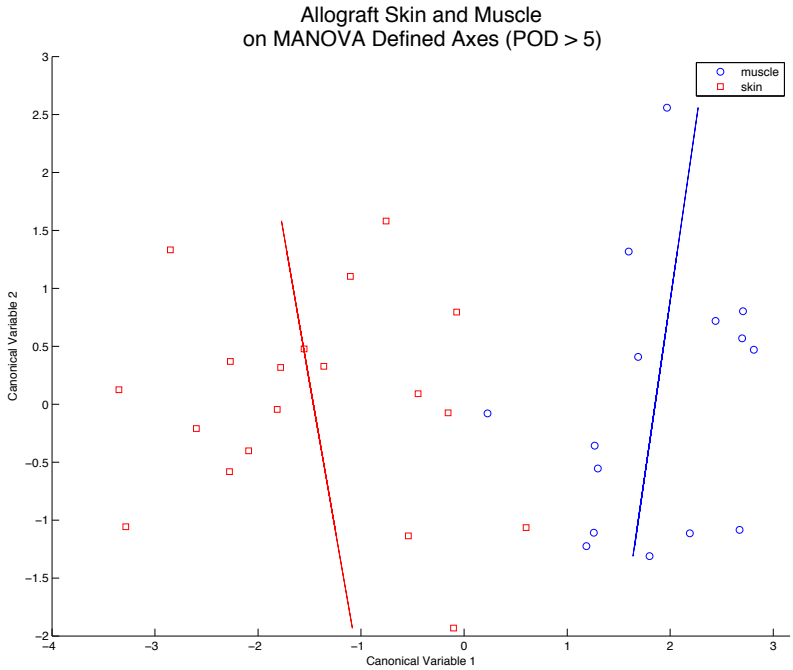

Figure 6.122

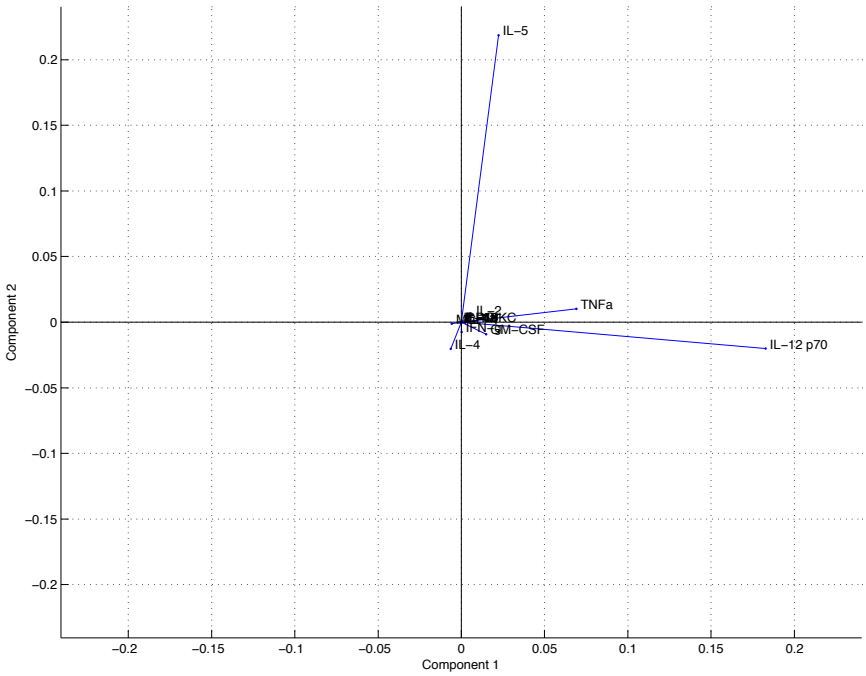

Figure 6.123

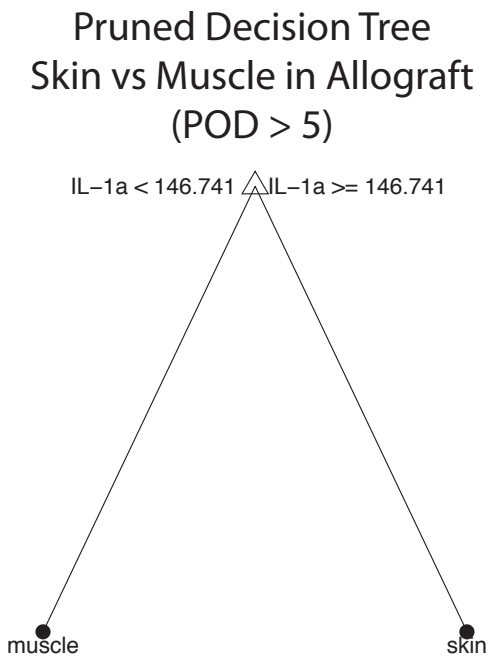

Figure 6.124

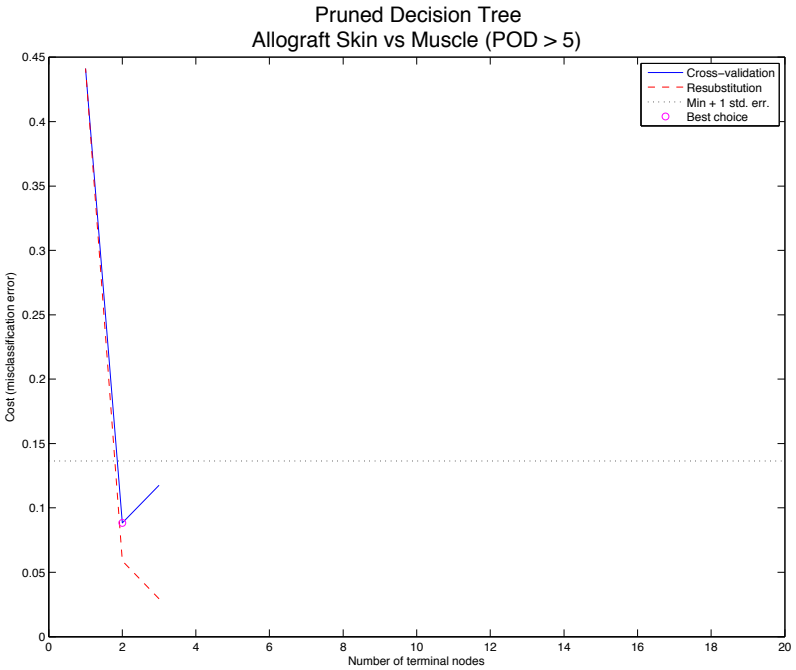

Figure 6.125

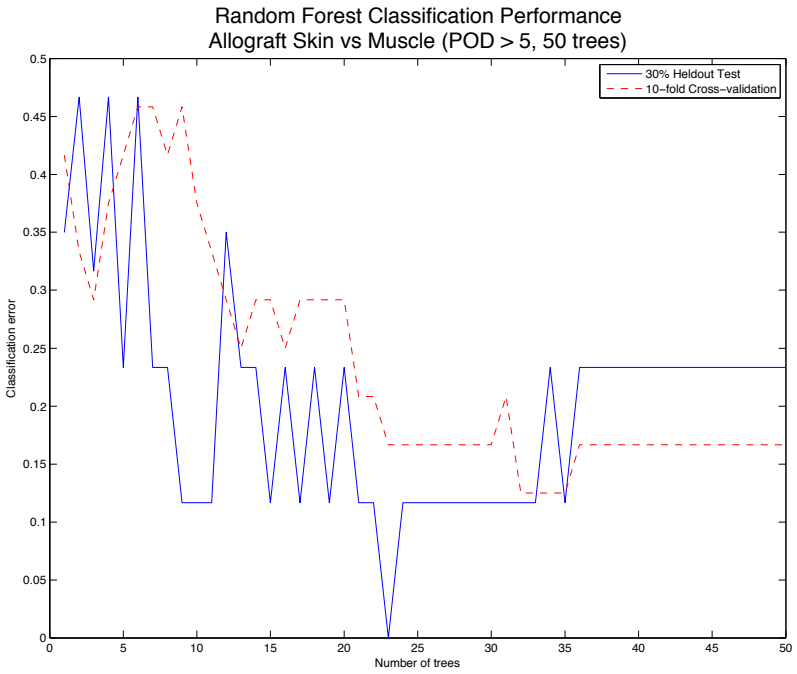

Figure 6.126

Skin vs Muscle in Isograft

All Time Points

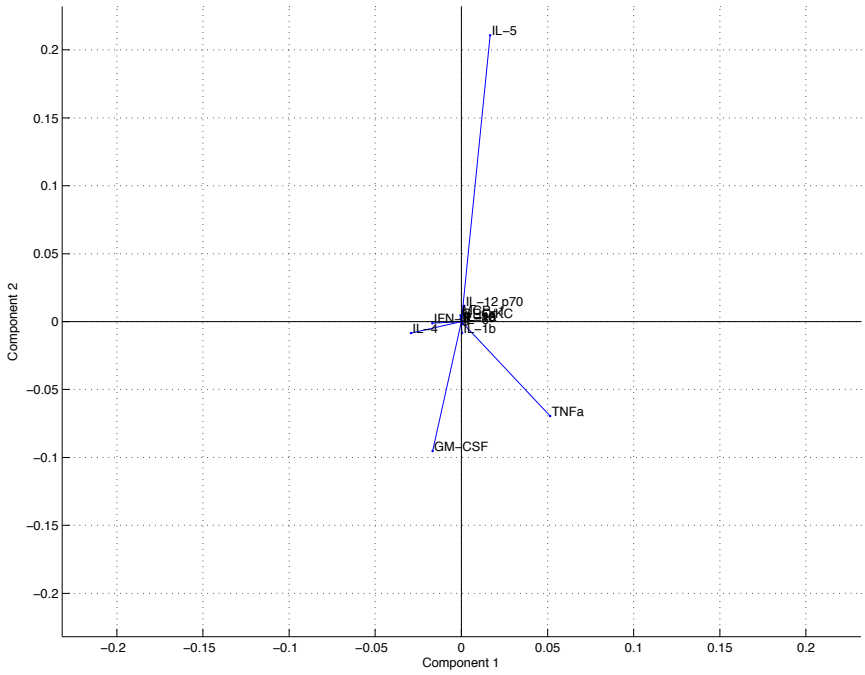

Figure 6.127 Cytokine contribution to MANOVA canonical variables 1 and 2 in isograft. Vector direction indicates which variable the cytokine is contributing to, while length indicates the strength of contribution.

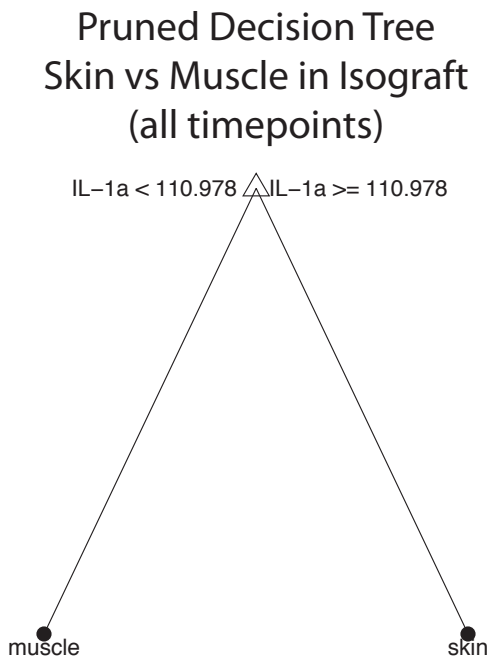

Figure 6.128

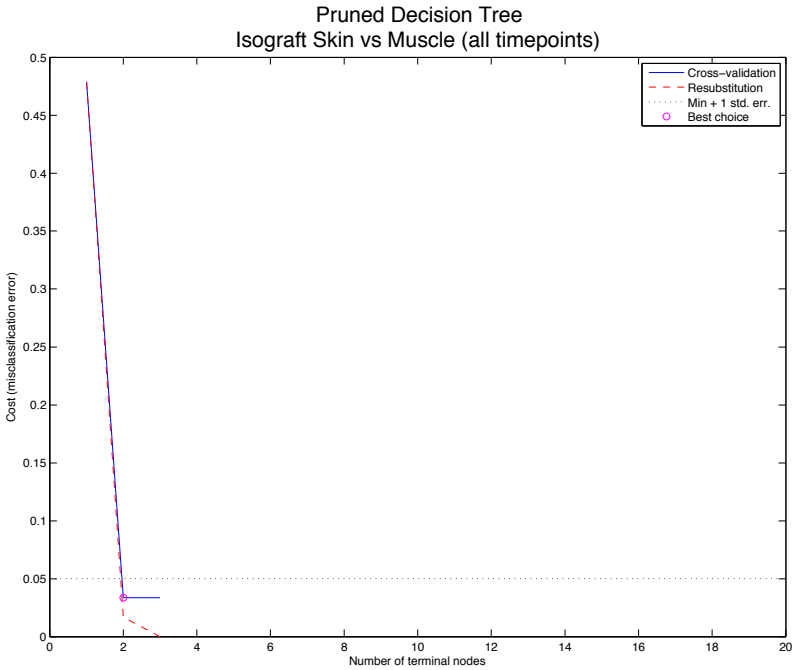

Figure 6.129

POD <= 5

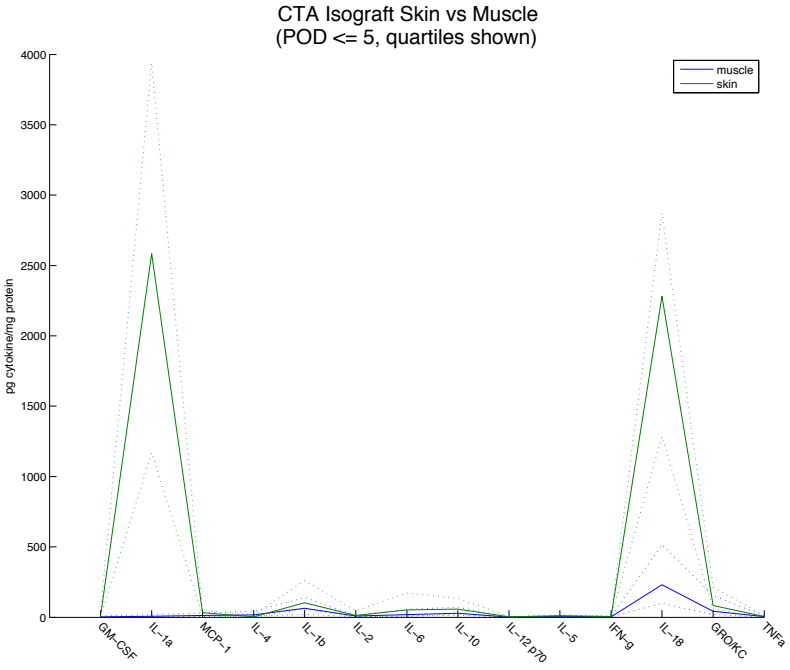

Figure 6.130

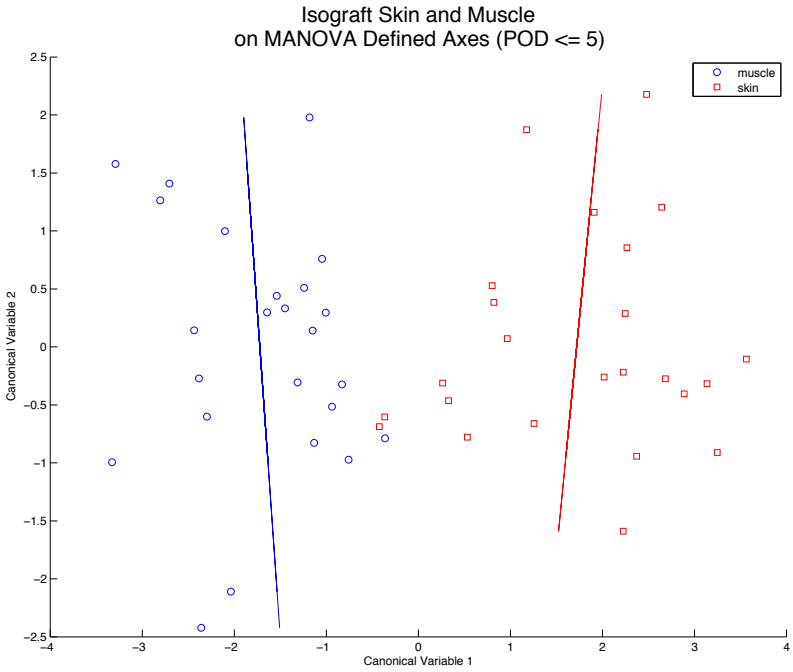

Figure 6.131

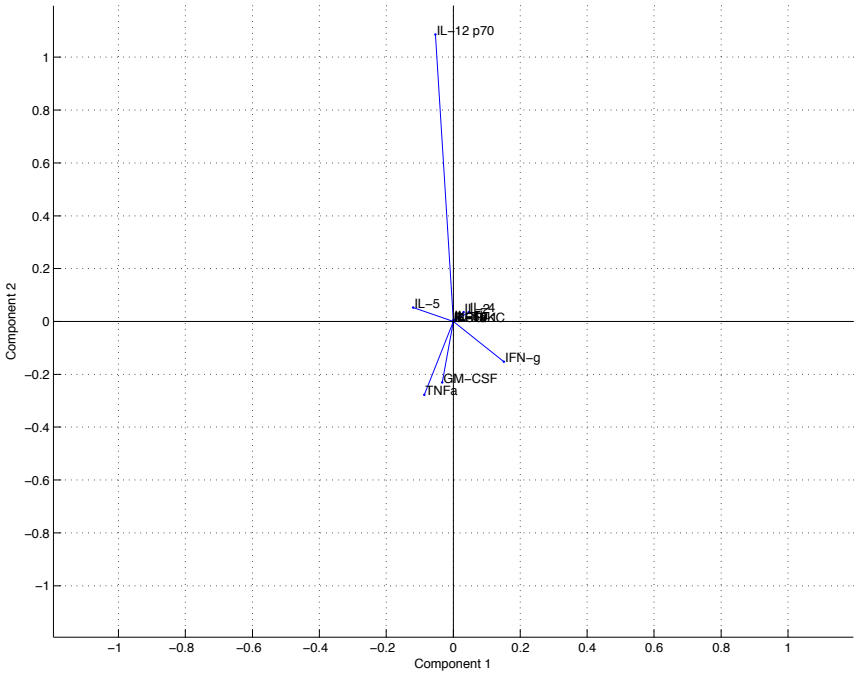

Figure 6.132

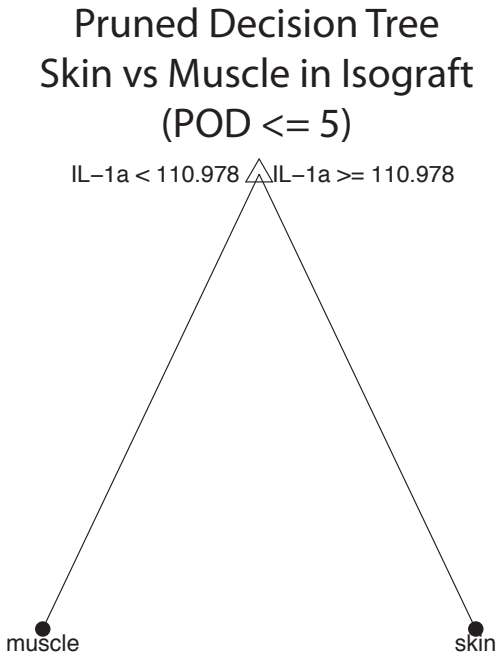

Figure 6.133

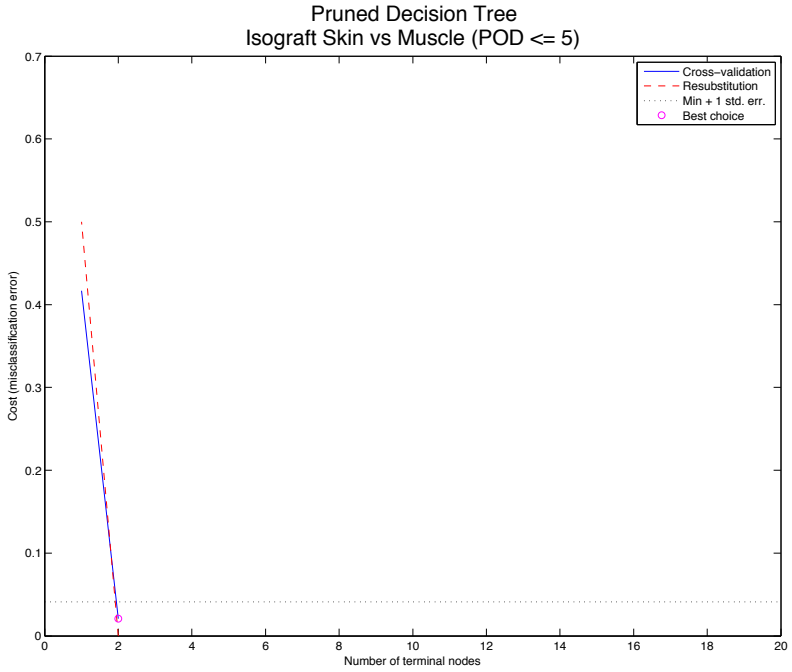

Figure 6.134

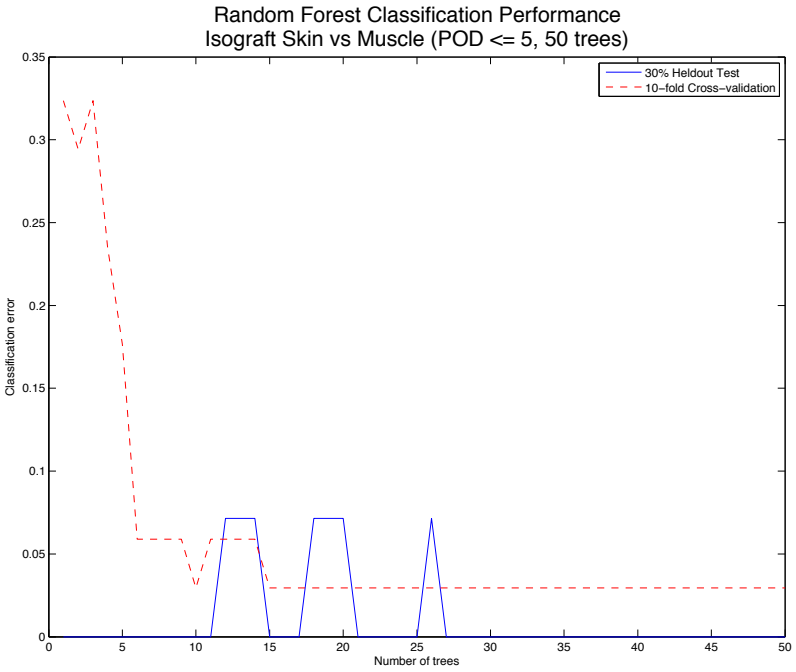

Figure 6.135

POD > 5

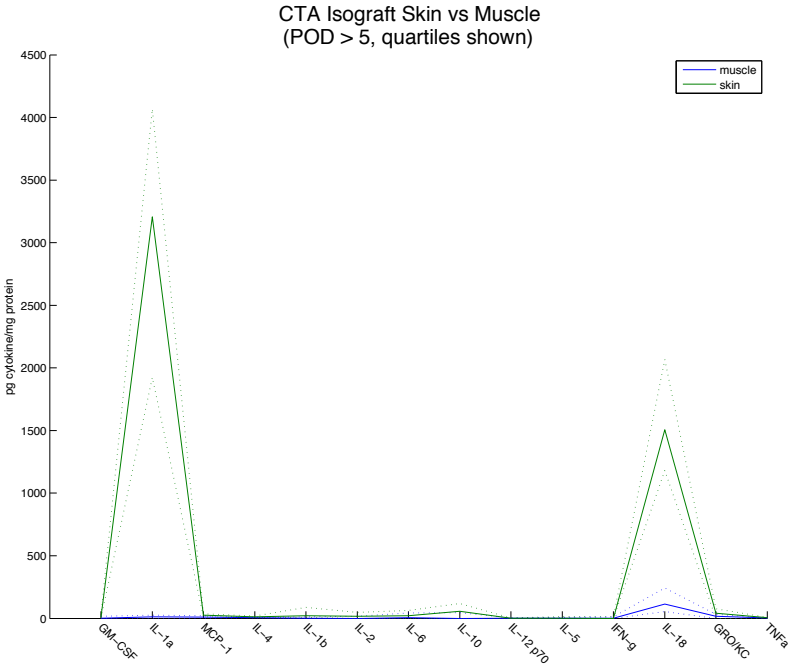

Figure 6.136

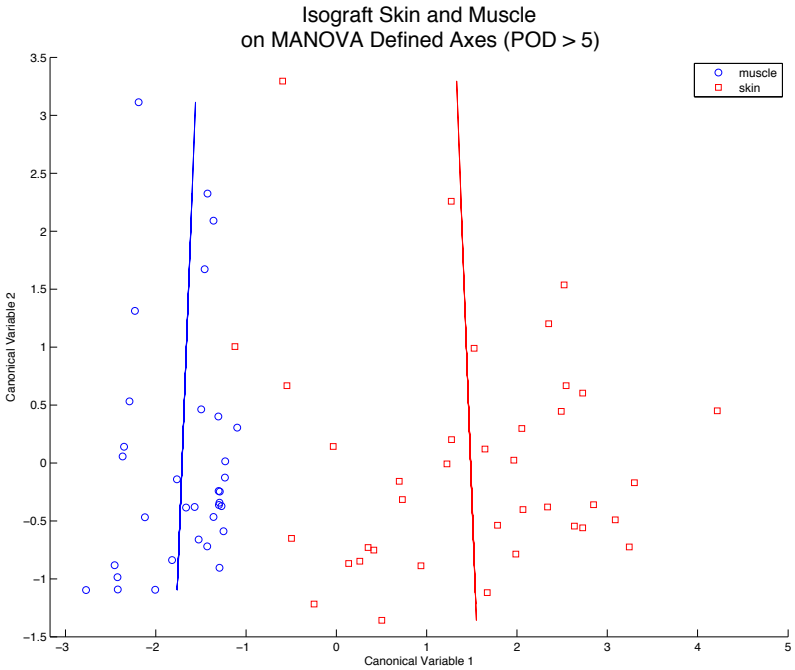

Figure 6.137

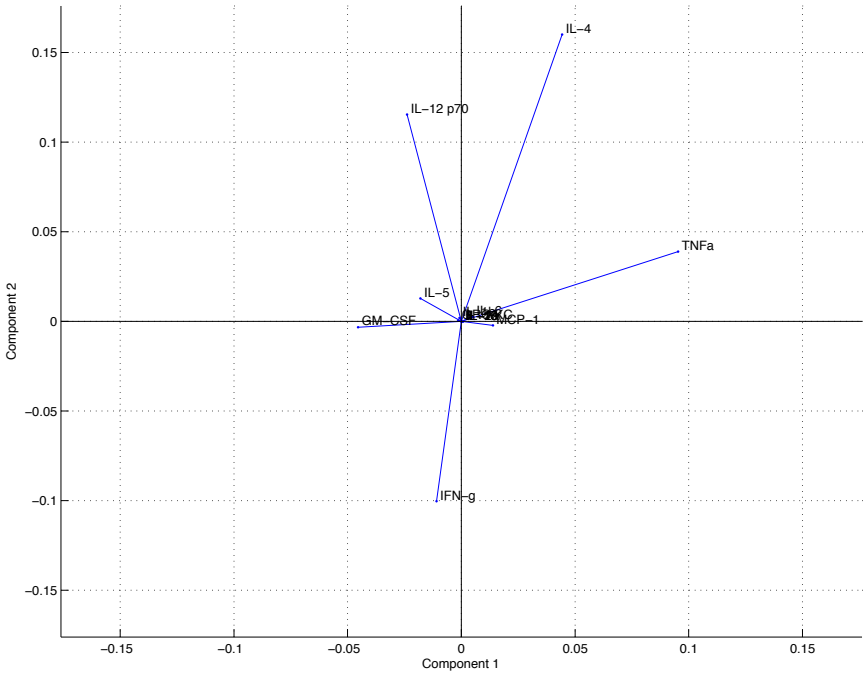

Figure 6.138

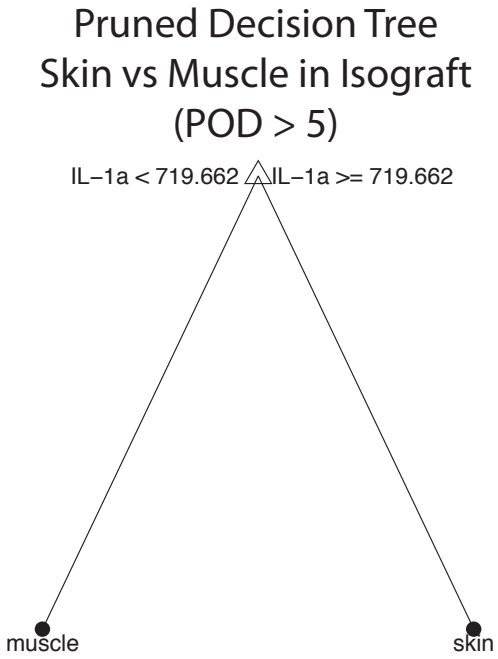

Figure 6.139

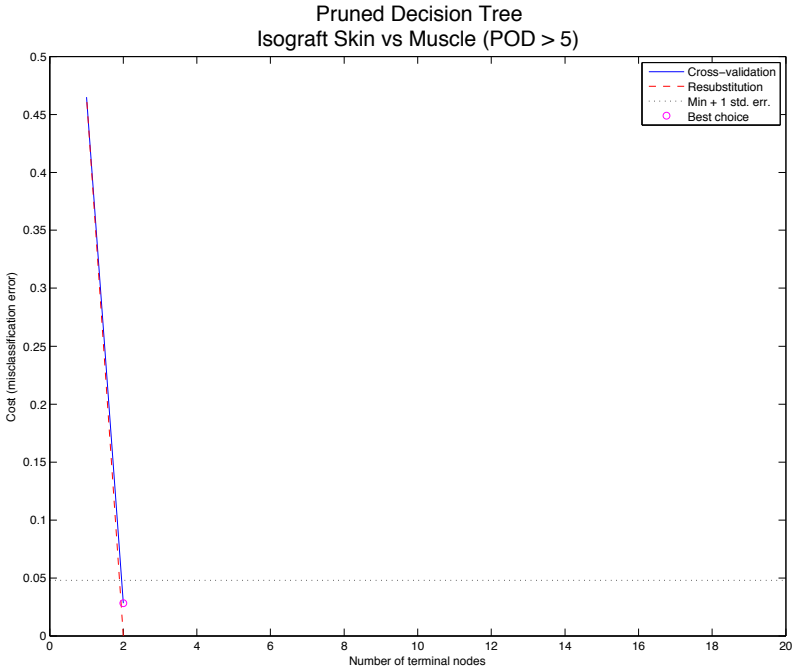

Figure 6.140

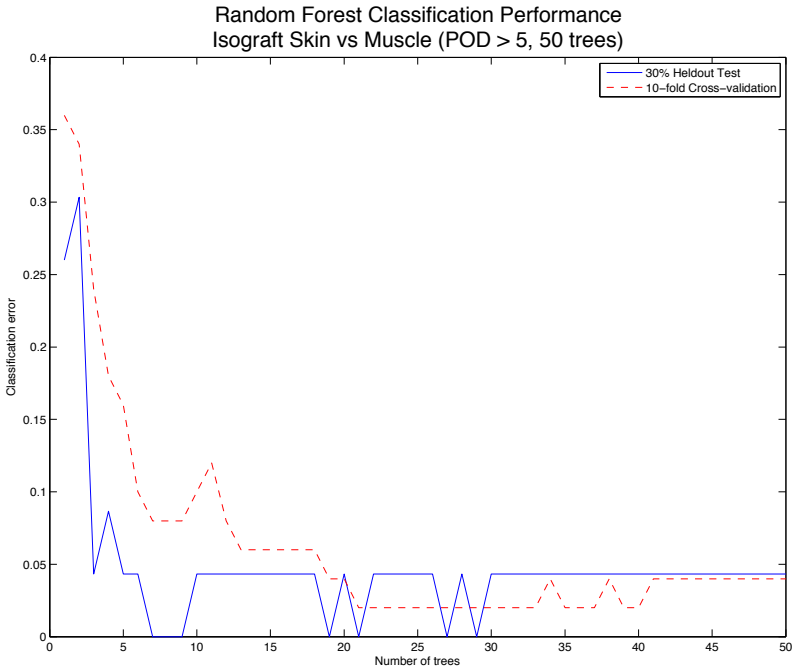

Figure 6.141

Skin vs Muscle in FK-Treated

All Time Points

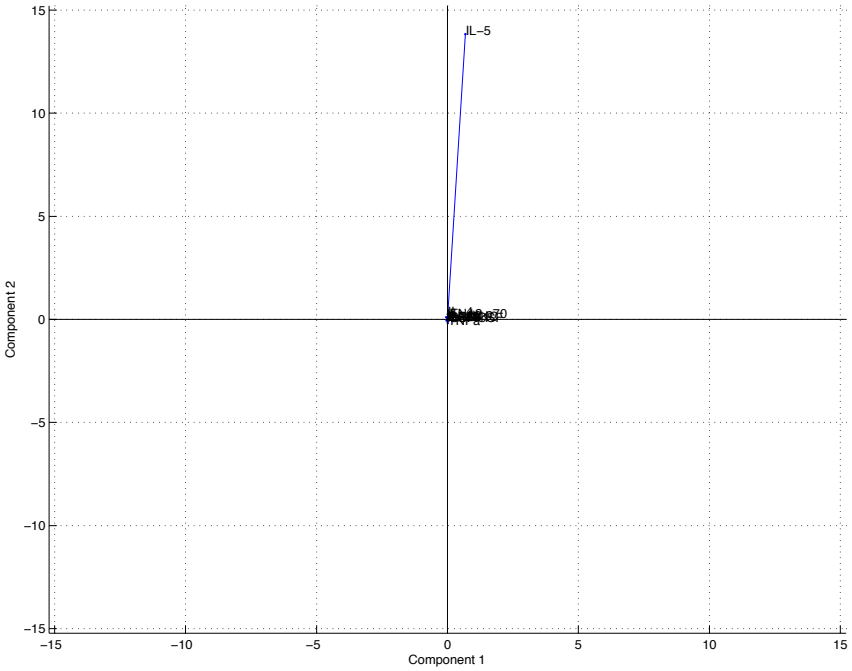

Figure 6.142 Cytokine contribution to MANOVA canonical variables 1 and 2 in FK-Treated. Vector direction indicates which variable the cytokine is contributing to, while length indicates the strength of contribution.

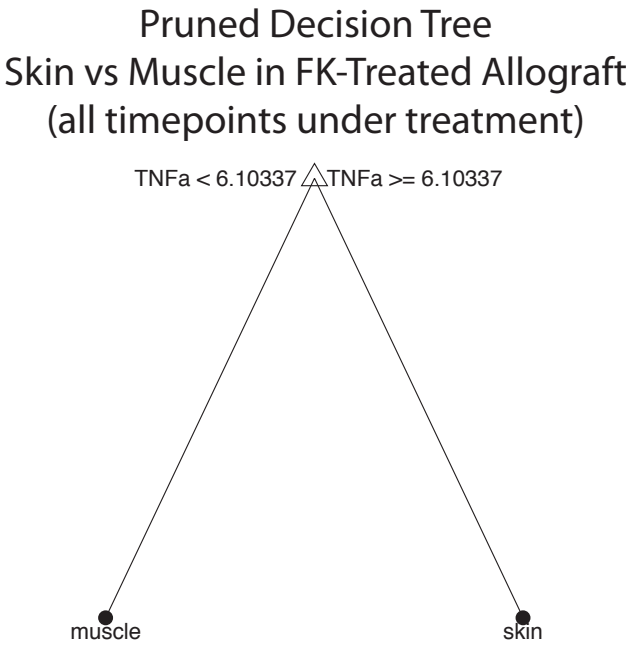

Figure 6.143

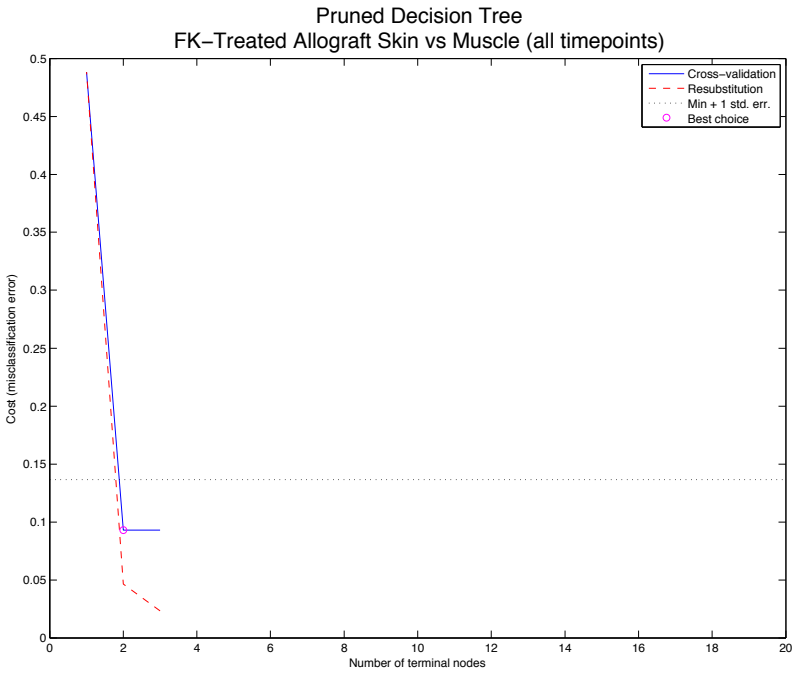

Figure 6.144

Skin vs Muscle in FK-Treatment Withdrawn

All Time Points

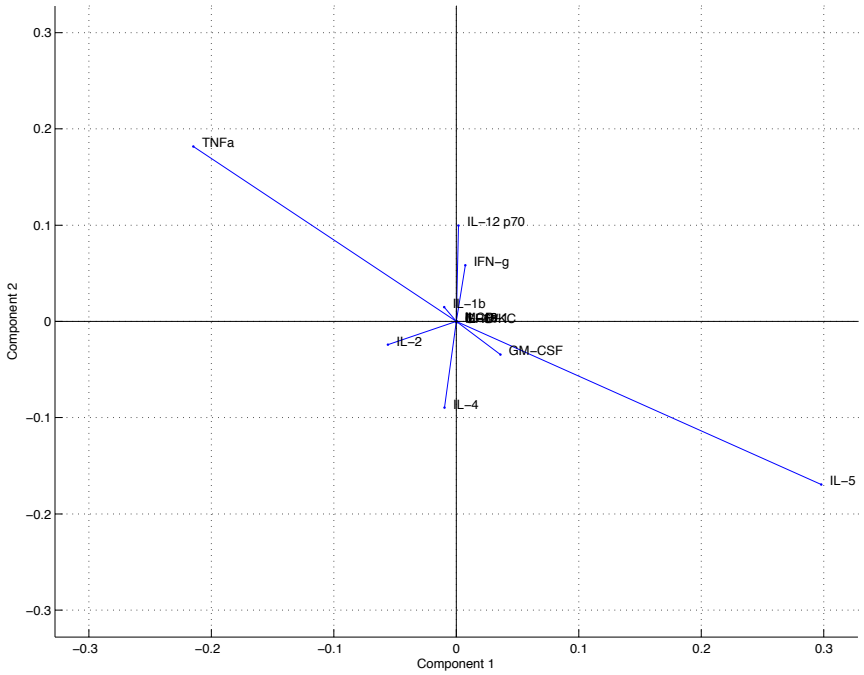

Figure 6.145 Cytokine contribution to MANOVA canonical variables 1 and 2 in FK-Treatment Withdrawn. Vector direction indicates which variable the cytokine is contributing to, while length indicates the strength of contribution.

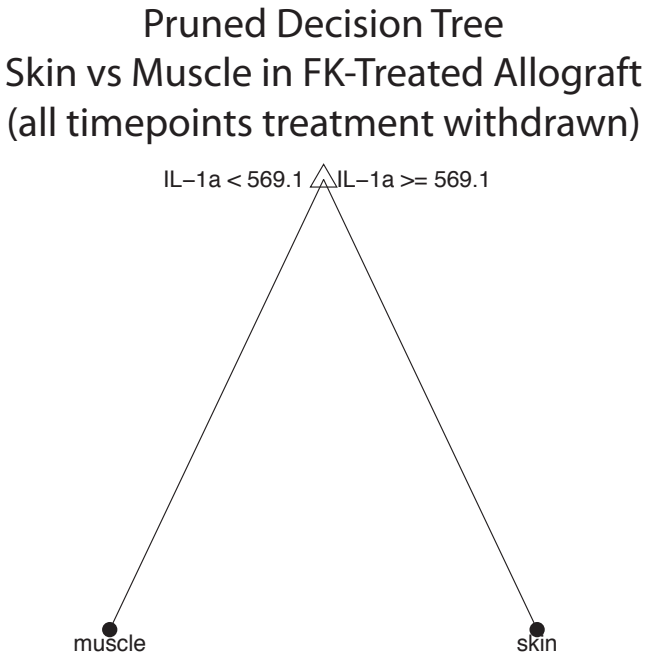

Figure 6.146

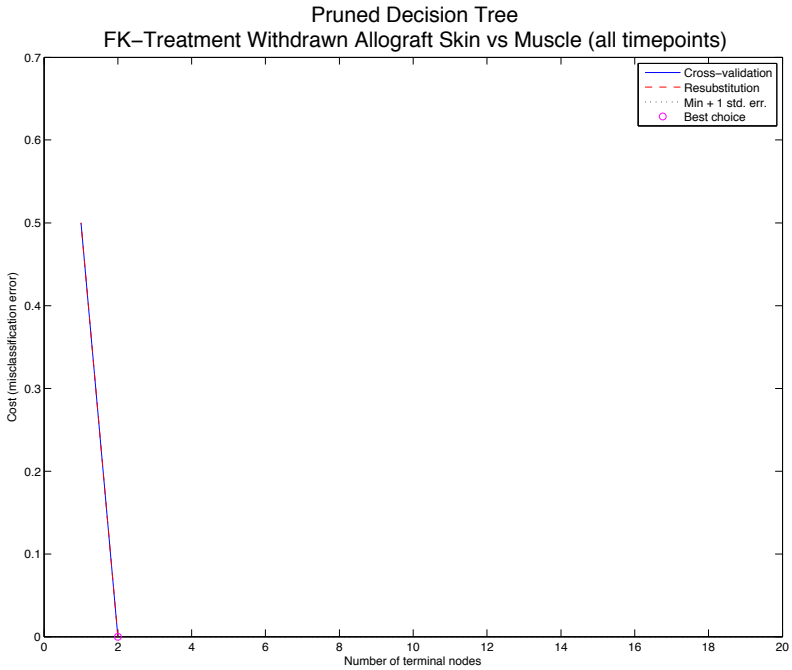

Figure 6.147

Skin vs Muscle in Naive

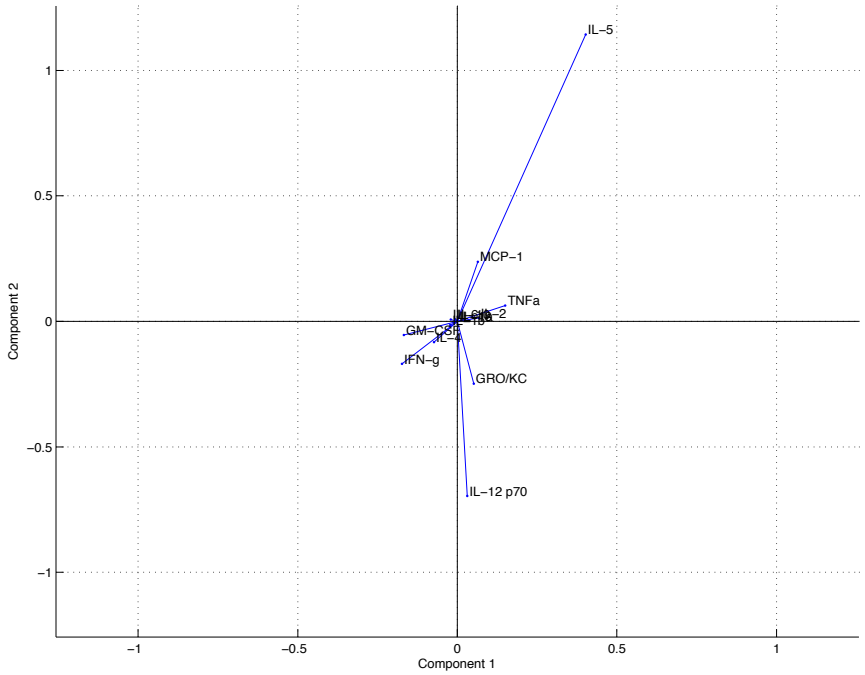

Figure 6.148 Cytokine contribution to MANOVA canonical variables 1 and 2 in naïve. Vector direction indicates which variable the cytokine is contributing to, while length indicates the strength of contribution.

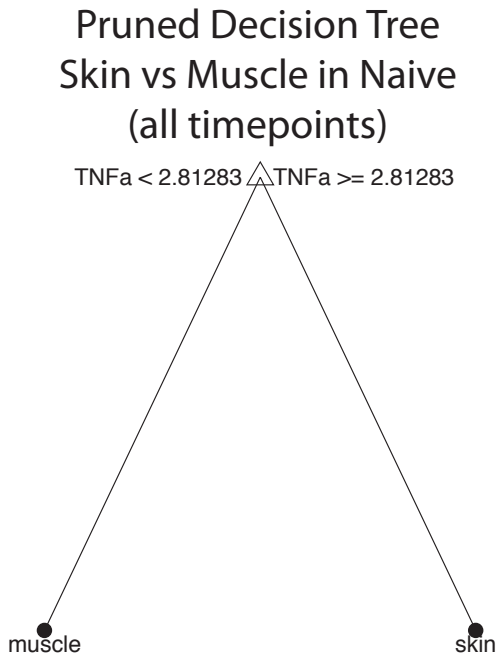

Figure 6.149

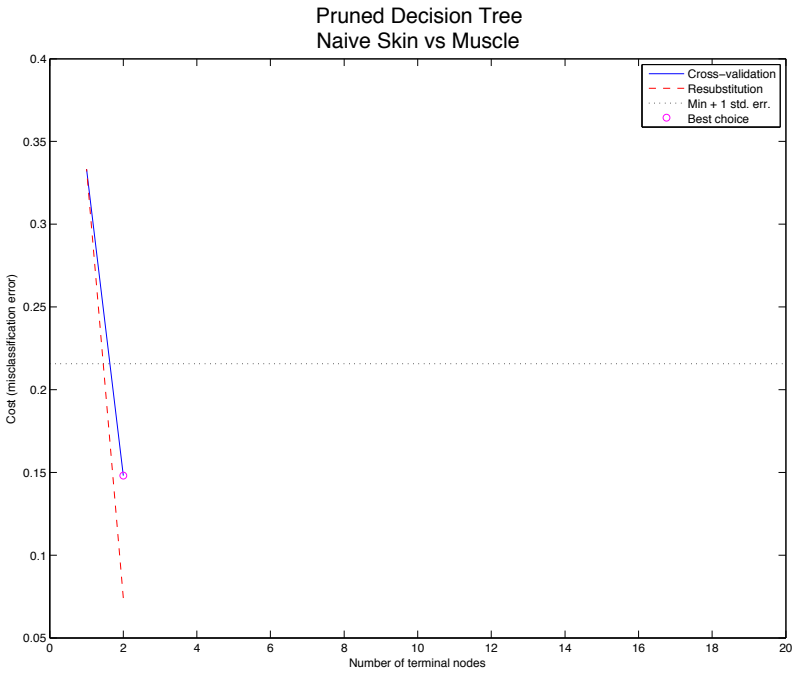
Pruned Decision Tree
Naive Skin vs Muscle
Cross−validation
Resubstitution
Min + 1 std. err.
Best choice
Cost (misclassification error)
Number of terminal nodes
0.4
0.35
0.3
0.25
0.2
0.15
0.1
0.05
0
2
4
6
8
10
12
14
16
18
20

Figure 6.150

Appendix D Hypothesis 3 Figures

Rejecting vs. Not Rejecting in Skin (all time points)

Original 14-Dimensional Feature Space

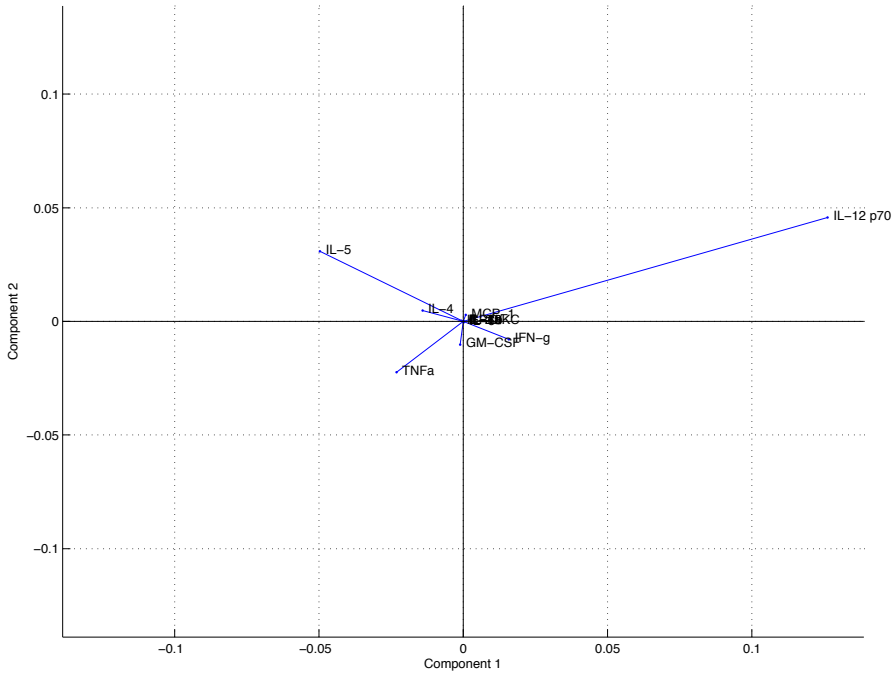

Figure 6.151

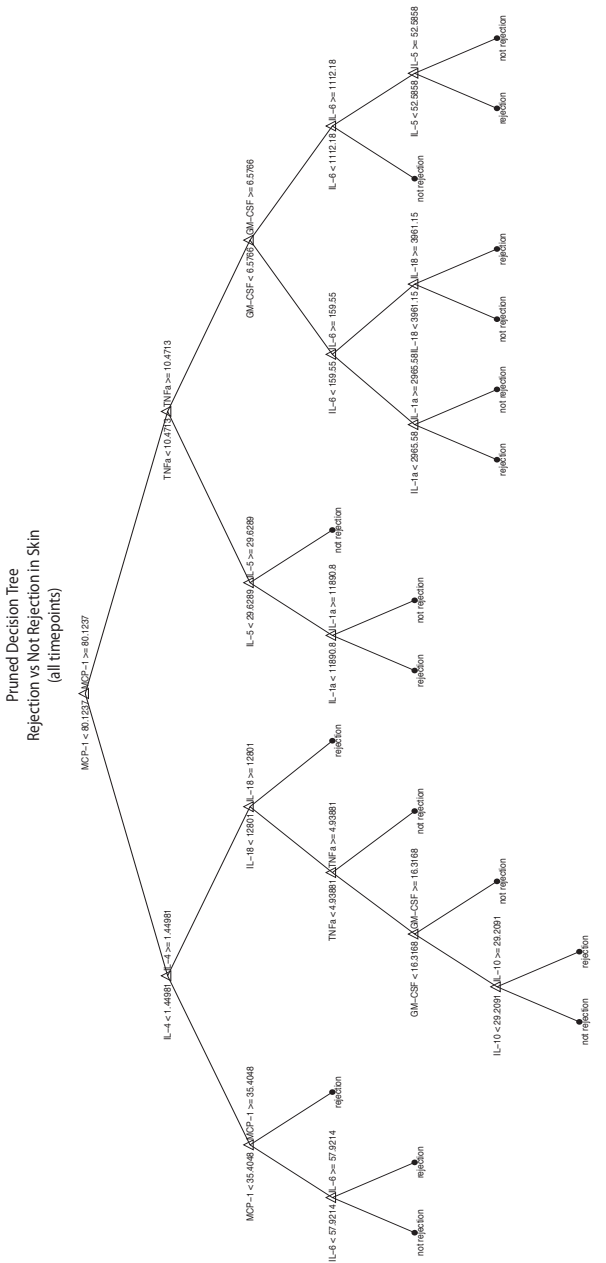
Pruned Decision Tree
Rejection vs Not Rejection in Skin
(all timepoints)
MCP−1 < 80.1232
MCP−1 >= 80.1237
IL−4 < 1.44981
IL−4 >= 1.44981
TNFa < 10.4713
TNFa >= 10.4713
MCP−1 < 35.4048
MCP−1 >= 35.4048
IL−6 < 57.9214
IL−6 >= 57.9214
rejection
not rejection
IL−18 < 12801
IL−18 >= 12801
TNFa < 4.93381
TNFa >= 4.93381
GM−CSF < 16.3168
GM−CSF >= 16.3168
IL−10 < 29.2091
IL−10 >= 29.2091
IL−5 < 29.6289
IL−5 >= 29.6289
IL−1a < 11890.8
IL−1a >= 11890.8
GM−CSF < 6.5766
GM−CSF >= 6.5766
IL−6 < 159.55
IL−6 >= 159.55
IL−6 < 1112.18
IL−6 >= 1112.18
IL−1a < 2965.58
IL−1a >= 2965.58
IL−18 < 3961.15
IL−18 >= 3961.15
IL−5 < 52.9858
IL−5 >= 52.9858

Figure 6.152

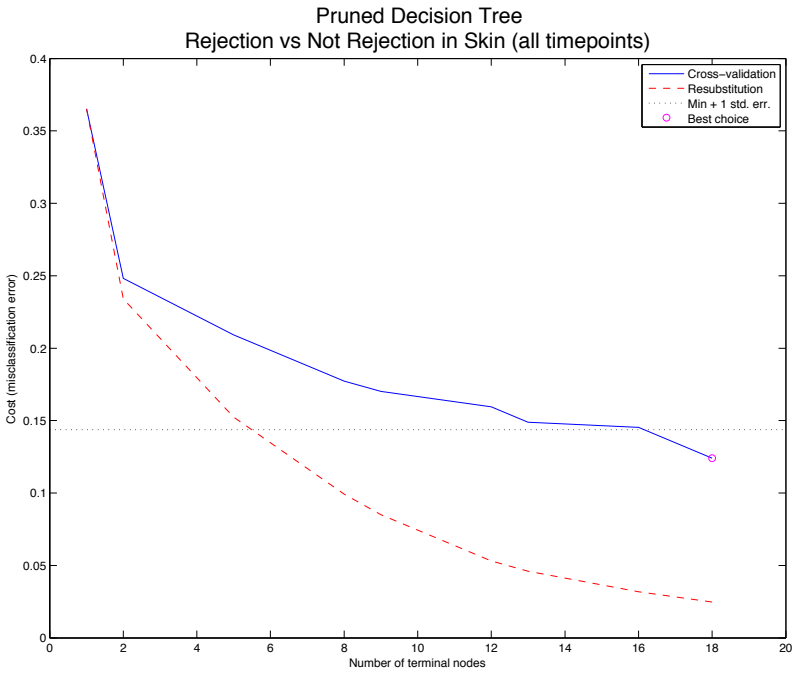

Figure 6.153

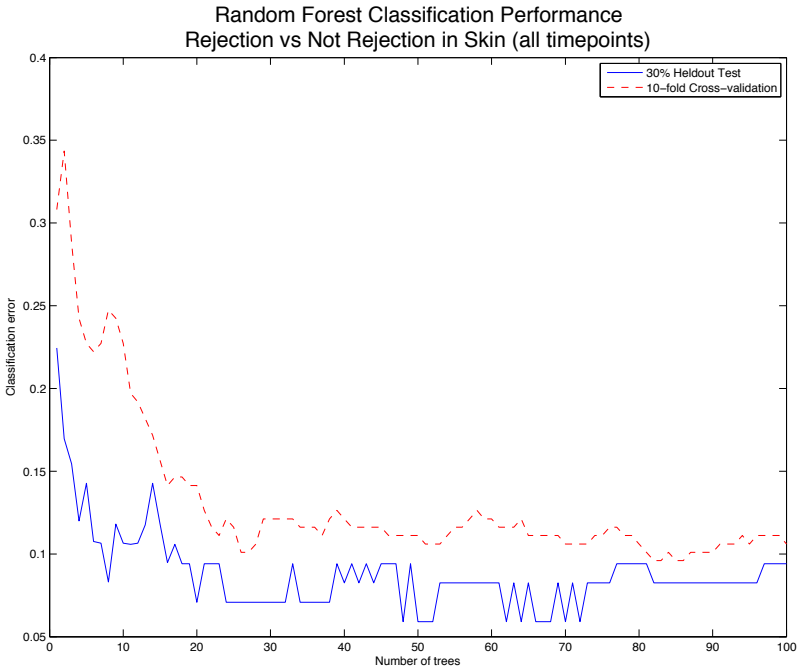

Figure 6.154

5-Dimensional Feature Selected Space

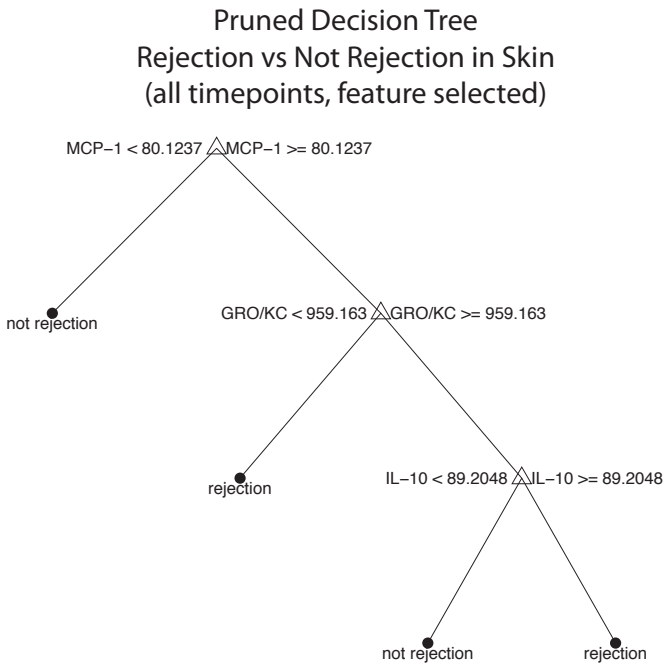

Figure 6.155

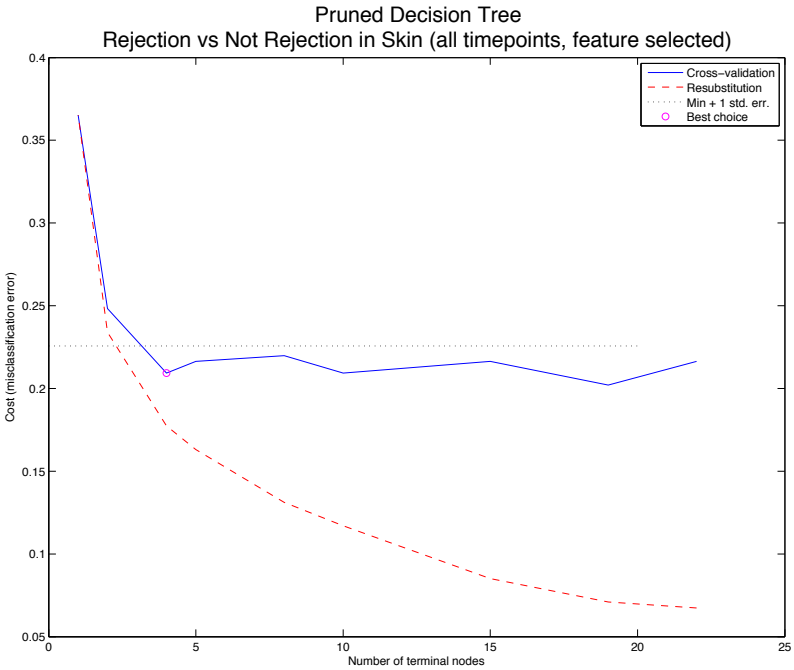

Figure 6.156

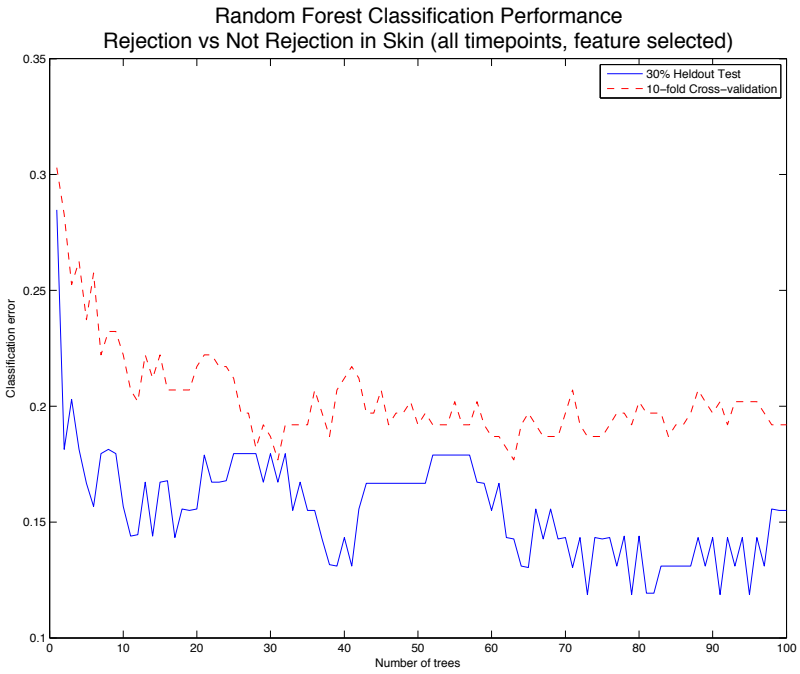

Figure 6.157

MANOVA Transformed Feature Space

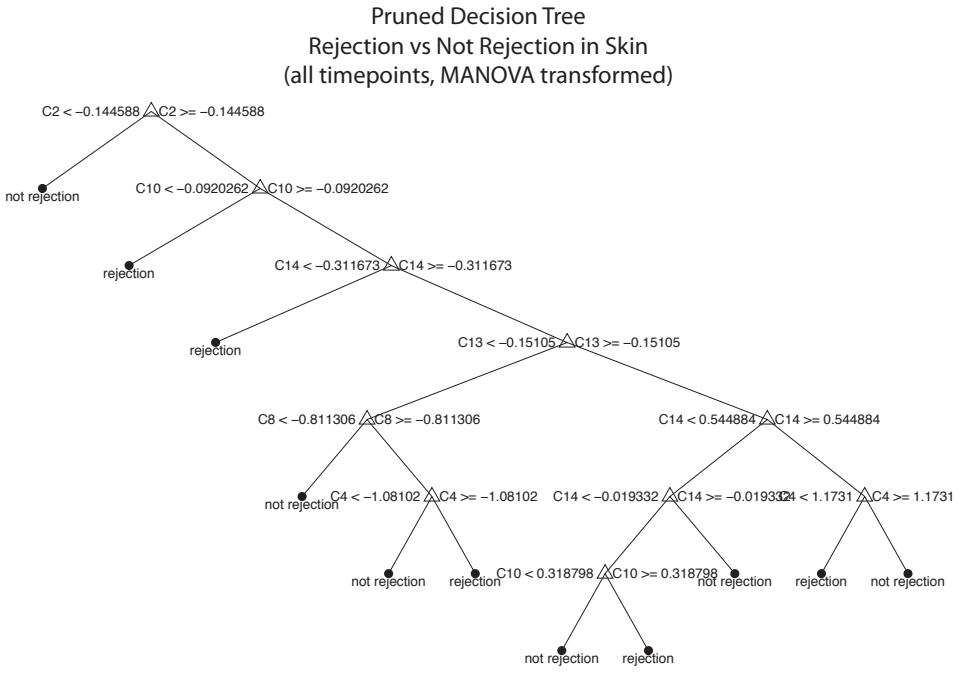

Figure 6.158

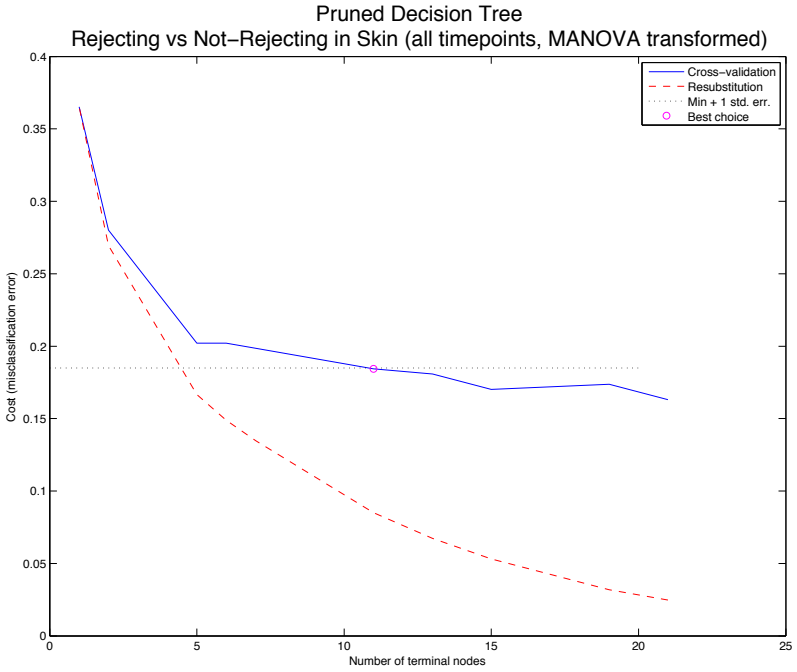

Figure 6.159

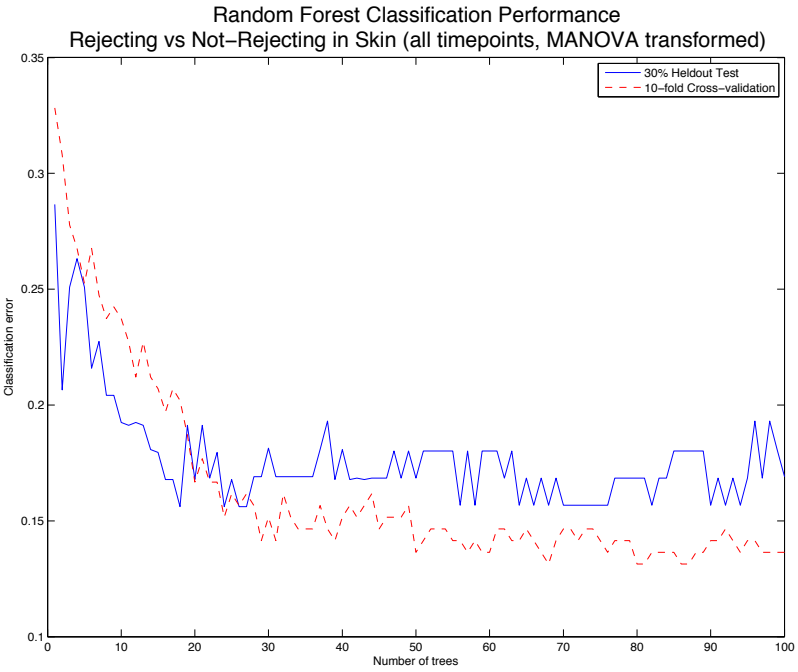

Figure 6.160

Hybrid Feature Space

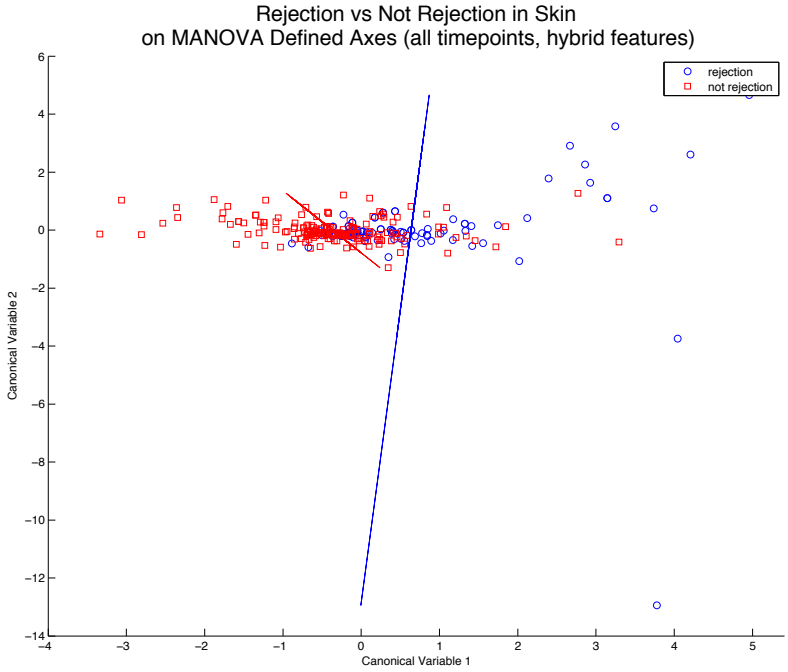

Figure 6.161

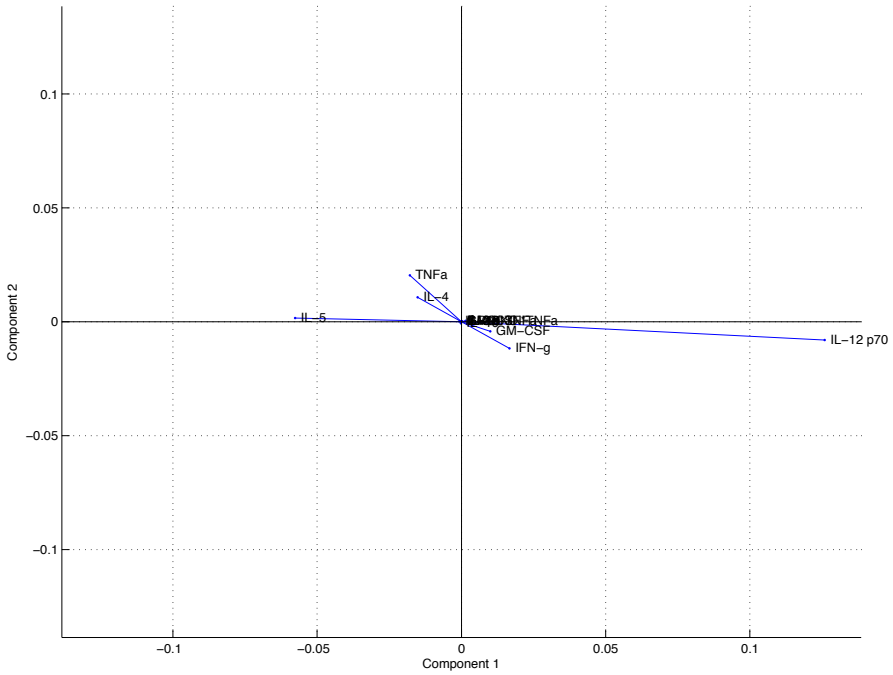

Figure 6.162

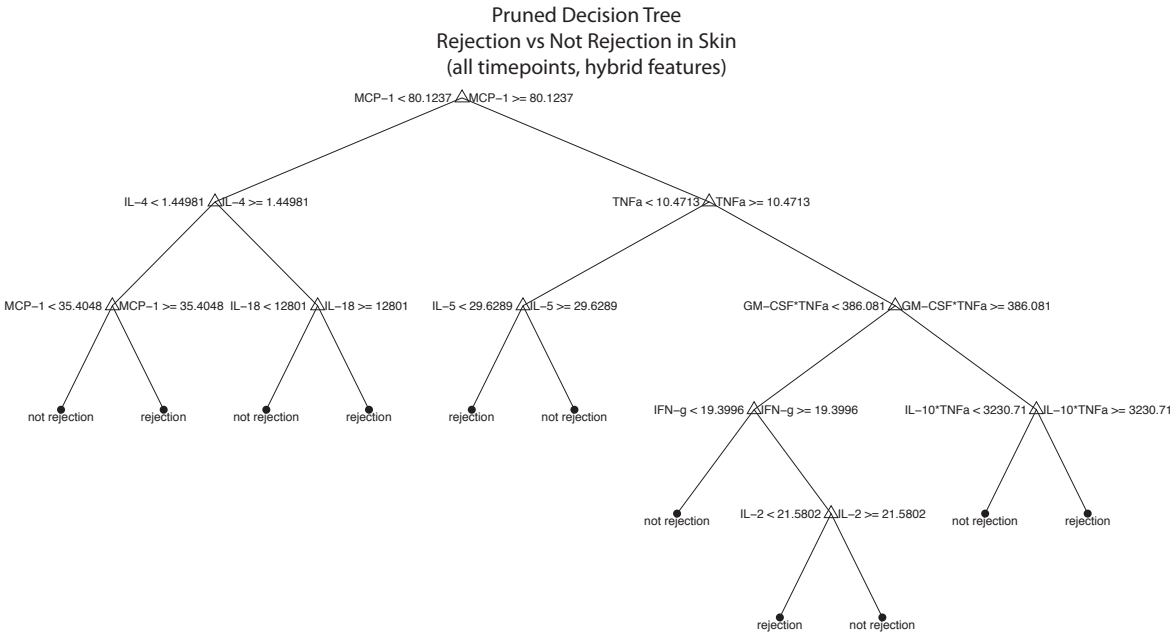

Figure 6.163

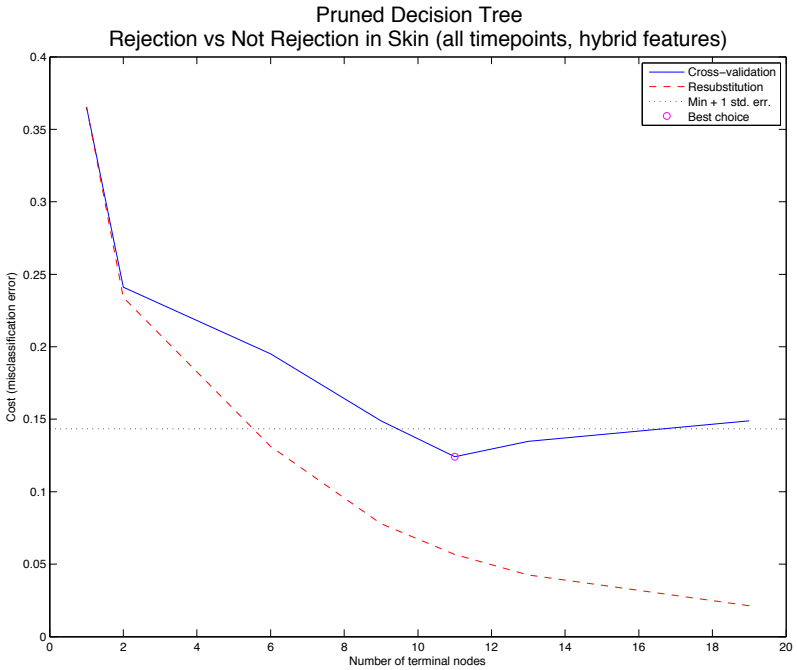

Figure 6.164

ROC Curves in Skin: Rejection

Rejection in Original Feature Space

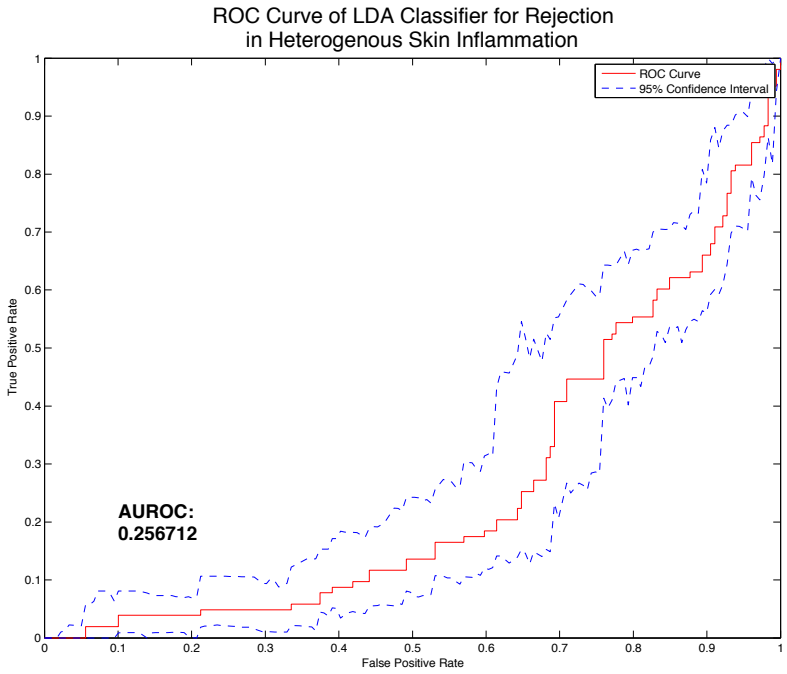

Figure 6.165

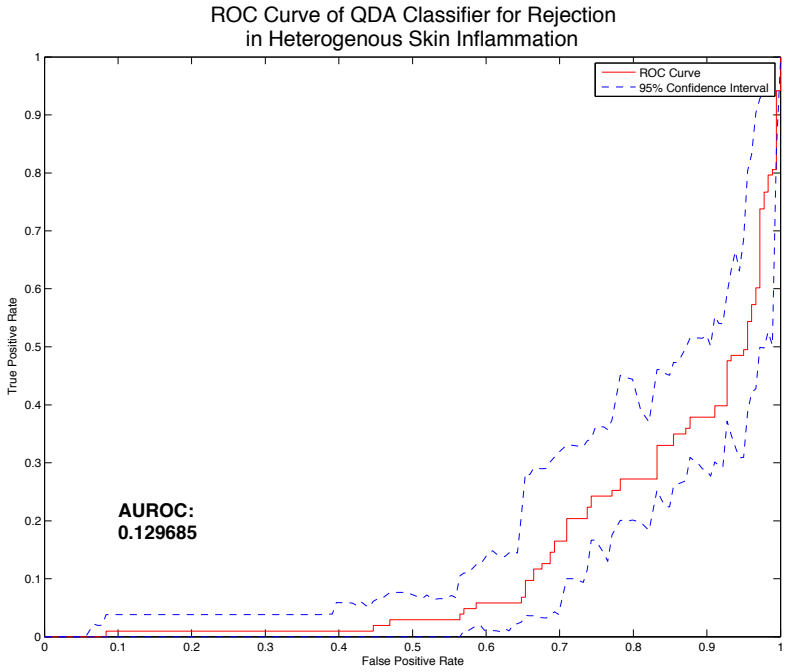

Figure 6.166

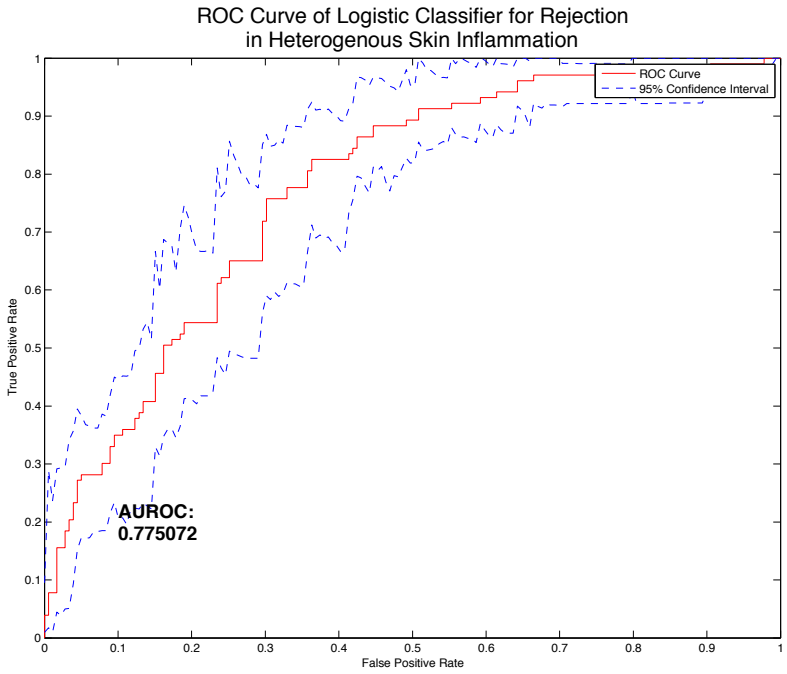

Figure 6.167

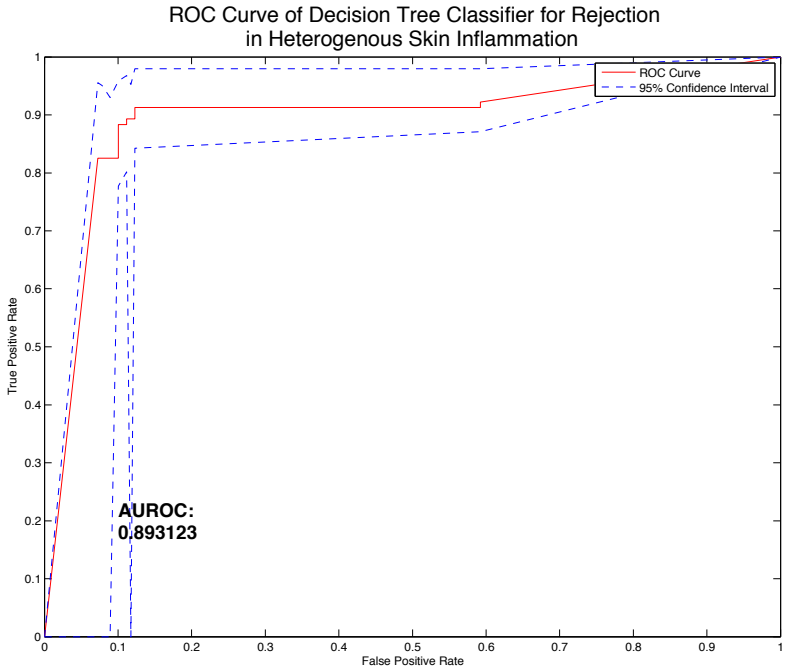

Figure 6.168

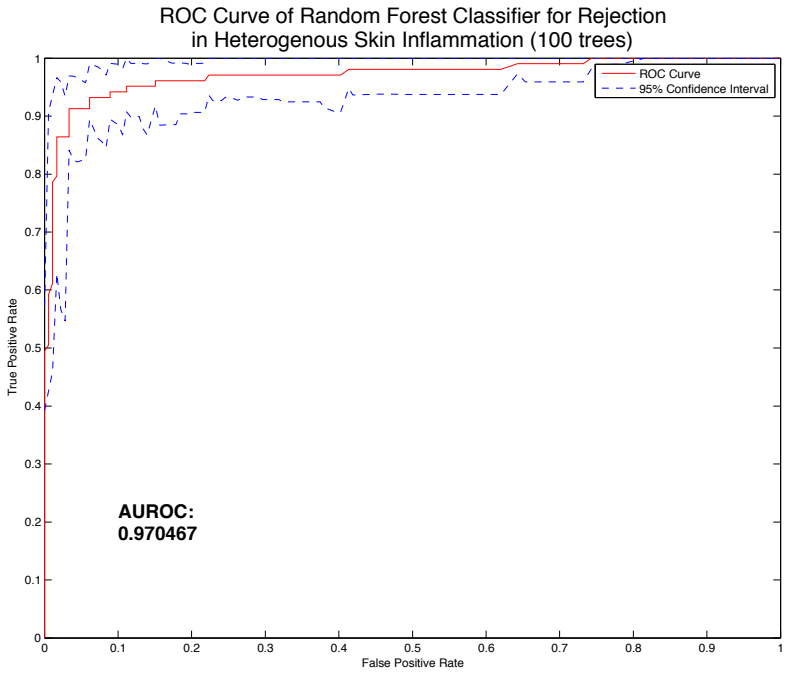

Figure 6.169

Rejection in Hybrid Feature Space

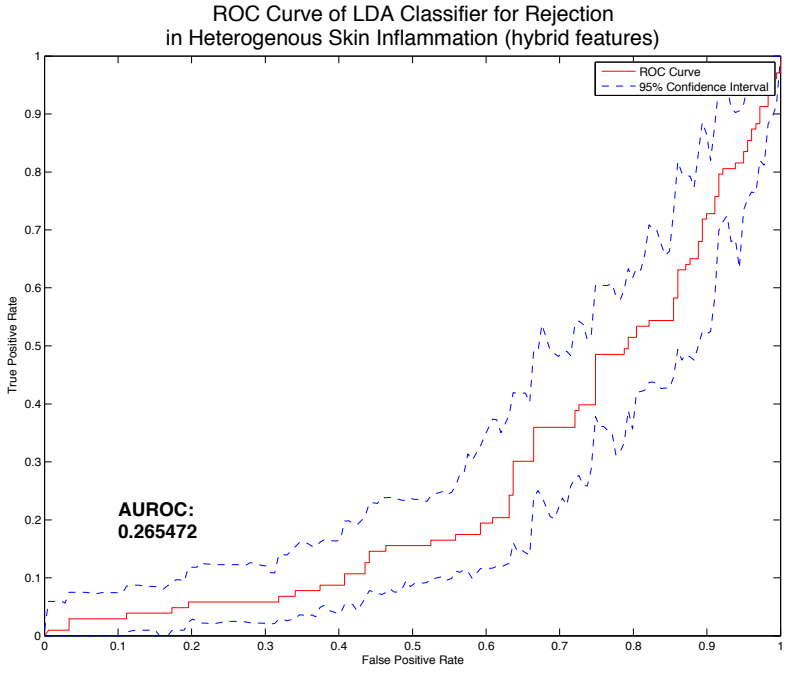

Figure 6.170

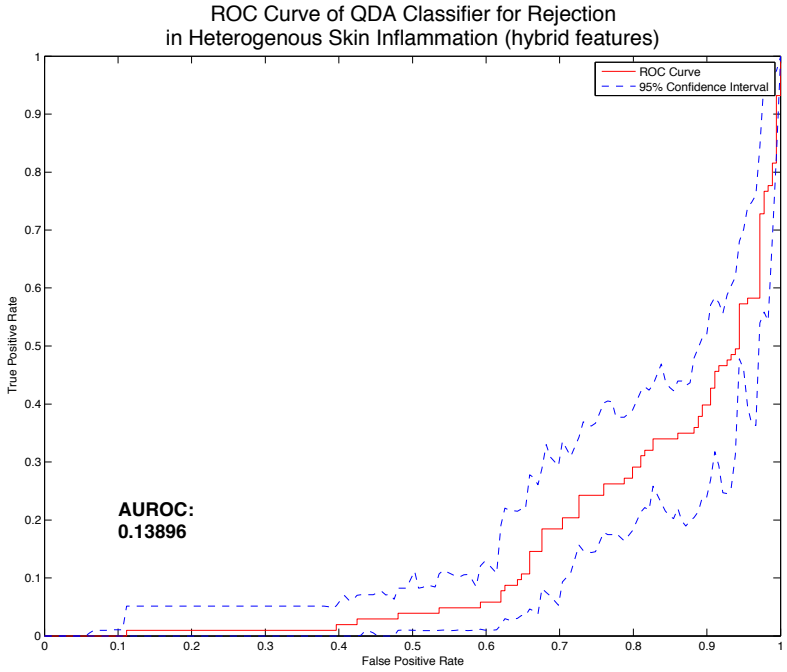

Figure 6.171

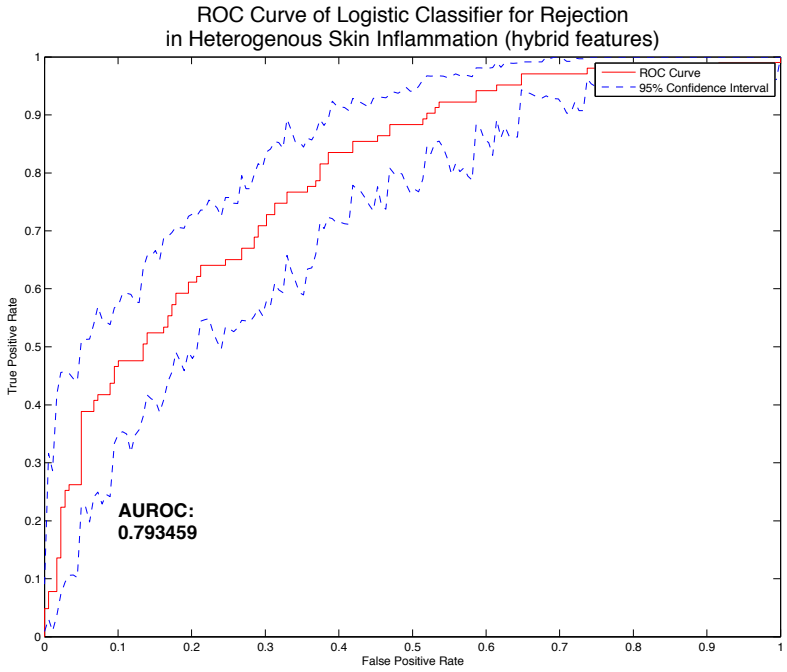

Figure 6.172

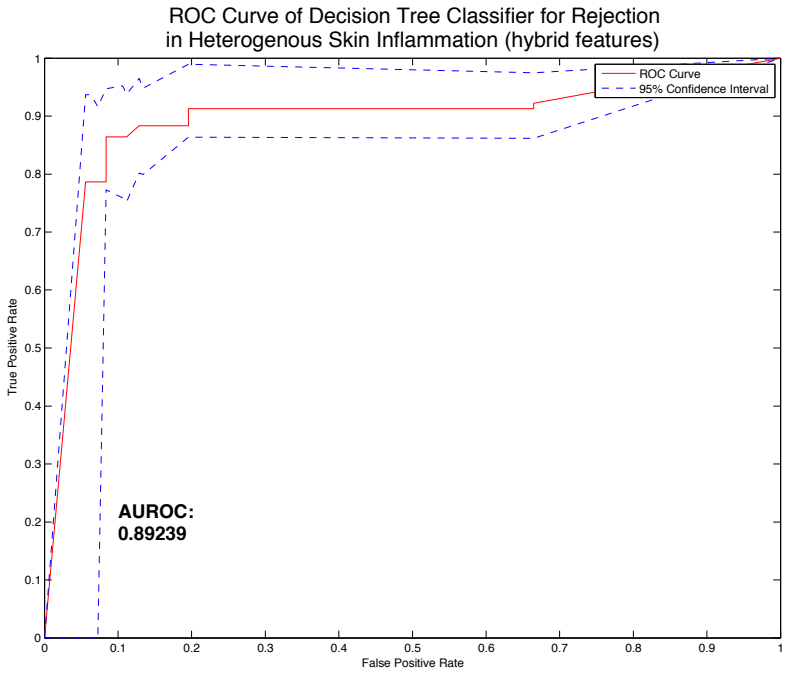

Figure 6.173

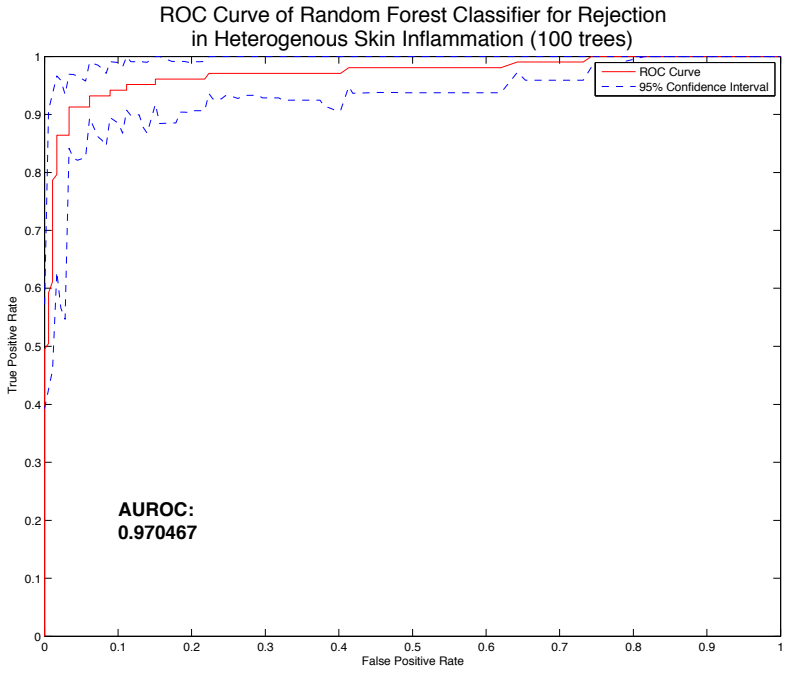

Figure 6.174

Rejection vs. Not Rejection in Skin (POD <= 5)

Original 14-Dimensional Feature Space

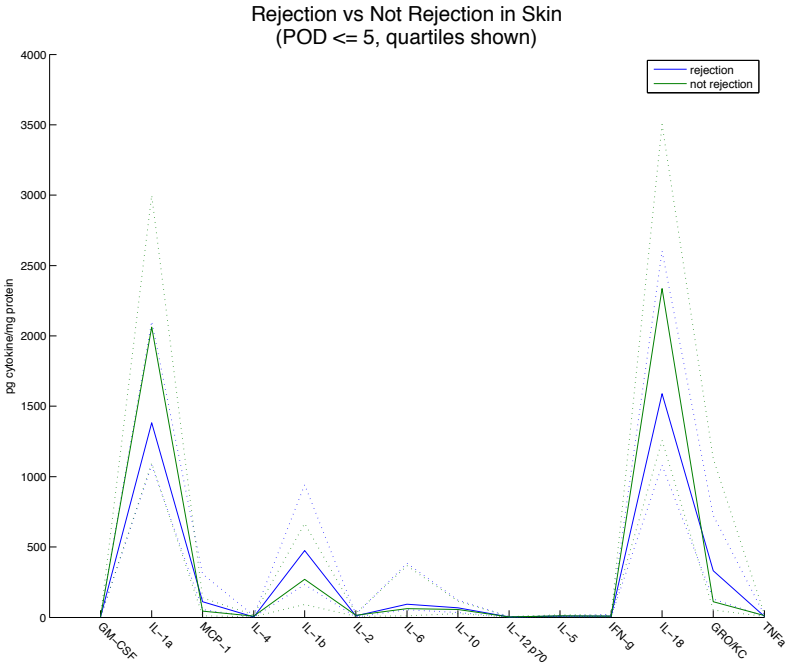

Figure 6.175

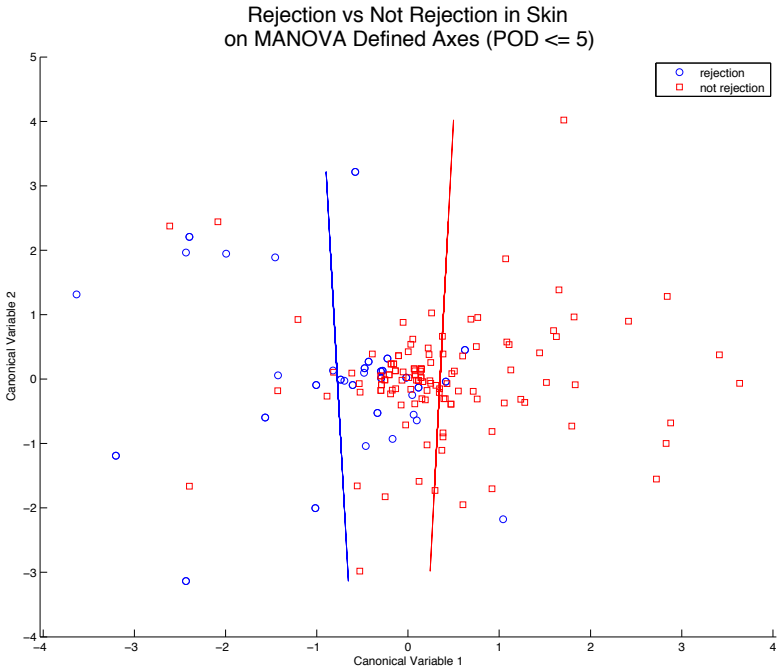

Figure 6.176

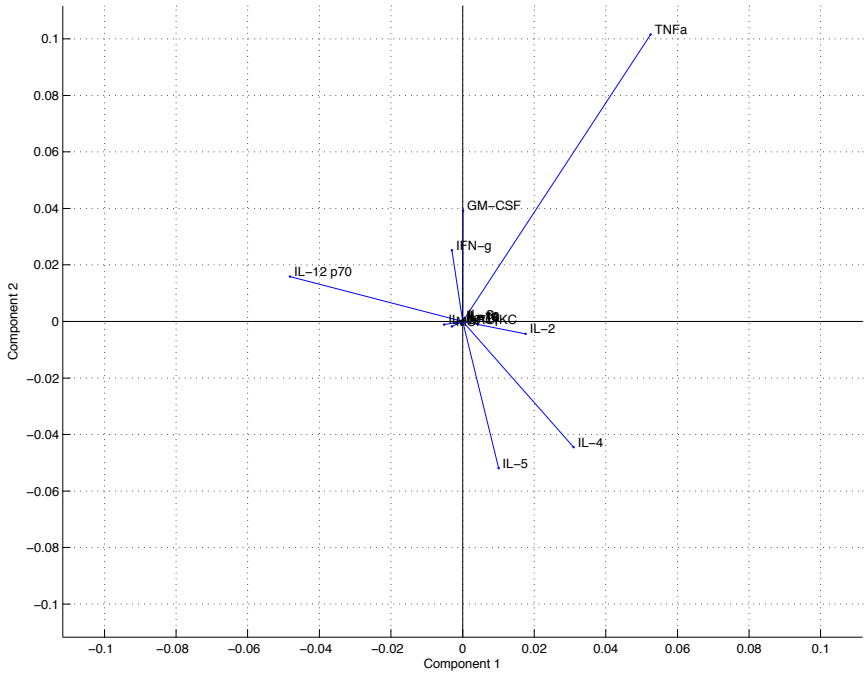

Figure 6.177

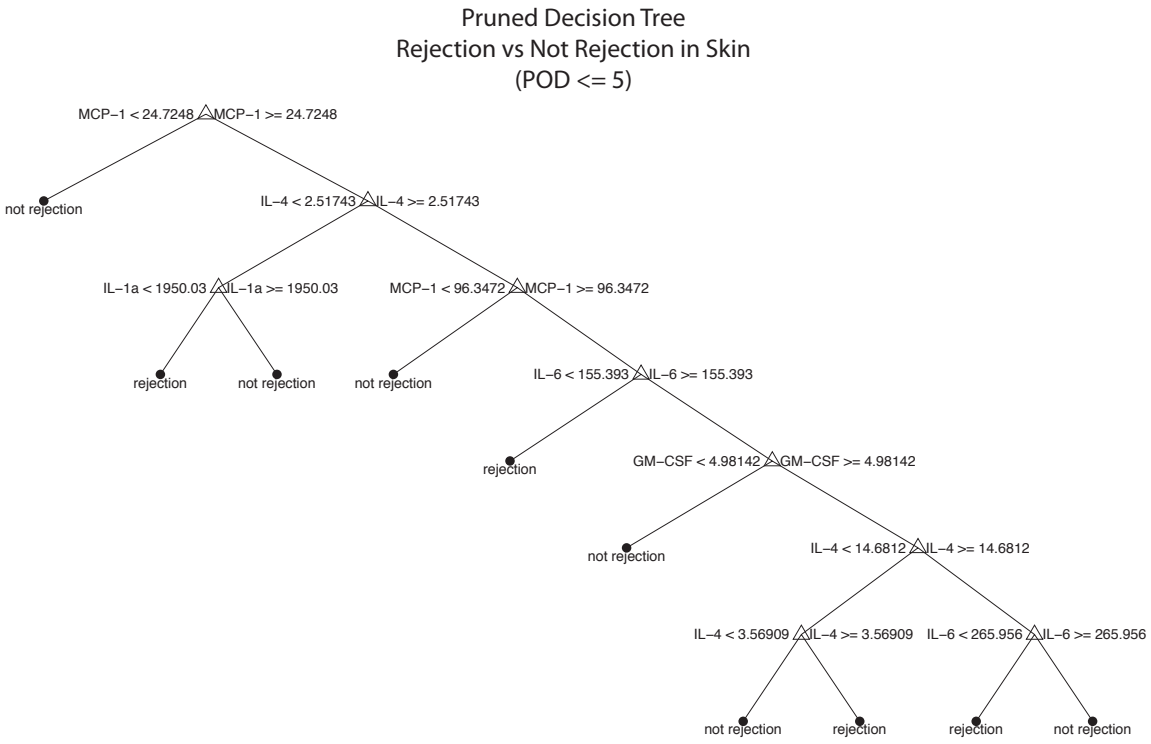

Figure 6.178

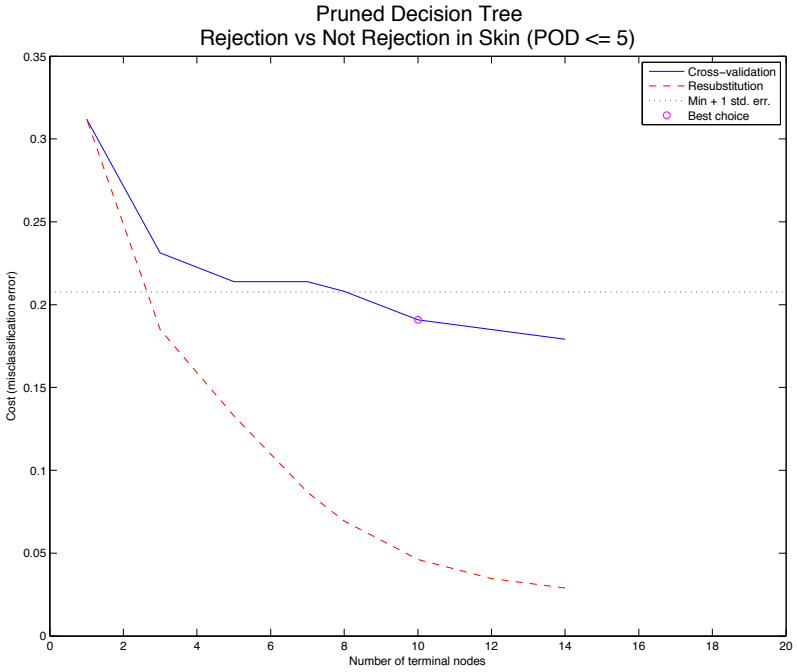

Figure 6.179

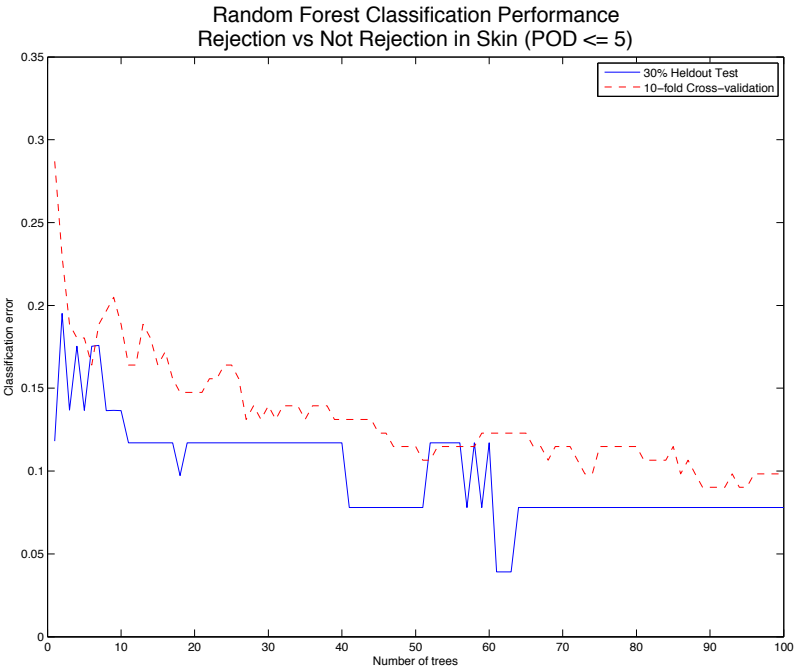

Figure 6.180

5-Dimensional Feature Selected Space

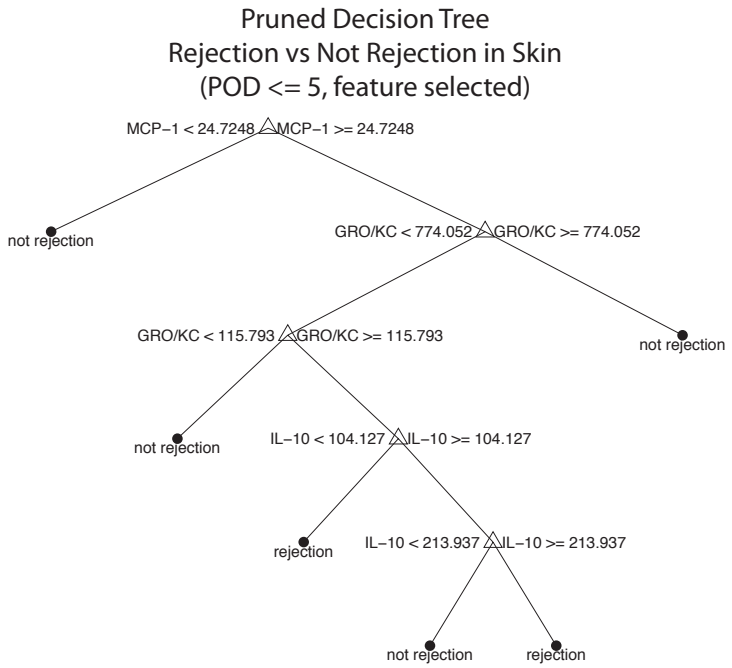

Figure 6.181

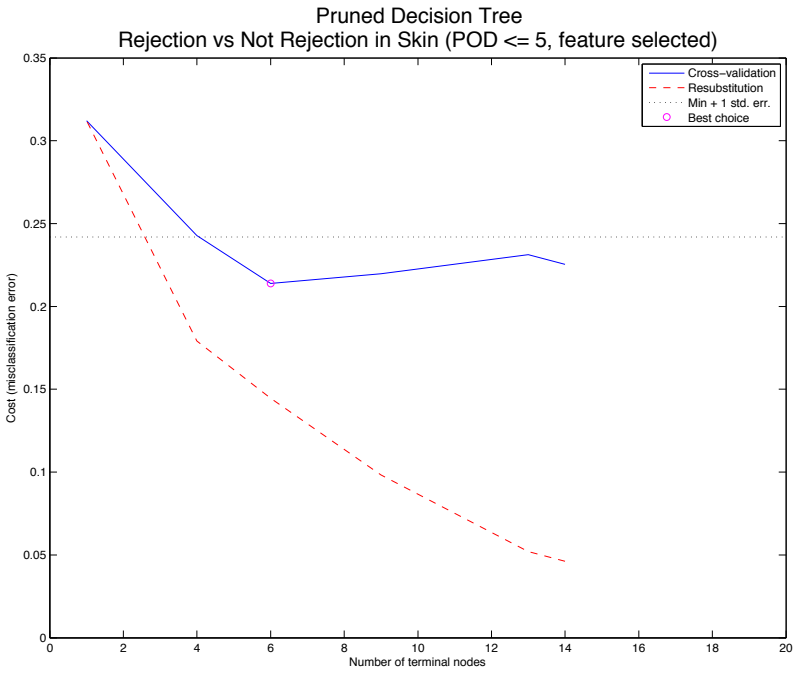

Figure 6.182

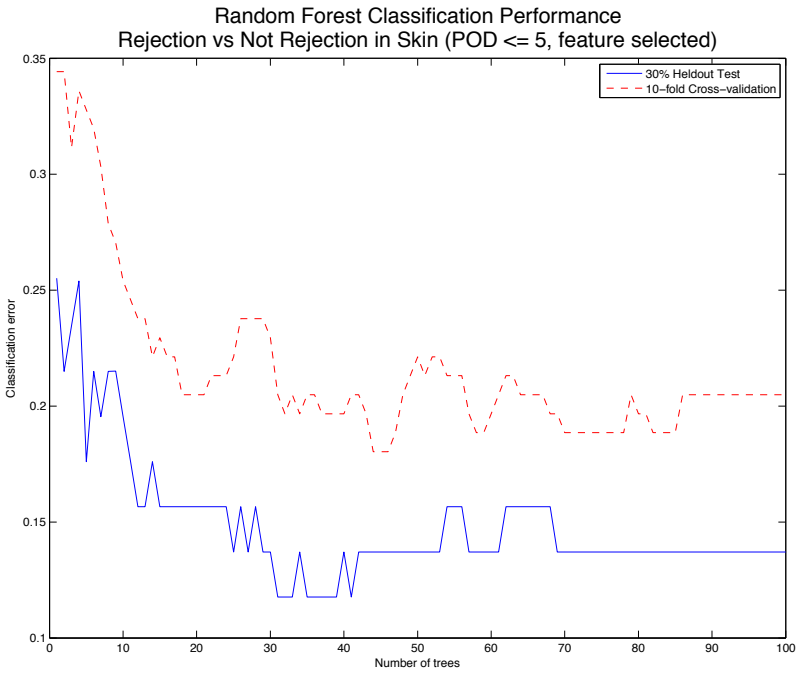

Figure 6.183

MANOVA Transformed Feature Space

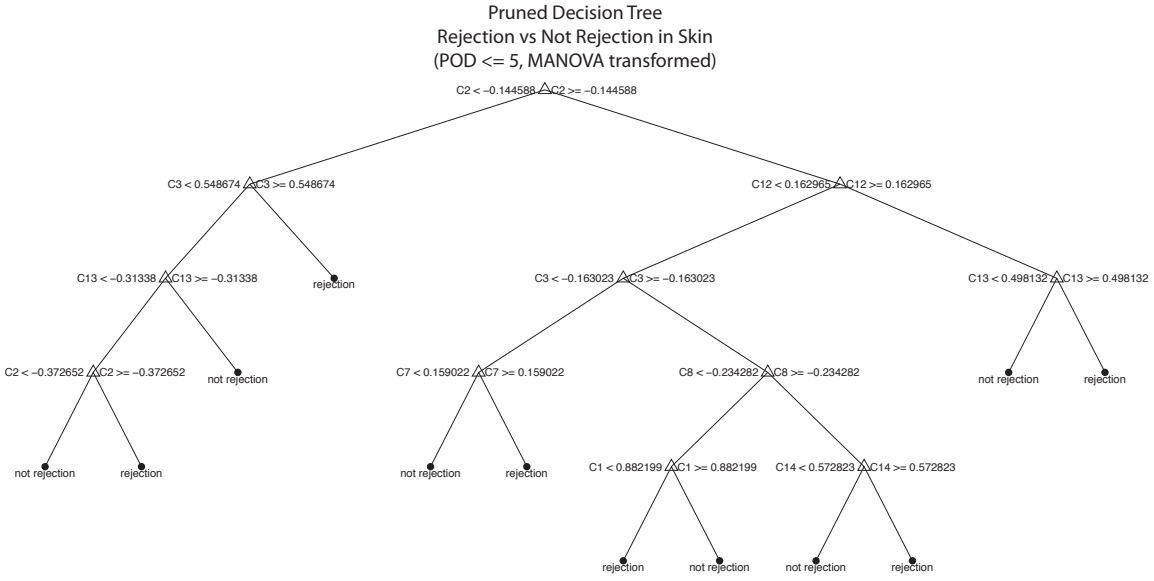

Figure 6.184

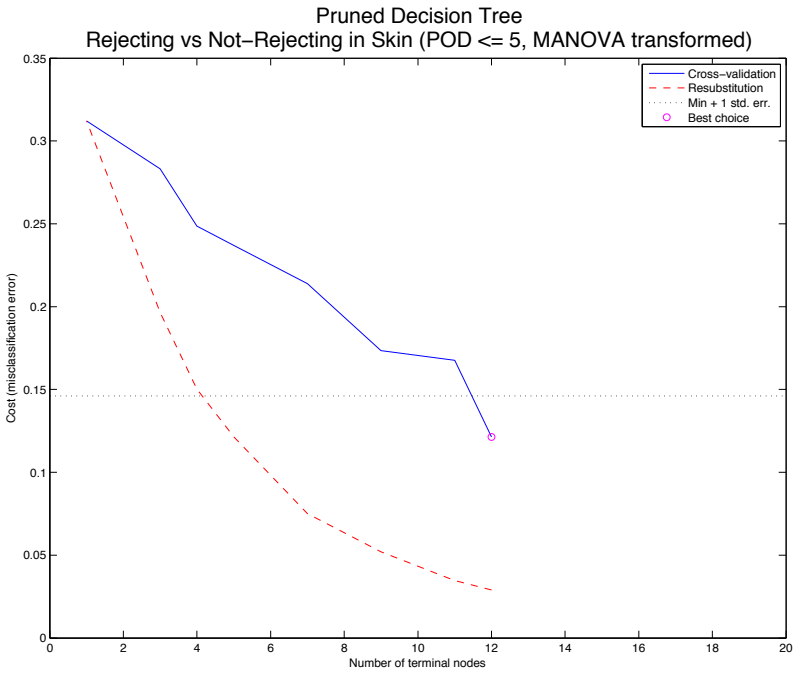

Figure 6.185

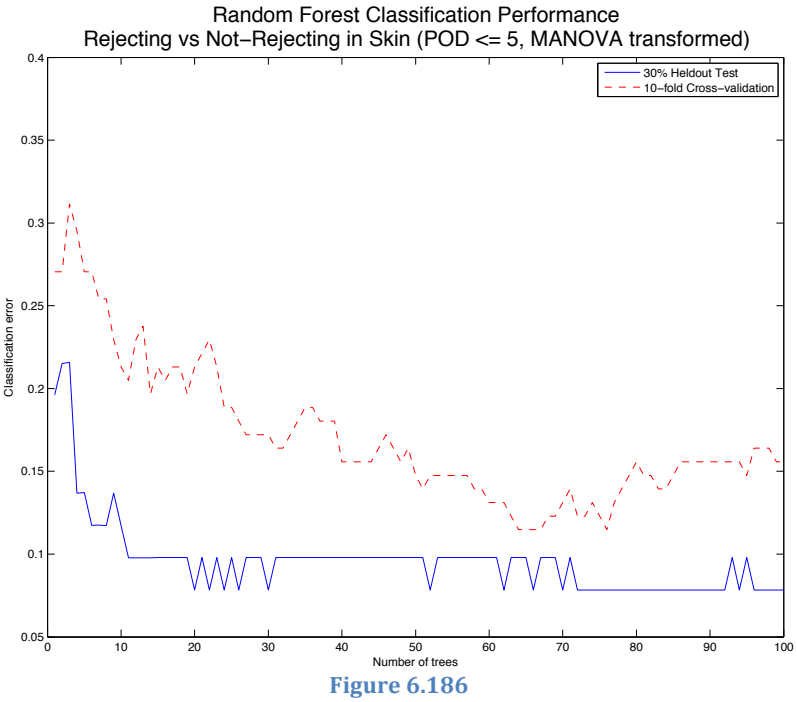

Figure 6.186

Rejecting vs. Not Rejecting in Skin (POD > 5)

Original 14-Dimensional Feature Space

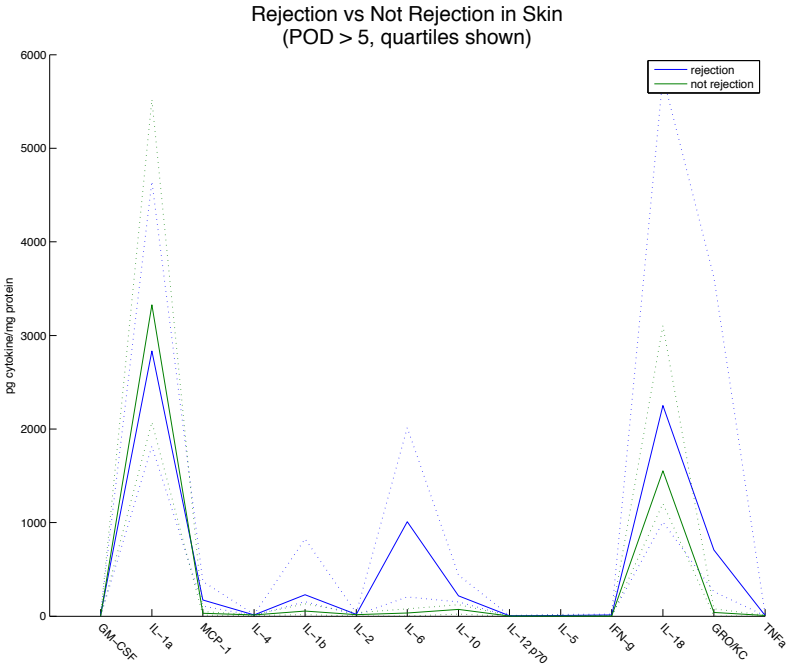

Figure 6.187

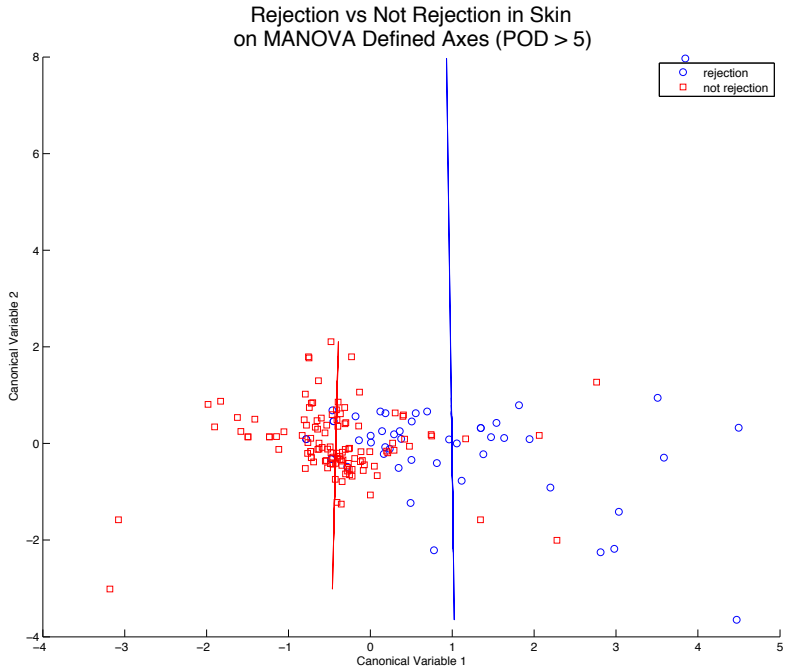

Figure 6.188

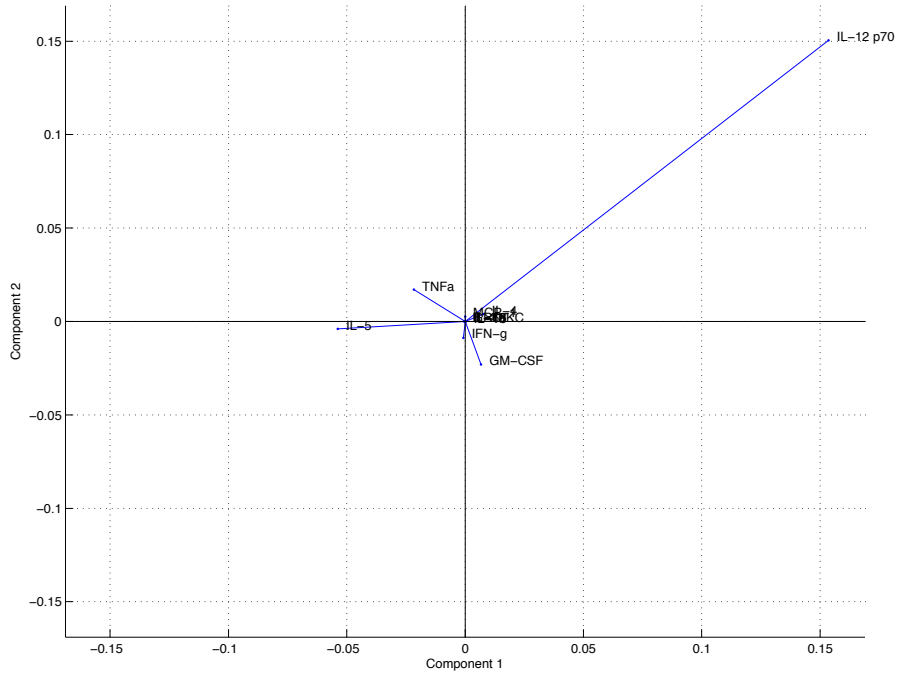

Figure 6.189

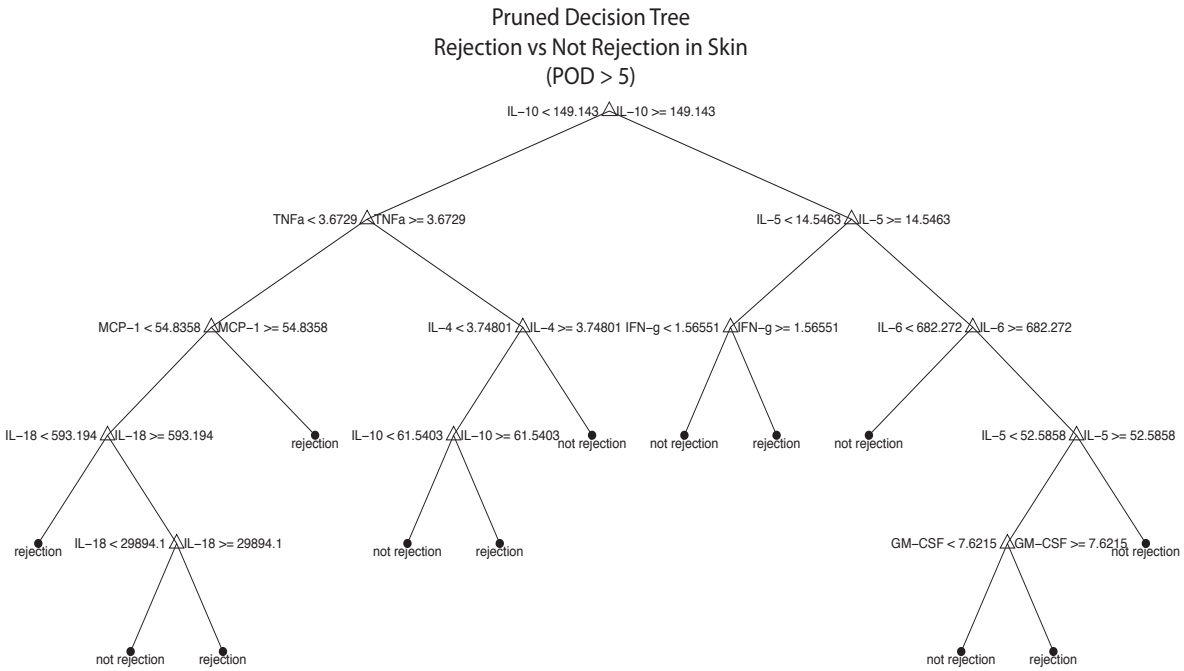

Figure 6.190

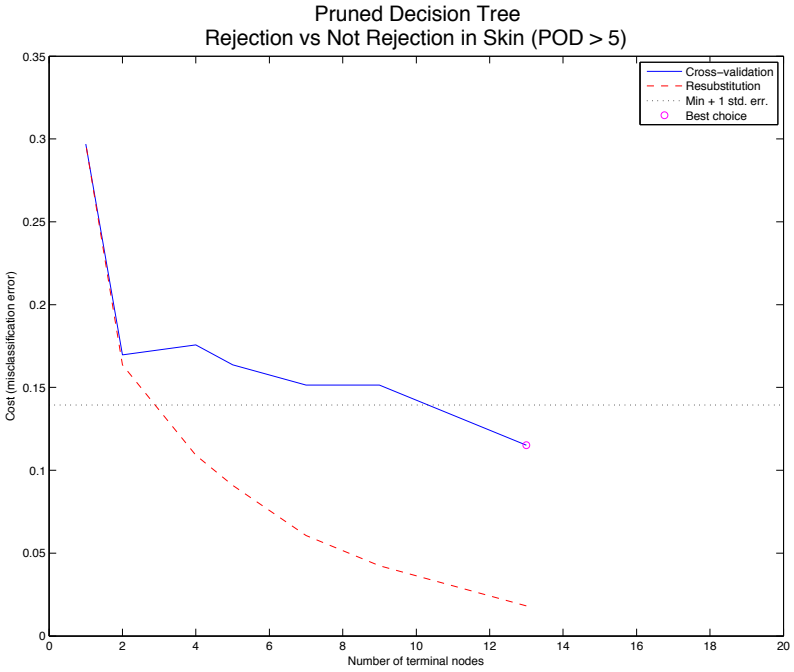

Figure 6.191

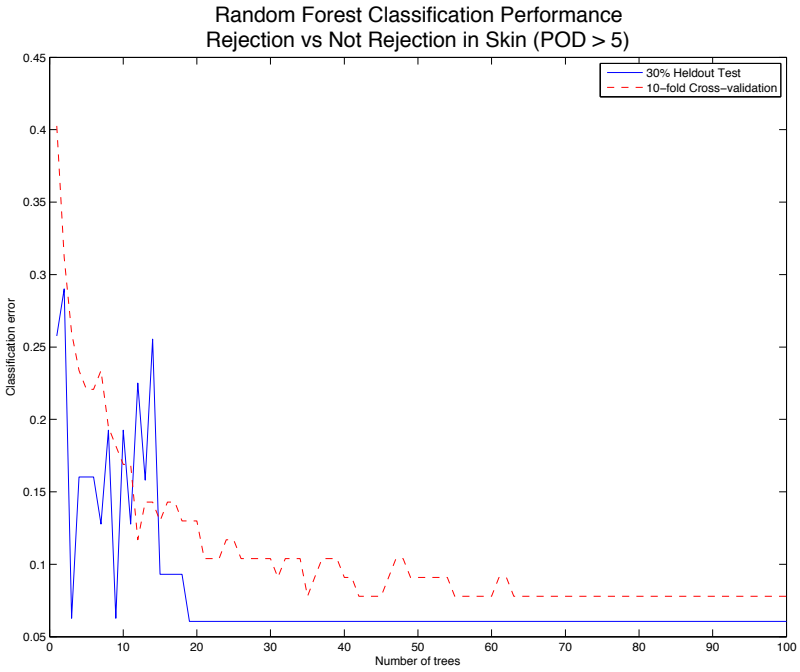

Figure 6.192

5-Dimensional Feature Selected Space

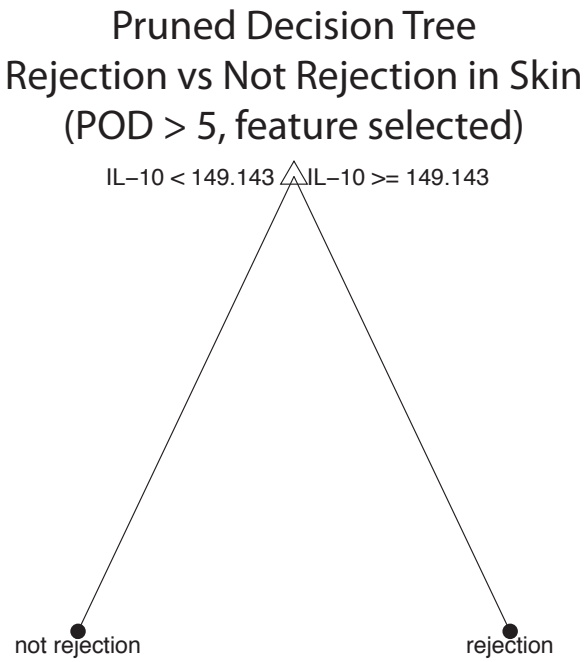

Figure 6.193

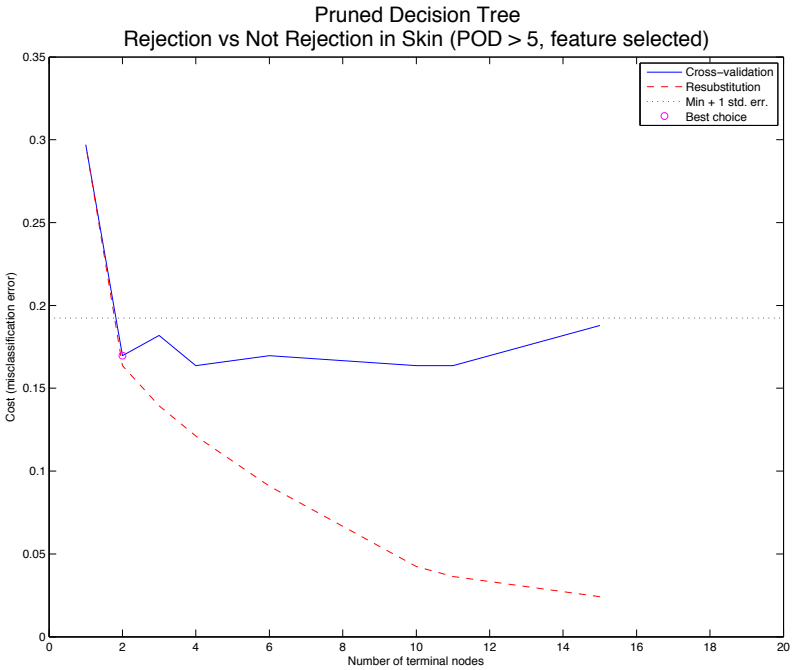

Figure 6.194

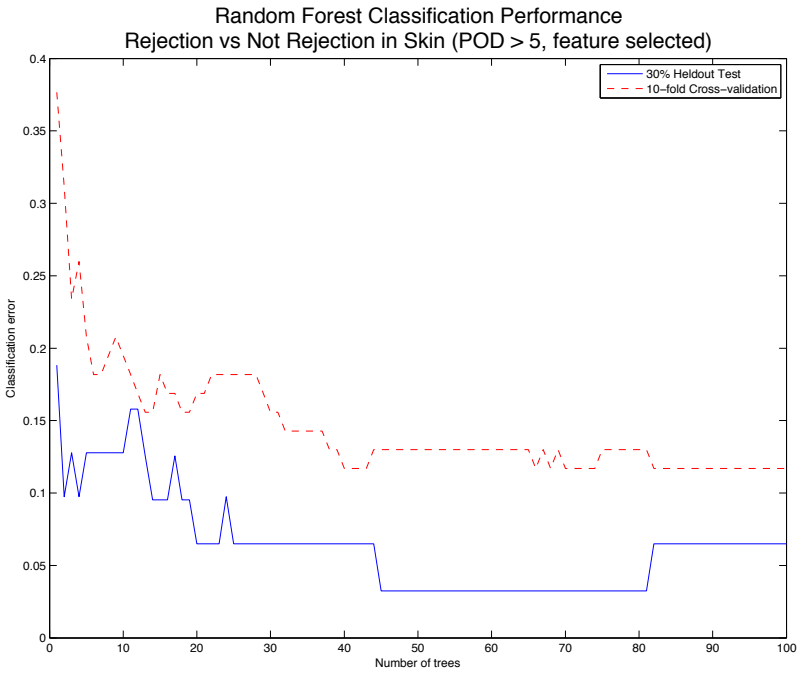

Figure 6.195

MANOVA Transformed Feature Space

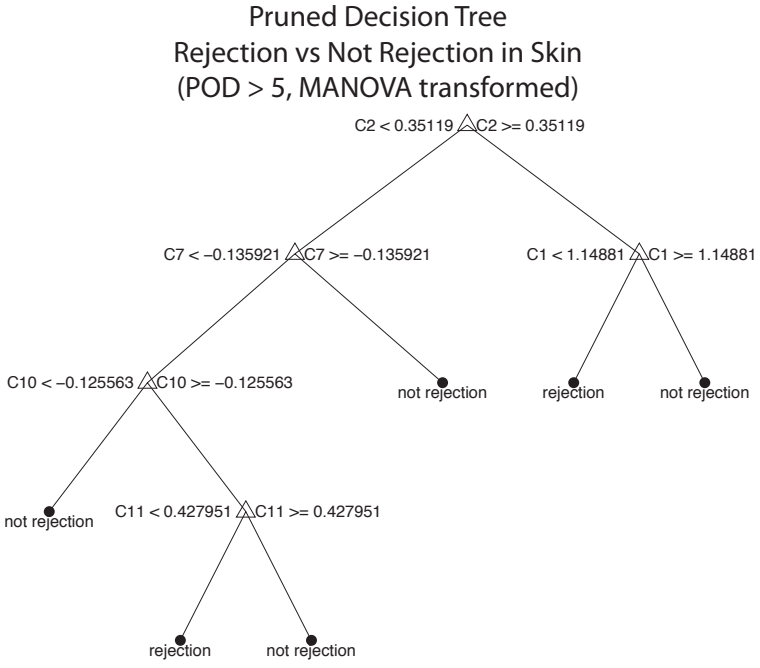

Figure 6.196

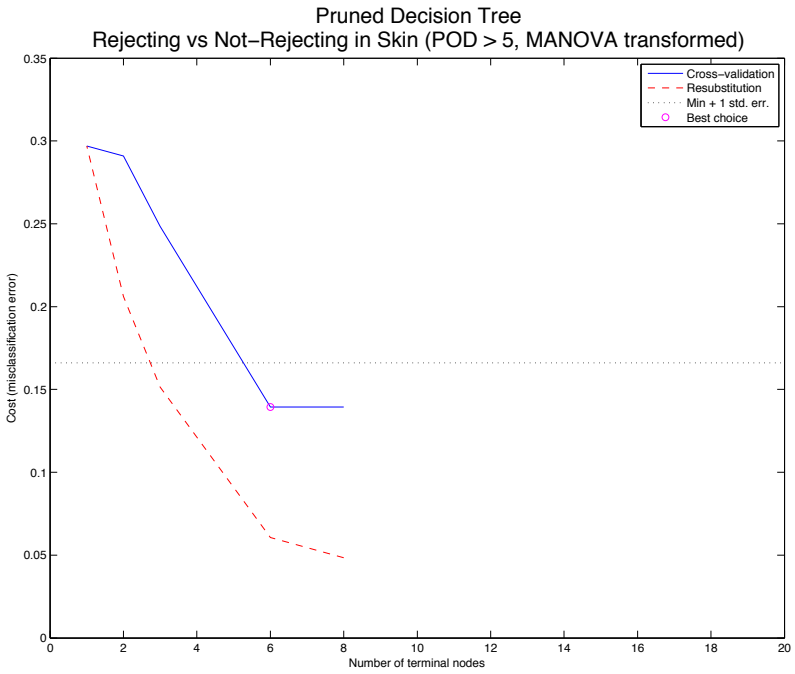

Figure 6.197

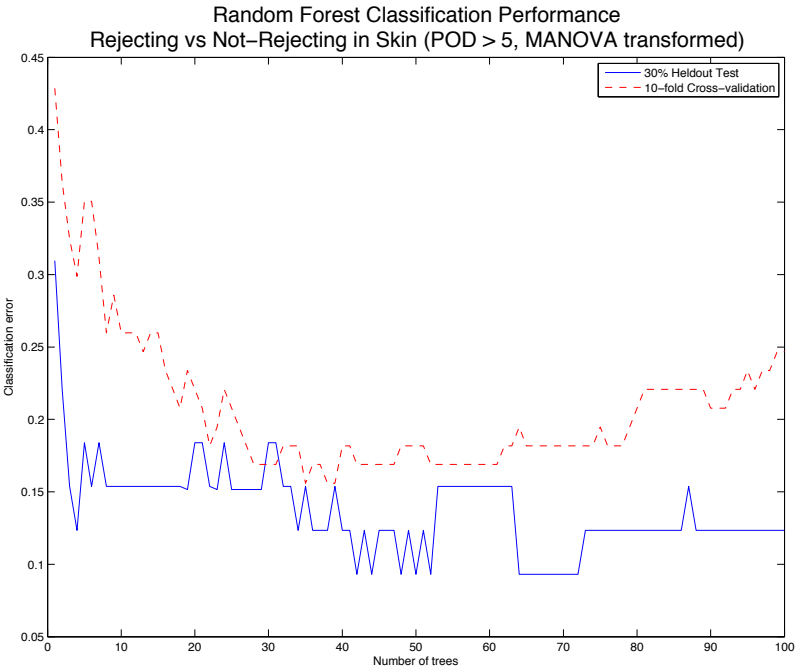

Figure 6.198

Rejecting vs. Not Rejecting in Muscle (all time points)

Original 14-Dimensional Feature Space

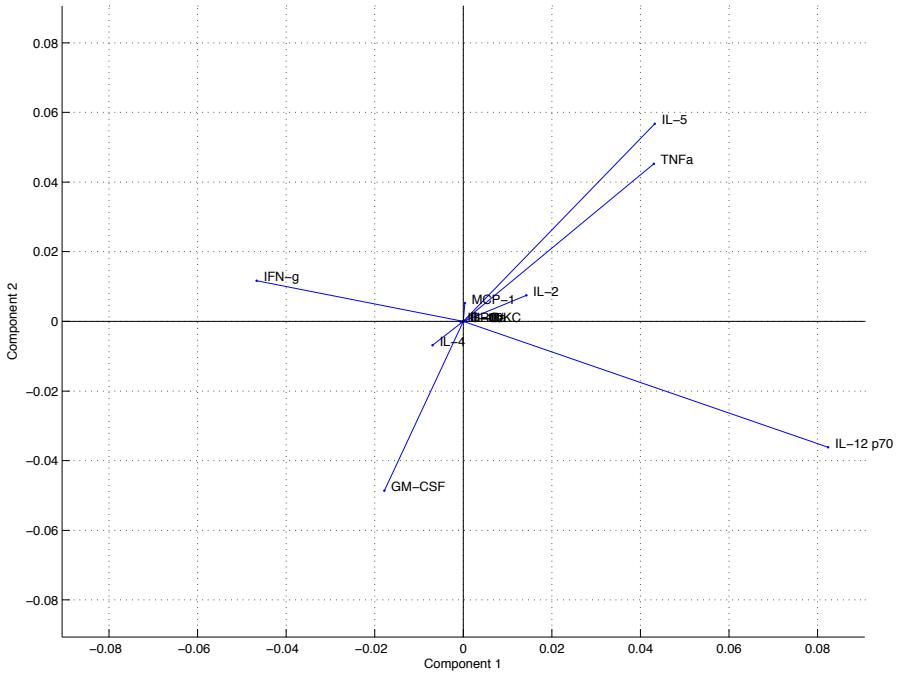

Figure 6.199

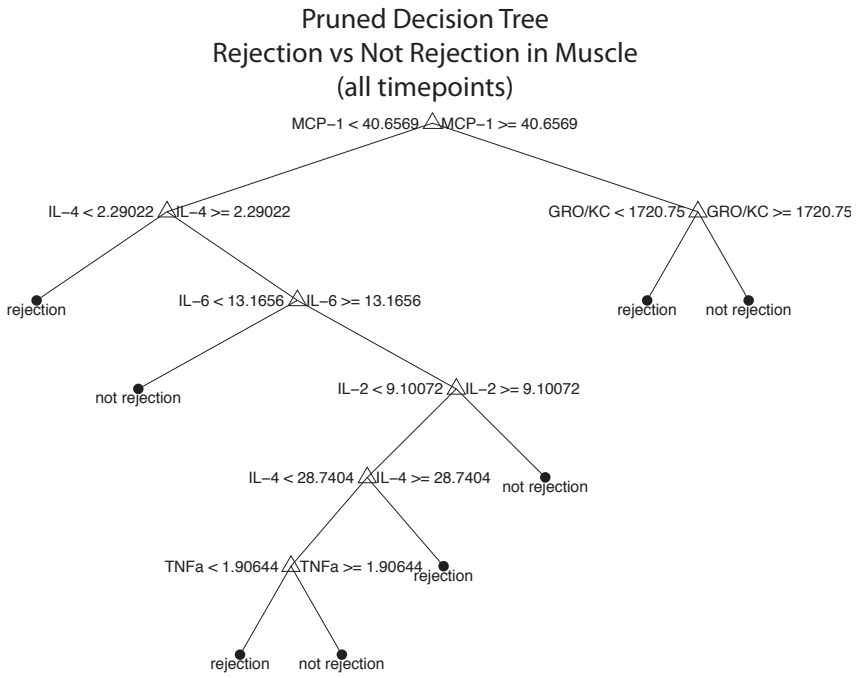

Figure 6.200

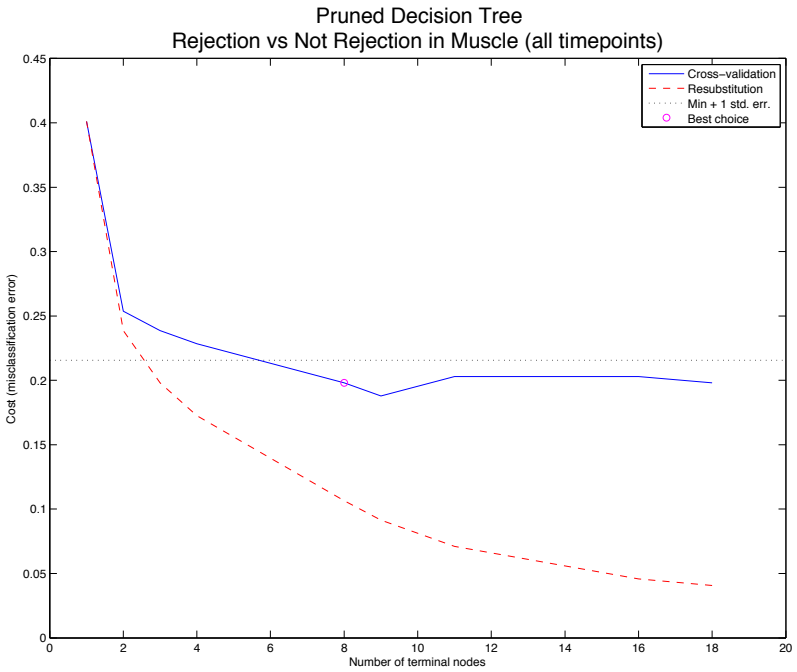

Figure 6.201

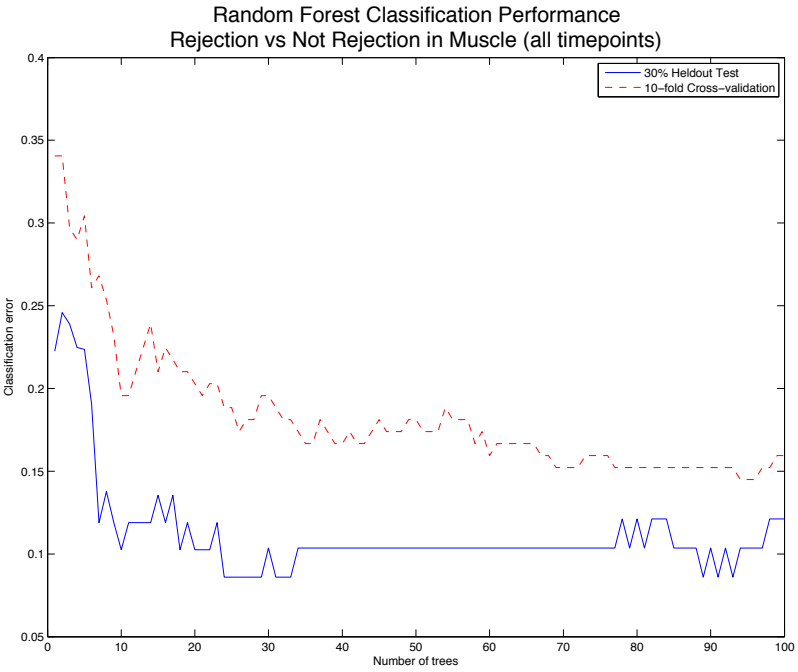

Figure 6.202

5-Dimensional Feature Selected Space

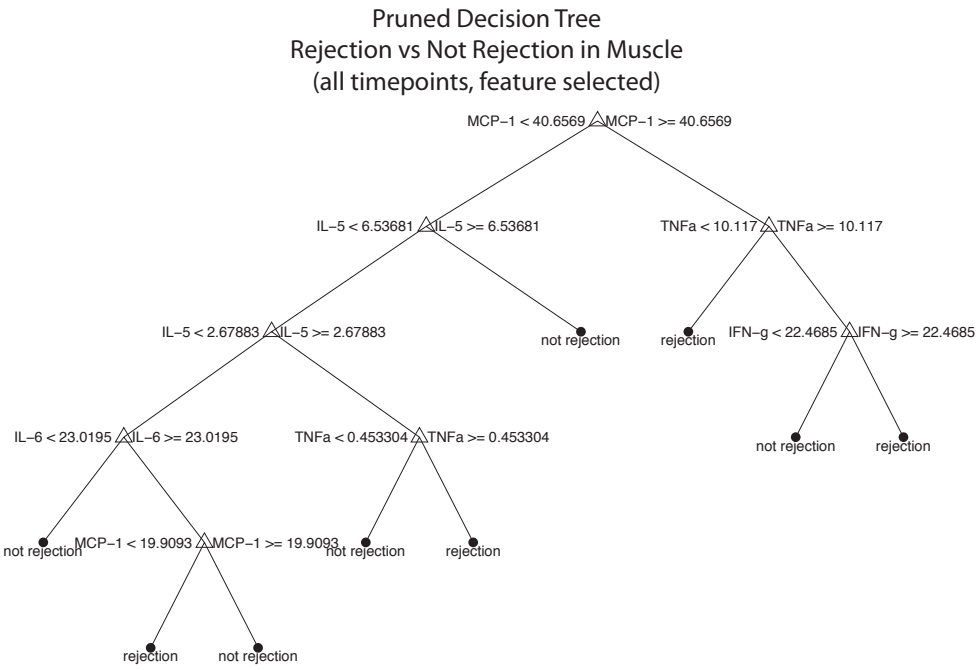

Figure 6.203

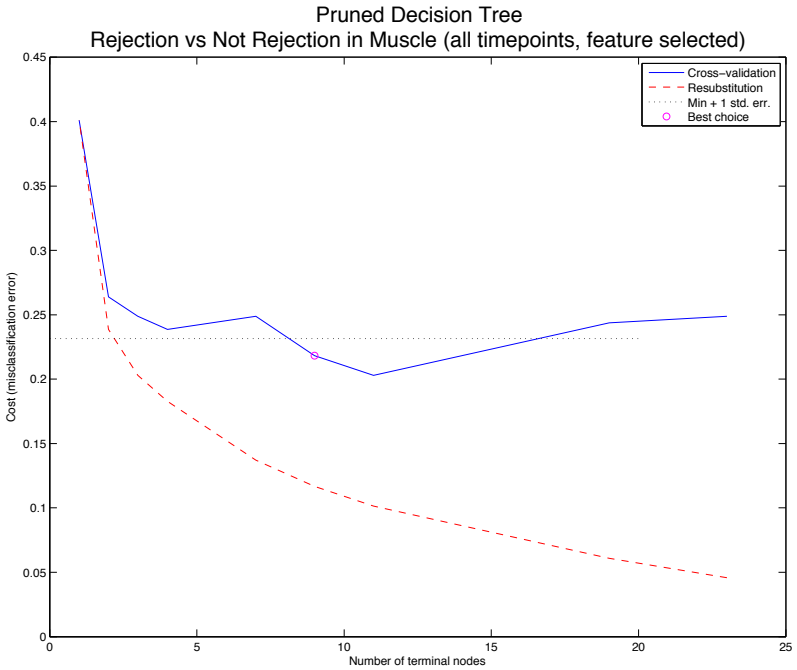

Figure 6.204

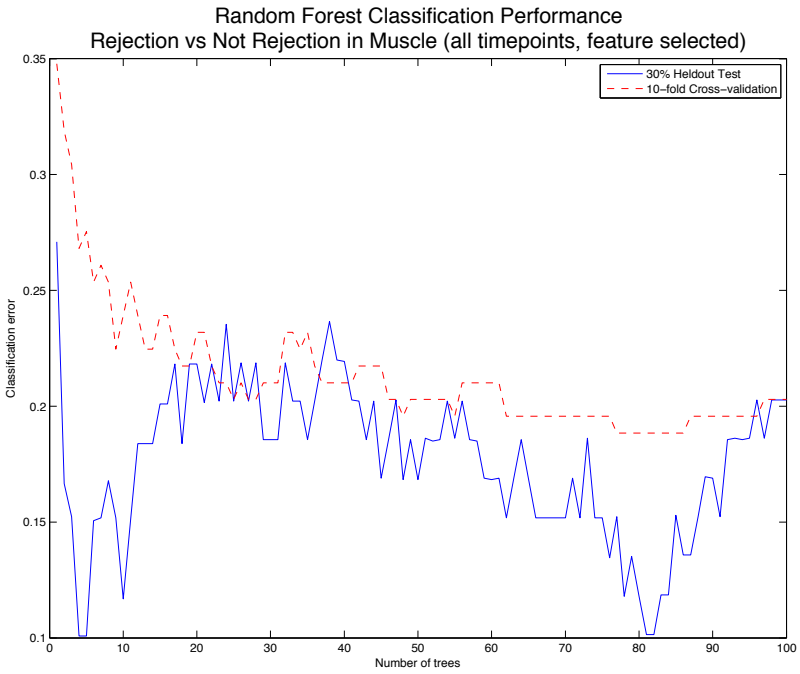

Figure 6.205

MANOVA Transformed Feature Space

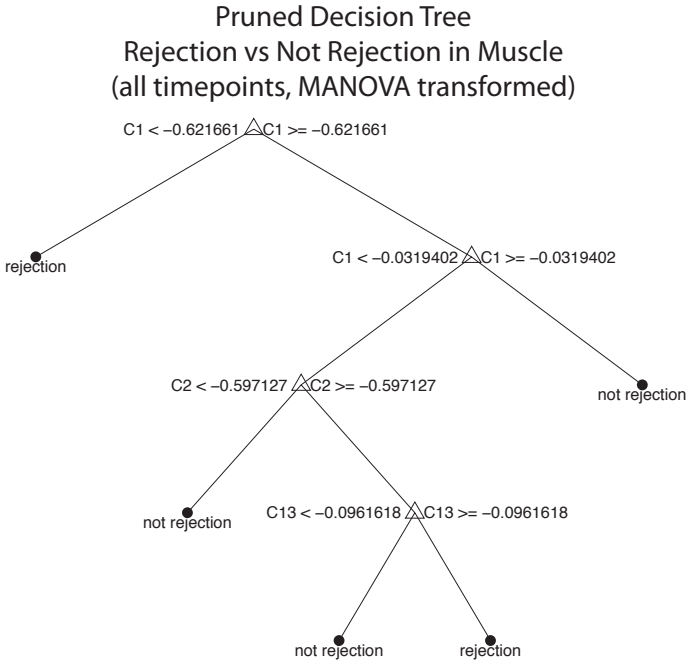

Figure 6.206

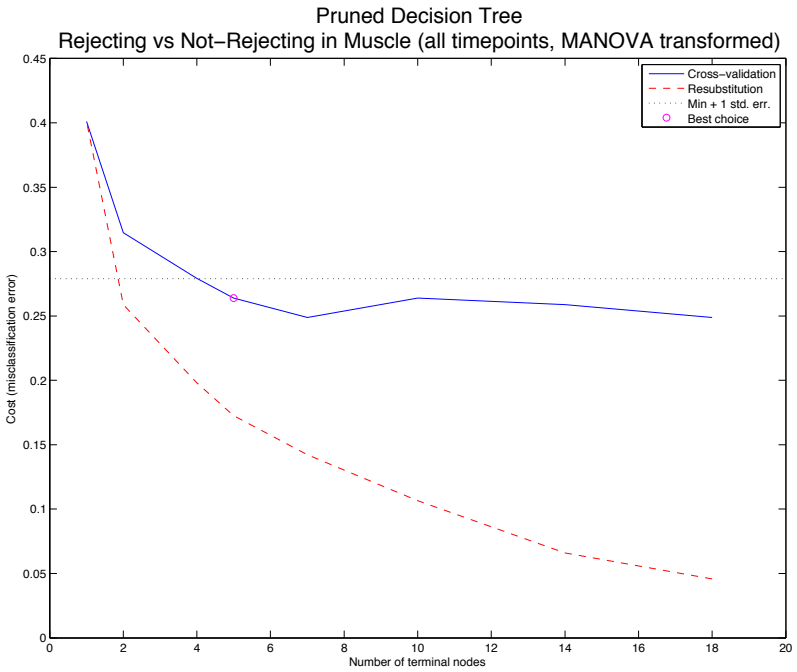

Figure 6.207

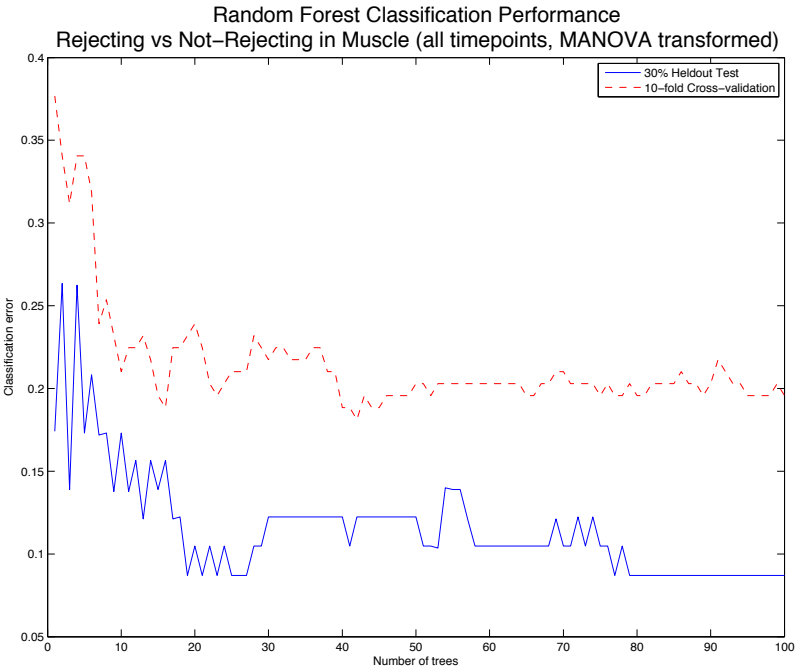

Figure 6.208

Hybrid Features

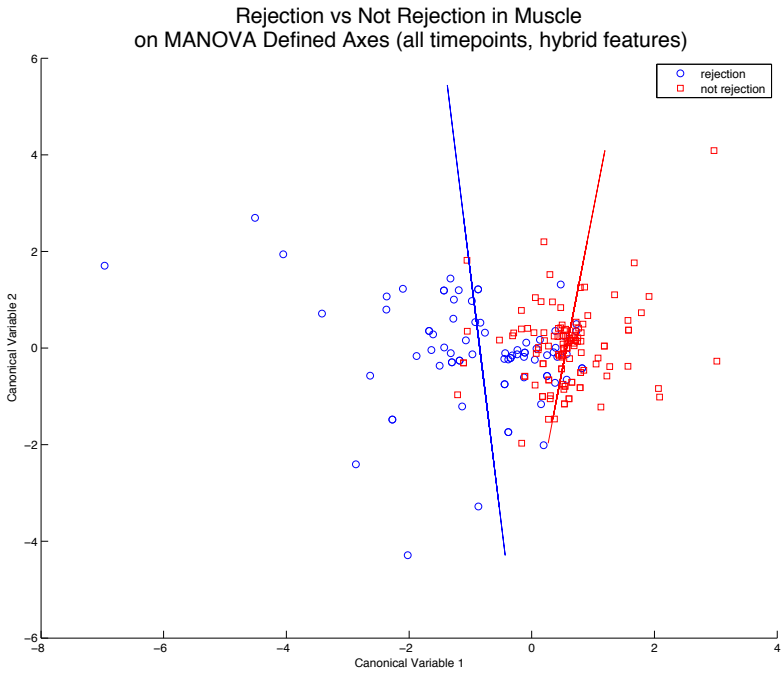

Figure 6.209

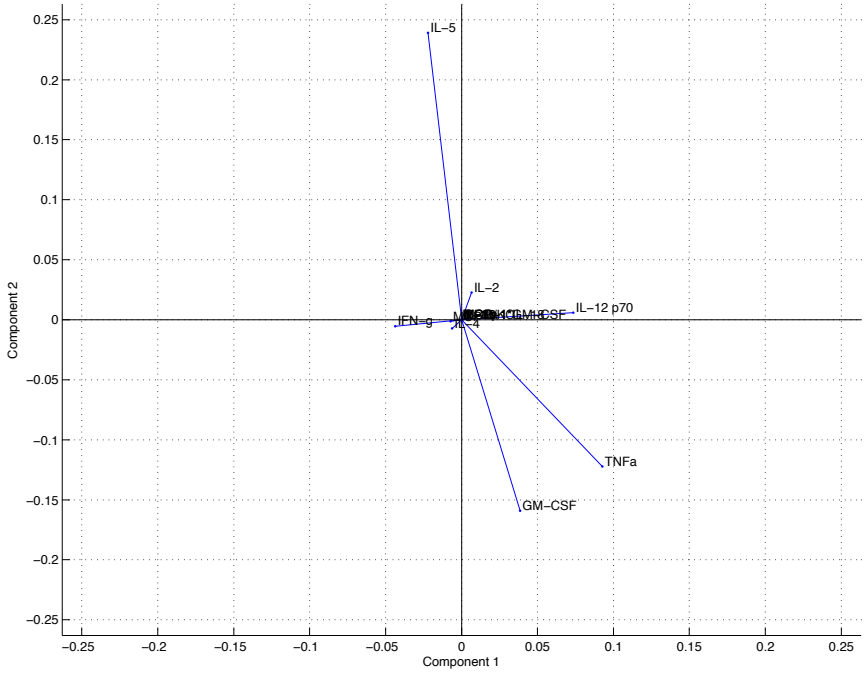

Figure 6.210

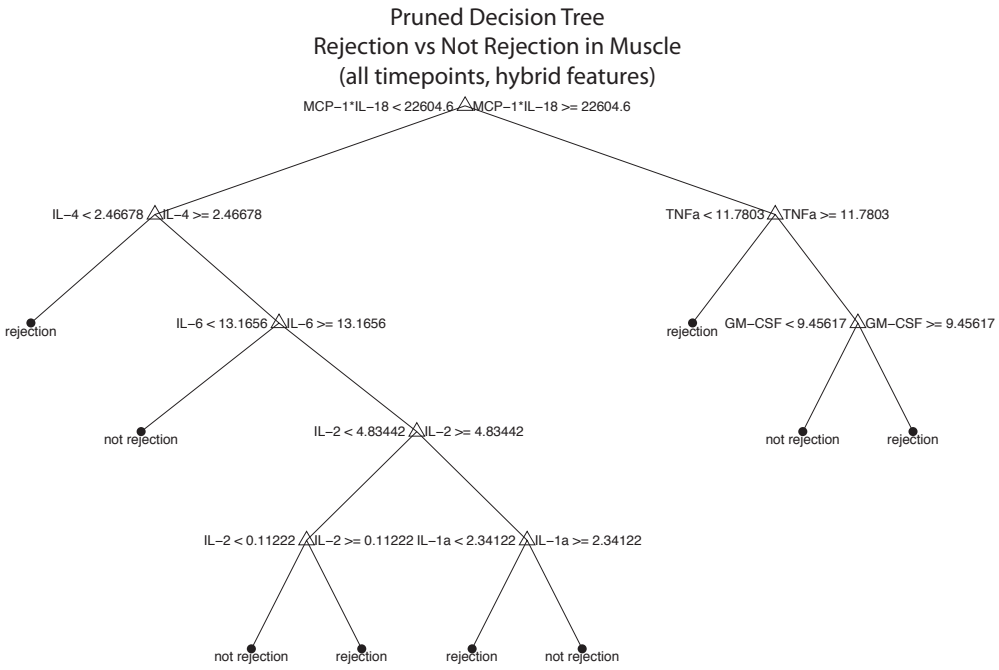

Figure 6.211

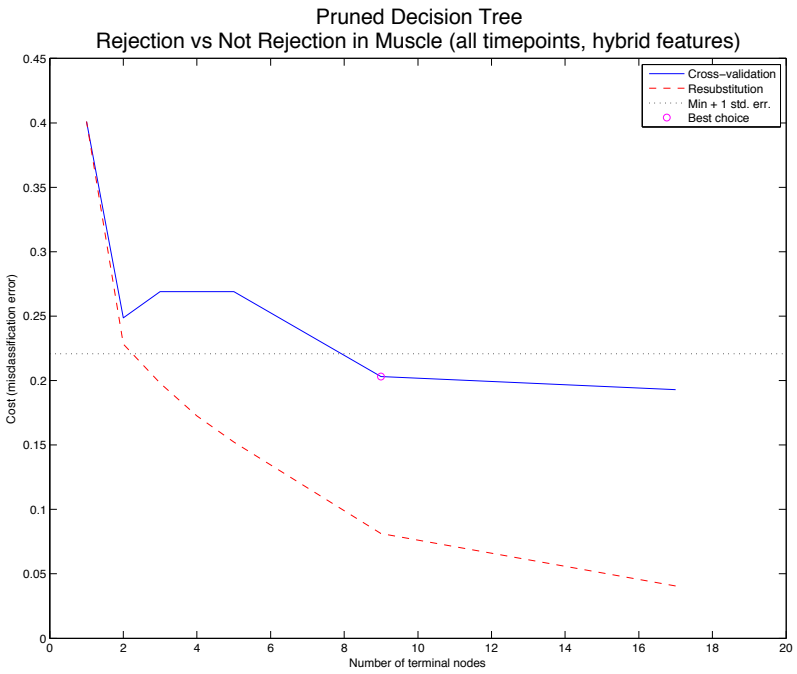

Figure 6.212

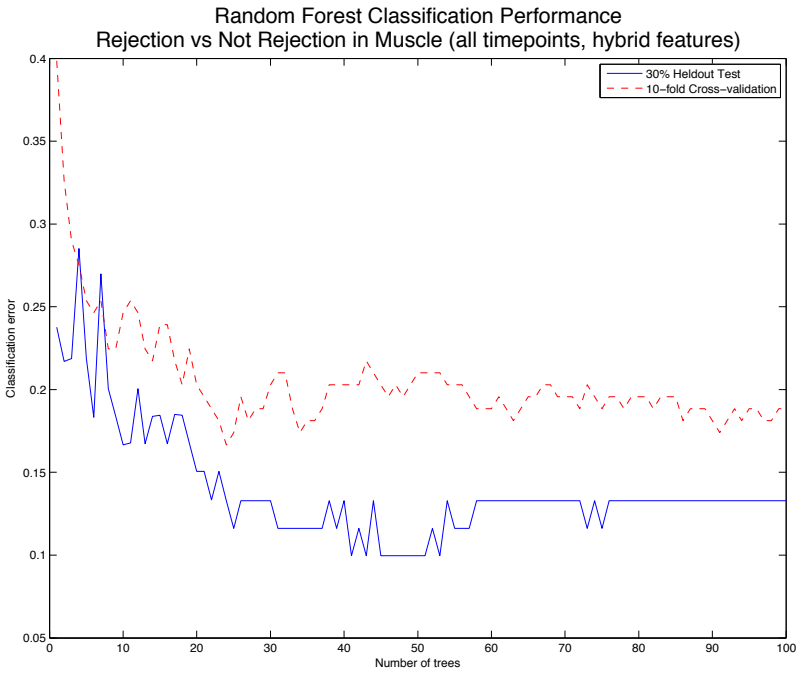

Figure 6.213

ROC Curves in Muscle: Rejection

Rejection in Original Feature Space

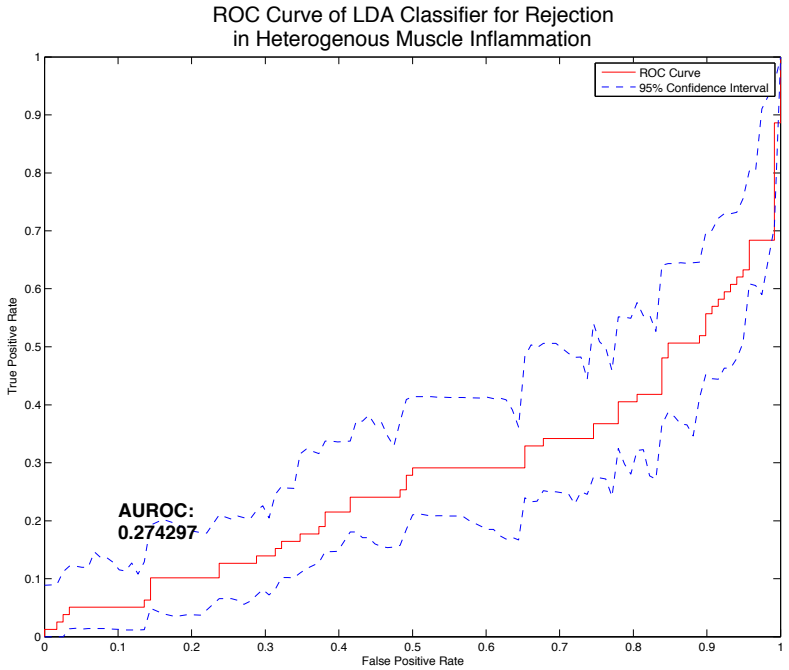

Figure 6.214

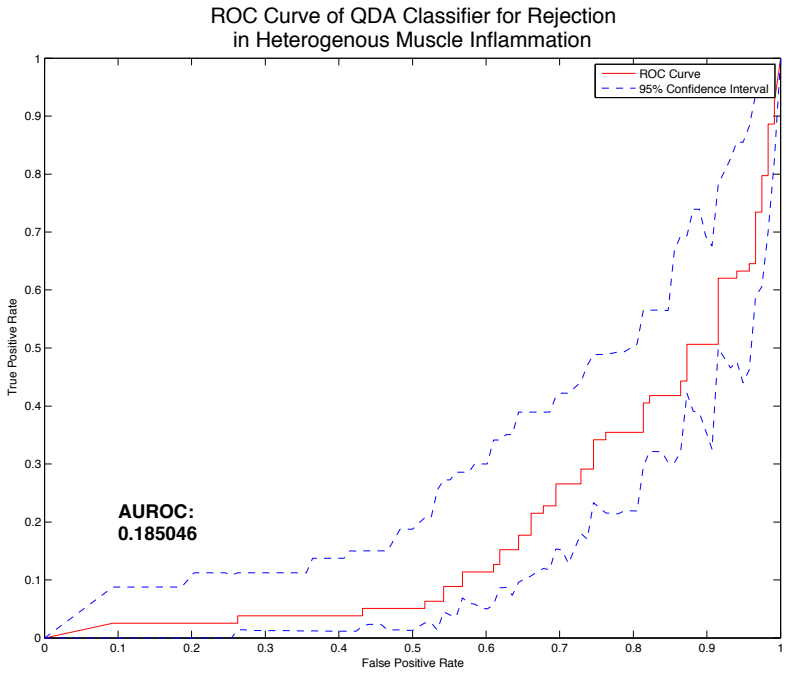

Figure 6.215

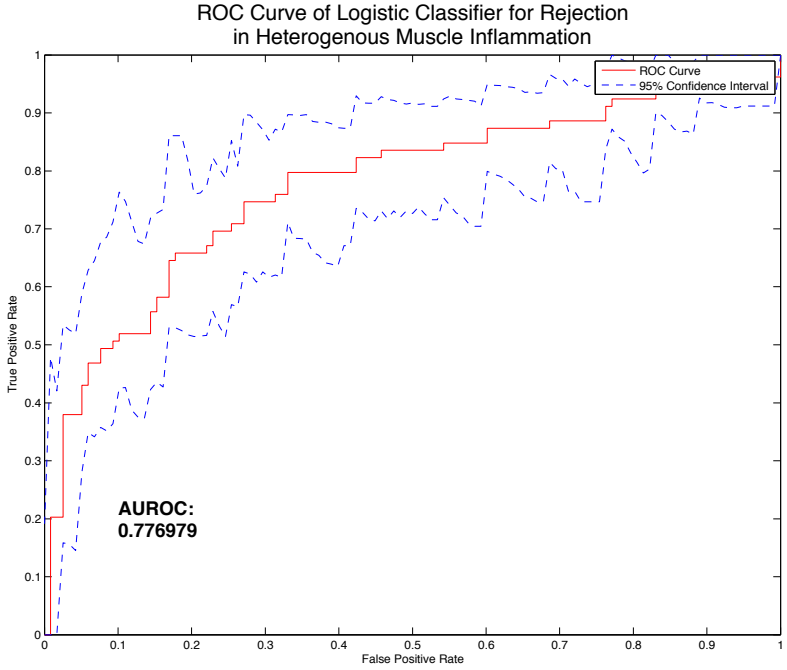

Figure 6.216

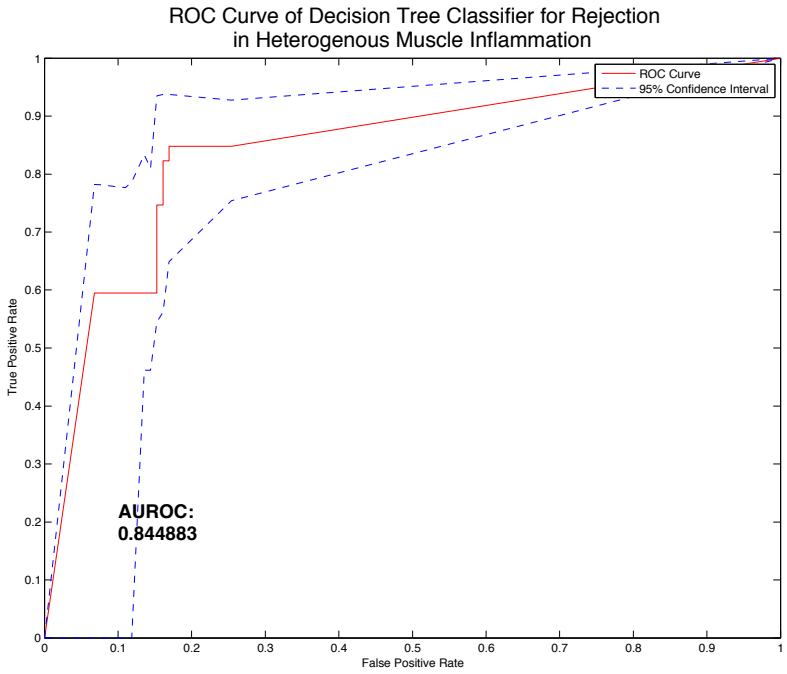

Figure 6.217

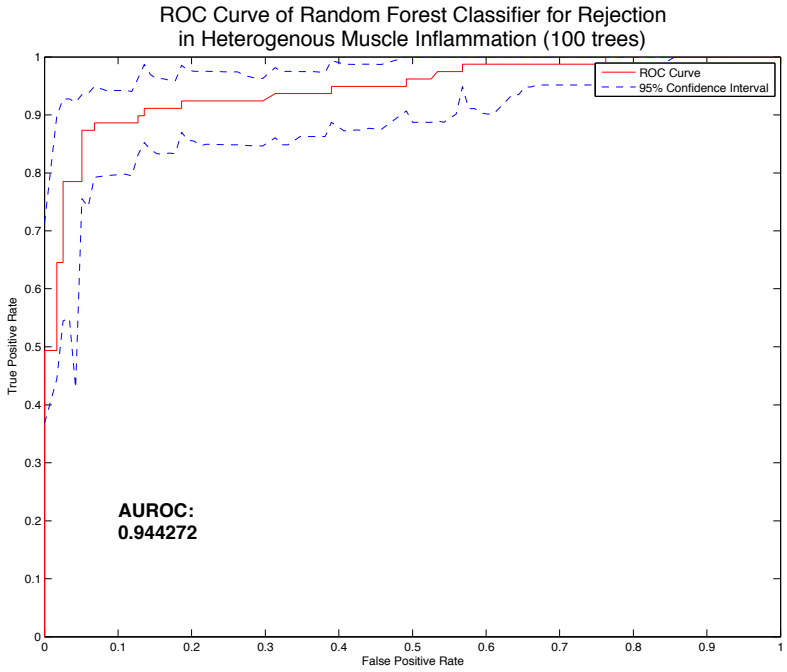

Figure 6.218

Rejection in Hybrid Feature Space

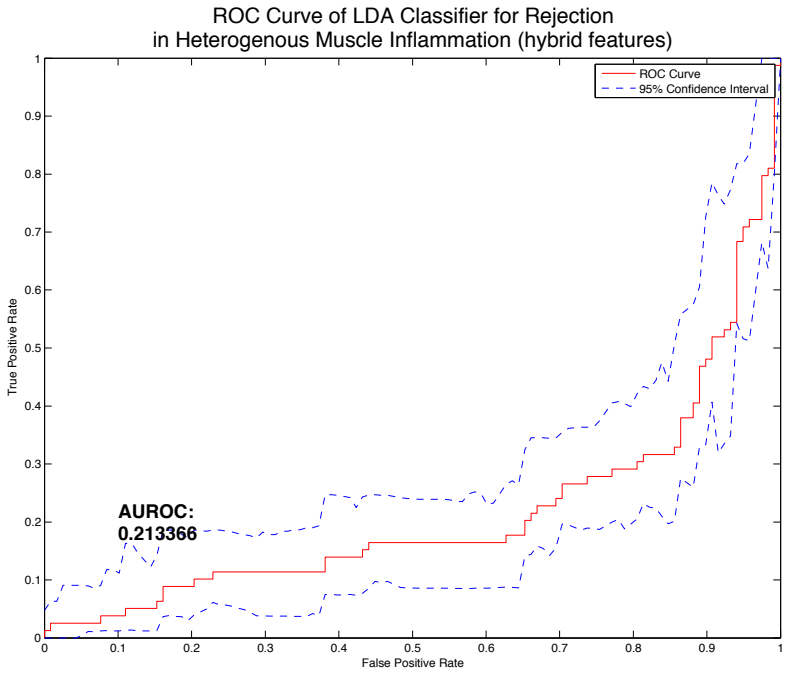

Figure 6.219

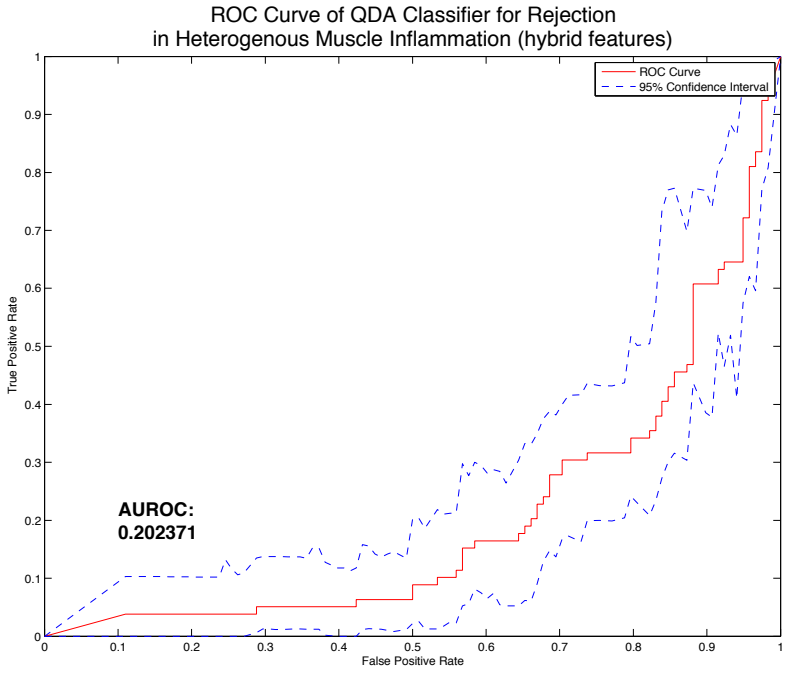

Figure 6.220

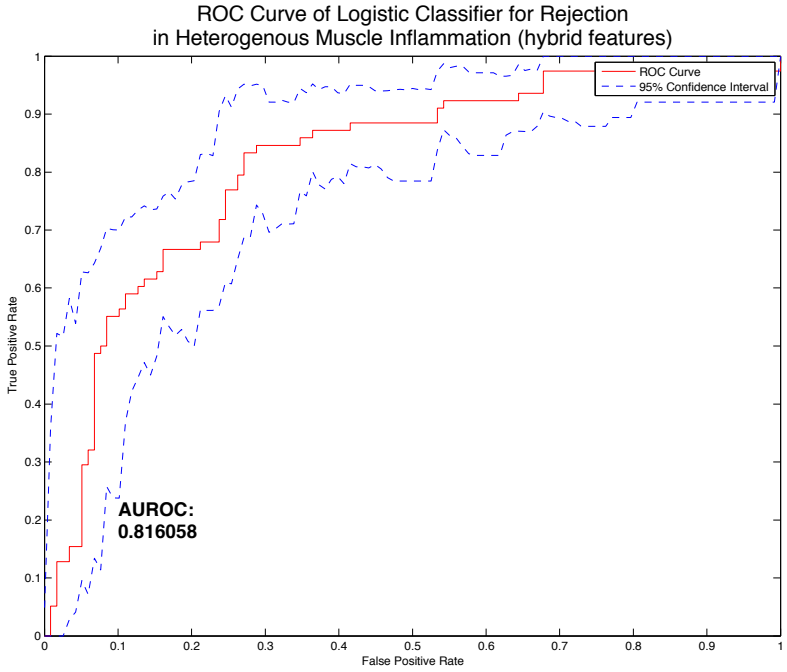

Figure 6.221

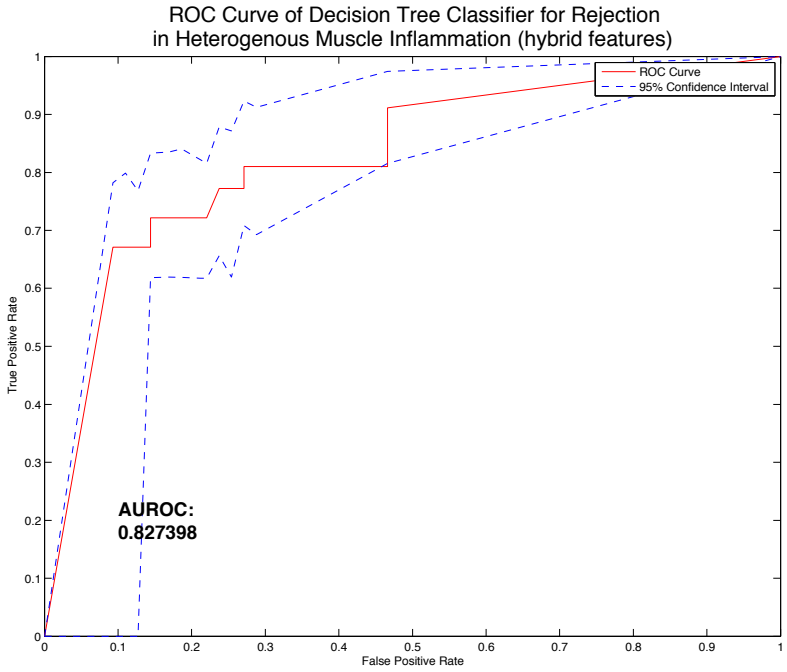

Figure 6.222

Rejection vs. Not Rejection in Muscle (POD <= 5)

Original 14-Dimensional Feature Space

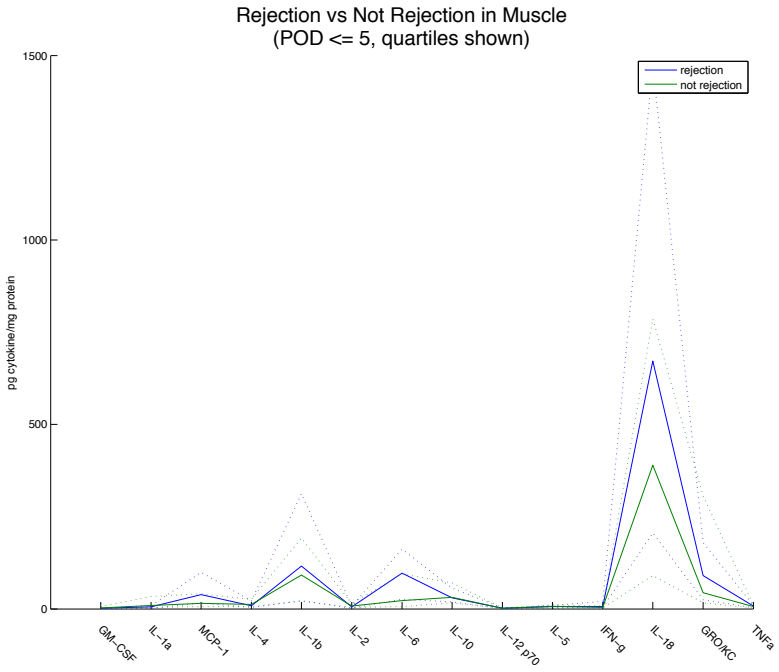

Figure 6.223

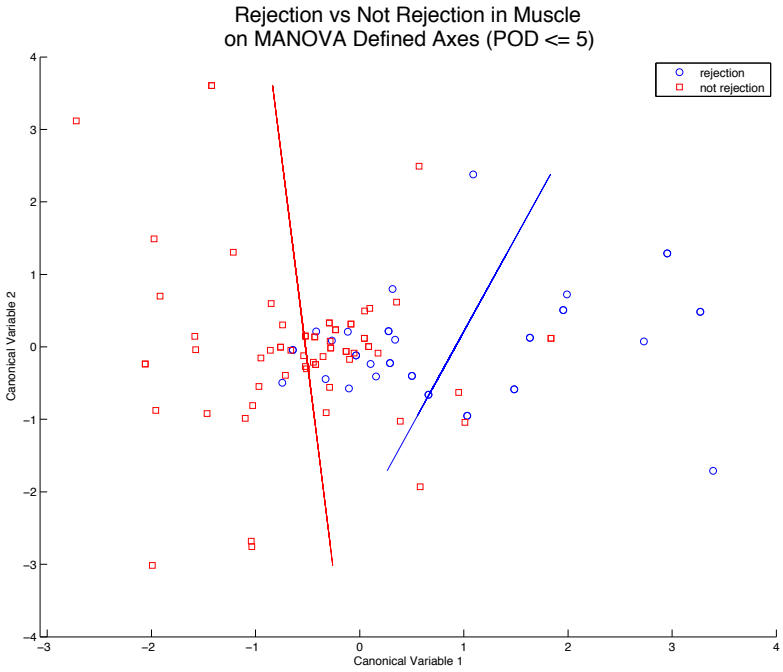

Figure 6.224

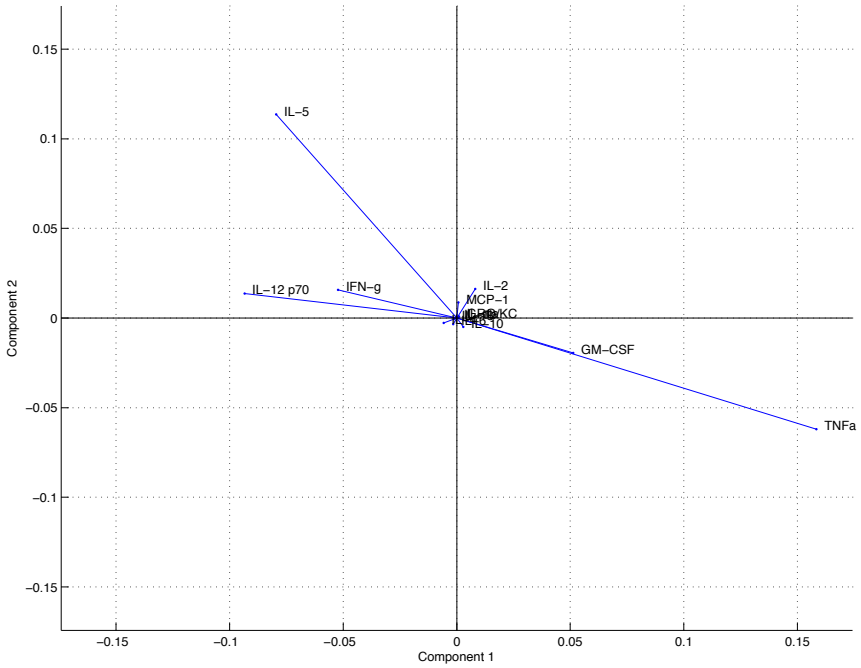

Figure 6.225

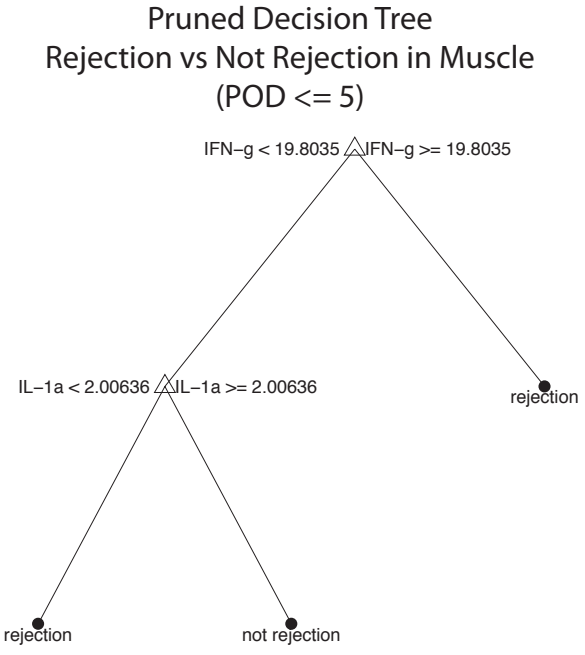

Figure 6.226

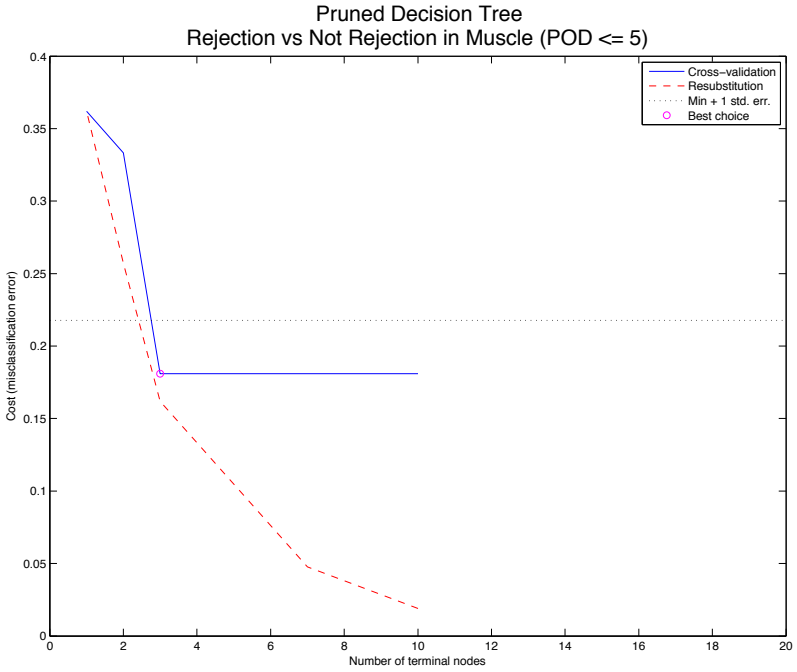

Figure 6.227

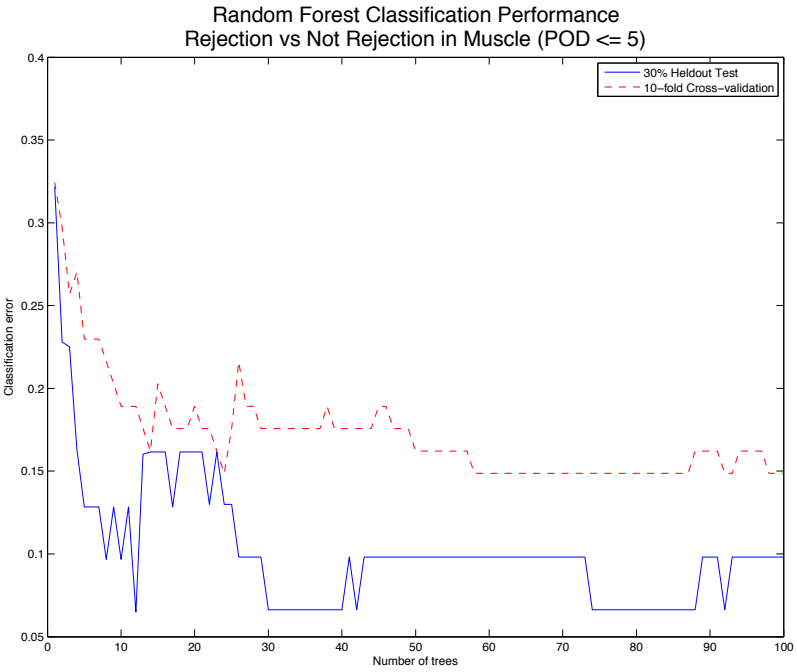

Figure 6.228

5-Dimensional Feature Selected Space

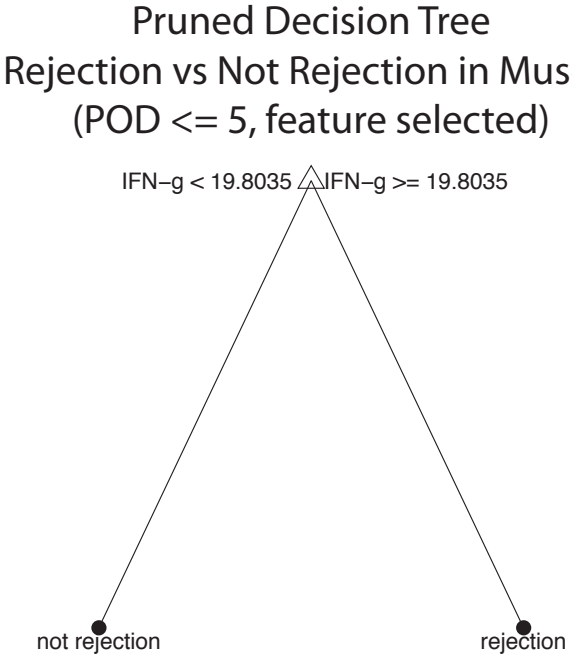

Figure 6.229

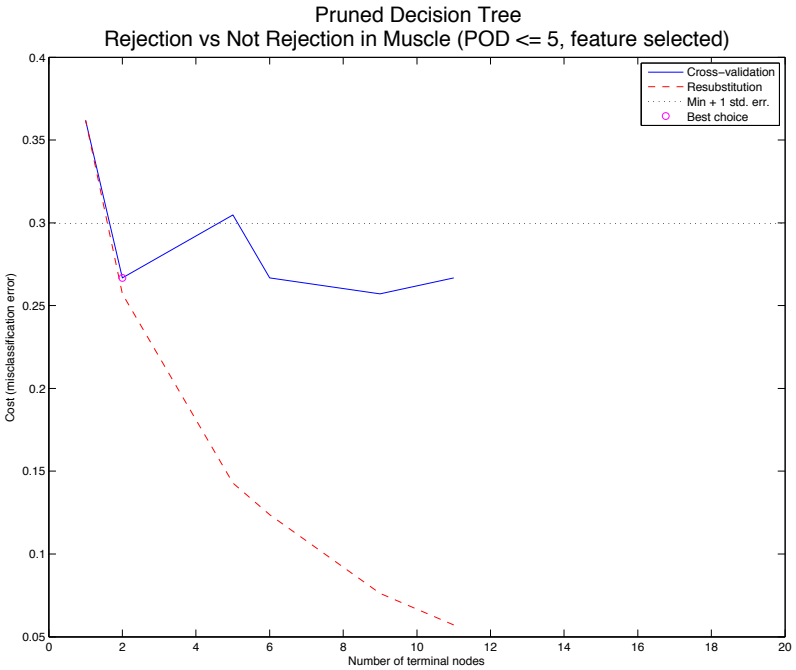

Figure 6.230

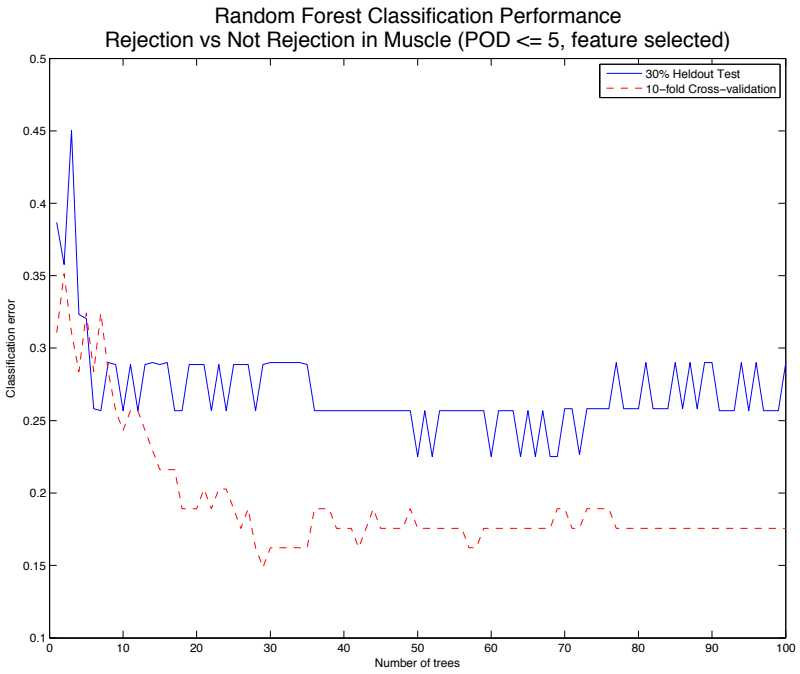

Figure 6.231

MANOVA Transformed Feature Space

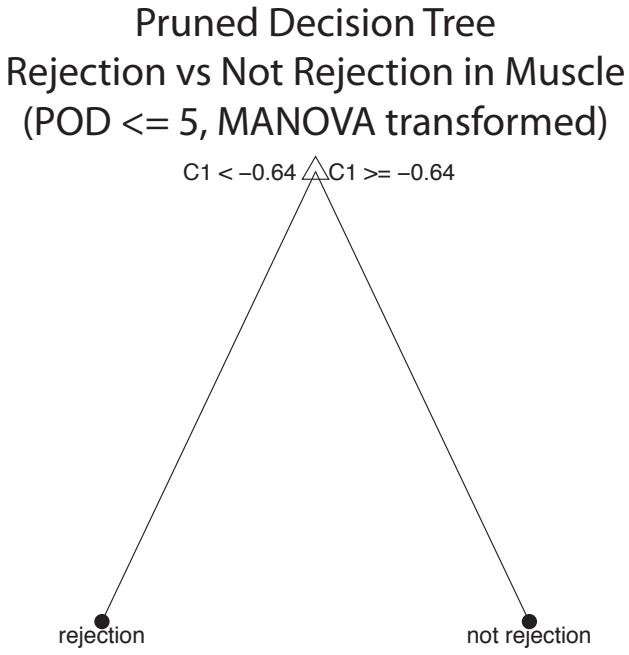

Figure 6.232

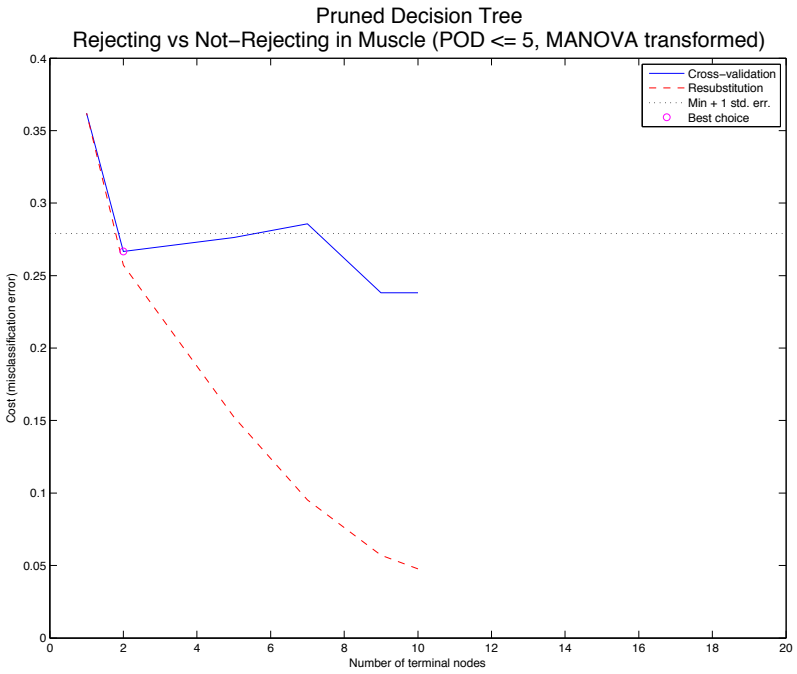

Figure 6.233

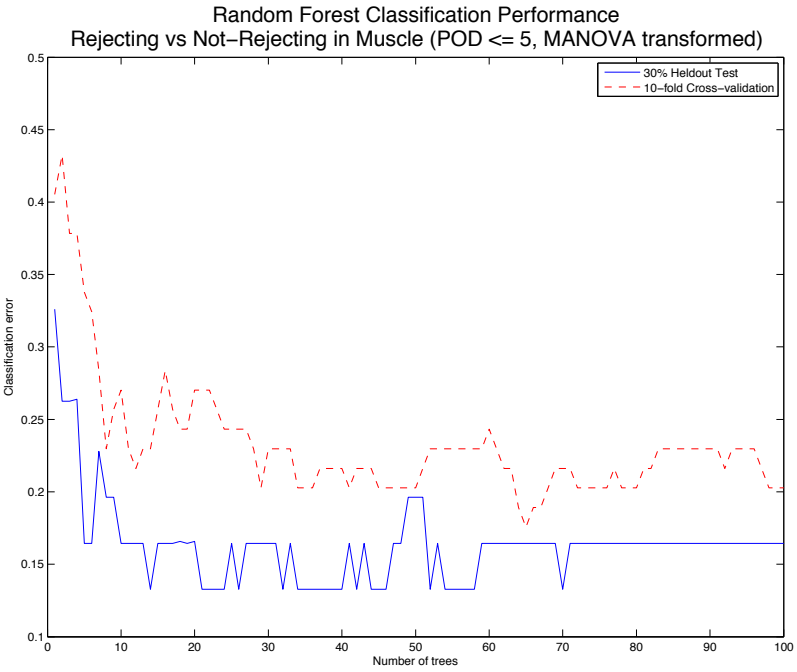

Figure 6.234

Rejection vs. Not Rejection in Muscle (POD > 5)

Original 14-Dimensional Feature Space

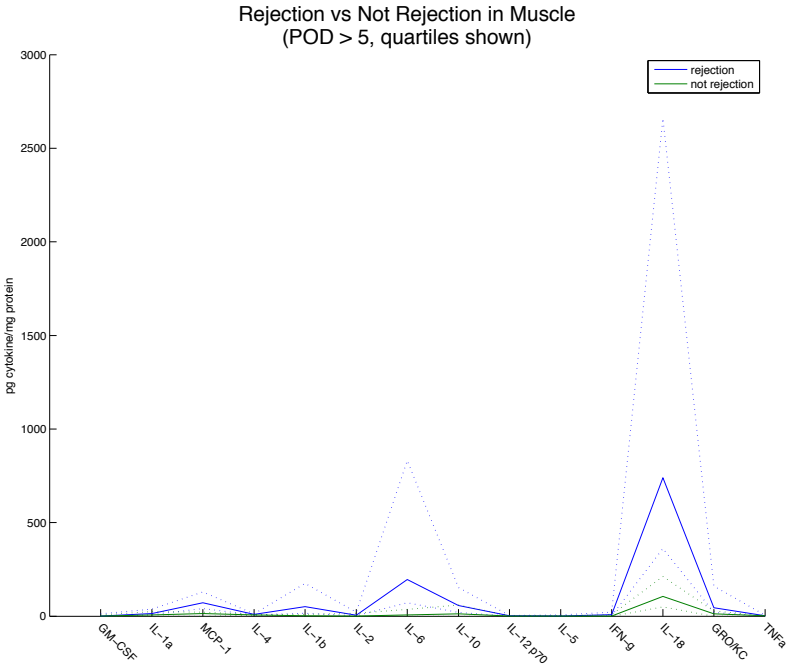

Figure 6.235

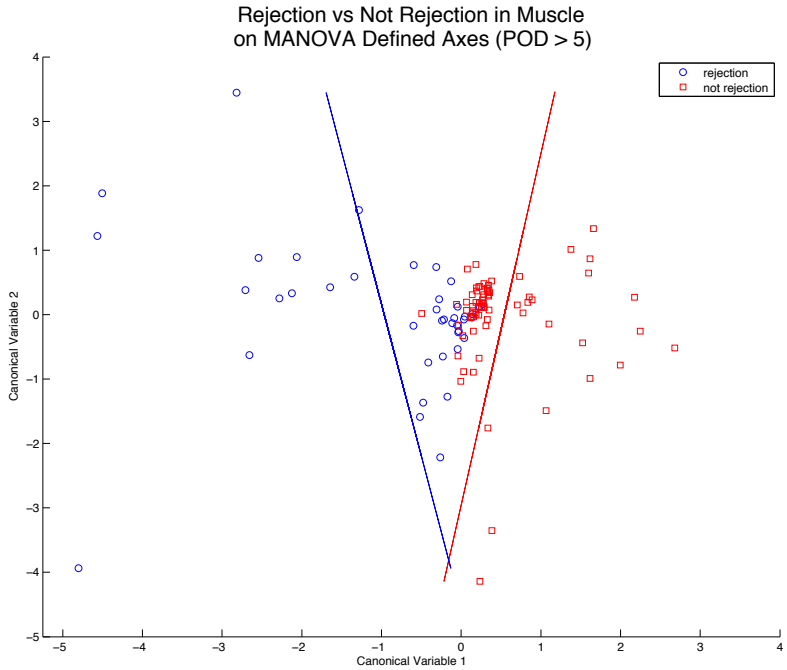

Figure 6.236

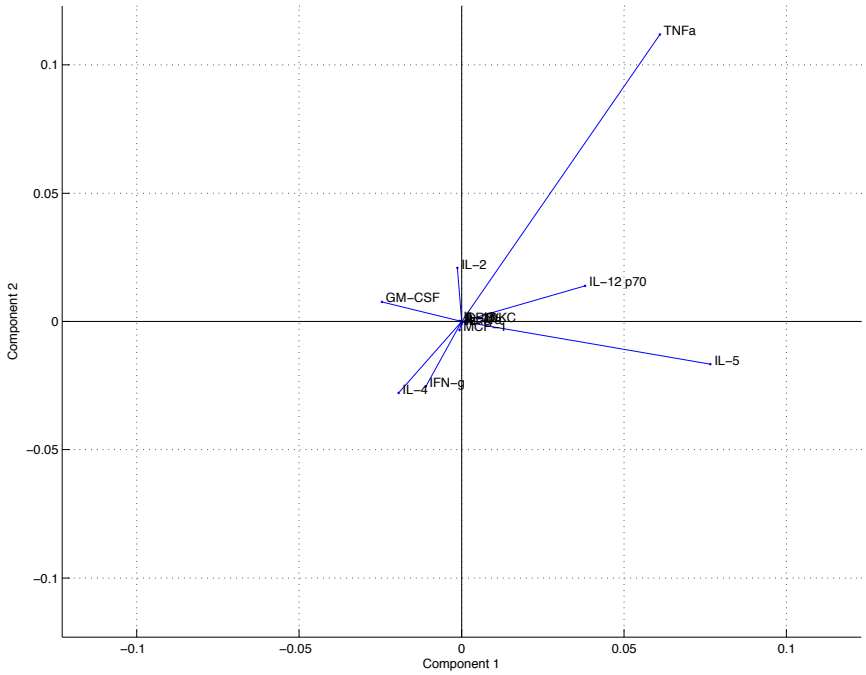

Figure 6.237

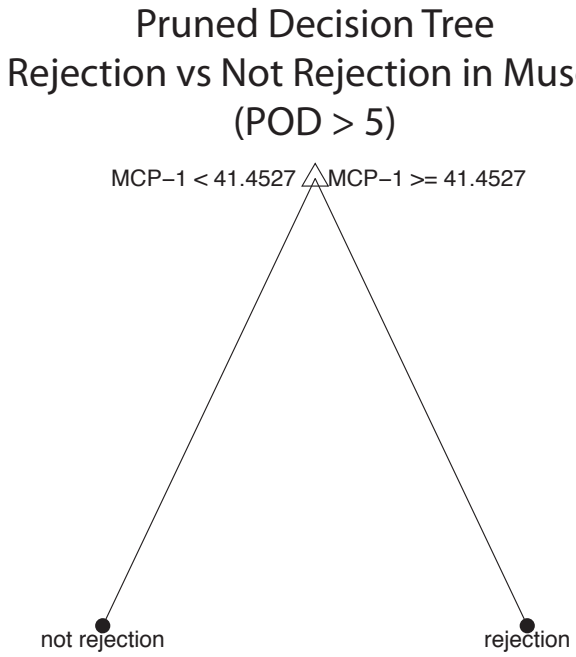

Figure 6.238

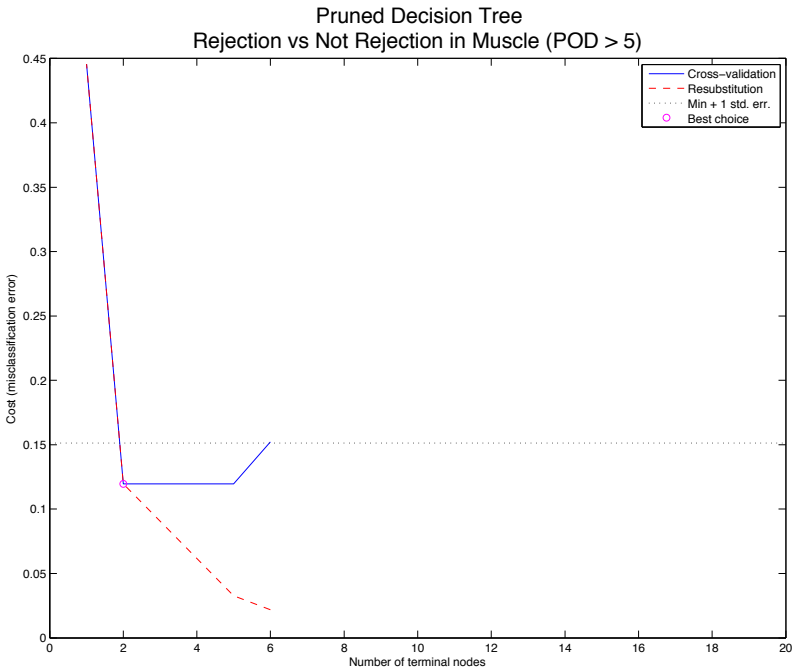

Figure 6.239

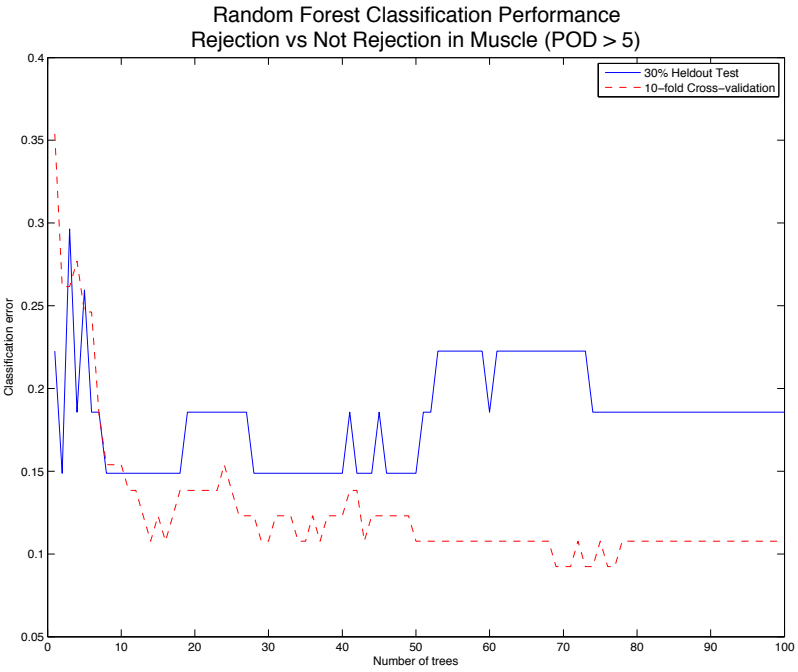

Figure 6.240

5-Dimensional Feature Selected Space

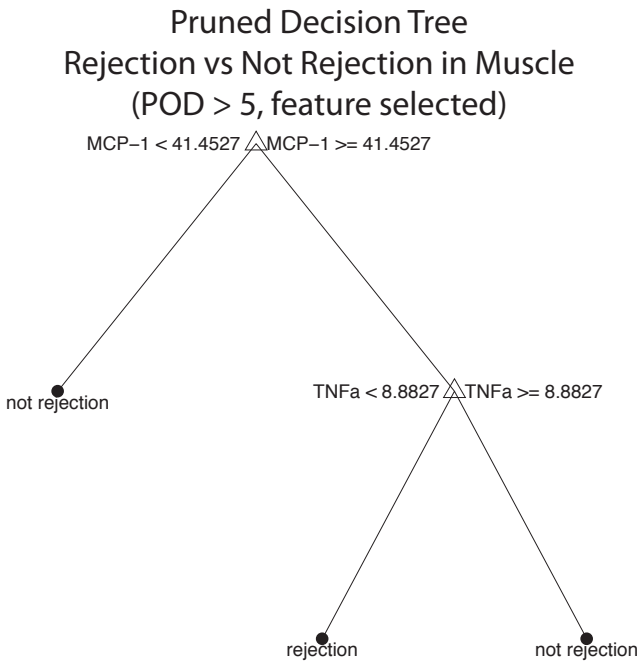

Figure 6.241

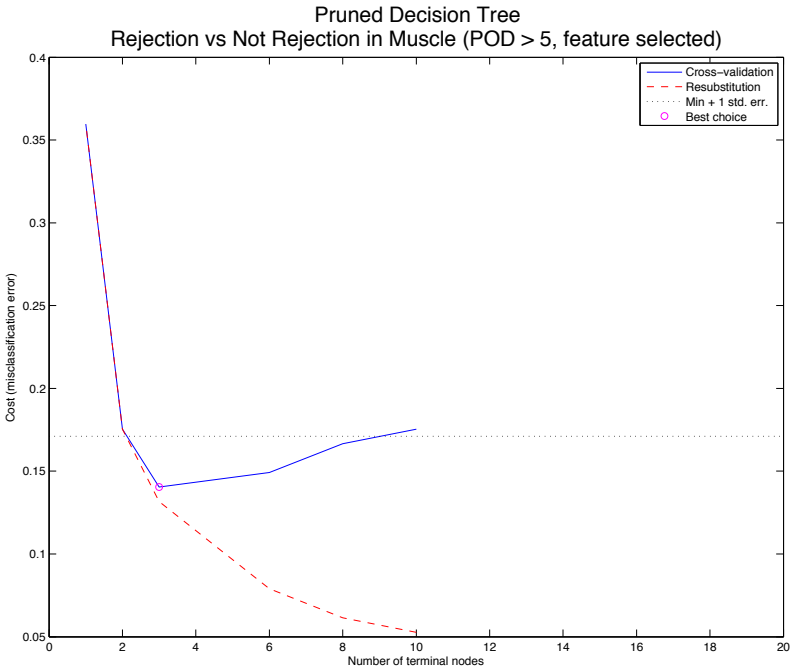

Figure 6.242

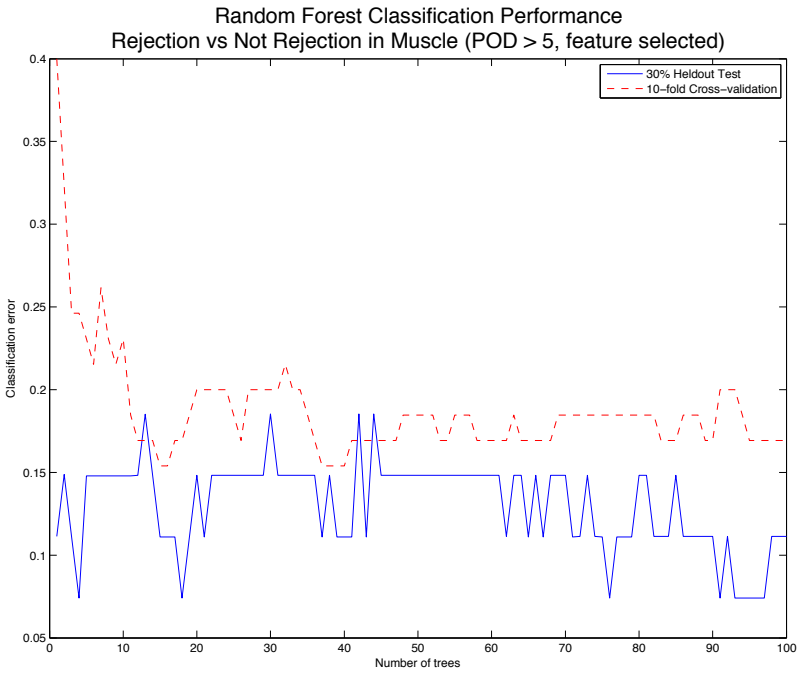

Figure 6.243

MANOVA Transformed Feature Space

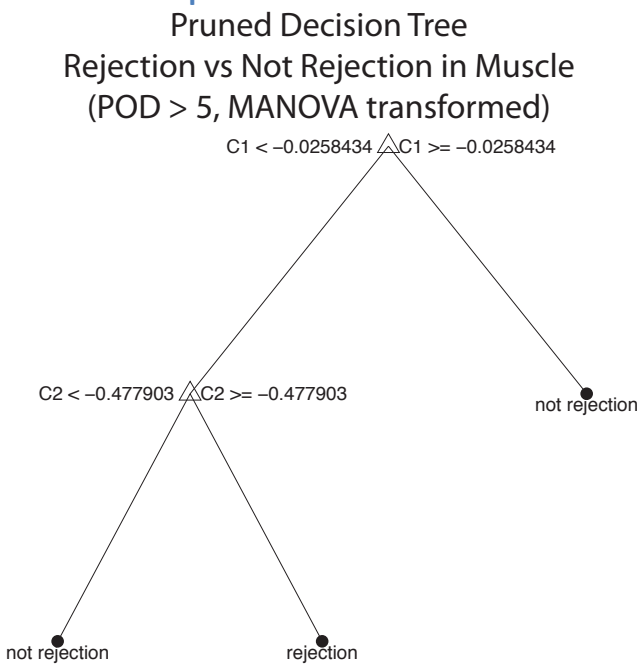

Figure 6.244

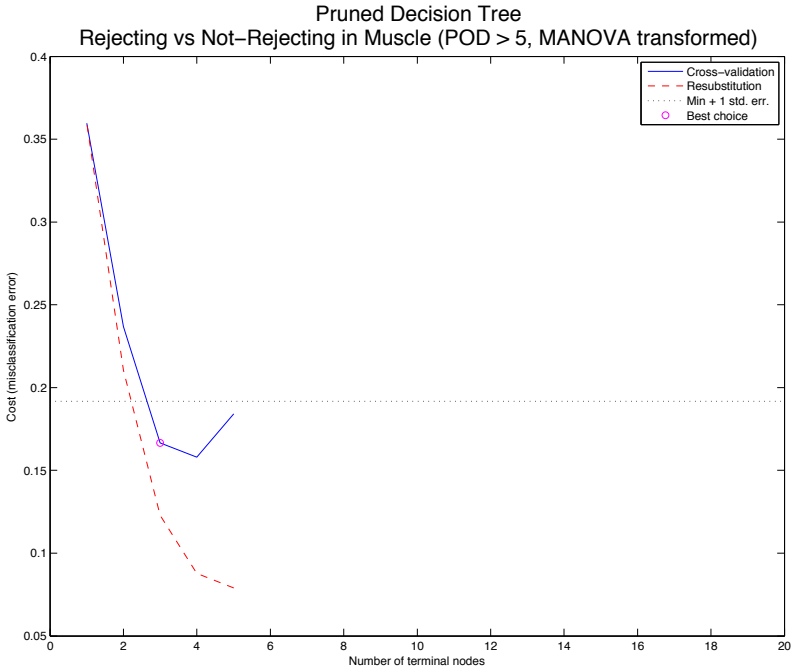

Figure 6.245

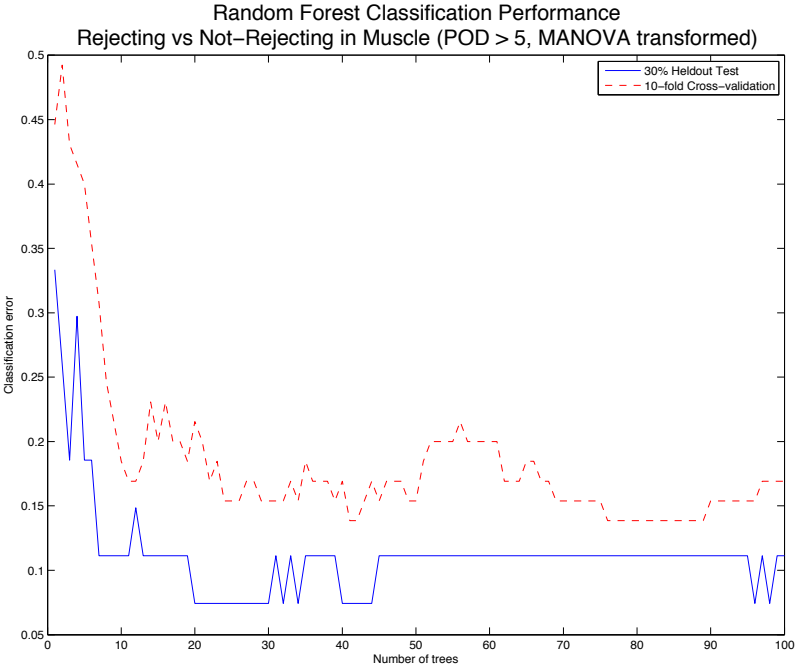

Figure 6.246

Type of Inflammation in Skin (all time points)

Original 14-Dimensional Feature Space

Figure 6.247

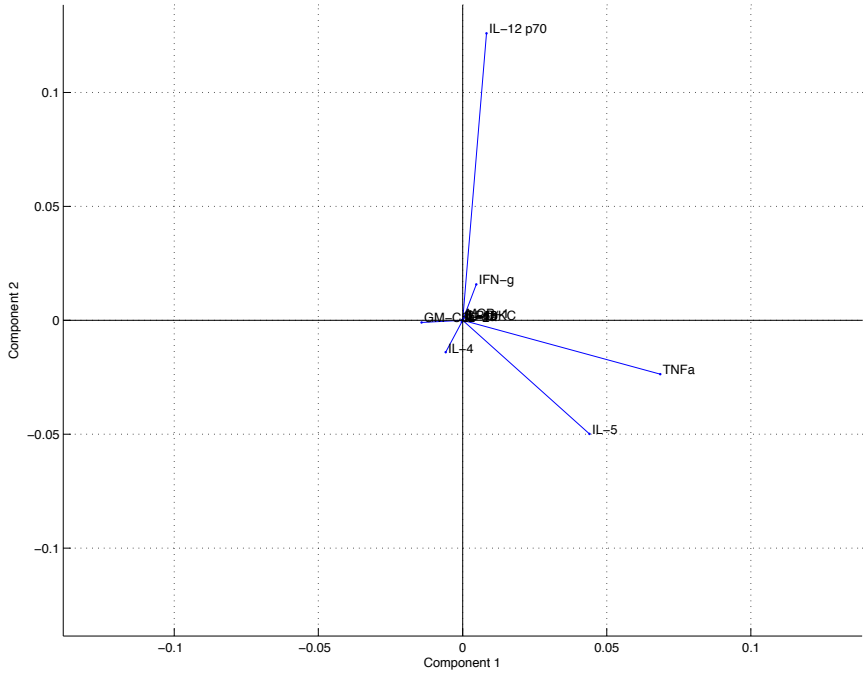

Figure 6.248

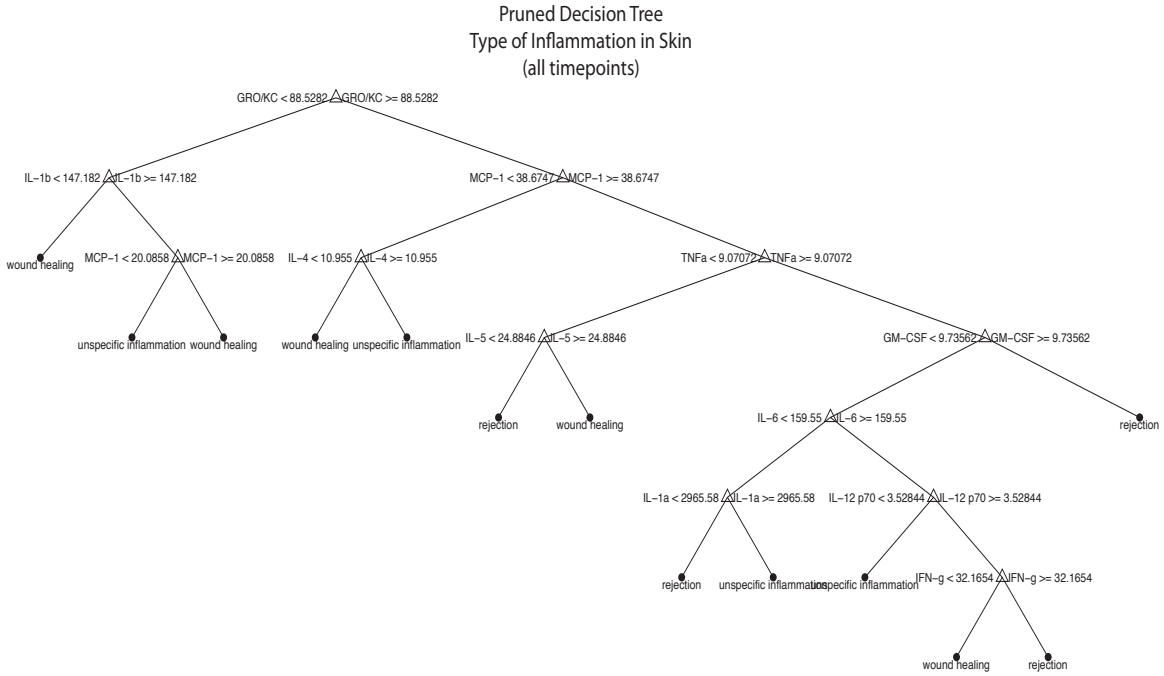

Figure 6.249

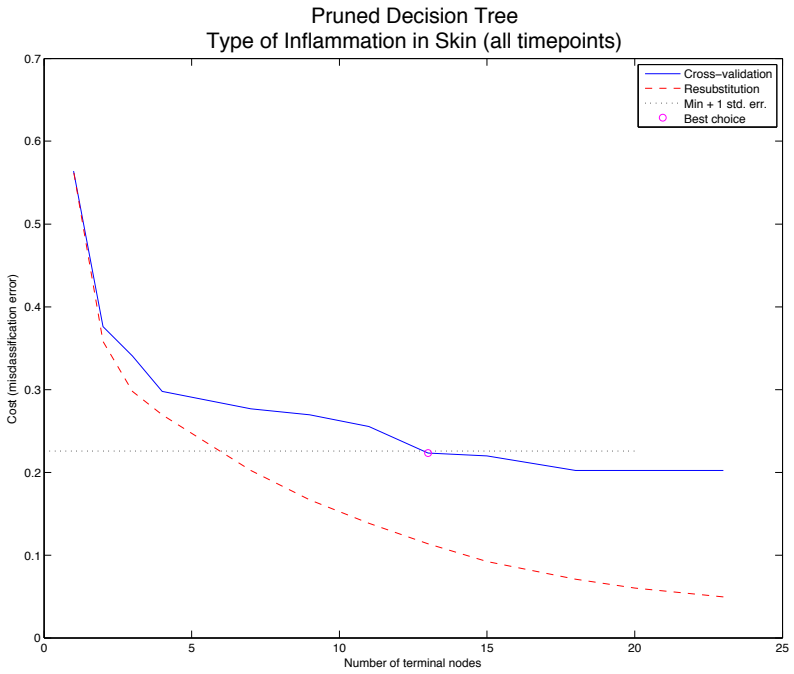

Figure 6.250

5-Dimensional Feature Selected Space

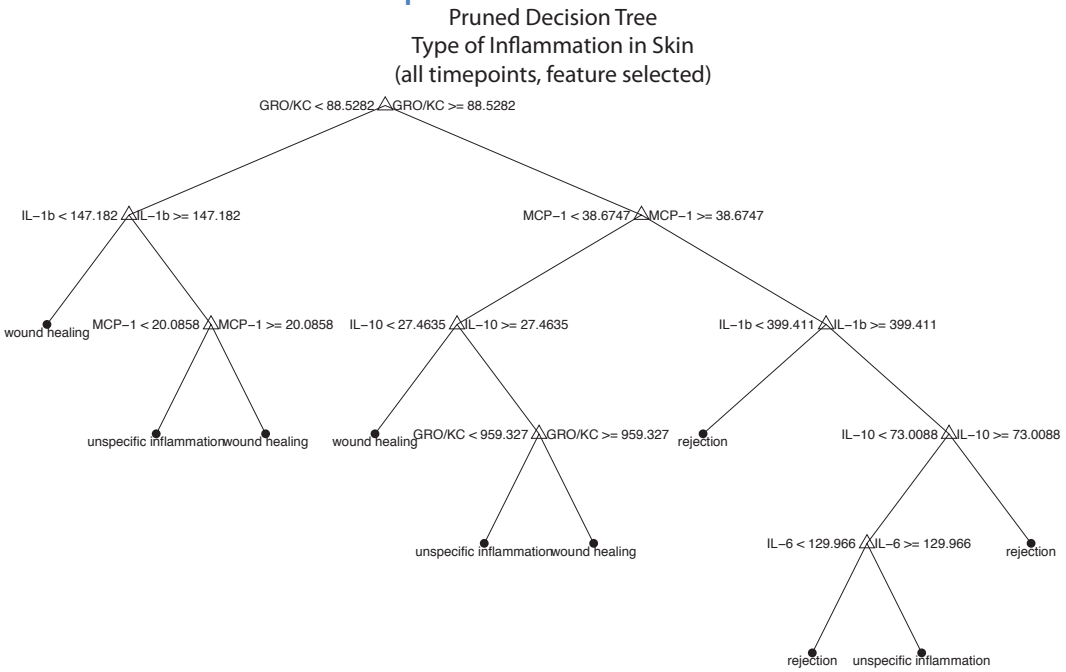

Figure 6.251

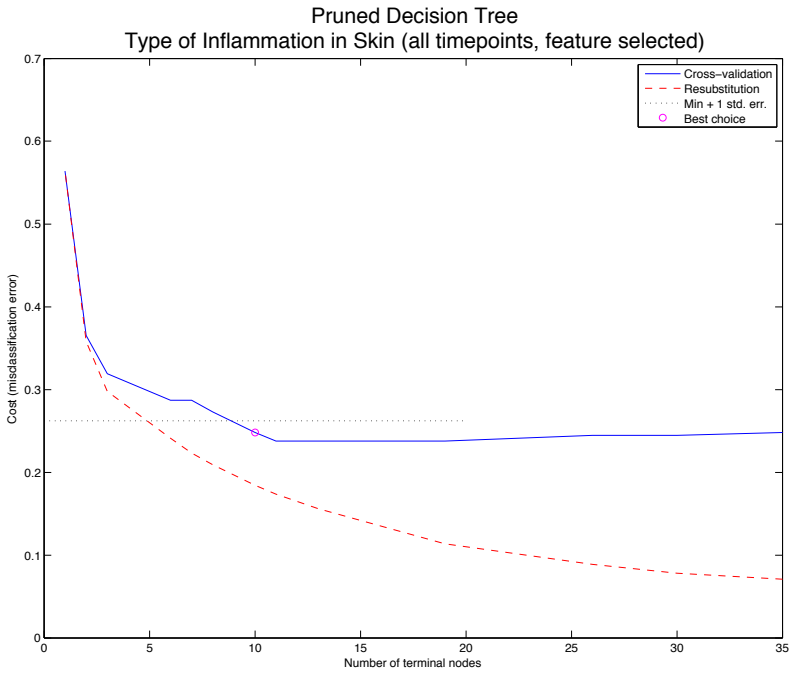

Figure 6.252

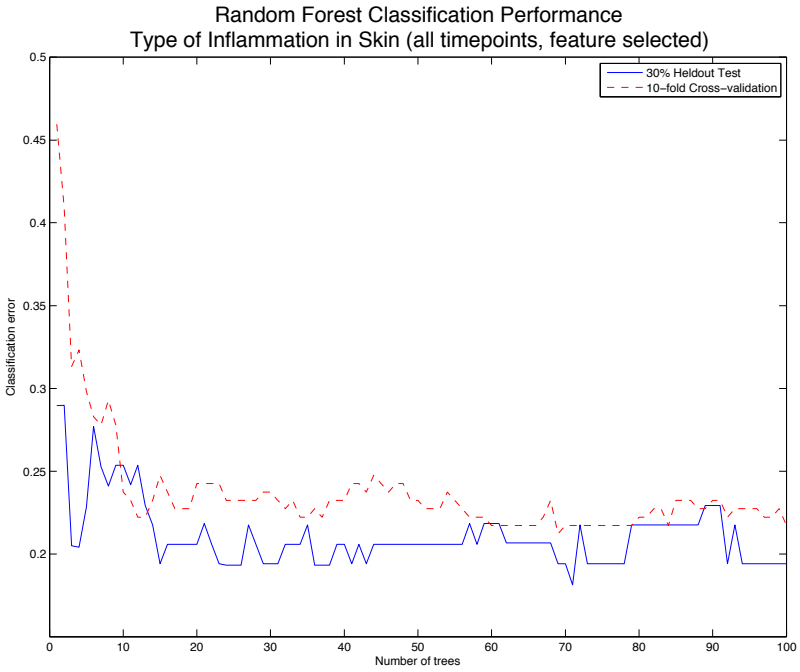

Figure 6.253

MANOVA Transformed Feature Space

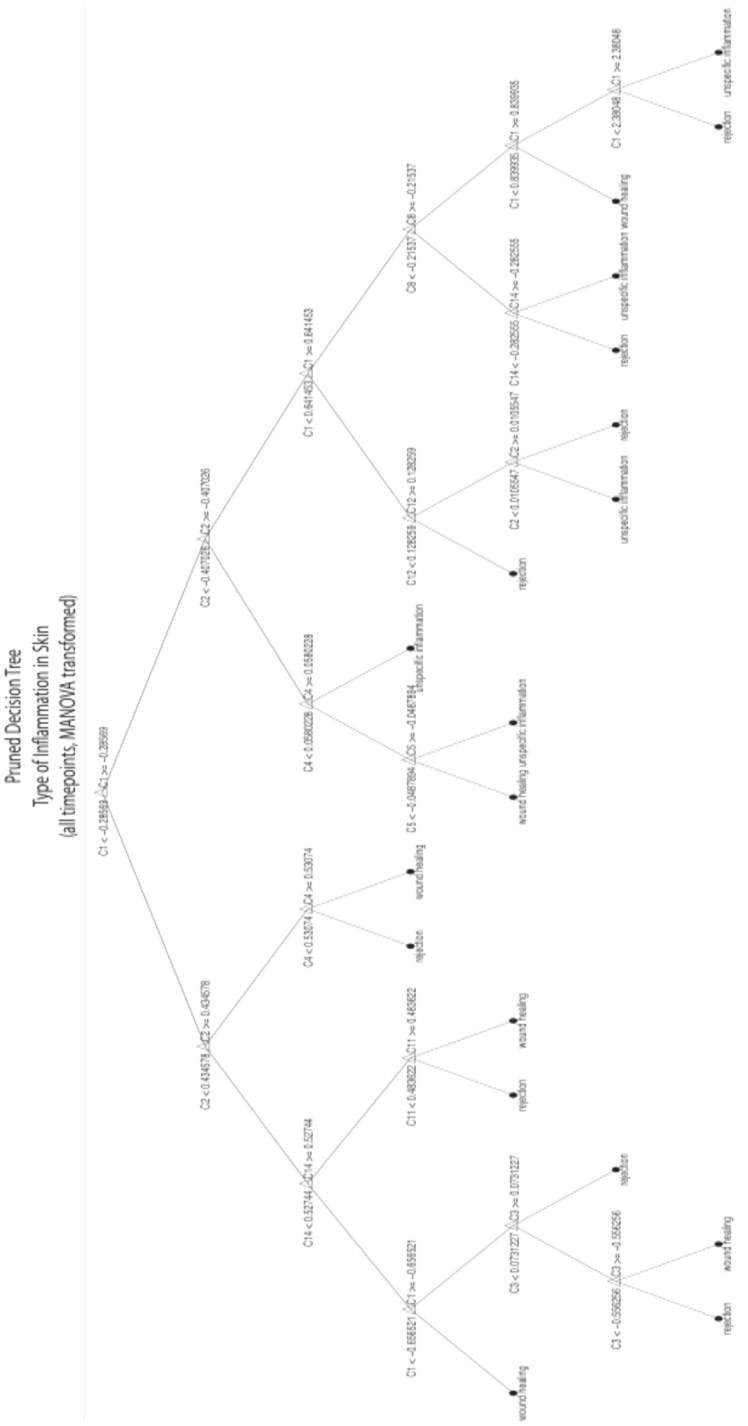
Pruned Decision Tree
Type of Inflammation in Skin
(all timepoints, MANOVA transformed)
C1 < -0.28569
C1 >= -0.28569
C2 < -0.407026
C2 >= -0.407026
C2 < 0.434578
C2 >= 0.434578
C1 < 0.6414453
C1 >= 0.6414453
C4 < 0.0868228
C4 >= 0.0868228
C4 < 0.530774
C4 >= 0.530774
C14 < 0.52744
C14 >= 0.52744
C12 < 0.126259
C12 >= 0.126259
C5 < -0.0467844
C5 >= -0.0467844
C11 < 0.463622
C11 >= 0.463622
C8 < -0.21537
C8 >= -0.21537
C2 < 0.0105547
C2 >= 0.0105547
C1 < 0.839935
C1 >= 0.839935
C14 < -0.282556
C14 >= -0.282556
C1 < 2.38048
C1 >= 2.38048
C1 < -0.656521
C1 >= -0.656521
C3 < 0.0731227
C3 >= 0.0731227
C3 < -0.556226
C3 >= -0.556226
wound healing
rejection
unspecific inflammation

Figure 6.254

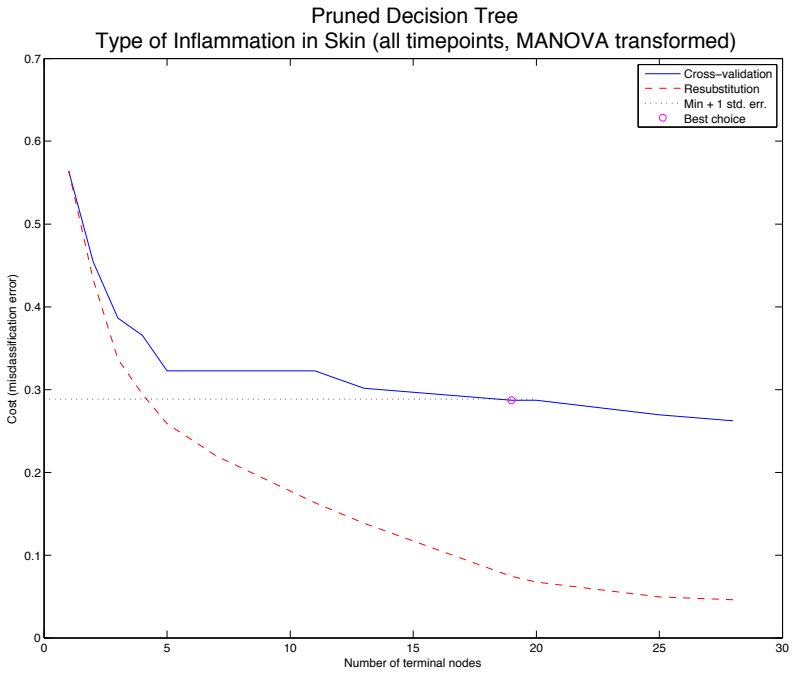

Figure 6.255

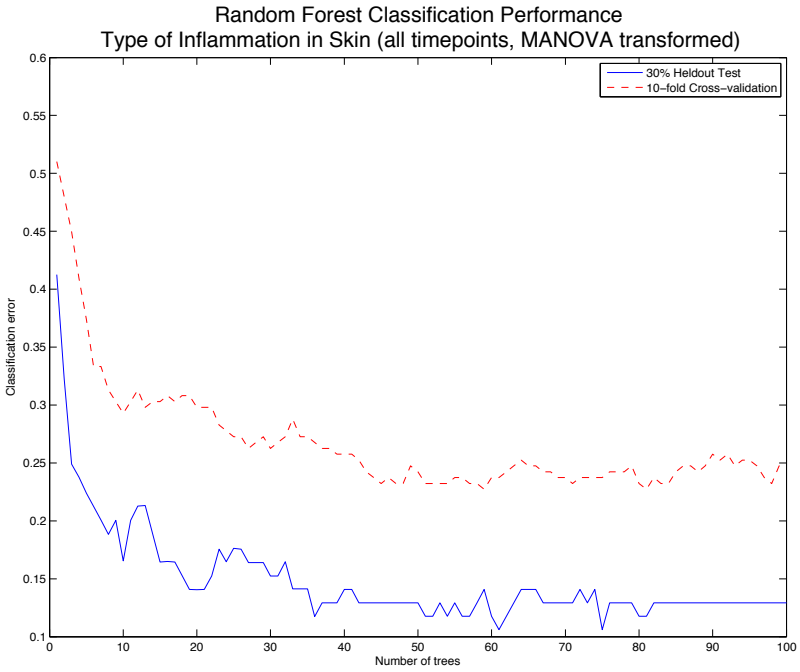

Figure 6.256

Hybrid Feature Space

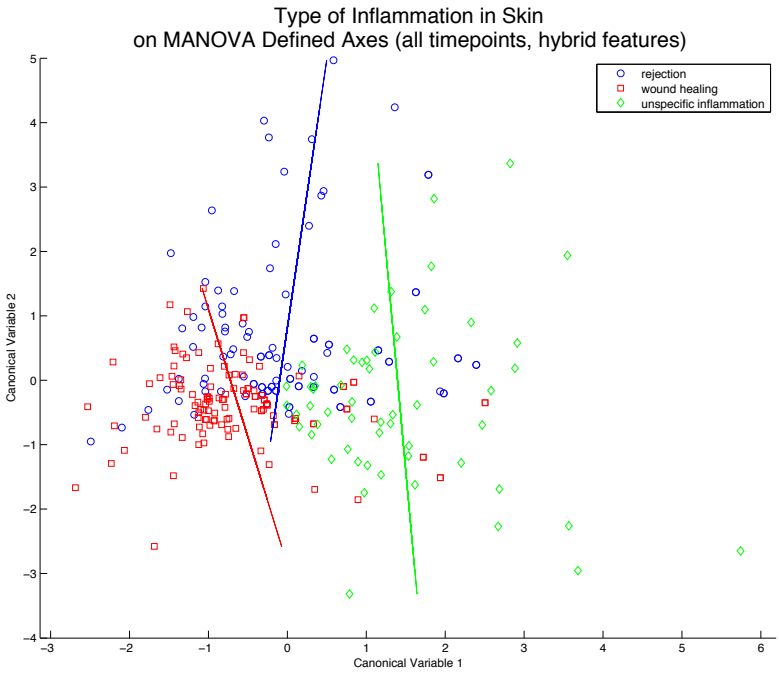

Figure 6.257

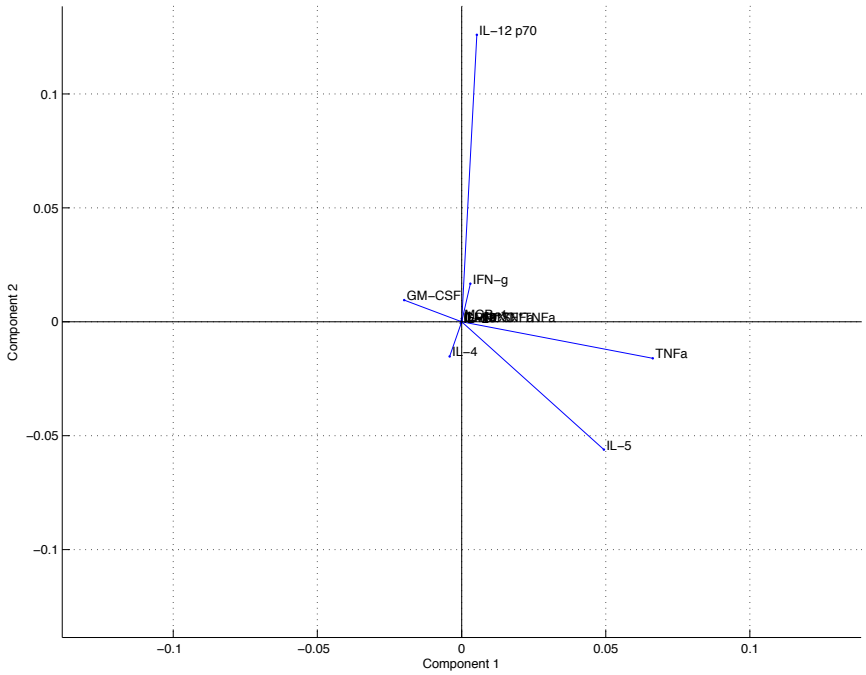

Figure 6.258

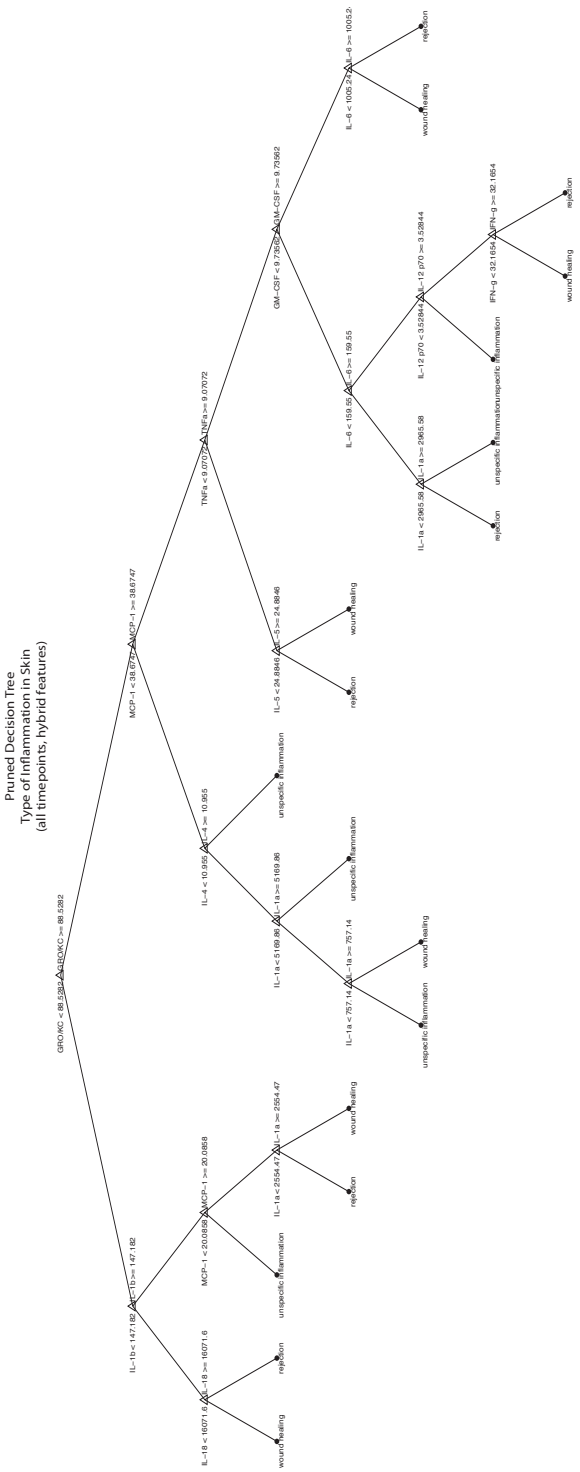
Pruned Decision Tree
Type of Inflammation in Skin
(all timepoints, hybrid features)
GRO/KC < 88.5282
GRO/KC >= 88.5282
IL−1b < 147.182
IL−1b >= 147.182
IL−18 < 16071.6
IL−18 >= 16071.6
wound healing
repair
MCP−1 < 20.0858
MCP−1 >= 20.0858
unspecific inflammation
IL−1a < 2554.47
IL−1a >= 2554.47
MCP−1 < 38.6747
MCP−1 >= 38.6747
IL−4 < 10.955
IL−4 >= 10.955
IL−1a < 5169.86
IL−1a >= 5169.86
IL−1a < 757.14
IL−1a >= 757.14
TNFa < 9.07072
TNFa >= 9.07072
IL−5 < 24.8946
IL−5 >= 24.8946
GM−CSF < 9.73562
GM−CSF >= 9.73562
IL−6 < 159.99
IL−6 >= 159.99
IL−1a < 2965.98
IL−1a >= 2965.98
IL−6 < 1005.27
IL−6 >= 1005.27
IL−12 p70 < 3.52844
IL−12 p70 >= 3.52844
IFN−g < 32.1654
IFN−g >= 32.1654

Figure 6.259

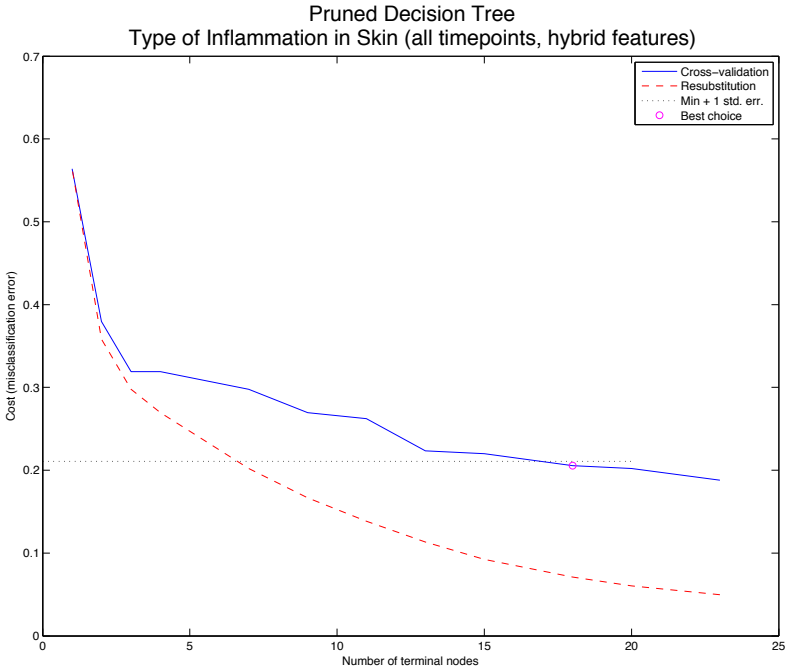

Figure 6.260

ROC Curves in Skin: Wound Healing and Unspecific Inflammation

Wound Healing in Original Feature Space

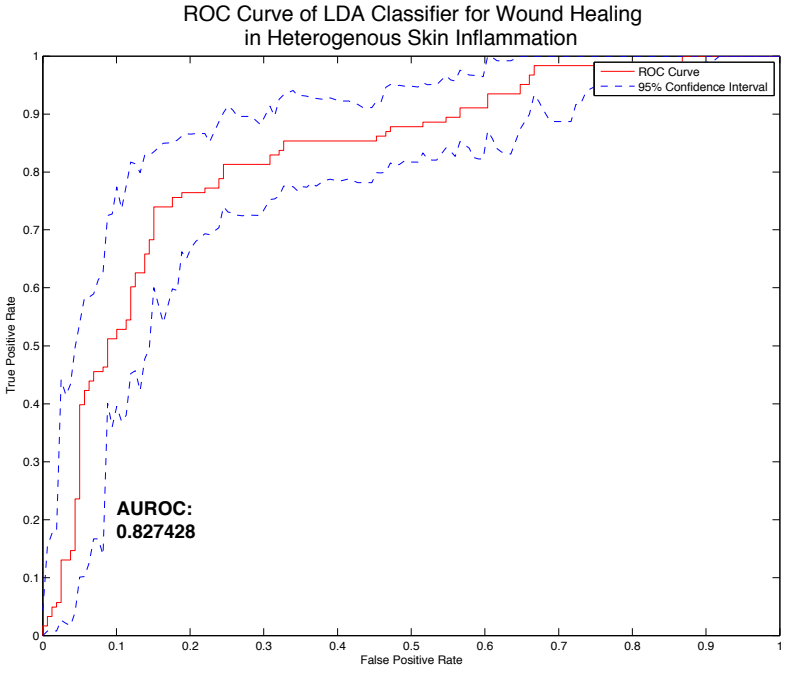

Figure 6.261

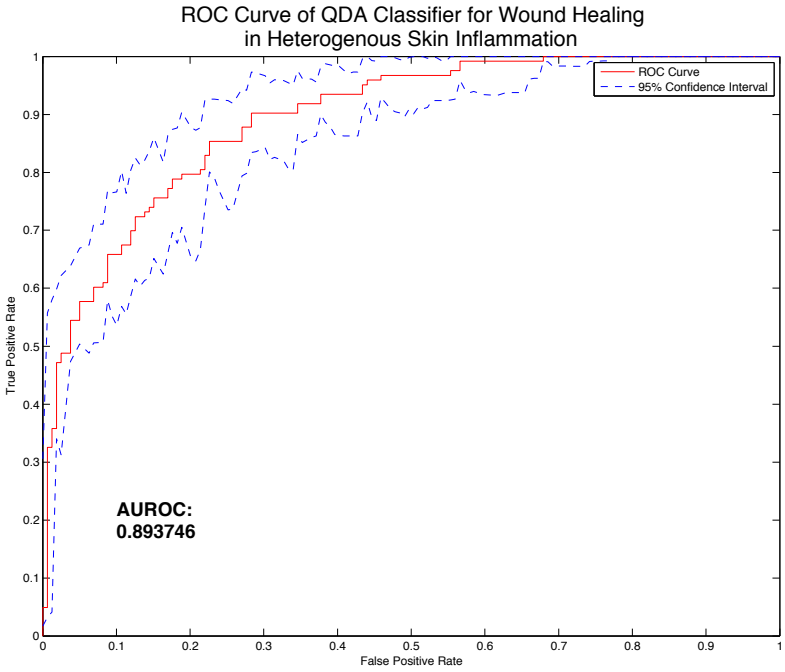

Figure 6.262

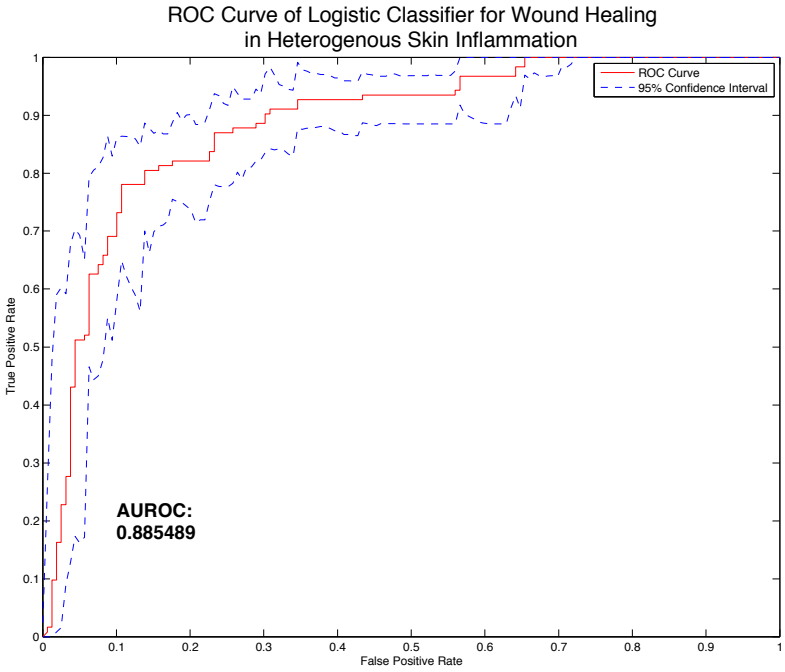

Figure 6.263

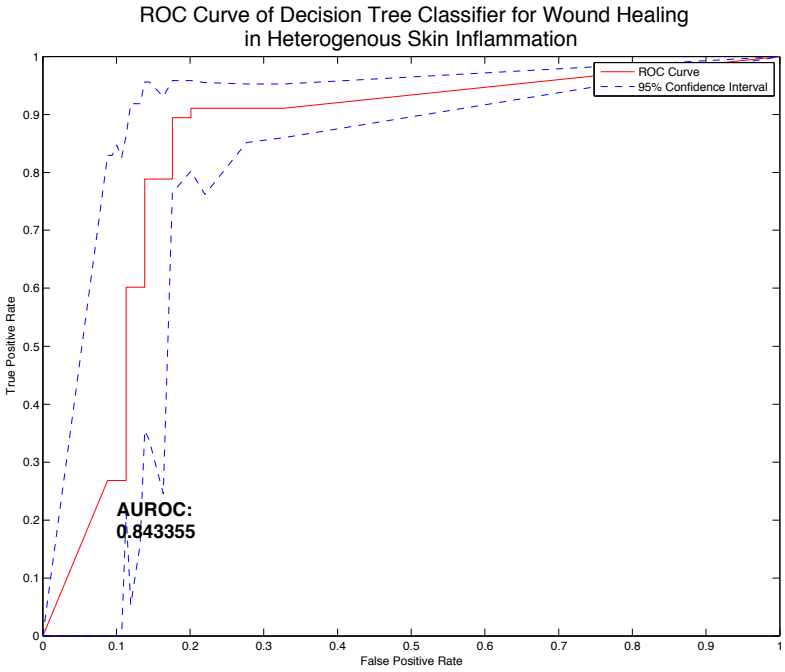

Figure 6.264

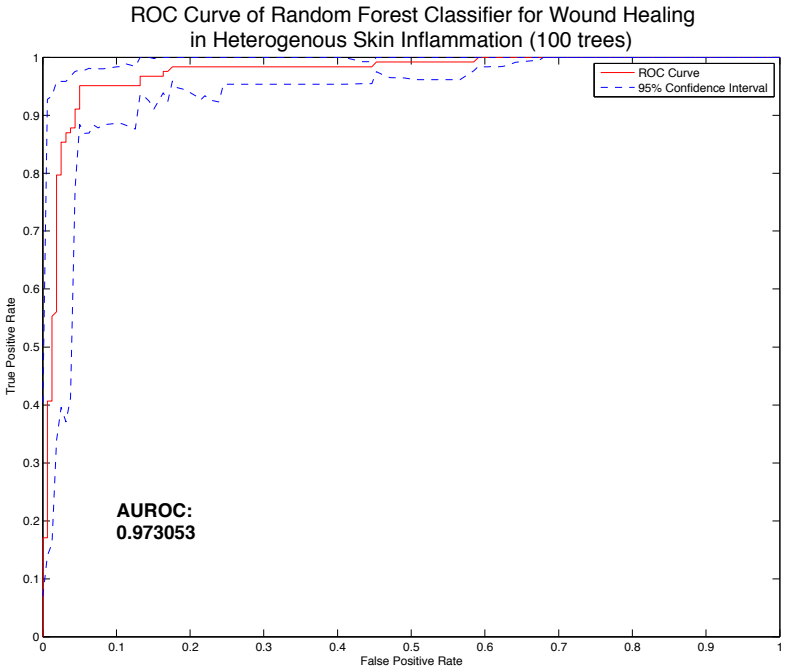

Figure 6.265

Wound Healing in Hybrid Feature Space

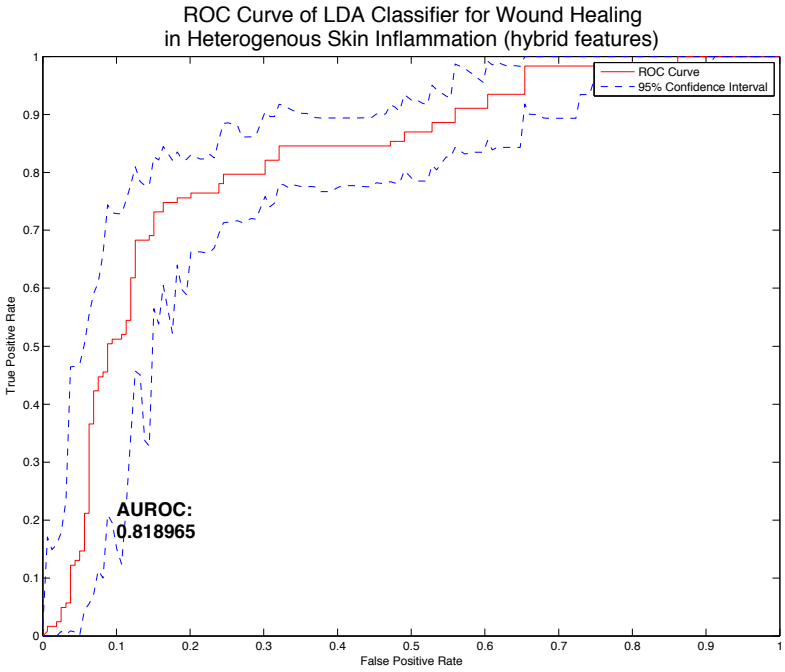

Figure 6.266

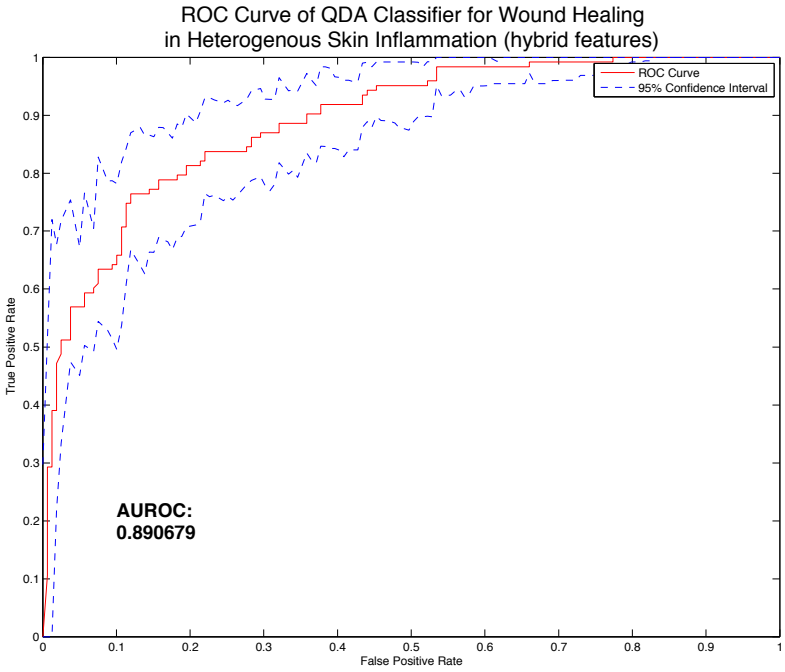

Figure 6.267

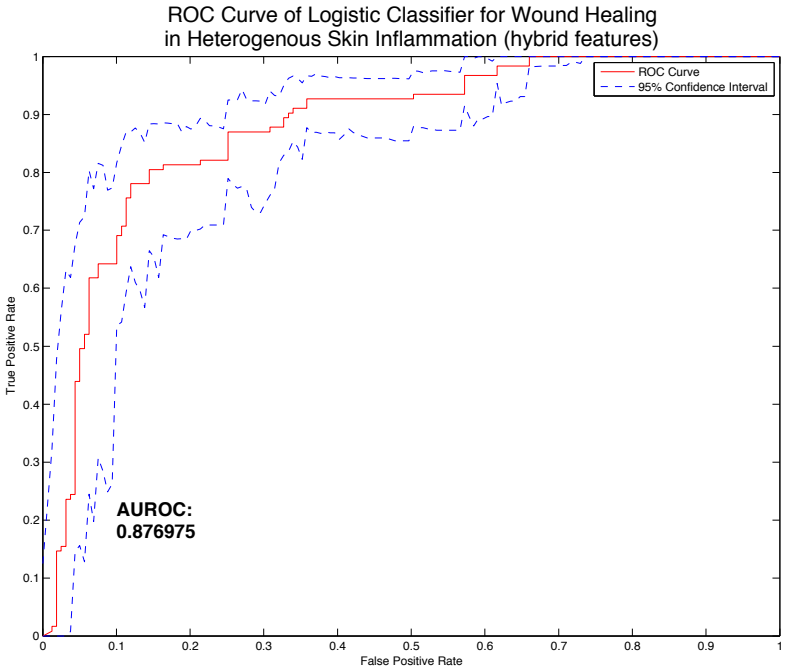

Figure 6.268

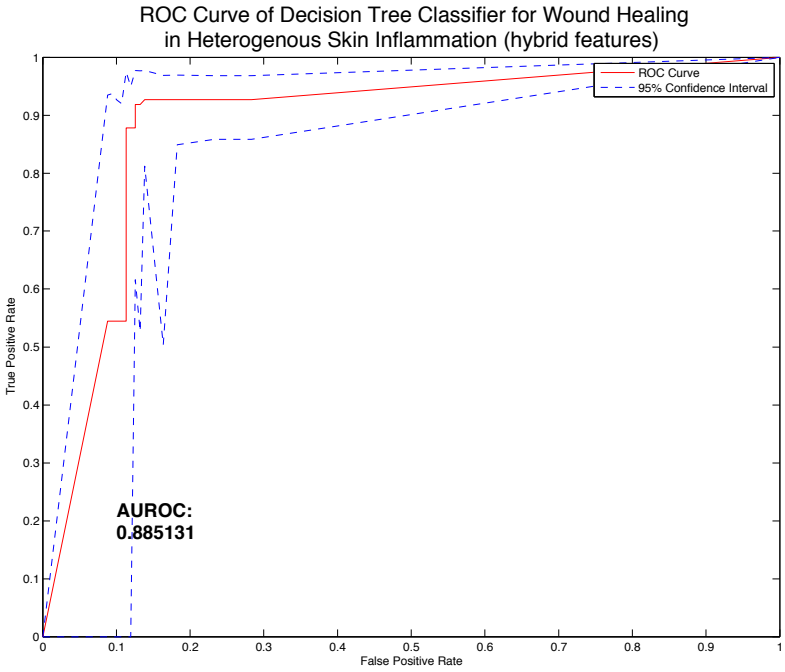

Figure 6.269

Unspecific Inflammation in Original Feature Space

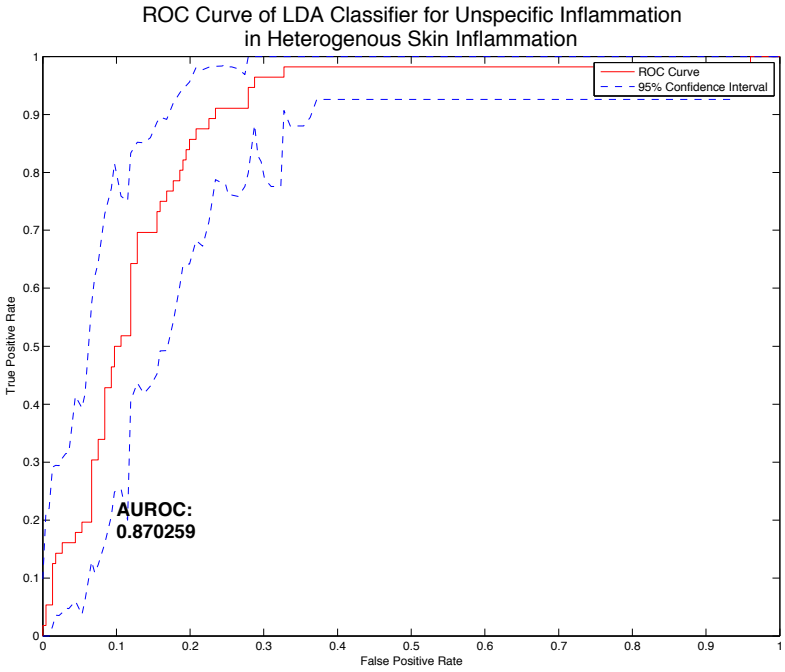

Figure 6.270

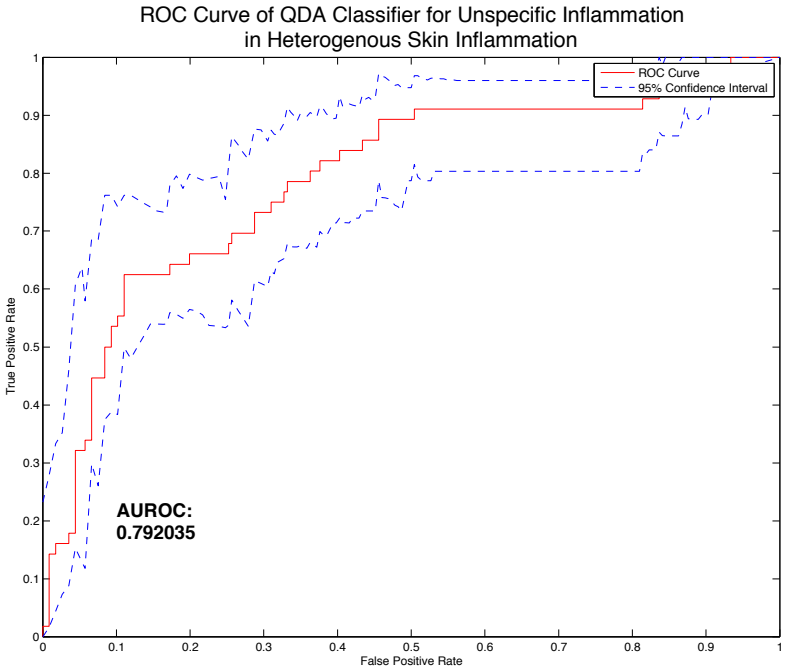

Figure 6.271

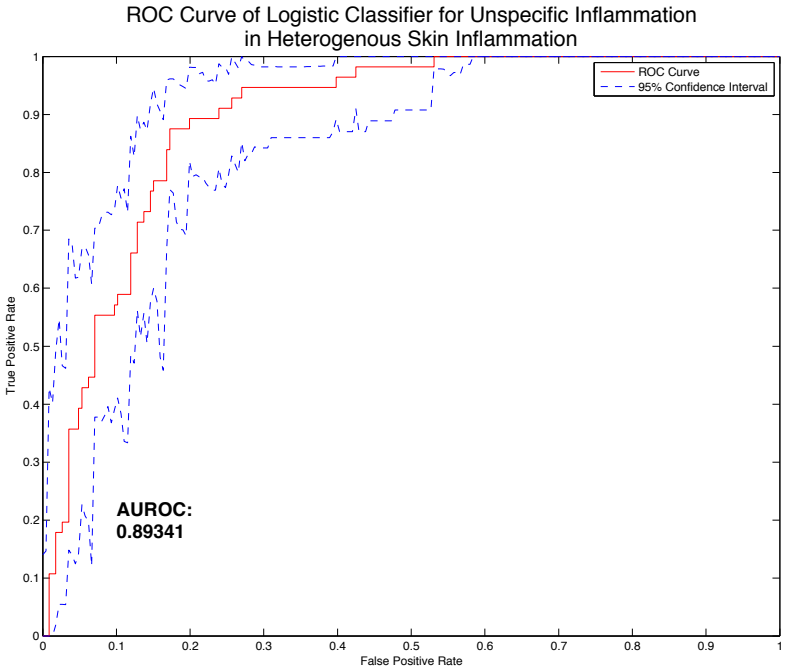

Figure 6.272

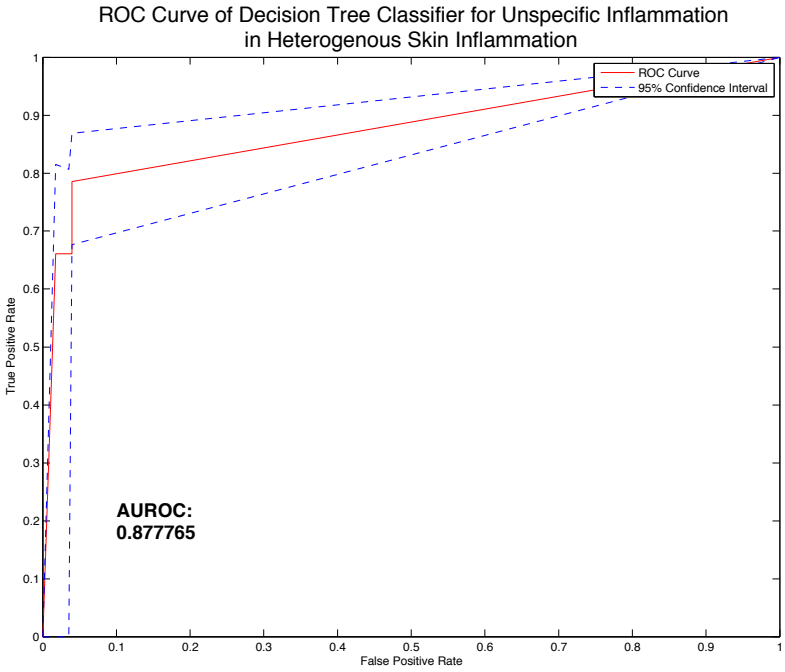

Figure 6.273

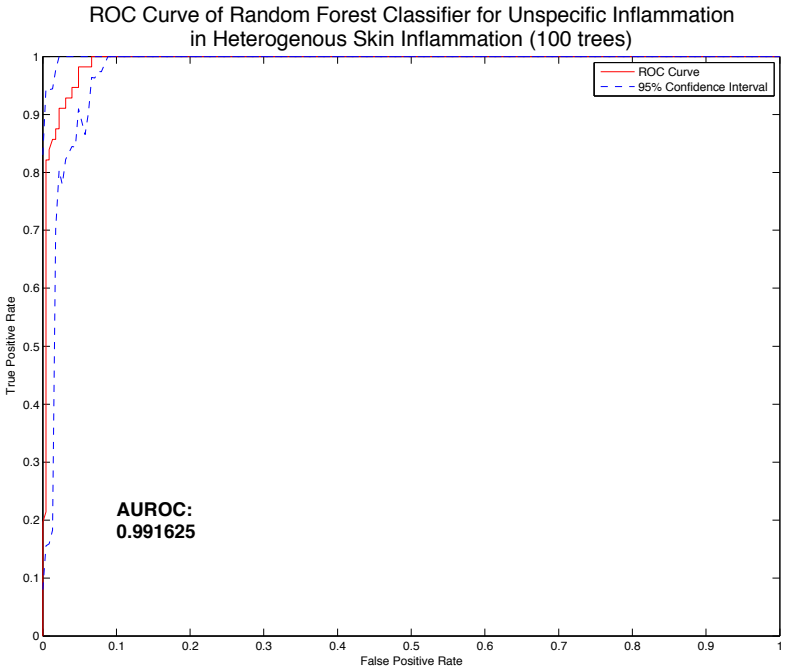

Figure 6.274

Unspecific Inflammation in Hybrid Feature Space

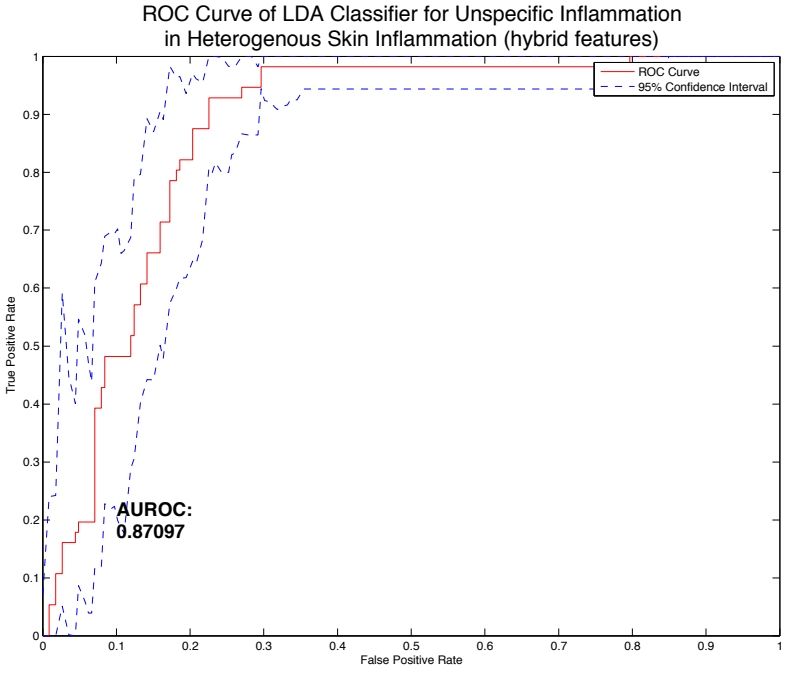

Figure 6.275

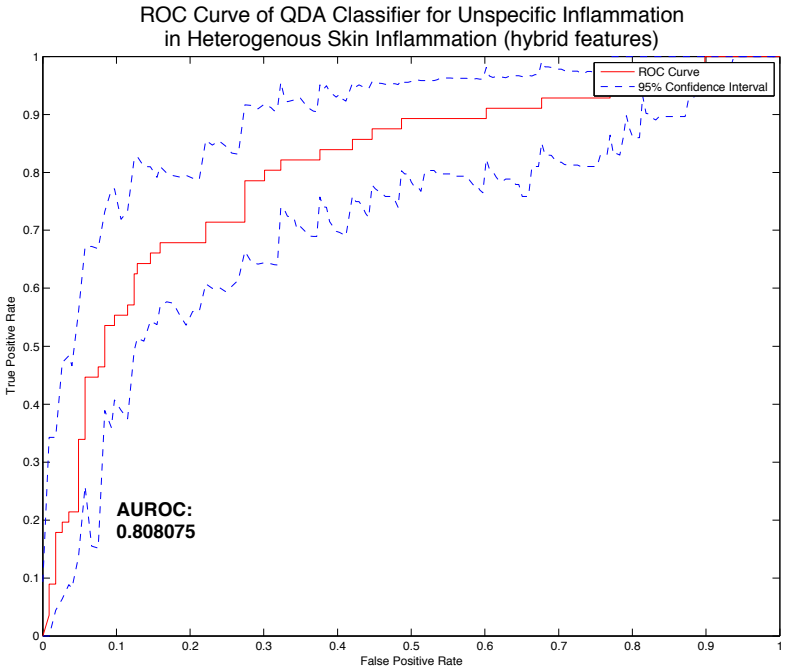

Figure 6.276

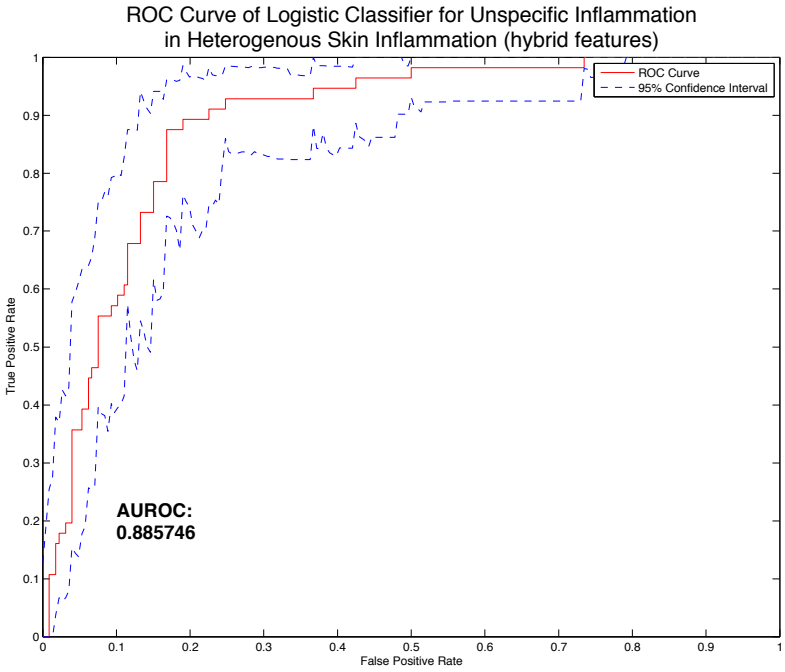

Figure 6.277

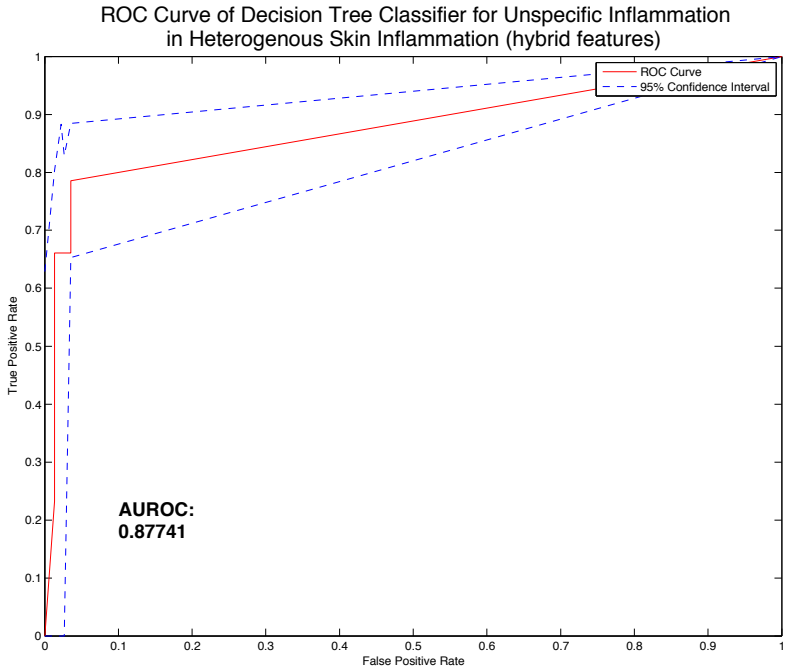

Figure 6.278

Type of Inflammation in Skin (POD <= 5)

Original 14-Dimensional Feature Space

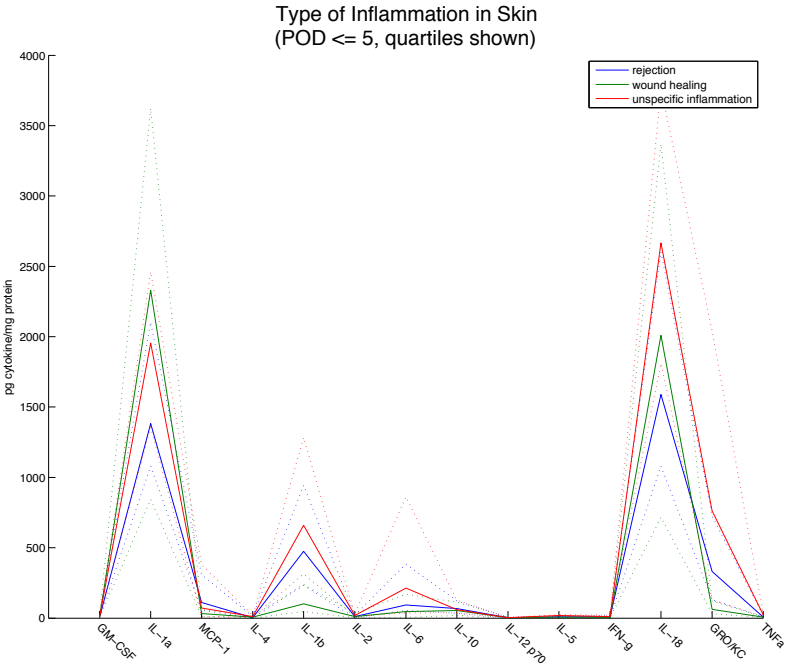

Figure 6.279

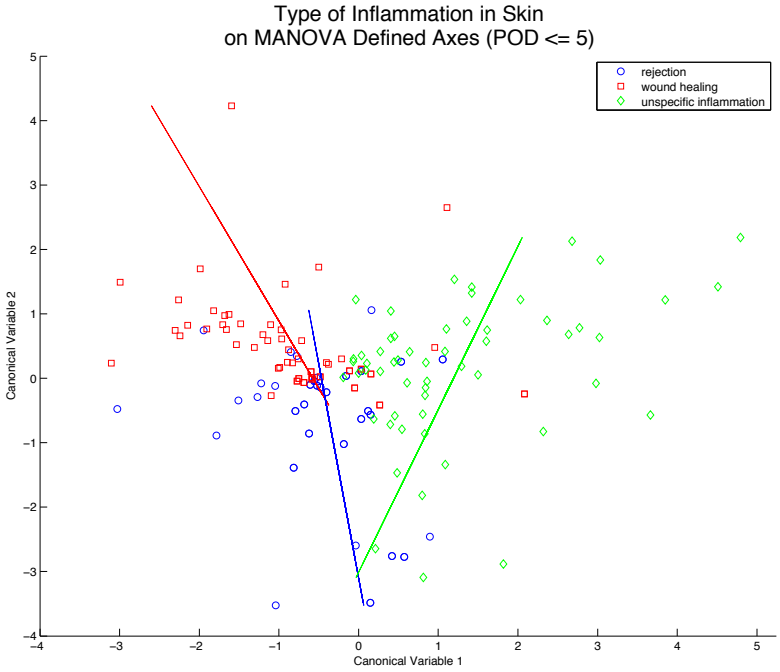

Figure 6.280

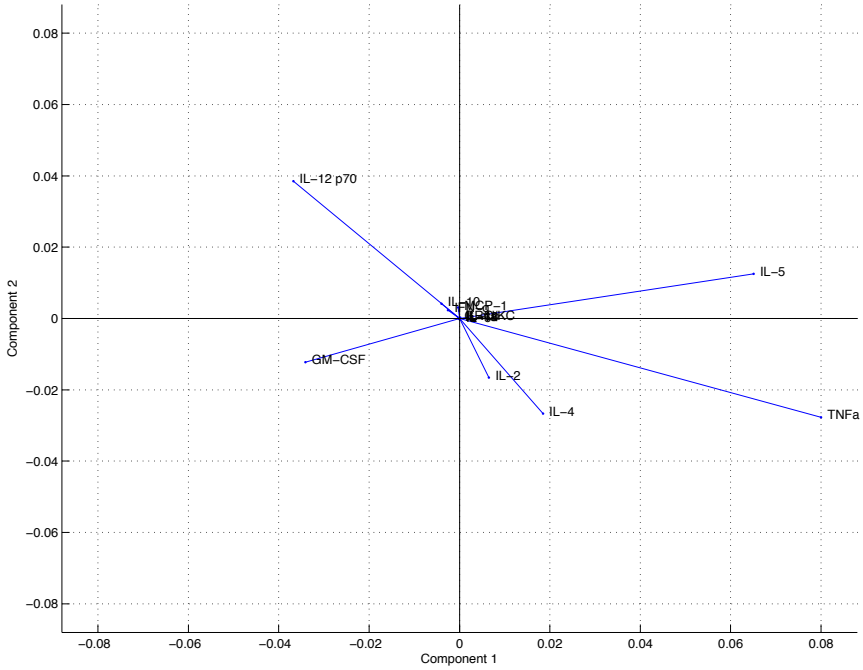

Figure 6.281

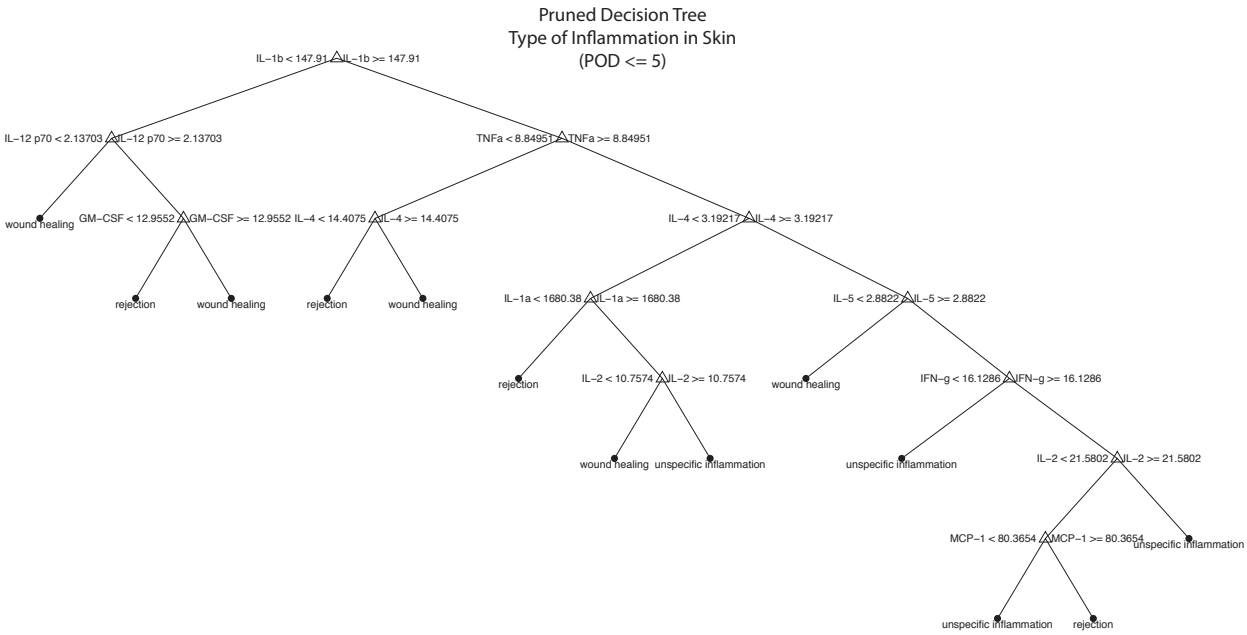

Figure 6.282

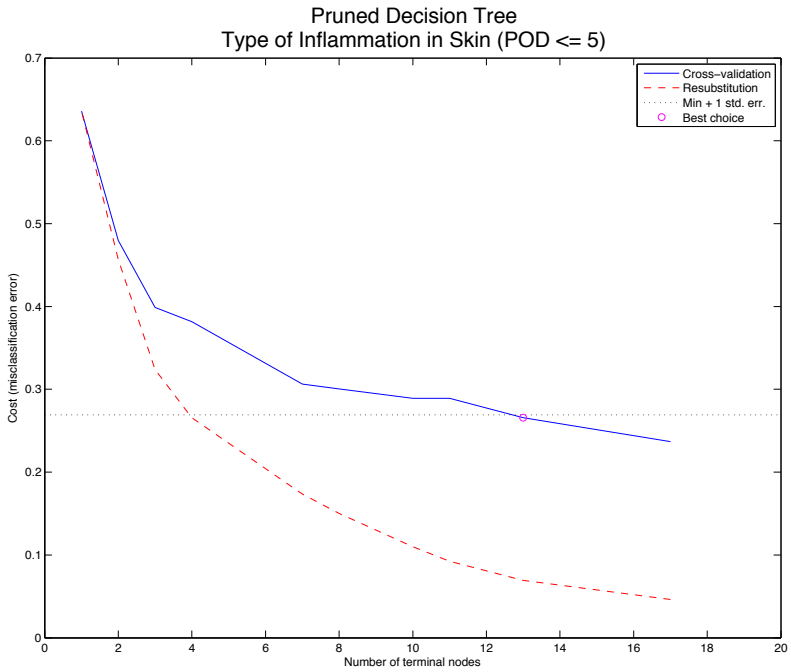

Figure 6.283

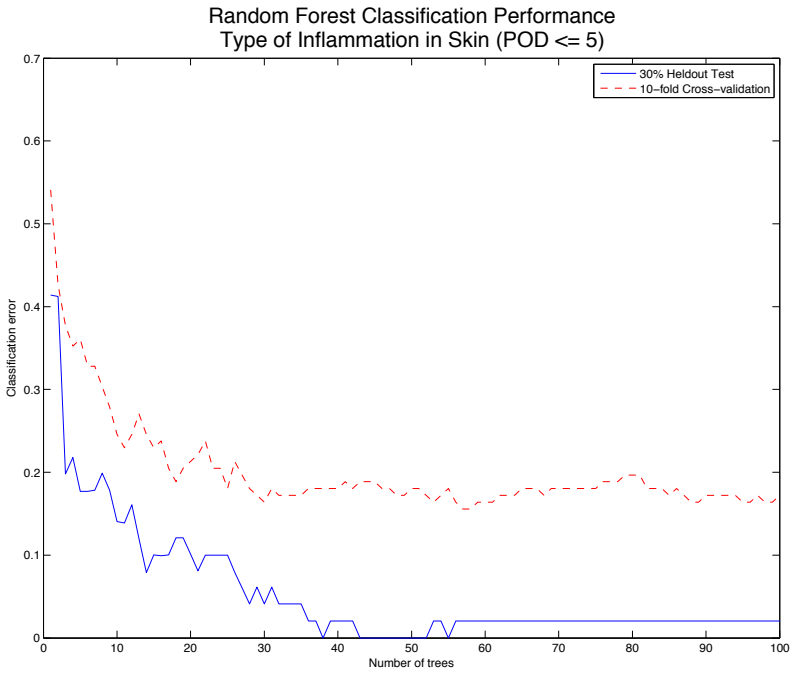

Figure 6.284

5-Dimensional Feature Selected Space

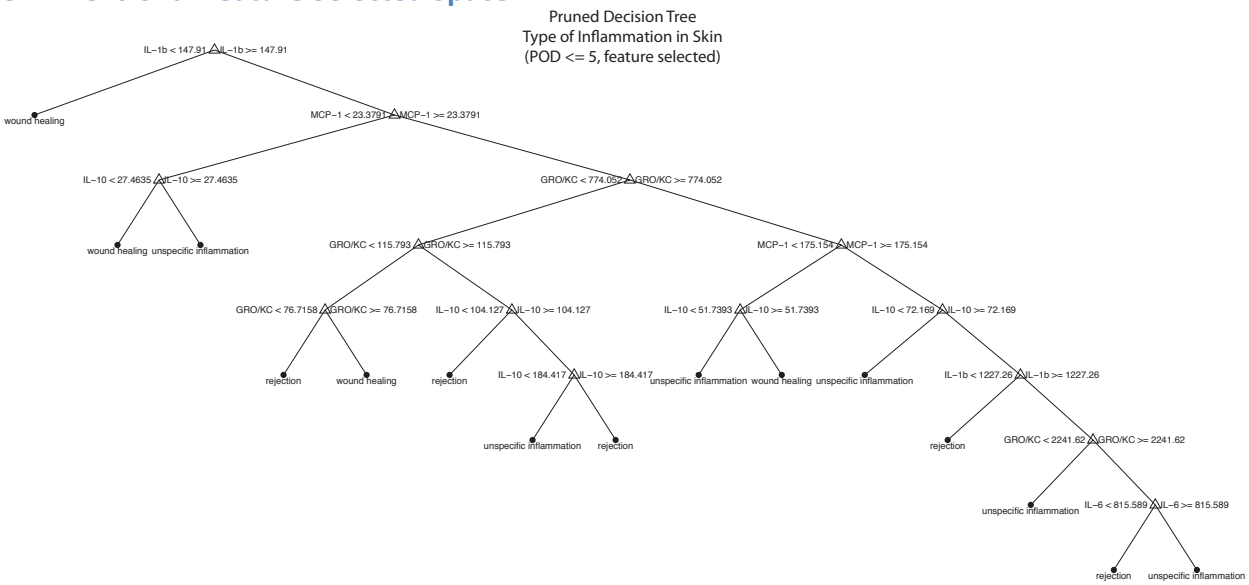

Figure 6.285

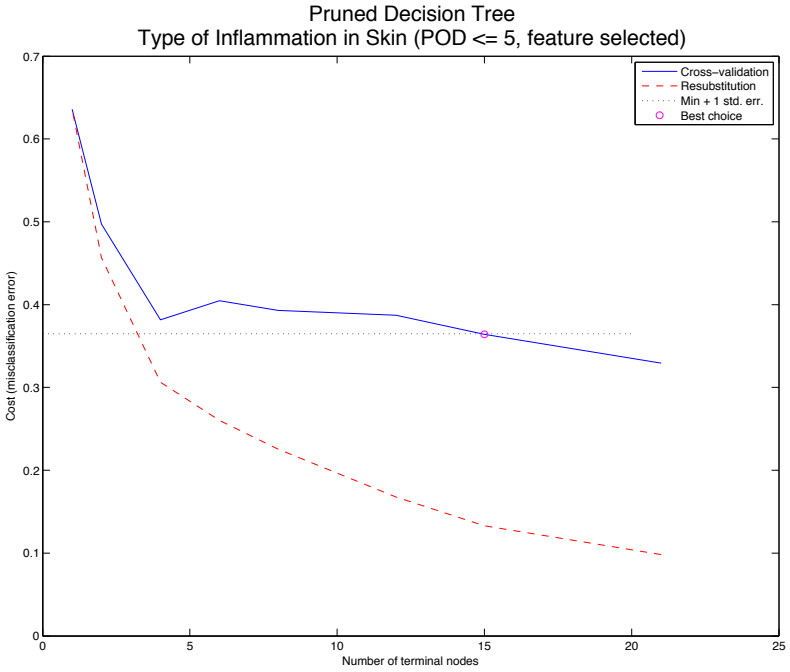

Figure 6.286

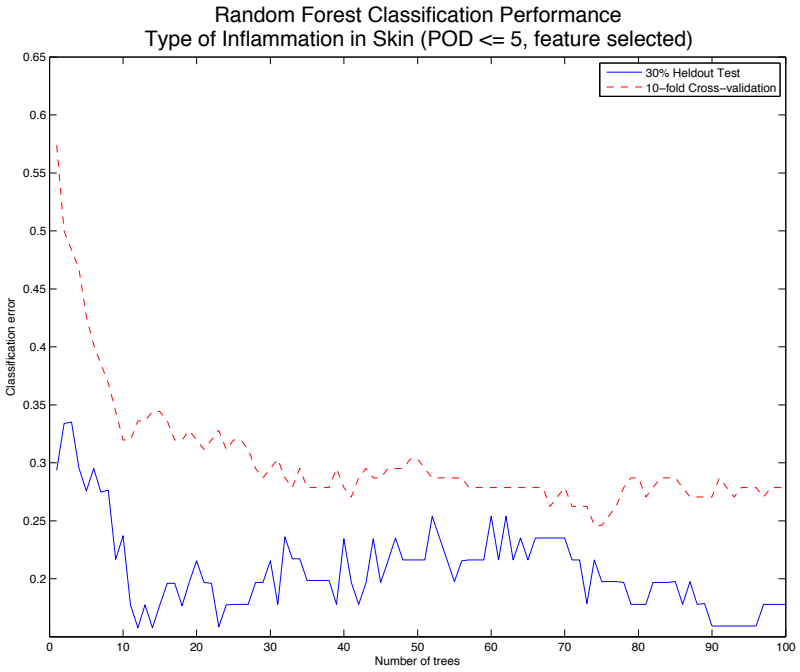

Figure 6.287

MANOVA Transformed Feature Space

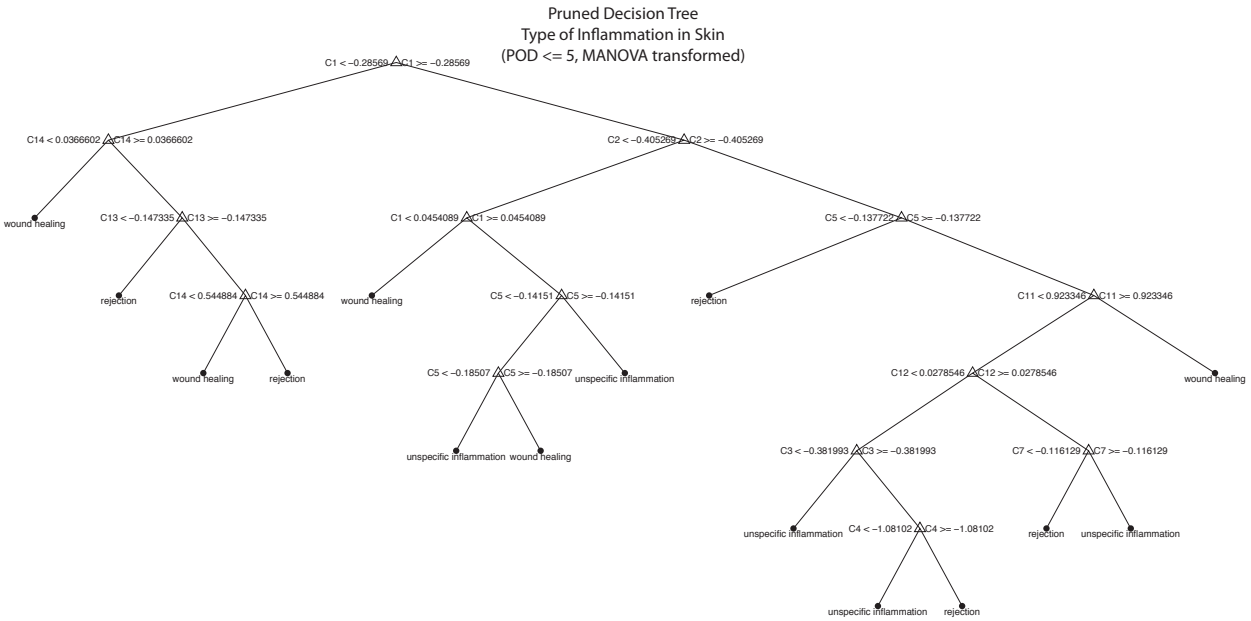

Figure 6.288

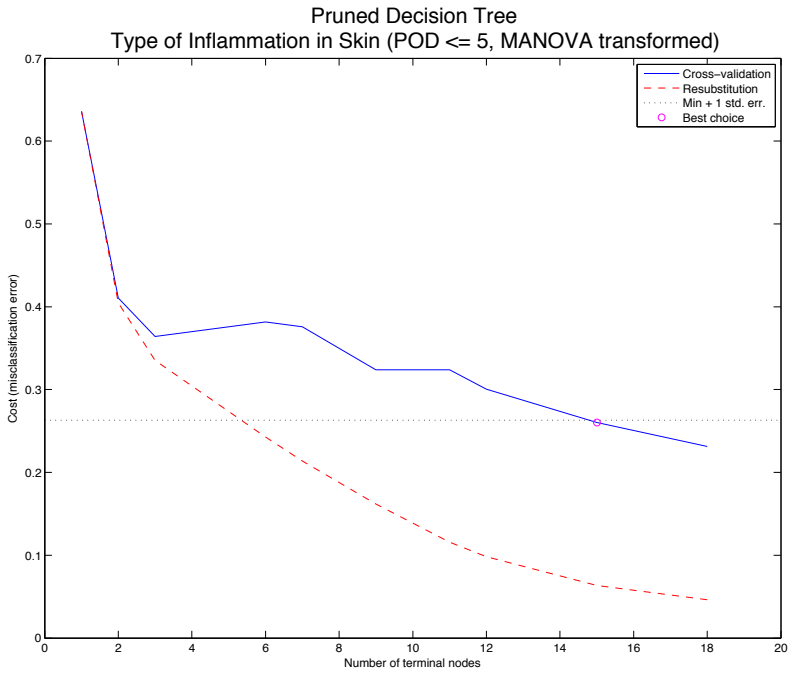

Figure 6.289

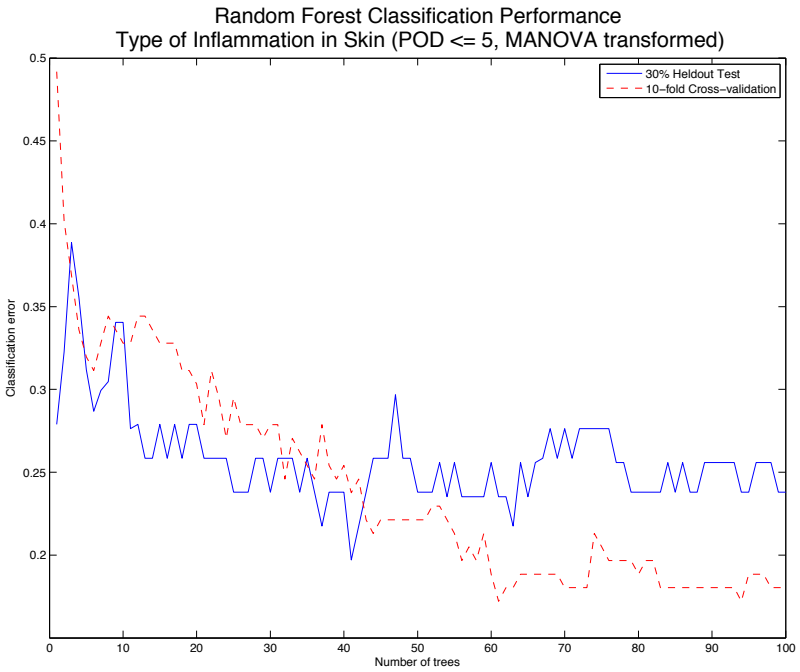

Figure 6.290

Type of Inflammation in Skin (POD > 5)

Original 14-Dimensional Feature Space

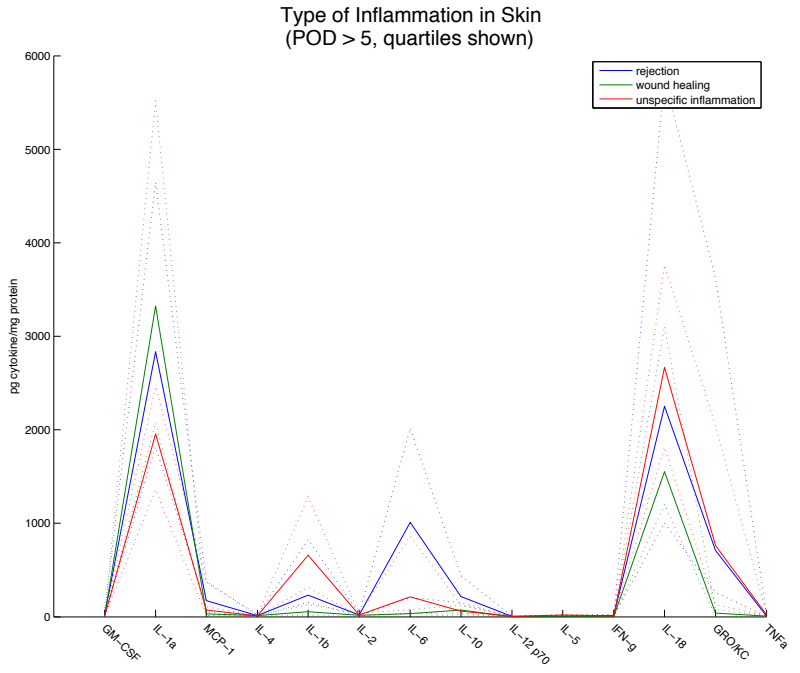

Figure 6.291

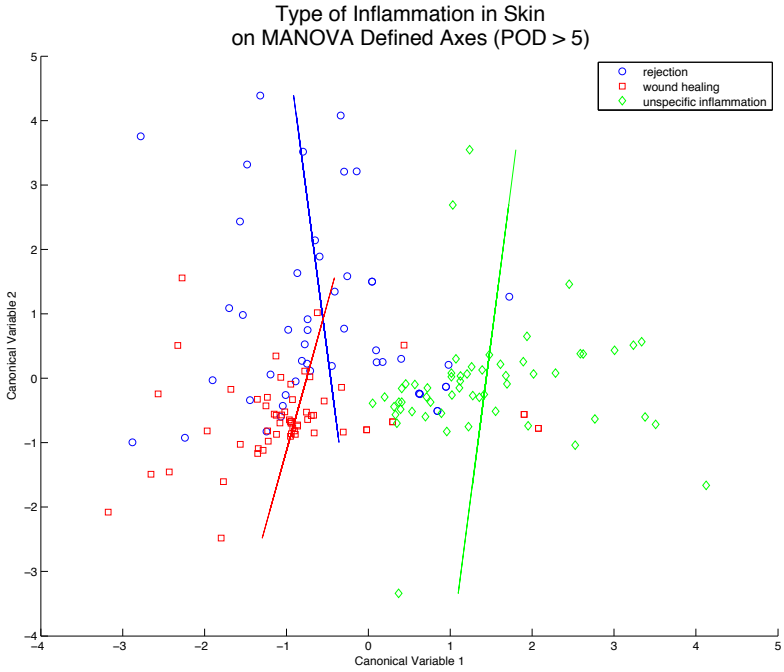

Figure 6.292

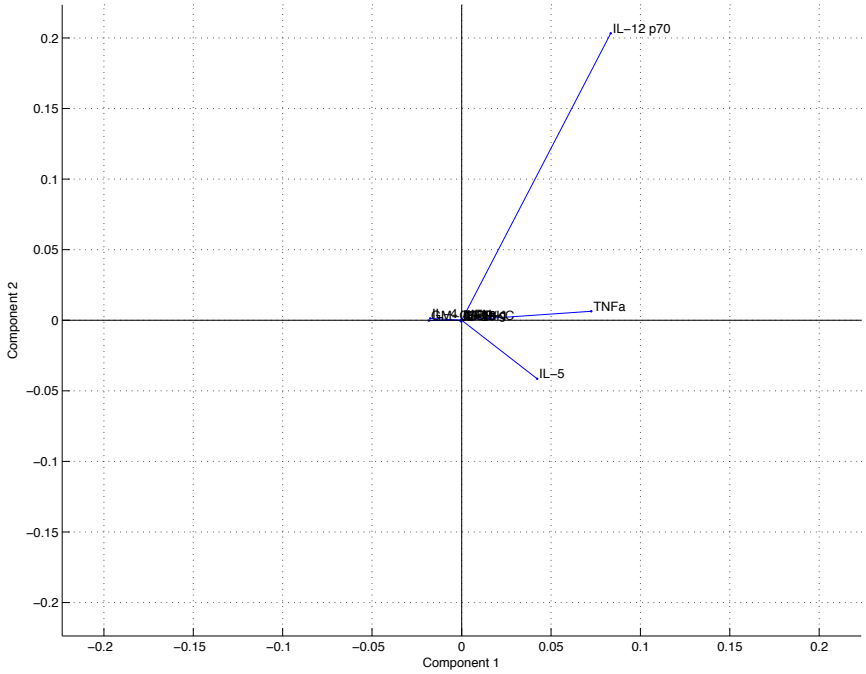

Figure 6.293

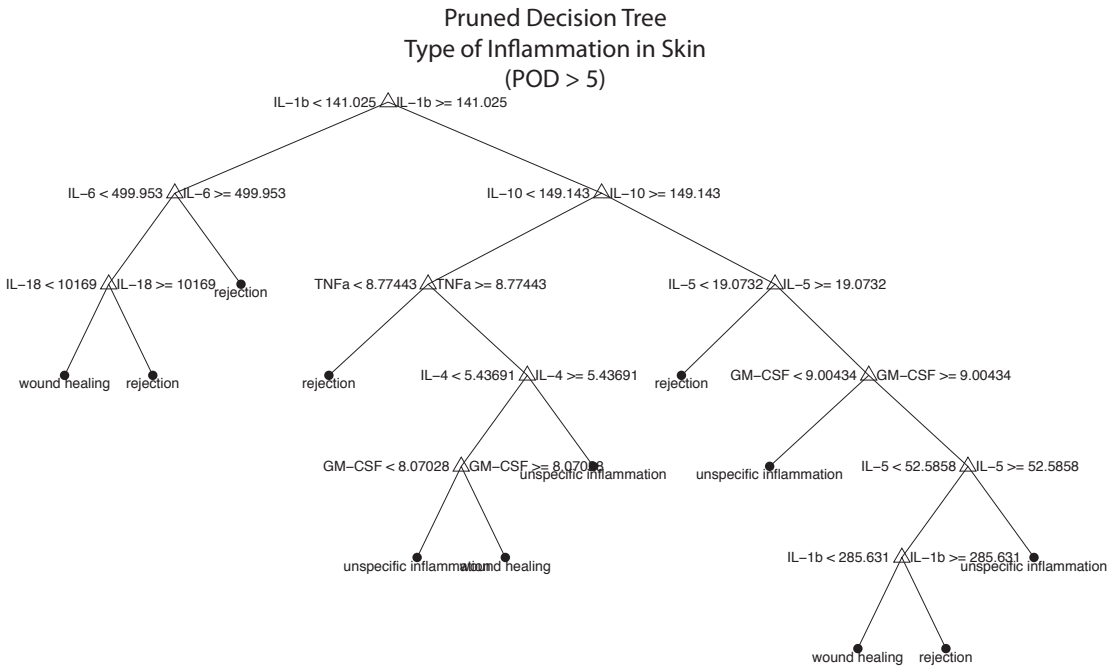

Figure 6.294

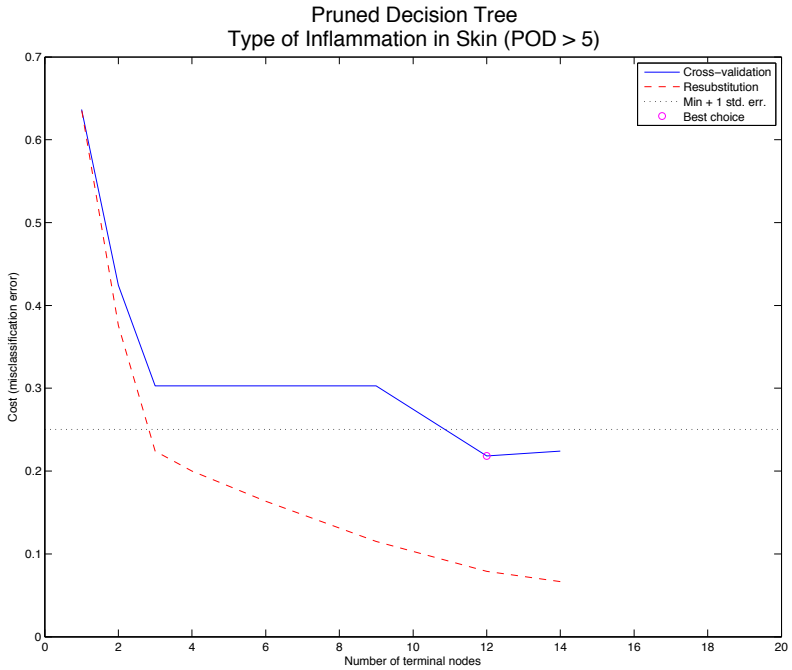

Figure 6.295

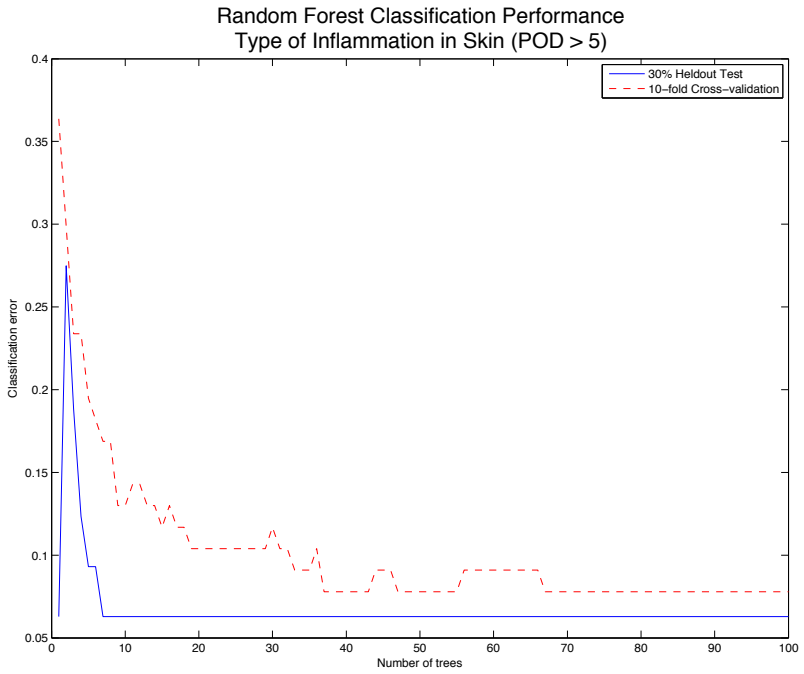

Figure 6.296

5-Dimensional Feature Selected Space

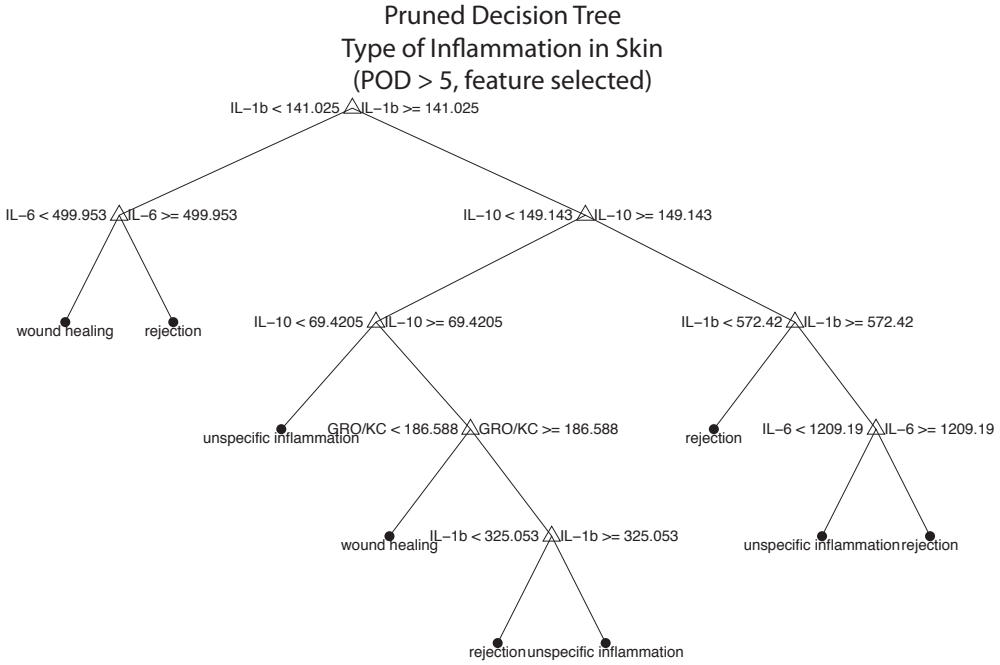

Figure 6.297

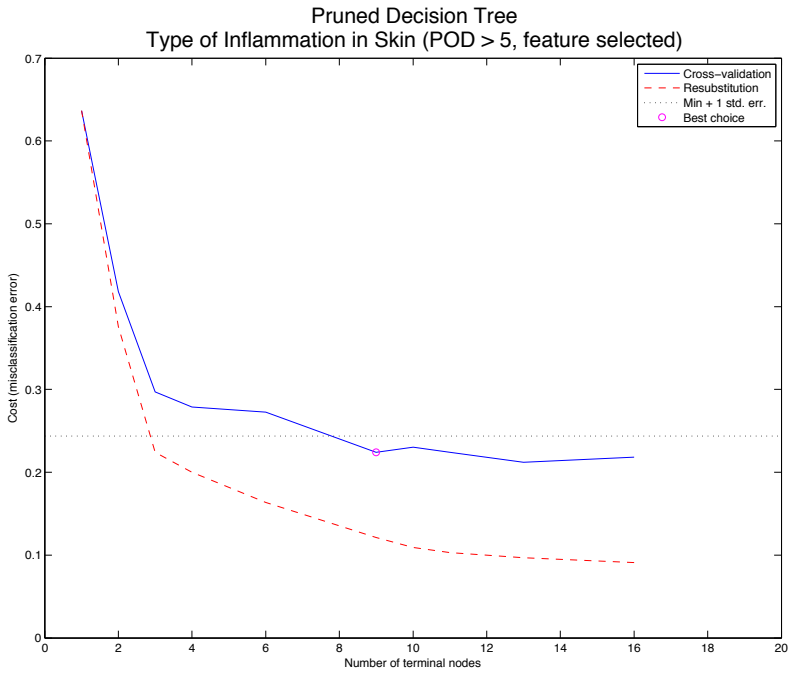

Figure 6.298

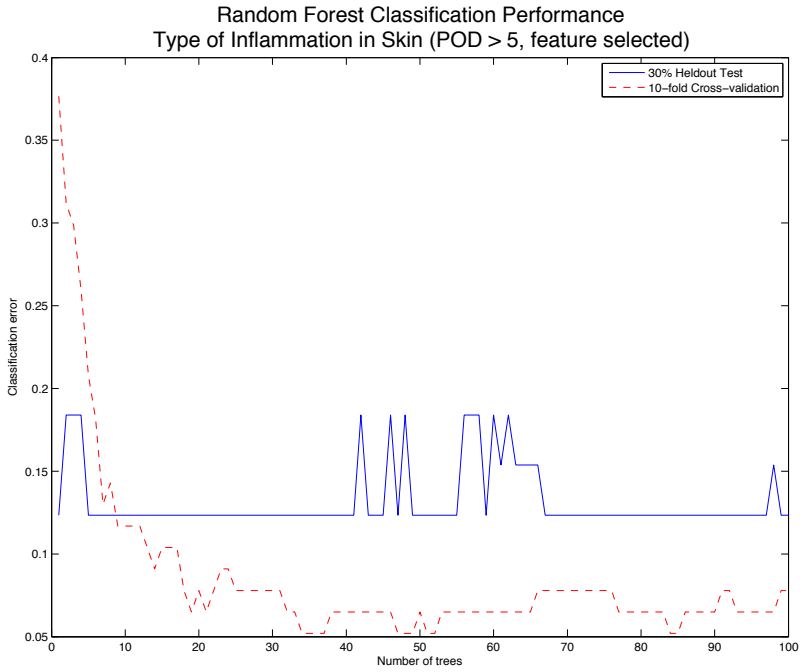

Figure 6.299

MANOVA Transformed Feature Space

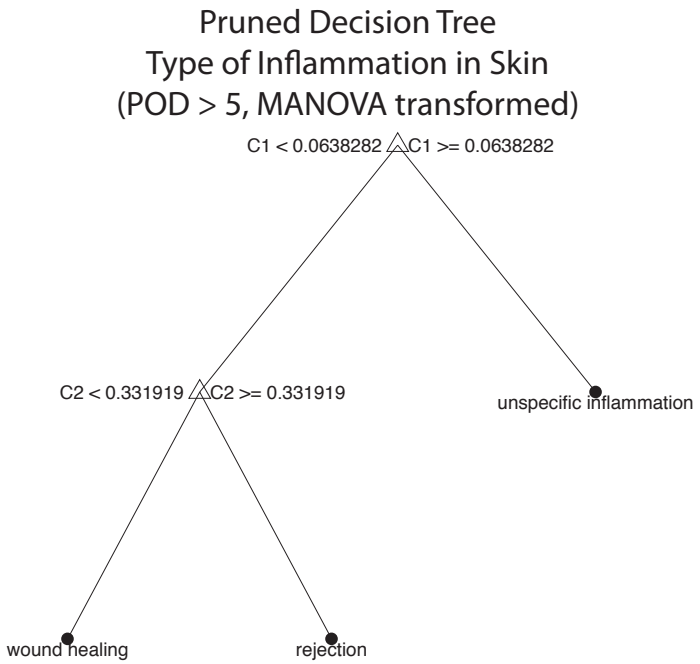

Figure 6.300

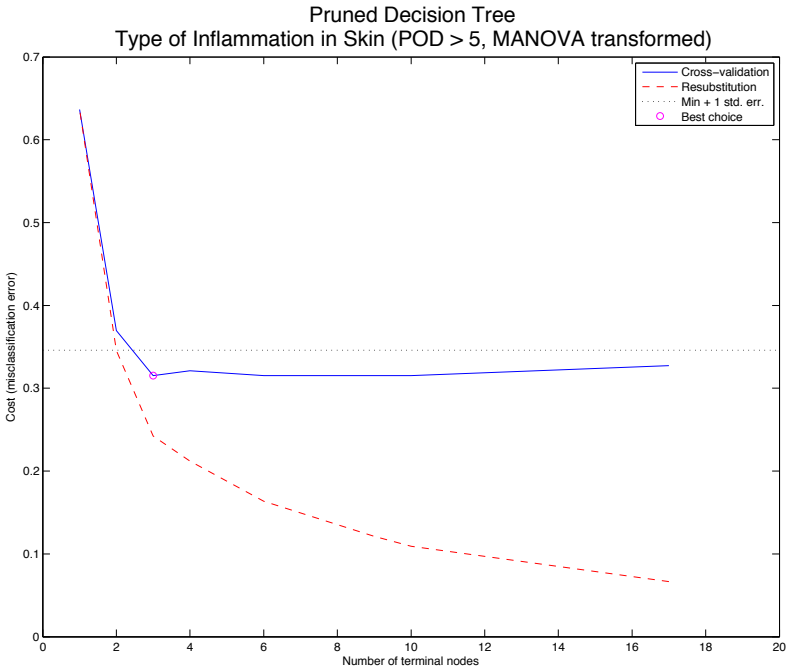

Figure 6.301

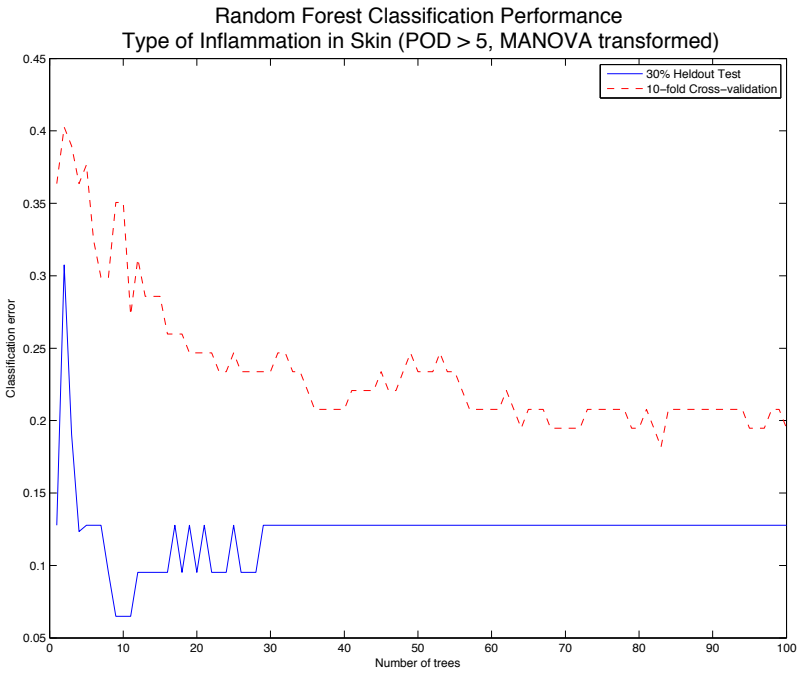

Figure 6.302

Type of Inflammation in Muscle (all time points)

Original 14-Dimensional Feature Space

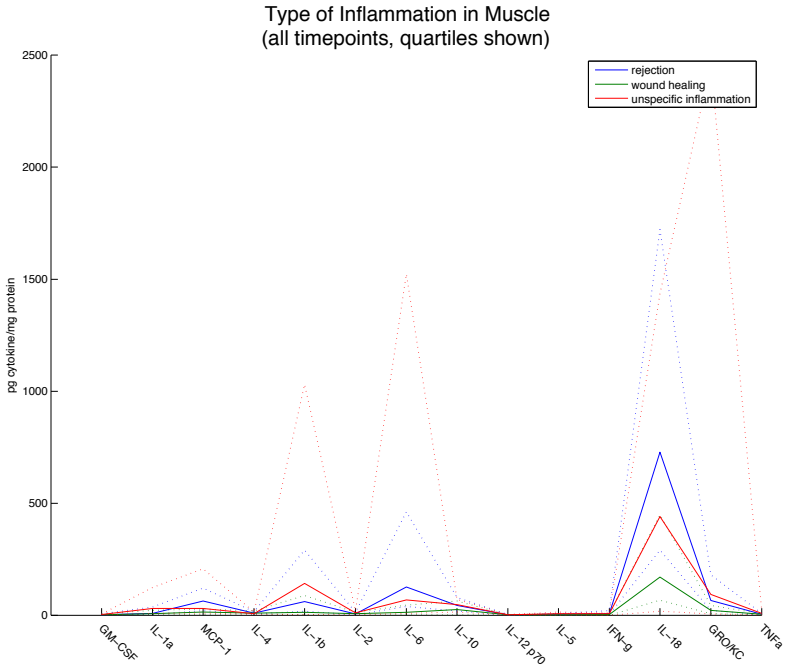

Figure 6.303

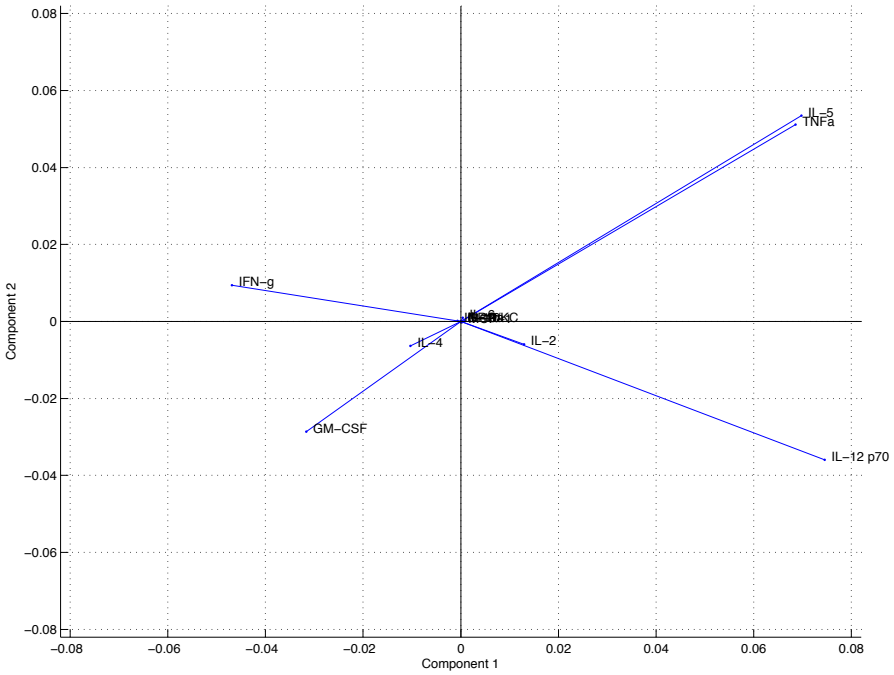

Figure 6.304

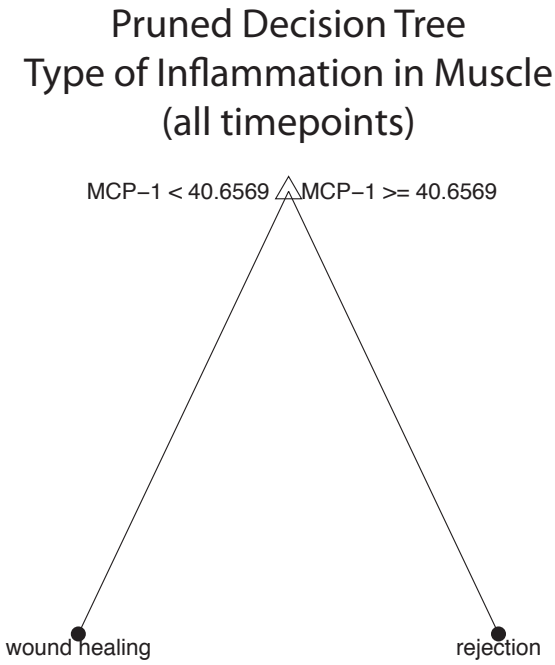

Figure 6.305

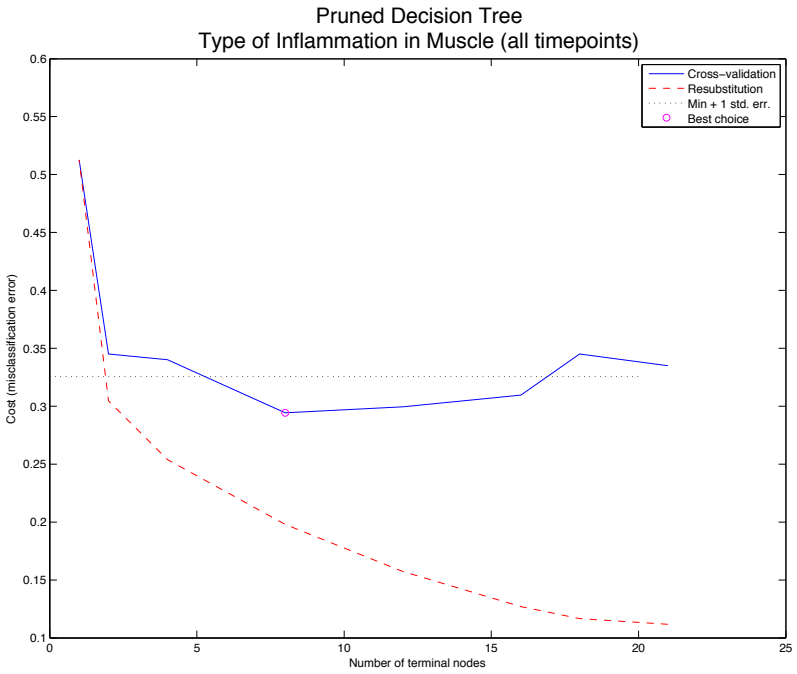

Figure 6.306

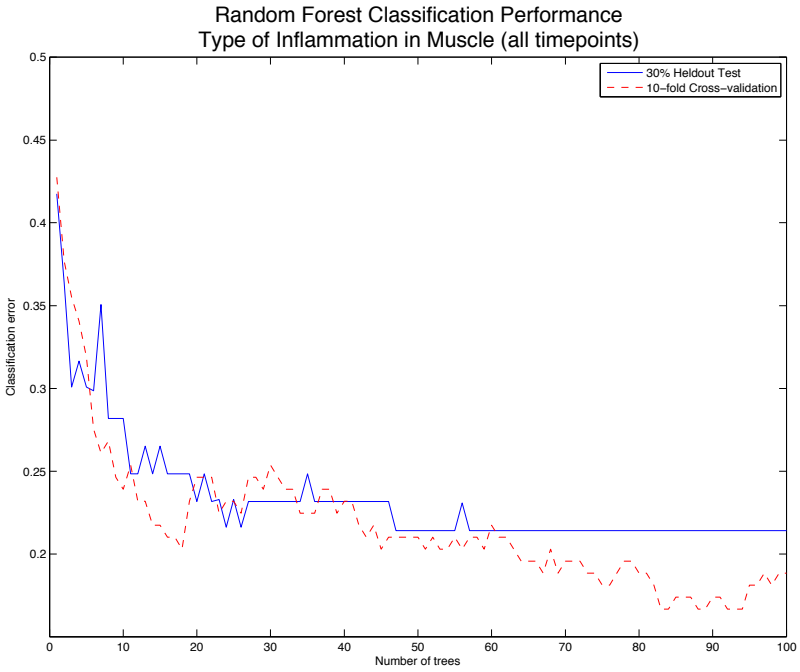

Figure 6.307

5-Dimensional Feature Selected Space

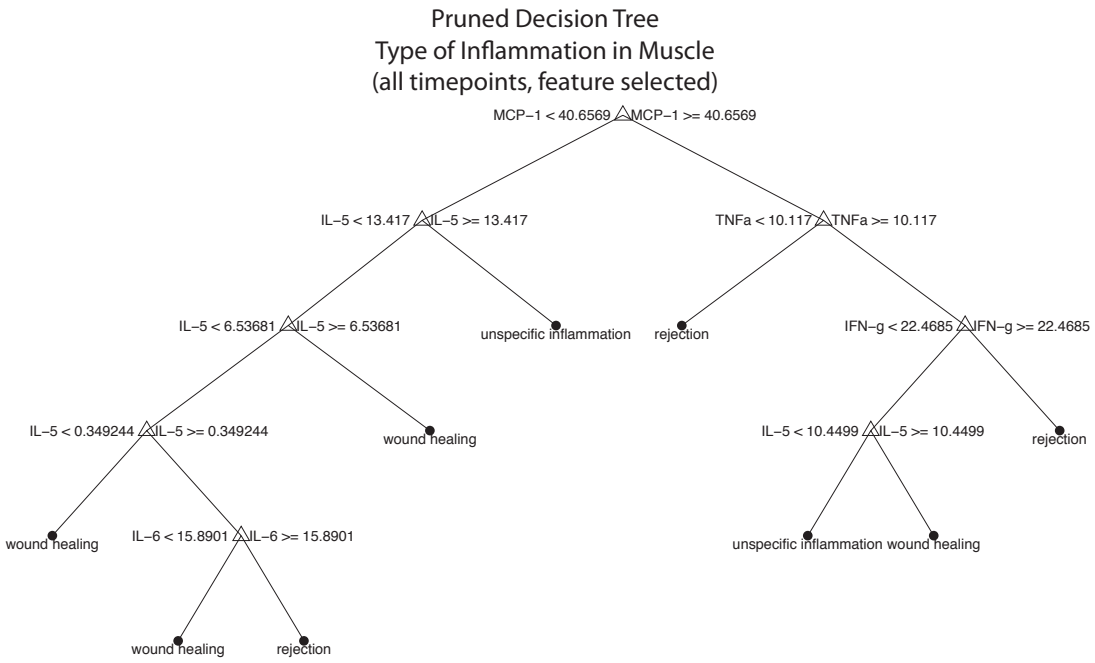

Figure 6.308

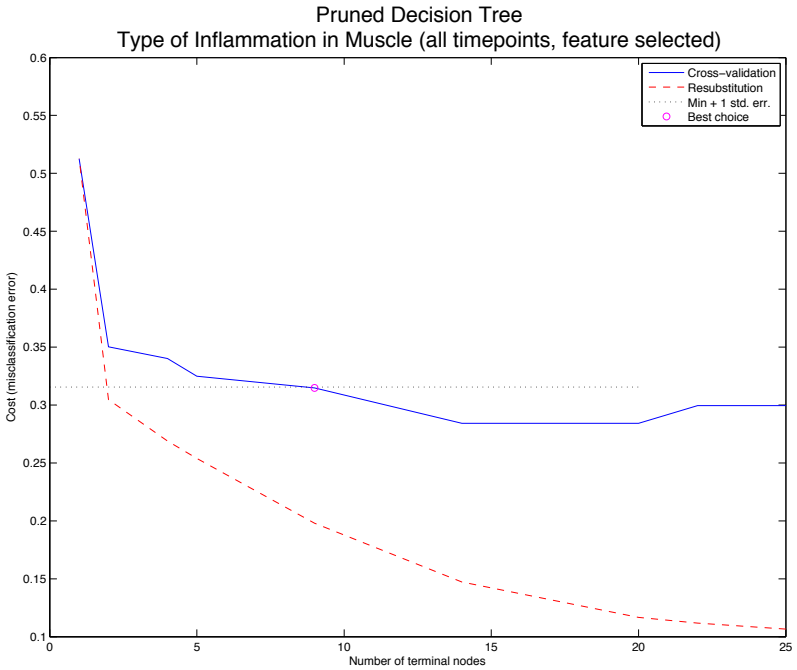

Figure 6.309

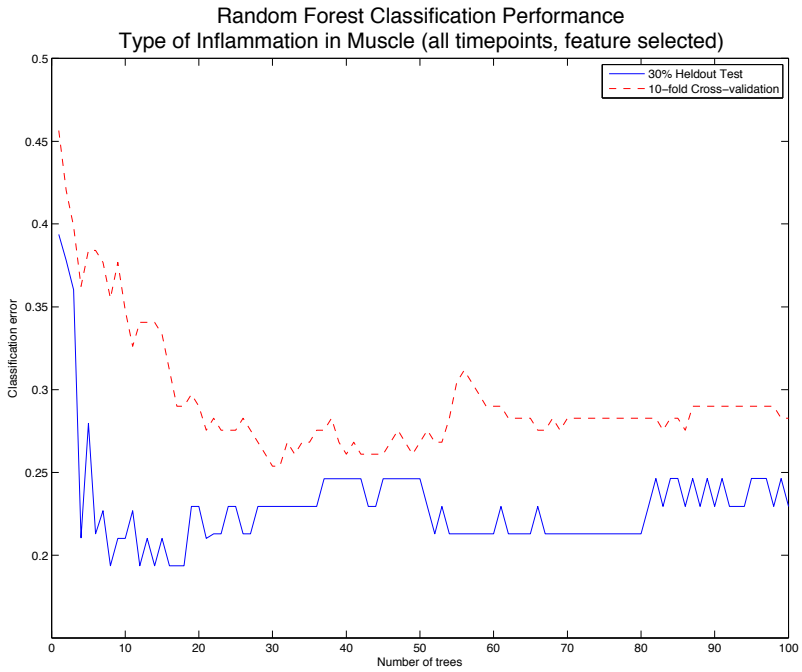

Figure 6.310

MANOVA Transformed Feature Space

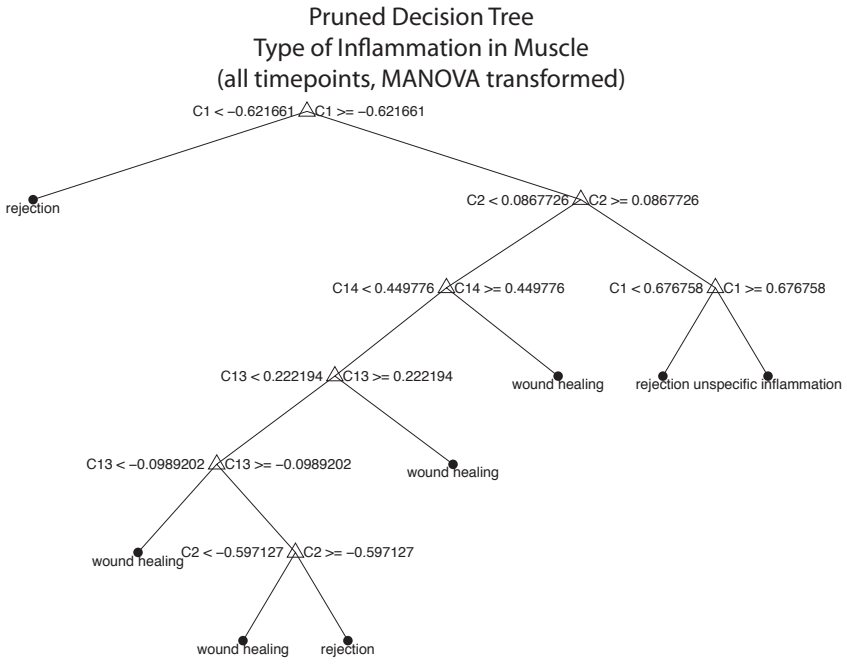

Figure 6.311

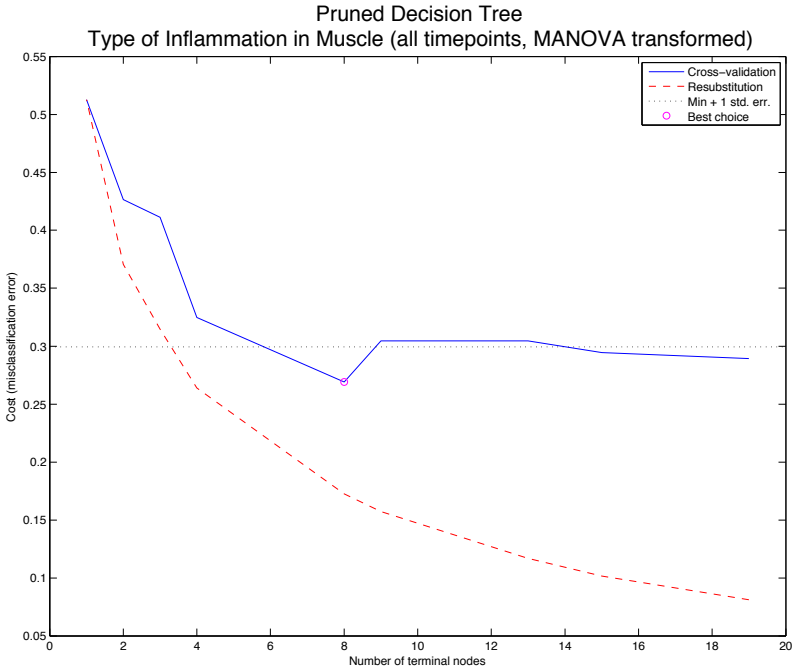

Figure 6.312

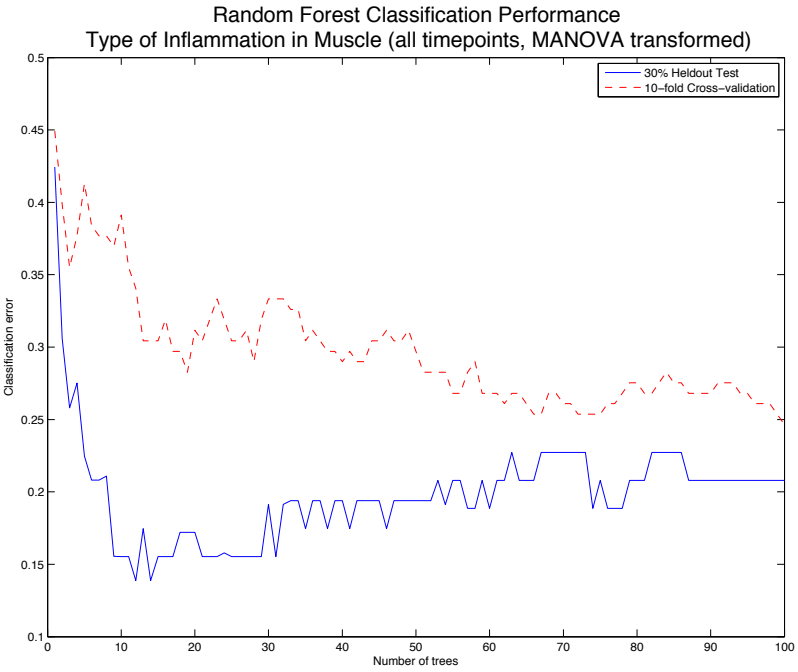

Figure 6.313

Hybrid Features

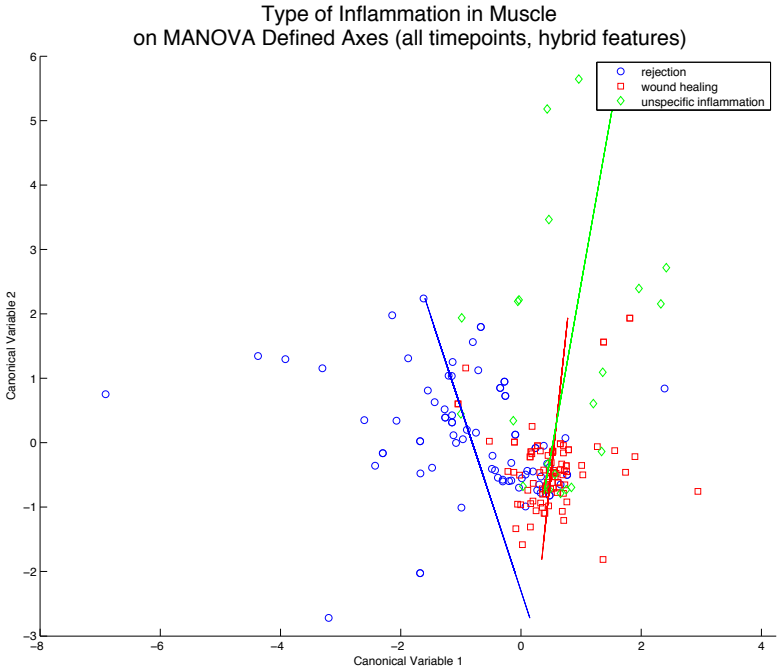

Figure 6.314

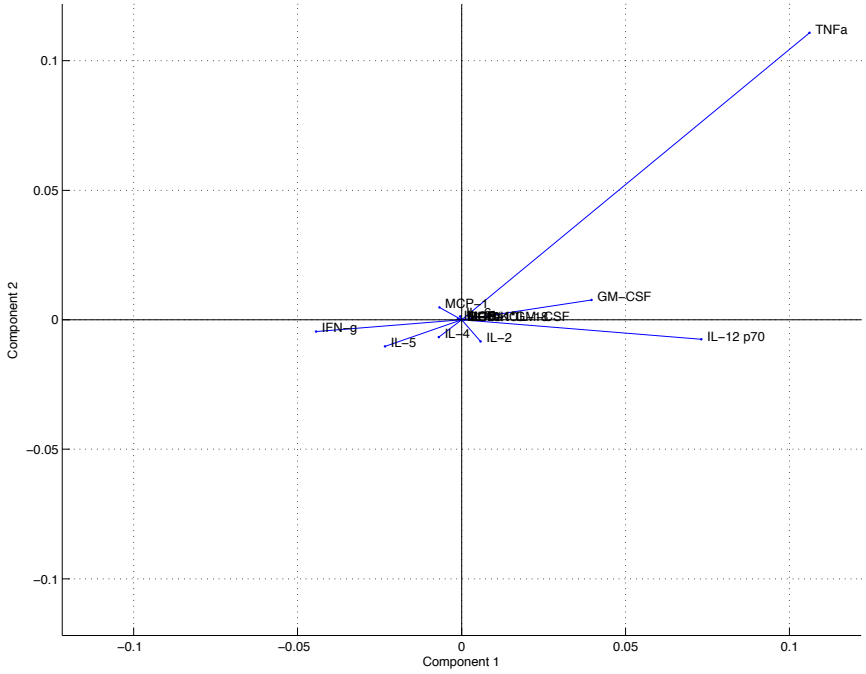

Figure 6.315

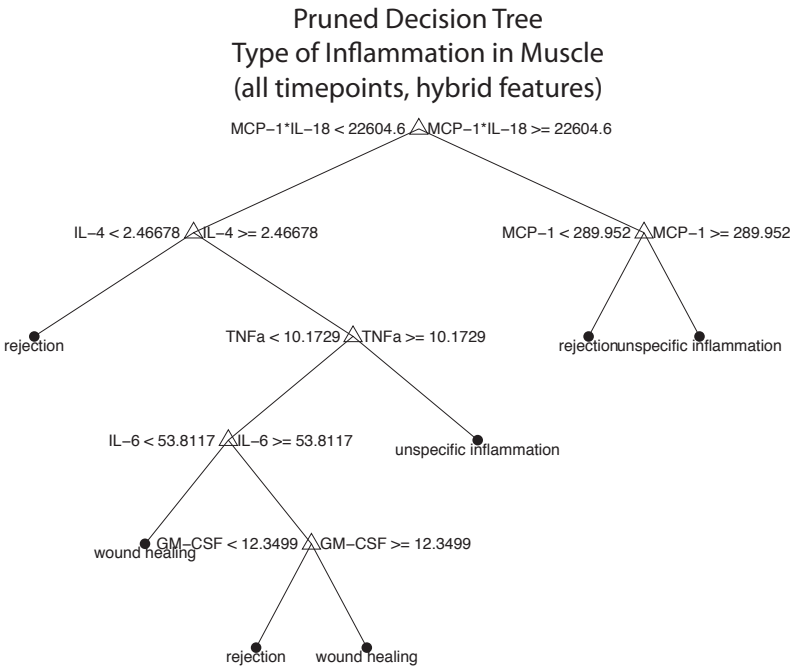

Figure 6.316

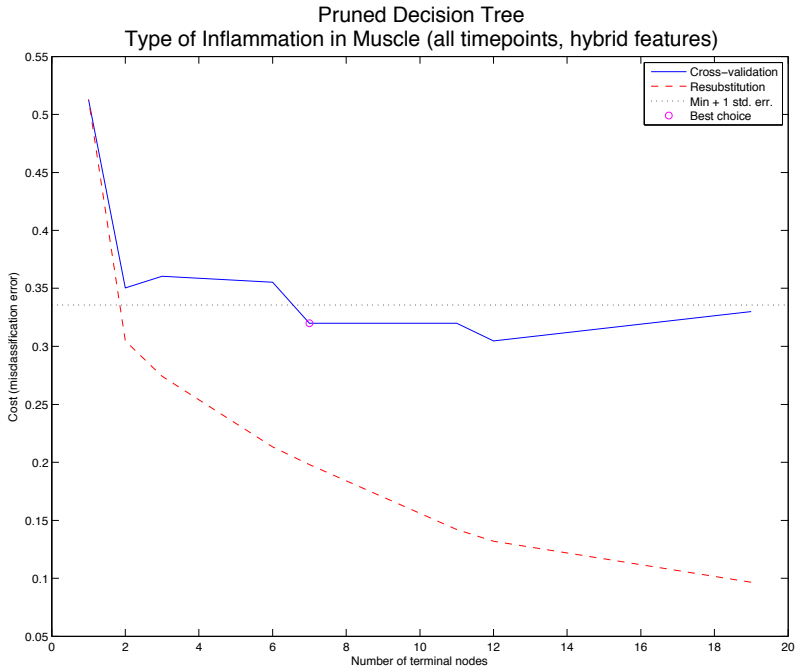

Figure 6.317

ROC Curves in Muscle: Wound Healing and Unspecific Inflammation

Wound Healing in Original Feature Space

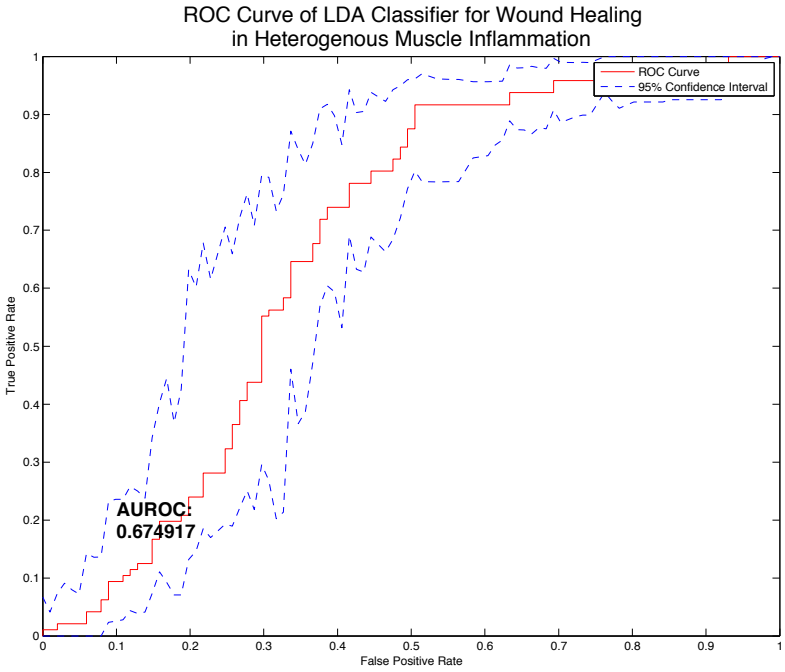

Figure 6.318

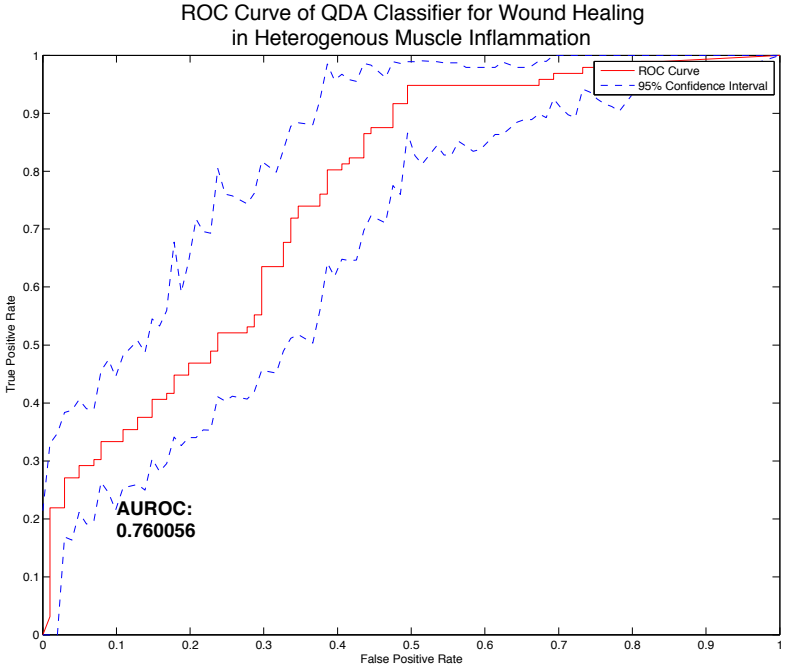

Figure 6.319

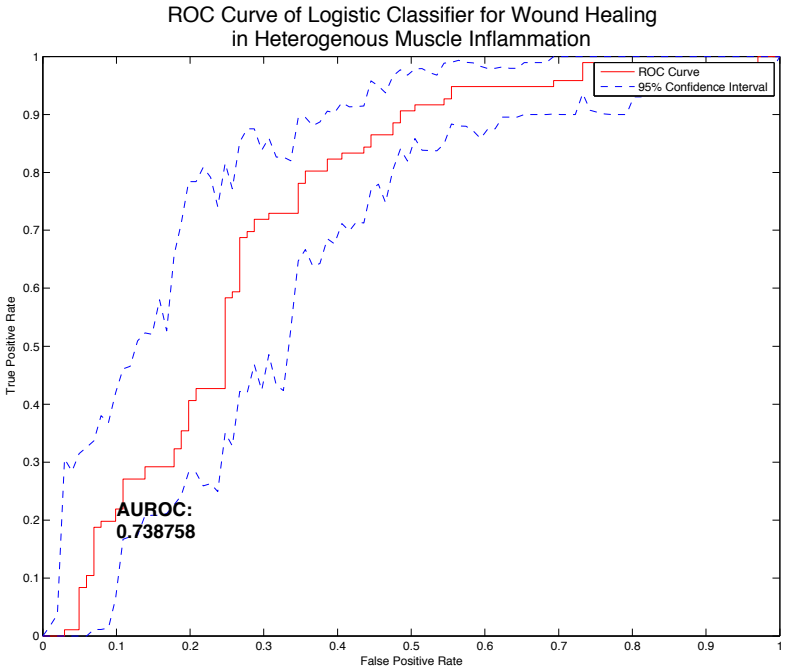

Figure 6.320

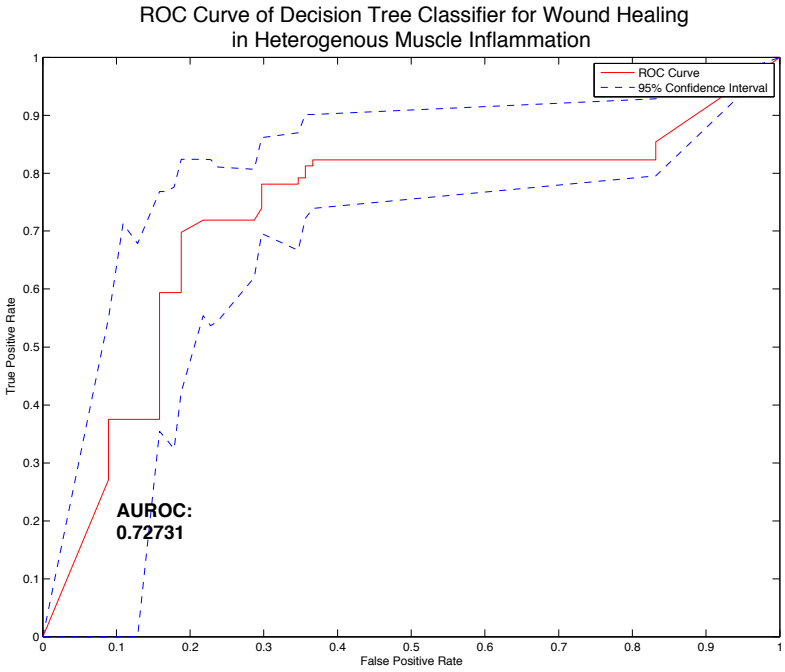

Figure 6.321

Wound Healing in Hybrid Feature Space

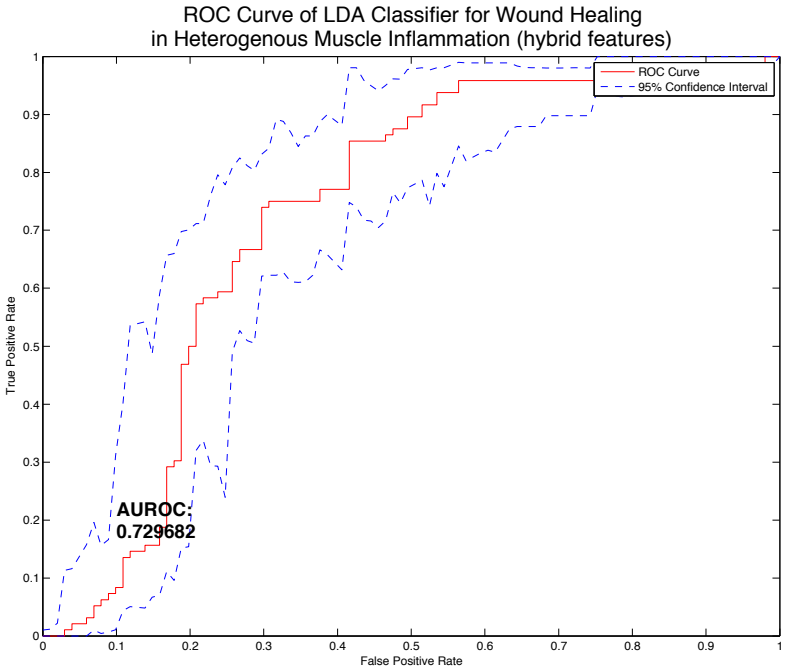

Figure 6.322

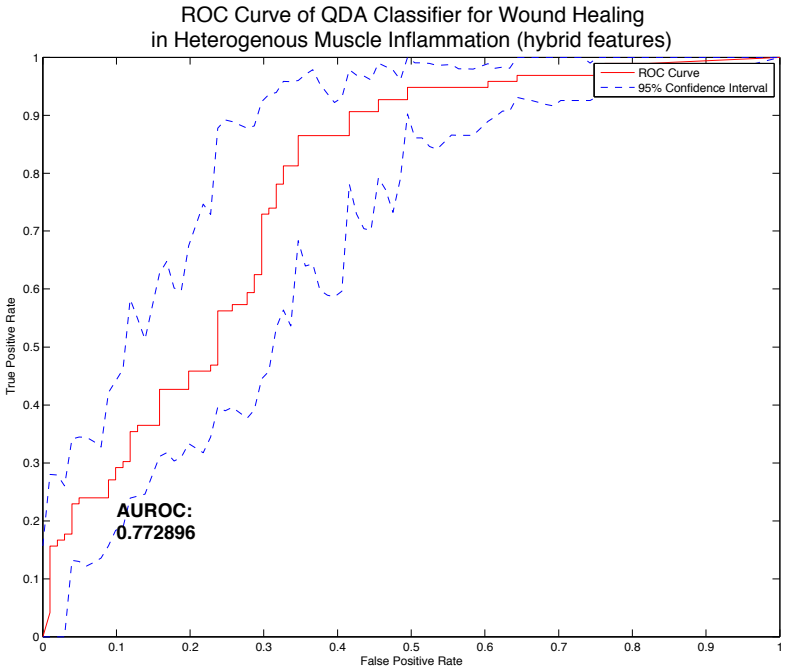

Figure 6.323

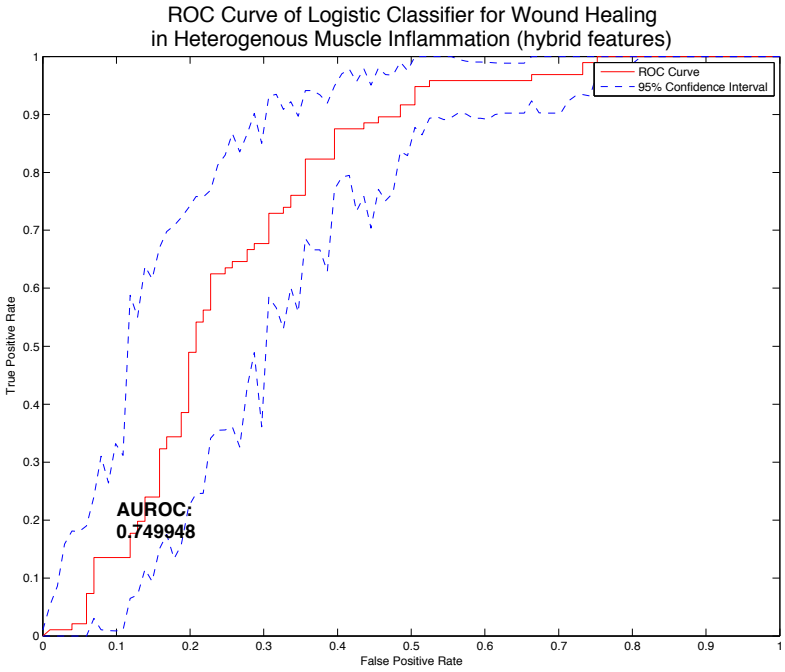

Figure 6.324

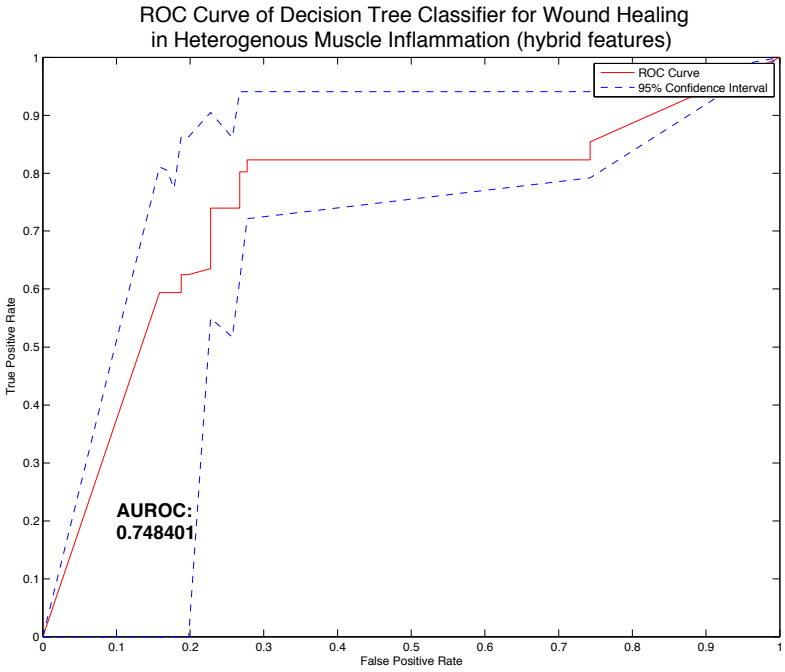

Figure 6.325

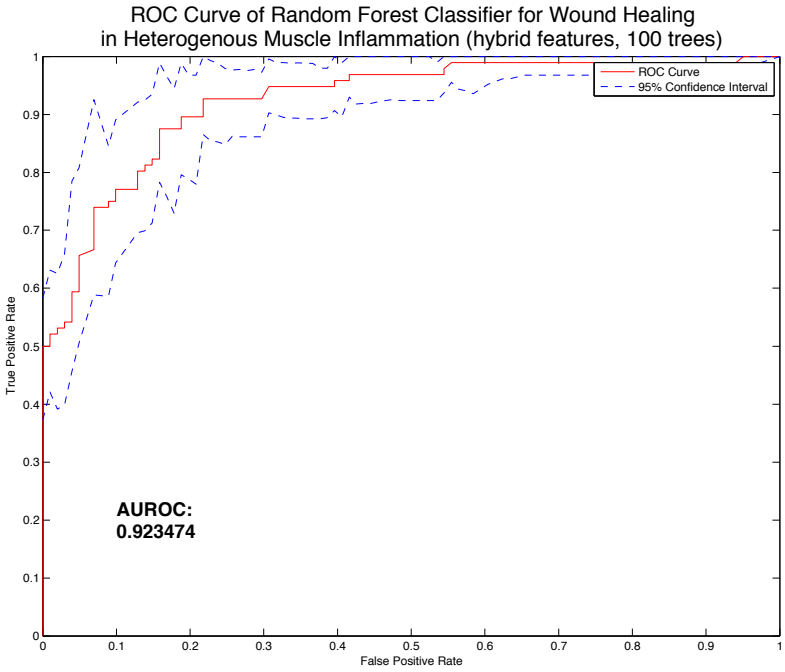

Figure 6.326

Unspecific Inflammation in Original Feature Space

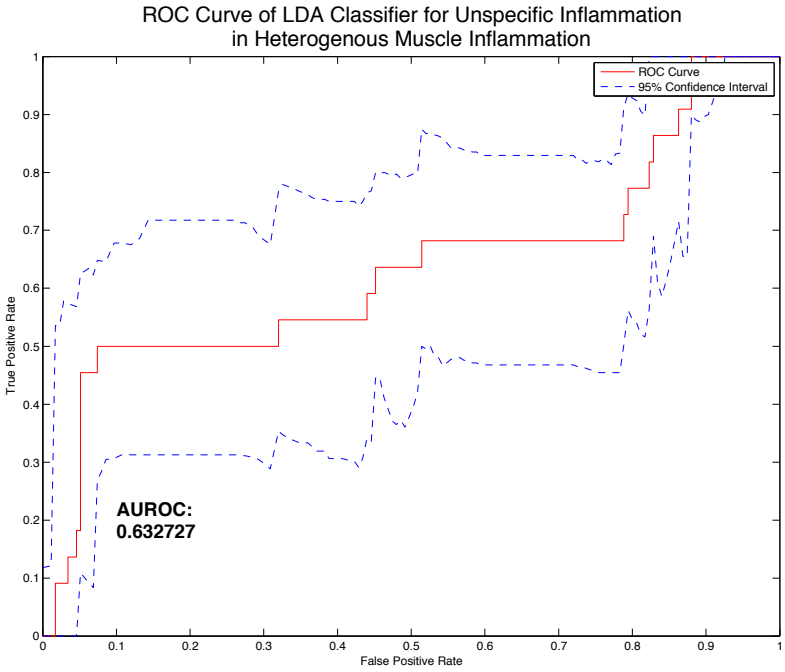

Figure 6.327

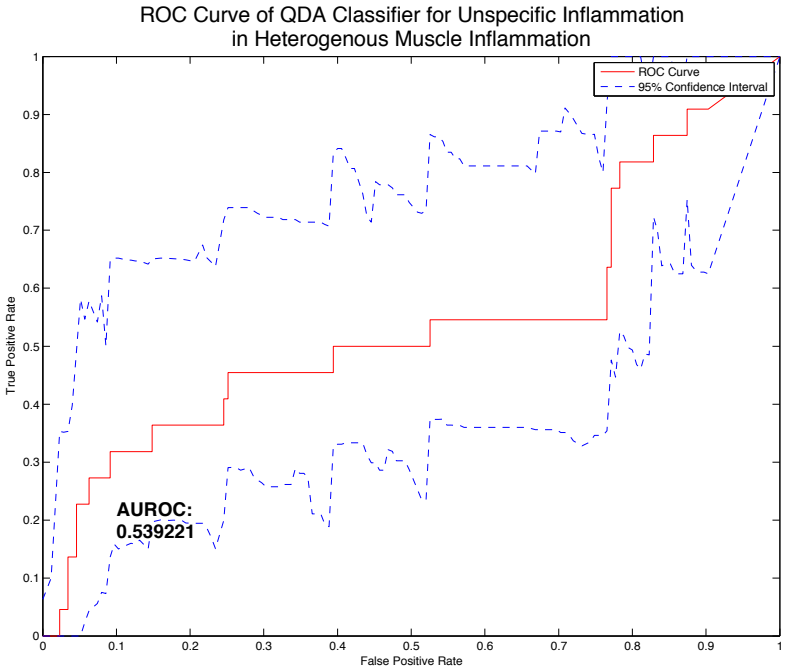

Figure 6.328

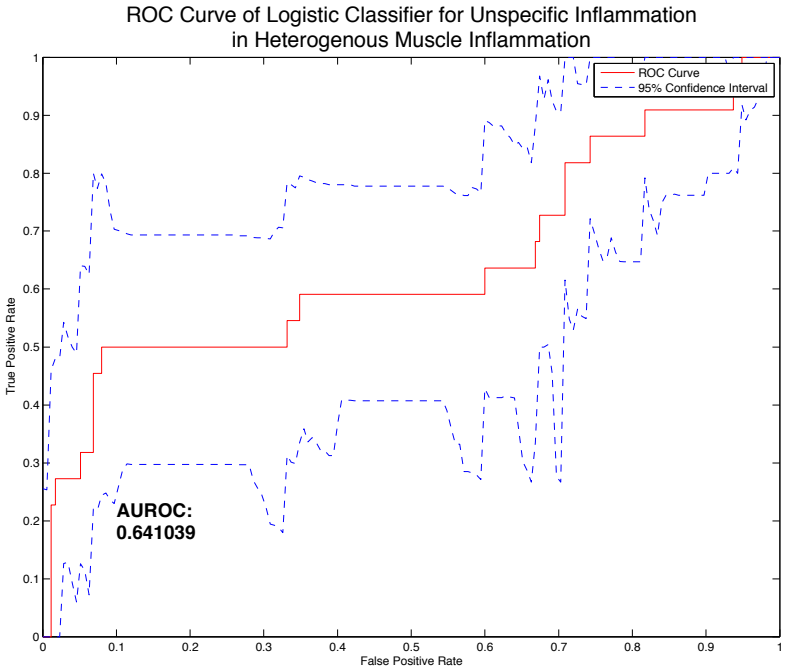

Figure 6.329

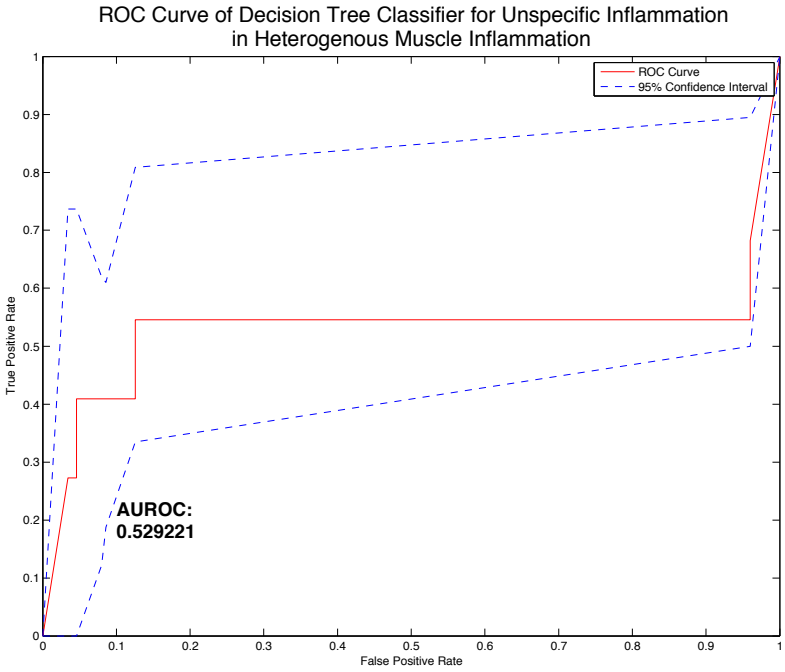

Figure 6.330

Unspecific Inflammation in Hybrid Feature Space

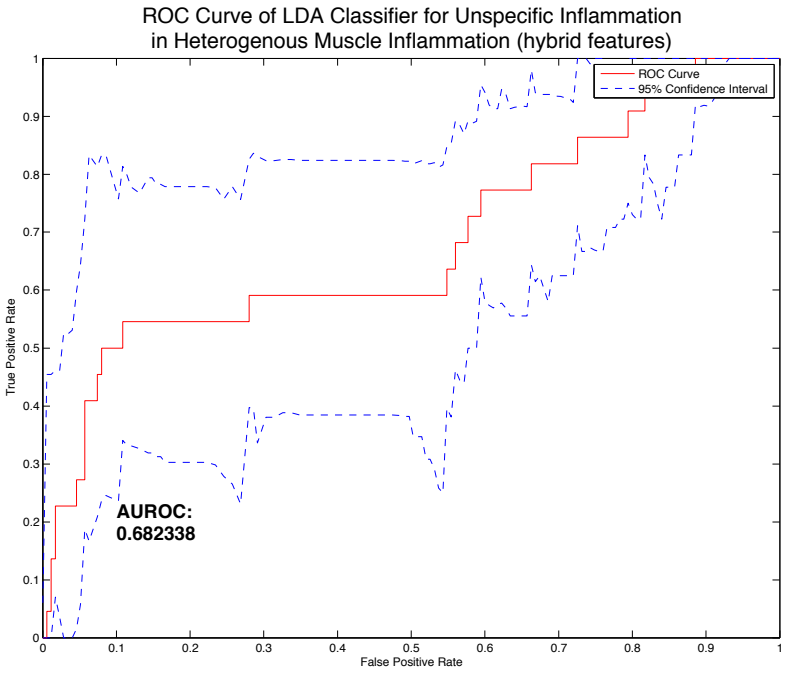

Figure 6.331

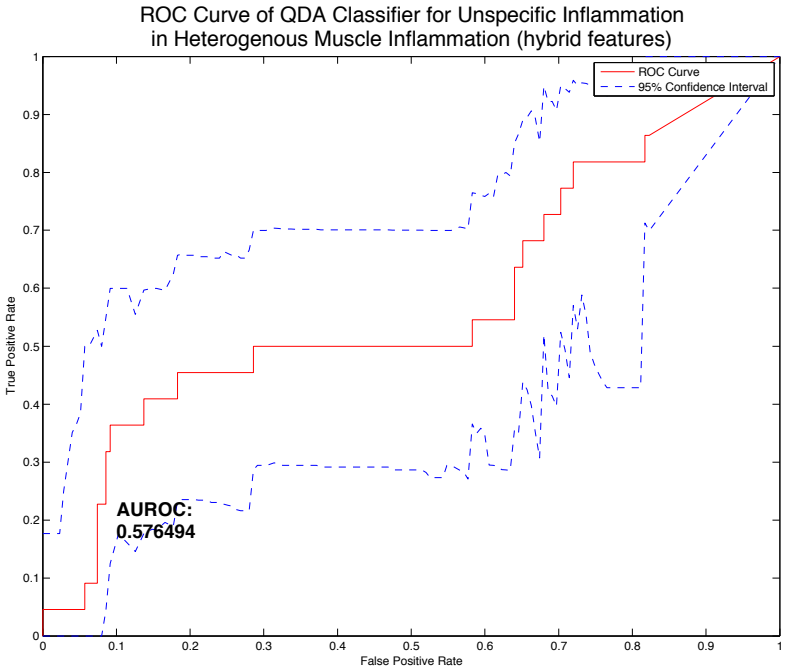

Figure 6.332

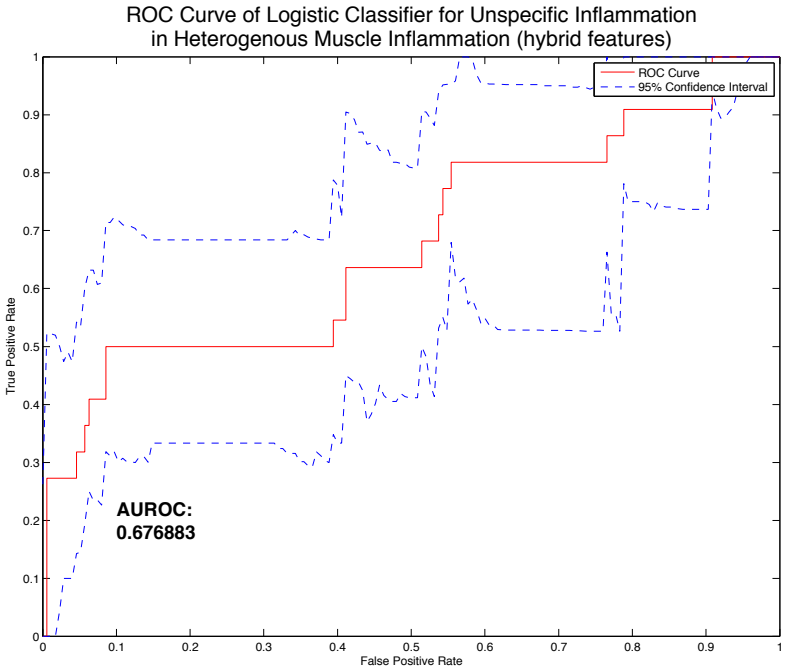

Figure 6.333

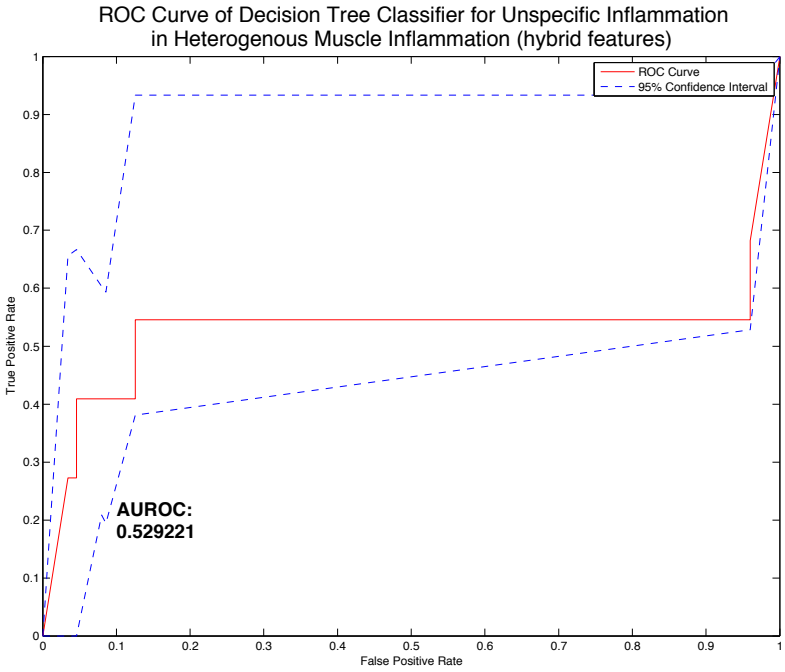

Figure 6.334

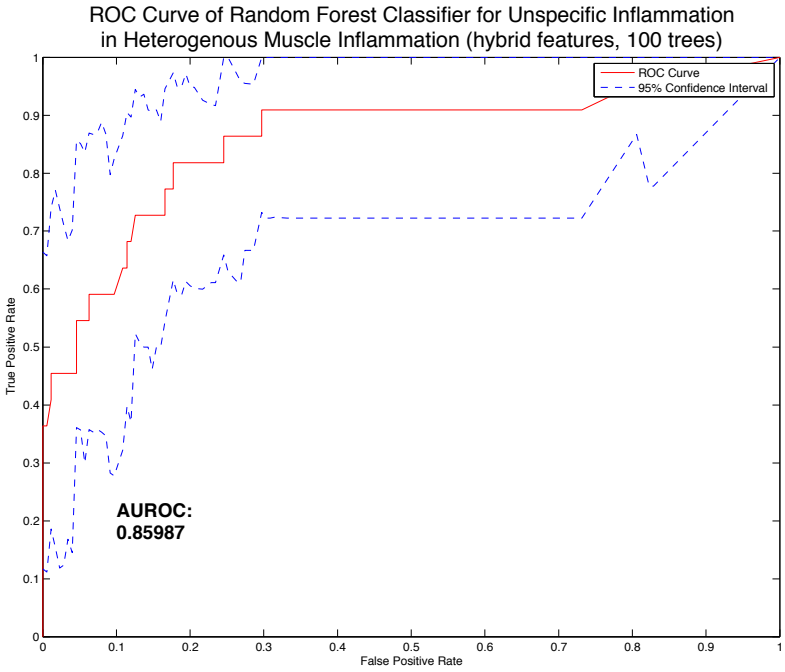

Figure 6.335

Type of Inflammation in Muscle (POD <= 5)

Original 14-Dimensional Feature Space

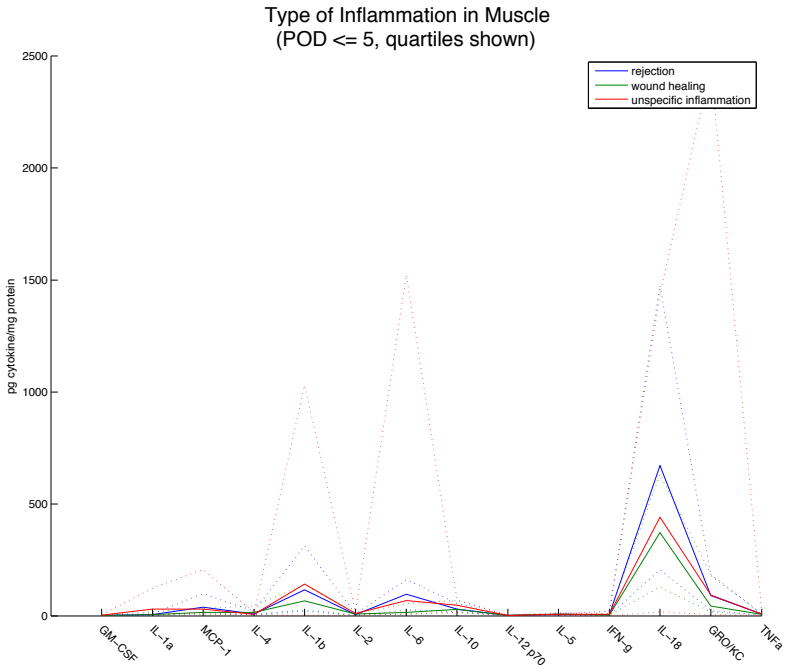

Figure 6.336

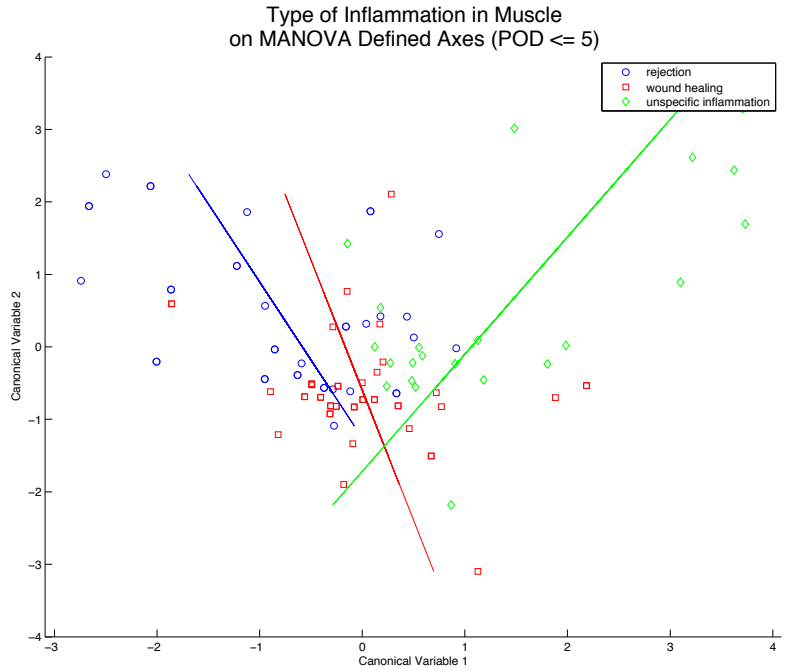

Figure 6.337

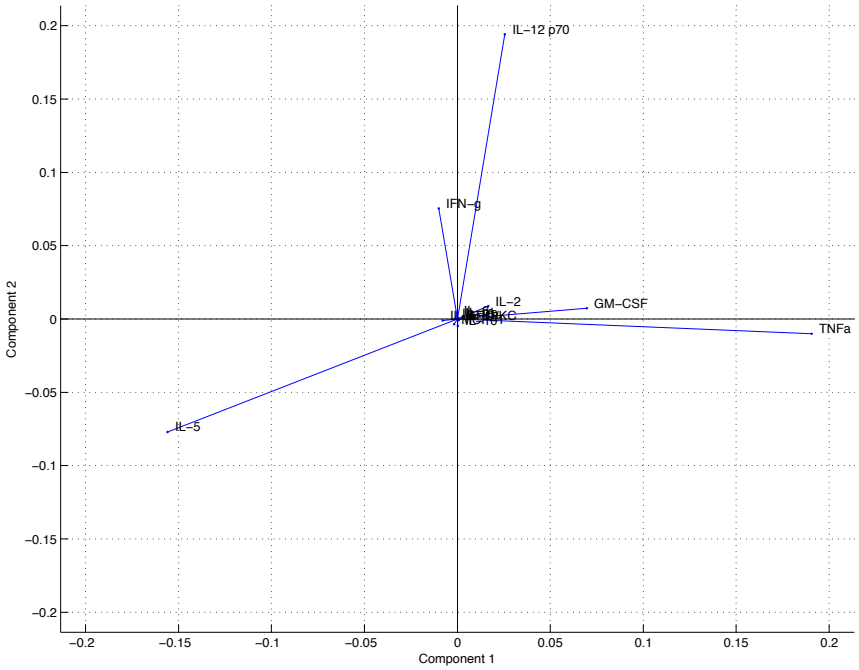

Figure 6.338

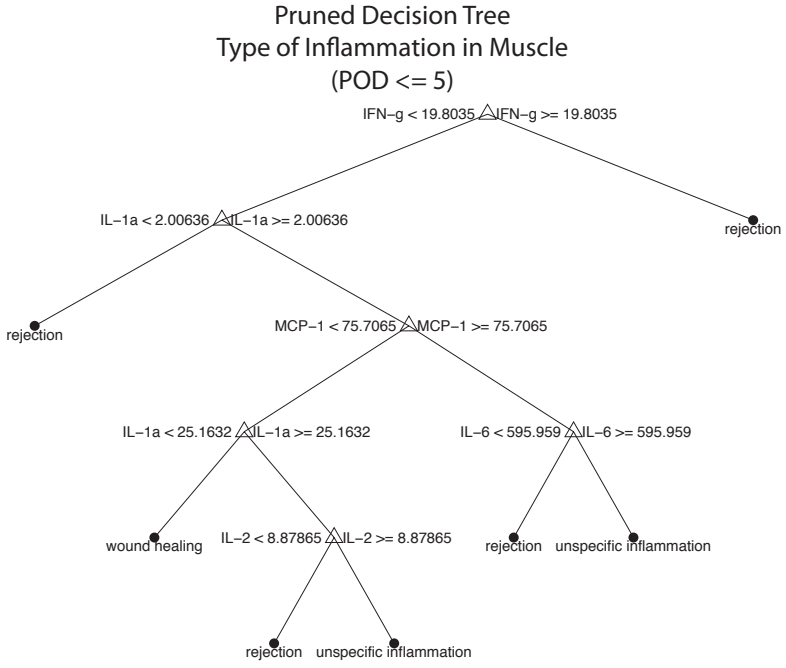

Figure 6.339

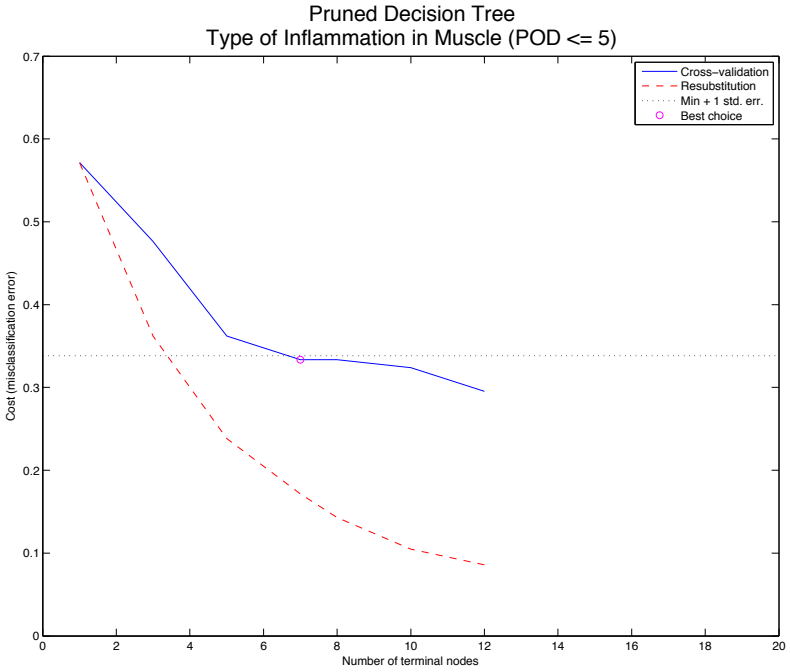

Figure 6.340

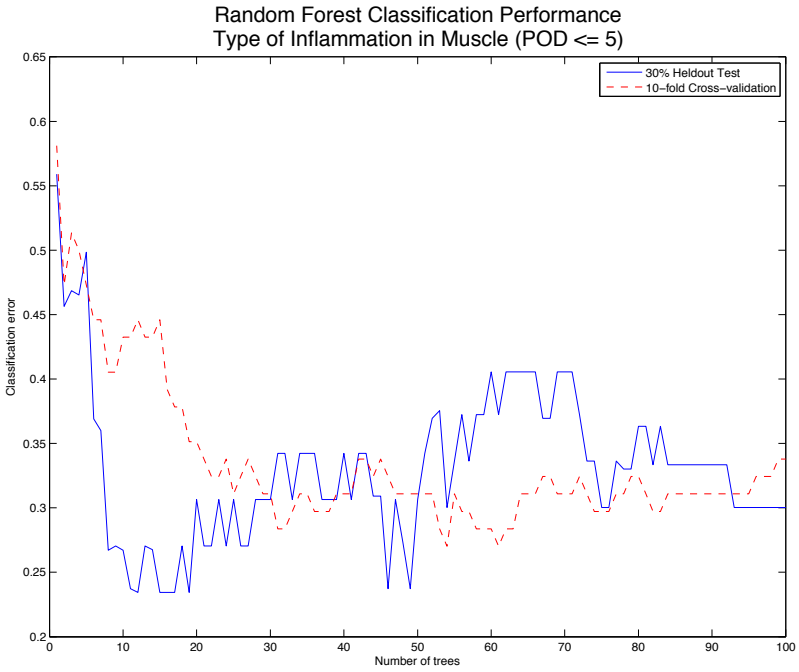

Figure 6.341

5-Dimensional Feature Selected Space

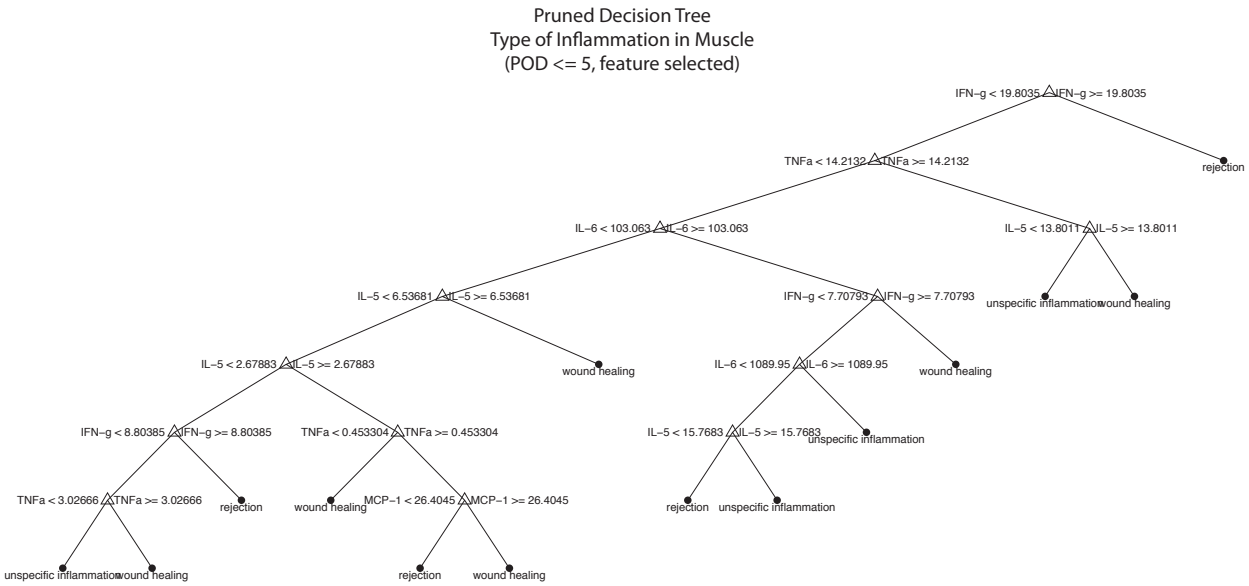

Figure 6.342

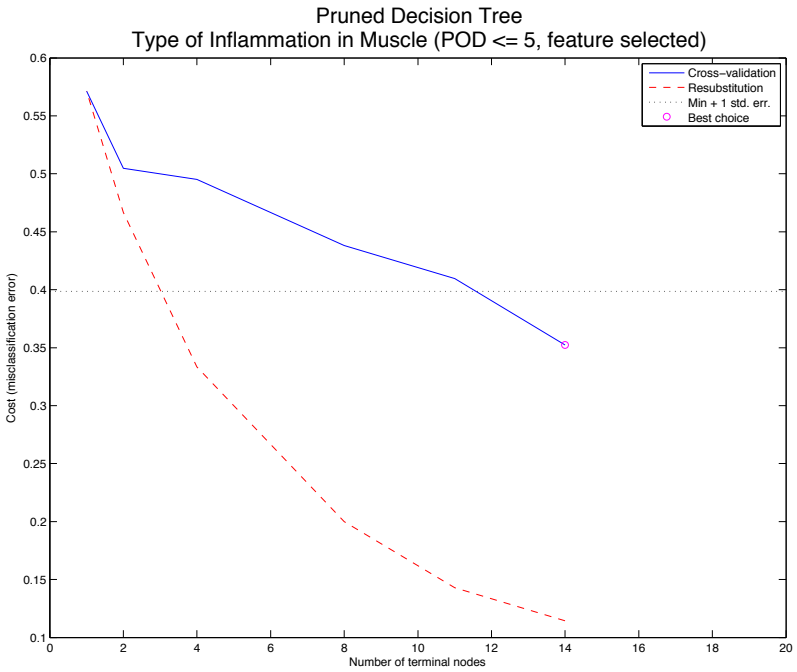

Figure 6.343

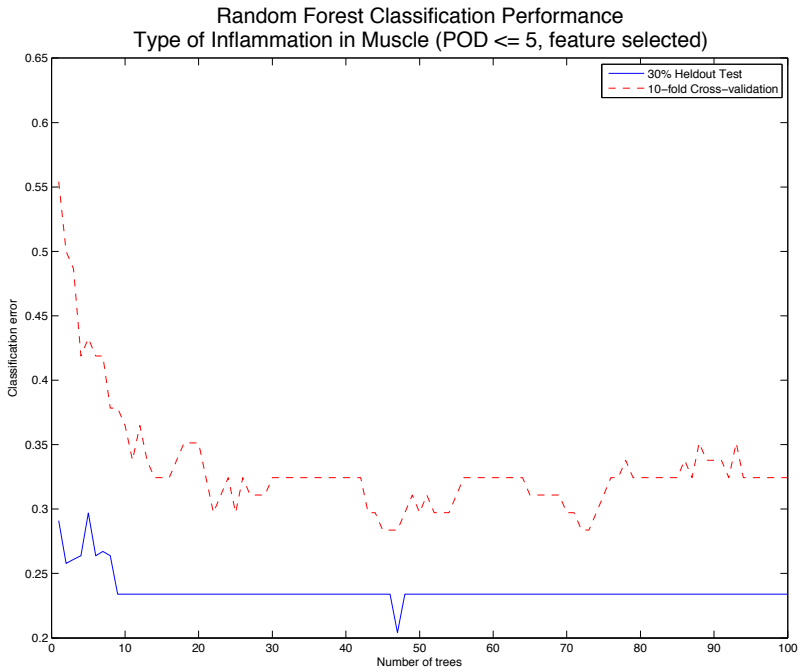

Figure 6.344

MANOVA Transformed Feature Space

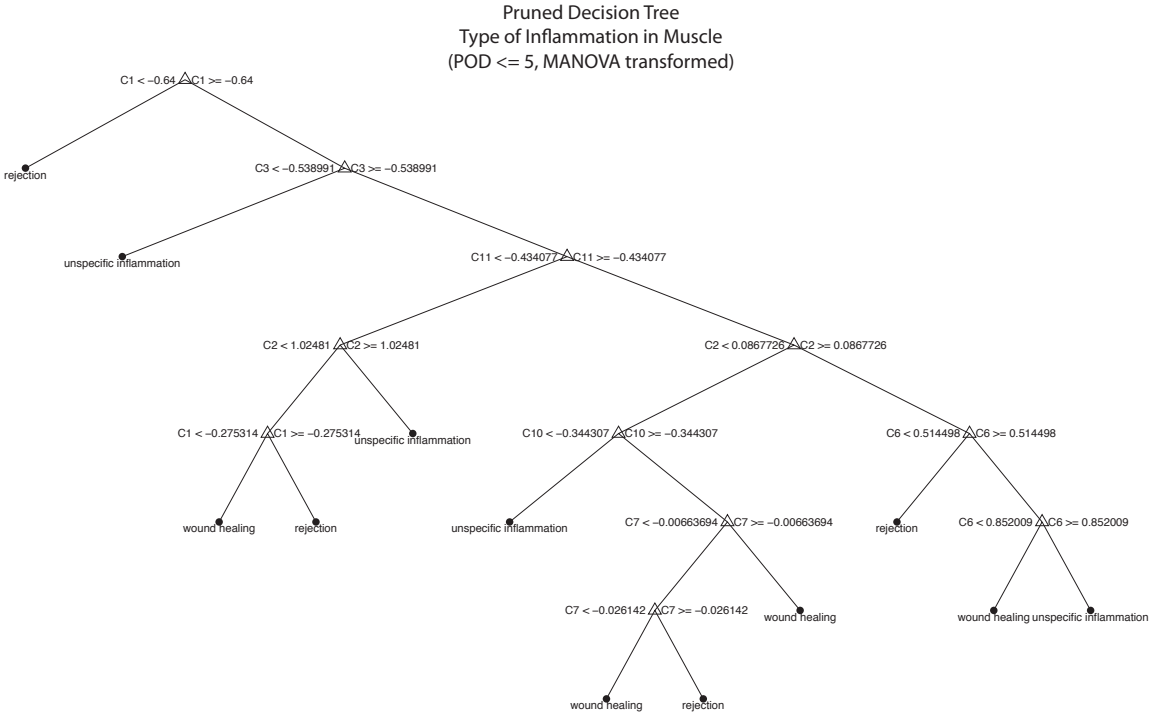

Figure 6.345

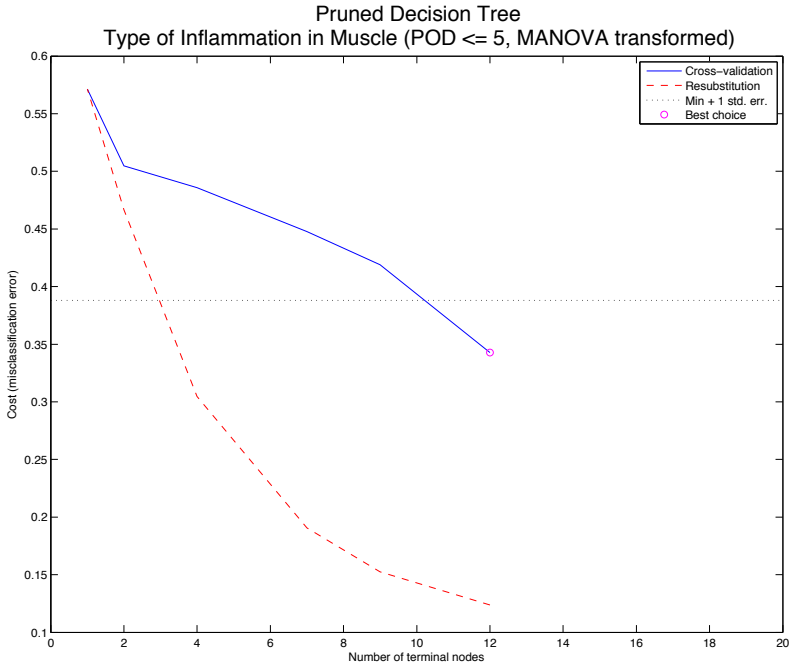

Figure 6.346

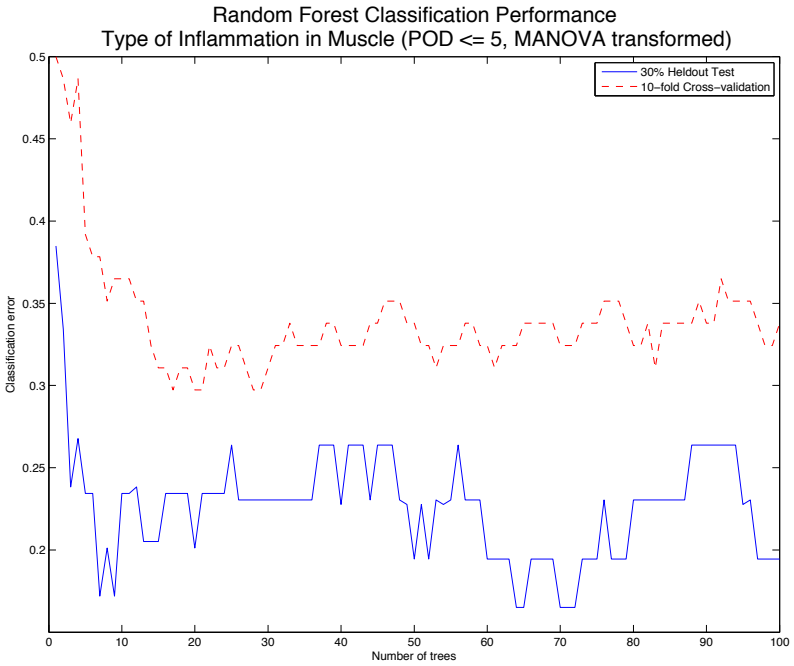

Figure 6.347

Type of Inflammation in Muscle (POD > 5)

Original 14-Dimensional Feature Space

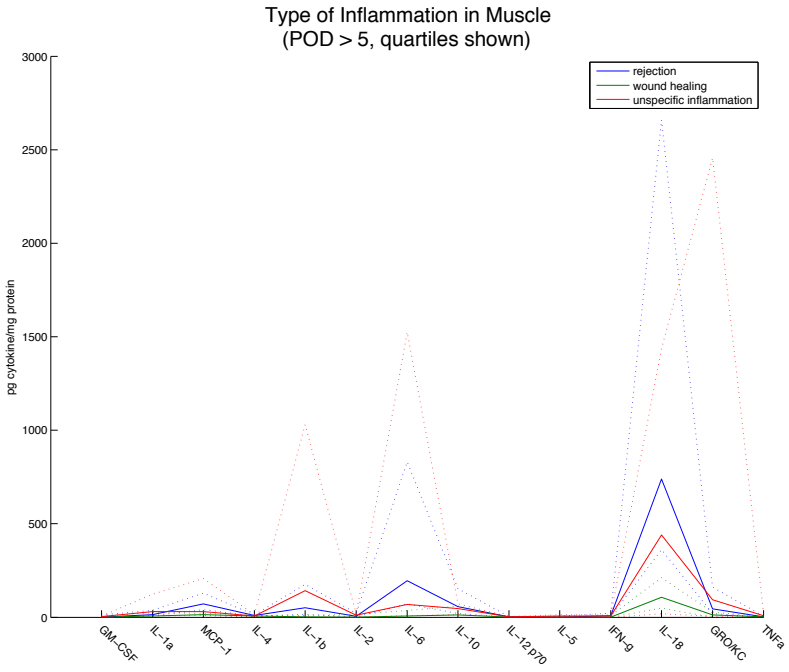

Figure 6.348

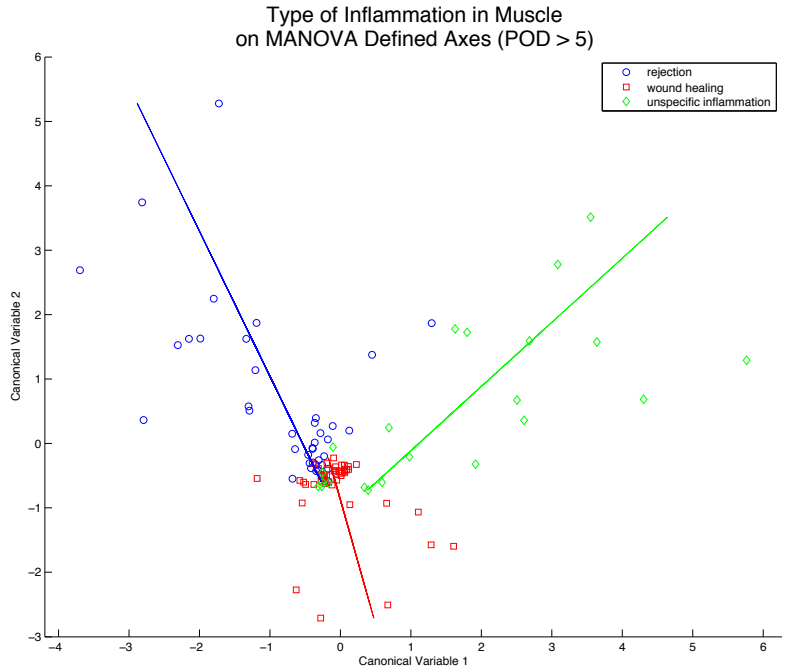

Figure 6.349

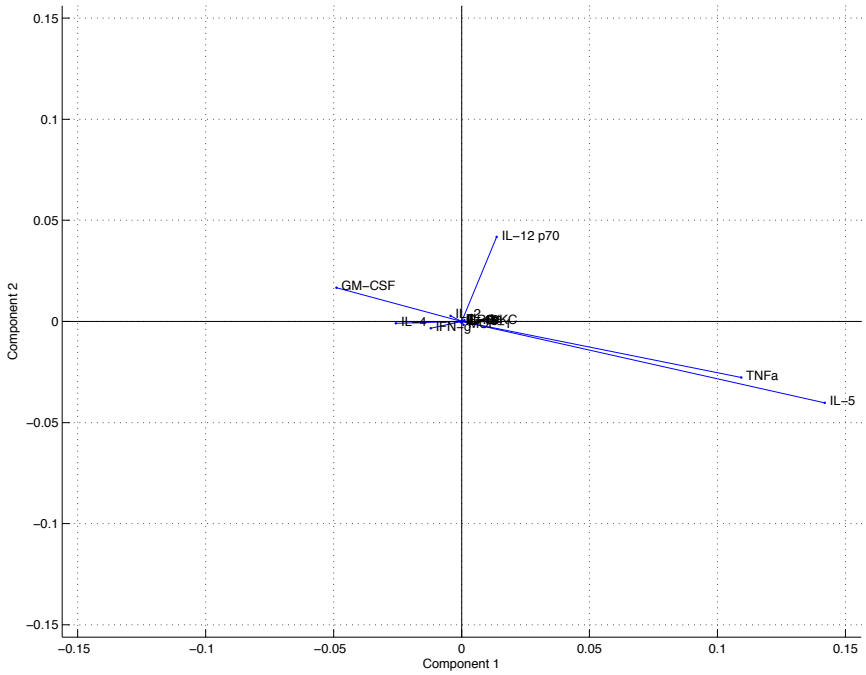

Figure 6.350

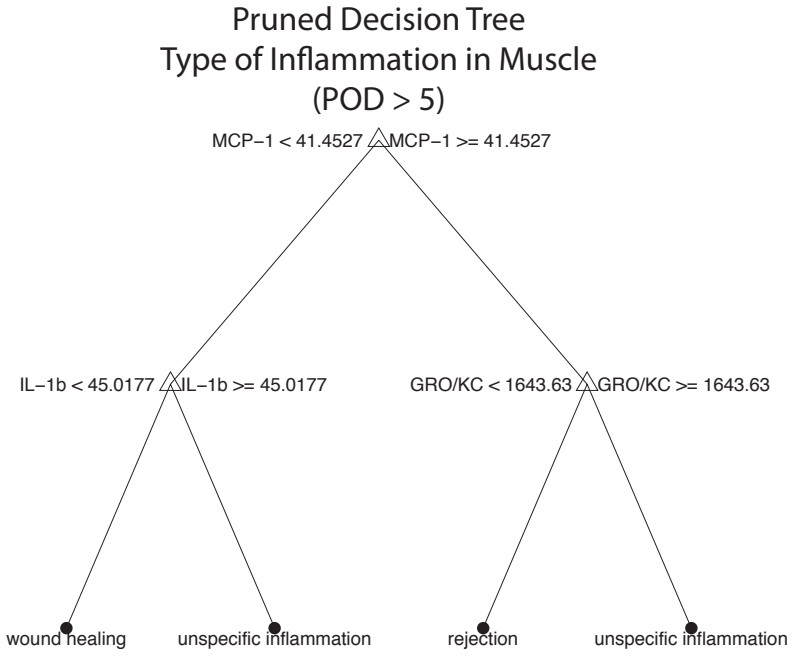

Figure 6.351

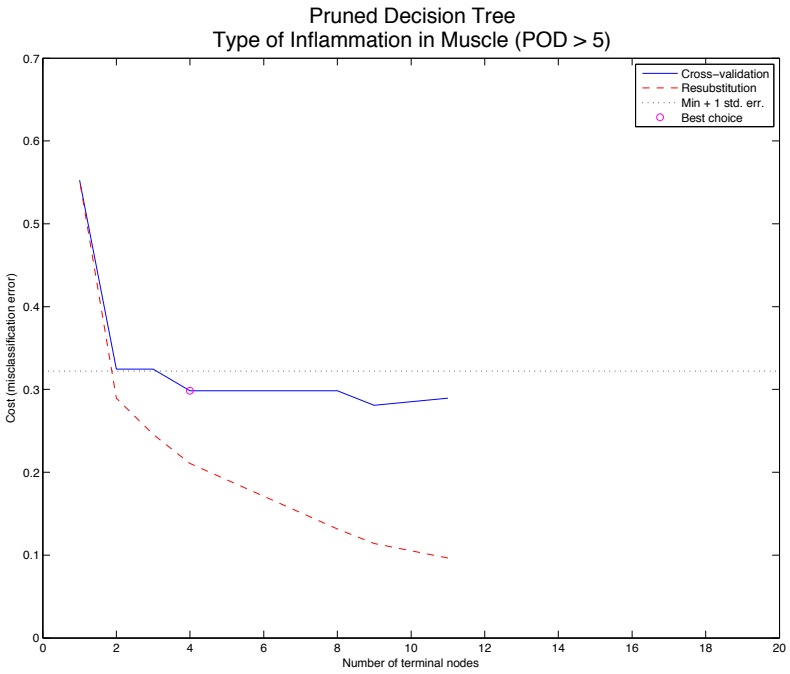

Figure 6.352

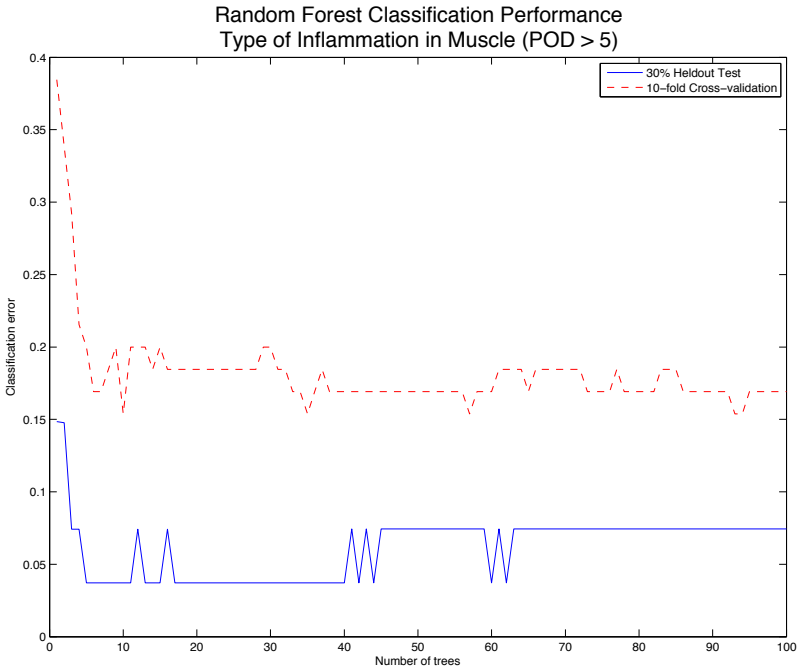

Figure 6.353

5-Dimensional Feature Selected Space

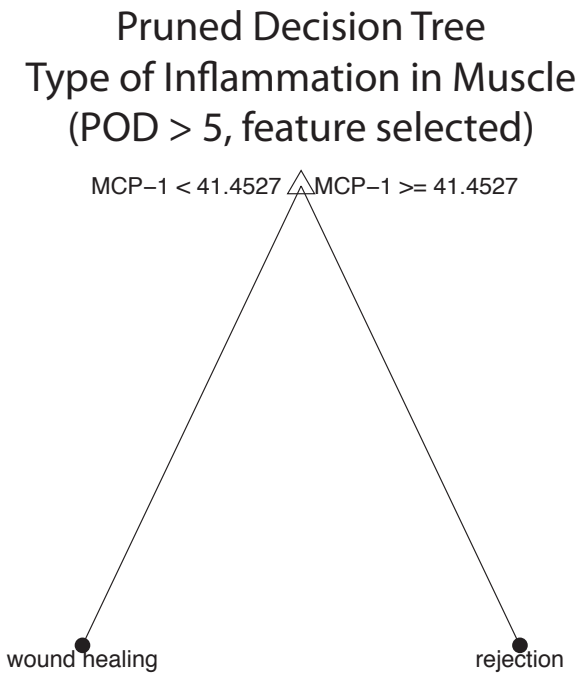

Figure 6.354

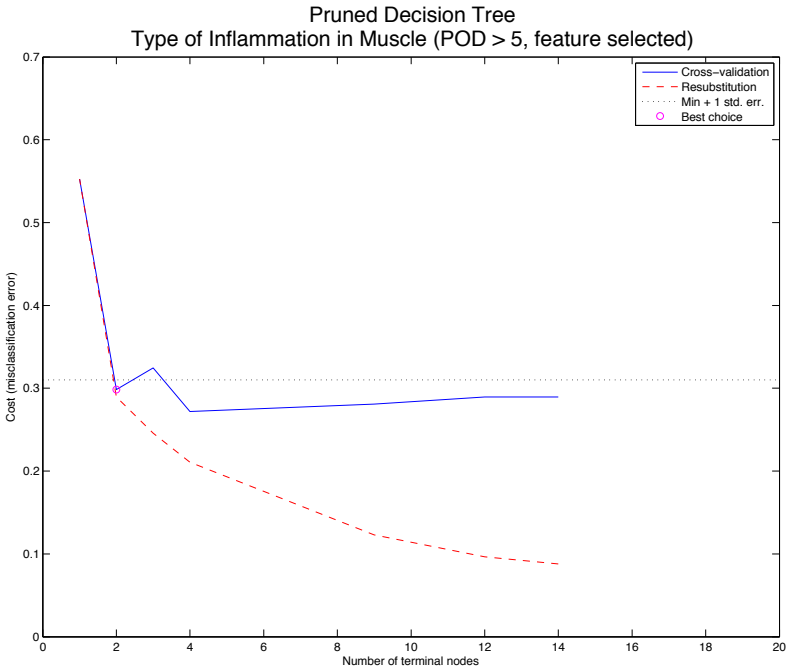

Figure 6.355

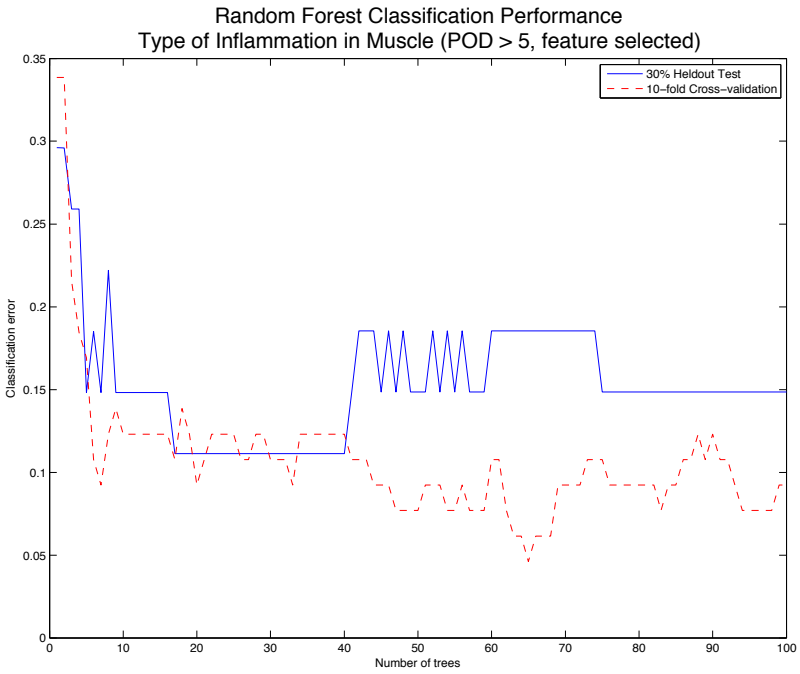

Figure 6.356

MANOVA Transformed Feature Space

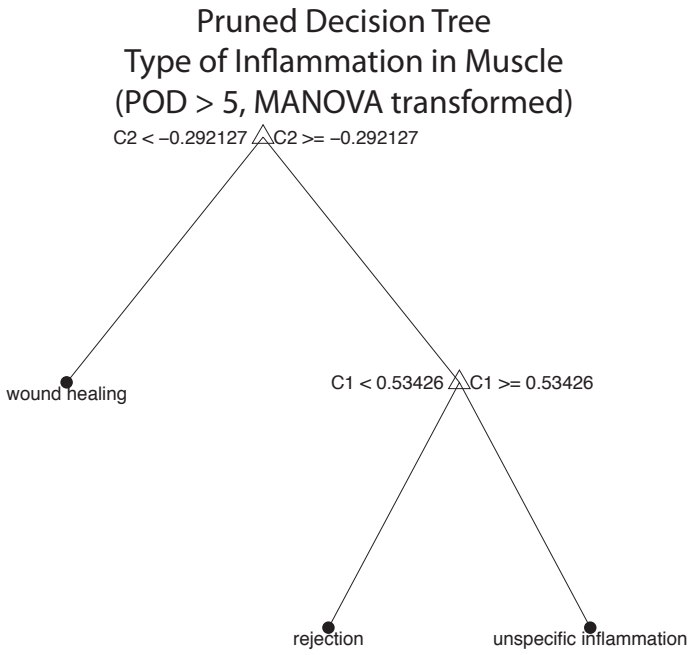

Figure 6.357

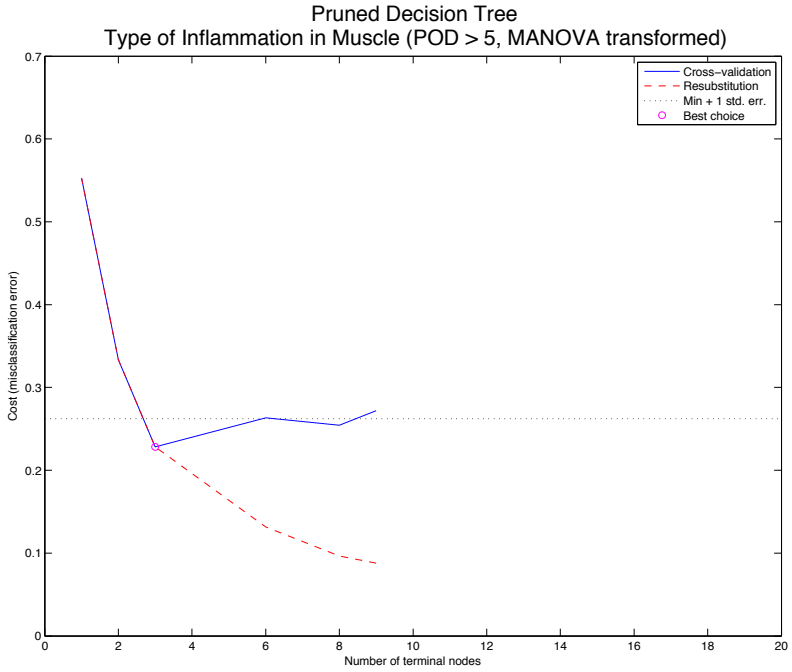

Figure 6.358

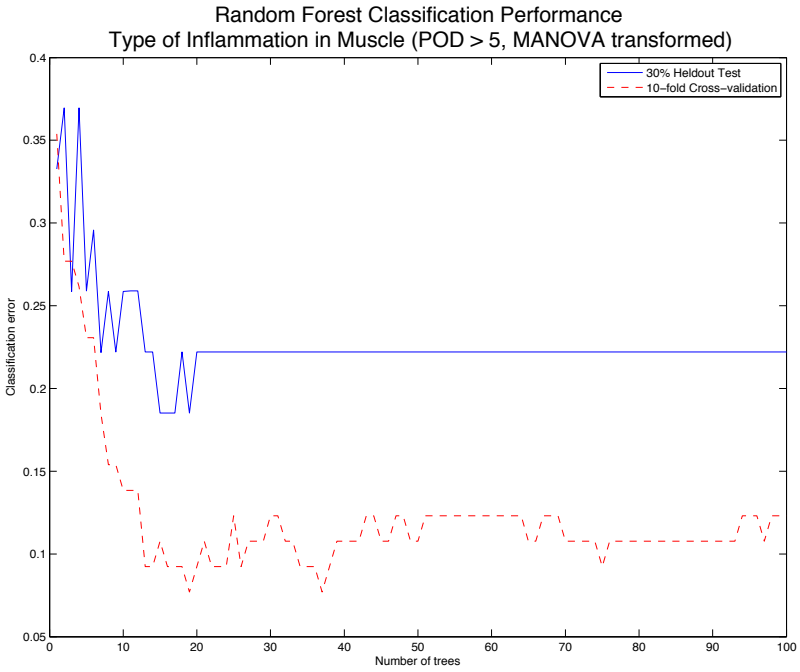

Figure 6.359

Appendix E Related Literature

The scientific literature is growing at an exponential rate. Highly active areas such as immunology, transplantation, and computer science seem to be growing even faster than most. This section provides references to literature, organized by area. This is not a comprehensive listing of all literature related to the themes in this thesis, but rather literature that was reviewed and most relevant to this work.

Cytokines, Chemokines, and Their Role in the Immune System

Bona, Constantin A, and Jean-Pierre Revillard. 2001. Cytokines and Cytokine Receptors: Physiology and Pathological Disorders. 1st ed. CRC Press, March 7.

Bondy, C, and D LeRoith, eds.C Bondy and D LeRoith to. 1997. Cytokines, Part A (Growth Factors & Cytokines in Health & Disease). 1st ed. Elsevier Science, May 2.

Miller, MD, and MS Krangel. 1992. "Biology and biochemistry of the chemokines: a family of chemotactic and inflammatory cytokines.." Critical reviews in immunology.

Epstein, FH. 1998. "Chemokines—chemotactic cytokines that mediate inflammation." New England Journal of Medicine.

Adams, DH. 1997. "Chemokines: leucocyte recruitment and activation cytokines." The Lancet.

Schall, TJ. 1994. "Chemokines, leukocyte trafficking, and inflammation." Current opinion in immunology.

Zlotnik, A, J Morales, and JA Hedrick. 1999. "Recent advances in chemokines and chemokine receptors.." Critical reviews in immunology.

Rollins, BJ. 1997. "Chemokines." Blood.

Gerard, C, and BJ Rollins. 2001. "Chemokines and disease." Nat Immunol.

Ward, SG, and K Bacon. 1998. "Chemokines and T lymphocytes: more than an attraction.." Immunity.

Mackay, CR. 2001. "Chemokines: immunology's high impact factors." Nature immunology.

Rossi, D. 2000. "The biology of chemokines and their receptors." Annual review of immunology.

Taub, DD, and JJ Oppenheim. 1994. "Chemokines, inflammation and the immune system.." Therapeutic immunology.

Beckerman, Martin. 2005. Molecular and cellular signaling. Springer Verlag.

Themes in Transplantation

Starzl, Thomas Earl, Carl-Gustav Groth, and Leonard Makowka. 1988. Liver transplantation.

Starzl, Thomas E, and John J Fung. 2010. Themes of liver transplantation. Hepatology (Baltimore, Md.). Vol. 51. June. doi:10.1002/hep.23595.

Petruzzo, PalminaMarco Lanzetta and Jean-Michel Dubernard to. 2007. Hand transplantation. Marco Lanzetta and Jean-Michel DubernardEds. 1st ed. Springer, January 19.

Brandacher, Gerald, and W P Andrew Lee. 2011. Hand Transplantation, an Issue of Hand Clinics. W B Saunders Co, November 28.

Lee, W P Andrew. 2008. Transplantation of composite tissue allografts. Springer Verlag.

Dubernard, Jean-Michel. 2001. Composite Tissue Allografts. John Libbey Eurotext.

Hakim, Nadey S, Earl Owen, and Jean-Michel Dubernard. 2006. Composite tissue allograft. Imperial College Pr.

Siemionow, M, M Bozkurt, and Y Kulahci. 2007. "Current status of composite tissue allotransplantation.." Handchirurgie, Mikrochirurgie, plastische Chirurgie : Organ der Deutschsprachigen Arbeitsgemeinschaft für Handchirurgie : Organ der Deutschsprachigen Arbeitsgemeinschaft für Mikrochirurgie der Peripheren Nerven und Gefässe : Organ der Vereinigung der Deutschen Plastischen Chirurgen 39 (3) (June): 145–155. doi:10.1055/s-2007-965233.

Gordon, Chad RCharles W Hewitt and W P Andrew Lee to. 2007. Transplantation of Composite Tissue Allografts. Charles W Hewitt and W P Andrew LeeEds. 1st ed. Springer, December 18.

Immunosuppression and Immunsuppressive Agents (specifically Tacrolimus)

Kino, T, H Hatanaka, and M Hashimoto. 1987. "FK-506, a novel immunosuppressant isolated from a Streptomyces. I. Fermentation, isolation, and physico-chemical and biological characteristics.." The Journal of ….

Kino, T, H Hatanaka, and S Miyata. 1987. "FK-506, a novel immunosuppressant isolated from a Streptomyces. II. Immunosuppressive effect of FK-506 in vitro.." The Journal of ….

Iwasaki, Yōji, Leonard Makowka, Thomas E Starzl, Satoru Todo, and European Society for Organ Transplantation. 1987. FK-506, a potential breakthrough in immunosuppression.

Goto, T, T Kino, H Hatanaka, and M Nishiyama. 1987. "Discovery of FK-506, a novel immunosuppressant isolated from Streptomyces tsukubaensis.." Transplantation ….

Fung, J, S Todo, and TE Starzl. 1991. "Pharmacokinetics of FK 506 in transplant patients." Transplantation ….

Kelly, PA, and GJ Burckart. 1995. "Tacrolimus: a new immunosuppressive agent." American journal of health- ….

Rejection and Markers of Rejection

Bishop, G A, B M Hall, G G Duggin, J S Horvath, A G Sheil, and D J Tiller. 1986. "Immunopathology of renal allograft rejection analyzed with monoclonal antibodies to mononuclear cell markers.." Kidney international 29 (3) (March): 708–717.

VERLAG, SPRINGER. 2010. Immunologic Signatures of Rejection. Springer Verlag, October 1.

Racusen, Lorraine C, Robert B Colvin, Kim Solez, Michael J Mihatsch, Philip F Halloran, Patricia M Campbell, Michael J Cecka, et al. 2003. "Antibody-mediated rejection criteria - an addition to the Banff 97 classification of renal allograft rejection.." American journal of transplantation : official journal of the American Society of Transplantation and the American Society of Transplant Surgeons 3 (6) (June): 708–714.

Lande, Jeffrey D, Jagadish Patil, Na Li, Todd R Berryman, Richard A King, and Marshall I Hertz. 2007. "Novel insights into lung transplant rejection by microarray analysis.." Proceedings of the American Thoracic Society 4 (1) (January): 44–51. doi:10.1513/pats.200605-110JG.

Tolerogenic and Minimal Immunosuppression Therapy

Starzl, TE, N Murase, K Abu-Elmagd, and EA Gray. 2003. "Tolerogenic immunosuppression for organ transplantation." The Lancet.

Demetris, AJ, JJ Fung, A Marcos, and TE Starzl. 2005. "Kidney transplantation under minimal immunosuppression after pretransplant lymphoid depletion with Thymoglobulin or Campath." Journal of the American ….

Classifiers and Statistical Learning

Mitchell, Tom M. 1997. Machine Learning. 1st ed. McGraw-Hill Science/Engineering/Math, March 1.

Witten, Ian H, and Eibe Frank. 2005. Data Mining: Practical Machine Learning Tools and Techniques, Second Edition (Morgan Kaufmann Series in Data Management Systems). 2nd ed. Morgan Kaufmann, June 22.

Sansone, Carlo, Josef Kittler, and Fabio Roli. 2011. Multiple Classifier Systems. 10th International Workshop, MCS 2011, Naples, Italy, June 15-17, 2011. Proceedings. Springer, June 29.

Cortes, C. 1995. "Support vector machine." Machine Learning.

Feature Transformation Methods

Golub, GH. 1970. "Singular value decomposition and least squares solutions." Numerische Mathematik.

Bunch, JR. 1978. "Updating the singular value decomposition." Numerische Mathematik.

Dunteman, George Henry. 1989. Principal components analysis. Sage Publications, Inc, May 1.

Bray, James H, and Scott E Maxwell. 1985. Multivariate analysis of variance. Sage Publications, Inc.

Harlow, Lisa L. 2005. The Essence of Multivariate Thinking. Basic Themes and Methods. Psychology Press, February 1.

De Lathauwer, L, and B De Moor. 2000. "A multilinear singular value decomposition." SIAM Journal on Matrix ….

Complexity, Efficiency, Signaling, and Systems

Nakanishi, Shigetada, Ryoichiro Kageyama, and Dai Watanabe, eds.Shigetada Nakanishi, Ryoichiro Kageyama, and Dai Watanabe to. 2009. Systems Biology: The Challenge of Complexity. 1st ed. Springer, May 15.

Hawkins, John A. 2004. Efficiency and complexity in grammars. Oxford University Press, USA.

Ricard, Jacques. 1999. Biological complexity and the dynamics of life processes. Elsevier Science, November 1.

Choi, Sangdun. 2010. Systems Biology of Signaling Networks. Springer Verlag, August 30.

Weng, G, and US Bhalla. 1999. "Complexity in biological signaling systems." Science.

Kriete, Andres, and Roland Eils. 2006. Computational systems biology. Academic Press.

Prior Publications and Refereed Conference Presentations in the Area

Wolfram-Raunicher, D; Starzl, R; Barclay, D; Vodovotz, Y; Levine, L; Wang, Y; Gorantla, V.; Brandacher, G; Lee, WPA; Schneeberger, S. "A Computational Model To Profile Cytokine Networks Mediating Acute Rejection After Composite Tissue Allotransplantation". Plastic & Reconstructive Surgery, June 2010, Vol. 125, Issue 6, pp. 24, doi: 10.1097/01.prs.0000371760.07150.cc

Wolfram D, Starzl R, Barclay D, Vodovotz Y, Wang Y, Brandacher G, Gorantla V, Lee WPA, Carbonell J, Schneeberger S. Profiling cytokine networks mediating acute rejection after composite tissue allotransplantation in a rat limb transplant model. Robert H. Ivy Society. Pittsburgh, April 2009. Invited Talk.

Starzl R, Brandacher G, Wolfram D, Barclay D, Vodovotz Y, Wang Y, Gorantla V, Pratschke J, Lee WPA, Carbonell J, Schneeberger S. Profiling cytokine expression and dynamics mediating acute rejection following composite tissue allotransplantation in a rat model. Univ. of Pittsburgh Research Day, May 2009. Poster Presentation.

Wolfram D, Starzl R, Barclay D, Vodovotz Y, Brandacher G, Lee WPA, Schneeberger S. Profiling cytokine networks mediating acute rejection after CTA in a rat model. Ohio Valley Meeting of Plastic Surgeons. May 2009. Invited Talk.

Wolfram-Raunicher D, Starzl R, Barclay D, Vodovotz Y, Levine L, Wang Y, Gorantla V, Brandacher G, Lee WPA, Schneeberger S. Profiling gene expression and cytokine networks mediating acute rejection after composite tissue allotransplantation. European Plastic Surgery Research Council 1st meeting. August 2009. Invited Talk.

Starzl R, Wolfram D, Barclay D, Vodovotz Y, Levine L.M., Uguroglu S., Wang Y, Gorantla V, Brandacher G, Lee WPA, Schneeberger S. Diagnosis of acute skin rejection in a rat limb allotransplant model utilizing a robust logistic classifer. 9th International Society of Hand and Composite Tissue Transplantation. Sept. 2009. Invited Talk.

Wolfram D, Starzl R, Barclay D, Vodovotz Y, Wang Y, Brandacher G, Lee WPA, Schneeberger S. Profiling gene expression and cytokine networks mediating acute rejection after composite tissue allotransplantation. Plastic Surgery Research Council 55th annual meeting. May 2010. Plenary Talk.

Starzl R, Brandacher G, Wolfram D, Barclay D, Vodovotz Y, Wang Y, Gorantla V, Pratschke J, Lee WPA, Schneeberger S. Analysis of genetic and proteomic factors of the immune response mediating cellular infiltration and trafficking in skin rejection of composite tissue allografts. XXIII International Congress of The Transplantation Society. August 2010. Poster Presentation.

Starzl R, Wolfram D, Barclay D, Vodovotz Y, Wang Y, Brandacher G, Pratschke J, Lee WPA, Schneeberger S. Allogeneic and syngeneic cytokine networks in skin muscle and composite tissue allografts. XXIII International Congress of The Transplantation Society. August 2010. Poster Presentation.